Organotetrelchalkogenidcluster mit Heteroadamantanstruktur

Kumulative Dissertationsschrift

zur Erlangung des akademischen Grades eines Doktors der Naturwissenschaften (Dr. rer. nat.)

dem Fachbereich Chemie der Philipps-Universität Marburg (Hochschulkennziffer 1180) vorgelegt von

Eike Dornsiepen, M. Sc.
aus Bad Wildungen

Marburg, 2019

Erstgutachterin: Prof. Dr. Stefanie Dehnen
Zweitgutachter: PD Dr. Ralf Tonner
Promotionsverfahren eröffnet: 22. 05. 2019
Prüfungstermin: 16. 07. 2019

Every experiment destroys some
of the knowledge of the system which
was obtained by previous experiments.
– Werner Heisenberg

Erklärung

Ich erkläre, dass eine Promotion noch an keiner anderen Hochschule als an der Philipps-Universität Marburg, Fachbereich Chemie, versucht wurde. Ich versichere, dass ich meine vorgelegte Dissertation:

„Organotetrelchalkogenidcluster mit Heteroadamantanstruktur“

selbst und ohne fremde Hilfe verfasst, nicht andere als die in ihr angegebenen Quellen oder Hilfsmittel benutzt, alle vollständig oder sinngemäß übernommenen Zitate als solche gekennzeichnet sowie die Dissertation in der vorliegenden oder einer ähnlichen Form noch bei keiner anderen in- oder ausländischen Hochschule anlässlich eines Promotionsgesuchs oder zu anderen Prüfungszwecken eingereicht habe.

Marburg, 21. Mai 2019 Eike Dornsiepen

Die vorliegende Arbeit wurde im Zeitraum von Februar 2016 bis Mai 2019 unter der Leitung von Prof. Dr. Stefanie Dehnen am Fachbereich Chemie der Philipps-Universität Marburg angefertigt.

Inhaltsverzeichnis

Abbildungsverzeichnis

Verzeichnis der Schemata

1 Einführung

Die vorliegende Arbeit berichtet über die Darstellung verschiedener Organotetrelchalkogenidcluster mit Heteroadamantanstruktur, deren Derivatisierung durch Umsetzung mit Übergangsmetallkomplexen sowie die Untersuchung der nichtlinearen optischen Eigenschaften der erhaltenen Verbindungen. Im Folgenden soll daher zunächst auf Vorarbeiten zu den verschiedenen Verbindungsklassen, die wichtigsten Grundlagen der nichtlinearen Optik sowie auf die unmittelbaren Vorarbeiten, welche zur Entstehung des Projekts führten, eingegangen werden.

1.1 Organotetrelchalkogenidcluster

Organotetrelchalkogenidcluster sind Moleküle, die sich aus einem anorganischen Grundgerüst, welches Atome der Elemente der Gruppen 14 und 16 enthält, sowie einer organischen Ligandenhülle zusammensetzen. Die anorganischen Kerne leiten sich formal von den entsprechenden Chalkogenidotetrelat-Anionen ab, bei denen die terminalen Chalkogenatome durch organische Substituenten ersetzt sind, welche über kovalente Tetrel-Kohlenstoffbindungen angebunden sind. Es handelt sich somit um Verbindungen, deren allgemeine Zusammensetzung mit der Formel $[(RT)_xE_y]$ (R = organischer Substituent; T = Si, Ge, Sn; E = O, S, Se, Te) beschrieben werden kann.
Das Interesse an solchen anorganisch-organischen Hybridverbindungen gründet auf der Verknüpfung der charakteristischen Eigenschaften der anorganischen und organischen Bestandteile, woraus Materialeigenschaften resultieren, welche nur mit den einzelnen Komponenten nicht zu erreichen wären.[1] Die elektrischen und optischen Eigenschaften werden häufig von Struktur und Zusammensetzung des anorganischen Kerns beeinflusst, wohingegen Löslichkeit und die Reaktivität gegenüber Molekülen (einschließlich katalytischer Aktivität[2]) und Oberflächen vor allem von den organischen Substituenten abhängen.[3]
Hinsichtlich der Strukturmotive der anorganischen Kerne soll hier zuerst auf die Chalkogenidotetrelate eingegangen werden. In der Natur finden sich vor allem deren leichteste Vertreter, die Silikate. Deren grundlegendes Strukturmotiv ist das Orthosilikat-Anion $[SiO_4]^{4-}$. Durch Eckenverknüpfung mehrerer SiO_4-Tetraeder entstehen räumlich begrenzte acyclische (Sorosilicate) und cyclische (Cyclosilicate) Strukturmotive sowie periodische Ketten (Inosilicate), Schichten (Phyllosilicate) und Gerüste (Tectosilicate). In all diesen Verbindungen sind die Si-Atome immer tetraedrisch koordiniert und es tritt ausschließlich Eckenverknüpfung der Tetraeder auf.[4]
Als schwere Homologe der Sorosilicate können die supertetraedrischen Tn-Clusteranionen aufgefasst werden, wobei n angibt, aus wie vielen TE_4-Tetraedern pro Supertetraederkante das Anion aufgebaut ist (siehe Abbildung 1). Solche Anionen sind bis zu einer Maxi-

malgröße von T5 bekannt,[5–7] dabei handelt es sich um Anionen der Zusammensetzung $[M_{35}E_{56}]^{q-}$ (M = Tetrel- oder ÜM-Atom, E = O, S, Se, Te). Solche großen Anionen sind nur durch Einbau niedrig geladener Kationen wie Cu^{+}, Zn^{2+} oder Cd^{2+} zugänglich, da andernfalls die Gesamtladung zu groß wird. Bei ausschließlichem Vorhandensein von Tetrelkationen entstehen in der Regel T2-Clusteranionen der Zusammensetzung $[T_4E_{10}]^{4-}$,[8,9] deren Struktur der des Adamantans entspricht.

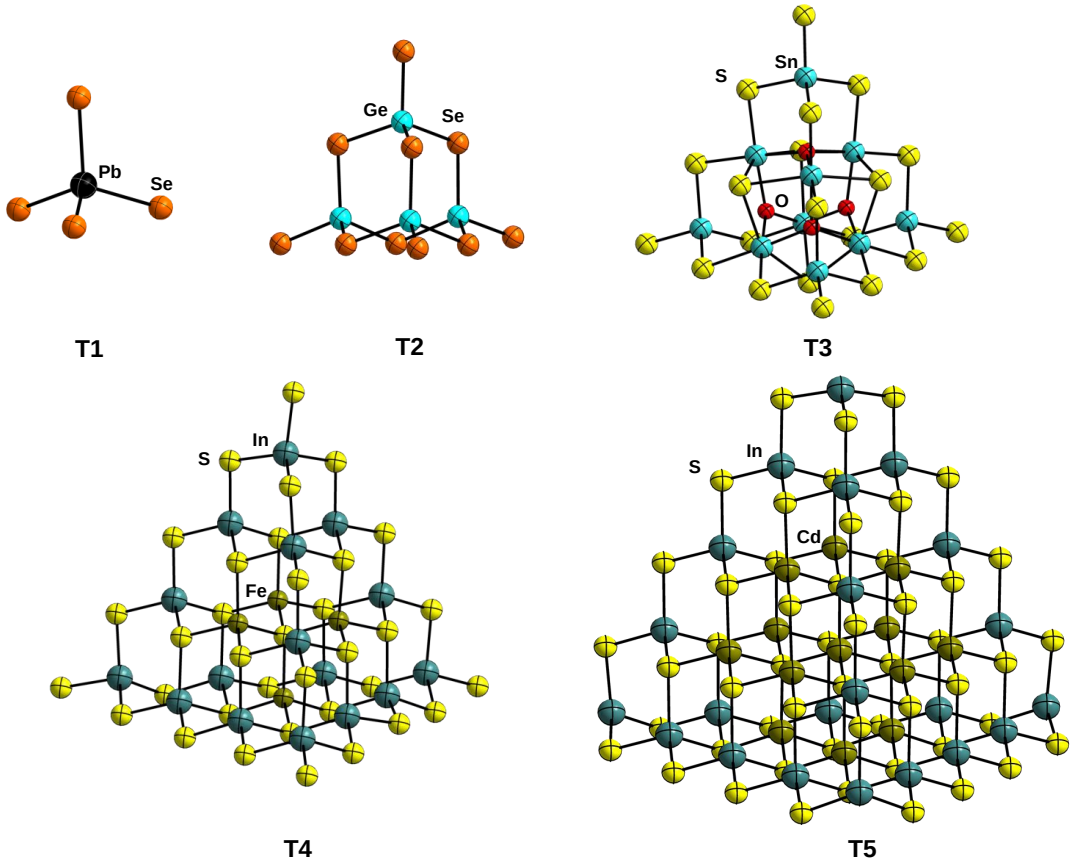

Abbildung 1: Beispiele für supertetraedrische Chalkogenidometallat-Anionen. Obere Reihe (v.l.n.r.): $[PbSe_4]^{4-}$,[10] $[Ge_4Se_{10}]^{4-}$,[11] $[Sn_{10}S_{20}O_4]^{8-}$.[12] Untere Reihe: $[H_2Fe_4In_{16}S_{35}]^{12-}$,[13] $[Cd_{13}In_{22}S_{52}]^{12-}$.[7]

Bei den schweren Chalkogenidotetrelaten treten neben dem Verknüpfungsmotiv der Eckenverknüpfung auch Kanten- und Flächenverknüpfung auf, was die strukturelle Vielfalt noch weiter erhöht. So entsteht durch Kantenverknüpfung zweier Tetraeder das $[T_2E_6]^{4-}$-Anion.[14–16] Durch Einbau von Übergangsmetallatomen kann noch eine andere Clusterfamilie aufgebaut werden, bei der vier $[TE_4]$-Tetraeder und ein zentrales $[T_4E]$-Tetraeder kombiniert werden, was zur Ausbildung pentasupertetraedrischer sogenannter P1-Cluster führt (siehe Abbildung 2, oben rechts).[17–24] Weitere häufig auftretende Strukturmotive sind das Defektheterokuban $[T_3E_7]^{q-}$[25] (siehe Abbildung 2, oben links) sowie

dessen über zwei Chalkogenatome verbrücktes Dimer, das Bisdefektheterokuban $[T_6E_{10}]^{q-}$ (siehe Abbildung 2, oben mittig), die sich dadurch auszeichnen, dass in ihnen das Tetrelatom nicht tetraedrisch, sondern trigonal bipyramidal koordiniert ist. Durch Kombination dieser Strukturmotive kann eine Vielzahl von Ketten-, Schicht- und Raumnetzstrukturen erhalten werden,[26] aber auch die Isolation großer diskreter Anionen, deren größten Vertreter das als „Zeoball“ bezeichnete $[Ge_{24}Sn_{36}Se_{132}]^{24-}$-Anion (siehe Abbildung 2, unten) darstellt, ist möglich.[27,28]

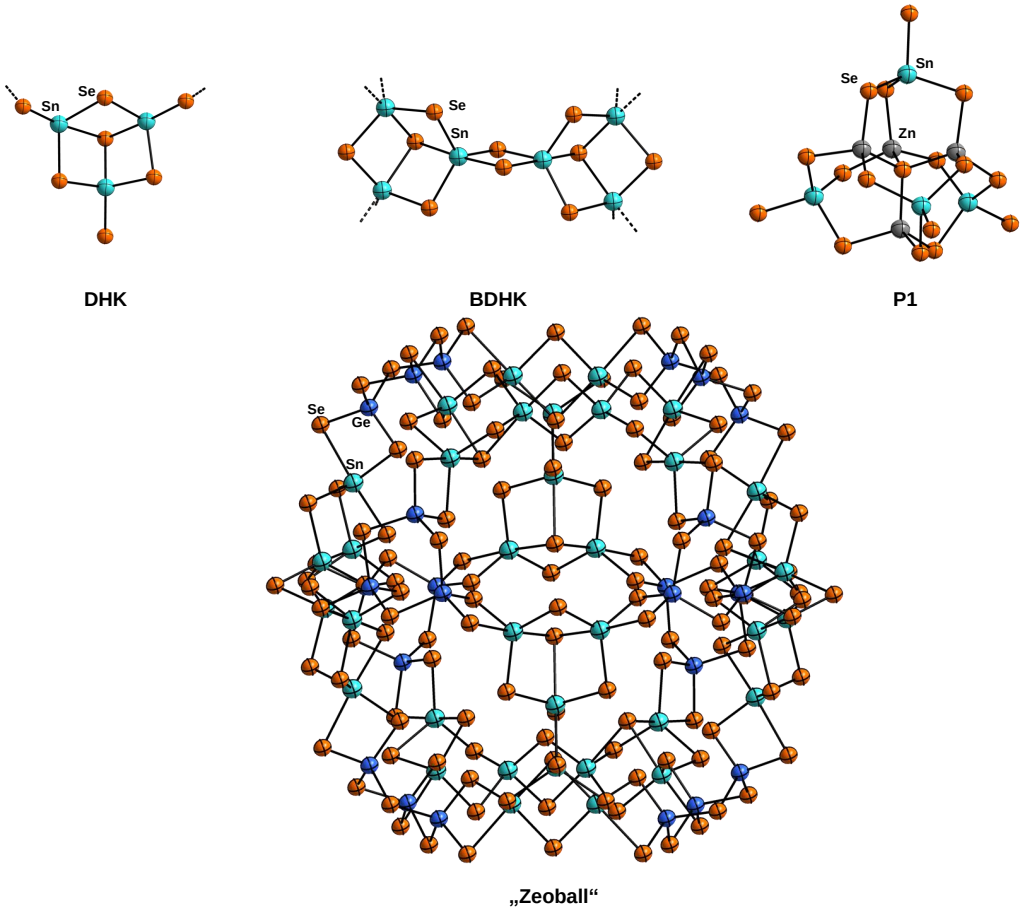

Abbildung 2: Weitere typische Bausteine bzw. Anionenstrukturen von Chalkogenidometallaten. Oben links: $[Sn_3Se_7]^{2-}$-Defektheterokuban-Anion.[25] Oben Mitte: $[Sn_6Se_{14}]^{4-}$-Bisdefektheterokuban-Anion.[29] Oben rechts: P1-Clusteranion der Zusammensetzung $[Sn_4Zn_4Se_{17}]^{10-}$.[18] Unten: „Zeoball“ -Anion der Zusammensetzung $[Ge_{24}Sn_{36}Se_{132}]^{24-}$.[28]

Chalkogenidotetrelate besitzen vielfältiges Anwendungspotential, etwa als Ionentauscher,[30] Ionenleiter,[31–35] Gasadsorptionsmaterialien,[36] oder Katalysatoren.[37] Durch (formale) Substitution der terminalen Chalkogenatome in den gerade vorgestellten Baugruppen durch organische Substituenten entstehen neutrale oder niedrig geladene Orga-

notetrelchalkogenidcluster. Auf deren Strukturen und Eigenschaften soll in Abschnitt 1.3 näher eingegangen werden. Hier sei zunächst der präparative Zugang zu dieser Verbindungsklasse dargelegt.

1.2 Präparative Zugangswege

Organotetrelchalkogenidcluster werden grundsätzlich durch Umsetzung eines Organotetrelsynthons mit einer Chalkogenidquelle synthetisiert. Als Organotetrel-Bausteine werden übli-cherweise die jweiligen Trichloride verwendet, welche die zum Aufbau von Käfigstrukturen erforderlichen drei Abgangsgruppen besitzen. Als Chalkogenidquelle kommen in der Regel die Alkalimetallchalkogenide oder die Bis(trimethylsilyl)chalkogenide in Frage; vereinzelt wurden auch Schwefelwasserstoff[38,39] oder Ammoniumpolysulfide[40] verwendet. Die Alkalimetallchalkogenide werden zweckmäßigerweise aus den Elementen in flüssigem Ammoniak dargestellt.[41,42] Durch Umsetzung der Alkalimetallchalkogenide mit Chlorotrimethylsilan und anschließende Destillation sind die Bis(trimethylsilyl)chalkogenide erhältlich. Alternativ ist die Darstellung der Alkalimetallchalkogenide auch in organischen Lösungsmitteln wie Tetrahydrofuran möglich, falls ein Elektronentransfer-Reagenz wie Naphthalin in katalytischen Mengen zugegeben wird;[43,44] hierbei stellt sich jedoch die vollständige Abtrennung des Naphthalins schwierig dar, sodass auf diesem Wege hergestellte Bis(trimethylsilyl)chalkogenide in der Regel mit ebendiesem verunreinigt sind.
Aufwendiger gestaltet sich in der Regel die Synthese der erforderlichen Organotetreltrichloride. Für die Tetrelelemente Silicium und Germanium erfolgt diese in der Regel durch Umsetzung von Organolithium- oder Grignard-Reagenzien mit einem Überschuss an $SiCl_4$ bzw. $GeCl_4$, wobei bei geeigneter Wahl der Reaktionsbedingungen in der Regel selektiv die einfach substituierte Spezies erhalten wird (vgl. Gleichung 1).[45,46] Natürlich ist hierbei die Auswahl der organischen Substituenten auf solche begrenzt, die gegenüber Organolithium- oder -Organomagnesium-Spezies inert sind; dies erschwert die Synthese von Organotetreltrichloriden mit funktionellen Gruppen, welche eine nachfolgende Derivatisierung erlauben. Im Falle des Zinns ist dieser Syntheseweg in der Regel wenig erfolgversprechend, da dort die Aktivierungsbarriere für die Zweit- und Drittsubstitution deutlich geringer ausfällt und somit in der Regel ein Gemisch aus $RSnCl_3$, R_2SnCl_2 und R_3SnCl erhalten wird, das sich aufgrund der nur geringen Unterschiede in Siedepunkten und Löslichkeiten nicht sinnvoll auftrennen lässt. Eine der wenigen Ausnahmen ist hierbei das Cyclopentadienylzinntrichlorid, welches sich sauber in einer Salzeliminierungsreaktion aus Natriumcyclopentadienid und Zinntetrachlorid im Verhältnis 1:1 herstellen lässt.[47] In der Regel werden Organozinntrichloride jedoch durch eine nach K. A. Kocheshkov benannte Redistributionsreaktion aus einer Tetraorganozinnverbindung und Zinntetrachlorid erhalten. Für einfache Alkyl- oder Arylsubstituenten ohne funktionelle Gruppen

wird zunächst in einer Grignard-Reaktion die symmetrische Tetraorganozinnspezies R_4Sn hergestellt und anschließend mit drei Äquivalenten Zinntetrachlorid zum gewünschten Organozinntrichlorid umgesetzt (vgl. Gleichung 2).[48–51] Organozinntrichloride mit funktionellen organischen Gruppen hingegen werden üblicherweise in einer Variante dieser Redistributionsreaktion erhalten, bei der eine gemischtsubstituierte Tetraorganozinnverbindung RR'_3Sn mit einem Äquivalent Zinntetrachlorid umgesetzt wird. Dabei wird ein Gemisch aus dem erwünschten Produkt $RSnCl_3$ und dem Nebenprodukt R'_3SnCl erhalten, welches durch Flüssig-Flüssig-Extraktion zwischen Acetonitril und Pentan aufgetrennt werden kann. Als „Dummy-Substituenten"R' kommen vor allem Cyclohexyl- oder *n*-Butyl-Substituenten zum Einsatz. Die gemischtsubstituierte Organozinnspezies RR'_3Sn kann durch Umsetzung von Organolithium- oder -Organomagnesiumverbindungen mit R'_3SnX (X = Cl, Br)[52–55] oder durch Einwirkung von R'_3SnLi auf RX dargestellt werden (vgl. Gleichung 3).[52,56,57] Ist eine Toleranz gegenüber funktionellen Gruppen wie Alkoholen oder Estern gefordert, kann RR'_3Sn auch durch radikalische Hydrostannierung terminaler Alkene oder Alkine mit Tricyclohexlyzinnhydrid synthetisiert werden (vgl. Gleichung 4).[52,58] Die Einführung von Substituenten mit Ketofunktion ist durch einen Cobalt(I)-katalysierten Halogen-Metall-Austausch mit Zink und anschließende Transmetallierung mit Tri-*n*-butylzinnchlorid möglich.[59] Die soeben beschriebenen Synthesewege sind in Schema 1 zusammengefasst.

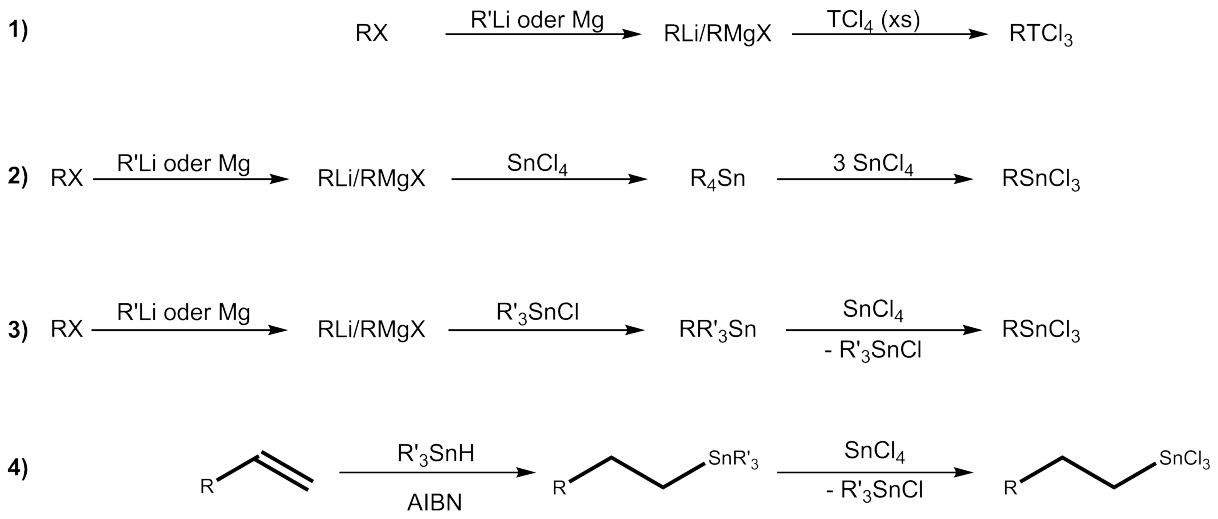

Schema 1: Mögliche Zugangswege zu Organotetreltrichloriden. 1) Direkte Darstellung durch Salzmetathese. 2) KOCHESHKOV-Redistribution. 3) KOCHESHKOV-Redistribution unter Verwendung von „Dummy-Substituenten". 4) Radikalische Hydrostannylierung mit anschließender KOCHESHKOV-Redistribution.

Einen weiteren Zugangsweg zu Organozinntrichloriden bietet die Hydrostannylierung aktivierter Alkene mit Trichlorstannan „$HSnCl_3$“ . Trichlorstannan liegt in koordinierenden Lösungsmitteln als Disolvat-Komplex vor und wird durch Einleiten von HCl-Gas in eine Suspension von Zinn(II)-chlorid im entsprechenden Lösungsmittel hergestellt; in der Regel wird hierfür Diethylether verwendet.[60,61] Allerdings hat diese Hydrostannylierung den Nachteil, dass sie zuverlässig nur für α-β-ungesättigte Carbonyle funktioniert.[60,62,63] Die Trichlorostannyl-Gruppe wird dabei regioselektiv in β-Position addiert, so dass es zur Ausbildung eines Fünfrings durch intramolekulare Lewis-Säure-Base-Addukt-Bildung des Zinnatoms mit dem Carbonylsauerstoff-Atom kommt, welche die erhaltenen Organozinntrichloride stabilisiert. Mechanistisch verläuft die Reaktion so, dass zunächst vom Carbonylsauerstoff das Proton vom $HSnCl_3$ abstrahiert wird, woraufhin das (nukleophile) Trichlorostannat-Fragment an der (elektrophilen) β-Position angreift. Durch anschließende Keto-Enol-Tautomerisierung wird das Keton zurückgebildet (siehe Schema 2). Formal entspricht diese Hydrostannylierung damit einer Michael-Addition.[61,64]

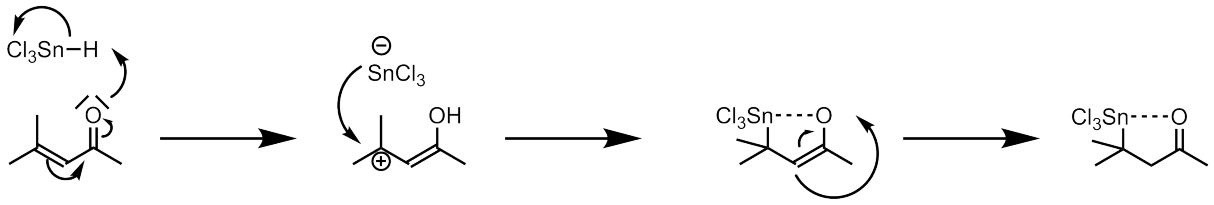

Schema 2: Reaktionsmechanismus der Hydrostannylierung am Beispiel der Reaktion von Mesityloxid mit Trichlorstannan.

Analog zur Hydrostannylierung können α-β-ungesättigte Carbonyle auch zu Organogermaniumtrichloriden hydrogermyliert werden. Die Hydrogermylierung erfolgt in gleicher Weise, allerdings wird das Trichlorgerman $HGeCl_3$ in der Regel durch Reduktion von $GeCl_4$ entweder mit Natriumdihydrogenphosphit in salzsaurer wässriger Lösung[65,66] oder mit 1,1,3,3-Tetramethyldisilan in Diethylether[67,68] hergestellt.
Die Darstellung von Organotetrelchalkogenidkomplexen und -clustern aus den entsprechenden Trichloriden erfolgt, indem Chlor- durch Chalkogenatome substituiert werden, welche zwei oder mehrere Zinnatome verknüpfen. Triebkraft hierbei ist, je nach verwendeter Chalkogenidquelle, die Bildung von Alkalimetallchloriden oder Trimethylsilylchlorid. Eine Kontrolle des Produktspektrums kann einerseits durch die vorgegebene Stöchiometrie der Edukte, andererseits aber auch durch die Löslichkeit der Produkte und dementsprechend die Wahl eines geeigneten Lösungsmittels erfolgen. Im Idealfall fällt das gewünschte Produkt unmittelbar nach seiner Bildung aus und kann damit nicht oder nur noch sehr langsam weiterreagieren. In unserer Arbeitsgruppe haben sich im Wesentlichen drei mögliche Syntheserouten etabliert (vgl. Schema 3):

- **Umsetzung von $RTCl_3$ mit $Na_2S{\cdot}9\,H_2O$ im Wasser-/Aceton-Gemisch** (vgl. Gleichung 5). Dabei fällt der gebildete Cluster aus und kann abfiltriert werden. Die Verwendung von Wasser ist dabei möglich, weil die Reaktion mit dem Natriumsulfid deutlich schneller abläuft als die Hydrolyse des Organozinntrichlorids und diese somit unterdrückt wird. Je nach Konzentration ist es möglich, dass das als Nebenprodukt gebildete Natriumchlorid teilweise mit ausfällt und durch gründliches Waschen des Produkts mit Wasser entfernt werden muss. Diese Reaktion ist nur zur Darstellung von Organogermanium- und zinnsulfidclustern geeignet, da sich sowohl Organosiliciumtrichloride als auch Alkalimetallselenide und -telluride in Wasser zu schnell zersetzen.[69,70]

- **Umsetzung von $RTCl_3$ mit Na_2E in THF** (vgl. Gleichung 6). Die Alkalimetallchalkogenide besitzen eine begrenzte Löslichkeit in THF und reagieren langsam ab.[67,68,71] Als alternatives Lösungsmittel kann auch flüssiger Ammoniak verwendet werden.[72,73] Da allerdings die als Nebenprodukt anfallenden Alkalimetallchloride ebenfalls eine nicht zu vernachlässigende Löslichkeit besitzen, ist zu deren Abtrennung in der Regel ein Lösungsmittelwechsel erforderlich, um den gewünschten Cluster durch Extraktion mit Toluol oder Dichlormethan zu isolieren. Daher ist diese Methode zur Darstellung von Clustern, die sich in Toluol oder Dichlormethan schlecht lösen, ungeeignet. Zur Synthese von Organosiliciumclustern ist dies allerdings - neben der Umsetzung von $RSiCl_3$ mit H_2E[74,75] - die einzig praktikable Methode, da bei der Umsetzung mit Bis(trimethylsilyl)chalkogeniden die Triebkraft fehlt. Hier stellt in der Regel auch die Löslichkeit kein Problem dar, da sich Organosiliciumchalkogenidcluster in der Regel deutlich besser lösen als ihre schwereren Homologen.[76,77]

- **Umsetzung von $RTCl_3$ mit $(Me_3Si)_2E$ in Toluol oder Dichlormethan** (vgl. Gleichung 7). Triebkraft ist hier die Bildung von Me_3SiCl. In der Regel fällt der gebildete Cluster aus und kann durch Filtrieren sauber erhalten werden. Aus Toluol werden, bedingt durch die mit der Clustergröße abnehmende Löslichkeit, in der Regel bevorzugt kleinere Cluster erhalten, aus Dichlormethan können größere Derivate synthetisiert werden.[78–80]

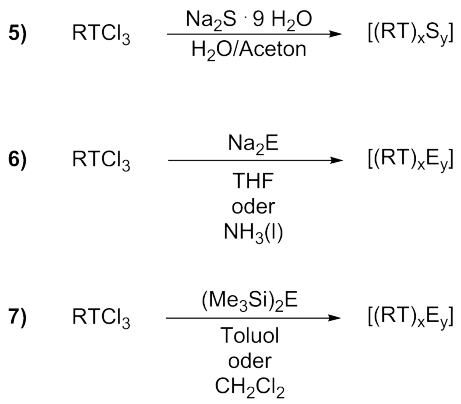

Schema 3: Verschiedene Wege zur Darstellung von Organotetrelchalkogenidclustern.

1.3 Binäre Organotetrelchalkogenidcluster

Durch die zuvor beschriebenen Synthesewege ist eine große Bandbreite verschiedener Organotetrelchalkogenidcluster zugänglich. Im Folgenden werden ausschließlich Verbindungen diskutiert, die aus Monoorganotetreltrihalogeniden erhalten wurden. Analoge Synthesen ausgehend von Diorganotetreldihalogeniden sind ebenfalls literaturbekannt,[69,81–88] dort treten als dominierendes Strukturmotiv Ringe verschiedener Größe auf. Die erste Verbindung dieser Art wurde 1903 von Pfeiffer und Lehnhardt dargestellt, es handelt sich dabei um ein Methylzinnsesquisulfid der Zusammensetzung $[(MeSn)_4S_6]$.[38] Während die Autoren für die Verbindung mangels geeigneter Analysemethoden die Zusammensetzung $(MeSn)_2S_3$ und eine Struktur mit einem μ-verbrückenden sowie zwei terminalen Schwefelatomen annahmen, konnten Scherer und Mitarbeiter 1968 durch Massenspektrometrie die korrekte Summenformel und durch Kristallstrukturanalyse die Molekülstruktur bestimmen.[89] Diese stellte sich als adamantanartige Struktur heraus, bei der die vier μ_3-verbrückenden Positionen durch mit je einer Methylgruppe abgesättigte Zinnatome, die sechs μ_2-verbrückenden Positionen durch Schwefelatome besetzt sind (vgl. Abbildung 3, links). In der Folge wurden zahlreiche alkyl- und arylsubstituierte Organotetrelsesquichalokgenide hergestellt und charakterisiert, die ebenfalls dieses Strukturmotiv besitzen.[40,69,72,90–96]

Die Existenz eines zweiten, zur adamantanartigen Struktur isomeren Strukturmotives für Organozinnsesquisulfidcluster, welches aus zwei zueinander parallelen T_2E_2-Vierringen besteht, die durch zwei weitere μ-verbrückende Chalkogenatome verknüpft sind, wurde mehrfach diskutiert,[89,91] konnte aber erst 1992 erstmalig experimentell an $[(t\mathrm{BuGe})_4S_6]$ nachgewiesen werden (vgl. Abbildung 3, mittig).[97]

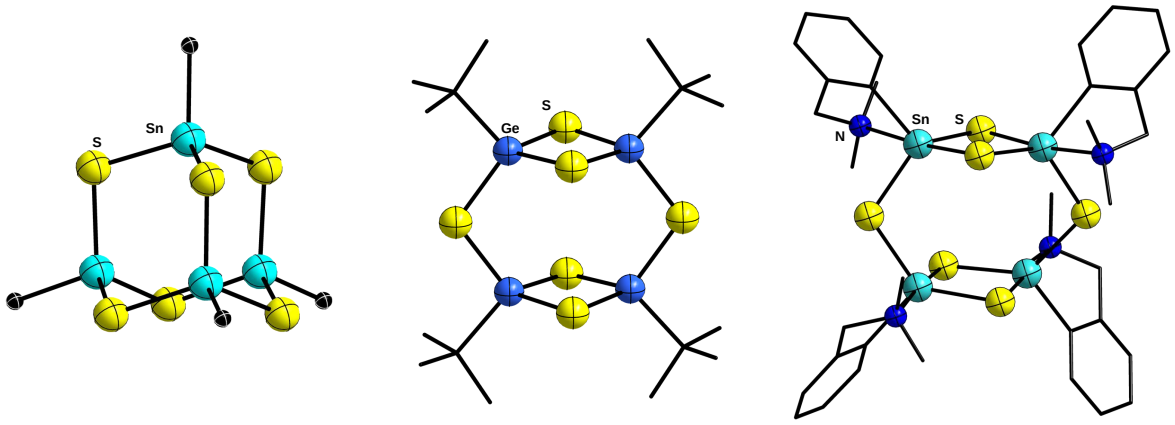

Abbildung 3: Links: Adamantanartige Molekülstruktur von $[(MeSn)_4S_6]$.[89] Mitte: Doppeldeckerartige Molekülstruktur von $[(t\text{BuGe})_4S_6]$.[97] Rechts: Doppeldeckerartige Molekülstruktur von $[\{o-(Me_2NCH_2)C_6H_4\}Sn_4S_6]$.[98]

Für dieses Strukturmotiv hat sich in der Literatur die Bezeichnung „Doppeldecker“ etabliert.[99] Durch Erhitzen lässt sich der doppeldeckerartige Käfig von $[(t\text{BuGe})_4S_6]$ in einen adamantanartigen Käfig überführen.[97] Dies wurde ebenfalls von Matsumoto und Mitarbeitern für Silicium- und Germaniumchalkogenidcluster $[(RT)_4E_6]$ (R = 1,1,2-Trimethyl-propyl; E = S, Se) bestätigt, was nahelegt, dass es sich beim doppeldeckerartigen Cluster um das kinetische, beim adamantanartigen Cluster hingegen um das thermodynamische Produkt handelt.[100] Ein ebenfalls doppeldeckerartiges Grundgerüst wurde auch von Varga und Silvestru für $[\{o\text{-}(Me_2NCH_2)C_6H_4\}Sn_4S_6]$ gefunden (vgl. Abbildung 3, rechts). Bei dieser Verbindung wird durch intramolekulare Lewis-Säure-Base-Wechselwirkung der Amin-Stickstoffatome mit den Zinnatomen die Koordinationszahl an diesen von vier auf fünf erhöht. Es ergibt sich damit für die Zinnatome eine (verzerrt) trigonal-bipyramidale Koordination statt der bei Koordinationszahl vier auftretenden tetraedrischen Koordination. Diese zusätzliche Wechselwirkung stabilisiert die doppeldeckerartige Molekülstruktur, sodass sie gegenüber der adamantanartigen Struktur bevorzugt auftritt.[98] Im Falle von $[(R^1Ge)_4S_6]$ ($R^1 = CMe_2CH_2COMe$) konnte in unserer Arbeitsgruppe sogar die umgekehrte Umwandlung einer adamantanartigen in eine doppeldeckerartige Struktur durch Erhitzen in siedendem Chloroform beobachtet werden. DFT-Rechnungen ergaben, dass in diesem Fall die doppeldeckerartige Struktur um 10 kJ/mol stabiler als das adamantanartige Isomer ist.[101] Organogermanium- und -zinnchalkogenidcluster mit dem organischen Substituenten R^1 sind in den vergangenen Jahren in unserer Arbeitsgruppe intensiv untersucht worden, da dessen Keto-Funktion neben der Stabilisierung des anorganischen Kerns die Möglichkeit zur Derivatisierung der organischen Ligandenhülle durch Umsetzung mit (metall-)organischen Molekülen komplementärer Reaktivität bietet.

In grundlegenden Studien wurden zunächst die Intermediate der Bildung der Organozinnsesquichalkogenidcluster durch schrittweise Kondensation des Organozinntrichlorids R^1SnCl_3 mit den Bis(trimethylsilyl)chalkogeniden untersucht. Durch Titration mit $(Me_3Si)_2E$ und Reaktionsverfolgung durch ^{119}Sn-NMR-Spektroskopie konnte sowohl für Schwefel als auch Selen und Tellur zunächst die Bildung eines zweikernigen, durch ein Chalkogenatom verbrückten, Zinnkomplexes $[(R^1SnCl_2)_2E]$ beobachtet werden. Bei weiterer Chalkogenid-Zugabe erfolgt die Ausbildung eines zweifach chalkogenidverbrückten zweikernigen Komplexes mit einem zentralen Sn_2E_2-Vierring ($[(R^1SnCl)_2E_2]$). Mit 1,33 Äquivalenten wird ein defektheterokubanartiger $[(R^1Sn)_3E_4Cl]$-Cluster gebildet, aus welchem durch weitere $(Me_3Si)_2E$-Zugabe schließlich die doppeldeckerartigen Organozinnsesquichalkogenidcluster $[(R^1Sn)_4E_6]$ entstehen. Diese Reaktionskaskade ist in Schema 4 zusammenfassend dargestellt. Mit Ausnahme des Organozinntellurid-Defektheterokubans $[(R^1Sn)_3Te_4Cl]$, welches nur massenspektrometrisch nachgewiesen werden konnte, wurden all diese Intermediate kristallisiert und vollständig charakterisiert.[78–80] Aus dem Organozinnsesquisulfidcluster $[(R^1Sn)_4S_6]$ kann, entweder durch lichtinduzierte Umlagerung oder gezielt durch Umsetzung mit Kohlenstoffdisulfid, ein gemischtvalenter Cluster der Zusammensetzung $[(R^1Sn)_6Sn_2S_{12}]$ gebildet werden, bei dem drei $(R^1Sn)_2S_4$-Baugruppen eine zentrale Sn-Sn-Hantel umgeben, in der die Zinnatome in der für Zinn selten beobachteten Oxidationsstufe +III vorliegen (vgl. Abbildung 4, links).[70,102]

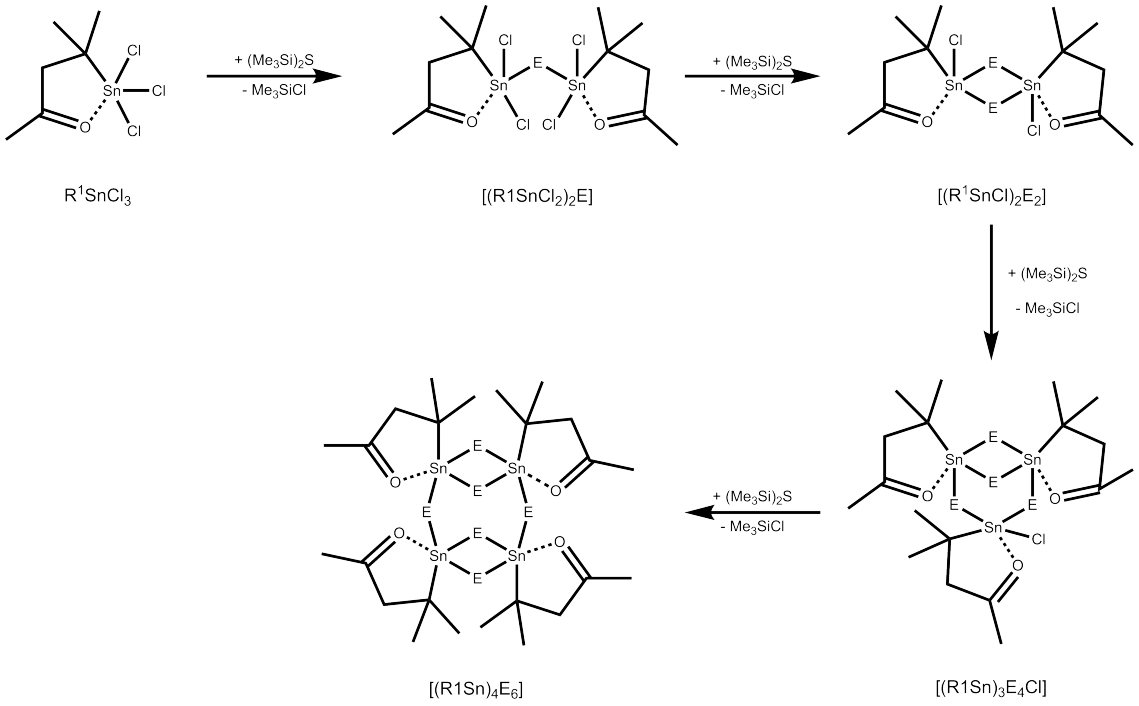

Schema 4: Schrittweise Bildung von Organozinnchalkogenidclustern durch Kondensationsreaktion von R^1SnCl_3 und $(Me_3Si)_2E$.

Im Falle des leichteren Homologen Germanium sind bisher nur die Sesquichalkogenidcluster $[(RGe)_4E_6]$ bekannt, die (in Abhängigkeit vom organischen Substituenten) eine adamantan- oder doppeldeckerartiger Struktur besitzen, da im Falle dieser Verbindungen stets nur Alkalimetallchalkogenide, aber keine Bis(trimethylsilyl)chalkogenide als Chalkogenidquelle zum Einsatz kamen.[67,68,103,104] Im Falle der Organogermaniumtelluridcluster wurde mehrfach die Bildung von Clustern der Zusammensetzung $[(RGe)_4Te_5]$ mit noradamantanartiger Struktur beobachtet. Diese Molekülstruktur leitet sich von einer adamantanartigen Struktur ab, der eine der μ-verbrückenden Chalkogenidpositionen fehlt. Hierdurch kommt es zur Ausbildung einer Ge-Ge-Bindung unter formaler Reduktion der beiden Germaniumatome von der Oxidationsstufe +(IV) zu +(III) (vgl. Abbildung 4, rechts).[103,104]

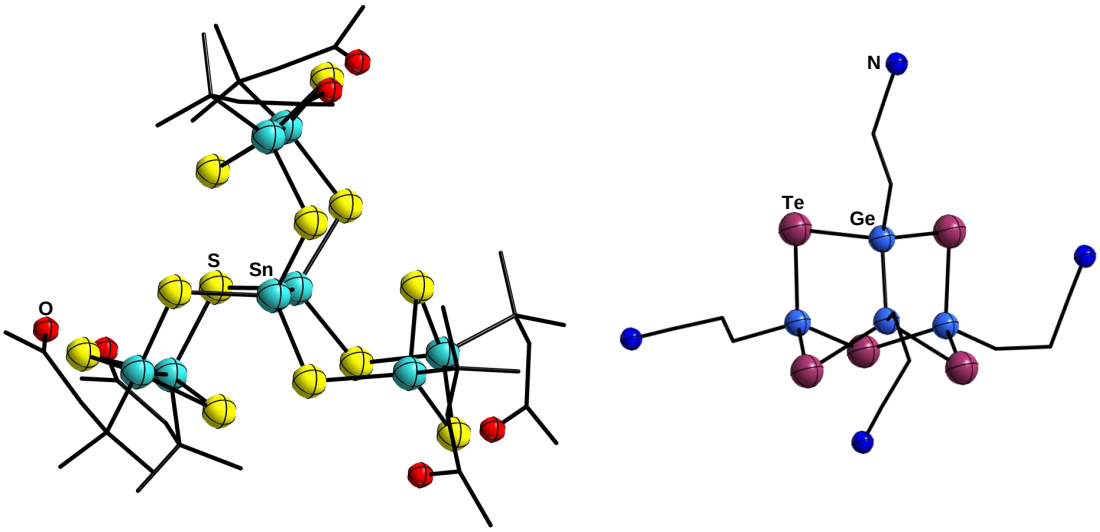

Abbildung 4: Links: Molekülstruktur von $[(R^1Sn)_6Sn_2S_{12}]$.[102] Rechts: Noradamantanartige Molekülstruktur von $[(RGe)_4Te_5]$ (R = (CH2)2CN).[68]

Ausgehend von den so erhaltenen Organotetrelchalkogenidclustern kann eine nachfolgende Derivatisierung der Ligandenhülle erfolgen. Die dafür in unserer Gruppe etablierte Syntheseroute basiert auf Kondensationsreaktionen von Carbonylgruppen mit Hydrazinen, Hydrazonen oder Hydraziden. Diese kann in zwei Varianten erfolgen:

- Umsetzung der ketofunktionalisierten Cluster $[(R^1Sn)_xE_y]$ mit Hydrazinen, Hydrazonen oder Hydraziden. Dies hat sich insbesondere für Hydrazine als problematisch herausgestellt, da diese oft dimerisieren, anstatt mit der Ketogruppe am Cluster zu reagieren.[105]

- Reaktion der ketofunktionalisierten Cluster mit Hydrazin (entweder als Hydrat oder als kommerziell erhältliche Lösung in THF eingesetzt) und anschließende Umsetzung mit Carbonylverbindungen, wobei hier in der Regel die Verwendung von Aldehyden erforderlich ist, da diese im Vergleich zu Ketonen deutlich reaktiver sind.[105]

Auf diese Weise ist es beispielsweise möglich, poly- und heteroaromatische Moleküle an die organische Ligandenhülle anzubinden. Die Polyaromaten sollen die Abscheidung der Cluster auf Oberflächen (Metalle, Halbleiter, Graphen) ermöglichen, während durch heteroaromatische (Chelat-)Liganden der Einfang von Übergangsmetallionen aus Lösung ermöglicht werden soll. Eine große Bandbreite an Clustern mit verschiedenen derartigen Substituenten konnte bisher erfolgreich dargestellt werden.[106–109] Bei der Anbindung sterisch anspruchsvoller Substituenten kommt es häufig zu einer Umlagerung des anorganischen Kerns zu einem bisdefektheterokubanartigen Grundgerüst Die so erhaltenen Moleküle entsprechen der allgemeinen Formel $[(RSn)_4Sn_2S_{10}]$. Durch Einsatz geeigneter heteroaromatischer Substituenten wie Benzothiazol konnten zudem photolumineszente Cluster erhalten werden.[109] Der Einfang von Übergangsmetallionen durch Chelatliganden am Cluster war bisher nur begrenzt erfolgreich. Bei Verwendung eines Bispyridin-Substituenten und Umsetzung mit Zinkhalogeniden kam es zur Umlagerung des Clusters unter Einbau von ZnX-Fragmenten (X = Cl, Br, I) ins anorganische Grundgerüst des Clusters (hierzu siehe Abschnitt 1.4).[106] Durch Ersatz von Bispyridin- durch Bipyridin-Substituenten hingegen konnte Zinkchlorid erfolgreich komplexiert werden, ohne dass dabei eine Umlagerung des Clusterkerns stattfindet.[110] In analogen Umsetzungen mit Platin- und Iridiumkomplexen hingegen kam es stets zur Zersetzung des Clusters.[111,112] Eine andere Möglichkeit, Metallionen an die Cluster anzubinden, besteht in der kovalenten Anbindung von Metallocenen. Durch Umsetzung von $[(R^1Sn)_4S_6]$ mit dem monofunktionaliserten Ferrocenderivat $H_2N{-}N{=}C(Me)Fc$ konnte ein bisdefektheterokubanartiger Cluster mit vier Ferrocenylsubstituenten synthetisiert werden. Das Cyclovoltammogramm dieser Verbindung zeigt zwei reversible Zwei-Elektronen-Oxidationen, was eine elektronische Kommunikation der Substituenten über den Clusterkern hinweg nahelegt (siehe Abbildung 5).[113] Mit difunktionalisierten Ferrocenen kommt es zur Verknüpfung jeweils zweier organischer Substituenten an einem Clustermolekül. Durch Variation der Anbindung des Ferrocenylsubstituenten, einerseits durch Umsetzung eines hydrazinfunktionalisierten Clusters mit Ferrocendialdehyd, andererseits durch Umsetzung des ketofunktionalisierten Clusters mit Ferrocendicarbonsäuredihydrazid, werden Verbindungen mit unterschiedlicher elektrochemischer Stabilität erhalten.[114] In der gleichen Weise konnte auch Ruthenocen an einen bisdefektheterokubanartigen Cluster angebunden werden; diese Verbindung wird allerdings elektrochemisch durch irreversible Oxidation zersetzt.[115] Adamantanartige Cluster mit Ferrocenylsubstituenten konnten durch direkte Umsetzung

von Ferrocenylzinntrichlorid mit Alkalimetallsulfiden und -seleniden dargestellt werden. Die analoge Reaktion mit Kaliumtellurid führte hingegen zur Bildung eines $[(FcSn)_3Te_2]$-Fünfrings (Fc = Ferrocenyl).[71,116] Auch die Zersetzung ferrocenylsubstituierter Cluster durch Hydrolyse und Einwirkung von Säuren und Basen wurde untersucht. Dabei wurden als Intermediate verschiedene Organozinnsulfidoxidcluster,[117] reine Organozinnoxidcluster - deren größten Vertreter die Verbindung $[(FcSn)_9(OH)_6O_8Cl_5]$ darstellt[118] - und, bei Zersetzung durch Salzsäure als Endprodukt das Hydrochlorid des entsprechenden Organozinntrichlorids $[(Fc(Me)CN_2C(Me)CH_2CMe_2)SnCl_3 \cdot HCl]$ erhalten.[113]

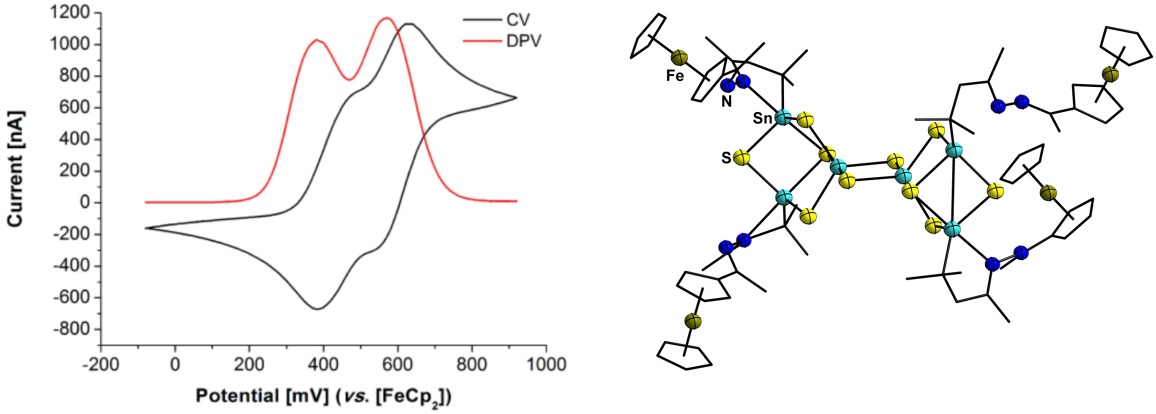

Abbildung 5: Links: CV- und DPV-Spektren von $[(R^{Fc}Sn)_4Sn_2S_{10}]$. Rechts: Molekülstruktur von $[(R^{Fc}Sn)_4Sn_2S_{10}]$ (R^{Fc} = $CMe_2CH_2C(Me)NNC(Me)Fc$).[113]

Während mit difunktionalisierten Ferrocenderivaten keine intermolekulare Verknüpfung stattfindet, kann eine solche durch Verwendung verbrückender organischer Dihydrazine erfolgen. Auf diese Weise konnte ein Cavitand mit zwei Bisdefektheterokuban-Käfigen, welche durch vier Naphthyldihydrazin-Substituenten verbunden sind, dargestellt werden (siehe Abbildung 6, links). Dieser lagert sich bei Umsetzung mit Trichlorstannan-Dietherat zu einer rugbyballartigen Kapsel der Zusammensetzung $[(Sn_3S_4)_2R_3]$ (R = $\{CMe_2CH_2C(Me)NNH\}_2Np$) um.[119] Analoge Kapselverbindungen mit Zinnselenidkäfigen sind ebenfalls bekannt, hierbei kam neben Naphthyldihydrazin auch Adipinsäuredihydrazid als verbrückender Substituent zum Einsatz (siehe Abbildung 6, rechts).[120]

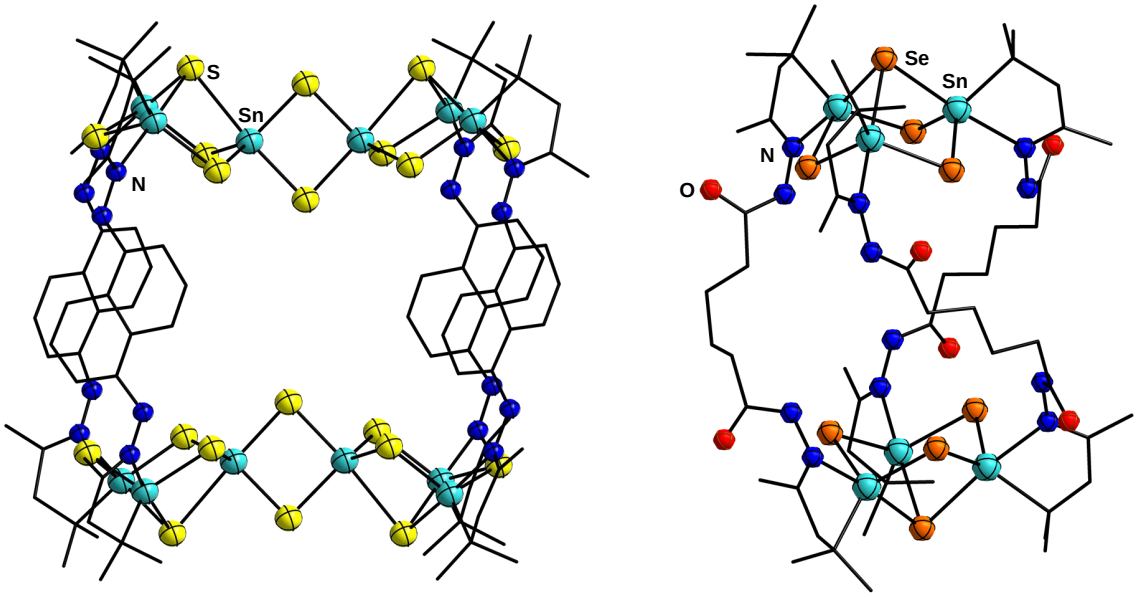

Abbildung 6: Links: Molekülstruktur von $[(Sn_6S_{10})_2R_4]$ (R = $\{CMe_2CH_2C(Me)NNH\}_2Np$).[119] Rechts: Molekülstruktur von $[(Sn_3Se_4)_2R_3]$ (R = $\{CMe_2CH_2C(Me)NNHCO\}_2(C_2H_4)_4$).[120]

Die sterisch anspruchsvollsten Substituenten, die bisher an Organozinnsulfidcluster angebunden werden konnten, sind organische Adamantan- und Diamantankäfige, die in einer Kooperation mit der Arbeitsgruppe Schreiner aus Gießen dargestellt wurden. Bei Verwendung von difunktionalisierten Diamantanen konnte ebenfalls eine Variation der rugbyball-artigen Kapselmoleküle erhalten werden.[121] Adamantan-Substituenten wurden zudem als Spacer zur Anbindung von Biomolekülen an Organozinnsulfidcluster genutzt. Dazu wurde ein Adamantylazidhydrazid durch Kondensation mit dem ketofunktionalisierten Organozinntrichlorid R^1SnCl_3 umgesetzt. Nach Darstellung des entsprechenden $[(RSn)_3S_4Cl]$-Clusters konnte die Azid-Funktion am Adamantylsubstituenten in einer ringspannungsinduzierten Azid-Alkin-Cycloaddition mit zwei verschiedenen Cyclooctinderivaten, die ihrerseits mit je einem Tripeptid substituiert waren, weiter umgesetzt werden (vgl. Schema 5).[122,123]

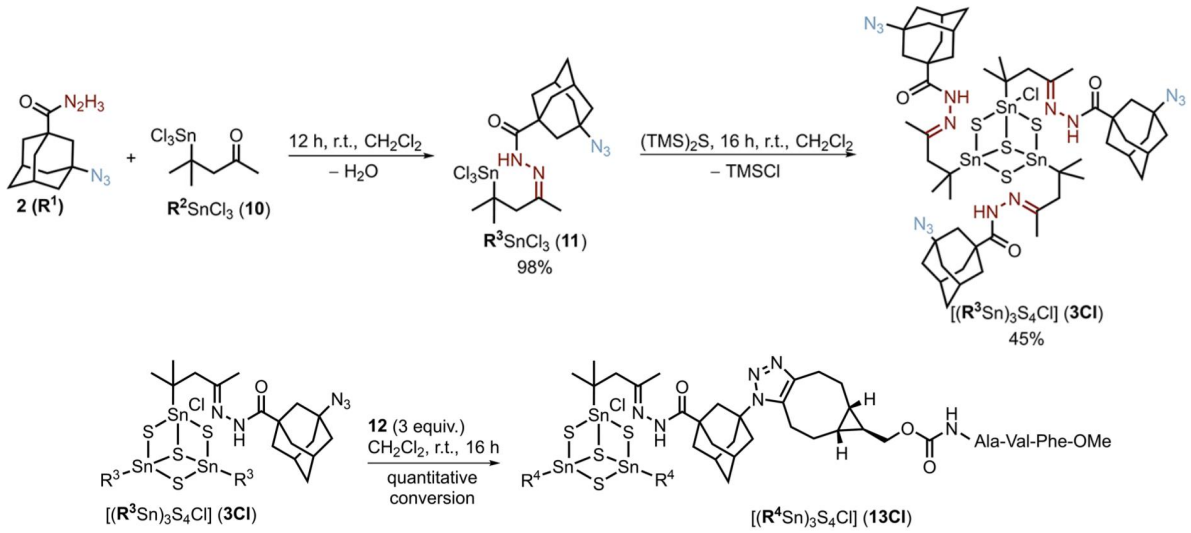

Schema 5: Oben: Darstellung eines adamantylazidfunktionalisierten Organozinnsulfidclusters. Unten: Peptidanbindung durch Azid-Alkin-Cycloaddition. Abbildungen entnommen aus Ref.[122].

Weitere Methoden zur Anbindung von Aminosäuren und Peptiden sind in unserer Arbeitsgruppe ebenfalls untersucht worden. Langfristiges Ziel dieser Studien soll es sein, die Eignung von Organozinnsulfidclustern als Cytostatika in der Krebstherapie zu untersuchen, indem die Cluster im relativ zu normalen Zellen deutlich saureren Milieu der Tumorzellen unter Freisetzung von Schwefelwasserstoff zersetzt werden. Eine biokompatible Ligandenhülle, welche die Moleküle zugleich hydrolyse- und oxidationsstabil macht, ist zur Einbringung der Moleküle in die Zellen erforderlich. Erste Vorarbeiten ergaben, dass bei Verwendung ungeschützter Aminosäuren eine intramolekulare Kondensationsreaktion auftritt, die unter Umlagerung des anorganischen Kerns verläuft.[124] Dies lässt sich jedoch durch Verwendung Boc-geschützter Aminosäuren umgehen. Hierzu wurde eine Syntheseroute etabliert, bei der zunächst aus dem Organozinntrichlorid R^1SnCl_3 und Aminosäurehydraziden funktionalisierte Organozinntrichloride synthetisiert werden, welche nachfolgend zu den entsprechenden Clustern umgesetzt werden (vgl. Schema 6).[125] Im Zusammenhang mit der geplanten Zersetzung in Tumorzellen und auch hinsichtlich der Möglichkeit der Entschützung und nachfolgenden Peptidsynthese am Cluster wurde das Verhalten aminosäurefunktionalisierter Cluster gegenüber Säuren untersucht.[126]

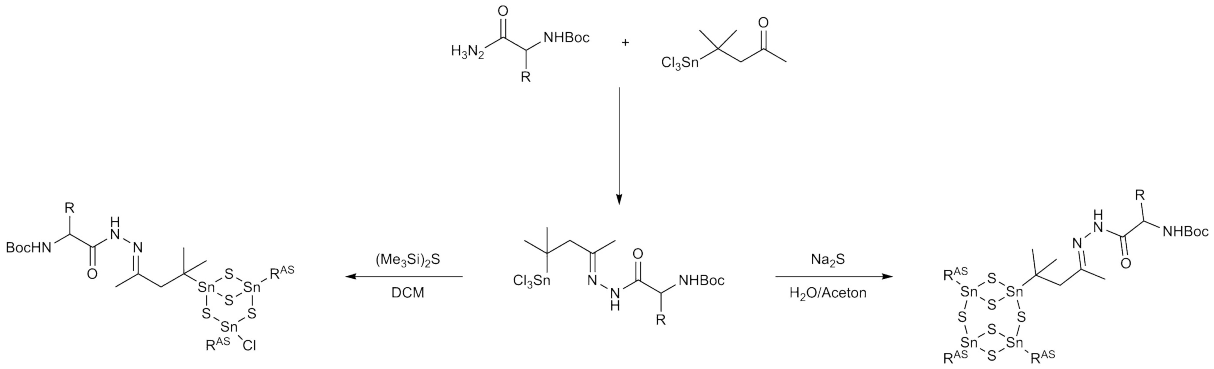

Schema 6: Darstellung aminosäurefunktionalisierter Organozinnsulfidcluster.[125]

Neben den zuvor besprochenen Verbindungen, welche alle ausgehend von Organozinn(IV)-halogeniden synthetisiert wurden, soll zusätzlich noch exemplarisch auf einige Verbindungen eingegangen werden, welche auf anderen Synthesewegen entstanden sind. Im Falle von Silicium kann durch oxidative Addition von elementarem Schwefel an ein Tetrasilan [$(RSi)_4$] (R = NDipp(TMS)) eine inverse Variante eines Defektheterokubans der Zusammensetzung [$(RSi)_4S_3$] erhalten werden.[127] Die Umsetzung von terphenylsubstituierten Monoarylstannanen $ArSnH_3$ mit elementarem Schwefel oder Selen liefert [2.1.1]- und [3.1.1]-Propellane der Zusammensetzung [$(ArSn)_2(Se_2)Se_2$] bzw. [$(ArSn)_2(E_3)E_2$] (E = S, Se).[128]

Mit Blei sind generell nur sehr wenige Chalkogenid-Käfigverbindungen bekannt, da Blei in der in solchen Käfigen üblichen Oxidationsstufe +IV ein starkes Oxidationsmittel ist, welches Chalkogenide zu den jeweiligen Elementen zu oxidieren vermag. Zu den wenigen bekannten organisch substituierten Bleichalkogenidkäfigen gehören [$Pb_4(OSiPh_3)_6$], ein adamantanartiger Käfig des zweiwertigen Bleis, der durch Protolyse von Plumbocen mit Triphenylsilanol erhalten werden kann,[129] sowie eine Reihe von Blei(II)-thiolaten, welche durch Umsetzung von Blei(II)-acetat mit 2,6-Dimethylthiophenol entstanden sind.[130]

1.4 Cluster mit ternärem anorganischem Grundgerüst

Durch Reaktion der zuvor beschriebenen Organotetrelchalkogenidcluster mit Übergangsmetallkomplexen können Cluster mit ternärem anorganischem Grundgerüst erhalten werden. Häufig ist bei diesen Reaktionen die zusätzliche Zugabe einer Chalkogenidquelle erforderlich, um das Grundgerüst des binären Clusters aufzubrechen und eine Umlagerung zu einem neuen, ternären Gerüst zu ermöglichen. Die bei weitem überwiegende Anzahl solcher ternärer Cluster wurde durch Umsetzung mit Münzmetallkomplexen dargestellt. So konnten Hauser und Merzweiler aus [$(PhSn)_4S_6$], Na_2S und [$(PPhMe_2)$(*bipy*)CuCl] (*bipy* = 2,2'-Bipyridin) einen Cluster der Zusammensetzung [$(PhSnS_3)_2(CuPPhMe_2)_6$] erhalten, dessen anorganisches Gerüst aus sechs zentralen Kupfer-Phosphan-Komplexfrag-

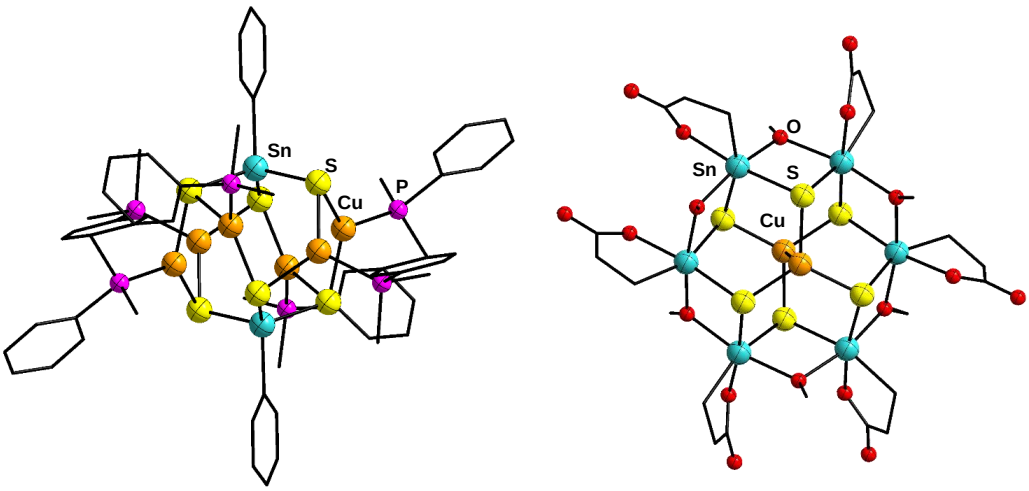

Abbildung 7: Links: Molekülstruktur von $[(PhSnS_3)_2(CuPPhMe_2)_6]$.[131] Rechts: Molekülstruktur von$[(RSn)_6(OMe)_6Cu_2S_6]^{4-}$(R=$C_2H_4COO^-$).[73]

menten besteht, welche durch zwei Phenyltrithiostannant-Gruppen ober- und unterhalb verknüpft werden. (vgl. Abbildung 7, links).[131] Wie die Autoren nachweisen konnten, wird zu Beginn der Reaktion zunächst aus dem Cluster und Natriumsulfid das Phenyltrithiostannant $Na_3[PhSnS_3]$[132] gebildet, welches dann mit dem Kupferkomplex reagiert.
In unserer Arbeitsgruppe konnten Cluster mit dem gleichen Strukturmotiv ausgehend von $[(RGe)_4S_6]$ (R = R^1, C_2H_4COOH) und $[(R^1Sn)_4S_6]$ dargestellt werden, zudem gelang die Synthese eines isostrukturellen Clusters $[(FcSn)_2(S/Se)_6(CuPPh_3)_6]$, in dem Schwefel und Selen nebeneinander vorliegen.[71] Wird hingegen der dianionische, defektheterokubanartige Cluster $Na_2[(RSn)_3S_4]$ (R = $C_2H_4COO^-$), welcher seinerseits aus Natriumsulfid und dem entsprechenden Organozinntrichlorid in flüssigem Ammoniak zugänglich ist, in flüssigem Ammoniak mit Kupfer(I)-chlorid umgesetzt, so wird ein anionischer Cluster mit einem neuartigen Strukturmotiv erhalten, der die Zusammensetzung $Na_4[(RSn)_6(OMe)_6Cu_2S_6]$ hat. Hierbei ist eine zentrale Cu_2S_6-Gruppe von sechs Organozinn-Einheiten umgeben, welche ihrerseits durch sechs Methanolat-Anionen verbrückt sind (siehe Abbildung 7, rechts).[73] Wird $[(R^1Sn)_4S_6]$ mit Carbodihydrazid umgesetzt, kommt es zu einer intramolekularen Verbrückung der organischen Substituenten jeweils zweier Zinnatome. Mit Natriumsulfid entsteht das Thiostannat $Na_2[RSn_2S_4]$ (R = $CO\{NNC(Me)CH_2CMe_2\}_2$), das mit $[(PPh_2Me)_3CuCl]$ zu einem ternären Cluster der Zusammensetzung $[R_2\{SnS_2Cu(PPh_2Me)\}_4]$ reagiert. Zwei der $SnCuS_2$-Einheiten bilden übereinander liegende Vierringe aus, welche durch die beiden anderen, gestrecktenSnCuS_2-Einheiten verknüpft werden (vgl. Abbildung 8, links).[133]

Gemischtvalente Cluster können durch Reaktion des defektheterokubanartigen Clusters $[(R^1Sn)_3S_4Cl]$ mit $[Cu(PPh_3)_3Cl]$ und $(Me_3Si)_2S$ erhalten werden. Diese besitzen die Zusammensetzung $[(R^1Sn^{IV})_4(Sn^{II}Cl)_2(CuPPh_3)_2S_8]$ und bestehen aus zwei zentralen Cu-Sn-Hanteln, welche durch zwei $(RSn)_2S_4$-Einheiten verbunden sind (siehe Abbildung 8, rechts).[134] Verbindungen mit dem gleichen Strukturmotiv konnten auch für die Elementkombinationen Ag/Sn/S,[134] Cu/Sn/Se[135] und Ag/Sn/Se[136] erhalten werden. Durch Umsetzung der Organozinn-Silbersulfid-Spezies mit Hydrazinhydrat kommt es, abgesehen von der Reaktion des organischen Substituenten, zu einer Umlagerung des anorganischen Kerns, wodurch ein Cluster mit deutlich größerem anorganischem Kern und der Zusammensetzung $[(R^2Sn)_{10}Ag_{10}S_{20}]$ ($R^2 = CMe_2CH_2C(Me)NNH_2$) entsteht (vgl. Abbildung 10, oben).[134] Mit dem schwereren Homologen Gold konnten lediglich kleinere Komplexe der Zusammensetzung $[(RSn)_2(SAuPR'_3)_2S_4]$ (R = R^1, R^2; R' = Ph, Me) erhalten werden, bei denen ein Sn_2S_2-Vierring an den Zinnatomen jeweils einen $SAuPR'_3$-Substituenten trägt. Die Orientierung dieser Substituenten hängt hierbei von der Wahl der Liganden an den Gold- (PPh_3 vs. PMe_3) und Zinnatomen (R^1 vs. R^2) ab.[134,137] Die Bildung größerer Cluster wird in diesen Fällen vermutlich dadurch verhindert, dass Gold(I) im Gegensatz zu seinen leichteren Homologen bevorzugt linear koordiniert auftritt, was die Entstehung entsprechender Käfigverbindungen erschwert.

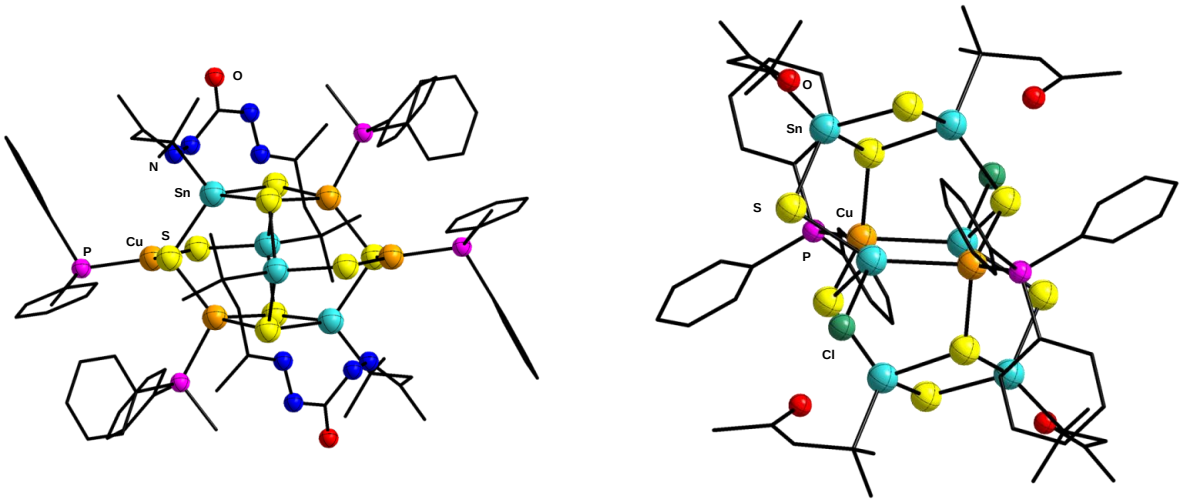

Abbildung 8: Links: Molekülstruktur von $[R_2\{SnS_2Cu(Ph_2PMe)\}_4]$.[133] Rechts: Molekülstruktur von$[(R^1Sn^{IV}))_4(Sn^{II}Cl)_2(CuPPh_3)_2S_8]$.[134]

Neben dem bereits erwähnten Cluster $[(R^1Sn)_4(SnCl)_2(CuPPh_3)_2Se_8]$, der aus $[(R^1Sn)_4Se_6]$ erhalten wird, konnten ausgehend von dem Organozinnselenidcluster $[(R^1Sn)_3Se_4Cl]$ durch Reaktion mit $[Cu(PPh_3)_{4-x}Cl_x]$ (x = 1, 2) und $(Me_3Si)_2Se$ weite-

re ternäre Cluster erhalten werden. All diese Moleküle bestehen aus einer oder mehreren $(RSn)_2Se_4$-Baugruppen, die mehrere Metallatome im Zentrum des anorganischen Kerns koordinieren. Der kleinste Vertreter dieser Reihe ist die Verbindung $[\{(R^1Sn)_2Se_4\}(CuPPh_3)_2]$, größere Varianten stellen die Cluster $[\{(R^2Sn)_2Se_4\}_2(CuPPh_3)_2Sn]$ und $[\{(R^1Sn)_2Se_4\}_3(CuPPh_3)_2SnCu_2]$ dar. Als Besonderheit kann die Verbindung $[\{(R^1SnCl)Se_2\}_2(CuPPh_3)_2(SnCl)_2]$ gelten, bei der die chelatisierenden $\{(RSn)_2Se_4\}$-Gruppen durch $\{(R^1Sn)Se_2\}$ ersetzt sind, und die als einzige ohne Zugabe einer zusätzlichen Chalkogenidquelle entsteht. Die genannten Verbindungen sind in Abbildung 9 zusammengefasst.[135]

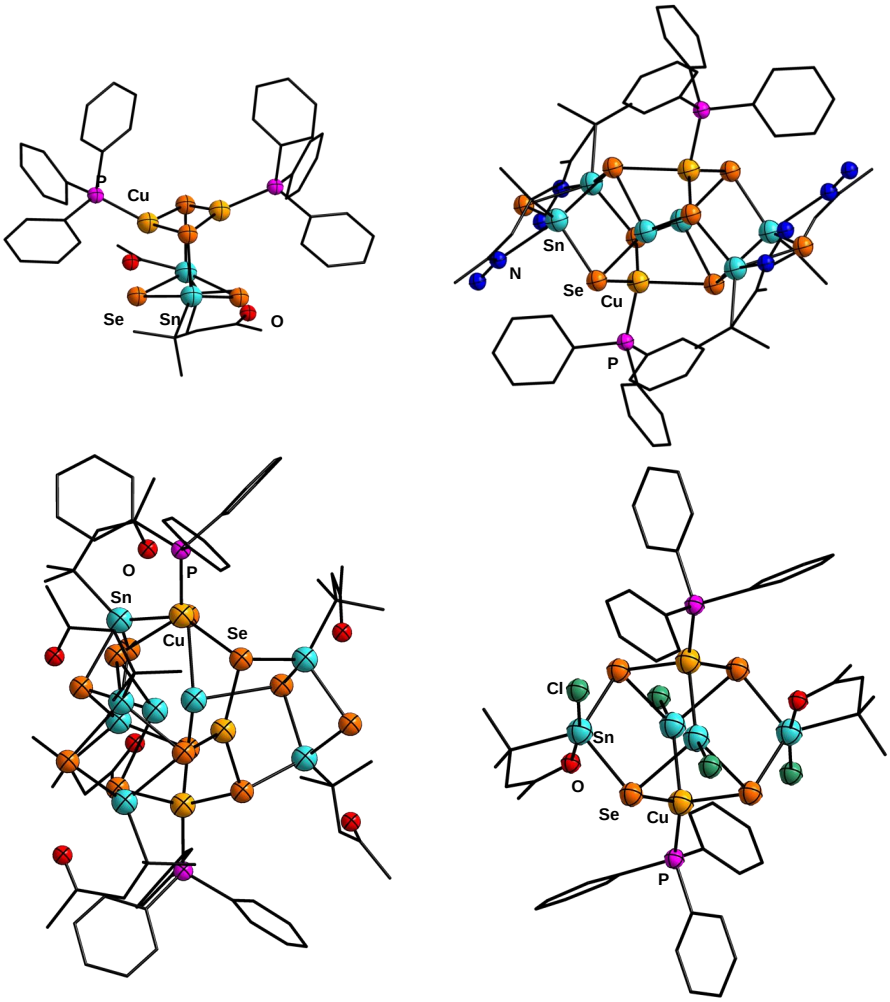

Abbildung 9: Oben links: Molekülstruktur von $[\{(R^1Sn)_2Se_4\}(CuPPh_3)_2]$. Oben rechts: Molekülstruktur von $[\{(R^2Sn)_2Se_4\}_2(CuPPh_3)_2Sn]$. Unten links: Molekülstruktur von $[\{(R^1Sn)_2Se_4\}_3(CuPPh_3)_2SnCu_2]$. Unten rechts: Molekülstruktur von $[\{(R^1SnCl)Se_2\}_2(CuPPh_3)_2(SnCl)_2]$.[135]

Für die Elementkombination Ag/Sn/Se sind zwei weitere Cluster bekannt, bei denen es sich um Isomere der gleichen Zusammensetzung $[(RSn)_{12}Ag_{14}Se_{25}]$ handelt. Eins der beiden Isomere trägt dabei den organischen Substituenten R^1 und zeichnet sich durch ein pseudooktaedrisches Grundgerüst aus, das um ein zentrales $SeAg_6$-Oktaeder aufgebaut ist. Dieses ist von einem Würfel aus acht Silberatomen umgeben, dessen Flächen von

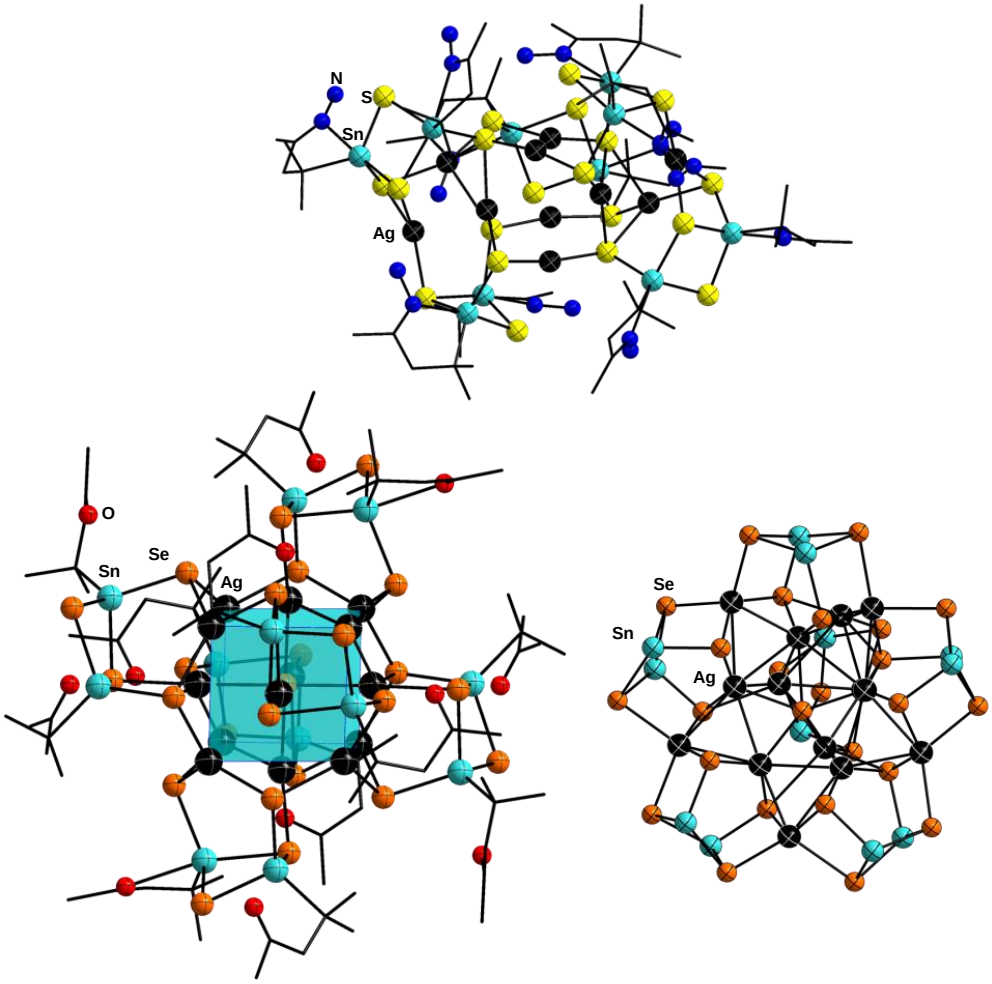

Abbildung 10: Oben: Molekülstruktur von $[(R^2Sn)_{10}Ag_{10}S_{20}]$.[134] Unten links: Molekülstruktur von $[(R^1Sn)_{12}Ag_{14}Se_{25}]$.[136] Unten rechts: Struktur des anorganischen Kerns von $[(R^2Sn)_{12}Ag_{14}Se_{25}]$.[136]

den bereits beschriebenen $\{(R^1Sn)_2Se_4\}$-Bausteinen überkappt sind (siehe Abbildung 10, unten links). Durch Zugabe von Hydrazinhydrat zur Reaktionslösung wird das andere Isomer erhalten, welches deutlich unsymmetrischer erscheint. Der anorganische Kern dieser Verbindung ist um einen *pseudo*-C_5-symmetrischen $SeAg_5$-Stern aufgebaut, der von fünf $\{(R^2Sn)_2Se_4\}$-Bausteinen umgeben ist, die zusätzlich durch fünf weitere Sil-

beratome verknüpft sind. Die potentiell fünfzählige Molekülsymmetrie wird durch eine $Ag_4\{(R^2Sn)_2Se_4\}$-Gruppe gebrochen, die eine Seite des sternförmigen Motives überkappt (siehe Abbildung 10, unten rechts).[136]

Einige weitere ternäre Cluster existieren mit anderen Übergangsmetallen jenseits der Gruppe 11, die im Folgenden beschrieben werden. So ist durch Umlagerung von $[(R^1Ge)_4S_6]$ nach Zugabe von Hydrazinhydrat ein anionisches Thiogermanat der Zusammensetzung $(N_2H_5)_2[(R^2Ge)_2S_4]$ zugänglich, welches mit $[(tmeda)Pd(NO_3)_2]$ zu einem Cluster der Zusammensetzung $[(R^2Ge)_4Pd_6S_{12}]$ reagiert. Dessen anorganischer Kern ist aus vier kantenverknüpften Pd_3GeS_3-Defektheterokubanen zusammengesetzt, deren Palladiumatome alle quadratisch-planar koordiniert sind (siehe Abbildung 11, links).[138] Ebenfalls mit Palladium konnten durch Reaktion von $[(R^1Sn)_4Se_6]$ und $[Pd(PPh_3)_2Cl_2]$ zwei trigonal-bipyramidale Cluster erhalten werden, deren Bildung mit vollständiger Zersetzung der eingesetzten binären Cluster einhergeht. In $[Pd_3Se_2(PPh_3)_5(SnCl_3)][SnCl_3]$ ist einer der Triphenylphos-phan-Liganden an einem der Palladiumatome durch eine Trichlorostannylgruppe ersetzt worden (siehe Abbildung 11, mittig).[139] Ähnliche Cluster mit einer M_3Se_2-Bipyrami-de sind auch mit Ruthenium und Osmium bekannt.[140] Ein ähnliches Strukturmotiv besitzt der Cluster $[Pd_2Se_2(R^2SnCl_2)(PPh_3)_3Cl]$, in dem eines der Palladiumatome durch eine R^2SnCl_2-Gruppe ersetzt ist (siehe Abbildung 11, links).[139] Dieses Strukturmotiv existiert auch mit Platin.[112,141]

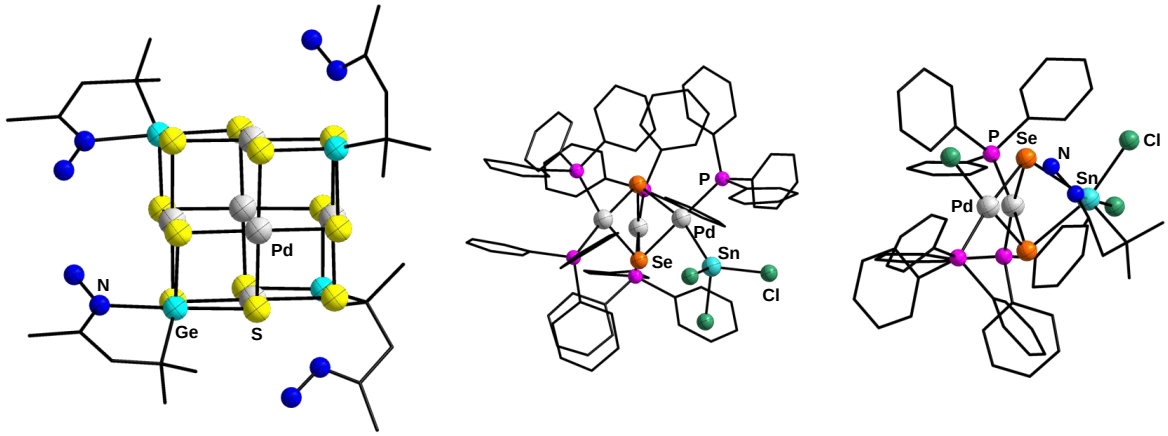

Abbildung 11: Links: Molekülstruktur von $[(R^2Ge)_4Pd_6S_{12}]$.[138] Mitte: Struktur des $[Pd_3Se_2(PPh_3)_5(SnCl_3)]$-Kations.[139] Rechts: Molekülstruktur von $[Pd_2Se_2(R^2SnCl_2)(PPh_3)_3Cl]$.[139]

Auch ein ternärer Cluster mit Iridium wurde unter vollständiger Zersetzung des Edukts dargestellt. Diese Verbindung hat die Zusammensetzung $[\{(cod)_3Ir_3S_2\}_2(SnCl)_2S_2]$ und besteht aus einem Sn_2S_2-Vierring, der an zwei gegenüberliegenden Seiten mit je einer Ir_3S_2-Pyramide überkappt ist, die durch Ir–Sn- und Ir–S-

Bindungen an den zentralen Ring angebunden ist (siehe Abbildung 12, links).[111] Wie bereits in Abschnitt 1.3 beschrieben, konnte eine Serie ternärer Cluster mit Zink beim Versuch, mit an den Cluster angebundenen Bispyridin-Substituenten Zinkionen aus Lösung einzufangen, erhalten werden. Die Verbindungen besitzen die Zusammensetzung $[(RSn)_4(ZnX)_8S_{10}]$ (R = $CMe_2CH_2C(Me)NHNC(2\text{-py})_2$; X = Cl, Br, I; vgl. Abbildung 12, rechts). Hier sind die Zinkionen zwar teilweise von den Bispyridin-Substituenten koordiniert, es kam gleichzeitig aber auch zum Einbau von Zinkatomen ins anorganische Grundgerüst des Clusters.[106]

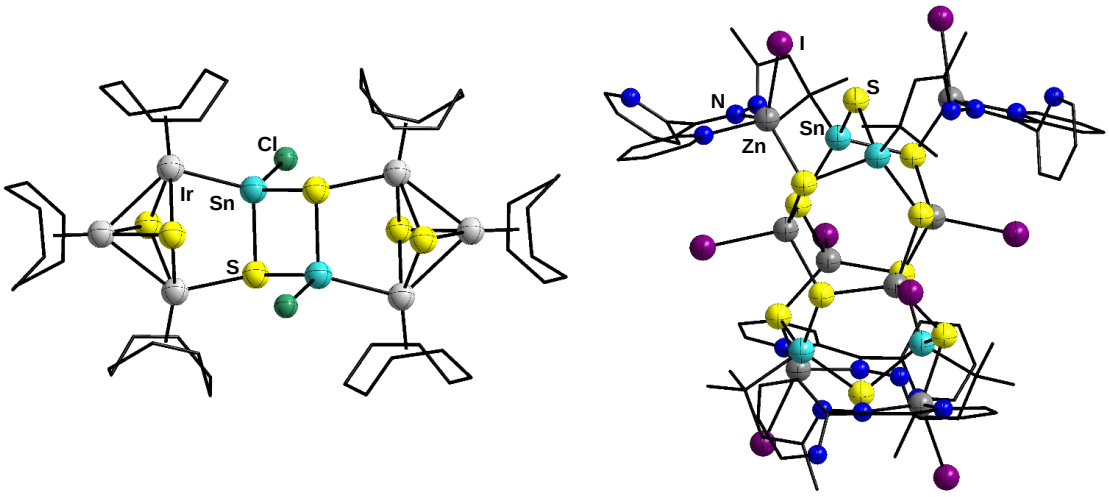

Abbildung 12: Links: Molekülstruktur von $[\{(cod)_3Ir_3S_2\}_2(SnCl)_2S_2]$.[111] Rechts: Molekülstruktur von $[(RSn)_4(ZnI)_8S_{10}]$ (R = $CMe_2CH_2C(Me)NHNC(2\text{-py})_2$).[106]

Abschließend soll noch kurz beispielhaft auf ternäre Cluster eingegangen werden, die nicht ausgehend von vorgeformten binären Clustern, sondern ausschließlich aus mononuklearen Präkursor-Verbindungen erhalten wurden. So konnte durch solvothermale Umsetzung von $Cl_3SnC_4H_8SnCl_3$ mit $[Cu(PPh_3)_3Cl]$ und Na_2S in Methanol ein Cluster der Zusammensetzung $[Cu_4Sn(BuSnS_2)_6(CuPPh_3)_6]$ dargestellt werden. Dieser ist aus einer zentralen Cu_4Sn-Bipyramide aufgebaut, die in eine $Cu_6Sn_6S_{12}$-Schale eingebettet ist, welche wiederum durch sechs PPh_3-Gruppen an den Kupferatomen und sechs Butylgruppen an den Zinnatomen abgesättigt wird (siehe Abbildung 13, links).[142] Eichhöfer und Mitarbeiter stellten aus $PhSnCl_3$, CuCl, PEt_2Ph, $(Me_3Si)_2S$ und Bu_4NCl einen anionischen Cluster her, der als Salz der Zusammensetzung $(Bu_4N)[(PhSn)_{12}Cu_{19}S_{28}(PEt_2Ph)_3]$ anfällt. Der anorganische Clusterkern besteht aus einer Kupfersulfid-Einheit, die nach außen durch PhSn-Gruppen abgesättigt wird (siehe Abbildung 13, mittig).[143] Werden CuOAc und PPh_2Et anstelle von CuCl und PEt_2Ph verwendet, entsteht ein Cluster der Zusammenset-

zung $[(PhSn)_2(CuPPh_2Et)_6S_6]$, der strukturell eng verwandt mit dem von Merzweiler publizierten $[(PhSnS_3)_2(CuPPhMe_2)_6]$-Cluster ist. Die schwereren Homologen mit Selen und Tellur sind ebenfalls bekannt und unterscheiden sich voneinander nur durch die Verbrückungsmodi der Chalkogenatome (siehe Abbildung 13, rechts). Die Tellurverbindung stellt zugleich den bisher einzigen organisch funktionalisierten ternären Cluster mit Tellur dar.[144]

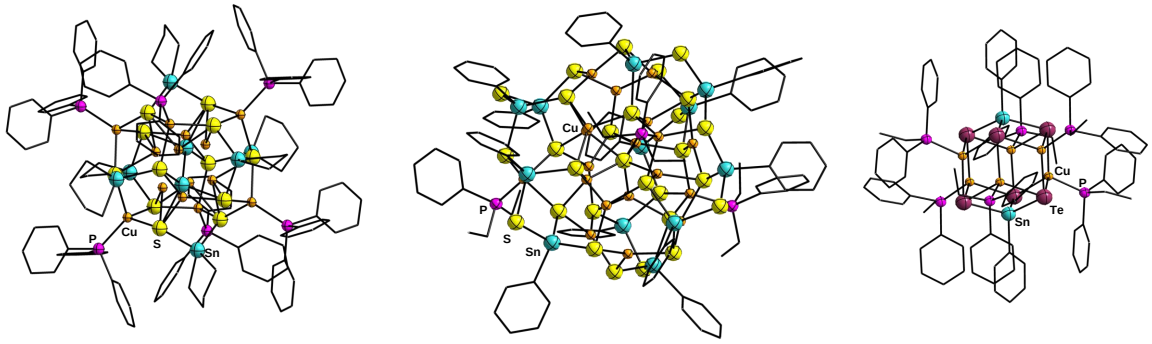

Abbildung 13: Links: Molekülstruktur von $[Cu_4Sn(BuSnS_2)_6(CuPPh_3)_6]$.[142] Mitte: Struktur des $[(PhSn)_{12}Cu_{19}S_{28}(PEt_2Ph)_3]^-$-Anions.[143]Rechts: Molekülstruktur von $[(PhSn)_2(CuPPh_2Et)_6Te_6]$.[144]

1.5 Nichtlineare Optik

Im Rahmen des Promotionsprojekts wurden Organotetrelchalkogenidcluster synthetisiert, deren nichtlineare optische Eigenschaften im Anschluss von der Arbeitsgruppe von Prof. Dr. Sangam Chatterjee in Gießen untersucht wurden. Vor diesem Hintergrund erscheint es notwendig, an dieser Stelle kurz die Grundlagen nichtlinearer optischer Effekte zu erläutern.

Wenn ein elektrisches Feld $\vec{E}$ mit einem Medium wechselwirkt, so wird in diesem Medium eine Polarisation $\vec{P}$ induziert. Für hinreichend niedrige Feldstärken besteht zwischen Feldstärke und Polarisation ein linearer Zusammenhang, der wie folgt beschrieben werden kann:

$$\vec{P} = \epsilon_0 \chi \vec{E} \text{ mit } \chi = (\epsilon(\omega) - 1) \tag{8}$$

Die elektrische Suszeptibilität χ ist also abhängig von der Dielektrizitätskonstanten ϵ, die ihrerseits frequenzabhängig ist. Für höhere Feldstärken kann dieser lineare Zusammenhang nicht gelten, da die Polarisation nicht beliebig ansteigen kann, sondern sich einem Sättigungswert annähert, der erreicht ist, wenn alle Dipole im Medium entlang der Feldlinien ausgerichtet sind. Somit muss die Suszeptibilität von der Feldstärke abhängig sein, was sich durch eine Potenzreihenentwicklung formulieren lässt:

$$\begin{aligned} P &= \epsilon_0(\chi_1 E + \chi_2 E^2 + \chi_3 E^3 + ...) \\ &= P_{lin} + \epsilon_0(\chi_2 E^2 + \chi_3 E^3 + ...) \\ &= P_{lin} + P_{NL} \end{aligned} \tag{9}$$

Die höheren Terme $\chi_2, \chi_3, ...$ werden dabei erst bei hohen Feldstärken relevant, wie sie etwa bei Einstrahlung von Lasern hoher Intensität erreicht werden. Wird das eingestrahlte elektrische Feld vereinfacht als ebene Welle $E = \frac{1}{2}E_0 \exp(i\omega t)$ angenommen und dessen vektoriellen Charakter vernachlässigt, so erhält man für die Polarisation folgenden Ausdruck:

$$P = \epsilon_0\chi_1 E_0 \cos(\omega t) + \frac{1}{2}\epsilon_0\chi_2 E_0^2[1 + \cos(2\omega t)] + \frac{1}{4}\epsilon_0\chi_3 E_0^3[3\cos(\omega t) + \cos(3\omega t)] + ... \tag{10}$$

Die Nichtlinearität zweiter Ordnung χ_2 beinhaltet sowohl einen zeitlich konstanten Anteil, als auch einen, der mit der doppelten Frequenz des eingestrahlten Feldes schwingt, während die Nichtlinearität einen mit der Grundfrequenz und einen mit der dreifachen Frequenz schwingenden Anteil enthält. Die Zeitabhängigkeit der Nichtlinearität zweiter Ordnung lässt sich demnach als eine Oszillation mit der Frequenz 2ω, also der doppelten Einfallsfrequenz, beschreiben. Dadurch kommt es zur Erzeugung von Licht der doppelten Frequenz (Frequenzverdopplung, *second harmonic generation*, SHG).
Die Frequenzverdopplung ist allerdings nicht der einzige nichtlineare Effekt zweiter Ordnung. Werden in das nichtlineare Medium zwei elektrische Felder unterschiedlicher Frequenzen ω_1 und ω_2 eingestrahlt, werden nicht nur die beiden zweiten Harmonischen $2\omega_1$ und $2\omega_2$ erzeugt, sondern auch die Summenfrequenz $\omega_1 + \omega_2$ und die Differenzfrequenz $|\omega_1 - \omega_2|$. Ob und wenn ja welcher dieser Effekte beobachtbar wird, hängt von der Phasenanpassung des verwendeten Mediums ab, da die einfallende Welle eine andere Ausbreitungsgeschwindigkeit im Medium hat als die von ihr erzeugten zweiten Harmonischen, Summen- oder Differenzfrequenzen. Dadurch kommt es zur Interferenz von einfallenden und im Medium erzeugten Frequenzen, so dass die Lichtintensität entlang der Strecke z, die die einfallende Welle durchläuft, oszilliert.[145,146]
Möchte man nun das nichtlineare Medium gezielt zur Frequenzverdopplung nutzen, so muss die Lichterzeugung phasenangepasst erfolgen, sodass die Brechungsindizes von Grundfrequenz und zweiter Harmonischer gleich sind. Dies wird durch Verwendung doppeltbrechender Medien, also Medien, deren Brechungsindex abhängig von der Polarisation des einfallenden Lichts ist, erreicht. Dadurch wird das einfallenden Licht in zwei senkrecht zueinander polarisierte Strahlenbündel aufgetrennt, deren Ausbreitungsgeschwindigkeit im Medium sich voneinander unterscheidet. Durch passende Ausrichtung des nichtlinea-

ren Mediums relativ zum einfallenden Licht kann nun eine phasenangepasste Frequenzverdopplung erfolgen, die im Idealfall nahezu verlustfrei ist.
Werden mehrere elektrische Felder gleichzeitig eingestrahlt, kann durch Wahl des jeweils geeigneten Phasenanpassungswinkels zwischen Frequenzverdopplung, Summen- und Differenzfrequenzerzeugung gewechselt werden. Die Summenfrequenzerzeugung kann auch umgekehrt verlaufen, also als Zerfall eines einfallenden Photons in zwei Photonen, deren Summenfrequenz der des einfallenden Photons entspricht. Dies wird als optisch parametrischer Prozess bezeichnet und etwa zur Erzeugung durchstimmbarer Laserpulse verwendet, da sich das Verhältnis der Frequenzen der beiden erzeugten Photonen durch Variation des Phasenanpassungswinkels einstellen lässt.[145,147]
Grundvoraussetzung für das Auftreten einer Nichtlinearität zweiter Ordnung ist, dass das verwendete Medium keine Inversionssymmetrie besitzt, da andernfalls nur Nichtlinearitäten ungerader Ordnung auftreten. Häufig verwendete Verbindungen sind anorganische Salze wie Kaliumdihydrogenphosphat, Lithiumniobat oder β-Bariumborat. Defekte in der Verbindung können aber auch in eigentlich inversionssymmetrischen Medien zur Aufhebung der Inversionssymemtrie führen, so dass auch in solchen Medien χ_2-Effekte auftreten können. Grundsätzlich besitzt jedes Medium eine solche Störstelle - die Oberfläche, an der es zu einer lokalen Symmetriereduktion kommt. Nichtlineare Effekte zweiter Ordnung können daher prinzipiell an der Oberfläche nahezu jeder Probe auftreten, sind aber üblicherweise deutlich schwächer ausgeprägt als solche aus dem Probenvolumen.
In inversionssymmetrischen Medien ist die Nichtlinearität dritter Ordnung, χ_3, die niedrigste beobachtbare Nichtlinearität. Die nichtlineare Polarisation dritter Ordnung enthält, wie in Gleichung 10 gezeigt, eine Komponente, die mit 3ω oszilliert. Somit ließe sich mit einem geeigneten inversionssymmetrischen Medium eine Frequenzverdreifachung erreichen. Da hier jedoch die Phasenanpassung schwieriger zu realisieren ist, wird eine Frequenzverdreifachung technisch in der Regel in einem zweistufigen Prozess erreicht. Zunächst wird die zweite Harmonische der Grundfrequenz ω erzeugt, anschließend wird in einem zweiten χ_2-Medium die Summenfrequenz aus ω und 2ω erzeugt. Damit lassen sich Ausbeuten von etwa 30 % erreichen.[145]
Ein weiterer technisch bedeutsamer nichtlinearer Effekt dritter Ordnung ist der optische Kerr-Effekt, der die Abhängigkeit des Brechungsindexes von der Lichtintensität beschreibt. Dieser Effekt führt beispielsweise zur Selbstfokussierung von Laserstrahlen. Ein von einem Laser emittierter Lichtpuls hat typischerweise eine gaußförmige Intensitätsverteilung. Tritt dieser nun in ein Medium ein, in dem der Kerr-Effekt auftritt, so wird das Intensitätsmaximum stärker gebrochen als die Flanken des Pulses. Dadurch kommt zu einer Fokussierung des Strahls. Eine Fokussierung noch innerhalb des Mediums ist dabei unerwünscht, da durch die starke Intensitätserhöhung im Fokus Nichtlinearitäten

höherer Ordnung induziert werden, was zur Zerstörung des Mediums führen kann; dies lässt sich jedoch durch Verwendung ausreichend großer Strahlquerschnitte vermeiden. Diese Selbstfokussierung kann jedoch auch erwünscht sein, um besonders kurze Laserpulse zu erzeugen. Dazu wird ein KERR-Medium mit einer Blende gekoppelt, sodass selektiv nur das intensive Pulsmaximum hinreichend fokussiert wird, um die Blende zu passieren. Dadurch, dass der KERR-Effekt nicht permanent ist, sondern sich die KERR-Linse nur bei Durchtritt eines hinreichend intensiven Laserpulses aufbaut und danach wieder verschwindet, kann ein in den Resonator eines Lasers eingebautes KERR-Medium zur selektiven Verstärkung eines bestimmten Photonenbündels genutzt werden, da nur dieses die Blende passieren kann. Durch diese Modenkopplung können sehr kurze Lichtpulse von ca. 10 fs erzeugt werden. Ein typisches KERR-Medium ist Titan-dotierter Saphir (Ti:Sa), welcher in entsprechenden Titan-Saphir-Lasern zur Anwendung kommt, bei denen ultrakurze Laserpulse aus dem einfallenden Licht eines (grünen) Pumplasers erzeugt werden. Als Pumplaser kommen hierbei in der Regel Ar-Laser (515 nm) oder frequenzverdoppelte Nd:YAG-Laser (532 nm) zum Einsatz.[145,148]

Im Bereich der Erzeugung ultrakurzer Laserpulse ist neben der Selbstfokussierung auch die Selbstphasenmodulation von Lichtpulsen ein bedeutsamer χ_3-Effekt. Durch die Abhängigkeit des Brechungsindexes von der Lichtintensität ändert sich bei Durchtritt eines Lichtpulses durch ein nichtlineares optisches Medium die Ausbreitungsgeschwindigkeit des Intensitätsmaximums relativ zu den Flanken des Pulses, dadurch kommt es zu einer Phasenverschiebung. Der Anfang des Pulses erfährt eine Rotverschiebung, zum Intensitätsmaximum hin tritt eine Blauverschiebung auf, und am Ende fällt die Frequenz wieder auf ω_0 ab. Somit entsteht eine spektrale Verbreiterung des Lichtpulses, die umso stärker ausfällt, je kürzer und intensiver der Lichtpuls ist. Auf diese Weise lassen sich Laserpulse erzeugen, die den gesamten sichtbaren Spektralbereich abdecken.[145,148]

1.6 Heteroadamantane mit nichtlinearen optischen Eigenschaften

Vor einigen Jahren stellte EUSSNER einen Organozinnsulfidcluster mit 4-Vinylphenyl-Substituenten (Styryl-Substituenten, im Folgenden Sty abgekürzt) dar. Da die Verbindung nicht kristallisierte, sondern stets reproduzierbar als amorphes Pulver anfiel, war eine Charakterisierung durch Kristallstrukturanalyse nicht möglich. Massenspektrometrisch konnte die Summenformel $[(StySn)_4S_6]$ nachgewiesen werden, und durch DFT-Rechnungen der beiden möglichen Isomere konnte gezeigt werden, dass die adamantanartige Struktur energetisch um 28.5 kJ/mol gegenüber der doppeldeckerartigen Konformation bevorzugt ist, so dass angenommen werden kann, dass die Verbindung als Heteroadamantan vorliegt (siehe Abbildung 14, links). Da solche Heteroadamantane durch ihre *pseudo-T_d*-Symmetrie nicht inversionssymmetrisch sind, war zu vermuten, dass an der Verbindung

nichtlineare optische Effekte wie etwa eine Frequenzverdopplung auftreten können. Durch Anregung einer Probe der Verbindung mit einer cw-Infrarot-Laserdiode wurde jedoch stattdessen die Emission eines Superkontinuums beobachtet, das sich über einen weiten Bereich des sichtbaren Spektrums erstreckt. Der Farbeindruck des emittierten Lichts entspricht bei genügend großen Anregungsleistungen mit einer Farbtemperatur von 2900 K dem einer Wolfram-Glühlampe (siehe Abbildung 14, rechts). Zu hohen Energien hin wird die Emission durch die Absorption der Verbindung selbst begrenzt, welche - durch UV-Vis-Spektroskopie und zeitabhängige DFT-Rechnungen (TD-DFT) ermittelt - bei etwa 3 eV einsetzt.

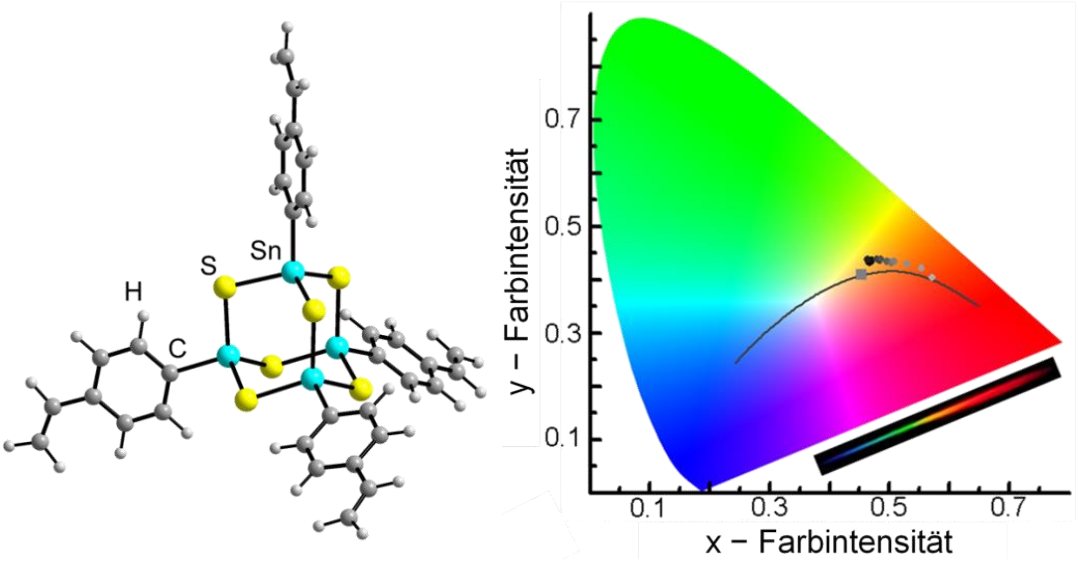

Abbildung 14: Links: DFT-optimierte Molekülstruktur von $[(StySn)_4S_6]$. Rechts: Normfarbtafel zur Darstellung der Farbmischung. Die Punkte stellen die Farbtemperatur des emittierten Weißlichts bei verschiedenen Anregungsleistungen dar. Zum Vergleich zeigt die graue Linie den Farbeindruck eines Schwarzkörperstrahlers, das graue Quadrat zeigt den Farbeindruck einer warmweißen Lichtquelle bei einer Farbtemperatur von 2856 K.[149]

Links in Abbildung 15 ist das Emissionsspektrum in Abhängigkeit von der Anregungsleistung des IR-Lasers (6 - 18 mW) aufgetragen. Es zeigt sich, dass bei einer Verdreifachung der Anregungsleistung die Intensität der Emission um drei Größenordnungen ansteigt, was einer Nichtlinearität achter Ordnung entspricht und einen thermischen Emissionsmechanismus ausschließt. Die Etendue, also die „Gerichtetheit“ des anregenden Laserstrahls wird weitestgehend beibehalten, wie in Abbildung 15 gezeigt. Dabei kommt es zu einer

gewissen Verbreiterung, da das emittierte Licht kürzere Wellenlängen enthält als der anregende Laserstrahl, welche stärker gestreut werden.[149,150]
Der Mechanismus der Weißlicht-Erzeugung ist bisher nicht vollständig geklärt, so dass weitere Studien erforderlich sind, um herauszufinden, was die notwendigen Voraussetzungen für die Beobachtung einer Weißlicht-Emission sind.

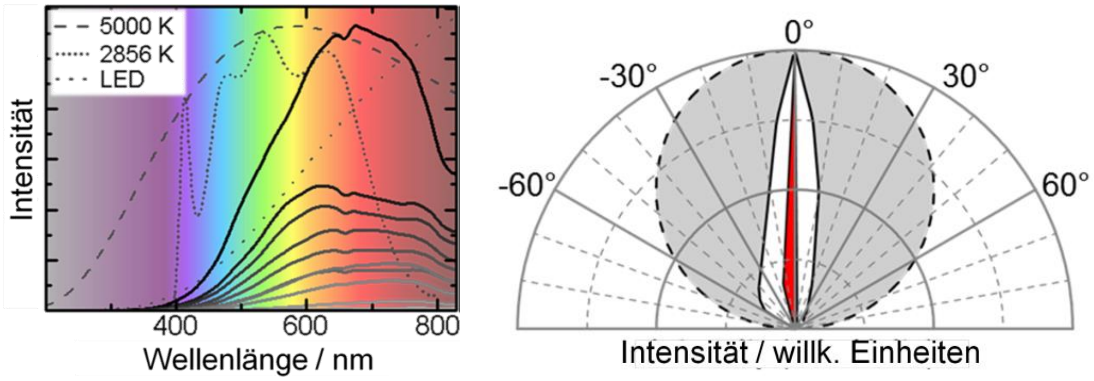

Abbildung 15: Links: Emissionsspektrum für verschiedene Anregungsleistungen von 6 bis 18 mW bei einer Anregungswellenlänge von 980 nm. Zum Vergleich sind die Emissionsspektren von Schwarzkörperstrahlern bei 2856 und 5000 K sowie das Emissionsspektrum einer weißen LED abgebildet. Rechts: Winkelabhängigkeit des emittierten Weißlichtspektrums im Wellenlängenbereich von 350 bis 800 nm (weiß), des anregenden IR-Lasers (rot) sowie eines idealen Lambertschen Emitters. (grau).[149]

2 Zielsetzung

Die Arbeit kann thematisch in drei Teile aufgeteilt werden. Im ersten Teilprojekt sollten aufbauend auf den Arbeiten von Eussner,[149,150] Organotetrelsesquichalkogenidcluster der Zusammensetzung $[(RT)_4E_6]$ mit heteroadamantanartiger Struktur dargestellt werden, um im Anschluss deren nichtlineare optische Eigenschaften zu untersuchen. Durch gezielte Variation sowohl der Kernzusammensetzung als auch der organischen Substituenten sollten zunächst Erkenntnisse über mögliche Voraussetzungen, Ursachen oder gar den Mechanismus der erstmals an $[(StySn)_4S_6]$ beobachteten Weißlichterzeugung gewonnen werden. Zudem sollte untersucht werden, inwiefern sich durch Variation der Zusammensetzung das Emissionsspektrum modifizieren lässt, was für potentielle technische Anwendungen als Lichtquelle, etwa in der medizinischen Diagnostik, bedeutsam ist. Die photophysikalischen Untersuchungen hierzu sollten in der Arbeitsgruppe Chatterjee in Gießen durchgeführt werden. Hierfür wurden zunächst präparative Zugangswege zu den als Edukt notwendigen Organotetreltrichloriden gefunden, um anschließend die jeweiligen Cluster darstellen und sauber isolieren zu können (vgl. Schema 7).

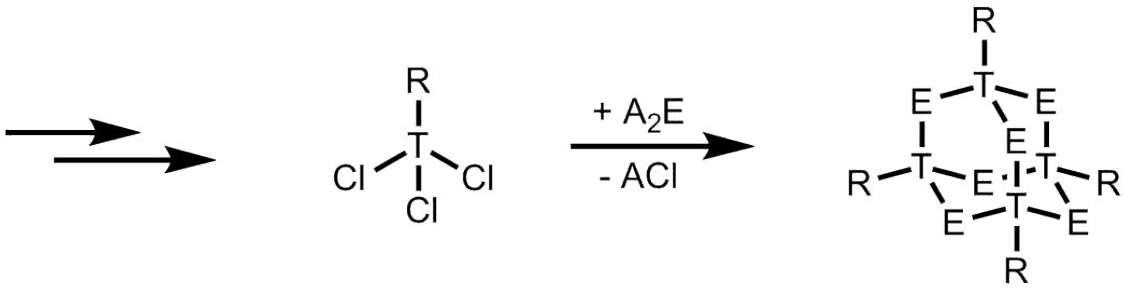

Schema 7: Darstellung binärer Organotetrelsesquichalkogenidcluster.

In einem zweiten, koordinationschemisch verorteten Teilprojekt sollte die Reaktivität der Cluster mit binärem anorganischem Grundgerüst gegenüber Übergangsmetall-komplexen untersucht werden. Als wesentlicher Parameter sollte hierbei neben der Wahl des jeweiligen Übergangsmetalls der Einfluss verschiedener (Phosphan-)Liganden an den eingesetzten Komplexen untersucht werden. Neben den für ähnliche Cluster bereits vielfach untersuchten Umsetzungen mit Münzmetallkomplexen (vgl. Abschnitt 1.4), war geplant, diese Reaktivitätsstudien auf elektronenärmere Übergangsmetalle auszudehnen. Zudem wurde die Reaktivität der bereits bekannten Cluster $[(R^1Sn)_3S_4Cl]$ und $[(R^1Sn)_4S_6]$ gegenüber verschiedenen Zinkkomplexen untersucht (vgl. Schema 8).

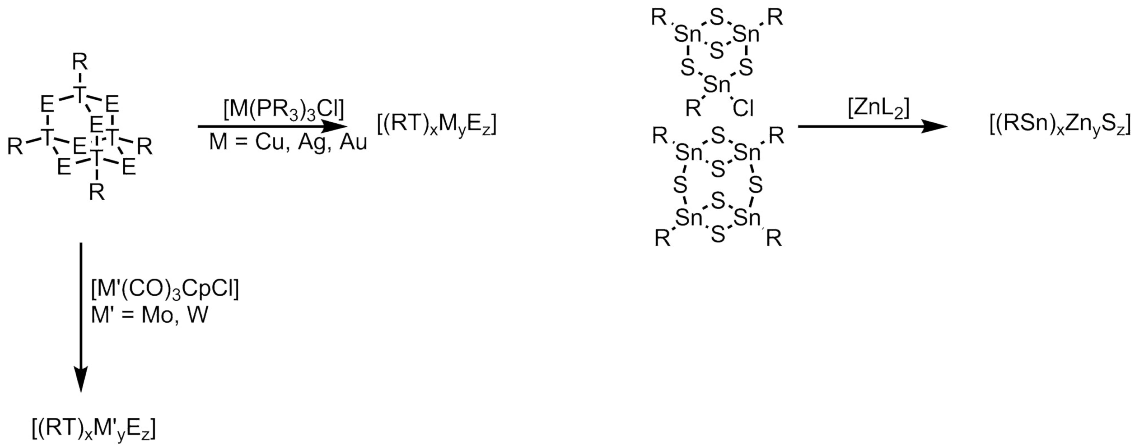

Schema 8: Darstellung von Clustern mit ternärem anorganischem Grundgerüst.

In einem dritten Teilprojekt wurde die Reaktivität des Organogermaniumtrichlorids R^1GeCl_3 gegenüber Bis(trimethylsilyl)chalkogeniden untersucht, um, wie für das schwere Homologe Zinn bereits durchgeführt, die Intermediate bei der Bildung der Organotetrelsesquichalkogenidcluster zu isolieren (vgl. Schema 9).

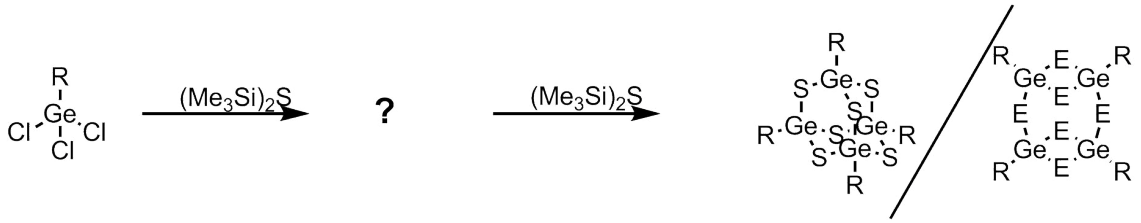

Schema 9: Isolierung von Intermediaten der Bildung der Organogermaniumsesquichalkogenidcluster.

3 Übersicht über die im kumulativen Teil enthaltenen Publikationen

Aus den Ergebnissen meines Promotionsprojekts sind bisher sieben publizierte, im Druck befindliche oder in Kürze einzureichende Publikationen hervorgegangen, die in diesem Kapitel kurz zusammengefasst werden sollen. Darüber hinaus bin ich Erstautor eines Übersichtsartikels über die Koordinationschemie von Tetrelchalkogeniden, der aber keine eigenen Forschungsergebnisse enthält. Zudem bin ich an fünf weiteren Publikationen als Coautor beteiligt, die entweder auf Ergebnissen aus meiner Masterarbeit basieren oder nicht in thematischem Zusammenhang zu meinem Promotionsprojekt stehen. Hierzu sei auf die vollständige Publikationsliste in Abschnitt 8 verwiesen.

3.1 "Organotetrel Chalcogenide Clusters: Between Strong Second-Harmonic and White-Light Continuum Generation"
N.W. Rosemann, J.P. Eußner, E. Dornsiepen, S. Chatterjee, S. Dehnen, *J. Am. Chem. Soc.* **2016**, *138*, 16224–16227.

3.2 "Controlling the White-Light Generation of $[(RSn)_4E_6]$: Effects of Substituent and Chalcogenide Variation"
E. Dornsiepen, F. Dobener, N. Mengel, S. Chatterjee, S. Dehnen, **2019**, *Manuskript in Vorbereitung.*

3.3 "White-Light Generation Upon In-Situ Amorphization of Single Crystals of $[\{(Me_3P)_3AuSn\}\{PhSn\}_3S_6]$ and $[\{(Et_3P)_3AgSn\}\{PhSn\}_3S_6]$"
E. Dornsiepen, F. Dobener, N. Mengel, O. Lenchuk, C. Dues, S. Sanna, D. Mollenhauer, S. Chatterjee, S. Dehnen, *Adv. Opt. Mater.* **2019**, 1801793

3.4 "Transition-Metal-Induced Rearrangement of $[(PhSn)_4S_6]$ Towards Ternary Cu^{I}/Sn/S or Cu^{II}/Sn/S Cluster"
E. Dornsiepen, F. Weigend, S. Dehnen, *Chem. Eur. J.* **2019**, *25*, 2486-2490.

3.5 "$[\{(PhSn)_3SnS_6\}\{(CpM)_3S_4\}]$ (M = Mo, W): Minimal Molecular Models of Covalent Attachment of Metalchalcogenide Clusters on Layered Transition Metal Dichalcogenides (TMDCs)"
E. Dornsiepen, S. Dehnen, **2019**, *Manuskript in Vorbereitung.*

3.6 "How Organotin Sulfide Clusters Behave in the Presence of Zinc Compounds – a Reactivity Study"
E. Dornsiepen, S. Dehnen, *Eur. J. Inorg. Chem.* **2019**, DOI: 10.1002/ejic.201900508.

3.7 "Dinuclear organogermanium chalcogenide complexes as intermediates towards functionalized clusters"
E. Dornsiepen, S. Dehnen, *Dalton Trans.* **2019**, *48*, 3671-3675.

3.1 Organotetrel Chalcogenide Clusters: Between Strong Second-Harmonic and White-Light Continuum Generation

Aufbauend auf den Untersuchungen an $[(StySn)_4S_6]$ wurde in dieser Arbeit adamantanartige Organotetrelsesquisulfidcluster untersucht, bei denen einerseits das Tetrelelement von Zinn über Germanium bis Silicium variiert wurde, andererseits wurden unterschiedliche organische Substituenten (Methyl, Phenyl, 1-Naphthyl) angebracht, um den bisher ungeklärten Mechanismus der Weißlichterzeugung zu untersuchen. Von den dargestellten Verbindungen ist lediglich $[(PhSi)_4S_6]$ kristallin, alle anderen Verbindungen liegen in amorphem Zustand vor. Bei Variation der Substituenten (siehe Abbildung 16, links) konnte für $[(PhSn)_4S_6]$ die von $[(StySn)_4S_6]$ bekannte Weißlichterzeugung beobachtet werden, während $[(MeSn)_4S_6]$ und $[(NpSn)_4S_6]$ (Np = 1-Naphthyl) stattdessen Frequenzverdopplung mit hoher Intensität zeigen. Für die methylsubstituierte Verbindung wurde dies auf das nicht vorhandene π-Elektronensystem zurückgeführt, wohingegen bei dem naphthylsubstituierten Cluster vermutlich eine durch π-*stacking* hervorgerufene, beginnende Fernordnung dafür sorgt, dass eine Emission in Phase erfolgt.

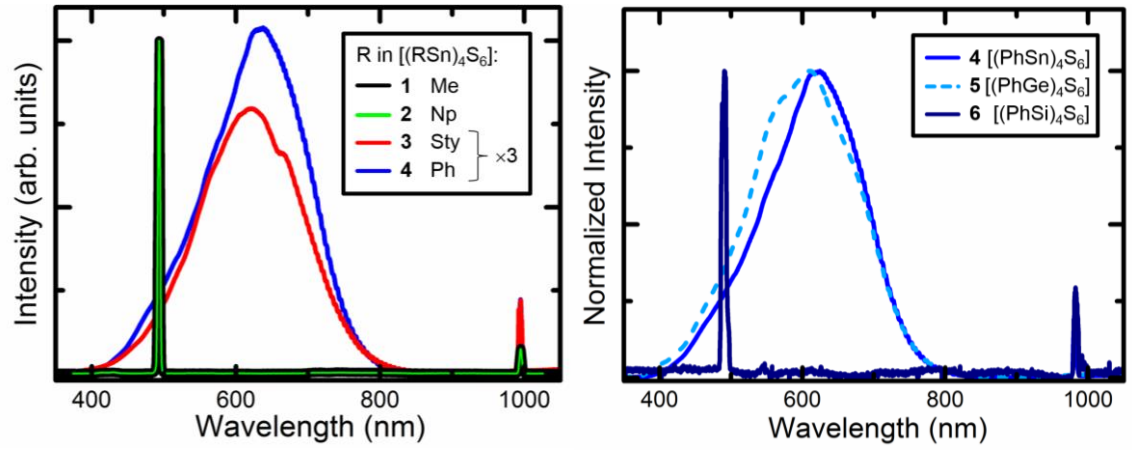

Abbildung 16: Links: Emissionsspektren von $[(MeSn)_4S_6]$ (schwarz), $[(NpSn)_4S_6]$ (grün), $[(StySn)_4S_6]$ (rot) und $[(PhSn)_4S_6]$ (blau) bei einer Anregungswellenlänge von 980 nm. Rechts: Emissionsspektren von $[(PhSn)_4S_6]$ (blau), $[(PhGe)_4S_6]$ (hellblau, gestrichelt) und $[(PhSi)_4S_6]$ (violett) bei einer Anregungswellenlänge von 980 nm.

Bei Variation des Tetrelelements (siehe Abbildung 16, rechts) zeigt $[(PhGe)_4S_6]$ analog zur Zinnverbindung Weißlichterzeugung, die allerdings leicht blauverschoben ist, während beim kristallinen $[(PhSi)_4S_6]$, Frequenzverdopplung auftritt. Zwar sind die Moleküle selbst nicht inversionssymmetrisch, allerdings kristallisiert die Verbindung in einer zentrosymmetrischen Raumgruppe, weshalb es sich vermutlich um einen Oberflächeneffekt handelt, der durch lokale Symmetriereduktion an der Kristalloberfläche hervorgerufen wird.

In dieser Arbeit konnten also, neben der nicht-inversionssymmetrischen Molekülstruktur als Grundvoraussetzung - zwei notwendige Voraussetzungen für eine Weißlichterzeugung identifiziert werden: Zum einen scheint ein π-Elektronensystem von grundlegender Bedeutung zu sein, zum anderen darf die Wechselwirkung zwischen den Molekülen auf keinen Fall zu einer Ausordnung bis hin zur Kristallinität führen, da andernfalls stattdessen phasengleiche Emission und damit Frequenzverdopplung auftritt.

3.2 Controlling the White-Light Generation of $[(RSn)_4E_6]$: Effects of Substituent and Chalcogenide Variation

Wie im vorigen Abschnitt beschrieben, eignen sich adamantanartige Organotetrelsesquisulfidcluster der Zusammensetzung $[(RT)_4S_6]$ (T = Ge, Sn) als kostengünstige Weißlichtemitter, indem sie infrarotes Laserlicht in gerichtetes Weißlicht umwandeln. Es konnte gezeigt werden, dass der Effekt der Weißlichterzeugung in erster Linie von der Morphologie der Verbindungen und der Art der organischen Substituenten abhängt. Um ein näheres Verständnis der Ursachen der Weißlichtemission zu erlangen, wurde in dieser Arbeit die Substanzbibliothek deutlich erweitert. Hierzu wurden adamantanartige Cluster $[(RSn)_4E_6]$ (R = Phenyl, Cyclopentadienyl, Cyclohexyl, Benzyl, $CH_2CH_2(C_6H_4)CO_2Et$ (R^4); E = S, Se) synthetisiert, charakterisiert und auf ihre nichtlinearen optischen Eigenschaften untersucht.

Die beiden benzylsubstituierten Cluster fallen als einzige der hier untersuchten Verbindungen kristallin an. Während das $[(BnSn)_4S_6]$ erwartungsgemäß kein Weißlicht erzeugt, sondern Frequenzverdopplung zeigt, kann beim entsprechenden Selenid Weißlicht beobachtet werden (siehe Abbildung 17), was jedoch auf das unterschiedliche thermische Verhalten der beiden Verbindungen zurückgeführt werden kann: Während der sulfidische Cluster sich bei 160 bis 180 °C zersetzt, ohne zuvor zu schmelzen, schmilzt $[(BnSn)_4Se_6]$ bei 141 °C unzersetzt und liegt infolge der Anregung mit Laserlicht vermutlich zumindest teilweise nicht mehr im kristallinen Zustand, sondern als Schmelze vor, wodurch eine Weißlichterzeugung möglich wird. Das Emissionsspektrum unterscheidet sich hierbei nicht signifikant von dem der Referenzverbindung $[(PhSn)_4S_6]$, zeigt aber erstmals, dass dieses Phänomen auch bei Schmelzen auftreten kann.

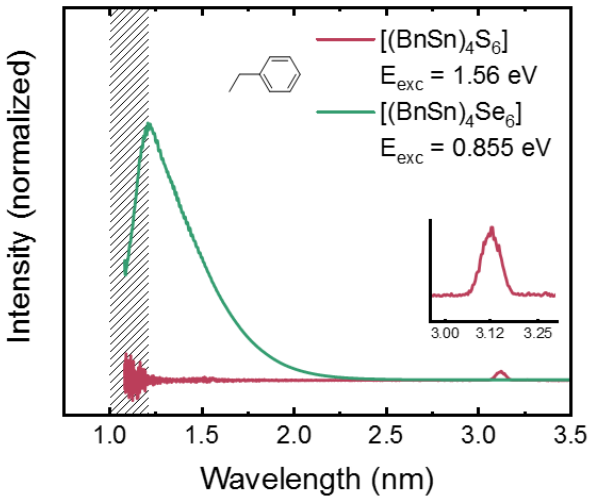

Abbildung 17: Emissionsspektren von $[(BnSn_4)S_6]$ (rot) und $[(BnSn)_4Se_6]$ (grün).

Weiterhin zeigt das Beispiel [$(BnSn)_4Se_6$], dass das aromatische System des Substituenten nicht zwingend direkt am Zinnatom angebunden sein muss, damit Weißlichterzeugung erfolgen kann. Dies wird ebenfalls durch die beiden Verbindungen [$(R^4Sn)_4S_6$] und [$(R^4Sn)_4Se_6$] bestätigt, bei welchen der aromatische Phenylrest durch eine Ethylen-Brücke an das Zinnatom angebunden ist, und die ebenfalls beide Weißlicht generieren. Auch hier scheint die Wahl des organischen Substituenten keinen Einfluss auf das Emissionsspektrum zu haben (siehe Abbildung 18), jedoch tritt durch Ersatz des Schwefels im anorganischen Kern durch Selen eine leichte Rotverschiebung auf.
Um die bisherige Hypothese, dass ein aromatisches π-Elektronensystem für die Weißlichterzeugung notwendig ist, zu testen, wurden im Anschluss cyclopentadienyl-substituierte Cluster untersucht, in denen die π-Elektronen in den C-C-Doppelbindungen lokalisiert sind. Auch hier tritt Weißlichterzeugung auf, wodurch die oben formulierte falsifiziert wurde. In den Emissionsspektren fällt auf, dass diese im Bereich hoher Energie steiler abfallen als bei den zuvor untersuchten Verbindungen, was in einem höheren Blauanteil des emittierten Lichts resultiert. Auch hier tritt bei Substitution der Schwefel- durch Selenatome eine Rotverschiebung des Spektrums auf.
In einem weiteren Schritt wurde gänzlich auf Substituenten mit π-Elektronen verzichtet, indem Cyclohexylreste an die Zinnatome angebunden wurden. Auch für diese beiden Verbindungen konnte Weißlichterzeugung gezeigt werden, sodass inzwischen ausgeschlossen werden kann, dass dieses Phänomen auf einer alleinigen Anregung von π-Elektronen beruht.
Aus diesen Erkenntnissen schließen wir, dass die Weißlichterzeugung auf einer Zwei-Photonen-Anregung in extrem kurzlebige virtuelle Zustände innerhalb des HOMO-LUMO-Gaps der Verbindungen beruht, aus denen die Moleküle unter Photonenemission in verschiedene schwingungsangeregte Zustände des elektronischen Grundzustandes relaxieren, wodurch die beobachteten breiten Emissionsspektren auftreten. Grundvoraussetzung hierfür ist ein hinreichend großes HOMO-LUMO-Gap, da andernfalls Anregungen in elektronisch angeregte Zustände mit deutlich längerer Lebensdauer dominieren, die auf anderen Wegen, etwa durch Photolumineszenz, relaxieren. Daher werden die Emissionsspektren am unteren Energielimit durch die Anregungsenergie, am oberen Limit durch das HOMO-LUMO-Gap begrenzt, wodurch beispielsweise die beobachtete Rotverschiebung beim [$(CpSn)_4Se_6$] erklärt werden kann, da hier die Emission durch ein gemäß DFT-Rechnungen mit 2.08 eV vergleichsweise kleines HOMO-LUMO-Gap limitiert wird.

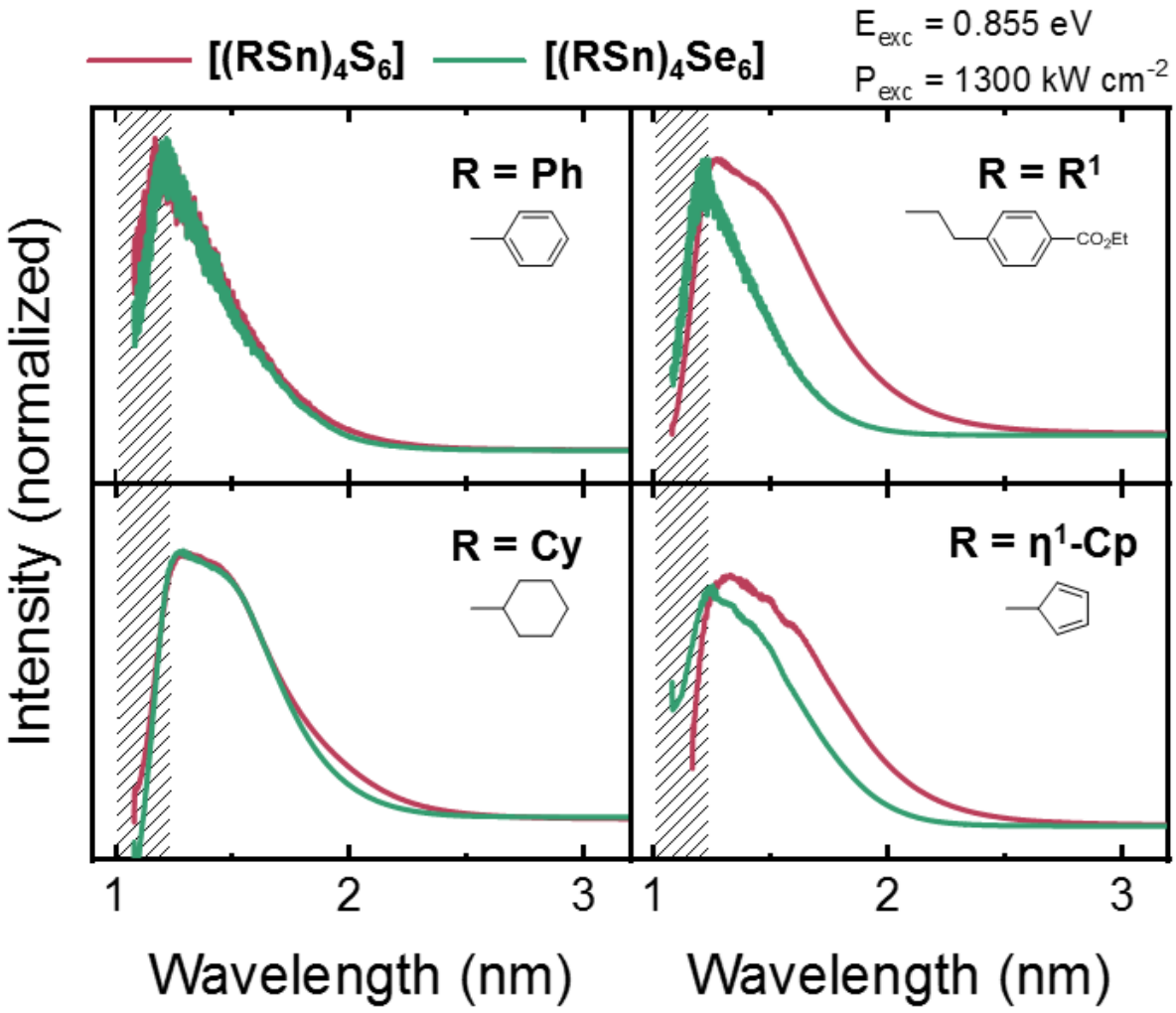

Abbildung 18: Oben links: Emissionsspektren von $[(PhSn_4)S_6]$ (rot) und $[(PhSn)_4Se_6]$ (grün). Oben rechts: Emissionsspektren von $[(R^4Sn_4)S_6]$ (rot) und $[(R^4Sn)_4Se_6]$ (grün). Unten links: Emissionsspektren von $[(CySn_4)S_6]$ (rot) und $[(CySn)_4Se_6]$ (grün). Unten rechts: Emissionsspektren von $[(CpSn_4)S_6]$ (rot) und $[(CpSn)_4Se_6]$ (grün).

3.3 White-Light Generation Upon In-Situ Amorphization of Single Crystals of [{(Me$_3$P)$_3$AuSn}{PhSn}$_3$S$_6$] and [{(Et$_3$P)$_3$AgSn}{PhSn}$_3$S$_6$]

Ausgehend von [(PhSn)$_4$S$_6$] wurde der Cluster [{(Me$_3$P)$_3$AuSn}{PhSn}$_3$S$_6$] (**1**) dargestellt, bei dem einer der Phenylreste der Ausgangsverbindung durch ein Goldphosphan-Komplexfragment substituiert wurde. Triebkraft für die Reaktion ist die Oxidation des Phenylrests zu Chlorbenzol bei gleichzeitiger Reduktion des betroffenen Zinnatoms von +IV zu +II. Versuche, alle vier Phenylreste zu substituieren, schlugen fehl. Sie führten stattdessen zur Umlagerung des Clusters und Bildung des dianionischen Defektheterokubanclusters [Au(PMe$_3$)$_4$][Au(PMe$_3$)$_2$][(PhSnCl)$_3$S$_4$] (**2**), in dem durch einen zusätzlichen Chlorid-Liganden an jedem Zinnatom die Koordinationszahl fünf auftritt, so dass die Bildung eines Defektheterokubans auch mit organischen Substituenten ohne σ-Donor-Funktion bevorzugt wird.

Der Versuch, die Reaktion auf das leichtere Homologe Silber zu übertragen, führte zunächst ebenfalls zur Zersetzung des Clusters unter Bildung von [(Me$_3$P)$_3$AgSnCl$_3$] (**3**). Mit dem sterisch anspruchsvolleren Phosphanliganden PEt$_3$ hingegen konnte erfolgreich der entsprechende Cluster [{(Et$_3$P)$_3$AgSn}{PhSn}$_3$S$_6$] (**4**) erhalten werden. DFT-Rechnungen zeigen, dass die vergleichsweise labile Zinn-Silber-Bindung in Verbindung **4** durch dispersive Wechselwirkungen zwischen den Ethylgruppen der Phosphanliganden und den Phenylresten an den Zinnatomen stabilisiert wird. Für den leichtesten Vertreter der Münzmetalle, das Kupfer, konnte wiederum auch mit dem kleineren Trimethylphosphan ein zu Verbindung **1** isostruktureller Cluster [{(Me$_3$P)$_3$CuSn}{PhSn}$_3$S$_6$] (**5**) erhalten werden. Alle genannten Verbindungen sind in Abbildung 19 zusammenfassend dargestellt.

Um den Einfluss der Münzmetall-Substituenten auf die photophysikalischen Eigenschaften im Vergleich zur Stammverbindung [(PhSn)$_4$S$_6$] zu untersuchen, wurden in der Arbeitsgruppe Chatterjee Emissions- und Photolumineszenzspektren der Verbindungen **1**, **4** und **5** aufgenommen. Die Verbindungen **1** und **4** zeigen Weißlicht-emission, allerdings erst nachdem sie durch den anregenden IR-Laser amorphisiert wurden. Die durch unterschiedliche Substitution der vier Zinnatome eingebrachte Asymmetrie reicht also offensichtlich nicht aus, um eine phasengleiche Emission zu verhindern und so eine Weißlichterzeugung im kristallinen Zustand zu ermöglichen. Das Emissionsspektrum selbst wird durch die Einbringung eines Münzmetallkomplexfragments nicht wesentlich beeinflusst (siehe Abbildung 20, links).

In der Kupferverbindung **5** hingegen wird die Weißlichterzeugung durch eine intensive grüne Photolumineszenz mit einem Lumineszenzmaximum bei 1.45 eV inhibiert (siehe Abbildung 20, rechts). In diesem Fall ist durch die Anwesenheit des Kupfer(I)-Komplexfrag-

ments die Besetzung langlebigerer Zustände, die unter Lumineszenz relaxieren, statistisch bevorzugt gegenüber der Besetzung extrem kurzlebiger virtueller Zustände, wie sie bei der Weißlichterzeugung auftreten.

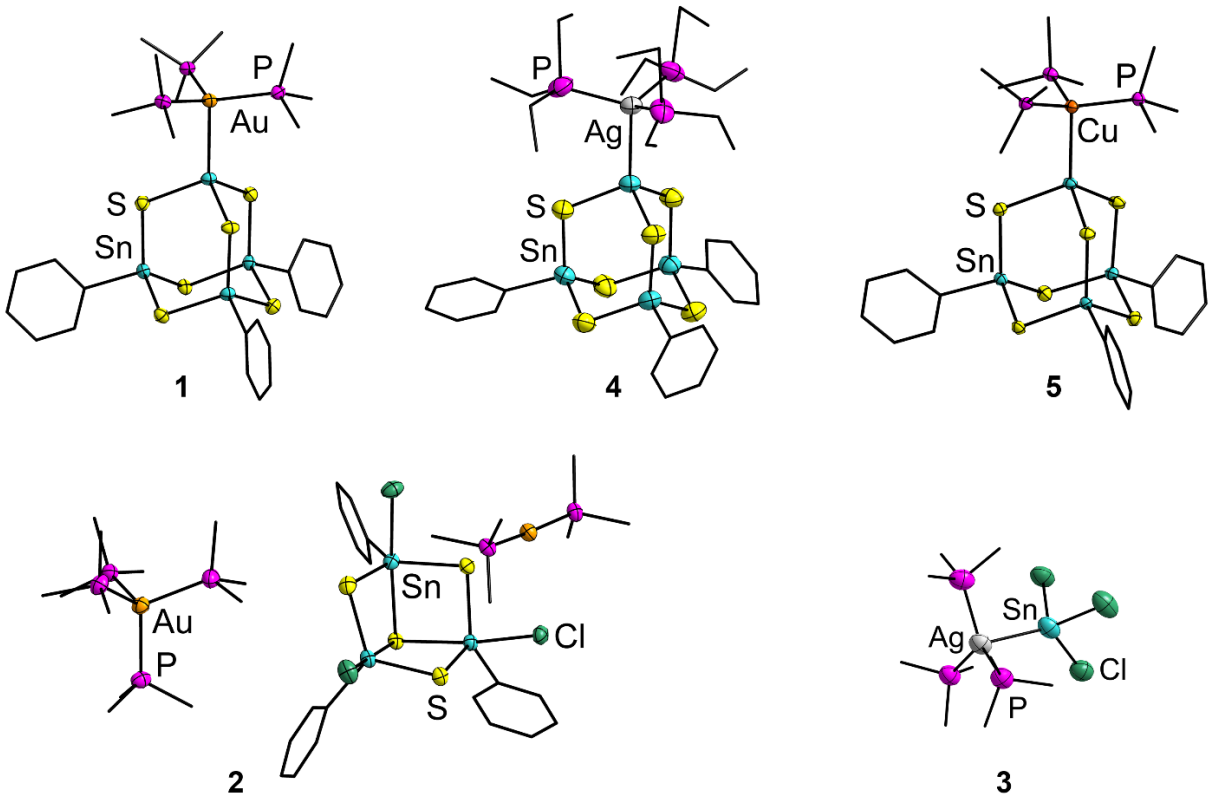

Abbildung 19: Molekülstrukturen der Verbindungen **1-5**. Die Ellipsoide sind mit 50 %-iger Aufenthaltswahrscheinlichkeit gezeigt, die Wasserstoffatome aus Gründen der Übersicht ausgeblendet.

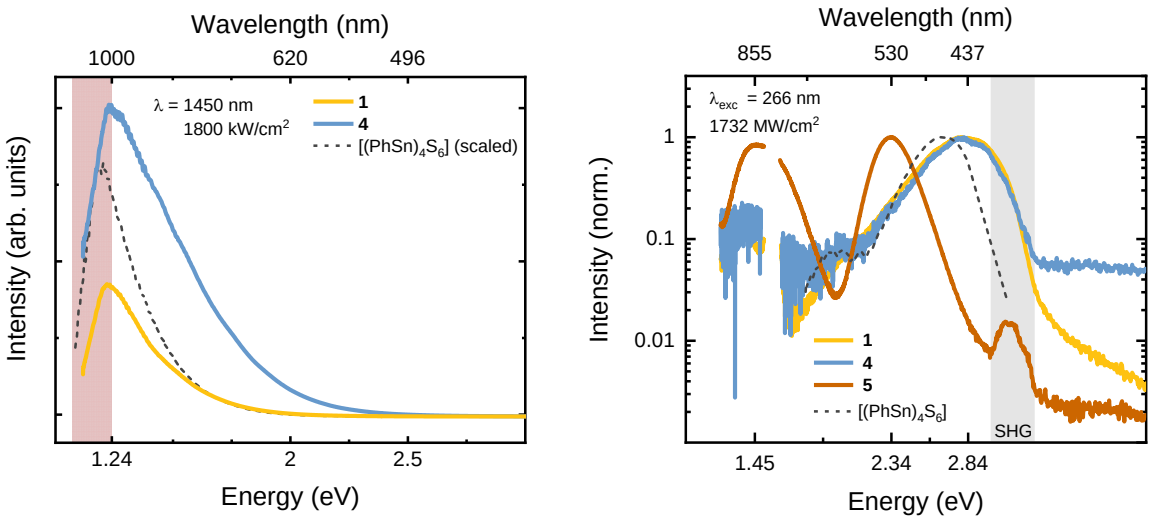

Abbildung 20: Links: Weißlichtemissionsspektren der Verbindungen **1** (gelb) und **4** (blau) bei einer Anregungswellenlänge von 1450 nm. Das Referenzspektrum von $[(PhSn)_4S_6]$ ist als gestrichelte Linie eingezeichnet. Rechts: Photolumineszenzspektren der Verbindungen **1** (gelb), **4** (blau) und **5** (braun) bei einer Anregungswellenlänge von 266 nm. Die Lücke bei 800 nm sowie der Peak bei 400 nm kommen durch die Grundfrequenz und die zweite Harmonische des anregenden frequenzverdreifachten Ti:Sa-Lasers zustande. Als Referenz ist das Photolumineszenzspektrum von $[(PhSn)_4S_6]$ als gestrichelte Linie gezeigt.

3.4 Transition-Metal-Induced Rearrangement of $[(PhSn)_4S_6]$ Towards Ternary $Cu^I/Sn/S$ or $Cu^{II}/Sn/S$ Clusters

Indem bei den im vorigen Abschnitt beschriebenen Reaktionen der Phosphanligand PMe_3 durch PPh_3 ersetzt wurde, konnten bei analoger Reaktionsführung aus $[(PhSn)_4S_6]$ und $[Cu(PPh_3)_3Cl]$ oder $[Cu(PPh_3)_2Cl_2]$ die ternären Cluster $[(CuPPh_3)_4(PhSn)_{18}Cu_6S_{31}Cl_2]$ (**1**) und $[\{Cu(PPh_3)_2\}(PhSn)_3(SnCl)S_8]$ (**2**) erhalten werden. Es handelt sich dabei um die ersten Beispiele, in denen Cluster mit ternärem anorganischem Grundgerüst ohne Zugabe einer zusätzlichen Sulfidquelle erhalten wurden. Verbindung **1** stellt den bisher größten neutralen ternären Cluster der Elementkombination Cu/Sn/S dar. Der Aufbau des ungewöhnlich unsymmetrischen anorganischen Kerns ist in Abbildung 21 unten schematisch dargestellt.

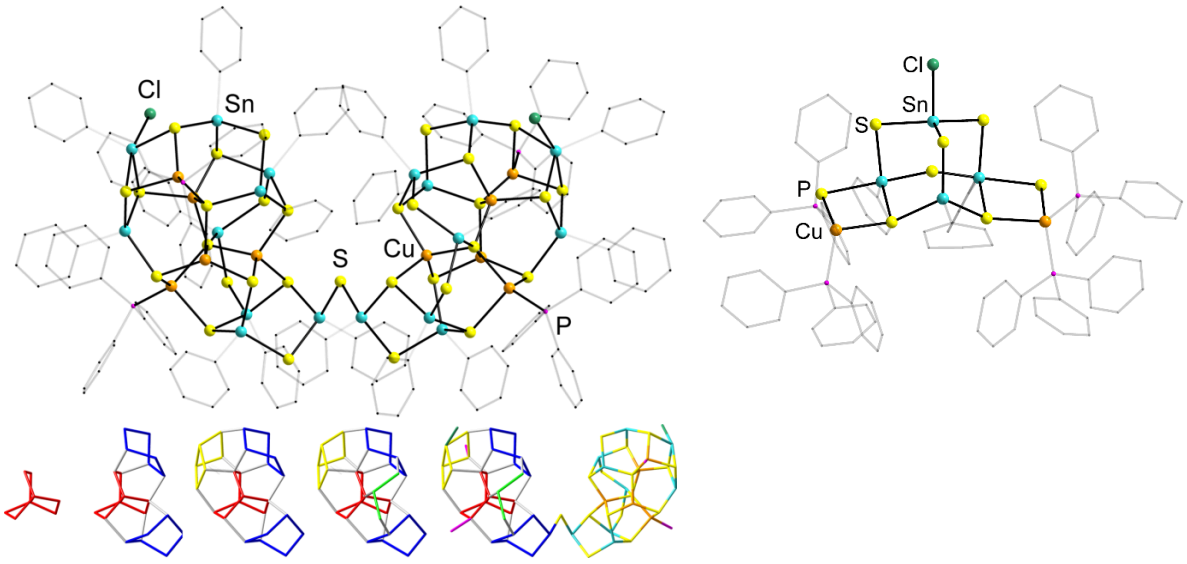

Abbildung 21: Links: Molekülstruktur von $[(CuPPh_3)_4(PhSn)_{18}Cu_6S_{31}Cl_2]$ (**1**). Rechts: Molekülstruktur von $[\{Cu(PPh_3)_2\}(PhSn)_3(SnCl)S_8]$ (**2**). Unten: Schematischer Aufbau des anorganischen Kerns von **1**.

Verbindung **2** hingegen stellt das erste Beispiel eines ternären Cu/Sn/E-Clusters (E = S, Se) dar, der Kupferatome in der Oxidationsstufe +II enthält. **2** kann als einer der ersten Schritte der Clusterbildung aufgefasst werden, da hier zwei Kupferkomplexfragmente an den noch weitgehend intakten binären Cluster koordinieren. Anscheinend reagiert der Kupfer(II)-komplex sehr langsam mit dem Organozinnsulfidcluster, sodass hier die Isolierung eines entsprechenden Intermediats möglich ist. **2** kann auch durch Oxidation der Reaktionslösung von **1** durch Luftsauerstoff erhalten werden.
Trotz der deutlich unterschiedlichen Clustergrößen besitzen die beiden Verbindungen sehr ähnliche optische Absorptionsenergien von 2.14 eV (**1**) bzw. 2.10 eV (**2**). Die Art der opti-

schen Anregung wurde durch TD-DFT-Rechnungen validiert. Für die geschlossenschalige Verbindung **1** ergab sich, dass dort hauptsächlich Anregungen aus den Cu(d)-Orbitalen in die Sn(s)-Orbitale auftreten, während bei der im Triplett-Zustand vorliegenden Verbindung **2** in erster Linie Übergänge von hohen besetzten Orbitalen am Schwefelatom S3 in die zwei niedrigsten unbesetzten Orbitale auftreten, die an den restlichen Schwefelatomen lokalisiert sind (vgl. Abbildung 22).

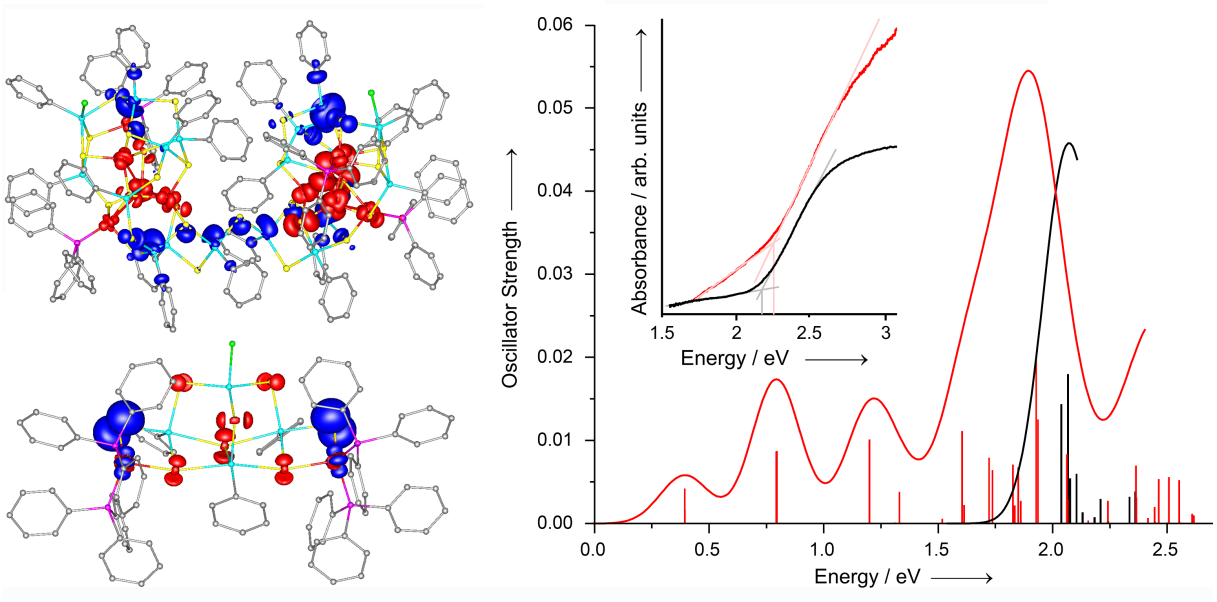

Abbildung 22: Links: Nicht relaxierte Differenzdichten für Verbindung **1** (oben) und **2** (unten) bei einem Konturwert von 0.001 a.u.. Rechts: Berechnete Anregungsenergien für **1** (schwarz) und **2** (rot). Zum Vergleich sind die gemessenen UV/Vis-Spektren eingefügt.

3.5 [{$(PhSn)_3SnS_6$}{$(CpM)_3S_4$}] (M = Mo, W): Minimal Molecular Models of Covalent Attachment of Metalchalcogenide Clusters on Layered Transition Metal Dichalcogenides (TMDCs)

Um die bisher unbekannte Abscheidung von Organozinnchalkogenidclustern auf Übergangsmetalldichalkogenid-Oberflächen (*transition metal dichalcogenide*, TMDC) zu simulieren, wurden molekulare Modellsysteme dafür synthetisiert und untersucht. Bei der Umsetzung von $[(PhSn)_4S_6]$ mit $[W(CO)_3CpCl]$ wurde zunächst der heterokubanartige Cluster $[(WCp)_3(SnCl_3)S_4]$ (**1**) erhalten, der sich in die Reihe literaturbekannter Cluster der Zusammensetzung $[(L_mM')_3S_4(ML'_n)]$ (M' = Element der Gruppe 13-15; M = Mo, W) einordnen lässt. Die dabei auftretende Zersetzung des Organozinnsulfidclusters kann durch Zugabe von $(Me_3Si)_2S$ zur Reaktionslösung unterdrückt werden, was zur Bildung des Organozinn-Sulfidowolframates $[\{(PhSn)_3SnS_6\}\{(CpW)_3S_4\}]$ (**2**) führt, bei dem das aus Verbindung **1** bekannte W_3S_4-Defektheterokuban als Ligand an einen adamantanartigen $[(PhSn)_3SnS_6]$-Käfig angebunden ist.

Formal handelt es sich um die gleiche Ligandenaustauschreaktion wie bei den in 3.3 beschriebenen Reaktionen mit Münzmetallkomplexen, bei denen ein Phenylrest unter Oxidation zu Chlorbenzol abgespalten und durch einen Metallkomplex substituiert wird. Es werden somit gemischtvalente Cluster erhalten, in denen das betroffene Zinnatom als Sn(II) vorliegt, während bei den anderen drei Zinnatomen die Oxidationsstufe +IV erhalten bleibt. Die Wolframatome liegen ebenfalls in der Oxidationsstufe +IV vor.

Der Transfer der Synthese auf das leichtere Homologe Molybdän funktioniert problemlos und führt entsprechend zur Bildung von $[\{(PhSn)_3SnS_6\}\{(CpMo)_3S_4\}]$ (**3**). In beiden Fällen können die Thiometallat-Käfige als Ausschnitt aus einer WS_2- bzw. MoS_2-Oberfläche betrachtet werden.

In den molekularen Systemen stellt sich die Wechselwirkung des Sn(II)-Atoms mit den Schwefelatomen des M_3S_4-Käfigs als 2e4z-Bindung zwischen dem freien Elektronenpaar am Sn(II) und unbesetzten Zuständen an den Schwefelatomen dar. Die freien Valenzelektronen der Mo- bzw. W-Atome sind in Mehrzentrenbindungen im Thiometallat-Käfig gebunden, wodurch im Molekül kein permanentes magnetisches Moment vorliegt, wie durch magnetische Messungen bestätigt werden konnte, was auch der Beschreibung ähnlicher M_3S_4-Käfige in der Literatur entspricht. Im Zinnsulfid-Käfig hingegen sind alle Elektronen in lokalisierten σ-Bindungen gebunden.

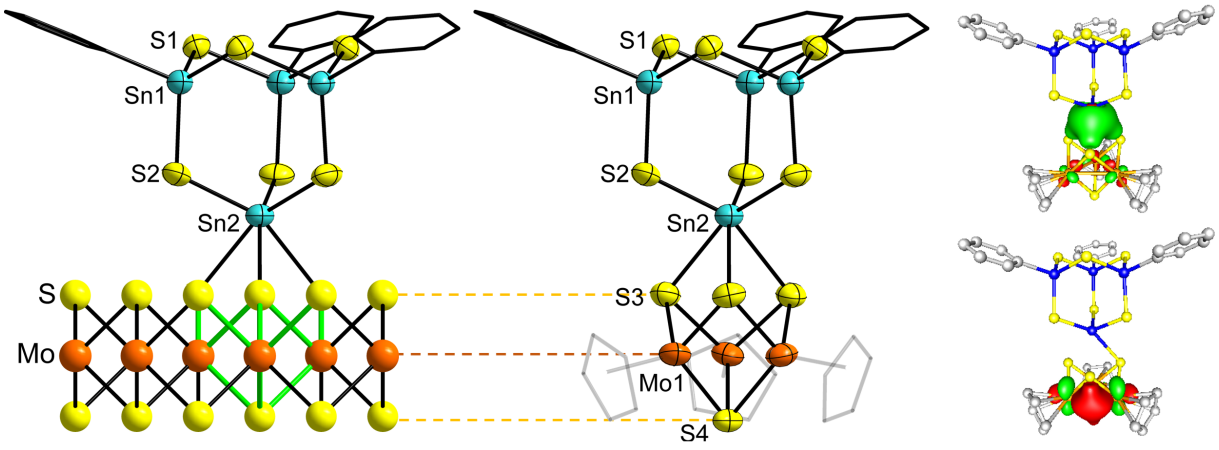

Abbildung 23: Oben Mitte: Molekülstruktur von **2**. Die Ellipsoide sind mit 50 %-iger Aufenthaltswahrscheinlichkeit gezeigt, die Wasserstoffatome aus Gründen der Übersicht ausgeblendet. Oben rechts: Die beiden LMOs mit den höchsten Energieerwartungswerten (Amplituden mit 0.05 a.u. dargestellt).

3.6 How Organotin Sulfide Clusters Behave in the Presence of Zinc Compounds – a Reactivity Study

Die Reaktivität der Organozinnsulfidcluster $[(R^1Sn)_3S_4Cl]$ ($R^1 = CMe_2CH_2COMe$) und $[(R^1Sn)_4S_6]$ gegenüber Münzmetall-Phosphan-Komplexen wurde in unserer Arbeitsgruppe in den letzten Jahren intensiv untersucht, wobei eine große Bandbreite verschiedener Cluster mit ternärem anorganischem Grundgerüst erhalten werden konnte. Demgegenüber sind für die Gruppe 12 nur die Cluster $[(RSn)_4(ZnX)_8S_{10}]$ ($R = CMe_2CH_2C(Me)NHNC(2\text{-}py)_2$, X = Cl, Br, I) als Beispiele bekannt. Um das Spektrum möglicher ternärer Cluster mit Zink zu erweitern, wurden die Cluster $[(R^1Sn)_3S_4Cl]$ und $[(R^1Sn)_4S_6]$ mit verschiedenen Zinkchlorid-Phosphan-Komplexen $[ZnCl_2(PR_3)_2]$ und Diphenylzink umgesetzt. Dabei wurde kein ter-närer Cluster erhalten, allerdings eine Vielfalt anderer bisher unbekannter Reaktionsprodukte (siehe Abbildung 24).

In Umsetzungen ausgehend von $[(R^1Sn)_3S_4Cl]$ blieb in der Regel das Defektheterokuban-Gerüst des Edukts erhalten. Unter Abspaltung des Chloridliganden wurden drei salzartige Verbindungen erhalten, bei denen $[(RSn)_3S_4]$-Kationen zusammen mit verschiedenen Chlorostannat- oder Chlorozinkat-Anionen kristallisieren, namentlich die Verbindungen $[(R^2Sn)_3S_4][SnCl_3]$ (**1**, $R^2 = CMe_2CH_2C(NNH_2)Me$), $[(R^3Sn)_3S_4]_2[dppe(ZnCl_3)_2]$ (**2**, $R^3 = CMe_2CH_2C(NNHPh)Me$) und $[(R^2Sn)_3S_4]_2[ZnCl_4]$ (**3**). Die Umsetzung von $[(R^1Sn)_3S_4Cl]$ mit $ZnCl_2$ und PMe_3 hingegen liefert das Phosphoniumsalz $[R^3PMe_3][HPMe_3][ZnCl_4]$ (**4**). Dieses entsteht, indem der organische Rest R^3 zunächst als R^3Cl vom Cluster abgespalten wird und anschließend mit $[ZnCl_2(PMe_3)]$ zum Phosphoniumsalz weiter reagiert, wie durch gezielte Darstellung von $[R^3PMe_3]_2[ZnCl_4]$ aus R^3Cl, $ZnCl_2$ und PMe_3 gezeigt werden konnte.

Bei Umsetzung von $[(R^1Sn)_4S_6]$ mit $ZnCl_2$ und Hydrazinhydrat kommt es zur teilweisen Hydrolyse des Clusters durch in situ entstehendes, stark saures $[ZnCl_2(H_2O)_2]$, wodurch sich ein gemischter Oxidsulfid-Cluster der Zusammensetzung $[(R^2Sn)_4S_5O]$ (**5**) bildet. Dieser besitzt eine verzerrt adamantanartige Struktur, bei der das Sauerstoffatom nach innen auf eine μ_3-verbrückende Position verschoben ist. Wird $[(R^1Sn)_4S_6]$ mit Diphenylzink umgesetzt, wird eine Transmetallierung des Phenylrests vom Zinkatom auf ein Zinnatom beobachtet. Unter partieller Zersetzung des Clusters $[(R^1Sn)_4S_6]$ entsteht dabei die Verbindung $[(R^2PhSn)_2S_2]$ (**6**), die strukturell verwandt ist mit dem bei der Darstellung von $[(R^1Sn)_3S_4Cl]$ und $[(R^1Sn)_4S_6]$ als Intermediat entstehenden $[(R^1SnCl)_2S_2]$.

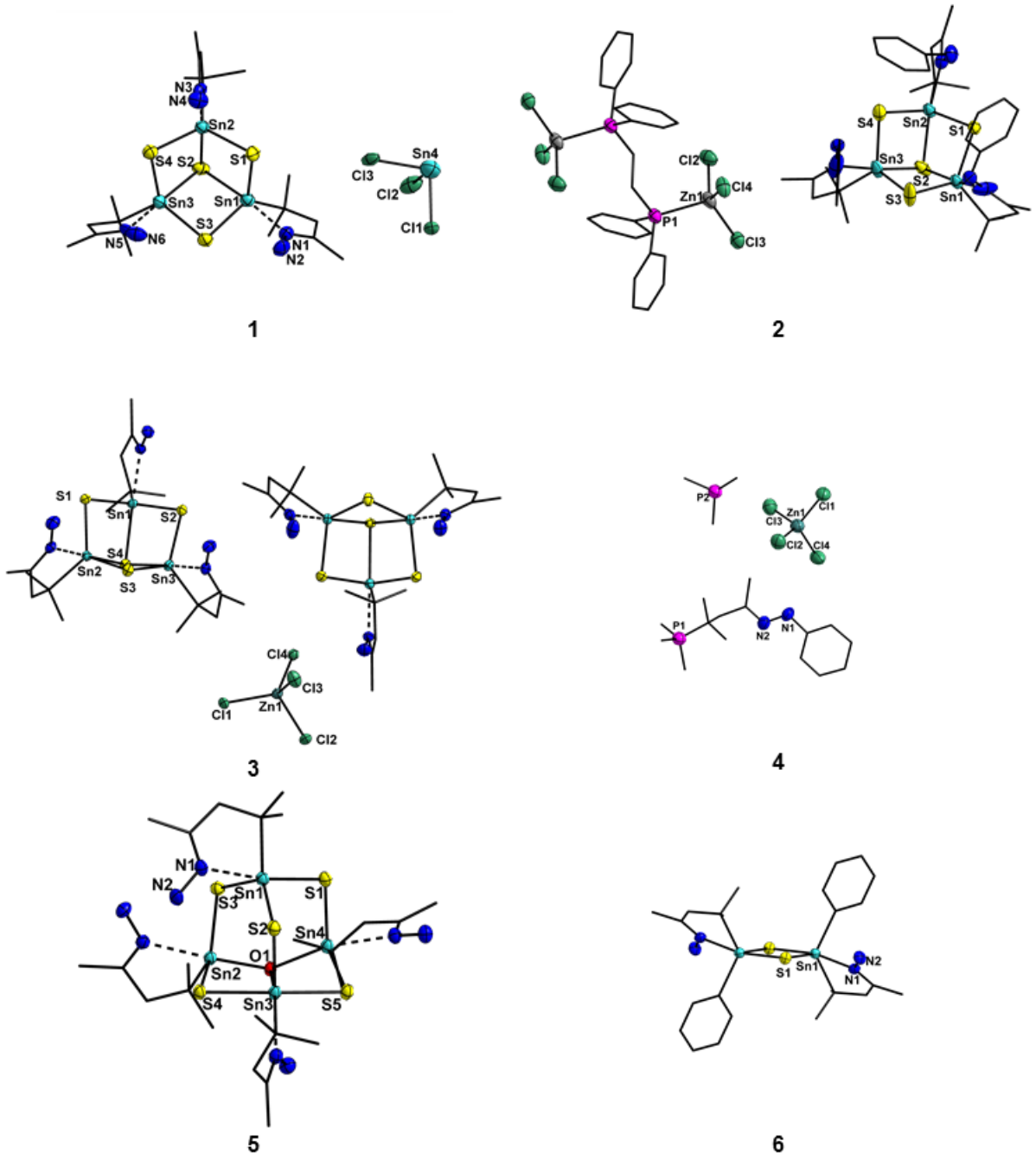

Abbildung 24: Molekülstrukturen der Verbindungen **1** - **6**. Die Ellipsoide sind mit 50 %-iger Aufenthaltswahrscheinlichkeit dargestellt, die Wasserstoffatome wurden aus Gründen der Übersicht weggelassen.

3.7 Dinuclear organogermanium chalcogenide complexes as intermediates towards functionalized clusters

Durch Umsetzung von R^1GeCl_3 mit $(Me_3Si)_2E$ (E = S, Se, Te) wurden drei zweikernige Organogermaniumchalkogenidkomplexe $[(R^1GeCl)_2E_2]$ (E = S (**1**), Se (**2**), Te (**3**)) erhalten, deren Zentrum jeweils ein Ge_2E_2-Vierring bildet. Durch Titrationsexperimente mit $(Me_3Si)_2E$ und Reaktionsverfolgung durch ^{1}H-NMR-Spektroskopie konnte gezeigt werden, dass es sich bei diesen Verbindungen um Intermediate der Bildung der Organogermaniumsesquisulfidcluster $[(R^1Ge)_4E_6]$ handelt (vgl. Abbildung 25). Im Gegensatz zum schweren Homologen Zinn, für das ähnliche Studien durchgeführt wurden,[78–80] treten hier die Intermediate $[(R^1GeCl_2)_2E]$ und $[(R^1Ge)_3E_4Cl]$ für E = S und Te gar nicht auf und werden für E = Se nur in Spuren gebildet.

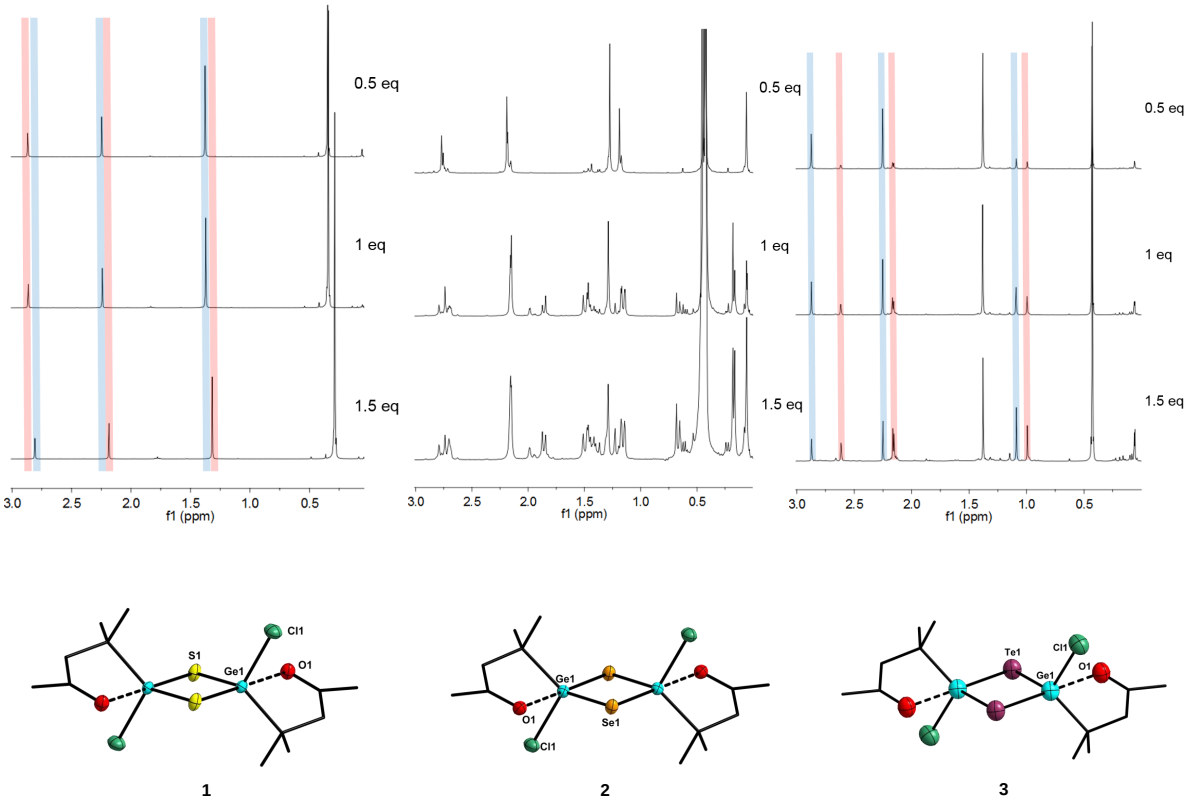

Abbildung 25: Molekülstrukturen und ^{1}H-NMR-Spektren der Titrationsexperimente der Verbindungen **1**-**3** (v.l.n.r.). Der jeweils rot markierte Signalsatz entspricht dem Intermediat **1** bzw. **3**, der blau markierte Signalsatz dem jeweiligen Sesquisulfidcluster.

Die optischen Anregungsenergien aller drei Verbindungen wurden durch UV/Vis-Spektroskopie bestimmt. Die ermittelten Werte von 3.95 eV (314 nm) und 3.25 eV (381 nm) für die farblosen Verbindungen **1** und **2** sowie 2.35 eV (528 nm) für die orangefarbene

Tellurverbindung **3** geben den allgemein erwarteten Trend sinkender Absorptionsenergien in homologen Reihen von Chalkogenidverbindungen wieder (siehe Abbildung 26).

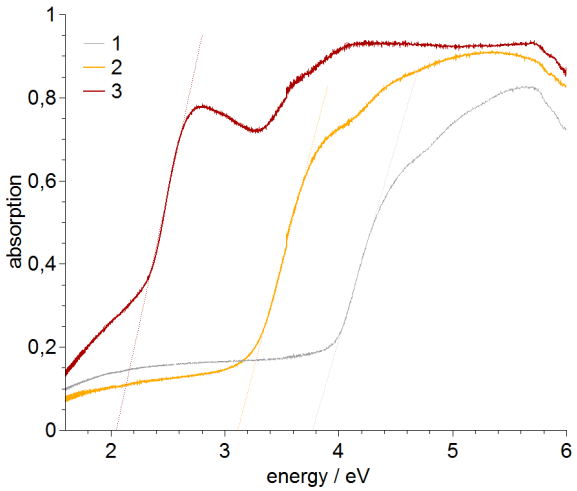

Abbildung 26: UV/Vis-Spektren der Verbindungen **1-3**.

Von den hier vorgestellten Publikationen gehören die ersten beiden zum ersten Teilprojekt, in dem durch gezielte Variation der Zusammensetzung adamantanartiger $[(RT)_4E_6]$-Cluster Voraussetzungen für das bisher noch nicht vollständig verstandene Phänomen der Weißlichterzeugung herausgearbeitet werden konnten. Die in Abschnitt 3.3 bis 3.6 zusammengefassten Publikationen gehören zum zweiten Teilprojekt, in dem die Koordinationschemie binärer Organozinnsulfidcluster gegenüber Übergangsmetallverbindungen untersucht wurde. Die in Abschnitt 3.7 vorgestellte Publikation schließlich gehört thematisch zum dritten Teilprojekt, der Isolierung von Intermediaten der Bildung der bereits bekannten Organogermaniumsesquichalkogenidcluster $[(R^1Ge)_4E_6]$.

4 Kumulativer Teil

4.1 Organotetrel Chalcogenide Clusters: Between Strong Second-Harmonic and White-Light Continuum Generation

Zitat: N.W. Rosemann, J.P. Eußner, E. Dornsiepen, S. Chatterjee, S. Dehnen, *J. Am. Chem. Soc.* **2016**, *138*, 16224–16227.

Abstract

Highly directional white-light generation was recently reported for the organotin sulfide cluster $[(StySn)_4S_6]$ (Sty = p-styryl). This effect was tentatively attributed to the amorphous nature of the material in combination with the specific combination of an inversionsymmetry-free T/E cluster core (T = tetrel, E = chalcogen) with the attachment of ligands that allow π delocalization of the electron density. Systematic variation of T and the organic ligand (R) that runs from T = Si through Ge to Sn and from R = methyl through phenyl and p-styryl to 1-naphthyl provides a more comprehensive view. According to powder X-ray data, only $[(PhSi)_4S_6]$ is single-crystalline among the named combinations. Here we demonstrate the fine-tuneability of the nonlinear response, i.e., changing from white-light generation to secondharmonic generation as well as controlling the whitelight properties. These are investigated as a function of T, π delocalization of the electron density within R, and the order within the molecular solids.

Eigener Anteil

Alle Synthesen wurden erstmals von Jan Christmann im Rahmen eines Forschungspraktikums unter Anleitung von Dr. Jens Eußner durchgeführt und in der Folge von mir reproduziert. Die Kristallstrukturanalyse von Verbindung **6**, die Aufnahme der TGA/DSC-Spektren und UV/Vis-Spektren sowie die DFT-Rechnungen wurden von Dr. Jens Eußner durchgeführt. ^{1}H-, ^{13}C- und ^{29}Si-NMR-Experimente wurden von der zentralen NMR-Abteilung des Fachbereichs Chemie an der Philipps-Universität unter Leitung von Dr. Xiulan Xie durchgeführt und von Dr. Jens Eußner ausgewertet. Pulverdiffraktogramme aller Verbindungen wurden von mir gemessen und ausgewertet. Alle photophysikalischen Untersuchungen wurden von Dr. Nils Rosemann in der Arbeitsgruppe von Prof. Dr. Sangam Chatterjee durchgeführt und ausgewertet. Das Manuskript wurde von allen Autoren gemeinsam verfasst.

JACS
JOURNAL OF THE AMERICAN CHEMICAL SOCIETY

Communication

pubs.acs.org/JACS

Organotetrel Chalcogenide Clusters: Between Strong Second-Harmonic and White-Light Continuum Generation

Nils W. Rosemann,[‡,§,∥] Jens P. Eußner,[†,∥] Eike Dornsiepen,[†,∥] Sangam Chatterjee,[‡,§] and Stefanie Dehnen*[,†]

[†]Fachbereich Chemie und Wissenschaftliches Zentrum für Materialwissenschaften (WZMW), Philipps-Universität Marburg, Hans-Meerwein-Straße 4, DE-35043 Marburg, Germany

[‡]Fachbereich Physik und Wissenschaftliches Zentrum für Materialwissenschaften (WZMW), Philipps-Universität Marburg, Renthof 5, DE-35032 Marburg, Germany

[§]Institute of Experimental Physics I, Justus-Liebig-University Giessen, DE-35392 Giessen, Germany

Supporting Information

ABSTRACT: Highly directional white-light generation was recently reported for the organotin sulfide cluster $[(StySn)_4S_6]$ (Sty = *p*-styryl). This effect was tentatively attributed to the amorphous nature of the material in combination with the specific combination of an inversion-symmetry-free T/E cluster core (T = tetrel, E = chalcogen) with the attachment of ligands that allow π delocalization of the electron density. Systematic variation of T and the organic ligand (R) that runs from T = Si through Ge to Sn and from R = methyl through phenyl and *p*-styryl to 1-naphthyl provides a more comprehensive view. According to powder X-ray data, only $[(PhSi)_4S_6]$ is single-crystalline among the named combinations. Here we demonstrate the fine-tuneability of the nonlinear response, i.e., changing from white-light generation to second-harmonic generation as well as controlling the white-light properties. These are investigated as a function of T, π delocalization of the electron density within R, and the order within the molecular solids.

Light-converting materials are continuously being developed for a multitude of applications, including advanced phosphors for bright white-light emission in light-emitting diodes.[1] These are nowadays omnipresent in diffuse illumination and display applications. Other light-converting materials target nonlinear optical processes such as second-harmonic generation (SHG).[2] Here, typically coherent laser radiation is upconverted into light of half the wavelength of the incident radiation. This is commonly achieved in crystalline materials lacking inversion symmetry.[3a] Microscopically, this enables the fundamental incident light to introduce a nonlinear polarization in the crystal. For phase-matching conditions, i.e., when the refractive index of fundamental and second-harmonic light are identical, both can exit the nonlinear medium and may later be separated.[3b] Currently, the search for advanced light conversion media is aiming at increased conversion efficiencies and extended accessible frequency regimes.[4]

Another class of highly nonlinear light-converting materials enhance effects such as self-phase modulation. These are used in extreme nonlinear processes such as the generation of highly brilliant (i.e., directional) broadband supercontinua. However, this process commonly requires intense, short-pulsed laser sources, confining their use to mostly scientific applications.[5]

In the course of our current research on tetrel chalcogenide hybrid compounds, clusters, and functional networks,[6] we recently showed that the organotin sulfide cluster compound $[(StySn)_4S_6]$ (Sty = *p*-styryl, 4-H_sC═CH−C_6H_4) produces spectrally broadband and highly brilliant white light. The observed vast optical nonlinearity even allows this process for low-fluence steady-state illumination generated from cost-effective near-infrared continuous-wave laser diodes. Tentatively, the white-light generation was identified as emission from coherently accelerated electrons in the delocalized π-electron system of the organic ligands combined with a strong transition dipole that is provided by the tetrel chalcogenide cluster core and a lack of phase matching.[7]

For a more comprehensive view of the nonlinear optical response, we studied the effect of slight variations of the system. For this, we prepared two series of compounds of the general formula $[(RT)_4S_6]$ (R = organic ligand; T = Si, Ge, Sn). All of these compounds were expected to exhibit (very) strong nonlinear optical properties, as they have similar compositions and structures as the proof-of-principle compound, included in this study as compound **3** for comparison.

One series addressed the effect of the ligands on the $[(RSn)_4S_6]$ scaffold. The ligands were varied from R = Me (**1**)[8a] through R = 1-naphthyl (Np) (**2**) and Sty (**3**)[7] to R = Ph (**4**)[8b] for exploration of the impact of the presence and the nature of the π-electron system. For this, it was either completely absent (Me) or decreased in size (Np → Sty → Ph). Changing the ligand particularly changes the intermolecular interactions, including the tendency of the solid material to exhibit no, short-range, or long-range order, which determines its amorphousness versus crystallinity. The second series addressed the composition of the inorganic cluster core. This affects the optical gap of the clusters, starting out from the Sn/S combination in **4** through Ge/S (**5**) to Si/S (**6**).[9] Overall, the two sample series reveal (i) whether and how the T/E/R

Received: October 19, 2016
Published: November 29, 2016

DOI: 10.1021/jacs.6b10738
J. Am. Chem. Soc. 2016, 138, 16224−16227

combination affects the orderliness or potential crystallization and (ii) how this affects the nonlinear optical properties.

All of the compounds were obtained upon reaction of the respective organotetrel halides $RTCl_3$ with sodium sulfide in an acetone/water solvent mixture or tetrahydrofuran at room temperature, with the formation of NaCl being the driving force for the cluster formation. Except for compound **6**, the compounds were obtained as amorphous powders under a large variety of reaction and crystallization conditions tested to date.[2] Hence, the molecular structures of the latter were elucidated via density functional theory (DFT) calculations (see the Supporting Information). According to these, all of the compounds are based on a heteroadamantane-type $[T_4S_6]$ scaffold, which is energetically favored over the "double-decker"-type isomer by 19.2−36.4 kJ/mol (see Table S1 and the Supporting Information). The organic substituents point away from the center of the inorganic cluster core in pseudotetrahedral fashion. As an exception, compound **6** could be obtained as single crystals. Thus, the structure of this compound was determined by single-crystal X-ray diffraction, thereby confirming the previous prediction for it.[8c] The structure was solved and refined in the monoclinic space group $P2_1/c$ with $Z = 4$ (see Figure 1 and the Supporting Information). In agreement with DFT calculations, the molecular structure of **6** is based on an inversion-free heteroadamantane-type inorganic scaffold with (idealized) T_d symmetry. The actual crystallographic symmetry is reduced by different orientations of the organic groups and by slight deformations of the inorganic core.

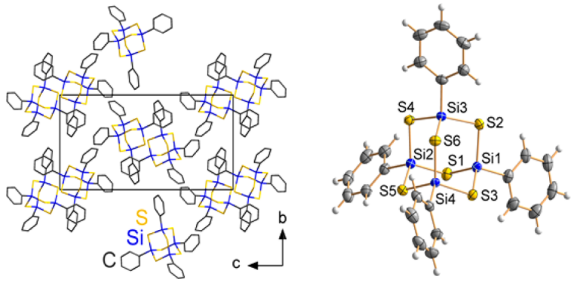

Figure 1. Fragment of (left) the crystal structure (wire representation, shown without H atoms) and (right) the molecular structure (ellipsoids drawn at the 70% probability level) of $[(PhSi)_4S_6]$ (**6**) according to X-ray diffraction studies. Selected structural parameters [Å, deg]: Si−S, 2.1184(5)−2.1476(5); C−Si, 1.854(1)−1.855(1); Si−S−Si, 102.86(2)−104.25(2); S−Si−S, 111.29(2)−113.27(2); C−Si−S, 103.85(5)−108.50(5).

Next, we investigated the nonlinear optical properties of the compounds. The samples were kept under high-vacuum conditions during laser irradiation. For excitation, a continuous-wave diode laser operating at a central wavelength of 980 nm was used. The optical power of 200 mW was focused on the sample in a confocal setup featuring a reflective microscope objective to avoid any chromatic aberrations (see the Supporting Information). This setup yielded a spot diameter of less than 10 μm on the sample. For detection, a Czerny−Turner-type spectrometer equipped with a thermoelectrically cooled back-illuminated deep-depletion Si-charge-coupled device camera was used. Residual scattered pump laser was attenuated using a heat-absorbing glass filter (Schott KG3).

Characteristic spectra of the first sample series (compounds **1**−**4**) are given in Figure 2. Clearly, the nature and extent of the

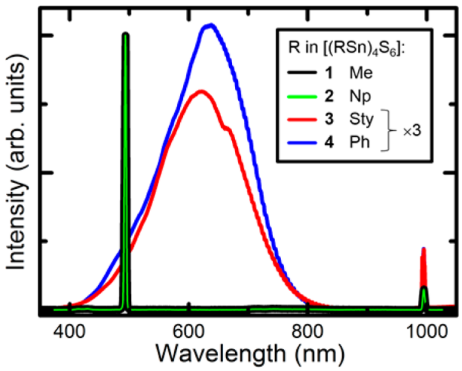

Figure 2. Emission spectra measured for an excitation wavelength of 980 nm. Compounds **1** (black) and **2** (green) exhibit intense SHG. Compounds **3** (red) and **4** (blue) exhibit strong white-light emission (scaled by a factor of 3).

π-electron system crucially influence the optical nonlinearity. Compounds **3** and **4** show pronounced white-light emission, while compounds **1** and **2** show intense SHG. The latter requires phase matching (which is not a precondition for white-light emission). Hence, the optical experiments infer a certain degree of order in the powders obtained for **1** and **2**. In **1**, both the low steric demand and the low flexibility of the ligand seem to allow for order—which can even lead to the formation of single crystals[8a]—although it is not visible in the X-ray diffraction diagrams of the powder studied herein (Figure S3). In the case of **2**, the pronounced π−π-stacking capability of the Np ligands apparently causes a relatively high degree of order in the amorphous powder. Hence, the two ligands, although significantly different in size and electronic nature, provoke similar nonlinear responses.

The situation changes upon attachment of ligands with a medium-sized extension of the π-electron system. Obviously, an effective intermolecular interaction does not take place between the cluster molecules in **3** (R = Sty), which we attribute to both the reduced π-stacking capability compared with Np ligands and the higher conformational flexibility of the Sty ligands compared with all of the other ligands involved herein. The smallest π-electron system in this series is present in the Ph groups in compound **4**. Like the Sty ligands in **3**, they hamper any intermolecular order when attached to the $[Sn_4S_6]$ core. Hence, phase matching is ruled out, and the nonlinear optical response changes from SHG to white-light generation.

The subtle yet crucial role of microscopic molecular order is further underlined by the slightly reduced white-light generation in **3** compared with **4**. In these compounds, the delocalization of the π-electron system is virtually identical. Nevertheless, the Sty ligands in **3** provide an increased potential for dispersive interactions between neighboring molecules and thus a potentially higher degree of order in the material, without reaching long-range order or crystallinity. Thus, the strength of the nonlinear optical response might in turn be used as a measure of the degree of intermolecular order in a macroscopically amorphous compound.

The strong nonlinear response found for all four compounds underlines the efficient enhancement of the nonlinearity by the transition dipole moment of the cluster core. Hence, even compound **1**, with its comparatively small electronic system, exhibits SHG, as the Me groups are in close proximity to the inorganic core.

DOI: 10.1021/jacs.6b10738
J. Am. Chem. Soc. 2016, 138, 16224−16227

The second group of samples comprises compounds **4**, **5**, and **6**. Here the inorganic cluster core is varied while the Ph ligands, which proved as most suitable for white-light generation in the first series, remain unchanged. In striking difference to the other two Ph-decorated compounds, **6** was obtained as clear and sizable single crystals (Figure S5). This difference in appearance is directly reflected in the measured spectra shown in Figure 3. SHG is exclusively observed for the crystalline compound whereas the other two exhibit broadband white-light emission, in perfect agreement with the assumption given above.

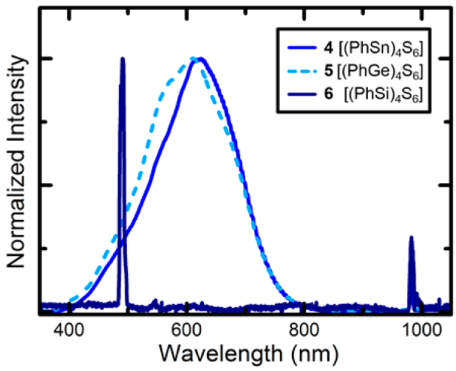

Figure 3. Spectra measured for an excitation wavelength of 980 nm. The amorphous compounds **4** (blue) and **5** (light blue, dashed) exhibit strong white-light emission. The crystalline compound **6** (dark blue) exhibits strong SHG.

The fact that Ph ligands, which perfectly exclude crystallization in the case of compounds **4** and **5**, do allow for the longer-range order in a crystal lattice in **6**, can be attributed to the different relative sizes of the three components T, E, and R. Obviously, four Ph ligands match well the steric demands of the $[Si_4S_6]$ scaffold to form a stable crystal structure with interdigitating Ph groups that, however, do not feature any typical π-stacking orientations with respect to each other. In contrast, a suitable crystal lattice seems to be lacking in the T/E/R = Sn/S/Ph and Ge/S/Ph combinations in **4** and **5**, respectively.

Comparison of the spectra of **4** and **5** reveals a blue shift of the maximum and of the high-energy flank when Sn is replaced with Ge. The white-light spectrum in both compounds is limited by reabsorption from the fundamental electronic transition of the cluster core. In accordance with the band gaps of SnS_2 and GeS_2 (2.18−2.44 eV[9] and 3.2 eV,[10] respectively), the reabsorption limit in compound **5** is blue-shifted relative to that in **4**. This is confirmed by UV/vis absorption spectroscopy (Figure S2). The white-light spectrum in both compounds is limited by reabsorption from the fundamental electronic transition of the cluster core.[1]

In conclusion, we have investigated the nonlinear optical response of two series of organotetrel chalcogenide cluster compounds of the general formula $[(RT)_4S_6]$ (R = Me, Np, Sty, Ph; T = Si, Ge, Sn) and identified prerequisites for either SHG or white-light generation. Variation of the ligand R showed that for a given size of the inorganic $[T_4S_6]$ cluster core, white-light generation is observed when R efficiently prevents any ordering of the solid compound. Opening a capability of ordering via intermolecular interactions reduces the efficiency of the white-light generation. Allowing for more order—in the case of T = Sn realized by small Me ligands or enhanced π-stacking capability—changes the nonlinear response from white-light generation to SHG. This was ultimately proven by SHG observed for a long-range-ordered system of a single crystal. The conditions for long-range order to occur are suitable relative sizes of the T, E, and R components and/or pronounced π-stacking capability.

For comparable systems that show the same type of nonlinear response, it was shown that changing T from Sn to Ge results in a blue shift of the absorption edge and thus in a blue shift of the white-light emission. Both findings underline the white-light generation mechanism proposed in previous studies.

■ ASSOCIATED CONTENT

Supporting Information

The Supporting Information is available free of charge on the ACS Publications website at DOI: 10.1021/jacs.6b10738.

Further information on synthesis and characterization (NMR, TGA/DSC, μRFA, PXRD, UV/vis, IR) (PDF)
Crystallographic data for **6** (CIF)

■ AUTHOR INFORMATION

Corresponding Author

*dehnen@chemie.uni-marburg.de

ORCID

Nils W. Rosemann: 0000-0002-7663-0397
Stefanie Dehnen: 0000-0002-1325-9228

Author Contributions

‖N.W.R, J.P.E., and E.D. contributed equally.

Notes

The authors declare no competing financial interest.

■ ACKNOWLEDGMENTS

This work was supported by the Deutsche Forschungsgemeinschaft within the framework of Grant GRK1782. We thank Jan Christman for his help with the synthesis and Vanessa Dahmen for her help with the spectroscopic experiments.

■ REFERENCES

(1) (a) Mueller-Mach, R.; Mueller, G.; Krames, M. R.; Höppe, H. A.; Stadler, F.; Schnick, W.; Juestel, T.; Schmidt, P. *Phys. Status Solidi A* **2005**, *202*, 1727−1732. (b) Nakamura, S. *Proc. SPIE* **1997**, *3002*, 26−35. (c) Kimme, F.; Brick, P.; Chatterjee, S.; Khanh, T. *Appl. Opt.* **2013**, *52*, 8779−8788.

(2) (a) Franken, P.; Hill, A.; Peters, C.; Weinreich, G. *Phys. Rev. Lett.* **1961**, *7*, 118−119. (b) Petrov, V.; Ghotbi, M.; Kokabee, O.; Esteban-Martin, A.; Noack, F.; Gaydardzhiev, A.; Nikolov, I.; Tzankov, P.; Buchvarov, I.; Miyata, K.; Majchrowski, A.; Kityk, I. V.; Rotermund, F.; Michalski, E.; Ebrahim-Zadeh, M. *Laser Photonics Rev.* **2010**, *4*, 53−98.

(3) (a) Nikogosyan, D. N. *Nonlinear Optical Crystals: A Complete Survey*; Springer: Berlin, 2005. (b) Boyd, R. W. *Nonlinear Optics*, 3rd ed.; Elsevier Science: New York, 2008.

(4) (a) Green, M. L. H.; Marder, S. R.; Thompson, M. E.; Bandy, J. A.; Bloor, D.; Kolinsky, P. V.; Jones, R. J. *Nature* **1987**, *330*, 360−362. (b) Alford, W. J.; Smith, A. V. *J. Opt. Soc. Am. B* **2001**, *18*, 524. (c) Muhammad, S.; Al-Sehemi, A. G.; Irfan, A.; Chaudhry, A. R. *J. Mol. Graphics Modell.* **2016**, *68*, 95−105. (d) Kanseri, B.; Bouillard, M.; Tualle-Brouri, R. *Opt. Commun.* **2016**, *380*, 148−153. (e) Canagasabey, A.; Corbari, C.; Gladyshev, A. V.; Liegeois, F.; Guillemet, S.; Hernandez, Y.; Yashkov, M. V.; Kosolapov, A.; Dianov, E. M.; Ibsen, M.; Kazansky, P. G. *Opt. Lett.* **2009**, *34*, 2483−2485.

DOI: 10.1021/jacs.6b10738
J. Am. Chem. Soc. 2016, 138, 16224−16227

(5) (a) Alfano, R. R. *The Supercontinuum Laser Source*; Springer: New York, 2016. (b) Birks, T. A.; Wadsworth, W. J.; Russell, P. S. J. *Opt. Lett.* **2000**, *25*, 1415−1417. (c) Husakou, A. V.; Herrmann, J. *Phys. Rev. Lett.* **2001**, *87*, 203901.
(6) (a) Santner, S.; Heine, J.; Dehnen, S. *Angew. Chem., Int. Ed.* **2016**, *55*, 876−893. (b) Thiele, G.; Franzke, Y.; Weigend, F.; Dehnen, S. *Angew. Chem., Int. Ed.* **2015**, *54*, 11283−11288. (c) Eußner, J. P.; Dehnen, S. *Chem. Commun.* **2014**, *50*, 11385−11388. (d) Bron, P.; Johansson, S.; Zick, K.; Schmedt auf der Günne, J.; Dehnen, S.; Roling, B. *J. Am. Chem. Soc.* **2013**, *135*, 15694−15697. (e) Lin, Y.; Massa, W.; Dehnen, S. *J. Am. Chem. Soc.* **2012**, *134*, 4497−4500. (f) Fard, Z. H.; Halvagar, M. R.; Dehnen, S. *J. Am. Chem. Soc.* **2010**, *132*, 2848−2849.
(7) Rosemann, N. W.; Eußner, J. P.; Beyer, A.; Koch, S. W.; Volz, K.; Dehnen, S.; Chatterjee, S. *Science* **2016**, *352*, 1301.
(8) (a) Crystal structure of **1**: Kobelt, D.; Paulus, E. F.; Scherer, H. *Acta Crystallogr., Sect. B: Struct. Crystallogr. Cryst. Chem.* **1972**, *28*, 2323. (b) Synthesis of **4**: Berwe, H.; Haas, A. *Chem. Ber.* **1987**, *120*, 1175−1182. (c) Synthesis of **6**: Fehér, F.; Lüpschen, R. *Z. Naturforsch., B: J. Chem. Sci.* **1971**, *26b*, 1191−1192.
(9) (a) Hu, S.; Song, G.; Li, W.; Peng, Y.; Jiang, L.; Xue, Y.; Liu, Q.; Chen, Z.; Hu, J. *Mater. Res. Bull.* **2013**, *48*, 2325. (b) Panda, S.; Antonakos, A.; Liarokapis, E.; Bhattacharya, S.; Chaudhuri, S. *Mater. Res. Bull.* **2007**, *42*, 576. (c) Deshpande, N.; Sagade, A.; Gudage, Y.; Lokhande, C.; Sharma, R. *J. Alloys Compd.* **2007**, *436*, 421.
(10) Nikolic, P. M.; Popovic, Z. V. *J. Phys. C: Solid State Phys.* **1979**, *12*, 1151.

DOI: 10.1021/jacs.6b10738
J. Am. Chem. Soc. 2016, 138, 16224−16227

Supporting Information

Organotetrel Chalcogenide Clusters: Between Strong Second-Harmonic and White-Light Continuum Generation

Nils W. Rosemann,[‡§] Jens P. Eußner,[†] Eike Dornsiepen,[†] Sangam Chatterjee,[‡§] and Stefanie Dehnen,[†*]

[†] *Fachbereich Chemie und Wissenschaftliches Zentrum für Materialwissenschaften (WZMW), Philipps-Universität Marburg, Hans-Meerwein-Straße, 35043 Marburg, Germany*

[‡] *Fachbereich Physik und Wissenschaftliches Zentrum für Materialwissenschaften (WZMW), Philipps-Universität Marburg, Renthof 7, 35032 Marburg, Germany*

[§] *Institute of Experimental Physics I, Justus-Liebig-University Giessen, DE-353992 Giessen, Germany*

Contents:

1. Syntheses

General

All manipulations were performed under argon atmosphere. All solvents were dried and freshly distilled prior to use. $[(MeSn)_4S_6]$ (**1**),[1] $[(NpSn)_4S_6]$ (**2**, Np = 1-naphthyl),[2] $[(StySn)_4S_6]$ (**3**, Sty = *para*-styryl),[3] and $[(PhSn)_4S_6]$ (**4**)[1] were prepared according to the reported methods. Reagents were purchased from Sigma–Aldrich. ^{1}H, ^{13}C, ^{29}Si and ^{119}Sn NMR spectroscopic measurements were carried out using Bruker DRX 300 MHz and DRX 500 MHz spectrometer at 25 °C. The chemical shifts were quoted in ppm relative to the residual protons of deuterated solvents in the ^{1}H NMR and ^{13}C NMR spectra. Me_4Si was used as external standard for ^{29}Si measurements. IR spectra were recorded on a Bruker Tensor 37 between 4000 and 400 cm^{-1} in attenuated total reflection. Elemental analysis was performed on an Elementar Vario Micro Apparatus. µRFA was done employing a Bruker Tornado M4.

Synthesis of 1,3,5,7-tetraphenyl-2,4,6,8,9,10-hexathia-1,3,5,7-tetragermana-adamantane, $[(PhGe)_4S_6]$ (5):

Phenyltrichlorogermane, $PhGeCl_3$, (1.52 g, 5.93 mmol) was added at room temperature to a solution of sodium sulfide nonahydrate, $Na_2S{\cdot}9H_2O$, (2.12 g, 8.90 mmol) in a solvent-mixture of water (10 mL) and acetone (8 mL). The resulting white precipitate was filtered and washed with water.

Yield: 0.63 g (0.80 mmol, 42% based on $PhGeCl_3$). ^{1}H NMR (300 MHz, DMF-d7, 25 °C): 7.41–8.04 (m, 20H) ppm. ^{13}C NMR (75 MHz, DMF-d7, 25 °C): 130.4, 131.7, 133.0, 133.9 ppm. IR: 420(m), 457(m), 537(m), 617(w), 690(s), 732(s), 815(s), 834(m); 883(w), 929(m), 996(w), 1024(w), 1087(w), 1099(w), 1159(w), 1184(w), 1260(w), 1305(w), 1332(w), 1432(m), 1438(w), 3050(w), 3070(w) cm^{-1}. Analysis (% calcd, % found for $C_{24}H_{20}Ge_4S_6$): C (36.43, 36.40), H (2.55, 2.64). µRFA (calcd, found for Ge_4S_6): Ge (0.67, 0.64), S (1.00, 1.00).

Synthesis of 1,3,5,7-tetraphenyl-2,4,6,8,9,10-hexathia-1,3,5,7-tetrasilana-adamantane, $[(PhSi)_4S_6]$ (6):

Anhydrous sodium sulfide, Na_2S, (0.906 g, 11.6 mmol) was suspended in tetrahydrofurane (18 mL). At a temperature of 0°C phenyltrichlorosilane, $PhSiCl_3$, (1.61 g, 7.75 mmol) was added dropwise under stirring. After two hours the reaction was continued at room temperature for 22 hours. The solvent was evaporated and the residue was extracted with toluene (18 mL). The solvent was slowly evaporated and the product was isolated as single crystalline material.

Yield: 0.38 g (0.62 mmol, 33% single crystalline yield based on $PhSiCl_3$). ^{1}H NMR (300 MHz, $CDCl_3$, 25 °C): 7.49–7.93 (m, 20H) ppm. ^{13}C NMR (75 MHz, $CDCl_3$, 25 °C): 129.1, 132.6, 133.1, 135.2 ppm. ^{29}Si NMR (99 MHz, $CDCl_3$, 25 °C): 8.5 ppm. IR: 442(w), 454 (w), 473(s), 492(m), 508(m), 555(s), 619(m), 688(s), 703(s), 738(s), 794(s), 863(m), 915(w), 925(w), 998(s), 1014(s), 1087(s), 1106(s), 1184(w), 1258(s), 1302(s), 1334(s), 1426(m), 1484(s), 1587(s), 2962(m), 3043(w), 3066(w) cm^{-1}. Analysis (% calcd, % found for $C_{24}H_{20}S_6Si_4$): C (36.43, 35.91), H (2.55, 2.52). µRFA (calcd, found for S_6Si_4): S (1.00, 1.00), Si (0.67, 0.66).

2. Thermogravimetric Analysis (TGA) and Differential Scanning Calorimetry (DSC)

Thermogravimetric analysis (TGA) and differential scanning calorimetry (DSC) were performed simultaneously on a Netzsch STA 400 in an aluminium oxide crucible in argon atmosphere with a heating rate of 10 K min^{-1}. The thermal decomposition of the compounds in inert Ar atmosphere with a heating rate of 10 K/min was observed at about 220 °C (**1**), 270 °C (**2**), 285 °C (**3**), 250 °C (**4**), 310 °C (**5**) and 370 °C (**6**), as shown in Figure S1. In all cases, the decomposition is an endothermic process.

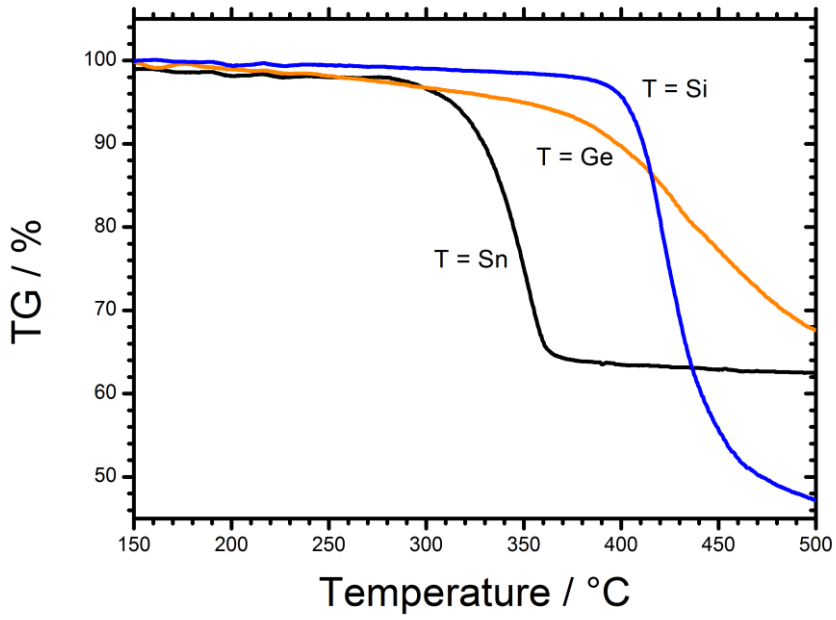

Figure S1. Thermogravimetric analysis (TGA) of compounds $[(PhT)_4S_6]$: **4** (T = Sn), **5** (T = Ge), and **6** (T = Si).

3. UV/Vis Spectroscopy

The linear optical absorption behavior was examined by means of UV-visible spectroscopy, measured as powder in reflectance mode on a Varian Cary 5000 spectrometer under ambient conditions. The spectra are shown in Fig. S2.

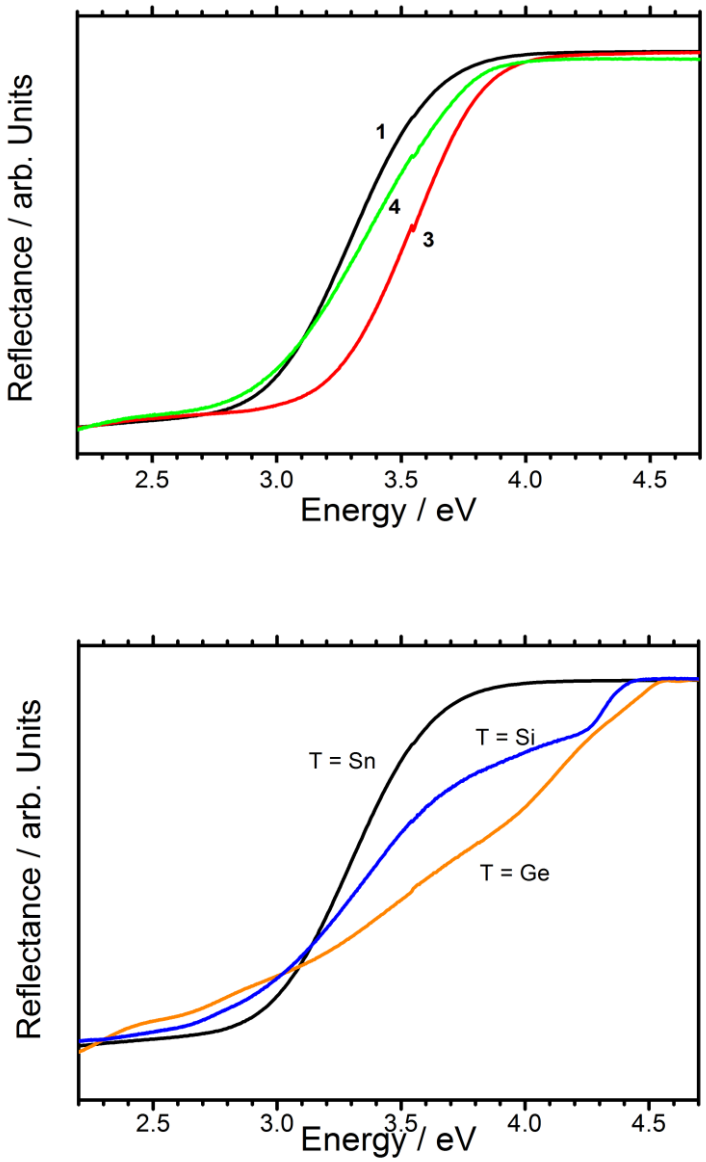

Figure S2. Solid state UV/Vis spectra. Top: Spectra of compounds **1** (red), **2** (green) and **4** (black). Bottom: Spectra of compounds **4** (black), **5** (orange), and **6** (blue).

4. X-Ray Powder Diffraction

In order to confirm the amorphous nature of compounds **1** to **5** as well as the crystallinity of compound **6**, all samples were examined by means of X-ray powder diffraction. The diffractograms are shown in Fig. S3. Powder X-ray diffraction patterns were measured on a StadiMP diffractometer by Stoe equipped with a Mythen 1K silicon strip detector and a Cu-K_α (λ = 1.54056 Å) x-ray source. Samples were measured in transmission between two layers of Scotch Tape (3M).

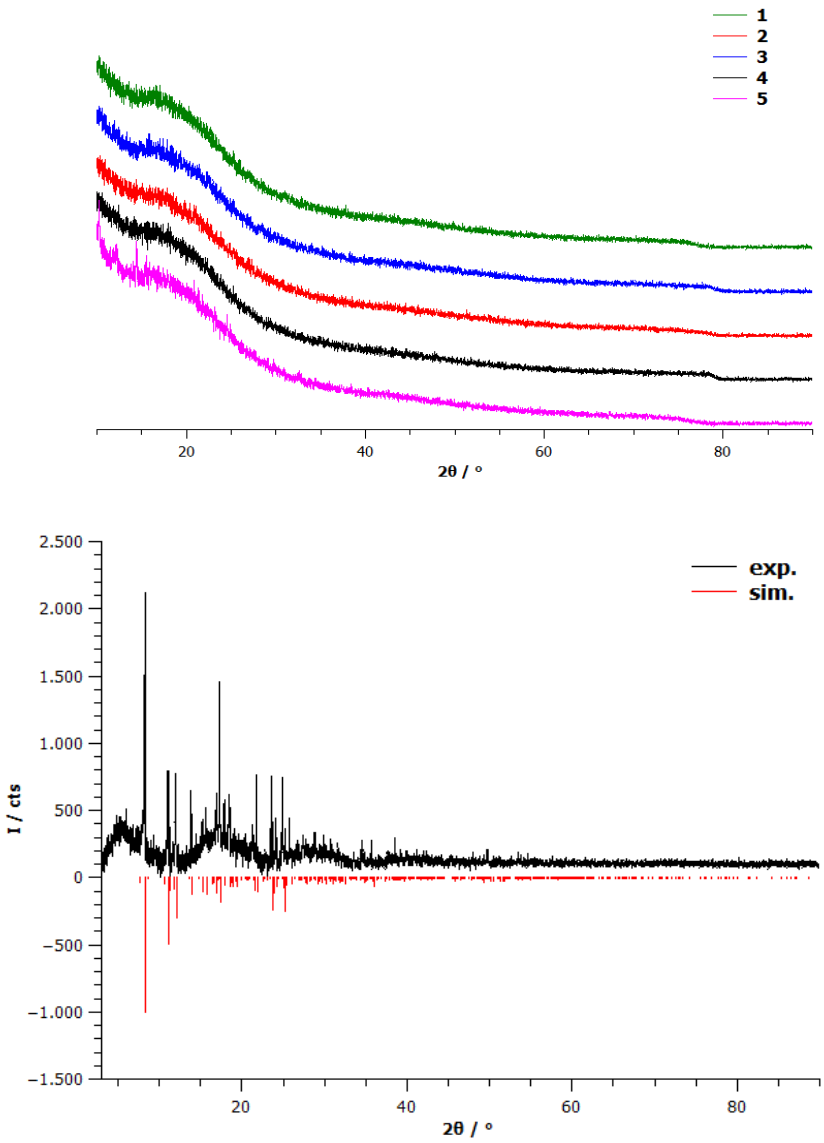

Figure S3. Top: X-ray powder diffractograms of compounds **1** (green), **2** (blue), **3** (red), **4** (black) and **5** (magenta), plotted one above the other in vertical direction for comparison. Bottom: X-ray powder diffractogram of compound **6** in comparison with a powder pattern simulated from the single crystal structure (see section 5). The slight angular shift between measured and simulated diffractograms can be attributed to the single crystal measurement being carried out at 100 K while the powder diffractograms were measured at 293 K.

5. Single Crystal X-Ray Crystallography of Compound 6

Data of the X-ray diffraction analyses were collected on a diffractometer equipped with a STOE imaging plate detector system IPDS2 using $Mo_{K\alpha}$ radiation with graphite monochromatization (λ = 0.71073 Å) at 100 K. Structure solution was performed by direct methods, full-matrix-least-squares refinement against F^2 using SHELXTL software.[4] Table S1 summarizes data collection and refinement details.

Table S1. X-ray data collection, structure solution and refinement data of **6**.

Empirical formula	$C_{24}H_{20}S_6Si_4$
Formula weight /g·mol^{-1}	613.12
Crystal color, shape	colorless, block
Crystal size /mm^3	0.20 × 0.16 × 0.16
Crystal system	monoclinic
Space group	$P2_1/c$
a /Å b /Å c /Å β /°	10.2415(3) 11.9566(5) 23.1774(8) 93.170(3)
V /Å^3	2833.81(17)
Z	4
ρ_{calc} /g·cm^{-3}	1.437
μ(MoK_α) /mm^{-1}	0.666
θ range /°	1.76–29.17
No. of measured reflections	26535
No. of independent reflections, R(int)	7616, 0.0424
No. of independent reflections ($I > 2\sigma(I)$)	5888
Parameters	307
Restraints	0
R_1 ($I > 2\sigma(I)$)	0.0277
wR_2 (all data)	0.0688
GOF (all data)	0.925
Max. peak/hole /e$^-$·Å^{-3}	0.561 / −0.225
Absorption correction type	none

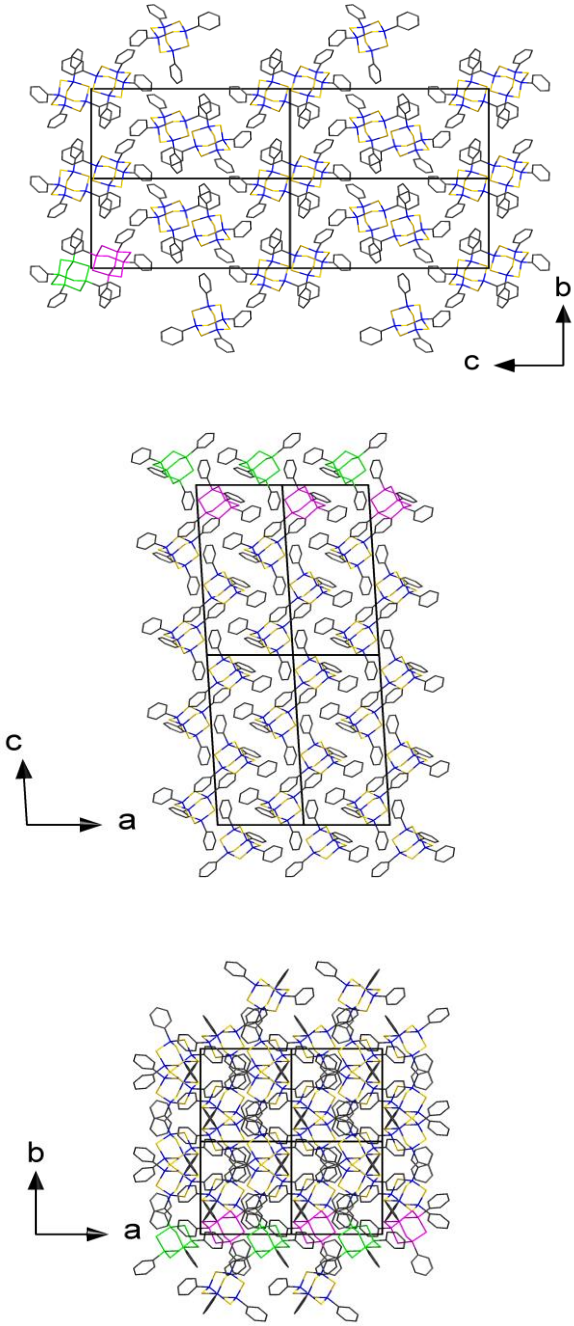

Figure S4. Packing of the molecules in **6**, shown as 2×2×2 supercells with view along [100] (top), [010] (center), and [001] (bottom). H atoms are omitted for clarity, Si, S, and C atoms drawn as blue, yellow, and grey wires, respectively. Cluster scaffolds with their inorganic cores drawn in green or pink color, respectively, indicate relative positions of neighboring cluster molecules in the different directions. The relative orientations of the phenyl rings do not indicate π stacking interactions.

6. Density Functional Theory (DFT) Calculations

Methods of the quantum chemical investigation: For the DFT calculations, the program system TURBOMOLE Version 6.5[5] using the RIDFT[6] program with the BP86 functional[7] and grid size m3 was applied. Basis sets were of def2-TZVP quality.[8,9] For Ge and Sn atoms, effective core potentials (ECP-28)[10] were employed. The simultaneous optimization of geometric and electronic structures were done without symmetry restrictions (C_1 symmetry). The accuracy of the structures was found within the typical error of the method.

According to the obtained general sum formula of $[(RT)_4S_6]$ (T = Si, Ge, Sn) two isomers for the organotetrel sulfide cluster exist. One isomer exhibits a hetero adamantane type scaffold with pseudo T_d symmetry, the other isomer exhibits a double-decker like scaffold with pseudo D_2 symmetry. DFT calculations show that the hetero adamantane topology is energetically favored in every case with various substituents (R = H, Me, Ph) by 20.7 to 41.0 kJ. For compounds **1**–**6** the calculated values are given in Table S2. For compound **5** the hetero-adamantane scaffold is energetically favored by 19.2 kJ/mol. For this reason we presume that only the hetero adamantane type scaffold is present at room temperature.

Table S2. Subtraction of the total energies of the calculated hetero-adamantane type clusters (AD) from the "double-decker" type clusters (DD). (Sty = *para*-styryl, Np = 1-naphthyl), indicating the energetic preference of the hetero-adamantane-type scaffold over the alternative one.

Compound	ΔE_{AD-DD} / kJ
$[(MeSn)_4S_6]$ (**1**)	–36.4
$[(NpSn)_4S_6]$ (**2**)	–19.2
$[(StySn)_4S_6]$ (**3**)	–28.5
$[(PhSn)_4S_6]$ (**4**)	–28.2
$[(PhGe)_4S_6]$ (**5**)	–30.4
$[(PhSi)_4S_6]$ (**6**)	–20.7

7. Optical Microscopy

Microscopy photographs of the compounds were taken with a stereo microscope (Carl Zeiss – STEMI SV 6) equipped with a standard CMOS camera. The compounds **4** and **5** are obtained as amorphous powders (cf. Fig. S5a-b). Compound **6** produces large crystallites as shown in Fig. S5c.

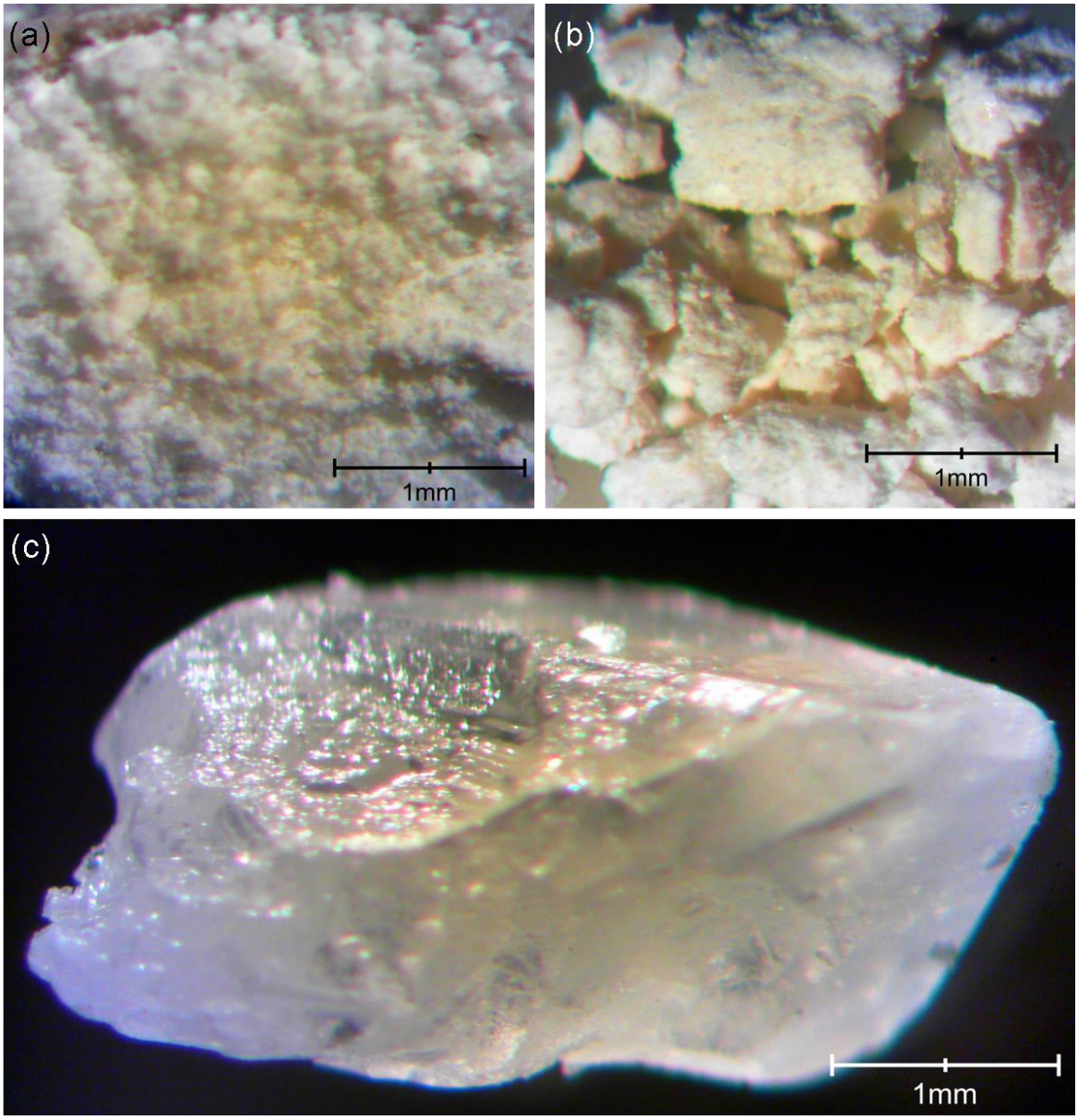

Figure S5. Microscopy photographs of the compounds **4**, **5** and **6**

8. Measurements of the Nonlinear Optical Response

The nonlinear responses of the samples are measured using the setup depicted in Fig. S6. The powders are kept inside a small vacuum cell with BK7 windows at pressures below 10^{-3}mbar. The continuous-wave 980 nm light from a laser diode is focused onto the samples using a 0.5 NA reflective microscope objective in a confocal geometry. A heat absorbing filter (Schott KG3) in the recollimated beam is used to block the residual pump laser. The remaining light, white-light or the second-harmonic, is then focused onto the entrance slit of a Czerny-Turner-type spectrometer where the dispersed spectrum is detected using a thermoelectrically cooled back-illuminated deep-depletion silicon charge-coupled device array sensor.

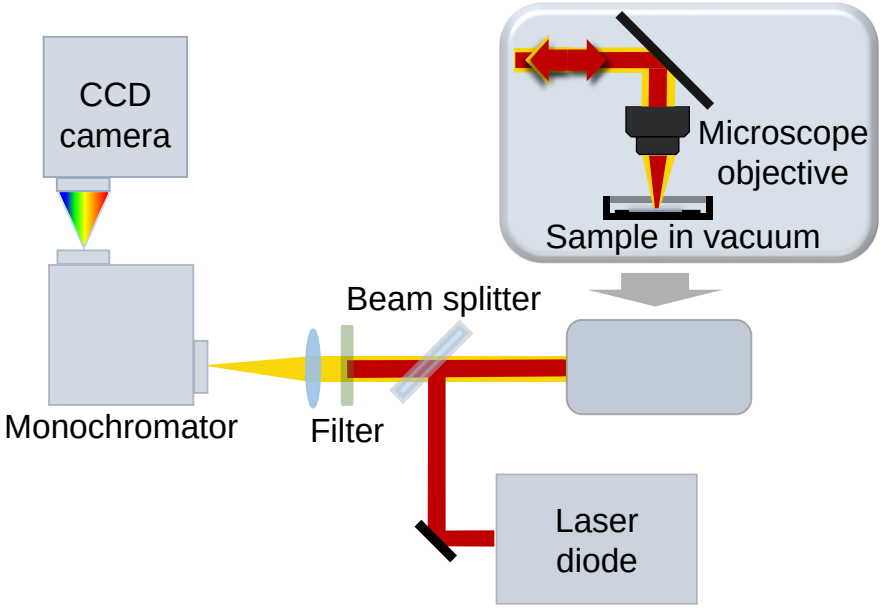

Figure S6. Setup for spectrally resolved measurements of the steady-state nonlinear response.

9. References for the Supporting Information

1. Costa, G. A. A.; Silva, M. C.; Silva, A. C. B, de Lima, G. M.; Lago, R.M.; Sansiviero, M. T. C. *Phys. Chem. Chem. Phys.* **2000**, *2,* 5708.
2. Berwe, H.; Haas, A. *Chem. Ber.* **1987**, *120*, 1175.
3. Rosemann, N. W.; Eußner, J. P.; Beyer, A.; Koch, S. W.; Volz, K.; Dehnen, S.; Chatterjee, S. *Science* **2016**, *352*, 1301–1304.
4. Sheldrick, G. M. *Acta Crystallogr.* **2008**, *A64*, 112.
5. TURBOMOLE V6.5, © TURBOMOLE GmbH. TURBOMOLE is a development of University of Karlsruhe and Forschungszentrum Karlsruhe 1989-2007.
6. Eichkorn, K.; Treutler, O.; Öhm, H.; Häser, M.: Ahlrichs, R. *Chem. Phys. Lett.* **1995**, *242*, 652; Eichkorn, K.; Weigend, F.; Treutler, O.; Ahlrichs, R. *Theor. Chim. Acta **1997***, *97*, 119.
7. Becke, A. D. *Phys. Rev. A* **1988**, *38*, 3098; Vosko, S. H., Wilk, L.; Nusair M. *Can. J. Phys.* **1980**, 58, 1200; Perdew, J. P.; Yue, W. *Phys. Rev.* **1986**, *B33*, 8800.
8. Weigend, F.;Ahlrichs, R. *Phys. Chem. Chem. Phys.* **2004**, *7*, 3297.
9. Weigend, F. *Phys. Chem. Chem. Phys.* **2006**, *8*, 1057.
10. Metz, B., Stoll, H.; Dolg, M. *J. Chem. Phys.* **2000**, *113*, 2563.

4.2 Controlling the White-Light Generation of $[(RSn)_4E_6]$: Effects of Substituent and Chalcogenide Variation

Zitat: E. Dornsiepen, F. Dobener, N. Mengel, S. Chatterjee, S. Dehnen, **2019**, *Manuskript in Vorbereitung.*

Abstract

Adamantane-type organotin sesquichalcogenides of the general composition $[(RT)_4S_6]$ (R = aromatic ligand, T = Si, Ge, Sn) were recently proven to a new class of materials with extreme non-linear optical properties that generate highly directed white-light upon irradiation with an inexpensive infrared laser diode. However, the mechanism behind this new type of supercontinuum generation is not yet understood. Furthermore, the nature of the organic ligands and the compounds' morphology are critical to the observation of either highly efficient second-harmonic generation (SHG) instead of the white-light generation (WLG). Therefore, there is an urgent need to massively expand the library of respective compounds and their thorough investigation to find and understand the crucial patterns and preconditions of the extreme non-linearity. Herein we present our most recent study on the series of novel compounds $[(RSn)_4E_6]$ (R = phenyl, cyclopentadienyl, cyclohexyl, benzyl, $CH_2CH_2(C_6H_4)CO_2Et$; E = S, Se), which were prepared, characterized and investigated for their nonlinear optical properties. With the exception of crystalline $[(BnSn)_4S_6]$, they all show WLG with similar emission spectra; slight blue shifts by introduction of cyclopentadienyl substituents or red shifts by introduction of Se in the inorganic core are observed. By these investigations, we present an important step forward in the knowledge of the new WLG property by disproving the initial assumption of an aromatic ligand as necessary precondition. We could show that also clusters with non-aromatic cyclohexyl and cyclopentadienyl ligands produce directed white-light. Hence, the necessary precondition seems to be just the presence of cyclic ligands, which we rationalized by means of in-depth quantum chemical studies.

Eigener Anteil

Alle Synthesen wurden von mir geplant und durchgeführt, mit Ausnahme der Verbindungen **B**, **C** und **4**, welche von Igor Müller im Rahmen eines von mir betreuten Forschungspraktikums hergestellt wurden. Die Aufnahme der röntgenographischen Daten sowie die Strukturlösung und -verfeinerung wurde von mir durchgeführt. IR-Spektren sowie ^{1}H- und ^{13}C-NMR-Spektren wurden von mir, ^{119}Sn-NMR-Spektren von der zentralen NMR-Abteilung des Fachbereichs Chemie an der Philipps-Universität unter Leitung von Dr. Xiulan Xie gemessen und von mir ausgewertet. Massenspektrometrie und CHNS-Analysen

wurden von der entsprechenden Serviceabteilung des Fachbereichs unter Leitung von Dr. Uwe Linne durchgeführt und von mir ausgewertet. Photolumineszenz- und Emissionsspektren wurden von Florian Dobener und Nils Mengel in der Arbeitsgruppe von Prof. Dr. Sangam Chatterjee an der Universität Gießen gemessen und ausgewertet. Das Manuskript wurde gemeinsam von allen Co-Autoren verfasst.

RESEARCH ARTICLE

Controlling the White-Light Generation of $[(RSn)_4E_6]$: Effects of substituent and chalcogenide variation

Eike Dornsiepen,[a] Florian Dobener,[b] Nils Mengel,[b] Sangam Chatterjee,[b] and Stefanie Dehnen[a]*

Abstract: Adamantane-type organotin sesquichalcogenide clusters of the general composition $[(RT)_4S_6]$ (R = aromatic substituent, T = Si, Ge, Sn) were recently proven to a new class of materials with extreme non-linear optical properties that generate highly directed white-light upon irradiation with an inexpensive infrared laser diode. However, the mechanism behind this new type of supercontinuum generation is not yet understood. Furthermore, the nature of the organic substituents and the compounds' morphology are critical to the observation of either highly efficient second-harmonic generation (SHG) instead of the white-light generation (WLG). Therefore, there is an urgent need to massively expand the library of respective compounds and their thorough investigation to find and understand the crucial patterns and preconditions of the extreme non-linearity. Herein we present our most recent study on the series of novel compounds $[(RSn)_4E_6]$ (R = phenyl, cyclopentadienyl, cyclohexyl, benzyl, $CH_2CH_2(C_6H_4)CO_2Et$; E = S, Se), which were prepared, characterized and investigated for their nonlinear optical properties. With the exeption of crystalline $[(BnSn)_4S_6]$, they all show WLG with similar emission spectra; slight blue shifts by introduction of cyclopentadienyl substituents or red shifts by introduction of Se in the inorganic core are observed. By these investigations, we present an important step forward in the knowledge of the new WLG property by disproving the initial assumption of an aromatic substituent as necessary precondition. We could show that also clusters with non-aromatic cyclohexyl and cyclopentadienyl substituents produce directed white-light. Hence, the necessary precondition seems to be just the presence of (cyclic) substituents providing enough electron density, which we rationalized by means of in-depth quantum chemical studies.

Introduction

Organotetrel chalcogenide clusters are organic/inorganic hybrid compounds consisting of an inorganic cage that is derived from chalcogenidotetrelate anions,[1,2] and features an organic substituent shell attached to the core by covalent tetrel-carbon bonds. Chalcogenidotetrelate salts have been actively investigated due to their tunable optoelectronic and semiconducting properties, resulting in diverse applications.[3-6] The decoration of such cluster anions with organic substituents does not only allow the isolation of compounds with discrete, neutral cluster molecules. It also enables further tailoring of material properties such as solubility in organic solvents or reactivity towards organic molecules, metal salts or surfaces.[7]

In the context of our investigation of functionalized organotetrelchalcogenide clusters,[8-13] we recently found an unprecedented, extreme non-linear optical behavior of the styryl-decorated cluster $[(StySn)_4S_6]$ (Sty = 4-vinylphenyl),[14] which belongs to the family of organotetrelsesquichalcogenide clusters of the general formula $[(RT)_4E_6]$ (R = organic substituent; T = Si, Ge, Sn; E = O, S, Se, Te).[15-19] $[(StySn)_4S_6]$ was obtained as an amorphous powder, but DFT calculations revealed the adamantane-type structure to be favored over the double-decker-type isomer by ca. 30 kJ/mol. While compounds that lack inversion symmetry are widely known for second harmonic generation (SHG), we observed white-light generation (WLG) upon irradiation with a commercially available CW infrared laser diode.[14] This unexpected phenomenon was intuitively attributed to the amorphous nature of the compound, as SHG requires phase-matched emission of photons. In the respective powders, this is clearly prohibited by random orientation of the molecules, which at the same time leads to an extreme broadening of the SHG emission. Yet, the exact mechanism of this non-linear response is still unknown. Therefore, we are currently about to expand the library of related compounds for getting more insight in the new WLG behavior.

Recently, we prepared a range of adamantane-type clusters with different organic substituents and tetrel elements: $[(PhSn)_4S_6]$ and $[(PhGe)_4S_6]$ exhibit WLG, while $[(PhSi)_4S_6]$, $[(MeSn)_4S_6]$ and $[(NpSn)_4S_6]$ do not emit white light; yet, these compounds still show non-linear optical properties by strong SHG instead.[20] For $[(PhSi)_4S_6]$, this is easily attributed to the crystallinity of the compound, which enables phase-matching. In the case of $[(MeSn)_4S_6]$, the organic substituent shell does not contain an aromatic π-electron system; as $[(MeSn)_4S_6]$ lacked any evidence for long-range but showed SHG, the presence of π-aromatic substituent molecules was intuitively assumed to be a necessary condition for WLG. The lack of WLG observed for the naphthyl-substituted $[(NpSn)_4S_6]$ was attributed to beginning long-range order in the amorphous powder due to π-stacking.[20]

Although the assumption of an aromatic π-electron system as a critical parameter seemed plausible, its role has remained unclear so far. So, we intended to further narrow down the chemical and electronic pre-conditions for WLG and designed a new series of compounds that have cyclic substituents R, hence including non-aromatic ones. Herein, we report on their synthesis and characterization as well as on the non-linear optical response that

[a] E. Dornsiepen, Prof. Dr. S. Dehnen
FB Chemie and WIssenschaftliches Zentrum für Materialwissenschaften (WZMW)
Philipps-Universität Marburg
Hans-Meerwein-Straße 4, D-35043 Marburg, Germany
E-mail: dehnen@chemie.uni-marburg.de

[b] F. Dobener, N. Mengel, Prof. Dr. S. Chatterjee
Institute of Experimental Physics I
Justus-Liebig-Universität Gießen
Heinrich-Buff-Ring 16, D-35392 Gießen, Germany

Supporting information for this article is given via a link at the end of the document.

was shown this way to be feasible with cyclic substituents lacking aromaticity, as well.

Clusters of the type $[(RSn)_4E_6]$ (R = phenyl, cyclopentadienyl, cyclohexyl, benzyl, $CH_2CH_2(C_6H_4)CO_2Et$) were prepared and fully characterized. The subtle influence of the substituent was probed by introducing either non-aromatic cyclic substituents, or an aliphatic linker to further separate the aromatic ring from the cluster core, or finally additional functionalization of the aromatic substituent. To gain further insight into the role of the cluster core's composition, the series of compounds was realized for both E = sulfur and selenium, with the latter being the first selenide clusters of this kind to be examined for non-linear optical properties. Scheme 1 summarizes the compounds synthesized and further studied herein.

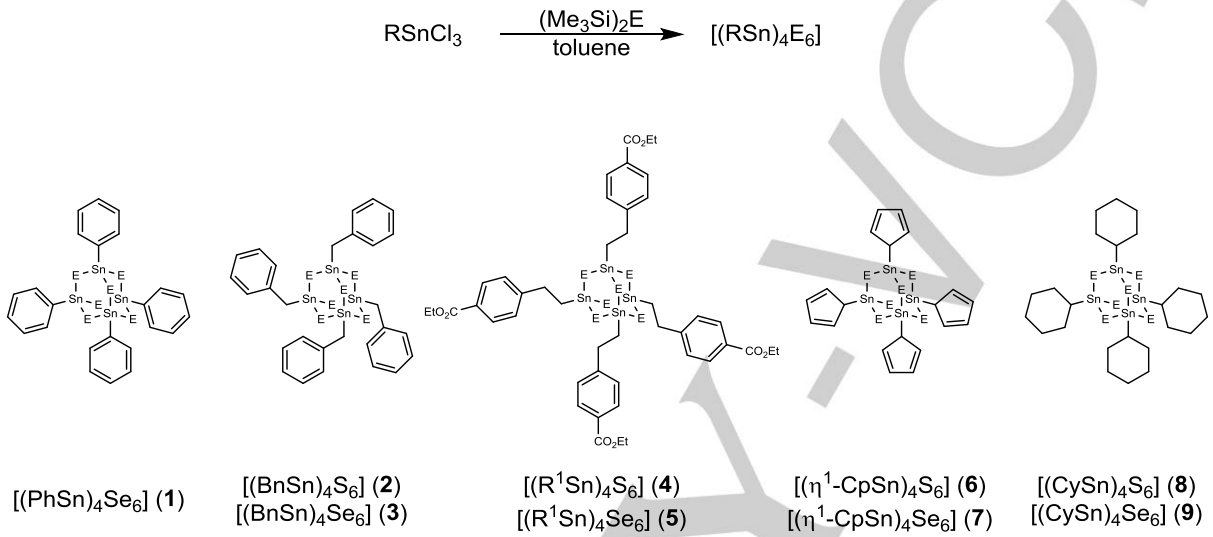

Scheme 1: Synthesis of compounds **1** – **9** (Ph = phenyl, Bn = benzyl, $R^1 = CH_2CH_2(C_6H_4)CO_2Et$, η^1-Cp = η^1-Cyclopentadienyl, Cy = cyclohexyl).

Results and Discussion

With the chosen series of compounds, we intended to gain more insight into the prerequisites for WLG by answering the following questions:

1) Is the emission spectrum affected by replacement of sulfur with selenium?

2) Does the aromatic substituent need to be bonded directly to the inorganic core, or is WLG also observed if an aliphatic spacer is inserted between the cluster core and the π-system?

3) Is a π-aromatic substituent necessary at all, or do π-electrons located in isolated double-bonds also lead to the observation of WLG?

4) Are substituents with any kinds of π-electrons generally needed for WLG, or can molecules that bear fully saturated organic substituents show WLG?

All compounds indicated in Scheme 1, which can be summarized as $[(RSn)_4E_6]$ (R = Ph, η^1-Cp, Cy, Bn, $CH_2CH_2(C_6H_4)CO_2Et$; E = S, Se), were prepared by reaction of the corresponding organotin trichlorides and $(Me_3Si)_2E$ in toluene. The clusters precipitated from solution and were isolated by filtration. Amorphousness versus crystallinity was probed by powder X-ray diffraction (see Figures S42-S50). To address the questions above, we collected emission spectra of all new compounds. The spectra of compounds **1** and **4**–**9** which are shown along with the spectrum of known compound $[(PhSn)_4S_6]$ (**A**) in Figure 1.In order to address question 1, we compared the emission spectra of all sulfide clusters with those of the selenide analogs. The observations will be discussed at each of the homologous pairs separately along this report, and summarized at the end. In case of compounds $[(PhSn)_4S_6]$ (**A**) and $[(PhSn)_4Se_6]$ (**1**), we did not see any significant change in the shape of the emission, thus concluding that the WLG is largely independent from the composition of the inorganic core here. This is similar to what has been reported for the variation of the tetrel element before.[20]

Regarding question 2, we investigated the benzyl-substituted clusters **2** and **3**, and also explored compounds **4** and **5**. The latter feature a $CH_2CH_2(C_6H_4)CO_2Et$ substituent, in which the phenyl moiety is separated from the tin atom by an CH_2 unit. Compounds **2** and **3** show a striking difference to the previously prepared clusters. While all other compounds were obtained as amorphous powders, **2** and **3** were isolated in crystalline form, suitable for single-crystal structural analysis. Apparently, the methylene groups in the benzyl substituents give the molecules the necessary flexibility to orient in a way that allows for an efficient packing in a crystal lattice. Hence, although enhanced flexibility of the substituents by free rotation about the Sn–C axes may cause the lack of long-range order in general, and lead to the remarkably amorphous powders of the clusters discussed herein, the clusters seem to make use of any possibility to order for a gain of lattice energy or alternate second order interaction energy. So far we identified three possible ways to do so: (a) beginning long-range order if the aromatic system is large enough for efficient π-

stacking (as found for naphthyl substituents in $[(NpSn)_4S_6]$),[20] (b) a relatively small size of the cluster core relative to (small) aromatic substituents, which in the sum allow for a sufficiently close approach of the clusters for efficient π-stacking (as found for $[(PhSi)_4S_6]$),[20] (c) setting apart a (small) aromatic groups from the cluster core by introducing an organic spacer group (as found for **2** and **3**). Although we did not expect compounds **2** and **3** to generate white-light owing to their crystalline nature, we investigated their structures, and also their non-linear optical response.

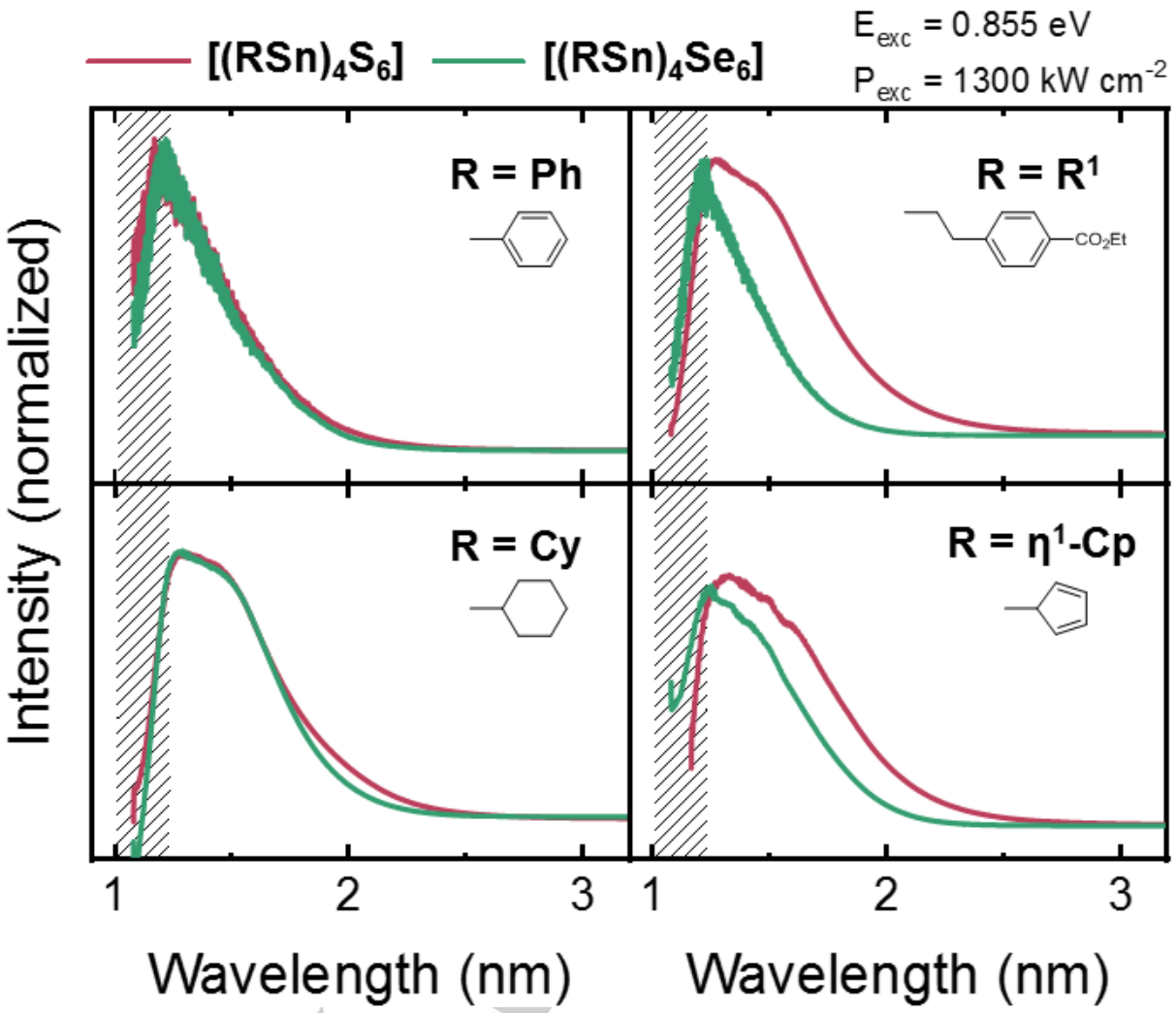

Figure 1. WLG emission spectra of organotin sulfide and selenide clusters **A** and **1** (R = phenyl), **4** and **5** (R = R^1 = $CH_2CH_2(C_6H_4)CO_2Et$), **6** and **7** (R = η^1-cyclopentadienyl), **8** and **9** (R = cyclohexyl).

2 crystallizes in the tetragonal crystal system in the space group $I\bar{4}$ with two formula units per unit cell. The Sn–S bonds show little variation, ranging from 2.3948(18) to 2.4086(19) Å, which is in the usual range for organotinsulfides.[9] The same holds for the bond angles within the inorganic core (103.60(11) – 115.71 (6)°), which are all in close proximity to an ideal tetrahedral angle. The selenide cluster **3** is isostructural to its lighter homologue. The Sn-Se bond lengths are 2.5227(9) – 2.5292(10) Å long, thus longer as in **2** and in the expected range for organotinselenides.[21] The variation in bond angles is slightly greater than in **2**, ranging from 100.82(5) to 117.13(3)°. For both of the compounds, the packing diagrams indicates the absence of π-stacking in spite of the presence of terminal phenyl rings (see Figure S33 for **2**, and Figure 2 for **3**). Instead, the benzyl substituents are well separated from each other. However, the packing of the molecules allows for another type of secondary interactions, which are found between the chalcogenide atoms in the cluster core and the phenyl rings of the neighboring molecules (shortest distance 3.5221(79) Å for **2** and 3.5303(81) Å for **3**).

The emission spectra of **2** and **3** are shown in Figure 3. While the sulfide cluster **2** showed SHG, as expected for a crystalline compound, the selenide compound **3** unexpectedly featured WLG. Yet, as WLG in the crystalline state is very unlikely to happen for the reasons given above, we also inspected the thermal behavior of both compounds. While **2** starts decomposing in the temperature range of 160–180°C without melting, **3** already melts at 141°C without decomposition. So, their different optical behavior can be put down to compound **3** melting under irradiation with the result that the order vanishes, which allows for WLG. This is similar to WLG upon amorphization in the solid state, which was observed for a series of unsymmetrically substituted clusters recently.[22]

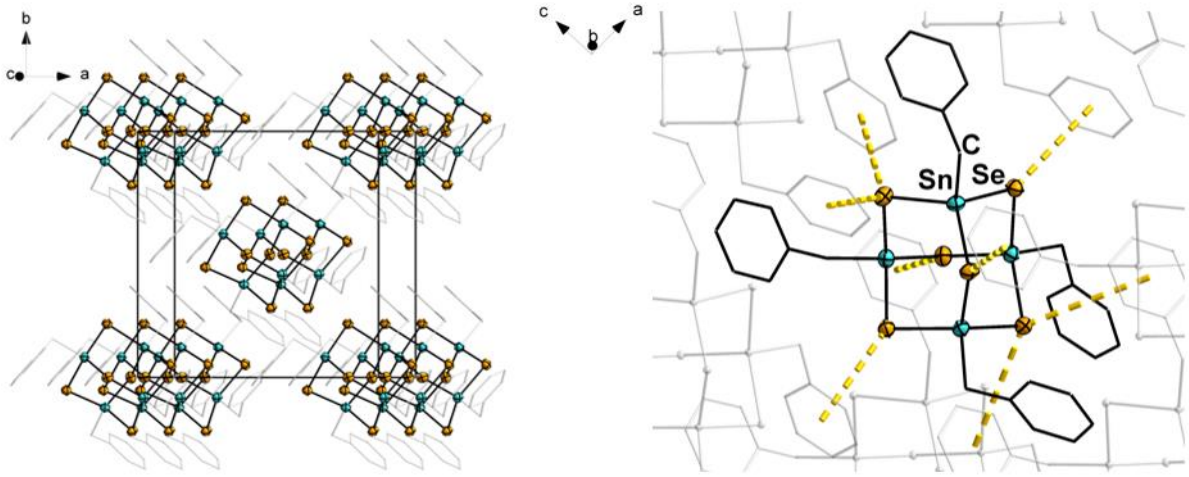

Figure 2. Packing of the cluster molecules in the crystal structure of **3** (left) and illustration of the intermolecular interaction of neighboring clusters (right). Ellipsoids are drawn at 50% probability; hydrogen atoms are omitted for clarity. The analogue structure of **2** is given in the Supporting Information (Figure S51).

To allow for amorphous solids with this kind of substituents, we explored compounds with a larger spacer length, namely compounds **4** and **5** comprising an ethylene group between the cluster core and the phenyl group (see Scheme 1, bottom). We hoped that the again enhanced flexibility of the substituents to inhibit crystallization this time, which indeed worked out. The emission spectra of these compounds are shown in the top right part of Figure 1. Both compounds exhibit WLG. The emission spectrum is not modified significantly in comparison to that of compounds **A** and **1** upon inclusion of a longer spacer. As for the quoted compounds, the emission sets in at energies slightly above those of the exciting laser, and drops off at the energy where SHG would be expected. However, by replacement of sulfur with selenium, we induce a red shift of the emission spectrum that was not observed for the phenyl-substituted clusters, which we cannot explain to date. Yet, to summarize our result regarding question 2, the final answer to question 2 is that in the case of amorphous solids, the aromatic substituents may be separated from the inorganic cluster core.

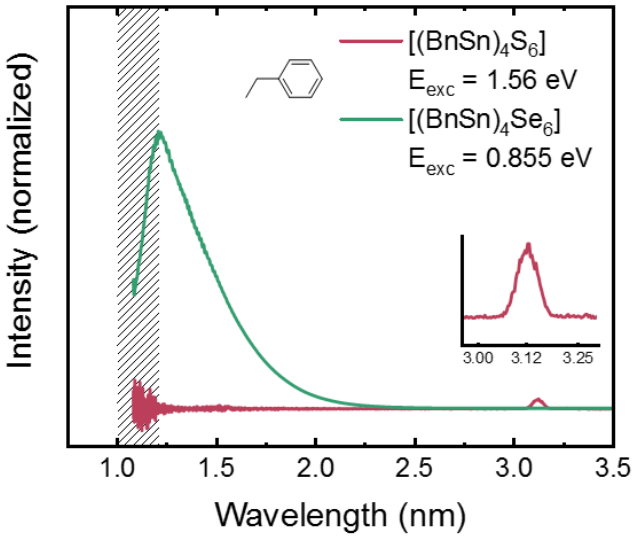

Figure 3. Emission spectra of compounds **2** (no WLG) and **3** (WLG).

Having learned that aliphatic spacers do not inhibit WLG in principle, we investigated if an aromatic π electron system is at all a necessary prerequisite for WLG. For this purpose, we prepared compounds with localized π-electrons in a non-aromatic system, namely the η^1-cyclopentadienyl-substituted clusters **6** and **7**. As shown in Figure 1 (bottom right), these compounds also show WLG, thus rendering the essential need for aromatic substituents obsolete. However, in both cases, we observed a steeper drop-off at the high-energy edge of the spectrum, resulting in a larger blue-portion of the emitted light. As for the other homologous pairs discussed above, a red shift is observed upon inclusion of selenium into the inorganic core of **7** as compared to the spectrum measured for **6**.

The last logical step in this study is to completely dispense with π-electrons in the substituents. As we knew from our previous studies that simple aliphatic substituents like methyl or butyl do not lead to WLG, but cause SHG instead, we probed the effect of a saturated, yet cyclic substituent. The substituent of choice here

was cyclohexyl for its relationship with the phenyl group regarding the number of C atoms, which was realized in compounds **8** and **9** (see Figure 1, bottom left). We observed WLG for both of these compounds, so our conclusion it that the WLG cannot be based on an electronic excitation of π electrons. In this case, we did not observe a red-shift between the spectrum of the sulfide cluster **8** and that of the selenide cluster **9**.

All these results together clearly showed that another explanation is needed for the observed phenomenon. Our explanation that takes into consideration the new findings is given as follows. The WLG process is based upon a two-photon excitation of the molecules into virtual states within the HOMO-LUMO gap, which have an extremely short lifetime (which prevents spectroscopic evidence of these states). From these virtual states, the molecules relax into the different vibrational excitation levels within the electronic ground state under emission of photons, yielding the observed broad emission spectra.

Hence, from all that we have learned in this work, the crucial requirement with respect to the electronic structure of potential white-light emitters is a large enough HOMO-LUMO gap. Otherwise electronic excitations into states with much longer lifetimes gain the upper hand, in which case other relaxation pathways like photoluminescence will be observed. Additionally, the amorphous nature of the compounds is key in deciding whether WLG or SHG is observed, because crystallinity allows for a preference of phase-matched SHG emission.

An observation that remains ununderstood is that the substitution of sulfur for selenium induces a red-shift of the emission in some cases, while in some cases no such effect occurs. In order to gain more insight into this, we looked into the electronic situation of the corresponding compounds. HOMO-LUMO gaps of all compounds were calculated by means of DFT calculations (see Table 1).

Table 1. HOMO-LUMO gaps of compounds **A** and **1**-**9**.

Compound	HOMO-LUMO gap / eV
A	3.15
1	2.69
2	2.90
3	2.61
4	3.19
5	2.75
6	2.25
7	2.08
8	3.16
9	2.74

In all cases, the selenide clusters have smaller gaps than the corresponding sulfides (as expected). For **7**, a gap of only 2.08 eV is calculated, which limits the light emission to ~2 eV, because photons with higher energy are reabsorbed by the sample, leading to occupation of excited electronic states with longer lifetime. Thus we can attribute the red-shift of the emission observed for the cyclopentadienyl-substituted clusters **6** and **7** to the extraordinarily small HOMO-LUMO gap. This explanation, however, does not serve to understand the red-shift observed in compound **5**. The gap of 2.75 eV is in the same range as for compounds **1**, **3** or **9**, where the replacement of sulfur with selenium did not cause a red-shift. Hence, we cannot rationalize why the observed emission is limited to a maximum energy of ~2.0 eV at this point.

Conclusion

In conclusion, we report on a study that allowed for a big step forward in the understanding of the new class of white-light emitters based on adamantane-type organotin chalcogenide clusters. While the previously stated precondition of the materials to be amorphous was confirmed once again, our new findings prompted us to re-phrase some of our former assumptions that were made based on a much smaller cohort of compounds. We could show that clusters of the type [(RSn_4E_6)] are capable of white-light generation (WLG) if they fulfill the following preconditions: they need to contain electron-rich (cyclic) substituents, which may – but do not need to – possess π-electrons, and which do not need to be directly bonded to the inorganic cluster core, as long the spacer group does not cause crystallization. A point that could no be clarified yet is the effect of a homologous replacement of sulfur atoms with its heavier congeners. Here, we need to refer to future comprehensive work into this direction.

Experimental Section

General: All synthetic steps were carried out under exclusion of oxygen and moisture by use of standard Schlenk techniques. Phenyltin trichloride,[23] bis(trimethylsilyl) sulfide[24] and selenide,[25] sodium cyclopentadienide,[26] tetracyclohexyltin,[27] benzyltributyltin,[28] 4-vinylethylbenzoate[29] and tricyclohexylstannane[30] were prepared according to literature procedures, $SnCl_4$ and AIBN were used as received from abcr. ^1H, ^{13}C, ^{31}P and ^{119}Sn NMR spectroscopy was carried out at 25°C using Bruker DRX 300 MHz and DRX 500 MHz spectrometers. The chemical shifts are given in ppm relative to the residual protons of deuterated solvents for ^1H spectra and relative to the solvent signal for ^{13}C spectra. ^{13}C, ^{31}P and ^{119}Sn spectra have been measured with ^1H decoupling. Me_4Sn was used as internal standard in ^{119}Sn NMR measurements. HR-ESI mass spectra were acquired with an LTQ-FT Ultra mass spectrometer (Thermo Fischer Scientific). The resolution was set to 100.000. Yields are based on the amount of Sn and refer to the amount of product isolated as single crystals. Powder X-ray diffraction patterns were measured on a StadiMP diffractometer by Stoe equipped with a Mythen 1K silicon strip detector and a Cu-Kα (λ = 1.54056 Å) x-ray source. Samples were measured in transmission between two layers of Scotch Tape (3M).

Synthesis of [$(PhSn)_4Se_6$] (1)

($Me_3Si)_2Se$ (1.20 mL, 4.79 mmol) was added at room temperature to a solution of $PhSnCl_3$ (0.50 mL, 3.04 mmol) in toluene (20 mL). After a few seconds, a light yellow precipitate formed that was filtered off after 5 minutes. Washing with toluene (5 mL) and drying *in vacuo* afforded **9** (915 mg, 0.73 mmol, 96%) as a light yellow powder.

^{1}H-NMR (CD_2Cl_2, 300 MHz)**:** δ = 7.53 (m, 12H, H_{ortho} + H_{para}), 7.69 (m, 8H, H_{meta}) ppm. **^{13}C-NMR** (CD_2Cl_2, 75 MHz)**:** δ = 129.5 (C_{arom}), 129.9 (C_{arom}), 131.7 (C_{arom}), 134.3 (C_{arom}) ppm. **^{119}Sn-NMR** (CD_2Cl_2, 112 MHz)**:** δ = –100 ($^{1}J_{SnC}$ = 130Hz, $^{1}J_{SnSe}$ = 683 Hz) ppm. **IR:** $\tilde{\nu}$ = 1573 (w), 1473 (w), 1439 (m), 1327 (w), 1296 (w), 1258 (w), 1887 (w), 1156 (w), 1064 (m), 1016 (w), 996 (m), 963 (w), 905 (w), 842 (w), 721 (s), 688 (s), 613 (w), 463 (w), 437 (s) cm^{-1}. **Elemental Analysis:** found (calcd.): C 23.41 (22.93), H 1.65 % (1.60 %).

Synthesis of $BnSnCl_3$ (A)

$BnSnCl_3$ was prepared by a modified literature procedure.[28] Benzyltributyltin (10.3 mL, 30.0 mmol) was cooled to –30°C. After addition of $SnCl_4$ (3.50 mL, 30.0 mmol), the reaction mixture was warmed to room temperature, dissolved in acetonitrile (25 mL) and stirred for 30 min. *n*-Pentane (20 mL) was injected into the solution, rapidly stirred for 3 min and then removed via PTFE cannula. This extraction was repeated ten times to remove Bu_3SnCl. The solvent was removed from the acetonitrile phase at reduced pressure, the remaining solid washed with *n*-pentane (20 mL) and dried *in vacuo*. **A** (6.59 g, 20.8 mmol, 69%) was obtained as a colorless solid. All analytical data are in agreement with reported data.[28]

Synthesis of $[(BnSn)_4S_6]$ (2)

A (1.00 g, 3.16 mmol) was dissolved in toluene (20 mL), $(Me_3Si)_2S$ (1.00 mL, 4.76 mmol) added and the solution stirred at room temperature. After 20 minutes, a colorless precipitate was formed that slowly turned yellow. After 35 minutes, the precipitate was filtered off. Leaving the filtrate standing for one day afforded **1** (280 mg, 0.27 mmol, 34%) as colorless crystals.

^{1}H-NMR (CD_2Cl_2, 300 MHz)**:** δ = 3.13 (s, 8H, -CH_2-), 7.14 (m, 12H, H_{ortho} + H_{para}), 7.28 (m, 8H, H_{meta}) ppm. **^{13}C-NMR** (CD_2Cl_2, 75 MHz)**:** δ = 36.9 (-CH_2-), 126.8 (C_{arom}), 128.9 (C_{arom}), 129.5 (C_{arom}) ppm. The quaternary carbon atom could not be detected. **^{119}Sn-NMR** (CD_2Cl_2, 112 MHz)**:** δ = 121 ($^{1}J_{SnC}$ = 110 Hz) ppm. **IR:** $\tilde{\nu}$ = 445 (s), 550 (m), 570 (m), 619 (w), 697 (s), 728 (s), 761 (s), 800 (m), 844 (w), 858 (m), 904 (m), 1028 (m), 1049 (m), 1109 (m), 1154 (w), 1179 (w), 1206 (m), 1259 (m), 1319 (w), 1334 (w), 1401 (m), 1451 (m), 1488 (m), 1509 (w), 1578 (w), 1595 (m) cm^{-1}. **Elemental Analysis:** found (calcd.): C 32.42 (32.60), H 2.79 (2.74), S 17.60 % (18.64 %).

Synthesis of $[(BnSn)_4Se_6]$ (3)

A (1.00 g, 3.16 mmol) was dissolved in toluene (20 mL), $(Me_3Si)_2Se$ (1.20 mL, 4.79 mmol) added and the solution stirred at room temperature. The solution immediately changed its color from colorless via yellow and orange to dark red, formation of a dark red precipitate occurred after 2-3 min. Filtration after 5 min afforded a clear red solution from which **2** (340 mg, 0.26 mmol, 33%) crystallized as orange blocks after one day.

^{1}H-NMR (CD_2Cl_2, 300 MHz)**:** δ = 3.27 (s, 8H, -CH_2-), 7.16 (m, 12H, H_{ortho} + H_{para}), 7.27 (m, 8H, H_{meta}) ppm. ^{13}C and ^{119}Sn NMR spectra could not be obtained due to the compound's low solubility. . **IR:** $\tilde{\nu}$ = 444 (s), 464 (w), 507 (w), 526 (w), 549 (m), 570 (m), 619 (w), 699 (s), 729 (s), 760 (s), 800 (m), 822 (w), 844 (m), 858 (m), 905 (m), 967 (w), 1029 (m), 1047 (m), 1109 (m), 1154 (w), 1205 (m), 1258 (m), 1319 (w), 1334 (w), 1400 (m), 1451 (m), 1488 (m), 1509 (w), 1588 (m), 1595 (m) cm^{-1}. **Elemental Analysis:** found (calcd.): C 24.98 (25.61), H 2.17 % (2.15 %),

Synthesis of R^1SnCy_3 (B)

4-Vinylethylbenzoate (600 mg, 3.38 mmol), tricyclohexylstannane (1.00 g, 2.70 mmol) and AIBN (10 mg, 0.06 mmol) were combined in a Schlenk tube und stirred at a temperature of 110°C for sixteen hours with addition of more AIBN (10 mg, 0.06 mmol) after eight hours. The residue was purified by column chromatography (SiO_2, petrol ether/ethyl acetate 9:1). **B** (909 mg, 1.66 mmol, 62%) was obtained as colorless oil.

^{1}H-NMR ($CDCl_3$, 300 MHz)**:** δ = 1.01 (m, 3H, -CH_3), 1.12-1.68 (m, 33H, C_6H_{11}), 1.79 (m, 2H, -$SnCH_2$-), 2.80 (m, 2H, -CH_2-) 4.29 (q, $^{1}J_{HH}$ =7.1 Hz, 2H, -OCH_2), 7.45 (d, $^{3}J_{HH}$ = 7.2 Hz, 2H, CH*arom*), 7.89 (d, $^{3}J_{HH}$ = 8.2 Hz, 2H, CH*arom*) ppm. **^{13}C-NMR** (CDCl3, 75 MHz)**:** δ = 8.4, 14.1, 26.1, 27.0, 29.0, 32.2, 33.3, 60.4, 127.3, 127.7, 129.5, 151.6, 166.5 ppm. **^{119}Sn-NMR** ($CDCl_3$, 187 MHz)**:** δ = –66 ppm. **HRMS (ESI+):** m/z calcd: 569.2417 $[C_{29}H_{46}O_2SnNa]^+$, found: 569.2420.

Synthesis of R^1SnCl_3(C)

B (909 mg, 1.66 mmol) was dissolved in *n*-pentane (24 mL). $SnCl_4$ (0.20 mL, 1.66 mmol) was slowly added and the reaction mixture stirred at room temperature for three hours. Acetonitrile (16 mL) was added and the stirring continued for 18 hours. The pentane layer was removed via PTFE cannula and the acetonitrile phase extracted three times with *n*-pentane (5 mL each). After solvent removal from the acetonitrile phase, **C** (490 mg, 1.22 mmol, 73%) was obtained as colorless solid.

^{1}H-NMR ($CDCl_3$, 300 MHz)**:** δ = 1.40 (t, $^{3}J_{HH}$ = 7.1 Hz, 3H, -CH_3), 2.62 (t, $^{3}J_{HH}$ = 7.8 Hz, 2H, -$SnCH_2$-), 3.26 (t, $^{3}J_{HH}$ = 7.8 Hz, 2H, -CH_2-) 4.38 (q, $^{1}J_{HH}$ = 7.1 Hz, 2H, -OCH_2), 7.33 (d, $^{3}J_{HH}$ = 8.3 Hz, 2H, -CH*arom*), 8.04 (d, $^{3}J_{HH}$ = 8.3 Hz, 2H, -CH*arom*) ppm. **^{13}C-NMR** (CDCl3, 75 MHz)**:** δ = 14.0, 30.3, 32.8, 60.9, 127.8, 129.6, 130.3, 144.5, 165.9 ppm. **^{119}Sn-NMR** ($CDCl_3$, 187 MHz)**:** δ = 2 ppm.

Synthesis of $[(R^1Sn)_4S_6]$ (4)

10 (370 mg, 0.92 mmol) was dissolved in toluene (15 mL). $(Me_3Si)_2S$ (0.30 mL, 1.43 mmol) was added and the solution stirred at room temperature for two hours. After solvent removal *in vacuo*, the residue was taken up in *n*-pentane (10 mL), filtered and dried. **3** (219 mg, 0.16 mmol, 69%) was obtained as a light yellow solid.

^{1}H-NMR ($CDCl_3$, 300 MHz)**:** δ = 1.39 (t, $^{3}J_{HH}$ = 7.1 Hz, 3H, -CH_3), 2.12 (t, $^{3}J_{HH}$ = 7.8 Hz, 2H, -$SnCH_2$-), 3.16 (t, $^{3}J_{HH}$ = 7.8 Hz, 2H, -CH_2-), 4.37 (q, $^{1}J_{HH}$ = 7.1 Hz, 2H, -OCH_2), 7.30 (d, $^{3}J_{HH}$ = 8.1 Hz, 2H, -CH*arom*), 8.00 (d, $^{3}J_{HH}$ = 8.2 Hz, 2H, -CH*arom*) ppm. **^{13}C-NMR** (CDCl3, 75 MHz)**:** δ = 14.9, 30.5, 31.2, 61.5, 128.6, 129.6, 130.7, 147.6, 167.1 ppm. **^{119}Sn-NMR** ($CDCl_3$, 187 MHz)**:** δ = 141 ($^{1}J_{SnC}$ = 109 Hz) ppm. **HRMS (ESI+):** m/z calcd: 1396.7962 $[C_{44}H_{52}O_8Sn_4S_6Na]^+$, found: 1396.7970. **IR:** $\tilde{\nu}$ = 3018 (w), 2957 (w), 2921 (w), 2847 (w), 1665 (w), 1590 (m), 1489 (m), 1451 (m), 1412 (m), 1333 (w), 1248 (w), 1203 (w), 1177 (w), 1152 (w), 1091 (w), 1043 (m), 1027 (m), 901 (m), 861 (m), 840 (w), 816 (w), 795 (w), 752 (m), 722 (m), 688 (m), 619 (w),563 (w), 548 (m), 622 (w), 561 (w), 548 (m), 497 (w), 476 (w), 400 (s) cm^{-1}. **Elemental Analysis:** found (calcd.): C 37.52 (38.40), H 4.12 (3.81), S 13.24 % (13.98 %).

Synthesis of $[(R^1Sn)_4Se_6]$ (5)

C (107 mg, 0.266 mmol) was dissolved in toluene (7 mL) and reacted with $(Me_3Si)_2Se$ (0.10 mL, 0.400 mmol). The clear yellow solution was stirred at room temperature for sixteen hours. Solvent removal *in vacuo* afforded **4** (97 mg, 0.058 mmol, 88%) as a dark orange solid.

^{1}H-NMR ($CDCl_3$, 300 MHz)**:** δ = 1.37 (t, 3H, -CH_3), 2.21 (t, 2H, -$SnCH_2$-), 3.09 (t, 2H, -CH_2-), 4.34 (q, 2H, -OCH_2-), 7.34 (d, 2H, CH_{arom}), 7.98 (d, 2H, CH_{arom}) ppm. **^{13}C-NMR** (CDCl3, 75 MHz)**:** δ = 14.7, 29.2, 32.0, 61.4, 128.8, 129.6, 130.5, 147.7, 166.8 ppm. **^{119}Sn-NMR** ($CDCl_3$, 187 MHz)**:** δ = –33 ($^{1}J_{SnC}$ = 133 Hz, $^{1}J_{SnSe}$ = 749 Hz) ppm. **IR:** $\tilde{\nu}$ = 2962 (m), 2907 (m), 2840

(m), 1708 (s), 1606 (m), 1574 (w), 1507 (w), 1455 (w), 1441 (w), 1413 (m), 1389 (w), 1362 (m), 1305 (w), 1258 (s), 1173 (m), 1095 (s), 1016 (s), 791 (s), 753 (m), 703 (m), 665 (w), 634 (w), 597 (w), 571 (w), 485 (w) cm^{-1}. **Elemental Analysis:** found (calcd.): C 32.25 (31.88), H 3.24 % (3.16 %).

Synthesis of $[(CpSn)_4S_6]$ (6)

NaCp (754 mg, 8.56 mmol) was suspended in toluene (20 mL), cooled to 0°C and a solution of $SnCl_4$ (1.00 mL, 8.56 mmol) in toluene (10 mL) was added dropwise. After stirring for 5 hours, the reaction mixture was filtered to remove NaCl. $(Me_3Si)_2S$ (2.70 mL, 12.86 mmol) was added to the filtrate. After ca. 10 min, a light yellow precipitate formed. Stirring was continued for one hour and the product collected by filtration and drying *in vacuo*. **5** (1.15 g, 1.24 mmol, 58%) was obtained as a yellow solid.

^{1}H-NMR (CD_2Cl_2, 300 MHz)**:** δ = 6.24 (s, 20H, C_5H_5) ppm. **^{13}C-NMR** (CD_2Cl_2, 75 MHz)**:** δ = 116.9 (s, C_5H_5) ppm. **^{119}Sn-NMR** (CD_2Cl_2, 112 MHz)**:** δ = 145 ($^1J_{SnC}$ = 100Hz) ppm **IR:** $\tilde{\nu}$ = 1380 (w), 1288 (w), 1250 (w), 1108 (w), 1085 (w), 1019 (w), 981 (w), 953 (w), 919 (m), 897 (m), 815 (w), 745 (s), 638 (m), 562 (w), 464 (w) cm^{-1}. **Elemental Analysis:** found (calcd.): C 21.91 (25.90), H 1.99 (2.17), S 21.08 % (20.74 %).

Synthesis of $[(CpSn)_4Se_6]$ (7)

NaCp (754 mg, 8.56 mmol) was suspended in toluene (20 mL), cooled to 0°C and a solution of $SnCl_4$ (1.00 mL, 8.56 mmol) in toluene (10 mL) was added dropwise. After stirring for 5 hours, the reaction mixture was filtered to remove NaCl. $(Me_3Si)_2Se$ (3.30 mL, 13.2 mmol) was added to the filtrate. Immediately, an orange precipitate was formed that was collected by filtration and dried *in vacuo*. **6** (1.22 g, 1.01 mmol, 47%) was obtained as an orange powder.

^{1}H-NMR (CD_2Cl_2, 300 MHz)**:** δ = 6.27 (s, 20H, C_5H_5) ppm. **^{13}C-NMR** (CD_2Cl_2, 75 MHz)**:** δ = 116.7 (s, C_5H_5) ppm. **^{119}Sn-NMR** (CD_2Cl_2, 112 MHz)**:** δ = –113 ($^1J_{SnC}$ = 153 Hz, $^1J_{SnSe}$ = 764 Hz) ppm. **IR:** $\tilde{\nu}$ = 1430 (w), 1377 (w), 1288 (w), 1223 (w), 1007 (w), 1083 (w), 1020 (w), 982 (w), 952 (w), 892 (m), 815 (w), 741 (s), 630 (m), 565 (w), 463 (w) cm^{-1}. **Elemental Analysis:** found (calcd.): C 19.73 (19.87), H 1.71 % (1.67 %).

Synthesis of $CySnCl_3$ (D)

Tetracyclohexyltin (6.93 g, 15.4 mmol) and $SnCl_4$ (5.40 mL, 46.2 mmol) were combined and heated to 140°C for 3 hours. During this time, the initially yellow suspension turned grey. Fractional distillation afforded **D** (7.40 g, 24.0 mmol, 39%) as a colorless oil.

Boiling point: 36°C/1.2·10^{-2} mbar. **^{1}H-NMR** ($CDCl_3$, 300 MHz)**:** δ = 0.99 (t, $^3J_{HH}$ = 7.3 Hz, 4H), 1.51 (m, 3H), 1.91 (dt, $^3J_{HH}$ = 12.6 , 7.5 Hz, 2H), 2.39 (t, $^3J_{HH}$ = 7.5 Hz, 2H) ppm.

Synthesis of $[(CySn)_4S_6]$ (8)

D (0.50 mL, 3.24 mmol) was dissolved in toluene (20 mL), $(Me_3Si)_2S$ (1.05 mL, 5.00 mmol) was added and the clear colorless solution stirred at room temperature for one day. Removal of all volatile components *in vacuo* afforded **7** (0.79 g, 0.79 mmol, 98%) as a colorless solid.

^{1}H-NMR (CD_2Cl_2, 300 MHz)**:** δ = 0.94 (m, 16H), 1.45 (m, 12H), 1.80 (m, 16H) ppm. **^{13}C-NMR** (CD_2Cl_2, 75 MHz)**:** δ = 13.9, 26.5, 27.6, 30.5 ppm. **^{119}Sn-NMR** (CD_2Cl_2, 112 MHz)**:** δ = 145 ($^1J_{SnC}$ = 100 Hz) ppm. **IR:** $\tilde{\nu}$ = 2954 (m), 2913 (m), 2850 (m), 1455 (m), 1375 (m), 1337 (m), 1287 (w), 1241 (m), 1171 (m), 1142 (m), 1072 (w), 1014 (m), 958 (m), 865 (w), 835 (m), 766 (w), 744 (w), 701 (m), 669 (s), 630 (w), 595 (w), 509 (w), 451 (w), 407 (w) cm^{-1}. **Elemental Analysis:** found (calcd.): C xx.xx (28.83), H x.xx (4.44), S xx.xx % (19.24 %).

Synthesis of $[(CySn)_4Se_6]$ (9)

D (0.50 mL, 3.24 mmol) was dissolved in toluene (20 mL), $(Me_3Si)_2Se$ (1.25 mL, 5.00 mmol) was added and the clear yellow solution stirred at room temperature. After 30 minutes, a light yellow precipitate was formed that was collected by filtration after an additional 30 min. Drying *in vacuo* afforded **8** (0.58 g, 0.45 mmol, 56%) as a light yellow solid.

^{1}H-NMR (CD_2Cl_2, 300 MHz)**:** δ = 0.94 (t, 4H),1.46 (m, 3H), 1.75 (m, 2H), 1.94 (t, 2H) ppm. **^{13}C-NMR** (CD_2Cl_2, 75 MHz)**:** δ = 13.7 (Sn*C*), 26.2, 28.3, 29.4 ppm. **^{119}Sn-NMR** (CD_2Cl_2, 187 MHz)**:** δ = –22 ($^1J_{SnC}$ = 123 Hz, $^1J_{SnSe}$ = 752 Hz) ppm. **IR:** $\tilde{\nu}$ = 2948 (m), 2910 (m), 2842 (m), 1452 (m), 1440 (w), 1372 (w), 1339 (w), 1289 (w), 1238 (m), 1160 (w), 1132 (m), 1069 (w), 1008 (w), 955 (w), 860 (w), 838 (m), 766 (w), 741 (w), 699 (w), 663 (s), 585 (w)m 491 (w), 409 (w) cm^{-1}. **Elemental Analysis:** found (calcd.): C xx.xx (22.50), H x.xx % (3.46 %),

Quantum Chemical Investigations: Density functional theory calculations were carried out with TURBOMOLE[31] using def2-TZVP basis sets[32] and taking advantage of the multipole-accelerated resolution-of the-identity method.[33] Structures were optimized with the functional BP86;[34] the B3-LYP functional[35] was employed for the calculation of the excitations.

Acknowledgements

This work was supported by the Deutsche Forschungsgemeinschaft in the framework of GRK1782.

Keywords: organotetrel chalcogenide clusters • white-light generation • second-harmonic generation • substituent effects • quantum chemical calculations

[1] M. G. Kanatzidis, *Adv. Mater.* **2007**, *19*, 1165-1181.
[2] W. Schiwy, B. Krebs, *Angew. Chem. Int. Ed. Engl.* **1975**, *14*, 436-436; *Angew. Chem.* **1975**, *87*, 451-452.
[3] N. Kamaya, K. Homma, Y. Yamakawa, M. Hirayama, R. Kanno, M. Yonemura, T. Kamiyama, Y. Kato, S. Hama, K. Kawamoto, A. Mitsui, *Nature Mater.* **2011**, *10*, 682–686.
[4] N. Zheng, X. Bu, B. Wang, P. Feng, *Science* **2002**, *298*, 2366–2369.
[5] S. Bag, P. N. Trikalitis, P. J. Chupas, G. S. Armatas, M. G. Kanatzidis, *Science* **2007**, *317*, 490–493.
[6] R. L. Glitzendanner, F. J. DiSalvo, *Inorg. Chem.* **1996**, *35*, 2623–2626.
[7] L. Nicole, C. Laberty-Robert, L. Rozes, C. Sanchez, *Nanoscale* **2014**, *6*, 6267–6292.
[8] J.P. Eußner, B.E.K. Barth, E. Leusmann, Z. You, N. Rinn, S. Dehnen, *Chem. Eur. J.* **2013**, *19*, 13792–13802.
[9] J.P. Eußner, S. Dehnen, *Chem. Commun.* **2014**, *50*, 11385–11388.
[10] J.P. Eußner, R.O. Kusche, S. Dehnen, *Chem. Eur. J.* **2015**, *21*, 12376–12388.
[11] E. Leusmann, F. Schneck, S. Dehnen, *Organometallics* **2015**, *34*, 3264–3271.
[12] N. Rinn, J.P. Eußner, W. Kaschuba, X. Xie, S. Dehnen, *Chem. Eur. J.* **2016**, *22*, 3094–3104.
[13] N. Rinn, L. Guggolz, J. Lange, S. Chatterjee, T. Block, R. Pöttgen, S. Dehnen, *Chem. Eur. J.* **2018**, *24*, 5840–5848.
[14] N. W. Rosemann, J. P. Eußner, A. Beyer, S. W. Koch, K. Volz, S. Dehnen, S. Chatterjee, *Science* **2016**, *352*, 1301-1304.
[15] P. Pfeiffer, R. Lehnardt, *Ber. Dtsch. Chem. Ges.* **1903**, *36*, 3027–3030.

[16] C. Dörfelt, A. Janeck, D. Kobelt, E. F. Paulus, H. Scherer, *J. Organomet. Chem.* **1968**, *14*, P22–P24.
[17] J. C. J. Bart, J. J. Daly, *J. Chem. Soc. Dalton Trans.* **1975**, 2063–2068.
[18] H. Berwe, A. Haas, *Chem. Ber.* **1987**, *120*, 1175–1182.
[19] C. Wagner, C. Raschke, K. Merzweiler, *Appl. Organomet. Chem.* **2004**, *18*, 147.
[20] N. W. Rosemann, J. P. Eußner, E. Dornsiepen, S. Chatterjee, S. Dehnen, *J. Am. Chem. Soc.* **2016**, *138*, 16224-16227.
[21] K. Wraage, T. Pape, R. Herbst-Irmer, M. Noltemeyer, H. G. Schmidt, H. W. Roesky, *Eur. J. Inorg. Chem.* **1999**, 869-872.
[22] E. Dornsiepen, F. Dobener, N. Mengel, O. Lenchuk, C. Dues, S. Sanna, D. Mollenhauer, S. Chatterjee, S. Dehnen, *Adv. Opt. Mater.* **2019**, *7*, DOI: 10.1002/adom.201801793.
[23] H. Zimmer, W. Sparmann, *Chem. Ber.* **1954**, *87*, 645-651.
[24] J. H. So, P. Boudjouk, P., *Synthesis* **1989**, 306-307.
[25] M. W. DeGroot, N. J. Taylor, J. F. Corrigan, *J. Mater. Chem.* **2004**, *14*, 654-660.
[26] T. K. Panda, M. T. Gamer. P. W. Roesky, *Ogranometallics* **2003**, *22*, 877-878.
[27] E. Krause, R. Pohland, *Ber. Dtsch. Chem. Ges.* **1924**, *58*, 532-544.
[28] D. V. Airapetyan, V. S. Petrosyan, S. V. Gruener, K.. V. Zaitsev, D. E. Arkhipov, A. A. Korlyukov, *J. Organomet. Chem.* **2013**, *747*, 241-248.
[29] S. Cho, B. Ma, S. T. Nguyen, J. T. Hupp, T. E. Albrecht-Schmitt, *Chem. Commun.* **2006**, *24*, 2563-2565.
[30] B. Jousseaume, M. Lahcini, M.-C. Rascle, *Organometallics* **1995**, *14*, 685-689.
[31] TURBOMOLE Version 7.3, TURBOMOLE GmbH 2018. TURBOMOLE is a development of University of Karlsruhe and Forschungszentrum Karlsruhe 1989 –2007, TURBOMOLE GmbH since 2007.
[32] K. Eichkorn, F. Weigend, O. Treutler, R. Ahlrichs, *Theor. Chem. Acc.* **1997**, *97*, 119.
[33] M. Sierka, A. Hogekamp, R. Ahlrichs, *J. Chem. Phys.* **2003**, *118*, 9136 – 9148.
[34] a) A. Becke, *Phys. Rev. A* **1988**, *38*, 3098 – 3100; b) J. Perdew, *Phys. Rev. B* **1986**, *33*, 8822 –8824.
[35] C. Lee, W. Yang, R. G. Parr, *Phys. Rev. B.* **1988**, *37*, 785 –789.

Supporting Information

Controlling the White-Light Generation of [(RSn)$_4$E$_6$]: Effects of substituent and chalcogenide variation

*Eike Dornsiepen, Florian Dobener, Nils Mengel, Sangam Chatterjee, and Stefanie Dehnen**

Content

1. NMR spectra

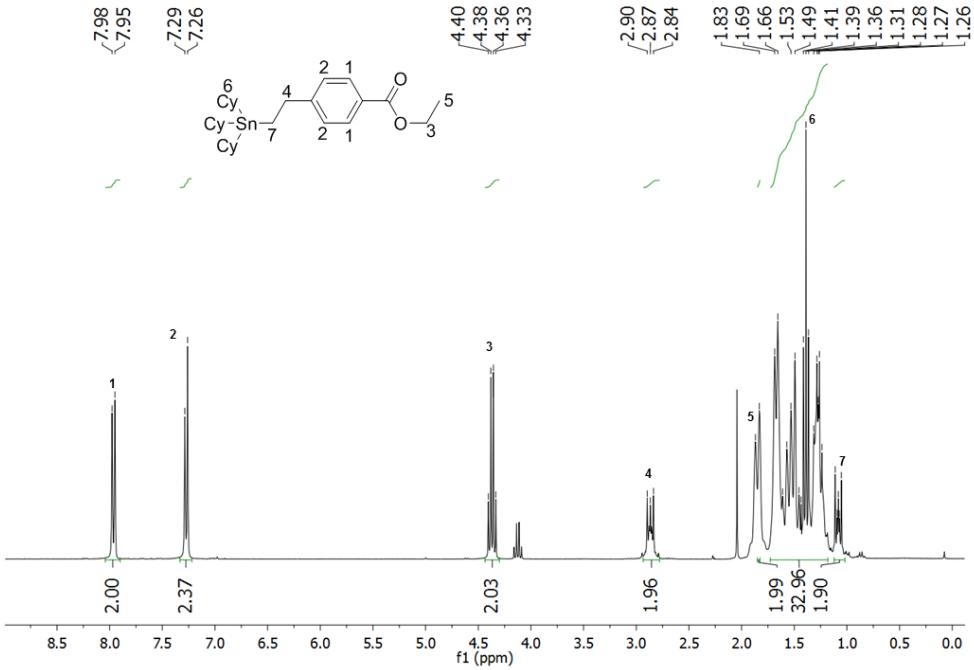

Figure S1: ^{1}H NMR spectrum of **B** (300 MHZ, 25°C, $CDCl_3$).

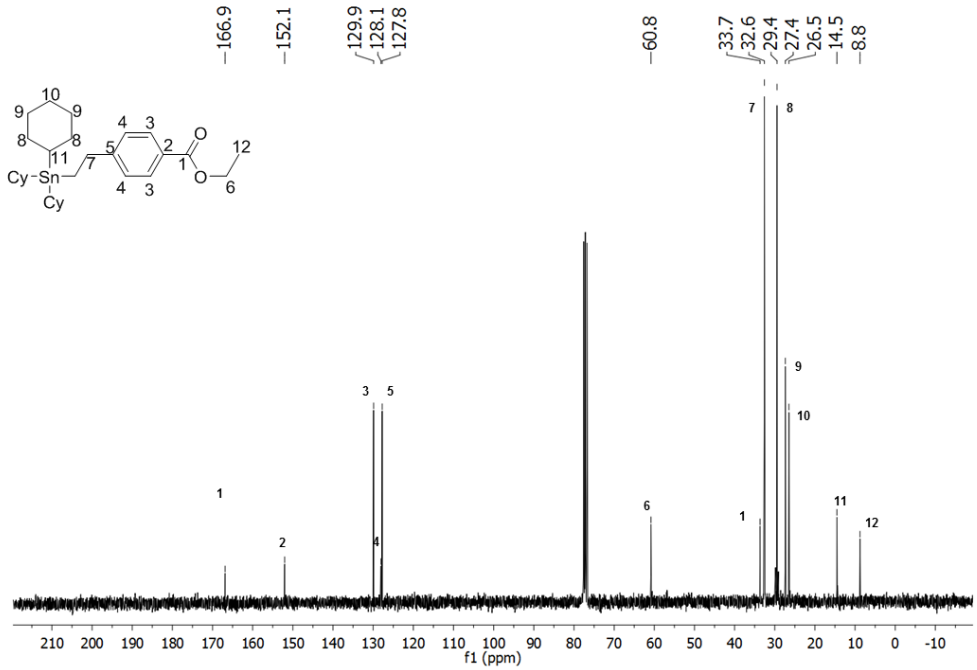

Figure S2: ^{13}C NMR spectrum of **B** (75 MHZ, 25°C, $CDCl_3$).

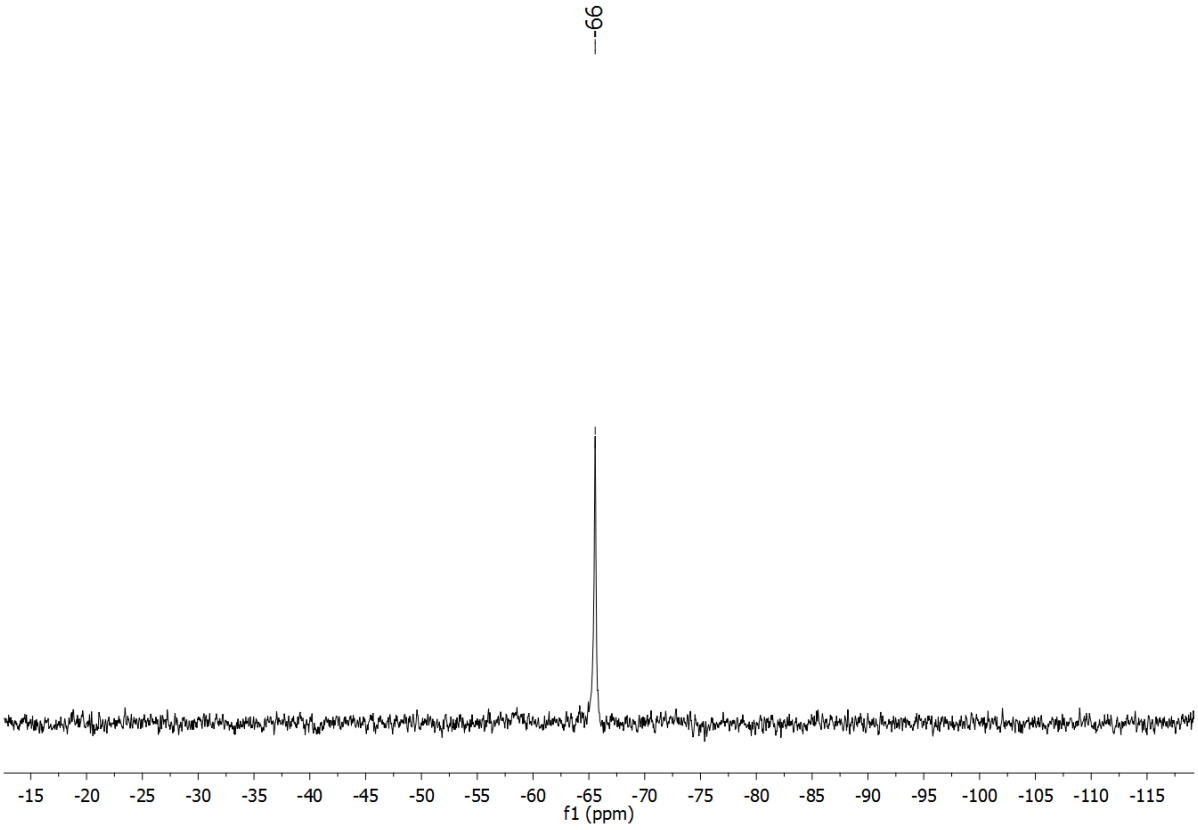

Figure S3: ^{119}Sn NMR spectrum of **B** (112 MHZ, 25°C, $CDCl_3$).

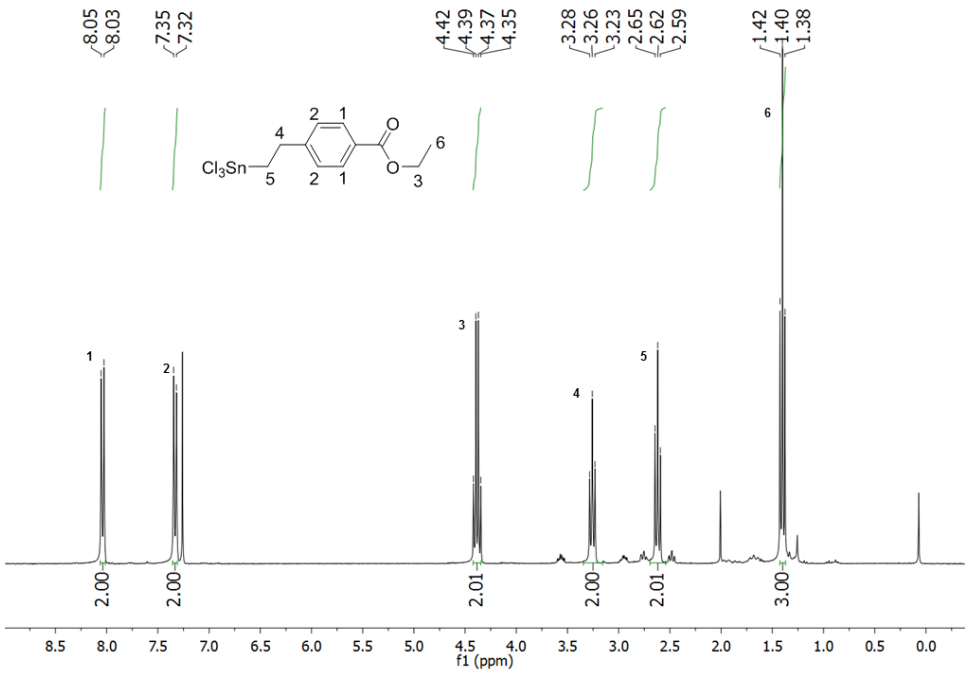

Figure S4: ^{1}H NMR spectrum of **C** (300 MHZ, 25°C, $CDCl_3$).

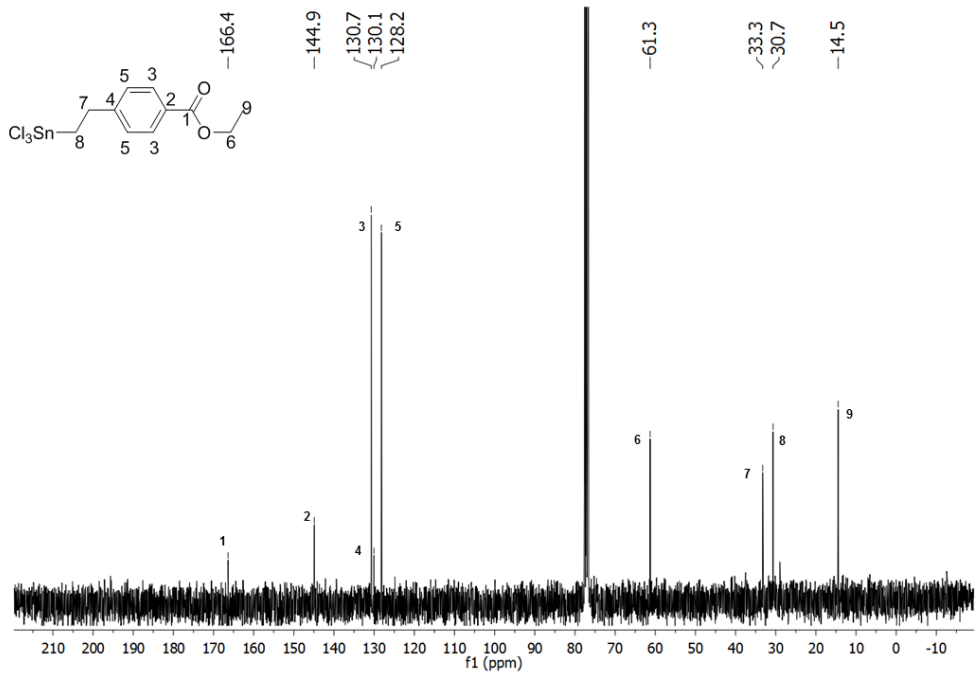

Figure S5: ^{13}C NMR spectrum of **C** (75 MHZ, 25°C, $CDCl_3$).

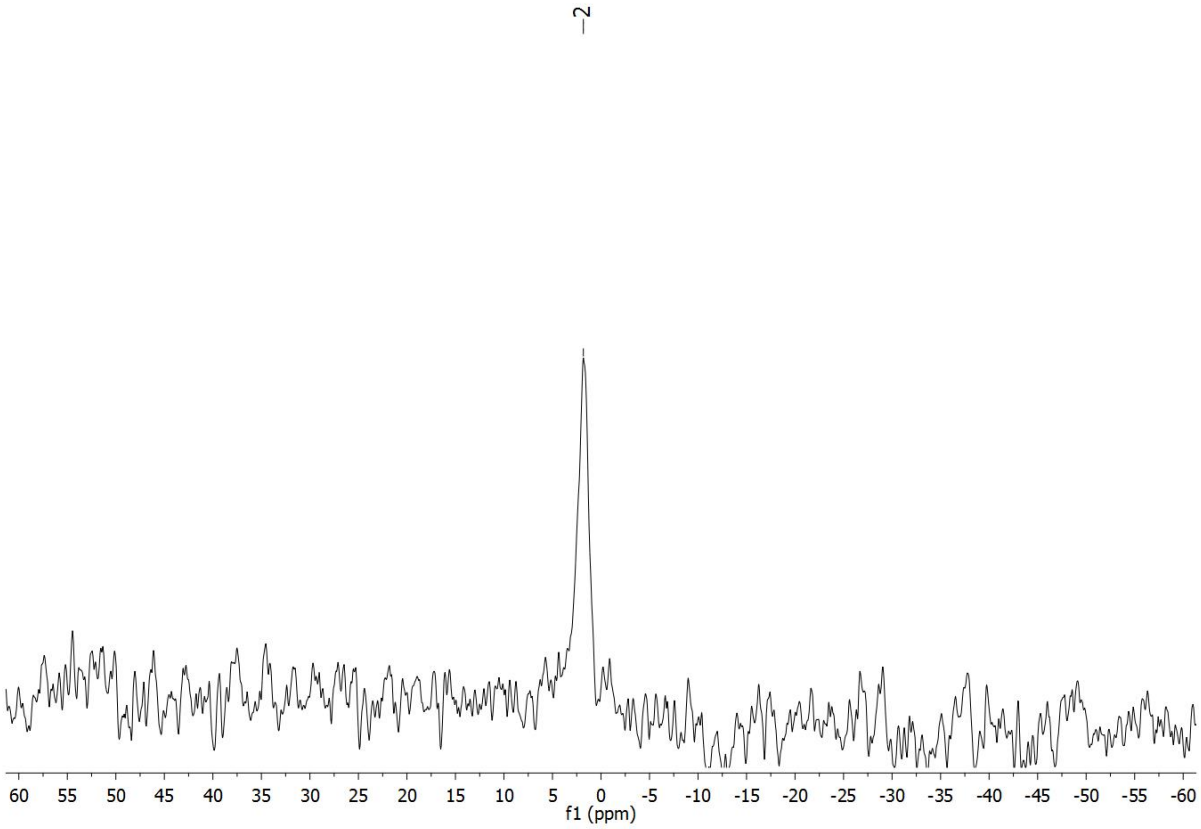

Figure S6: ^{119}Sn NMR spectrum of **C** (112 MHZ, 25°C, $CDCl_3$).

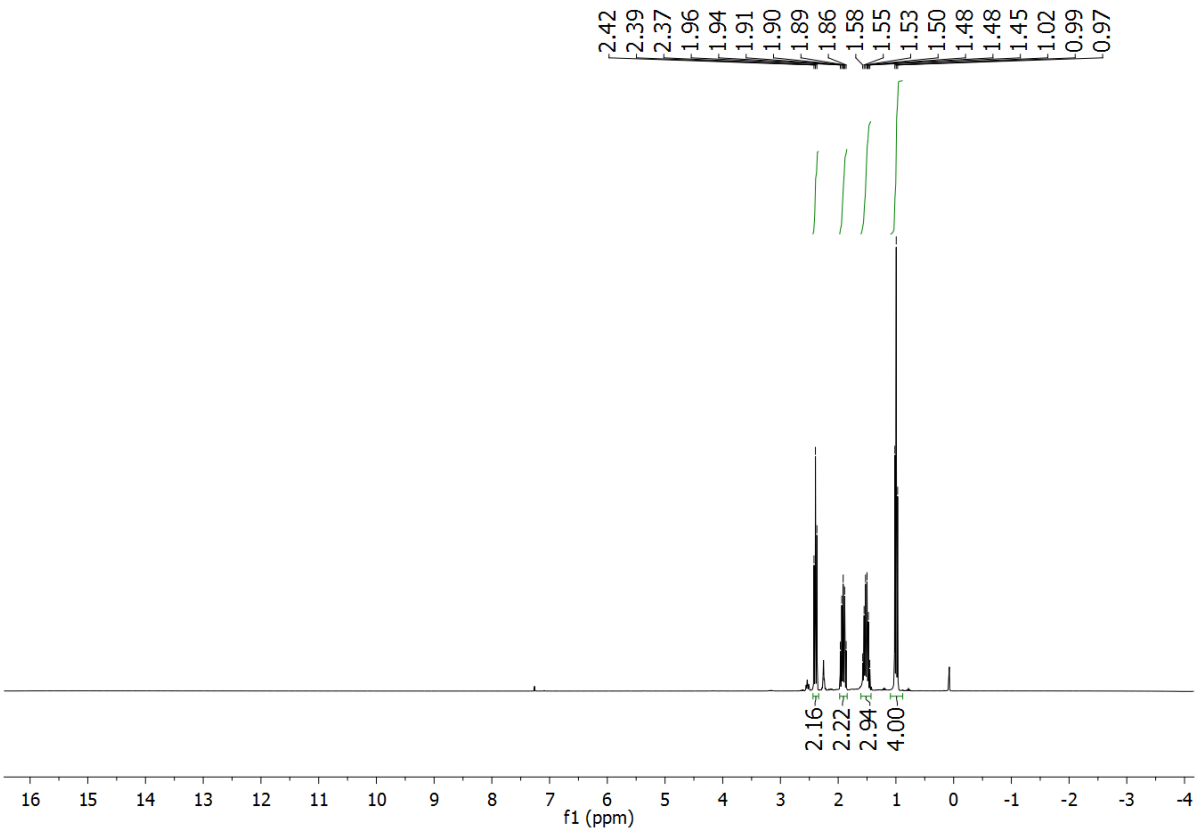

Figure S7: ^{1}H NMR spectrum of **D** (300 MHZ, 25°C, $CDCl_3$).

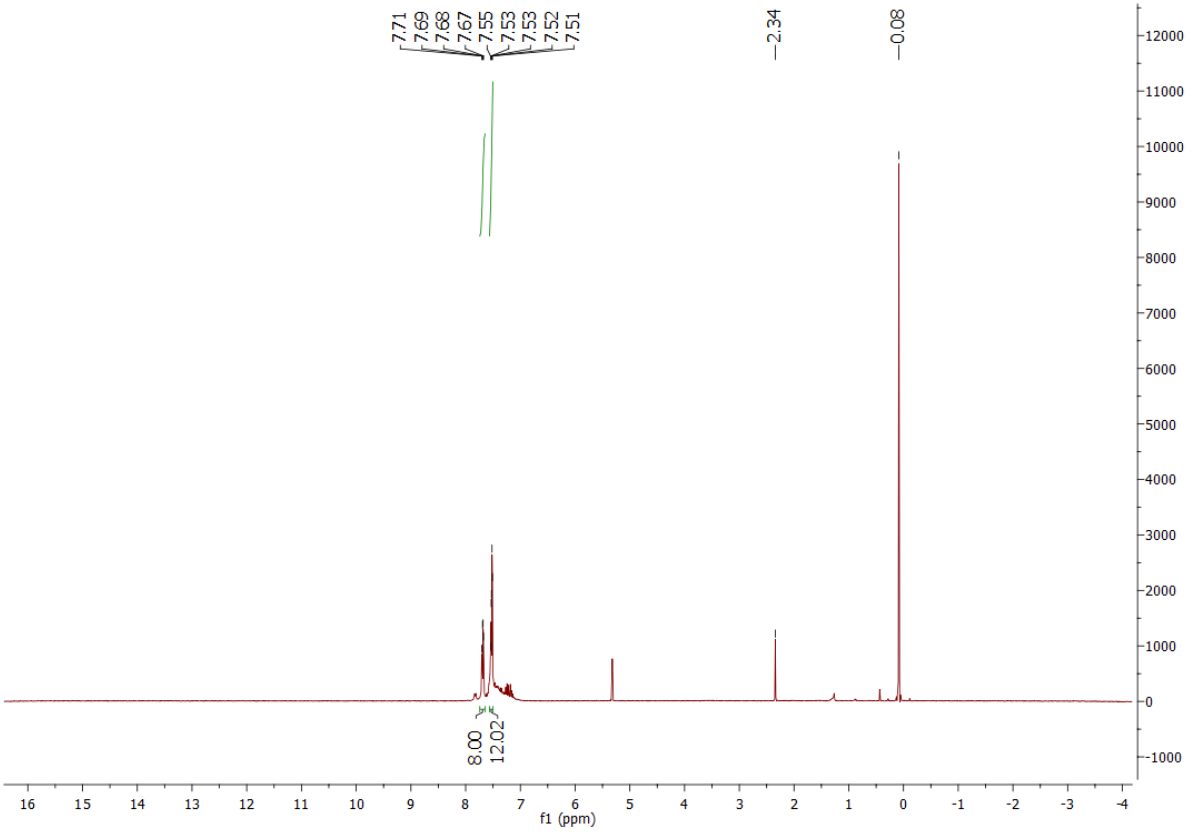

Figure S8: ^{1}H NMR spectrum of **1** (300 MHZ, 25°C, CD_2Cl_2).

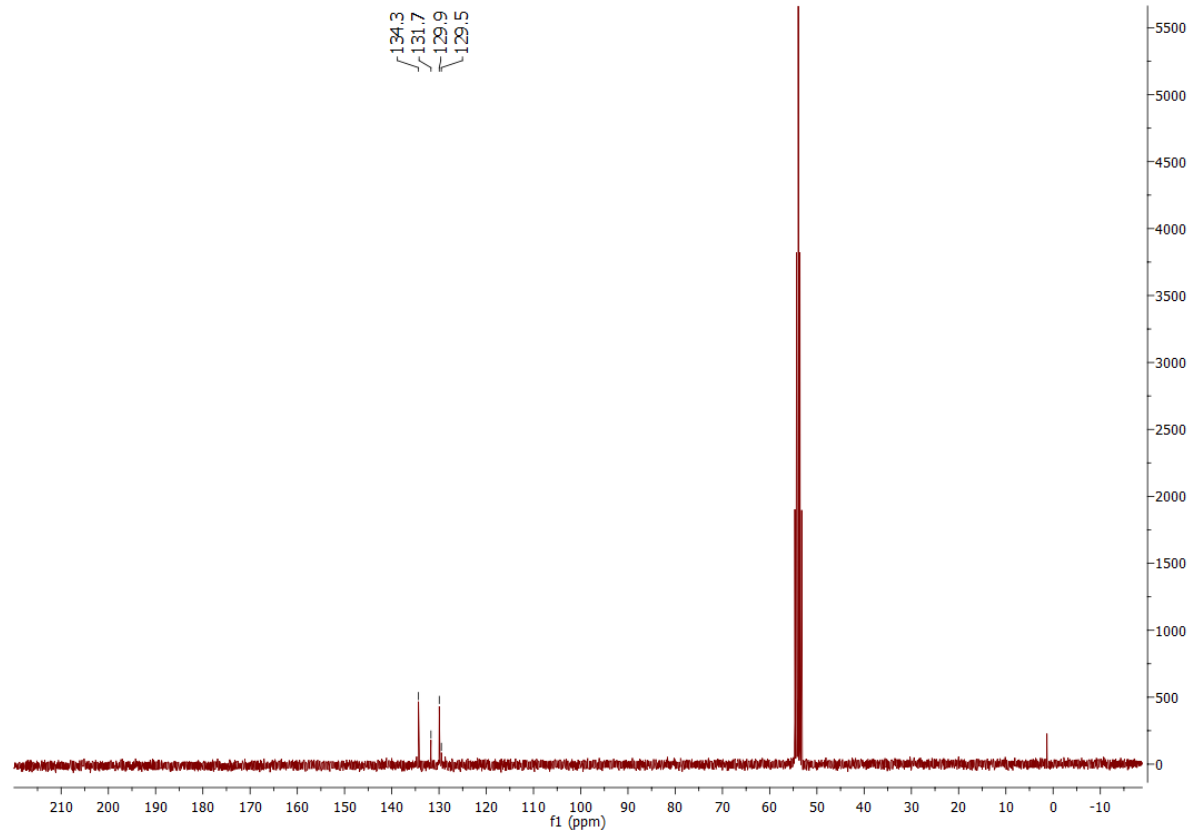

Figure S9: ^{13}C NMR spectrum of **1** (75 MHZ, 25°C, CD_2Cl_2).

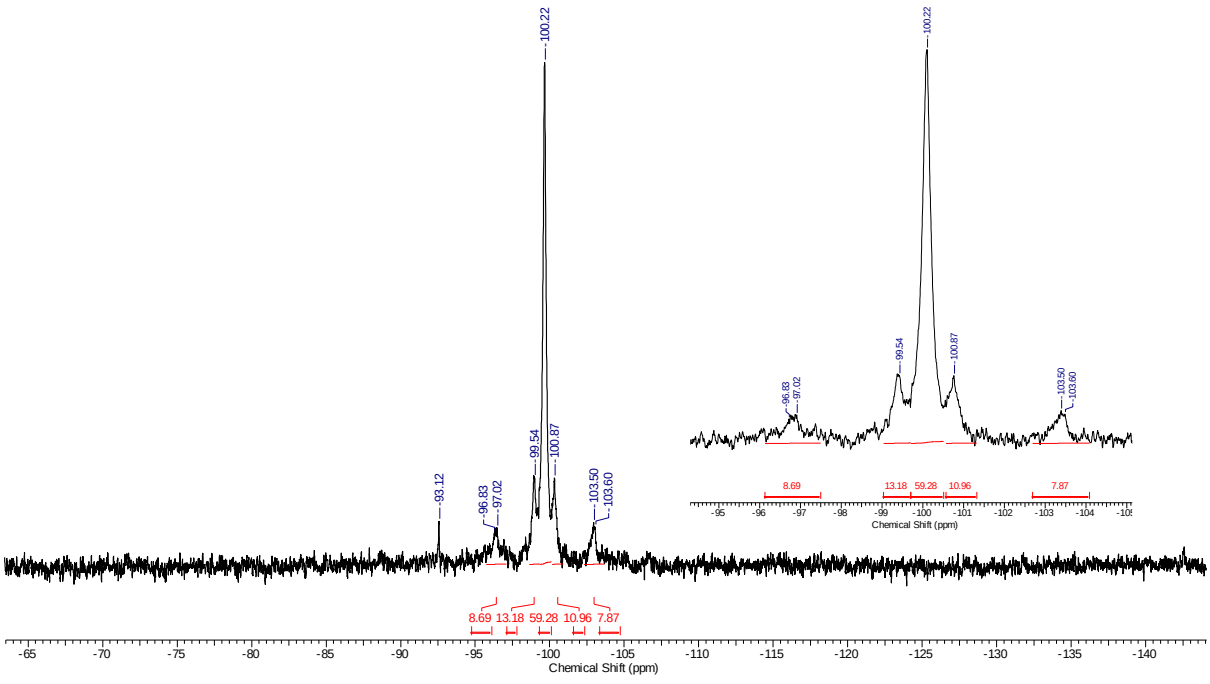

Figure S10: ^{119}Sn NMR spectrum of **1** (196 MHZ, 25°C, CD_2Cl_2).

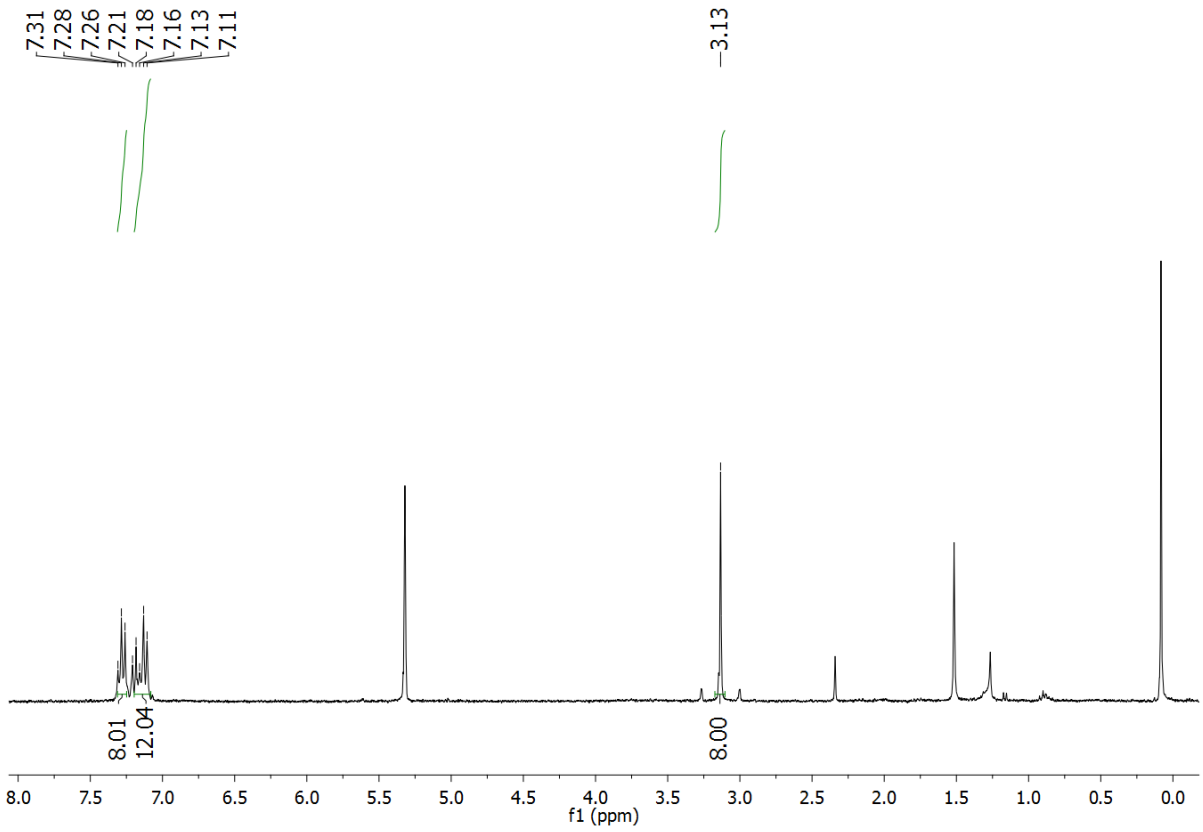

Figure S11: ^{1}H NMR spectrum of **2** (300 MHZ, 25°C, CD_2Cl_2).

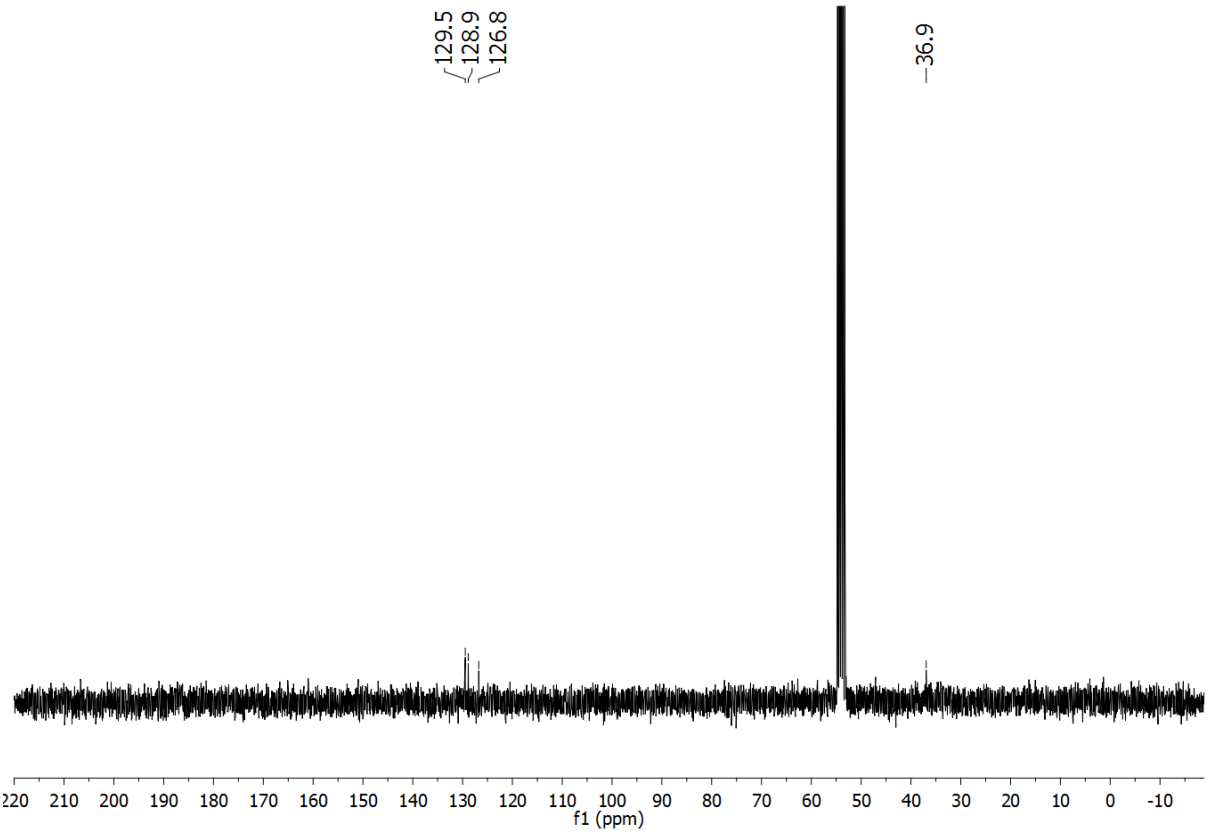

Figure S12: ^{13}C NMR spectrum of **2** (75 MHZ, 25°C, CD_2Cl_2).

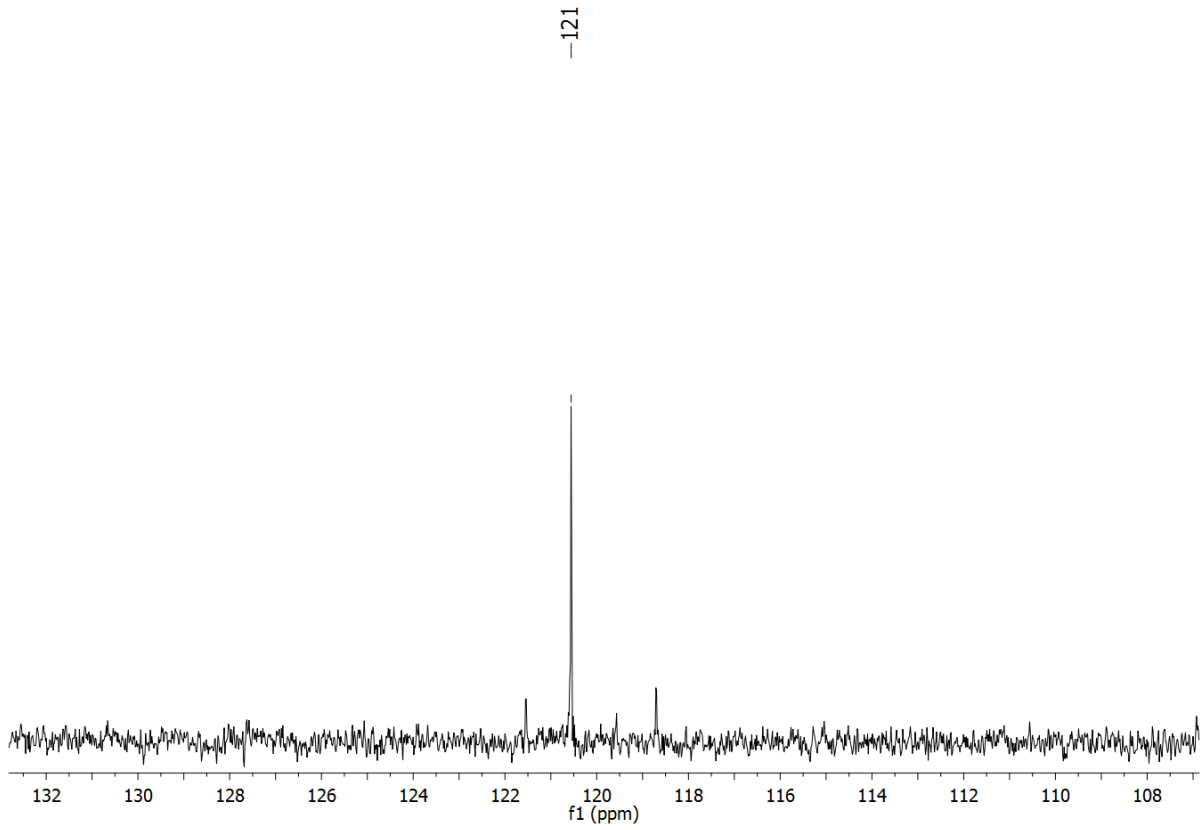

Figure S13: ^{119}Sn NMR spectrum of **2** (112 MHZ, 25°C, CD_2Cl_2).

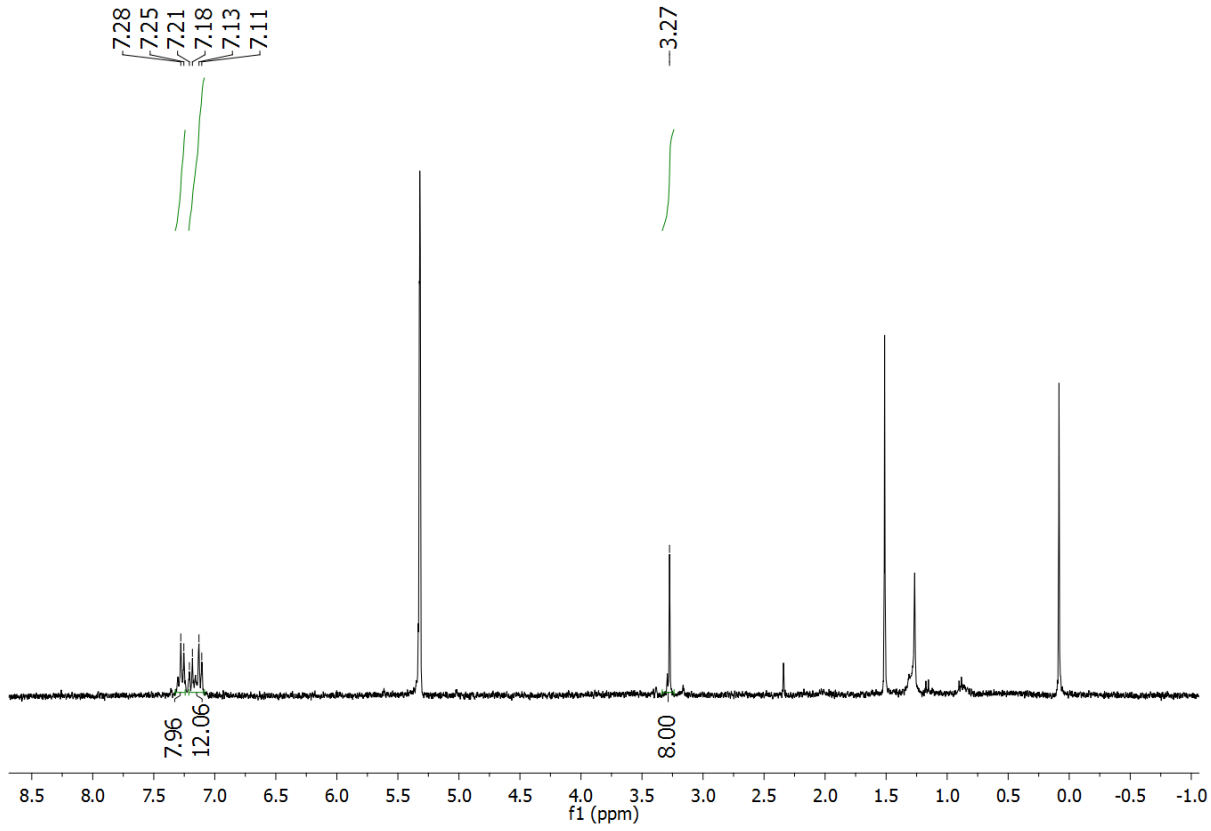

Figure S14: ^{1}H NMR spectrum of **3** (300 MHZ, 25°C, CD_2Cl_2).

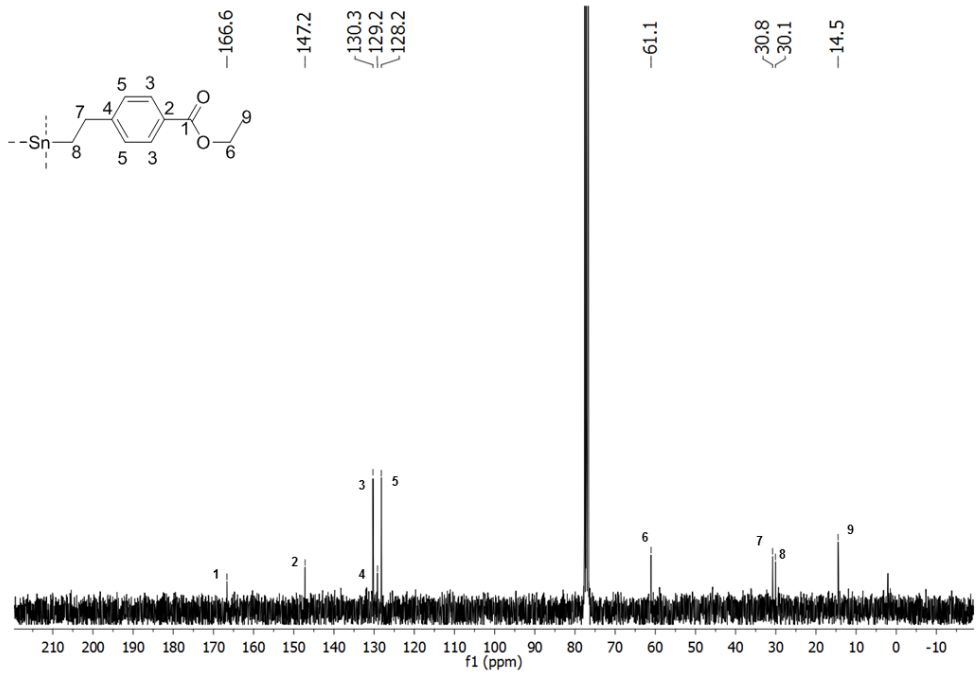

Figure S15: ^{1}H NMR spectrum of **4** (300 MHZ, 25°C, $CDCl_3$).

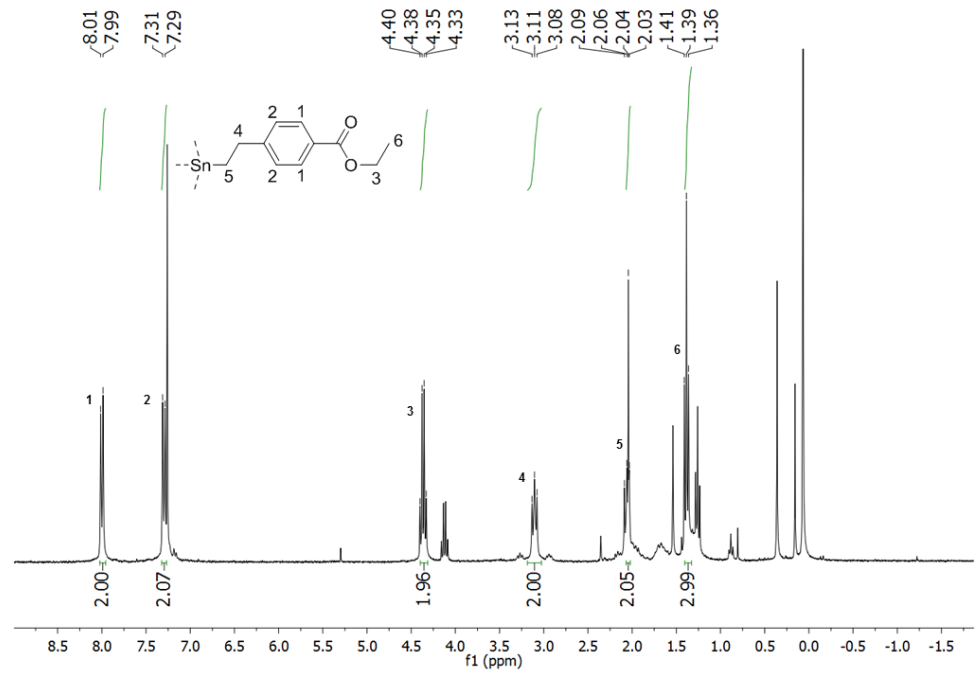

Figure S16: ^{13}C NMR spectrum of **4** (75 MHZ, 25°C, $CDCl_3$).

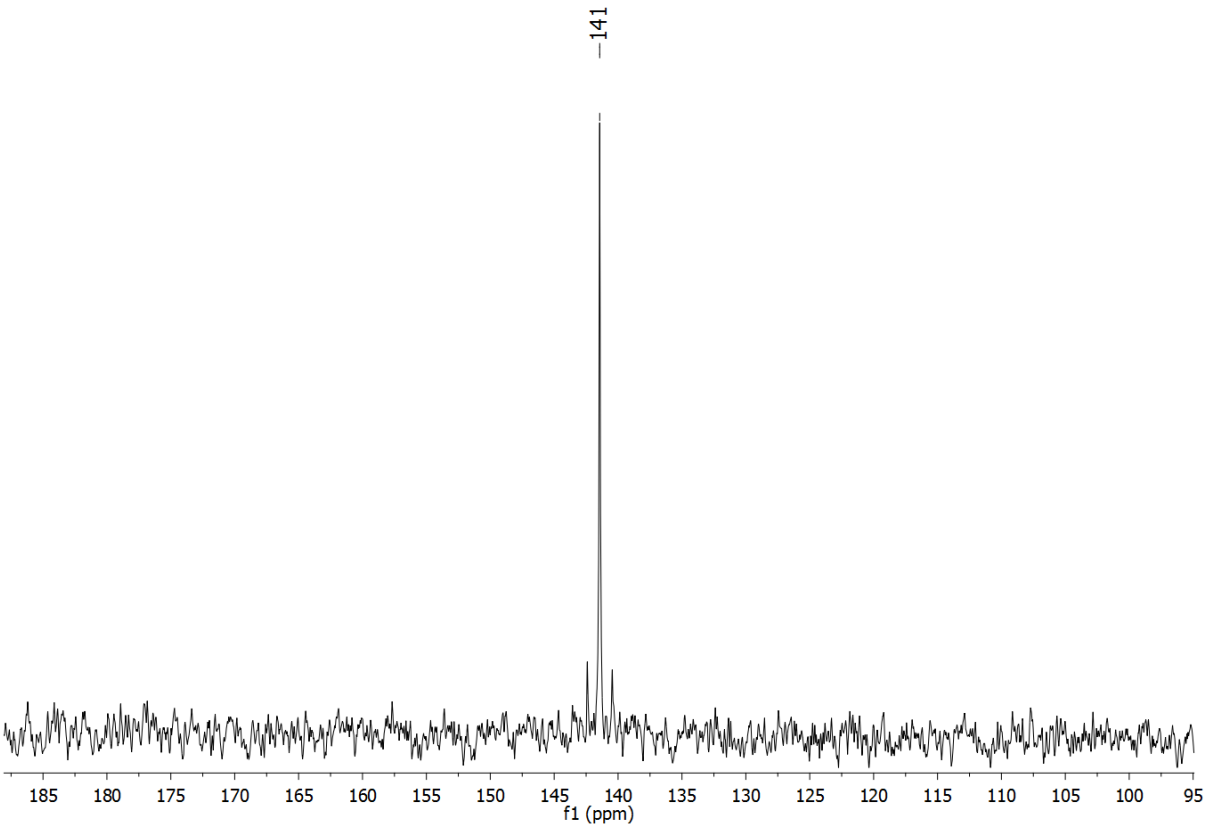

Figure S17: ^{119}Sn NMR spectrum of **4** (112 MHZ, 25°C, $CDCl_3$).

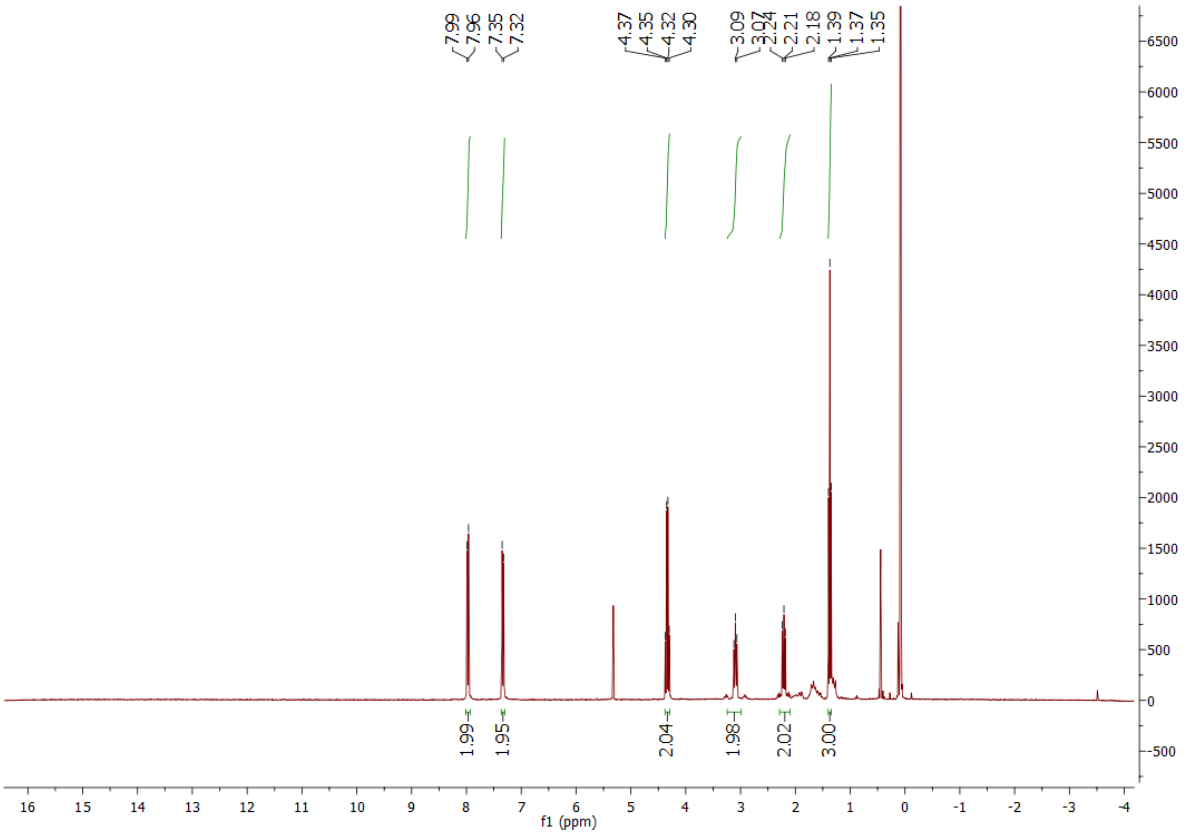

Figure S18: ^{1}H NMR spectrum of **5** (300 MHZ, 25°C, CD_2Cl_2).

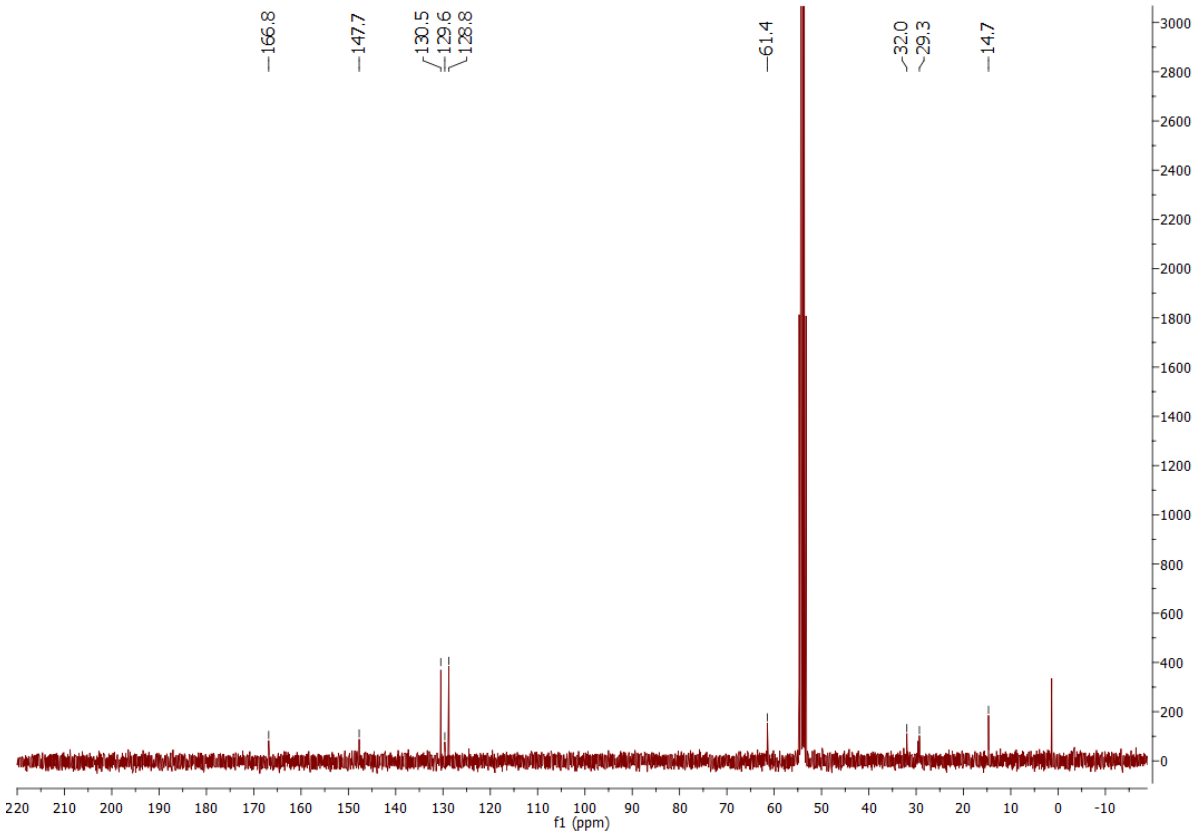

Figure S19: ^{13}C NMR spectrum of **5** (75 MHZ, 25°C, CD_2Cl_2).

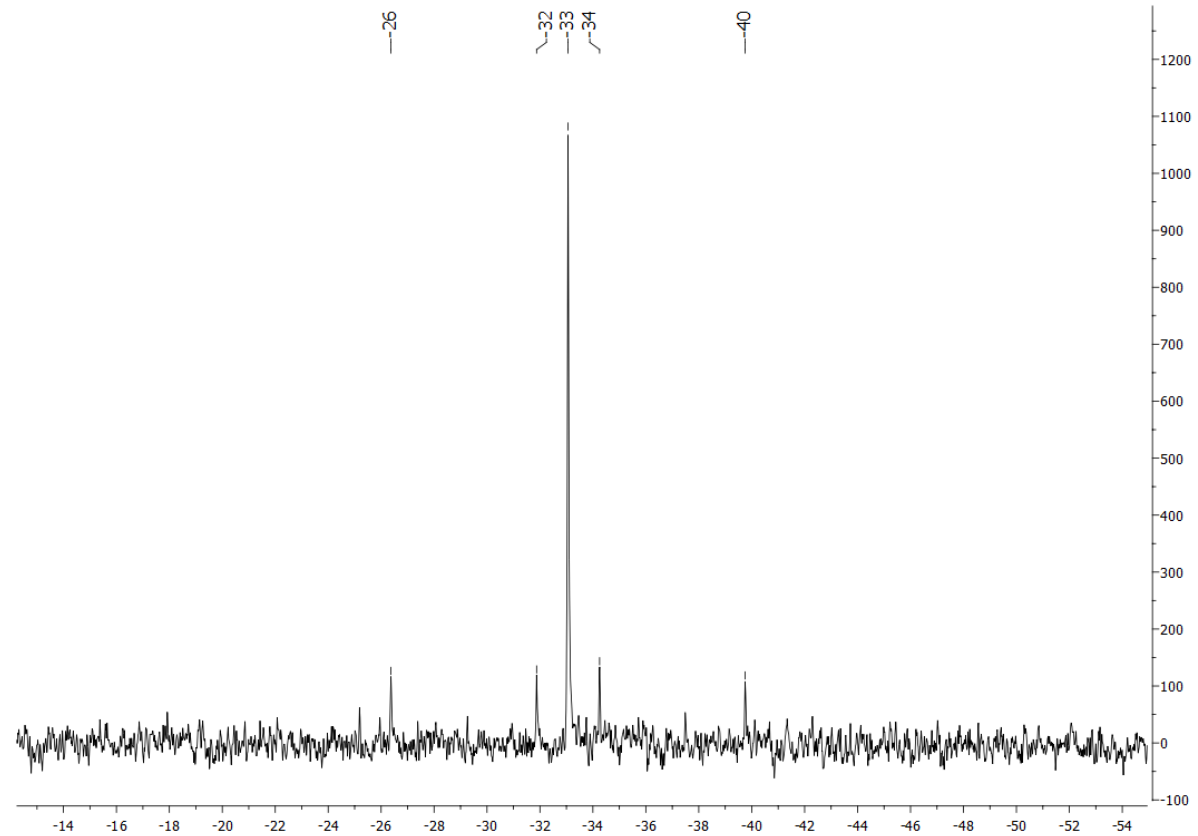

Figure S20: ^{119}Sn NMR spectrum of **5** (112 MHZ, 25°C, CD_2Cl_2).

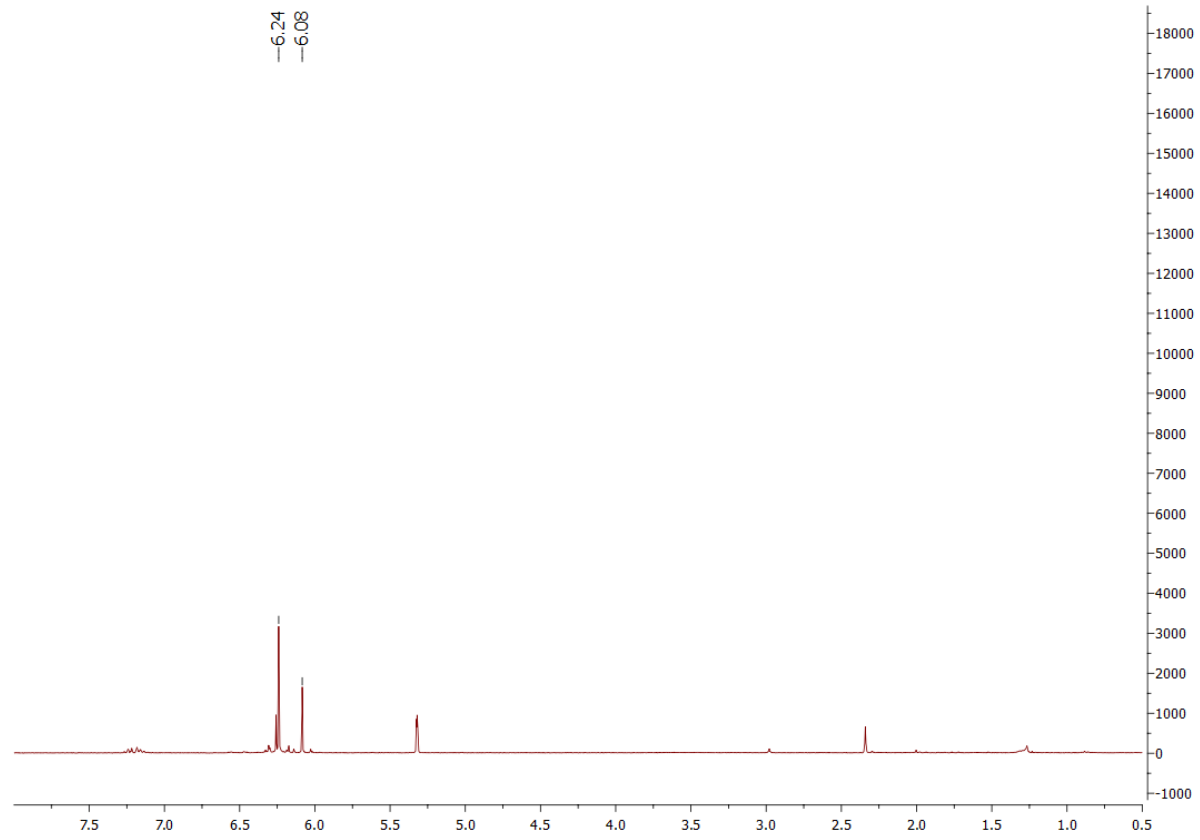

Figure S21: ^{1}H NMR spectrum of **6** (300 MHZ, 25°C, CD_2Cl_2)

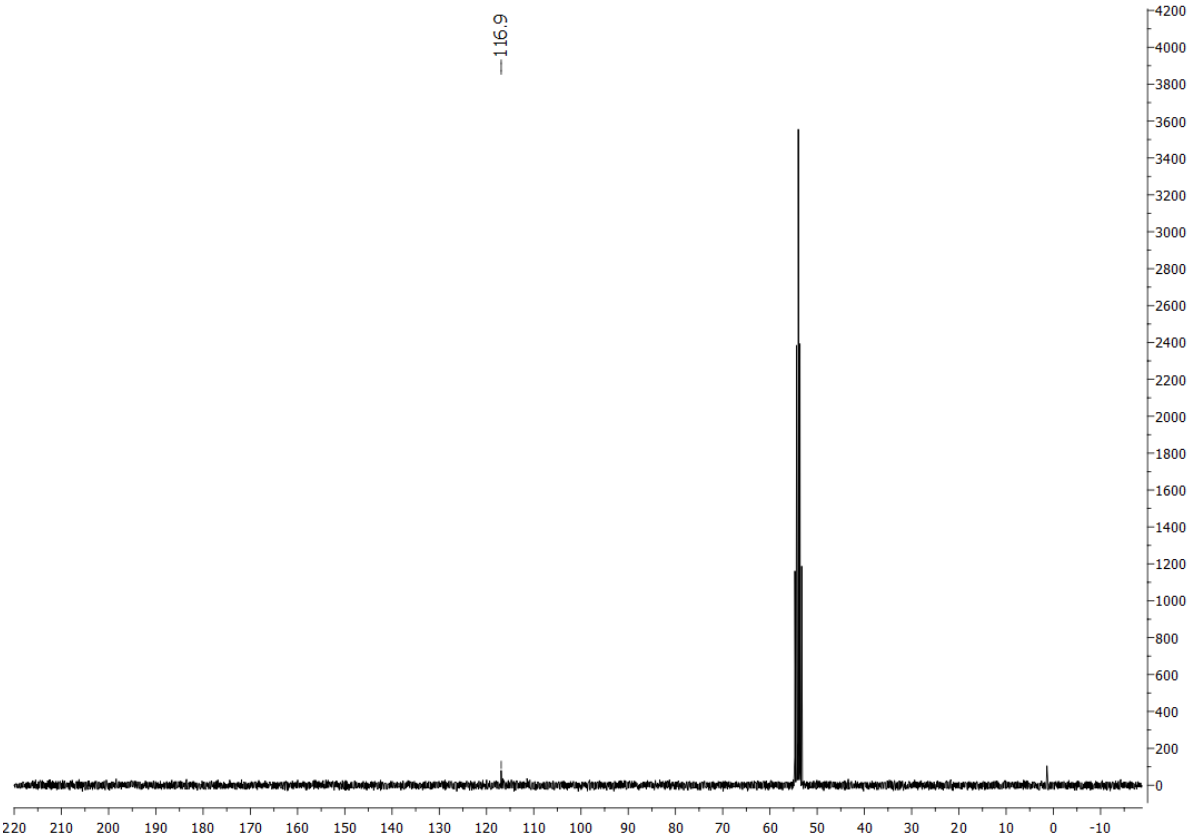

. **Figure S22:** ^{13}C NMR spectrum of **6** (75 MHZ, 25°C, CD_2Cl_2)

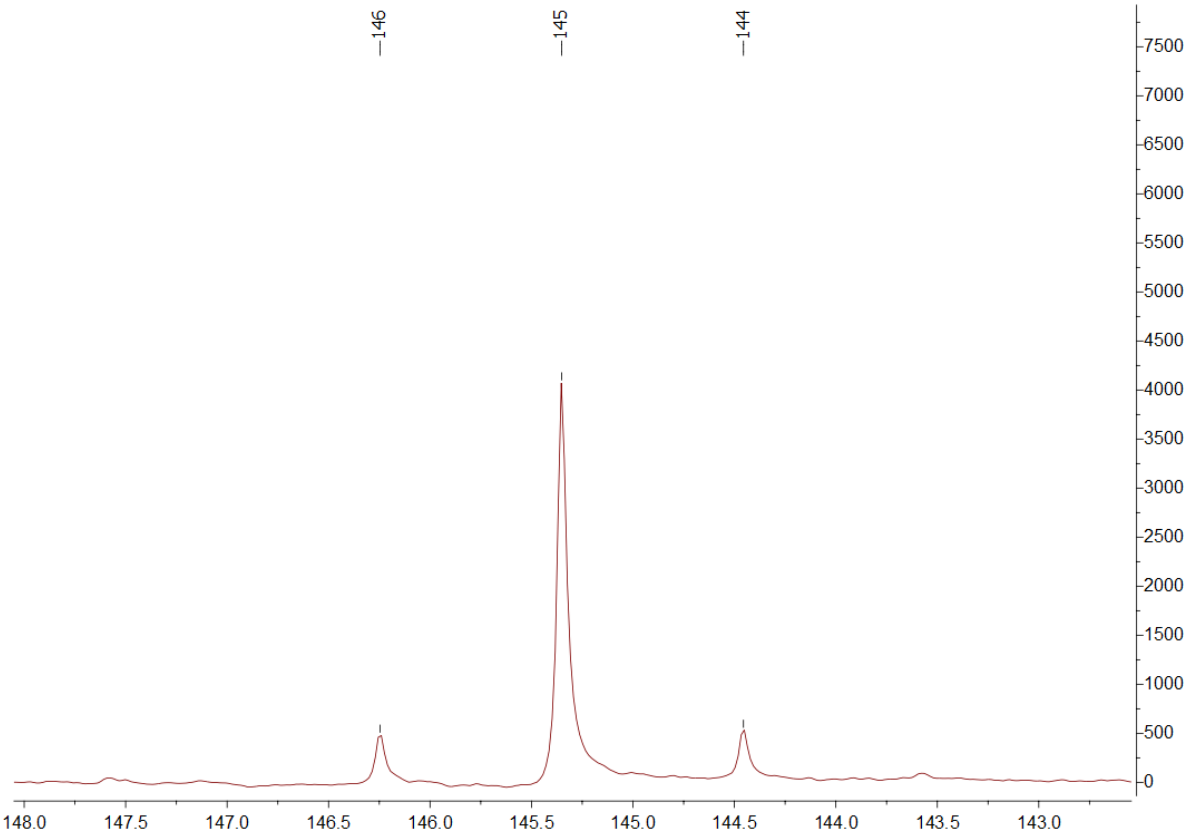

Figure S23: ^{119}Sn NMR spectrum of **6** (112 MHZ, 25°C, CD_2Cl_2)

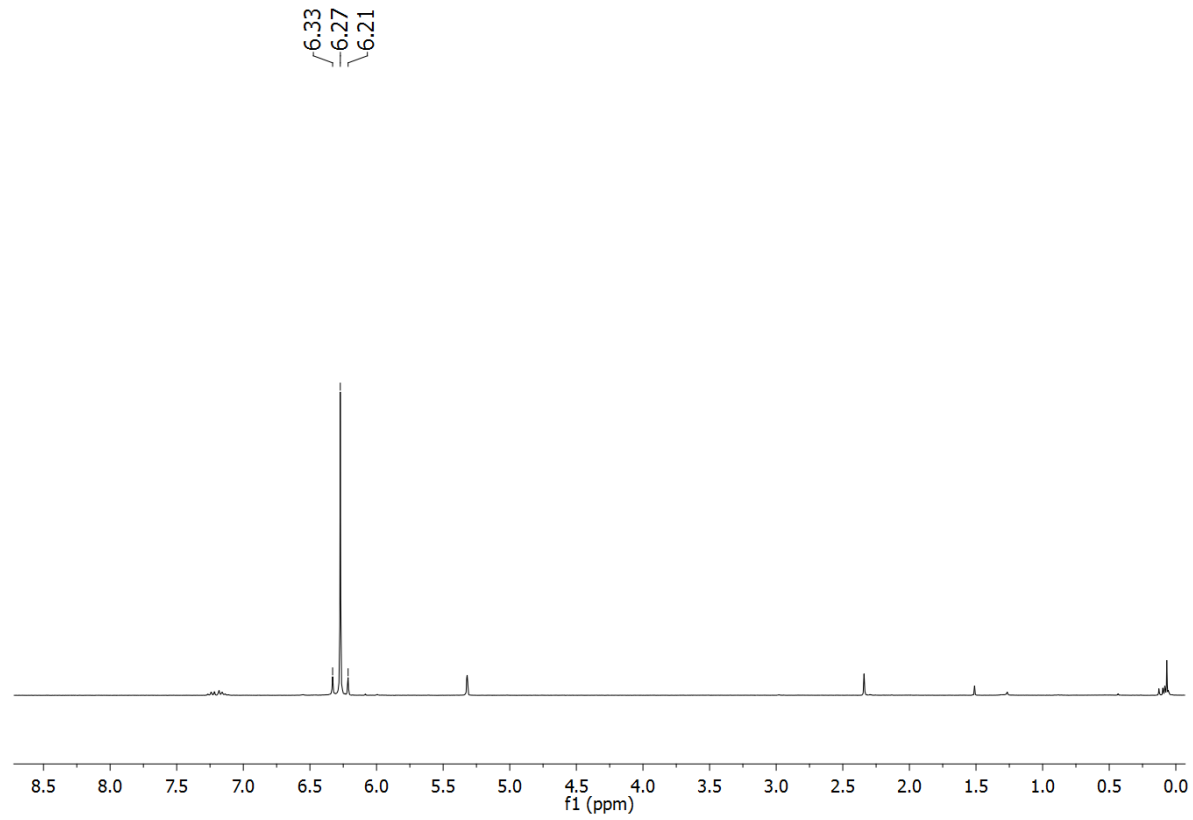

Figure S24: ^{1}H NMR spectrum of **7** (300 MHZ, 25°C, CD_2Cl_2).

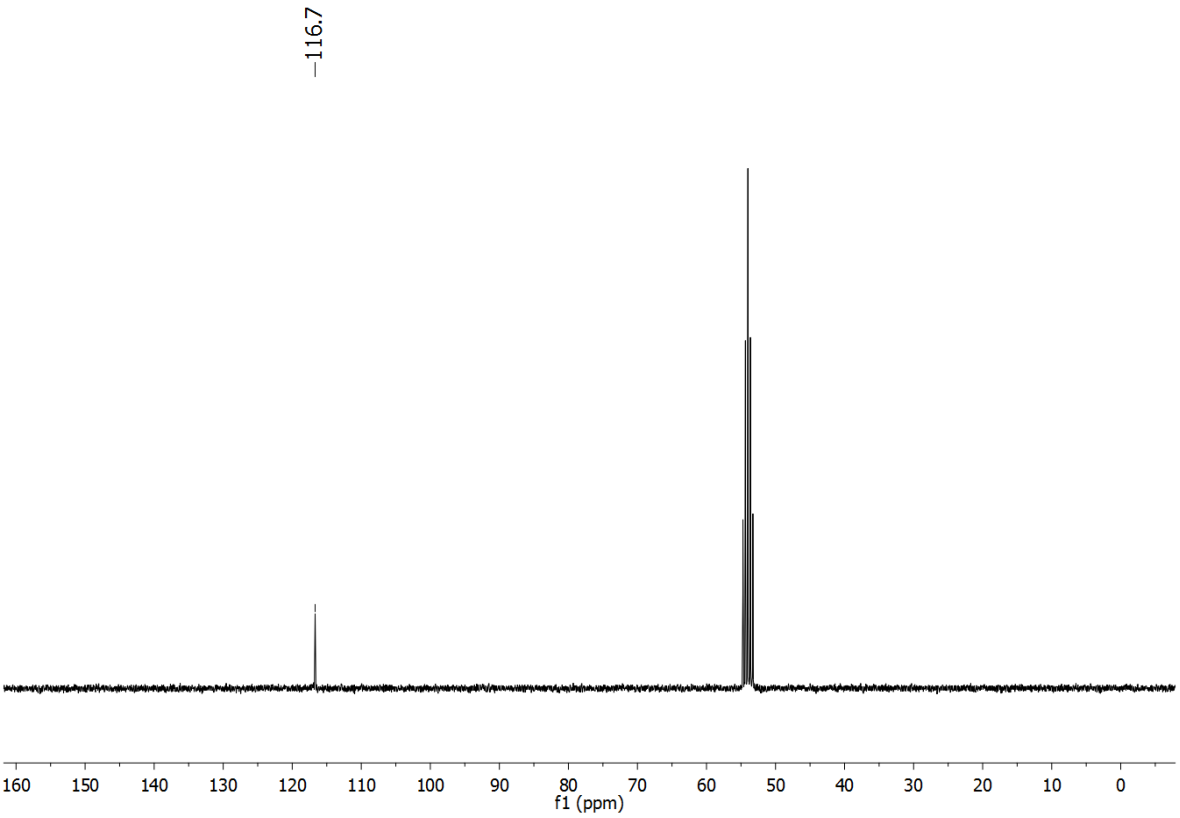

Figure S25: ^{13}C NMR spectrum of **7** (75 MHZ, 25°C, CD_2Cl_2).

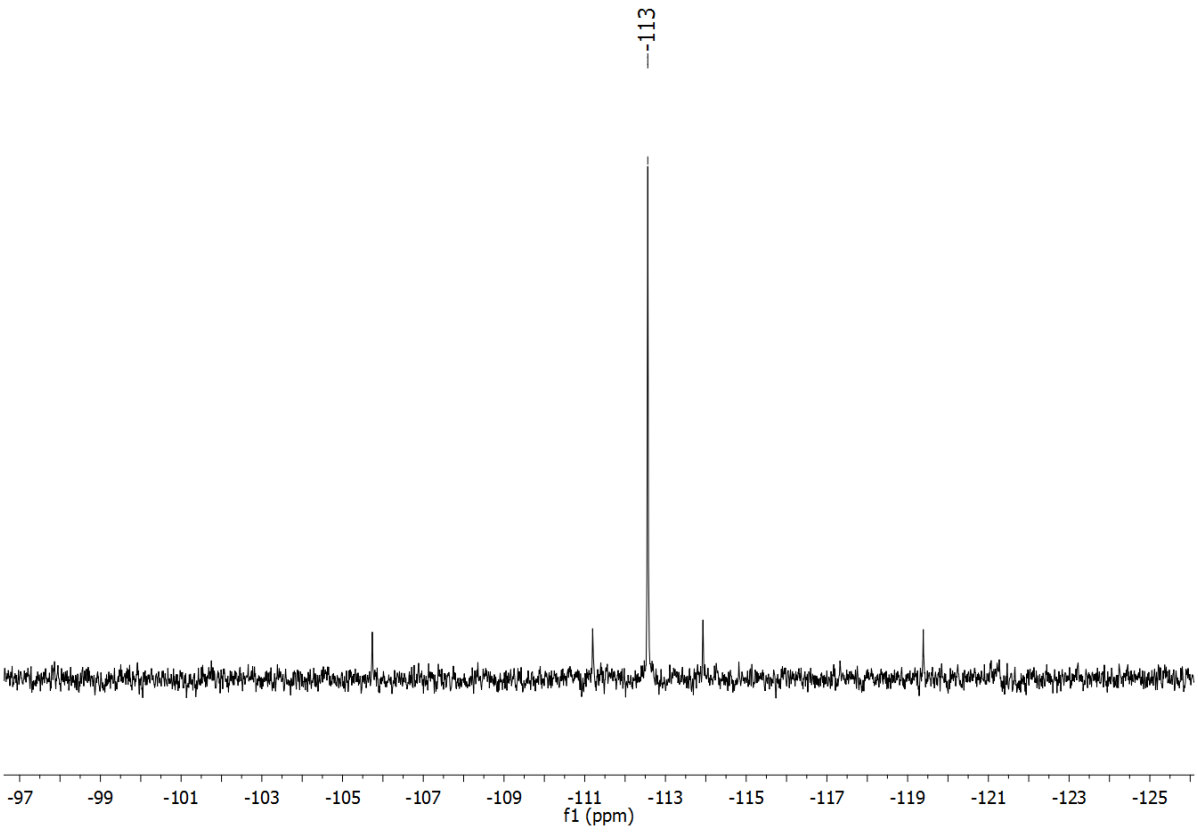

Figure S26: ^{119}Sn NMR spectrum of **7** (112 MHZ, 25°C, CD_2Cl_2).

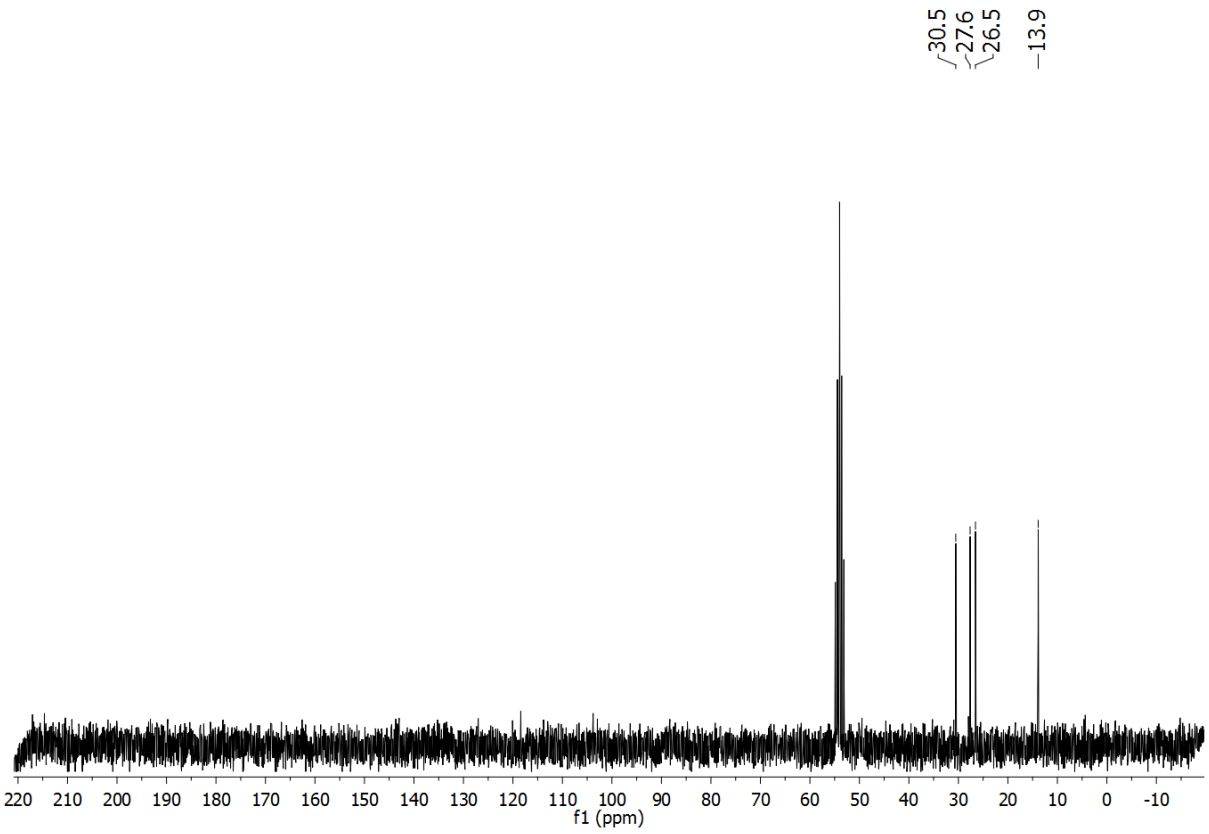

Figure S27: ^{1}H NMR spectrum of **8** (300 MHZ, 25°C, CD_2Cl_2).

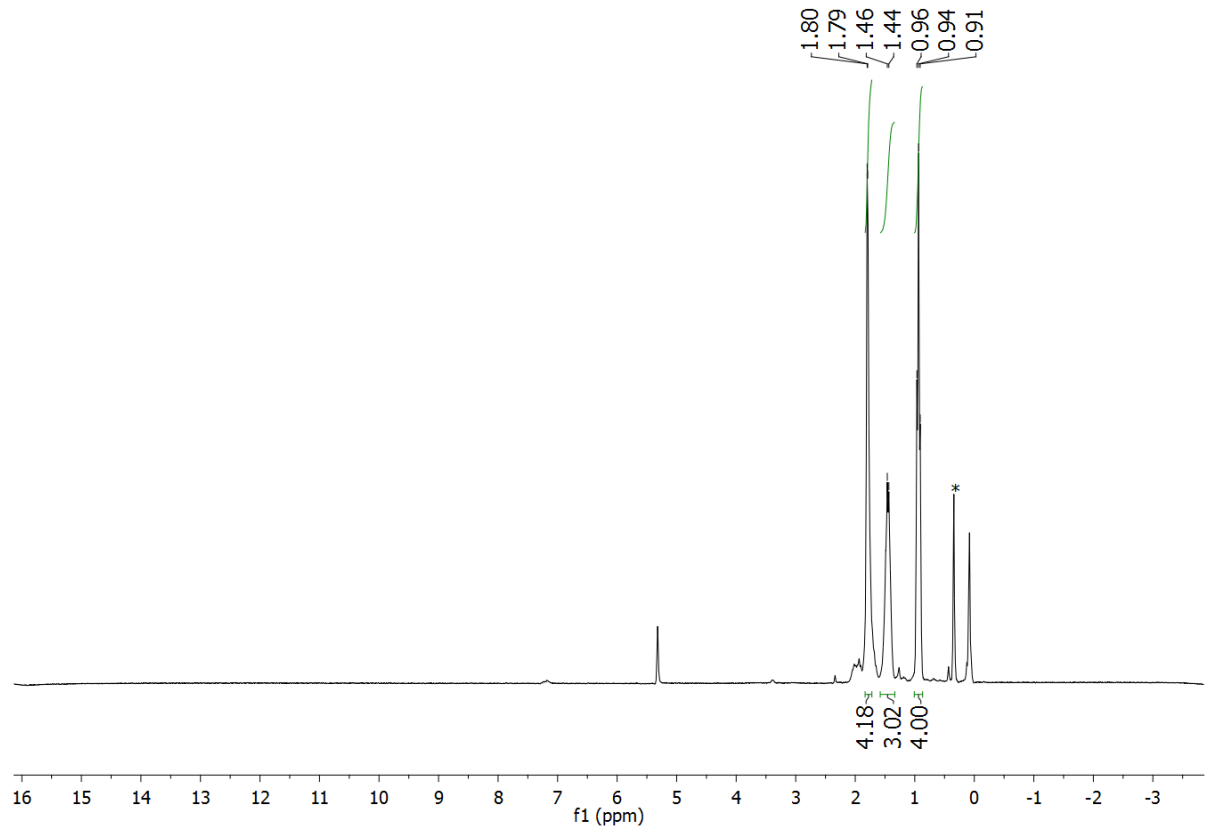

Figure S28: ^{13}C NMR spectrum of **8** (75 MHZ, 25°C, CD_2Cl_2).

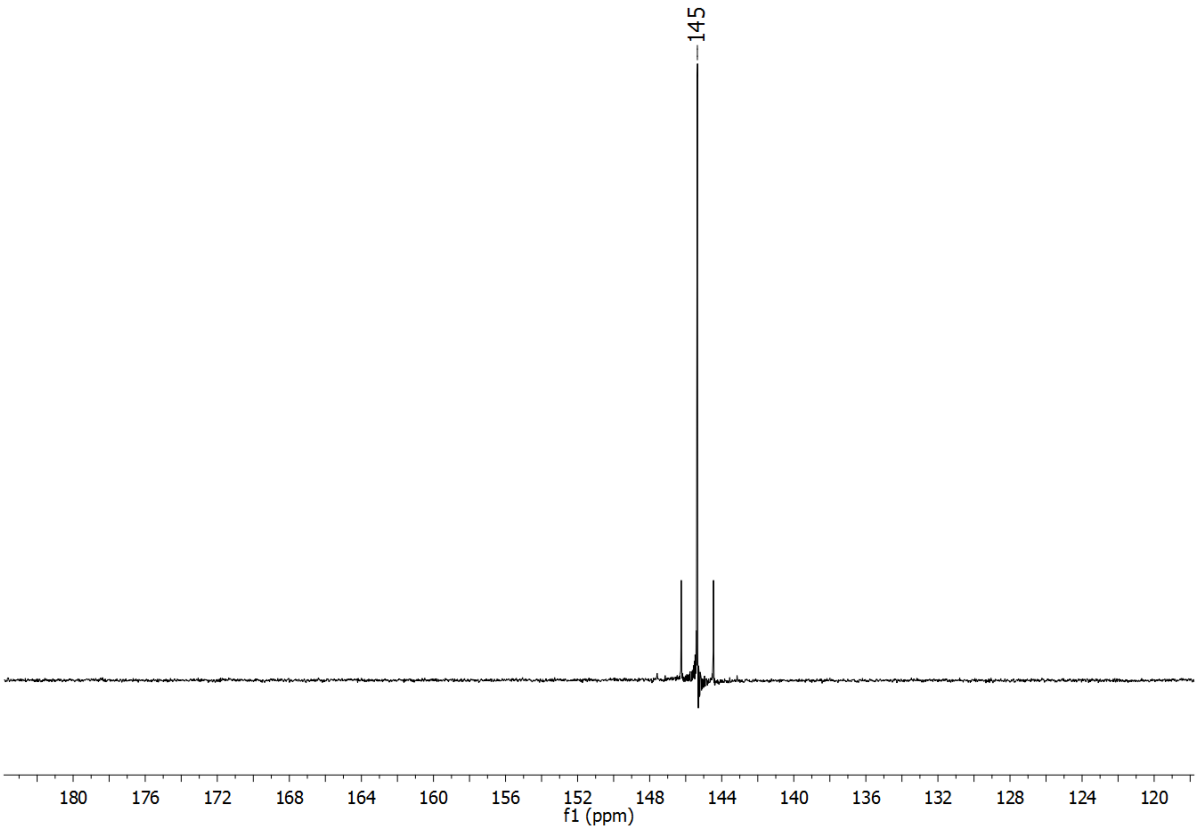

Figure S29: ^{119}Sn NMR spectrum of **8** (112 MHZ, 25°C, CD_2Cl_2).

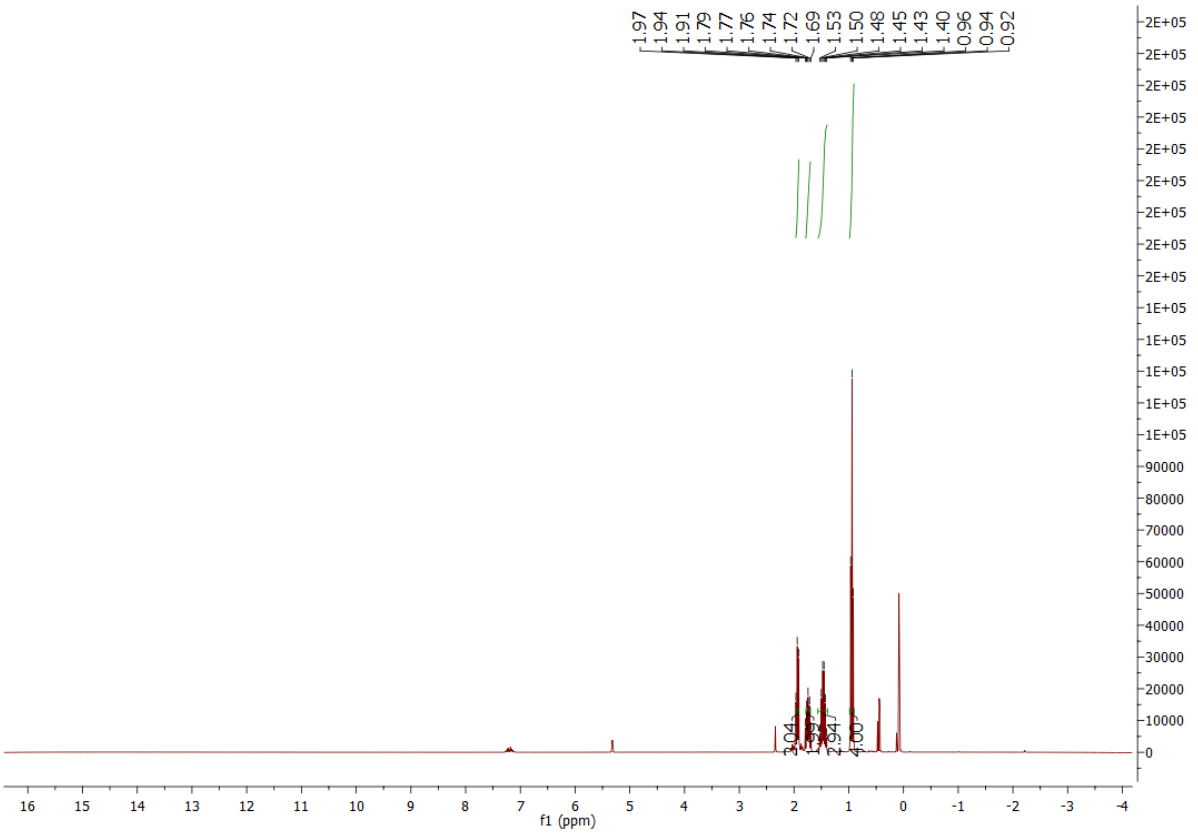

Figure S30: ^{1}H NMR spectrum of **9** (300 MHZ, 25°C, CD_2Cl_2).

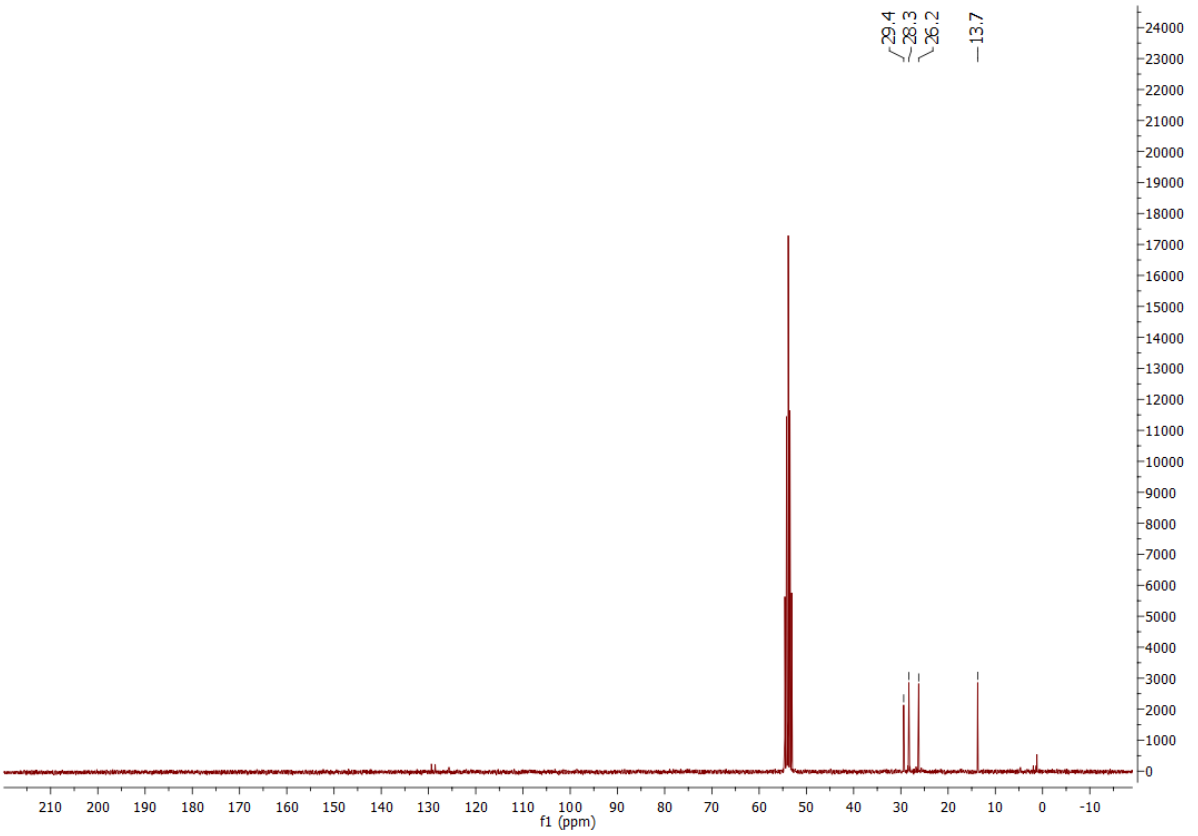

Figure S31: ^{13}C NMR spectrum of **9** (300 MHZ, 25°C, CD_2Cl_2).

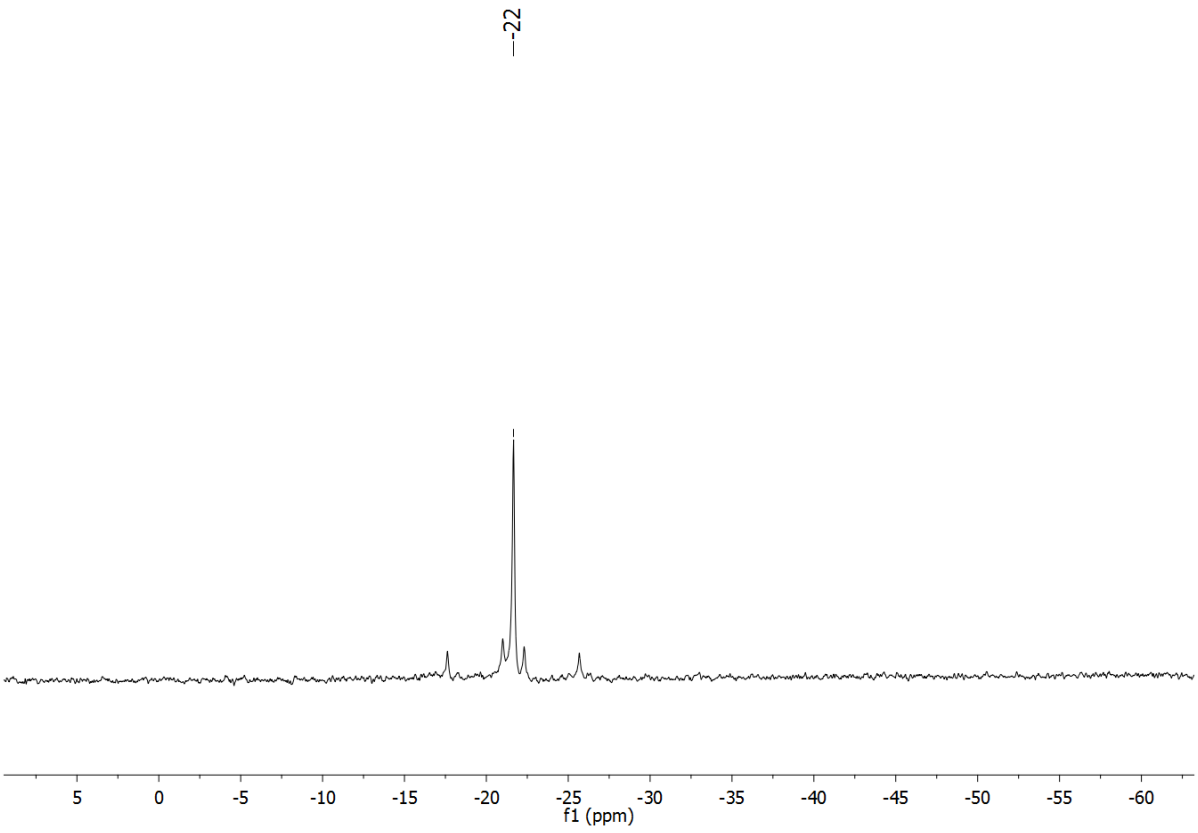

Figure S32: ^{119}Sn NMR spectrum of **9** (187 MHZ, 25°C, CD_2Cl_2).

2. IR spectra

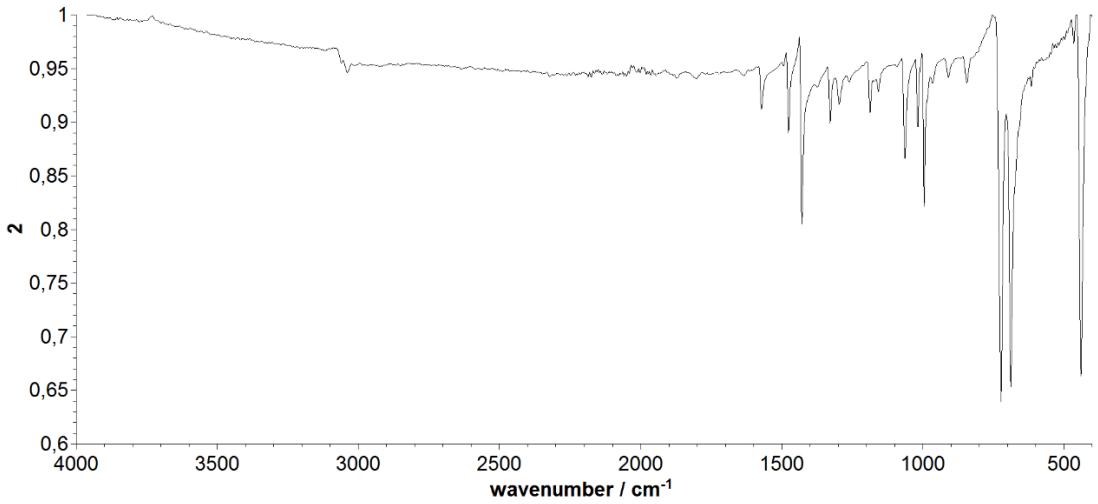

Figure S33: IR spectrum of **1**.

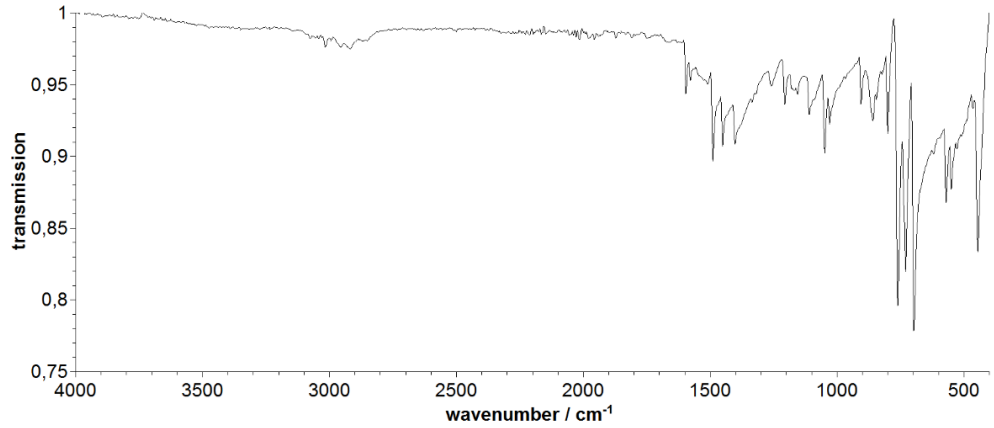

Figure S34: IR spectrum of **2**.

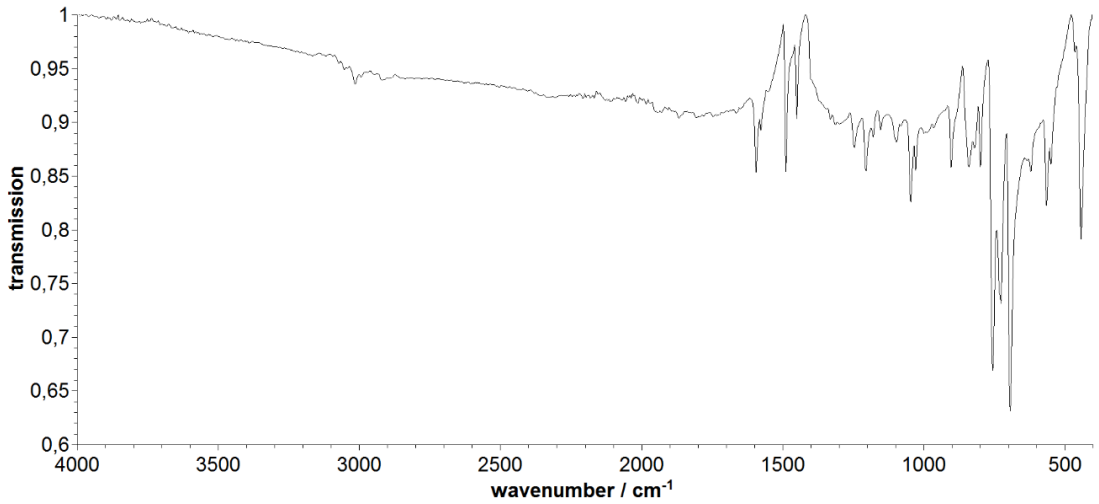

Figure S35: IR spectrum of **3**.

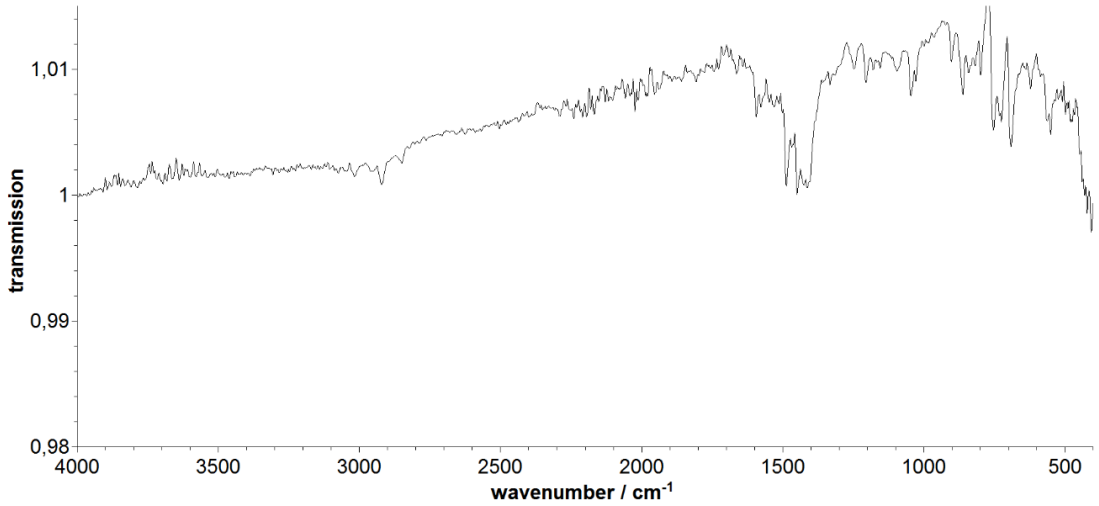

Figure S36: IR spectrum of **4**.

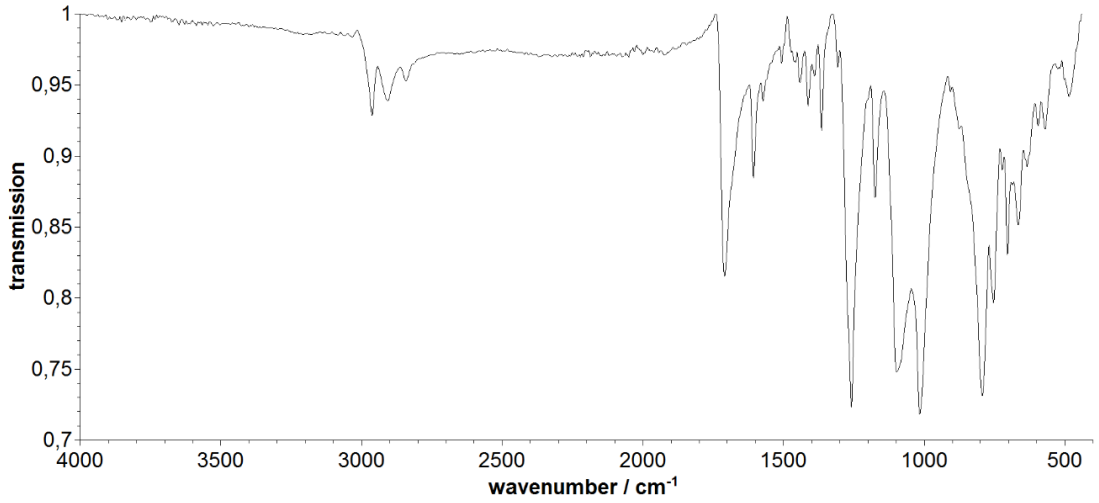

Figure S37: IR spectrum of **5**.

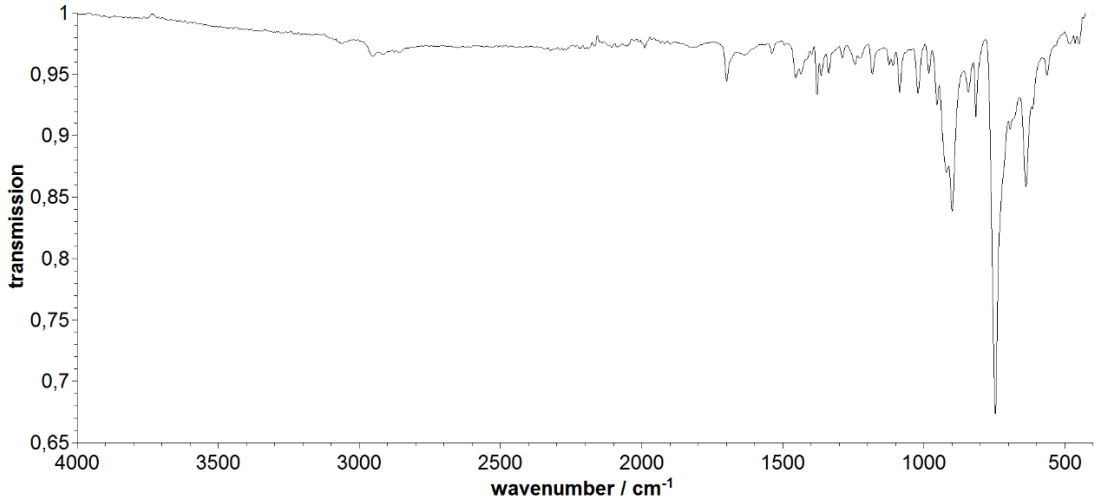

Figure S38: IR spectrum of **6**.

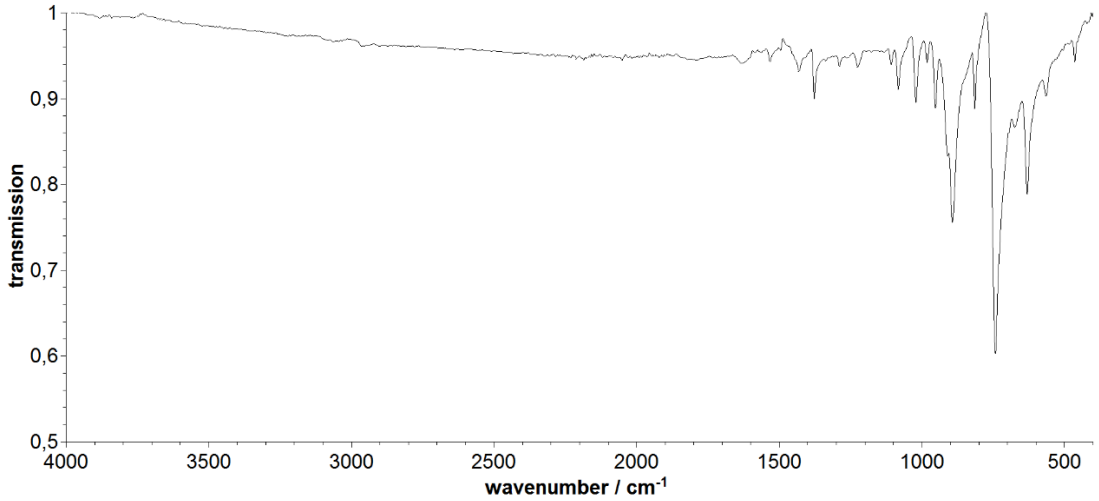

Figure S39: IR spectrum of **7**.

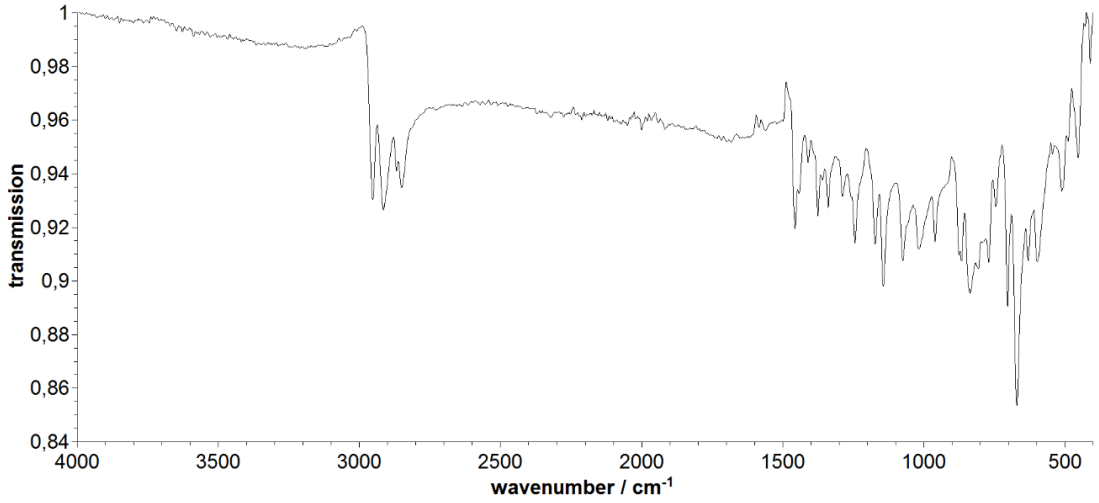

Figure S40: IR spectrum of **8**.

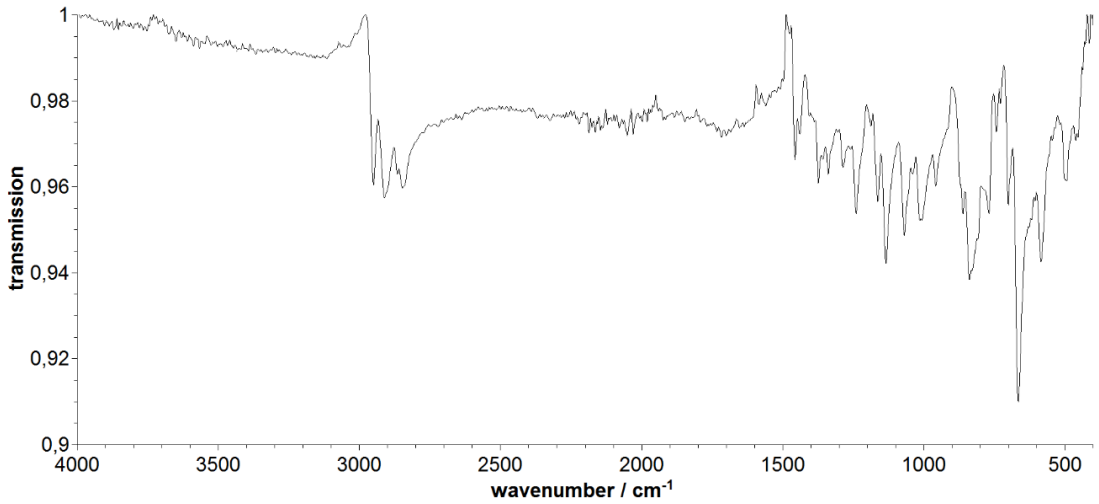

Figure S41: IR spectrum of **9**

3. X-Ray Powder Diffraction

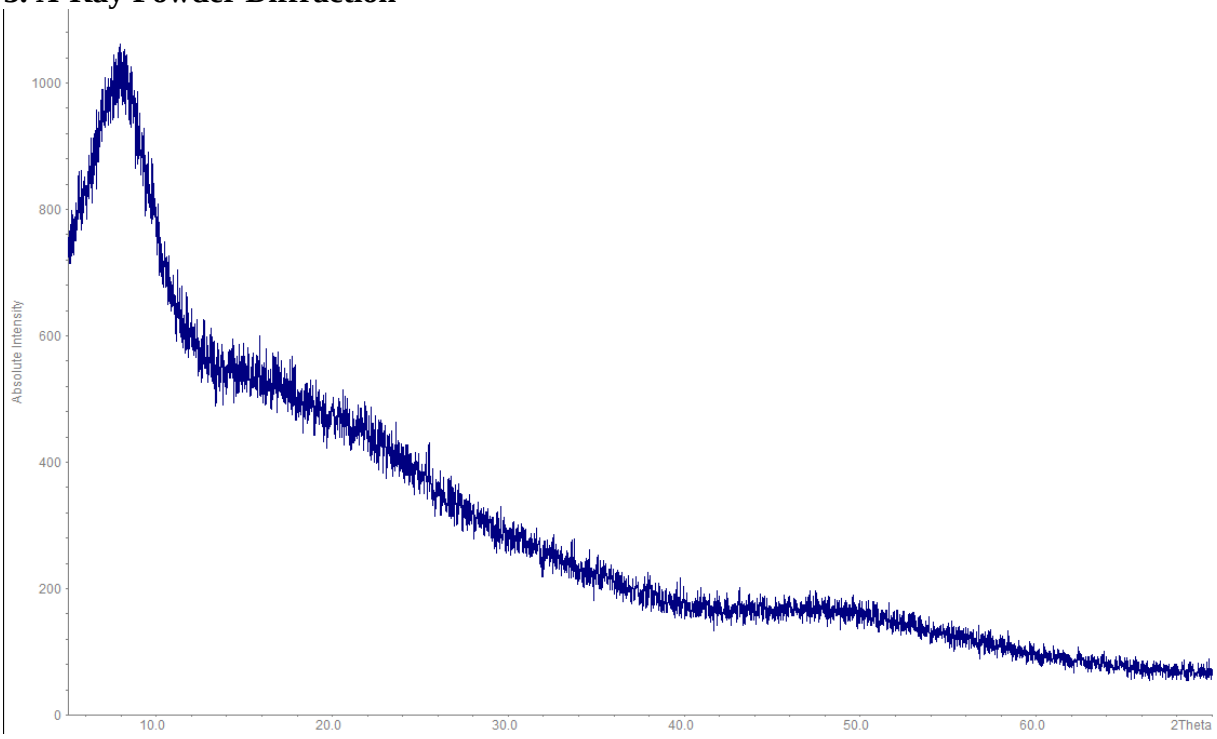

Figure S42: X-Ray powder diffractogram of **1**.

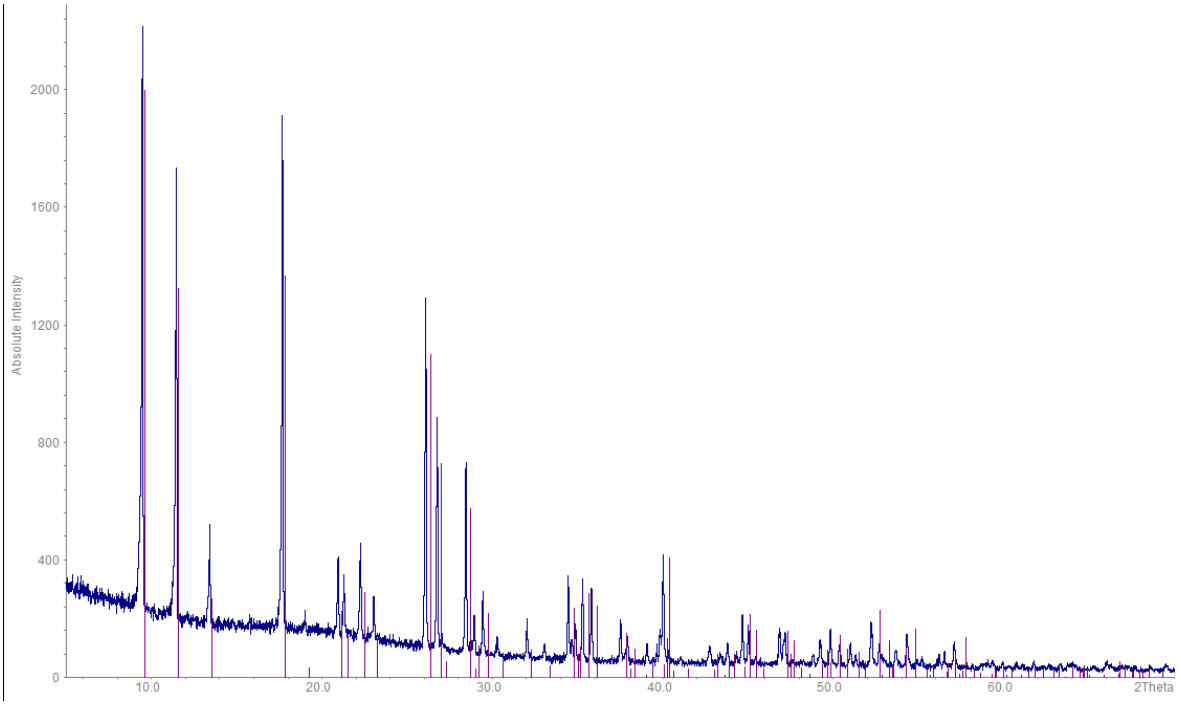

Figure S43: X-Ray powder diffractogram of **2**, compared with a simulated diffractogram obtained from the crystal structure of **2**. The angular shift arises from the temperature difference between powder (room temperature) and single-crystal measurement (100 K).

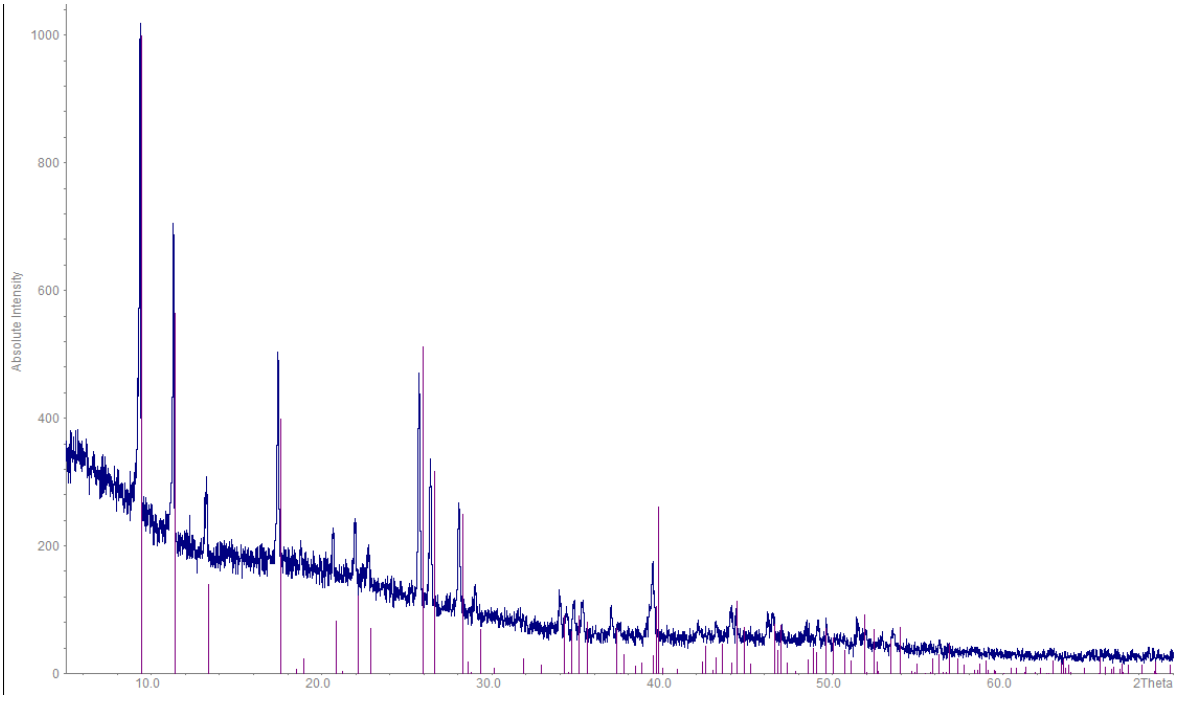

Figure S44: X-Ray powder diffractogram of **3**, compared with a simulated diffractogram obtained from the crystal structure of **3**. The angular shift arises from the temperature difference between powder (room temperature) and single-crystal measurement (100 K).

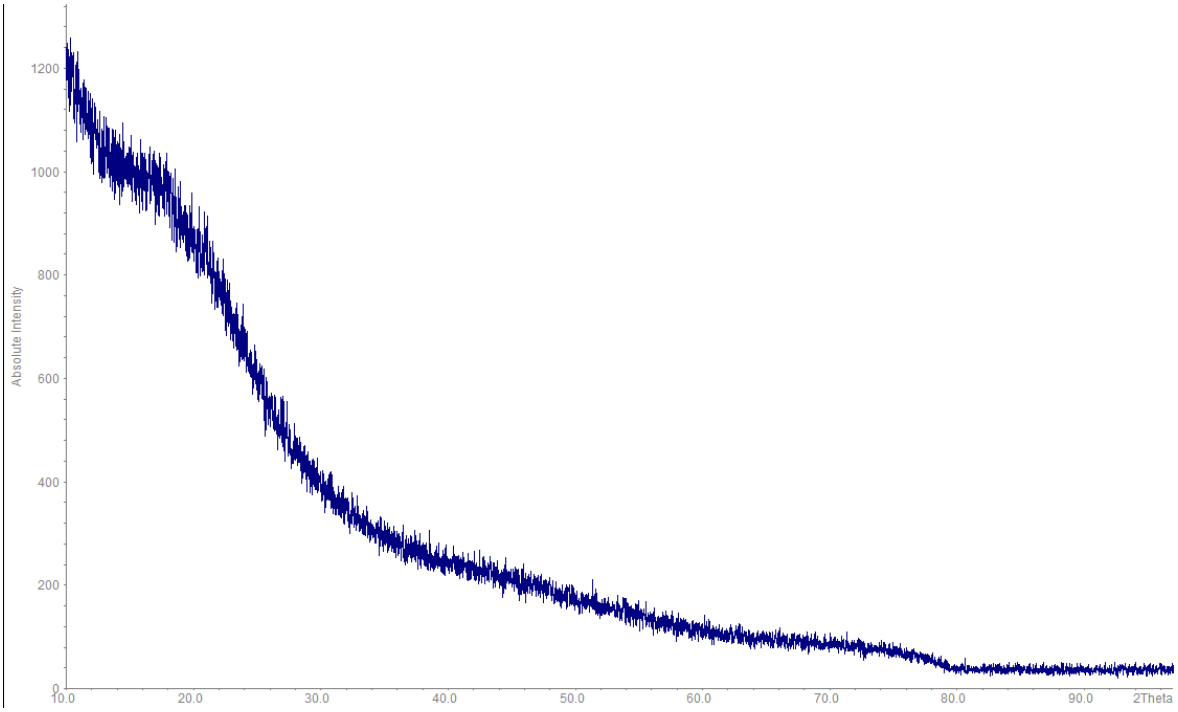

Figure S45: X-Ray powder diffractogram of **4**.

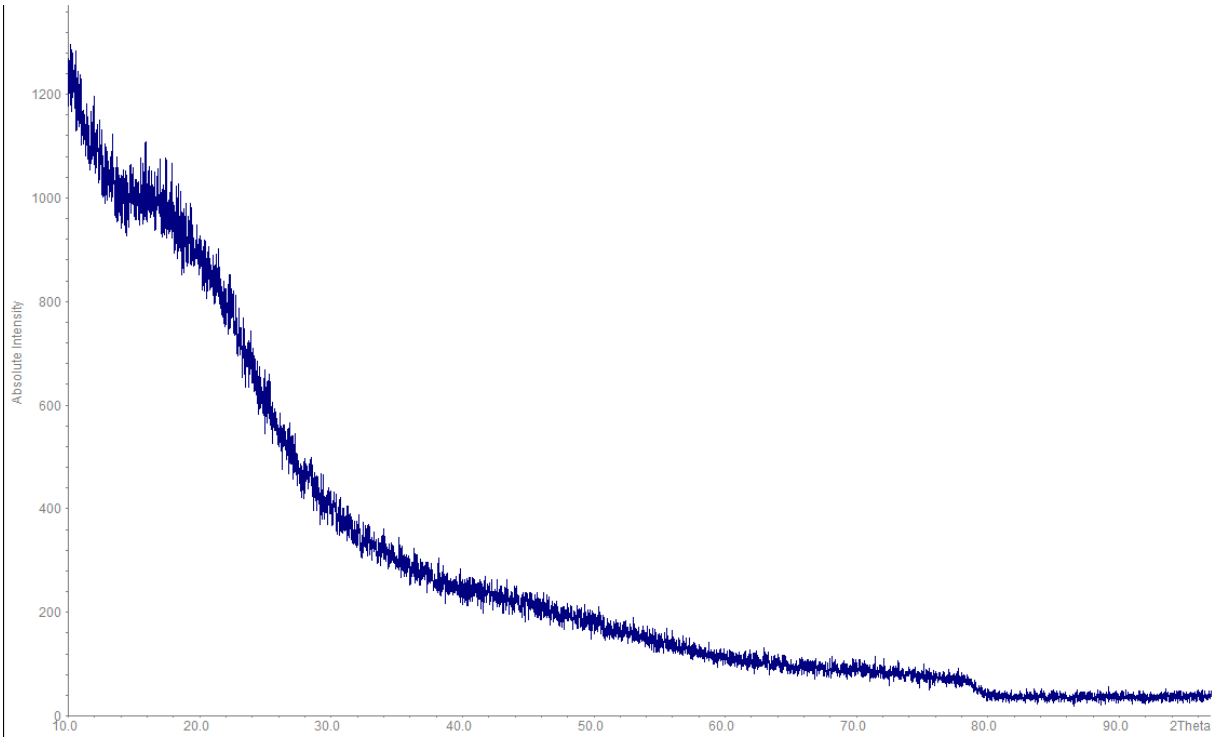

Figure S46: X-Ray powder diffractogram of **5**.

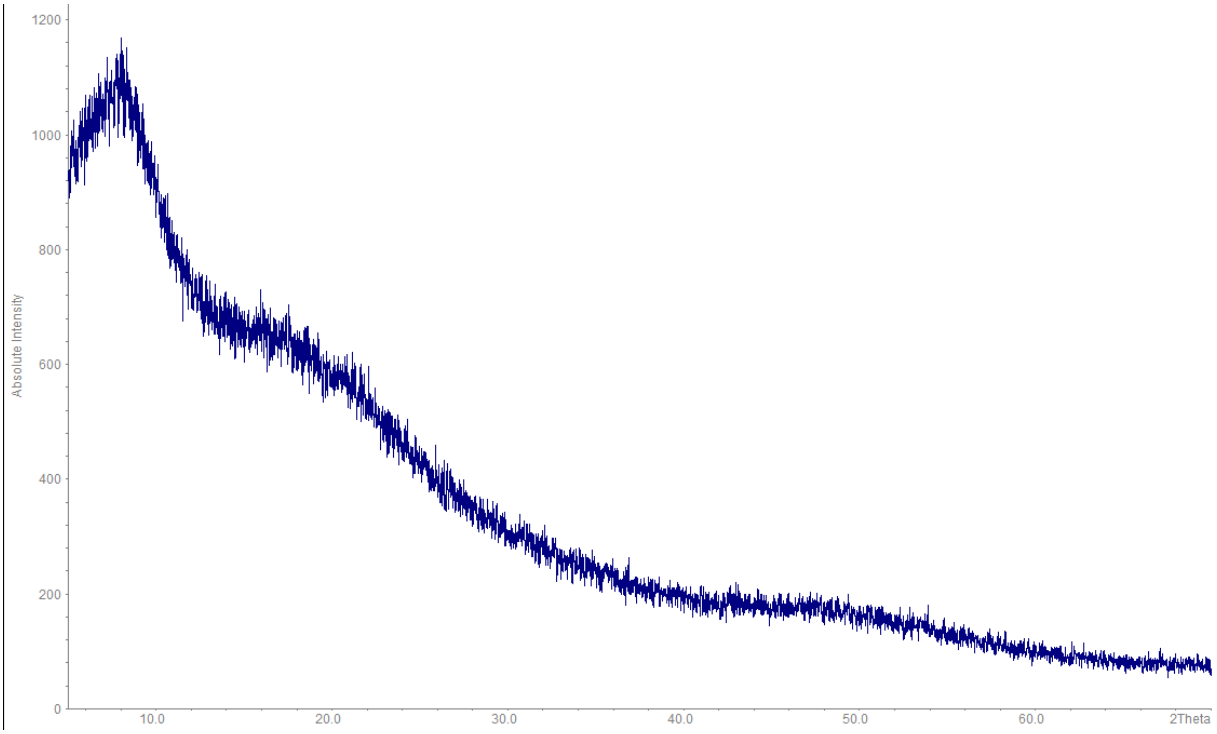

Figure S47: X-Ray powder diffractogram of **6**.

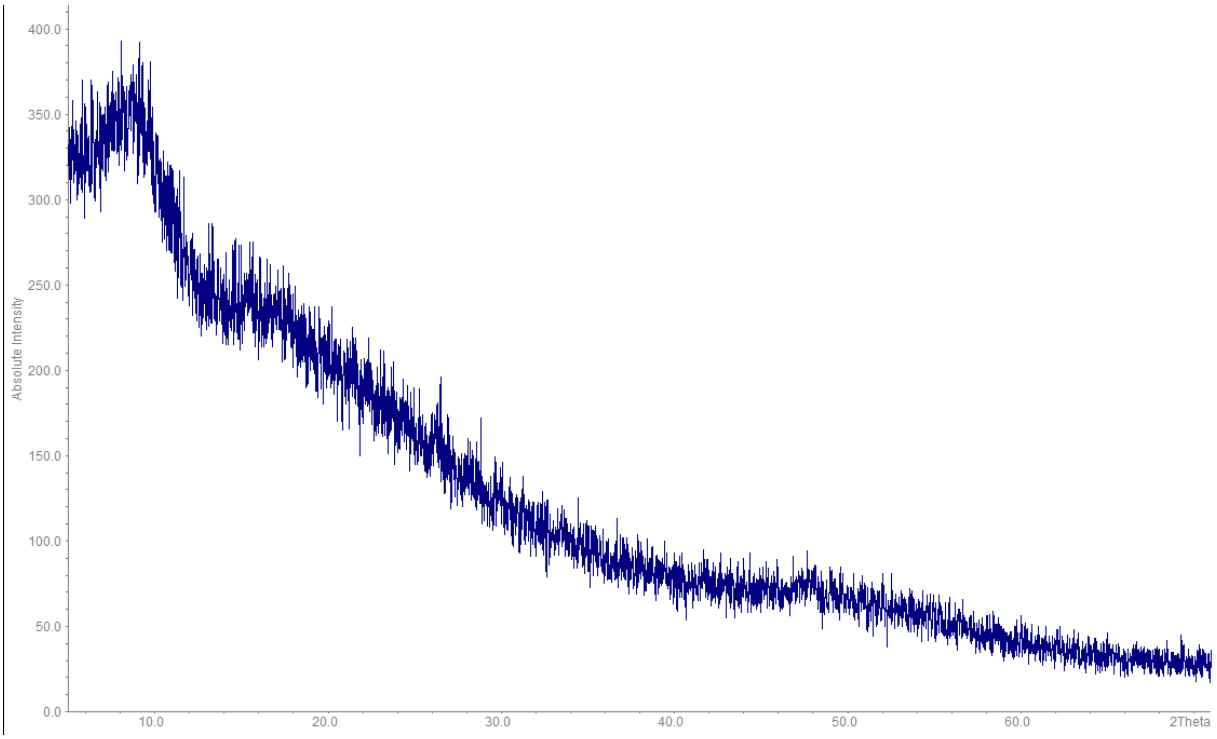

Figure S48: X-Ray powder diffractogram of **7**.

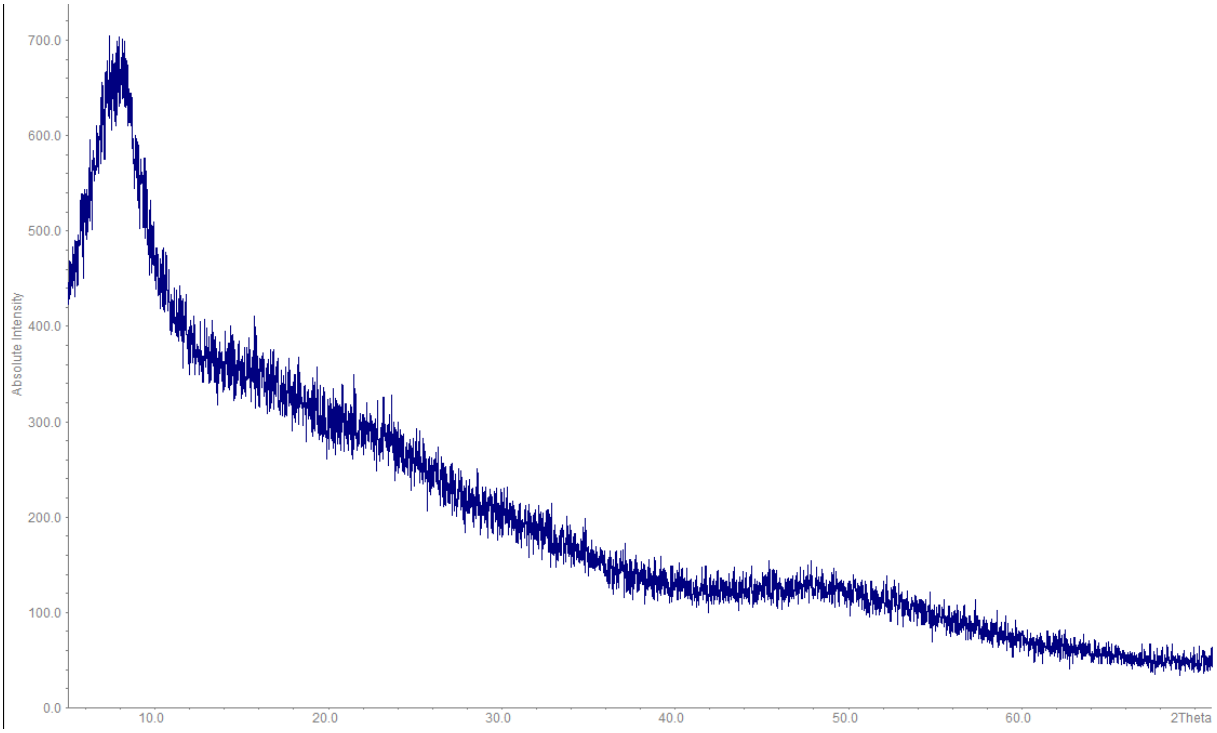

Figure S49: X-Ray powder diffractogram of **8**.

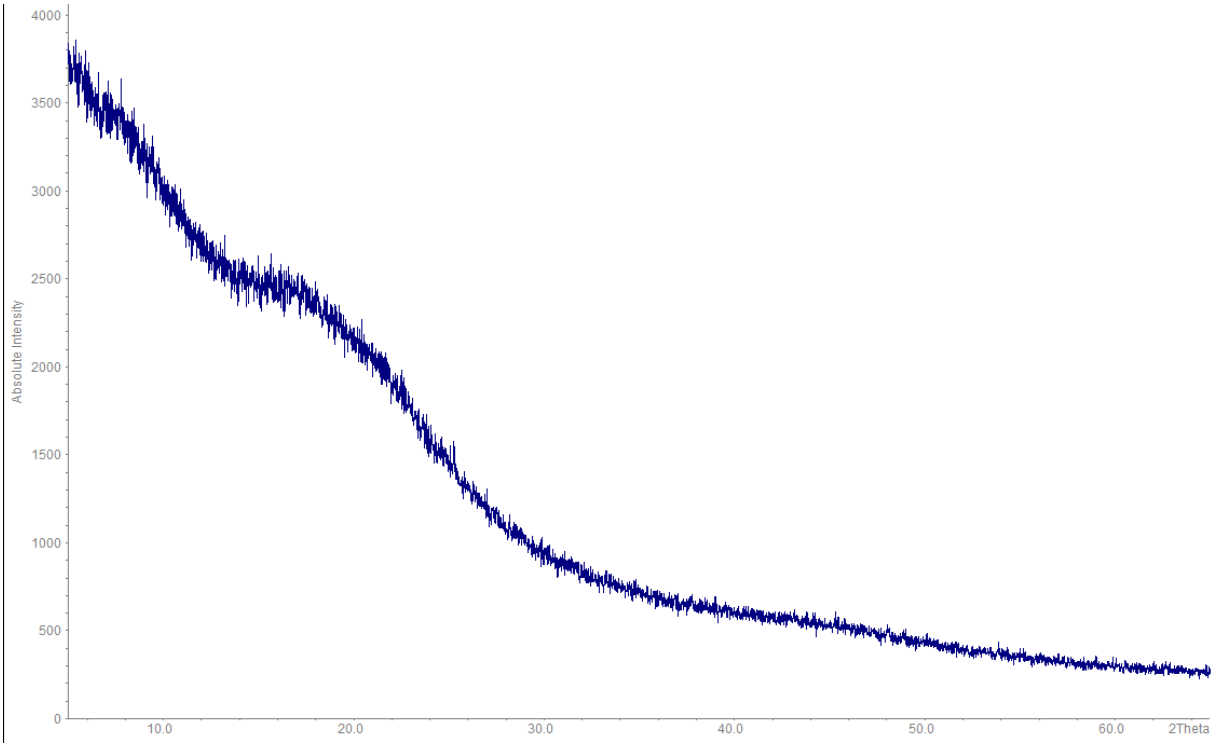

Figure S50: X-Ray powder diffractogram of **9**.

4. Single-Crystal X-Ray Crystallography of Compound 2

Data of the X-Ray diffraction analyses were collected on a STOE STADIVARI four-circle diffractometer using $Cu_{K\alpha}$ radiation (λ = 1.54186 Å) at 100 K. Reflection data were processed with X-Area 1.77.[1] Structure solution was performed by direct methods and full-matrix-least-squares refinement against F^2 using SHELXT[2] and SHELXL-2014[3] software.

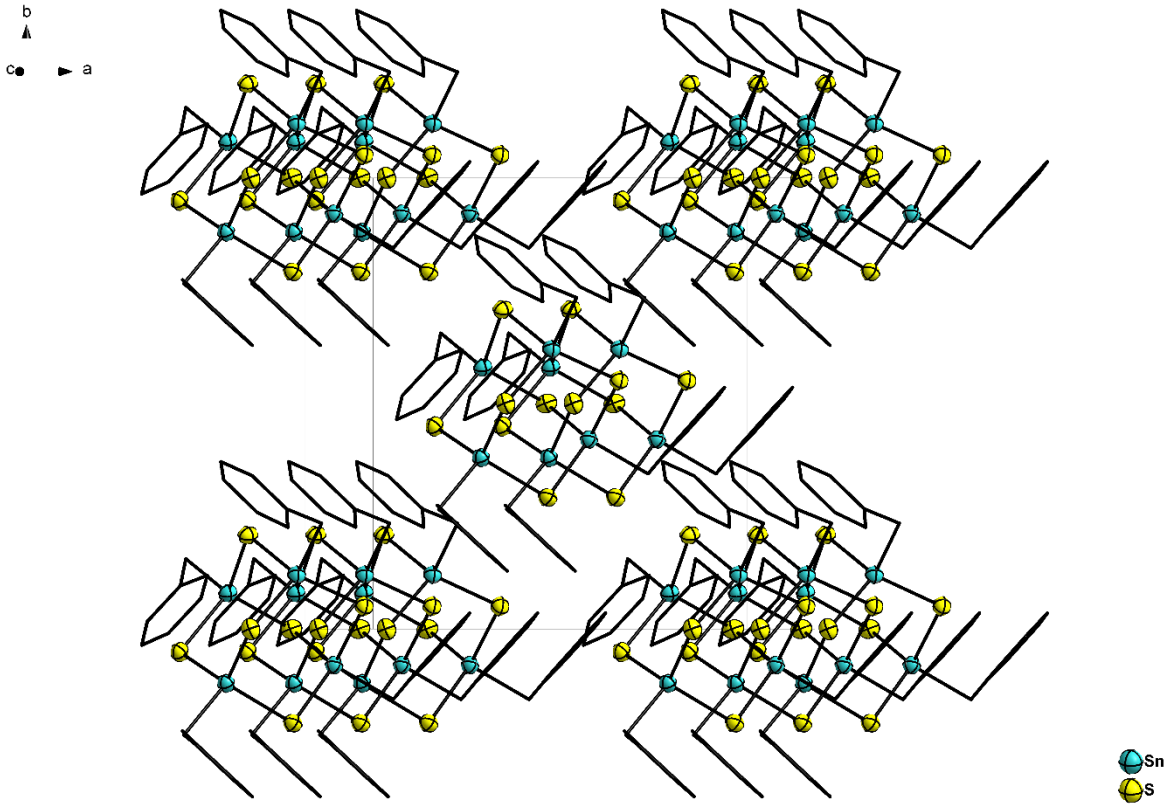

Figure S51: Crystal structure of **2**, showing the ordering of the molecules along the crystallographic *c* axis. Ellipsoids are drawn at 50% probability, hydrogen atoms are omitted for clarity.

Table S1: Crystal data and structure refinement for **2**.

Empirical formula	$C_{28}H_{28}S_6Sn_4$	
Formula weight	1031.62	
Temperature	100(2) K	
Wavelength	1.54178 Å	
Crystal system	Tetragonal	
Space group	$I\bar{4}$	
Unit cell dimensions	a = 13.0446(3) Å	α = 90°.
	b = 13.0446(3) Å	β = 90°.
	c = 9.4366(4) Å	γ = 90°.
Volume	1605.75(10) $Å^3$	
Z	2	
Density (calculated)	2.134 Mg/m^3	
Absorption coefficient	28.243 mm^{-1}	
F(000)	984	
Crystal size	0.15 x 0.13 x 0.10 mm^3	
Theta range for data collection	4.794 to 71.972°.	
Index ranges	-14<=h<=16, -16<=k<=14, -10<=l<=11	
Reflections collected	12918	
Independent reflections	1553 [R(int) = 0.0570]	
Completeness to theta = 67.679°	100.0 %	
Absorption correction	Sphere	
Max. and min. transmission	0.0105 and 0.0014	
Refinement method	Full-matrix least-squares on F2	
Data / restraints / parameters	1553 / 0 / 87	
Goodness-of-fit on F2	0.832	
Final R indices [I>2sigma(I)]	R1 = 0.0292, wR2 = 0.0869	
R indices (all data)	R1 = 0.0296, wR2 = 0.0877	
Absolute structure parameter	-0.025(17)	
Largest diff. peak and hole	0.776 and -0.467 e.Å-3	

Table S2: Atomic coordinates (x 104) and equivalent isotropic displacement parameters (Å2x 103) for **2.** U(eq) is defined as one third of the trace of the orthogonalized Uij tensor.

	x	y	z	U(eq)
Sn(01)	5798(1)	6202(1)	1440(1)	26(1)
S(002)	4492(2)	7086(2)	117(2)	30(1)
S(003)	5000	5000	3009(3)	30(1)
C(004)	6191(7)	7258(6)	5295(10)	34(2)
C(005)	4644(6)	8711(6)	5087(11)	37(2)
C(006)	6559(6)	7346(6)	2707(9)	28(2)
C(007)	5960(6)	7663(5)	3964(9)	32(2)
C(008)	5681(6)	7587(6)	6485(11)	37(2)
C(009)	4909(7)	8309(7)	6395(11)	42(2)
C(00A)	5169(6)	8398(6)	3871(9)	33(2)

Table S3: Bond lengths [Å] and angles [°] for **2**.

Sn(01)-C(006)	2.155(8)	Sn(01)-S(003)-Sn(01)#3	103.60(11)
Sn(01)-S(003)	2.3948(18)	C(008)-C(004)-C(007)	120.8(8)
Sn(01)-S(002)	2.405(2)	C(008)-C(004)-H(004)	119.6
Sn(01)-S(002)#1	2.4086(19)	C(007)-C(004)-H(004)	119.6
C(004)-C(008)	1.375(13)	C(009)-C(005)-C(00A)	120.0(7)
C(004)-C(007)	1.395(13)	C(009)-C(005)-H(005)	120.0
C(004)-H(004)	0.9300	C(00A)-C(005)-H(005)	120.0
C(005)-C(009)	1.385(15)	C(007)-C(006)-Sn(01)	113.3(5)
C(005)-C(00A)	1.396(13)	C(007)-C(006)-H(00A)	108.9
C(005)-H(005)	0.9300	Sn(01)-C(006)-H(00A)	108.9
C(006)-C(007)	1.479(12)	C(007)-C(006)-H(00B)	108.9
C(006)-H(00A)	0.9700	Sn(01)-C(006)-H(00B)	108.9
C(006)-H(00B)	0.9700	H(00A)-C(006)-H(00B)	107.7
C(007)-C(00A)	1.411(11)	C(004)-C(007)-C(00A)	118.1(8)
C(008)-C(009)	1.381(13)	C(004)-C(007)-C(006)	120.1(7)
C(008)-H(008)	0.9300	C(00A)-C(007)-C(006)	121.8(7)
C(009)-H(009)	0.9300	C(004)-C(008)-C(009)	121.1(10)
C(00A)-H(00C)	0.9300	C(004)-C(008)-H(008)	119.5
C(006)-Sn(01)-S(003)	108.1(2)	C(009)-C(008)-H(008)	119.5
C(006)-Sn(01)-S(002)	106.4(2)	C(008)-C(009)-C(005)	119.6(9)
S(003)-Sn(01)-S(002)	109.10(5)	C(008)-C(009)-H(009)	120.2
C(006)-Sn(01)-S(002)#1	106.1(2)	C(005)-C(009)-H(009)	120.2
S(003)-Sn(01)-S(002)#1	115.71(6)	C(005)-C(00A)-C(007)	120.4(8)
S(002)-Sn(01)-S(002)#1	110.96(4)	C(005)-C(00A)-H(00C)	119.8
Sn(01)-S(002)-Sn(01)#2	104.38(8)	C(007)-C(00A)-H(00C)	119.8

Symmetry transformations used to generate equivalent atoms:

#1 y,-x+1,-z #2 -y+1,x,-z #3 -x+1,-y+1,z

5. Single-Crystal X-Ray Crystallography of Compound 3

Data of the X-Ray diffraction analyses were collected on a STOE STADIVARI four-circle diffractometer using $Cu_{K\alpha}$ radiation (λ = 1.54186 Å) at 100 K. Reflection data were processed with X-Area 1.77.[1] Structure solution was performed by direct methods and full-matrix-least-squares refinement against F^2 using SHELXT[2] and SHELXL-2014[3] software.

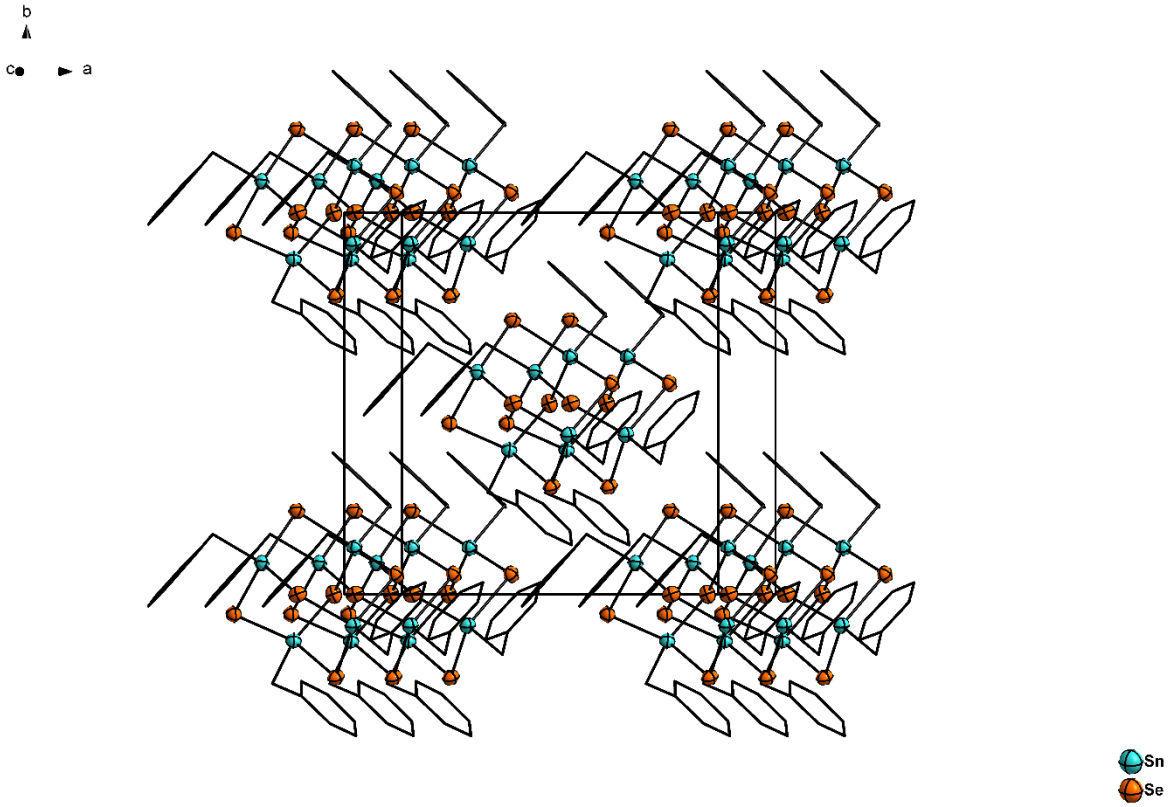

Figure S52: Crystal structure of **3**, showing the ordering of the molecules along the crystallographic *c* axis. Ellipsoids are drawn at 50% probability, hydrogen atoms are omitted for clarity.

Table S4: Crystal data and structure refinement for **3**.

Empirical formula	$C_{28}H_{28}Se_6Sn_4$
Formula weight	1313.02
Temperature	100(2) K
Wavelength	1.54178 Å
Crystal system	Tetragonal
Space group	$I\bar{4}$
Unit cell dimensions	a = 13.24260(10) Å α = 90°.
	b = 13.24260(10) Å β = 90°.
	c = 9.5754(2) Å γ = 90°.
Volume	1679.20(4) $Å^3$
Z	2
Density (calculated)	2.597 Mg/m^3
Absorption coefficient	30.959 mm^{-1}
F(000)	1200
Crystal size	0.25 x 0.20 x 0.15 mm^3
Theta range for data collection	4.722 to 71.461°.
Index ranges	-16<=h<=10, -16<=k<=15, -11<=l<=11
Reflections collected	14136
Independent reflections	1625 [R(int) = 0.0365]
Completeness to theta = 67.679°	100.0 %
Absorption correction	Sphere
Max. and min. transmission	0.0005 and 0.0000
Refinement method	Full-matrix least-squares on F2
Data / restraints / parameters	1625 / 0 / 87
Goodness-of-fit on F2 0.879	
Final R indices [I>2sigma(I)]	R1 = 0.0318, wR2 = 0.0910
R indices (all data)	R1 = 0.0319, wR2 = 0.0912
Absolute structure parameter	-0.015(7)
Largest diff. peak and hole	1.581 and -1.310 e.Å-3

Table S5: Atomic coordinates (x 104) and equivalent isotropic displacement parameters (Å2x 103) for **3**. U(eq) is defined as one third of the trace of the orthogonalized Uij tensor.

	x	y	z	U(eq)
Sn(01)	5818(1)	6219(1)	8541(1)	28(1)
Se(02)	5000	5000	6862(1)	32(1)
Se(03)	4476(1)	7177(1)	9872(1)	31(1)
C(004)	4690(7)	8706(7)	4994(12)	41(2)
C(005)	4934(8)	8326(8)	3696(13)	45(2)
C(006)	6195(7)	7278(7)	4748(11)	39(2)
C(007)	5202(7)	8386(6)	6184(11)	37(2)
C(008)	6576(6)	7338(7)	7291(9)	31(2)
C(009)	5983(6)	7668(6)	6059(10)	33(2)
C(00A)	5682(8)	7620(8)	3580(11)	42(2)

Table S6: Bond lengths [Å] and angles [°] for **3**.

Sn(01)-C(008)	2.153(9)	C(005)-C(004)-H(004)	119.6
Sn(01)-Se(02)	2.5227(9)	C(007)-C(004)-H(004)	119.6
Sn(01)-Se(03)#1	2.5283(9)	C(00A)-C(005)-C(004)	119.5(10)
Sn(01)-Se(03)	2.5292(10)	C(00A)-C(005)-H(005)	120.2
C(004)-C(005)	1.379(16)	C(004)-C(005)-H(005)	120.2
C(004)-C(007)	1.392(14)	C(00A)-C(006)-C(009)	120.7(9)
C(004)-H(004)	0.9300	C(00A)-C(006)-H(006)	119.6
C(005)-C(00A)	1.366(16)	C(009)-C(006)-H(006)	119.6
C(005)-H(005)	0.9300	C(004)-C(007)-C(009)	119.6(9)
C(006)-C(00A)	1.384(16)	C(004)-C(007)-H(007)	120.2
C(006)-C(009)	1.386(14)	C(009)-C(007)-H(007)	120.2
C(006)-H(006)	0.9300	C(009)-C(008)-Sn(01)	113.4(6)
C(007)-C(009)	1.410(12)	C(009)-C(008)-H(00A)	108.9
C(007)-H(007)	0.9300	Sn(01)-C(008)-H(00A)	108.9
C(008)-C(009)	1.483(12)	C(009)-C(008)-H(00B)	108.9
C(008)-H(00A)	0.9700	Sn(01)-C(008)-H(00B)	108.9
C(008)-H(00B)	0.9700	H(00A)-C(008)-H(00B)	107.7
C(00A)-H(00C)	0.9300	C(006)-C(009)-C(007)	118.4(9)
C(008)-Sn(01)-Se(02)	106.7(2)	C(006)-C(009)-C(008)	120.3(8)
C(008)-Sn(01)-Se(03)#1	104.6(2)	C(007)-C(009)-C(008)	121.3(9)
Se(02)-Sn(01)-Se(03)#1	117.13(3)	C(005)-C(00A)-C(006)	120.9(11)
C(008)-Sn(01)-Se(03)	105.2(2)	C(005)-C(00A)-H(00C)	119.5
Se(02)-Sn(01)-Se(03)	109.89(3)	C(006)-C(00A)-H(00C)	119.5
Se(03)#1-Sn(01)-Se(03)	112.32(2)		
Sn(01)-Se(02)-Sn(01)#2	100.82(5)		
Sn(01)#3-Se(03)-Sn(01)	101.64(4)		
C(005)-C(004)-C(007)	120.8(9)		

Symmetry transformations used to generate equivalent atoms:

#1 y,-x+1,-z+2 #2 -x+1,-y+1,z #3 -y+1,x,-z+2

6. References for the Supporting Information

[1] Stoe and Cie GmbH, *X-Area*, *Version 1.77*, **2016**.

[2] G. M. Sheldrick, *Acta Crystallogr A* **2015**, *71*, 3-8.

[3] C. B. Hübschle, G. M. Sheldrick, B. Dittrich, *J. Appl. Cryst.* **2011**, 1281-1284.

4.3 White-Light Generation Upon In-Situ Amorphization of Single Crystals of $[\{(Me_3P)_3AuSn\}\{PhSn\}_3S_6]$ and $[\{(Et_3P)_3AgSn\}\{PhSn\}_3S_6]$

Zitat: E. Dornsiepen, F. Dobener, N. Mengel, O. Lenchuk, C. Dues, S. Sanna, D. Mollenhauer, S. Chatterjee, S. Dehnen, *Adv. Opt. Mater.* **2019**, *7*, 1801793.

Abstract

In order to gain more information on the white-light generation by amorphous molecular materials, the influence of metal complex substituents on the photophysical properties of potential white-light emitters is investigated. Three compounds of the general type $[\{(R_3P)_3MSn\}\{PhSn\}_3S_6]$, with R/M = Me/Au (**1**), Et/Ag (**4**), and Me/Cu (**5**) are produced by reactions of the organotin sulfide cluster $[(PhSn)_4S_6]$ (**A**) with the corresponding coinage metal complexes $[M(PR_3)_3Cl]$. Excess of the gold complex in the reaction leads to rearrangement and formation of $[Au(PMe_3)_4][Au(PMe_3)_2][(PhSnCl)_3S_4]$ (**2**). The use of PMe_3 instead of PEt_3 in the reaction with the silver salt causes decomposition and affords $[(Me_3P)_3AgSnCl_3]$ (**3**). All compounds are structurally characterized, and the necessity of sterically stabilizing PEt_3 groups at the silver complex in **4** are rationalized by DFT calculations. Measurements of the photophysical properties of **1**, **4** and **5** show that the introduction of the metallo-ligands indeed affects the materials properties, and at the same time confirm that the reduction of the molecular symmetry alone is not a sufficient condition for white-light generation, which still requires amorphicity of the compound. This was realized for **1** and **4** in situ, while reabsorption processes inhibit white-light generation in case of the copper compound **5**.

Eigener Anteil

Alle Synthesen wurden von mir geplant und durchgeführt. Die Aufnahme der röntgenographischen Daten sowie die Strukturlösung und -verfeinerung wurde von mir durchgeführt. IR-Spektren sowie ^{1}H- und ^{13}C-NMR-Spektren wurden von mir, ^{31}P- und ^{119}Sn-NMR-Experimente von der zentralen NMR-Abteilung des Fachbereichs Chemie an der Philipps-Universität unter Leitung von Dr. Xiulan Xie gemessen und von mir ausgewertet. Massenspektren und CHN-Analysen wurden von der entsprechenden Serviceabteilung des Fachbereichs unter Leitung von Dr. Uwe Linne aufgenommen und von mir ausgewertet. Röntgenfluoreszenzspektren wurden von Bertram Peters aufgenommen und ausgewertet. Photolumineszenz- und Emissionsspektren wurden von Florian Dobener und Nils Mengel in der Arbeitsgruppe von Prof. Dr. Sangam Chatterjee an der Universität Gießen gemessen

und ausgewertet. Die quantenchemischen Rechnungen ohne periodische Randbedingungen wurden von Olena Lenchuk in der Arbeitsgruppe von Prof. Dr. Doreen Mollenhauer (Universität Gießen), jene mit periodischen Randbedingungen von Christof Dues in der Arbeitsgruppe von Prof. Dr. Simone Sanna (ebenfalls Universität Gießen) durchgeführt und ausgewertet. Das Manuskript wurde gemeinsam von allen Co-Autoren verfasst.

ADVANCED OPTICAL MATERIALS

www.advopticalmat.de

White-Light Generation Upon In-Situ Amorphization of Single Crystals of $[\{(Me_3P)_3AuSn\}(PhSn)_3S_6]$ and $[\{(Et_3P)_3AgSn\}(PhSn)_3S_6]$

*Eike Dornsiepen, Florian Dobener, Nils Mengel, Olena Lenchuk, Christof Dues, Simone Sanna, Doreen Mollenhauer, Sangam Chatterjee, and Stefanie Dehnen**

In order to gain more information on the white-light generation by amorphous molecular materials, the influence of metal complex substituents on the photophysical properties of potential white-light emitters is investigated. Three compounds of the general type $[\{(R_3P)_3MSn\}\{PhSn\}_3S_6)]$, with R/M = Me/Au (1), Et/Ag (4), and Me/Cu (5), are produced by reactions of the organotin sulfide cluster $[(PhSn)_4S_6]$ (A) with the corresponding coinage metal complexes $[M(PR_3)_3Cl]$. Excess of the gold complex in the reaction leads to rearrangement and formation of $[Au(PMe_3)_4][Au(PMe_3)_2][(PhSnCl)_3S_4]$ (2). The use of PMe_3 instead of PEt_3 in the reaction with the silver salt causes decomposition and affords $[(Me_3P)_3AgSnCl_3]$ (3). All compounds are structurally characterized, and the necessity of sterically stabilizing PEt_3 groups at the silver complex in 4 are rationalized by density functional theory (DFT) calculations. Measurements of the photophysical properties of 1, 4, and 5 show that the introduction of the metallo-ligands indeed affects the materials properties, and at the same time confirm that the reduction of the molecular symmetry alone is not a sufficient condition for white-light generation (WLG), which still requires amorphicity of the compound. This is realized for 1 and 4 in situ, while reabsorption processes inhibit WLG in case of the copper compound 5.

1. Introduction

During the last few decades, a large number of metal chalcogenide clusters has been prepared that vary in the composition of the metal and chalcogen atoms, as well as in the nature of the shielding ligands, which are introduced to prevent the cluster growth reactions from continuing toward bulk metal chalcogenides by kinetic stabilization.[1] In most cases, phosphine ligands were used for this purpose,[2] sometimes being supported by additional organic substituents on the chalcogen atoms.[3] Ternary clusters have also been reported that include a second type of metal atoms,[4] which enables tuning of structural and physical features within the range of the respective binary compounds.[5] Diversity can be further enhanced by attachment of functional organic ligands to the metal atoms of the clusters for tailoring material properties for optoelectronics or solar cells.[6]

Recently, our group has reported on the outstanding nonlinear optical properties of adamantane-type clusters with the general composition $[(RT)_4S_6]$ (R = organic substituent; T = Si, Ge, Sn).[7] We found that amorphous compounds with aromatic ligands transform infrared laser light into highly directional white light, while crystalline compounds or those with aliphatic ligands show strong second harmonic generation. Yet, the prerequisites for white-light generation are still under debate, and it is not clear whether the strong optical nonlinearities are an inherent molecular property or have their origin in the cluster habitus.

To shed light onto this physical scenario, we combined the adamantane-type clusters with metal complexes.[8] This allowed

E. Dornsiepen, Prof. S. Dehnen
Fachbereich Chemie and Wissenschaftliches Zentrum für Materialwissenschaften
Philipps-Universität Marburg
Hans-Meerwein-Straße, D-35043 Marburg, Germany
E-mail: dehnen@chemie.uni-marburg.de

F. Dobener, Dr. N. Mengel, Prof. S. Chatterjee
Institute of Experimental Physics I and Center for Materials Research (LaMa)
Justus Liebig University Giessen
Heinrich-Buff-Ring 16, D-35392 Giessen, Germany

The ORCID identification number(s) for the author(s) of this article can be found under https://doi.org/10.1002/adom.201801793.

Dr. O. Lenchuk, Prof. D. Mollenhauer
Institute of Physical Chemistry
Justus Liebig University Giessen
Heinrich-Buff-Ring 17, D-35392 Giessen, Germany

Dr. O. Lenchuk, Prof. D. Mollenhauer
Center for Materials Research (LaMa)
Justus Liebig University Giessen
Heinrich-Buff-Ring 16, 35392 Giessen, Germany

C. Dues, Prof. S. Sanna
Institute of Theoretical Physics and Center for Materials Research (LaMa)
Justus Liebig University Giessen
Heinrich-Buff-Ring 16, 35392 Giessen, Germany

DOI: 10.1002/adom.201801793

us to explore I) the effect of metallo-ligands on cluster stability and the particular optical properties, (II) the impact of the molecular symmetry-breaking by metallo-ligands on the optical response, and III) whether crystalline compounds are intrinsically unsuitable for white-light generation or whether they might become white-light emitters by appropriate modifications.

To this end, we performed reactions of $[(PhSn)_4S_6]$ (**A**) with coinage metal phosphine complexes, similar to those reported by the Merzweiler group under employment of copper complexes.[9] However, while Merzweiler and coworkers always added a sulfide source in order to rearrange the cluster core, in this work we substituted the organic ligands under retention of the inorganic core. Reactions of **A** with in situ-formed $[Au(PMe_3)_3Cl]$ yielded the ternary complex $[\{(Me_3P)_3AuSn\}(PhSn)_3S_6]$ (**1**), where one of the phenyl substituents of **A** was replaced with a gold complex fragment. Attempts to substitute all of the organic substituents failed, but yielded the ionic compound $[Au(PMe_3)_4][Au(PMe_3)_2][(PhSnCl)_3S_4]$ (**2**). Corresponding reaction with the lighter coinage metal phosphine complexes afforded the salt $[(Me_3P)_3AgSnCl_3]$ (**3**) and, upon utilization of another phosphine ligand, $[\{(Et_3P)_3AgSn\}(PhSn)_3S_6]$ (**4**), as well as the copper homologue of **1**, $[\{(Me_3P)_3CuSn\}(PhSn)_3S_6]$ (**5**). All syntheses are summarized in **Scheme 1**. With the help of corresponding DFT calculations, we explain this experimental finding by stabilizing dispersion interactions between the silver complex and the cluster. Optical spectroscopy measurements reveal that compounds **1** and **4** are rather efficient white-light emitters, while white-light generation is completely hindered by reabsorption processes in **5**.

The results lead to three main conclusions. I) Metallo-ligands do affect the cluster stability, and the group 11 atom co-controls the product spectrum, but the PL emission pattern and the capability and onset of white-light generation in general are not substantially affected by the presence of metallo-ligands for those compounds where white-light generation is observed. II) The symmetry breaking at molecular level as introduced by a metallo-ligand at one of the group 14 atoms alone is not a sufficient prerequisite for white-light generation, which seems to strictly require the presence of intermolecular disorder (amorphousness). III) The group 11 atom itself does have strong impact on the PL emission.

2. Results and Discussion

2.1. Syntheses and Crystal Structures

The reaction of **A** with one equivalent of gold(I) chloride and three equivalents of trimethylphosphine in tetrahydrofurane (THF) affords colorless crystals of $[\{(Me_3P)_3AuSn\}(PhSn)_3S_6]\cdot 2$ THF (**1**·2 THF) within one day. **1** crystallizes in the orthorhombic crystal system in the space group $Cmc2_1$ with four formula units per unit cell. In contrast to results of corresponding experiments with copper complexes reported by Merzweiler and coworkers, the gold ions are not incorporated into the inorganic cluster core. Instead, the phenyl substituent at one of the tin atoms is replaced by an $\{Au(PMe_3)_3\}$ fragment. The reaction taking place is a redox reaction where the respective tin atom is reduced from the (formal) +IV oxidation state to +II. The phenyl substituent, on the other hand, is oxidized to chlorobenzene. This can be described by the following reaction scheme (Equation (1))

$$\left[(PhSn)_4S_6\right] + AuCl + 3\,PMe_3 \rightarrow \mathbf{1} + PhCl \quad (1)$$

The inorganic core of **1** shows a slightly distorted adamantane-type structure (**Figure 1**, top left). Bond lengths and angles are summarized in **Table 1** together with calculated values, and reported in detail in the Supporting Information. While the Au substituent causes elongation of the adjacent Sn–S bond lengths (also with respect to other adamantane-type tin sulfide clusters like $[(C_6F_5Sn)_4S_6]$),[10] the bond angles are in the usual range for adamantane-type structures.[10] The Sn–Au bond length of 2.7162(7) Å is close to the respective length in $[(Me_3P)_3AuSnCl_3]$ (2.724 Å).[11] The same holds true for the Au–P bond lengths and the Sn–Au–P bond angles.

After obtaining compound **1**, we were left with the question if the substitution of more than one phenyl substituent was possible. Reactions with up to two equivalents of gold(I)

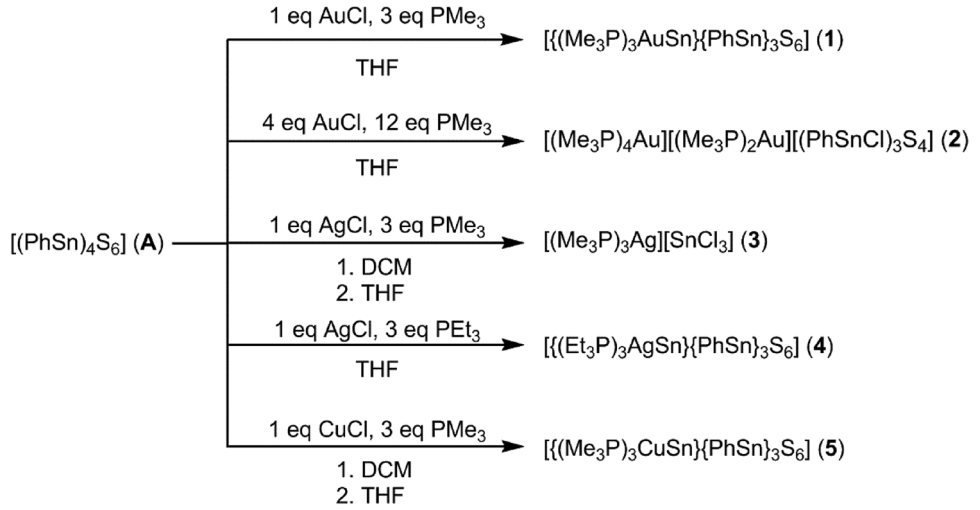

Scheme 1. Synthesis of compounds **1–5**.

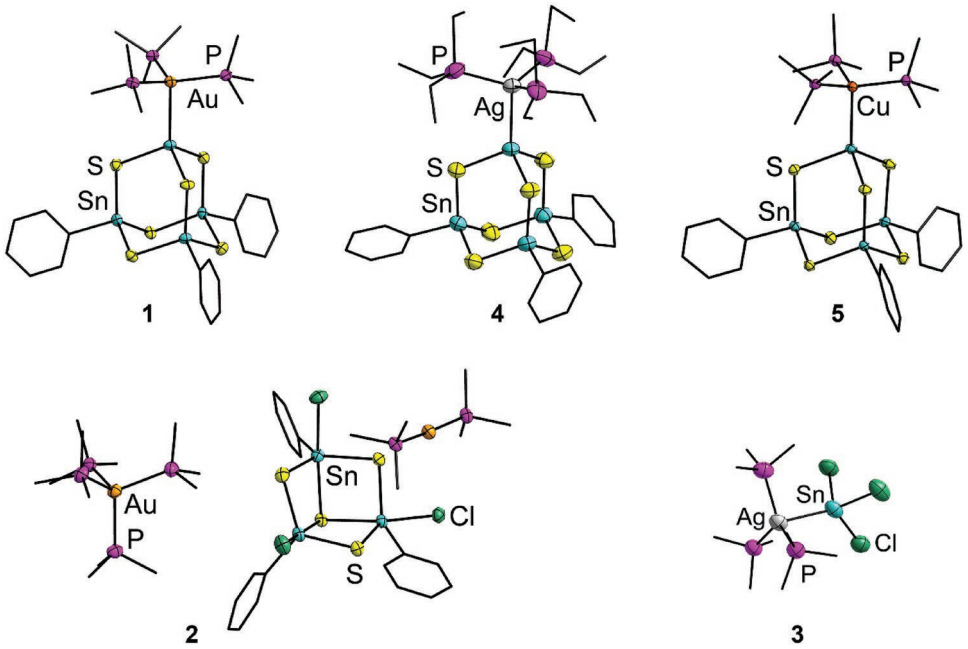

Figure 1. Molecular structures of compounds **1–5**. Ellipsoids (Sn, S, Au, Ag, Cu, P, Cl) are drawn at 50% probability. Organic groups are shown as black wires. Hydrogen atoms are omitted for clarity. For figures including the atom labeling scheme, see the Supporting Information.

chloride always yield **1**, while the use of a larger relative amount of the in situ-formed gold phosphine complex lead to the formation of a new compound, $[Au(PMe_3)_4][Au(PMe_3)_2][(PhSnCl)_3S_4]$ (**2**). Here, the gold phosphine complexes are not attached to the tin sulfide cluster, but instead serve as counterions for a dianionic tin sulfide cluster featuring a defect-heterocubane topology. This topology was, until now, known only for clusters where the organic substituent contains a σ-donor group that stabilizes this topology by coordination to the tin atom.[12] In this case, the organic ligand does not possess such a group, but the additional chloride substituent at each of the tin atoms also raises the corresponding coordination number to five, which also serves to stabilize the defect-heterocubane topology. The formation of **2** can be described by the following reaction scheme (Equation (2))

$$3\left[(PhSn)_4S_6\right] + 12\,AuCl + 26\,PMe_3 \rightarrow 4\,\mathbf{2} + 4\,Au + 2\,SPMe_3 \quad (2)$$

Elemental gold that formed as side-product was identified via PXRD of the precipitate from the reaction solution (see Figure S30, Supporting Information),[13] while the trimethyl phosphine sulfide was identified in the ^{31}P-NMR spectrum of the reaction solution (see Figure S14, Supporting Information).[14]

2 crystallizes in the monoclinic crystal system in the space group $P2_1/n$ with four formula units per unit cell. The $[(PhSnCl)_3S_4]^{2-}$ anion features pseudo-C_3 symmetry along an axis perpendicular to an Sn_3S_3 six-membered ring (Sn1, S3, Sn2, S2, Sn3, and S4), which runs through S3. Figure 1 (bottom left) illustrates the asymmetric unit of **2**, with the gold atom within the $[Au(PMe_3)_2]^+$ cation coordinated in an almost linear fashion. A detailed discussion of its structural features can be found in the Supporting Information.

As a subsequent step of our study, we transferred the synthesis of **1** to the homologous coinage metals Ag and Cu. Upon performing the previously described reaction with silver(I) chloride, we did not obtain an isostructural silver complex. Instead, $[(Me_3P)_3AgSnCl_3]$ (**3**) was obtained, containing a coinage metal complex known for the lighter and heavier homologues, but not yet for silver.[11,15] It crystallizes in the triclinic crystal system in the space group $P\bar{1}$ with four formula units per unit cell.

The Ag–P and Ag–Sn bond lengths are longer than the reported values of the M–Sn bonds in the corresponding Au and Cu complexes, showcasing the notably weaker metal–metal bond for M = Ag. The coordination geometry of the silver atom is distorted from an ideal tetrahedron more than in the copper and gold homologues and thus renders it a trigonal pyramidal rather than a pseudo-tetrahedral coordination. The molecular structure of **3** is shown in Figure 1, bottom right.

Upon changing the phosphine ligand to triethylphosphine, a complex that is analogous to compound **1** was finally obtained: $[\{(Et_3P)_3AgSn\}(PhSn)_3S_6]$ (**4**) crystallizes in the trigonal crystal system in the space group *P*-3 with two formula units per unit cell. The adamantane cage (Figure 1, top center) shows the same slight distortion as in **1**; however, the Sn–Ag bond is longer by 5.5 pm than the Sn–Au bond in **1**. It can be assumed that this is a sign of a comparably weak metal–metal bond, and also rationalizes that a slightly larger steric demand of triethylphosphine (Tolman cone angle: 132° vs 118° for PMe_3)[16] is needed to kinetically stabilize the cluster. We note that **4** is one of the rare compounds featuring a direct Ag–Sn bond, beside $[(RSn)_4(AgPPh_3)_2(SnCl)_2S_8]$ (R = $CMe_2CH_2C(O)Me$)[4c] and some stannaborate-decorated silver clusters.[17]

While it was not possible to synthesize a silver-substituted adamantane-type complex using PMe_3 as phosphine ligand,

this reaction succeeded for the lighter homologue. This way we obtained [{$(Me_3P)CuSn$}$(PhSn)_3S_6$] (**5**), hence, a complex isostructural to **1** (Figure 1, top right). **5** also crystallizes in the orthorhombic crystal system in the space group $CmC2_1$ with four formula units per unit cell. The inorganic core also shows a distortion of Sn3 from the position it would have in an ideal adamantane structure, as shown in the elongated Sn–S bond lengths of 2.500(2) and 2.516(4) Å, versus 2.355(2) to 2.411(2) Å for all other Sn–S bonds. The Sn–Cu bond length of 2.5818(18) Å is similar to the reported value in the known complex [$(Me_3P)_3CuSnCl_3$] (2.600 Å).[15] Further structural details can be found in the Supporting Information.

2.2. Quantum Chemical Investigation of the Cluster Structures

In order to understand the observation of different structures for the Ag versus the Cu and Au compounds, and to gain more insight into the geometric and electronic structures, we have performed DFT calculations of the clusters **1**, **4**, and **5**. Furthermore, we have calculated the hypothetical cluster [{$(Me_3P)_3AgSn$}$(PhSn)_3S_6$] (**4a**). The crystal structures have been used as starting points for the structure optimization. The calculated bond lengths and angles at both BP86-D3/cc-pVTZ(-PP) and PBE-D3/pw level of theory agree well with the experimental structures (see Table 1). Among the clusters, **1** shows the largest deviations from the experimental values. Though, the deviation is at most 1.4% and 2.3% for M–Sn and M–P bond lengths, respectively, and up to 3.1% for the angles. In further agreement with the experiment, the Sn–S bond length next to the connected coinage metal complex is similarly elongated for all clusters. The other structural parameters are very similar for all investigated clusters and close to the adamantane-type cluster core compounds such as [$(PhSn)_4S_6$]. The excellent agreement between cluster calculations with a localized basis set [BP86-D3/cc-pVTZ (-PP)] and periodic calculations within the supercell method employing a plane wave basis (PBE-D3/pw) shows that the latter approach is suitable for upcoming calculations of the crystalline phase.

Table 1. Calculated structural parameters (DFT) at BP86-D3/cc-pVTZ (-PP) (first line) as well periodic PBE-D3/pw (second line) level of theory of the isostructural cluster compounds [{$(R_3P)_3MSn$}{$PhSn$}$_3S_6$] with R/M = Me/Au (**1**), Et/Ag (**4**), or Me/Cu (**5**). Experimental values are given in parentheses for comparison.

	1 [Å, deg]	**4** [Å, deg]	**5** [Å, deg]
M	Au	Ag	Cu
Sn–S	2.41–2.44; 2.40–2.44 (2.35–2.41)	2.40–2.44; 2.42–2.44 (2.36–2.41)	2.41–2.44; 2.40–2.44 (2.36–2.41)
Sn–S (close to M)	2.52; 2.52 (2.50–2.51)	2.52–2.53; 2.47–2.49 (2.50)	2.52; 2.52 (2.52)
Sn–C	2.15; 2.16 (2.11–2.12)	2.15; 2.15–2.16 (2.12)	2.15; 2.15 (2.11–2.12)
M–Sn	2.73; 2.75 (2.72)	2.73; 2.76 (2.77)	2.56; 2.58 (2.58)
M–P	2.38 – 2.39; 2.38 (2.36–2.37)	2.44–2.46; 2.47 – 2.52 (2.45–2.48)	2.25; 2.24 (2.25)
Sn–S–Sn	103.0–109.1; 102.9–109.3 (101.9–112.6)	102.3–111.0; 102.0–109.5 (102.4–113.2)	103.1–109.1; 102.9–109.5 (102.0–112.7)
S–Sn–S	106.7–113.8; 106.3–114.2 (104.3–114.7)	105.1–114.6; 103.5–116.7 (102.8–115.6)	106.6–114.4; 106.3– 14.5 (100.5–114.6)
Sn–M–P	97.9–100.6 99.0–99.3 (100.06– 102.44)	102.8–105.3 100.0–100.2 (103.21–125.17)	100.7–101.0 101.2–101.4 (101.64–104.20)

Dispersion corrections improve the agreement between theory and experiment concerning the structural parameters shown in Table 1 (see Supporting Information for the values calculated without D3). However, the phenyl orientation changes by applying dispersion correction compared to the crystal structure, as shown in **Figure 2**. This effect concerns in particular cluster **4**. Here, we can conclude that intramolecular dispersion interactions between the larger phosphine ligands and the phenyl rings are important. Neglecting the crystal environment (intermolecular interactions) in our calculations results in changed phenyl orientations of the single cluster molecules due to intramolecular interactions.

For a direct comparison with **1** and **5**, we have furthermore calculated the hypothetical Ag cluster **4a** (which could not be synthesized) based on the crystal structure data of **1**. The corresponding structural parameters are shown in Table S17 in the Supporting Information. In the [{$(Me_3P)_3MSn$}$(PhSn)_3S_6$] series with M = Cu, Ag, Au, the M–Sn and M–P bond lengths increase in the order Cu < Au < Ag. However, while Au–Sn and Ag–Sn are very similar, the Au–P and Ag–P distances differ. The difference is in agreement with the development of corresponding bond lengths in coinage metal phosphine (PH_3) complexes and coinage metal dimers.[18,19] The origin of the obtained deviation of the subgroup order is due to relativistic effects for the gold atom, which increase the gold electron affinity and lead to stronger binding for Au–P and Au–Au bonds. This can be transferred to the Au–PMe_3 and Au–Sn moieties within this study.

The Sn–M–P angle is the only structural parameter that significantly differs between the hypothetical cluster **4a** and the experimentally found cluster **4**. Indeed, its value in the molecule with an [$Ag(PEt_3)_3$] substituent (102.8–105.3°, according to our BP86-D3/cc-pVTZ(-PP) calculations) is larger by about 4.8° than in the cluster with the [$Ag(PMe_3)_3$] group (98.0–100.5°, according to our BP86-D3/cc-pVTZ(-PP) calculations), and thus even larger than in cluster **5** featuring a terminal [$Cu(PMe_3)_3$] complex.

Notably, while the hypothetical **4a** cluster structure was calculated (based on the crystal structure data of **1**) to be most stable in a staggered orientation of phenyl rings and PMe_3 groups (**Figure 3**, left), the experimentally confirmed cluster **4** prefers an eclipsed orientation, in agreement with the calculations. Thus, we conclude that the maximal dispersion interaction of the cluster with the larger PEt_3 ligands is reached

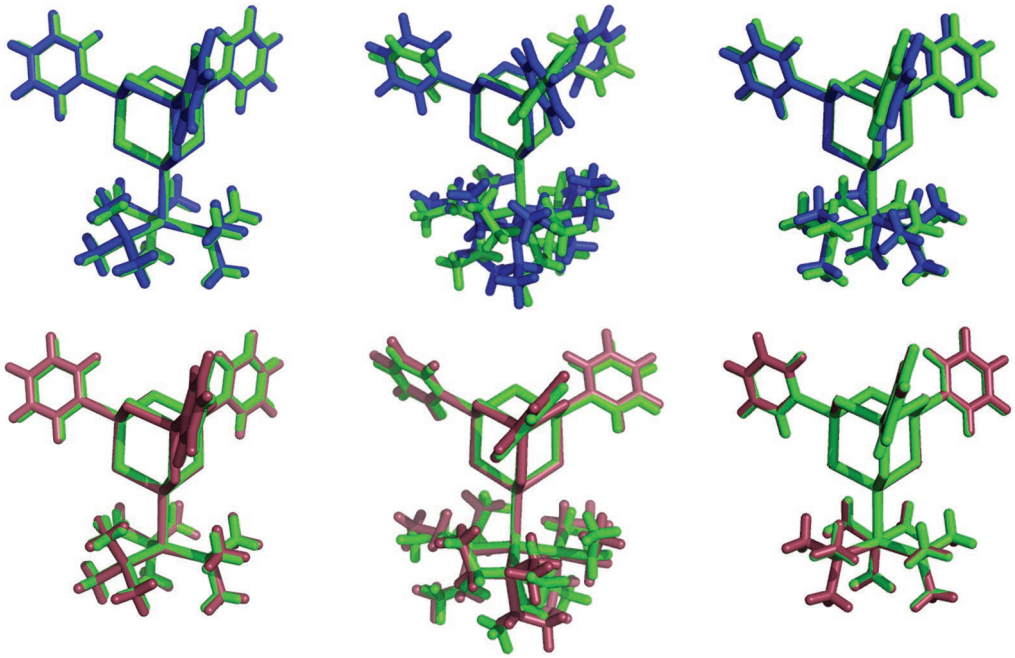

Figure 2. Overlay of crystal structures (green) with structures calculated at BP86-D3/cc-pVTZ(-PP) (blue, top row) and BP86/cc-pVTZ(-PP) (raspberry, bottom row) level of theory, indicating a better fit without consideration of dispersion interactions. Left: **1**. Center: **4**. Right: **5**.

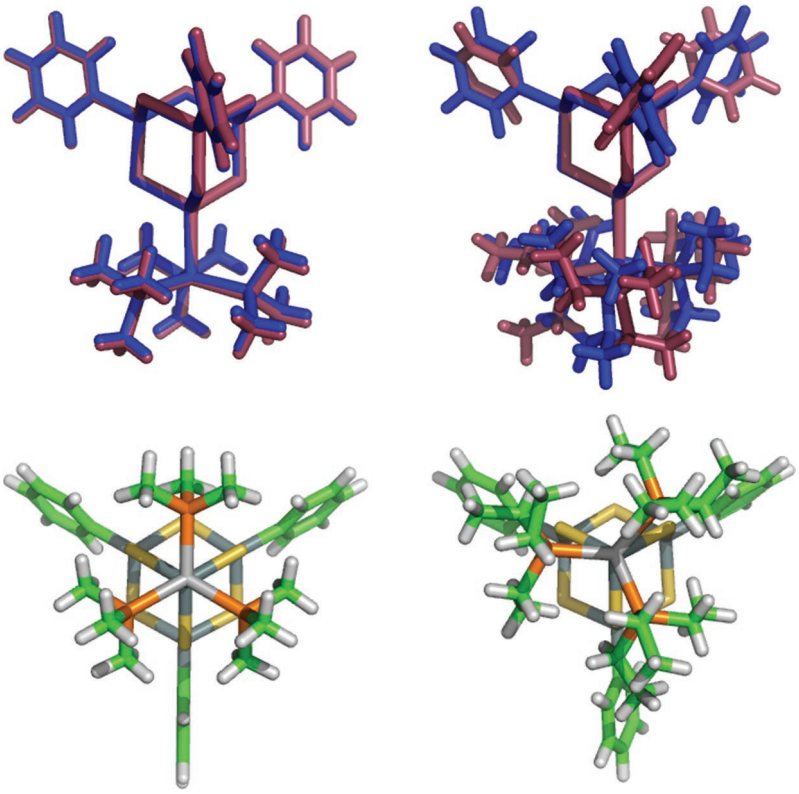

Figure 3. Overlay of the structures calculated at BP86-D3/cc-pVTZ(-PP) (blue) level of theory with the ones calculated at BP86/cc-pVTZ(-PP) (raspberry) level of theory. Furthermore, the structures calculated with dispersion corrections are shown in a different orientation (color code for the latter: Sn (blue grey), S (yellow), C (green), P (orange), H (white), and Ag (gray)). Left: **4a**. Right: **4**.

when the phosphine groups orient along the phenyl rings of the cluster (Figure 3, right). This changed orientation comes along with larger Sn–Ag–P angles for a better match.

Finally, we compare in Figure 3 the structures calculated with and without dispersion correction to investigate the intramolecular dispersion interaction between the PEt_3 ligands and phenyl rings. The orientations of both phosphine ligands and phenyl groups change clearly for the cluster with PEt_3 ligands, whereas there are no significant changes for the cluster with PMe_3 ligands. These stabilizing dispersion interactions between the silver complex and the cluster might explain why cluster **4** was isolated, while cluster **4a**, which additionally comprised the weakest M–Sn interaction as compared to M = Cu and Au, could not be isolated in the absence of these intramolecular interactions. Interestingly, the staggered orientation of PMe_3 ligands and phenyl rings is also obtained for cluster **1**, but cluster **5** yields an orientation between staggered and eclipsed.

The mass spectra of **1**, **4**, and **5** reflect a trend in the stability of the Sn–M bond (see Figures S1–S8, Supporting Information). While in **4** and **5**, fragments with intact Sn–M bond can be detected in the ESI(+) mass spectra, the Sn–Au bond is cleaved in **1**, so that an anionic tin sulfide fragment is observed in the ESI(–) spectrum, while the

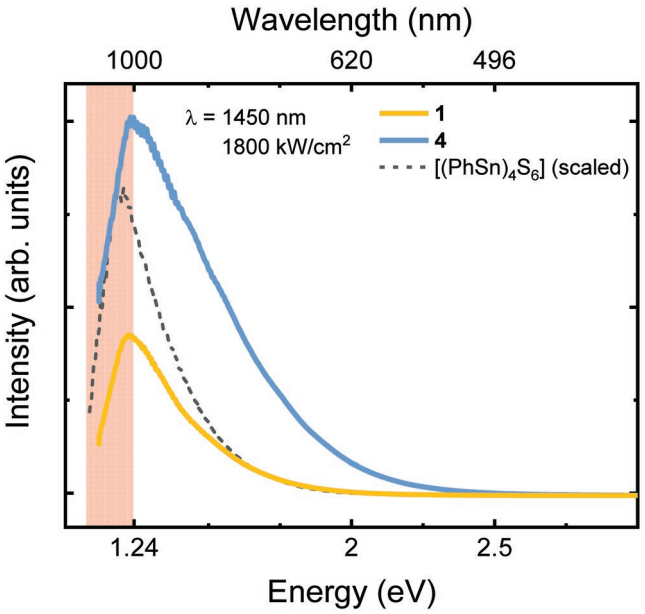

Figure 4. White-light emission of compounds **1** (yellow) and **4** (blue). Additionally, the dashed line shows the $[(PhSn)_4S_6]$ reference emission (scaled, excitation power density was 400 kW cm^{-2}). A continuous wave 1450 nm IR laser diode was used as the excitation source. In the red area, i.e., above 1000 nm, instrument response effects of the used silicon charge-coupled device array detector, which was cooled down to –60 °C, have to be considered.

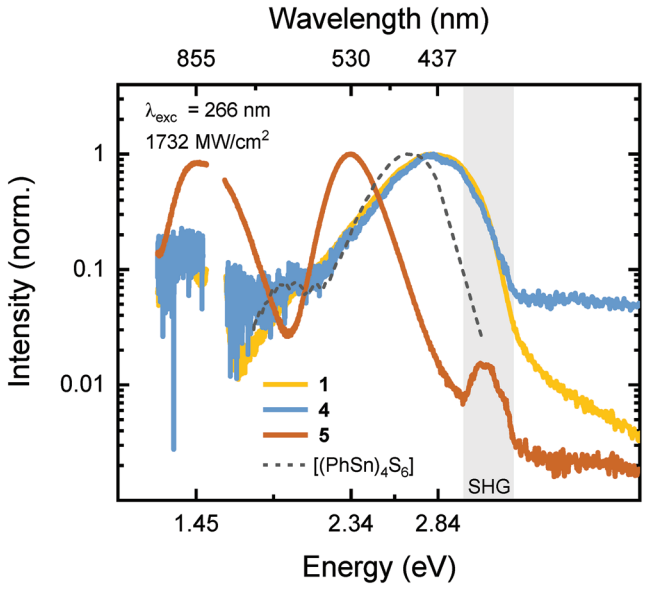

Figure 5. Normalized photoluminescence of compounds **1** (yellow), **4** (blue), and **5** (brown). Additionally, the dashed line represents the photoluminescence of $[(PhSn)_4S_6]$ as a reference system (from ref. [7]). The missing points at 800 nm are due to the fundamental Ti:Sapphire laser line which was frequency-tripled to reach the excitation wavelength of 266 nm. The second harmonic (SHG) peak at 400 nm is a residual from the third harmonic generation process of the exciting laser.

gold complex fragments form a new $[AuP(PMe_3)H]^+$ cluster during the ionization process.

2.3. Measurement of Optical Properties

Adamantane-type clusters have been recently shown to possess strong nonlinear optical properties. The previously studied cluster $[(PhSn)_4S_6]$, for instance, exhibits very efficient white-light generation, which was tentatively attributed to the delocalized π-systems provided by the four phenyl ligands. However, the effect was so far only detected for samples missing long-range order, thus for amorphous compounds. We were interested to see whether the introduction of molecular asymmetry would also cause white-light generation even in a crystalline sample. We, therefore, measured the white-light generated by such nonlinear interactions (**Figure 4**), and the photoluminescence (**Figure 5**) in the single-crystalline compounds **1**, **4**, and **5**, which differ from $[(PhSn)_4S_6]$ solely in the replacement by one of the phenyl ligands by a coinage metal complex.

Although being single-crystalline upon synthesis, **1** and **4** show white-light emission beginning at 2.25 eV (Figure 4). However, as confirmed by powder diffraction (see Figures S27–S29, Supporting Information), the samples undergo amorphization upon irradiation, which was hence confirmed a necessary condition for the white-light generation. The lower-energy boundary of the WL band could not be determined due to the instrument-limited responsivity of the used silicon deep-depletion charge-coupled device array detector (red area in Figure 4).

Intriguingly, compound **5** does not show any emission under irradiation of light with an excitation energy below its highest occupied molecular orbital (HOMO)–lowest occupied molecular orbital (LUMO) transition energy (2.34 eV). Hence, we also irradiated the samples above the HOMO–LUMO transition energy to measure the photoluminescence (PL) properties of **1**, **4**, and **5** (Figure 5). The first two show a very similar PL around 2.84 eV. A very weak second emission band is observed around 1.45 eV. Here, the structure of the substituted ligand does not appear to affect the emission profile at all. The PL of **5** is distinctly different: two pronounced peaks are observed at 1.45 and 2.34 eV, respectively; the peak around 1.45 eV is significantly enhanced as compared to **1**, **4**. Consequently, this emission pattern hinders the white-light generation, since it provides a reabsorption channel for photons with energies in the visible spectrum.

2.4. Quantum Chemical Studies of the Optical Properties

For a deeper insight into the optical properties of the clusters, lowest singlet and triplet excitations of the synthesized clusters **1**, **4**, and **5** were calculated by using time-dependent DFT (TD-DFT) and different functionals. The results are summarized in **Table 2**.

The calculated triplet excitations (BP86 functional) are close to the one calculated for $[(StySn)_4S_6]$ (2.8 eV), and they increase slightly along Au > Cu > Ag. The lowest singlet excitation is in each case about 0.1 eV higher in energy. Thus, the difference between singlet and triplet excitation is smaller than that for $[(StySn)_4S_6]$ (Sty = 4-vinylphenyl), where it is 0.35 eV. By

Table 2. Lowest triplet and singlet excitations (eV) calculated with TD-DFT for different density functionals and cc-pVTZ(-PP) basis sets.

	BP86-D3	TPSS-D3	B3LYP-D3
		1	
Triplet	2.62	2.74	2.97
singlet	2.70	2.81	3.27
		4	
triplet	2.82	2.94	3.33
singlet	2.91	3.03	3.50
		5	
triplet	2.72	2.83	3.23
singlet	2.79	2.91	3.42

applying the TPSS functional, the calculated excitation energies are shifted toward higher energies by 0.1 eV and by applying the B3LYP functional by 0.3–0.6 eV. For the latter, also the difference between the lowest singlet and triplet excitation energy is increased. Furthermore, we compared the orbitals that are relevant for the excitations to the ones of the $[(PhSn)_4S_6]$ cluster. The HOMO exhibits σ_{AuSn}-like character with the main contribution from an Au 6s orbital and small contributions of sulfur p-orbitals next to the complex, whereas the LUMO shows σ^*_{SnS}-like character at atoms most distant from the metal complex substituent (**Figure 6**). Corresponding MOs calculated at the PBE-D3/pw level of theory are in qualitative agreement, and are shown in Figures S28–S31 in the Supporting Information. The HOMO and LUMO are very similar for the clusters **1**, **4**, and **5**. Thus, the character of the excitations changes compared to the $[(PhSn)_4S_6]$ cluster due to the attached complex. This leads to a shift of the excitation energies.

We note that our calculated results of excitation energies consider the Franck–Condon excitation and, thus, cannot be compared directly to the experimental photoluminescence data. However, the excitation values of the clusters **1** and **4** are similar to the PL values. The changed photoluminescence of cluster **5** compared to **1** ad **4** hints toward a more complex potential energy surfaces of the excited states and/or the ground states. The calculations further indicate that the ionization energies of the clusters **1**, **4**, and **5** lie between 5.7 and 5.9 eV, which is indicative of the limit of their stability against irradiation.

3. Conclusion

Asymmetrically substituted clusters $[\{(R_3P)_3MSn\}\{PhSn\}_3S_6)]$, with R/M = Me/Au (**1**), Et/Ag (**4**), and Me/Cu (**5**) were obtained upon exchange of one phenyl ligand in $[(PhSn)_4S_6]$ by $[M(PR_3)_3Cl]$, while an excess of the gold complex afforded the ionic compound $[Au(PMe_3)_4][Au(PMe_3)_2][(PhSnCl)_3S_4]$ (**2**). With PMe_3 instead of PEt_3 ligands, compound $[(Me_3P)_3AgSnCl_3]$ (**3**) was obtained, as rationalized by means of DFT calculations. The photophysical properties of **1**, **4**, and **5** were measured and compared with each other. The results indicate three points. First, the molecular asymmetry introduced by a metallo-ligand at one of the group 14 atoms is not a sufficient condition for white-light generation, which still requires the presence of an intermolecularly disordered (amorphous) compound. Second, the presence of metallo-ligands does not affect the PL emission pattern and the capability and onset of white-light generation in general, but, third, the group 11 atom itself does have strong impact on the PL emission. Consequently, in this case the white-light generation is completely hindered for the copper compound **5**, due to reabsorption processes. These results put the analysis of the still not understood white-light generation by means of amorphous molecular materials one step forward.

4. Experimental Section

General: All synthetic steps were carried out under exclusion of oxygen and moisture by use of standard Schlenk procedures. Phenyltin trichloride, sodium sulfide, trimethylphosphine, triethylphosphine, and copper(I) chloride were prepared according to literature procedures.[20] Gold(I) chloride (abcr) and silver(I) chloride (Carl Roth) were used as

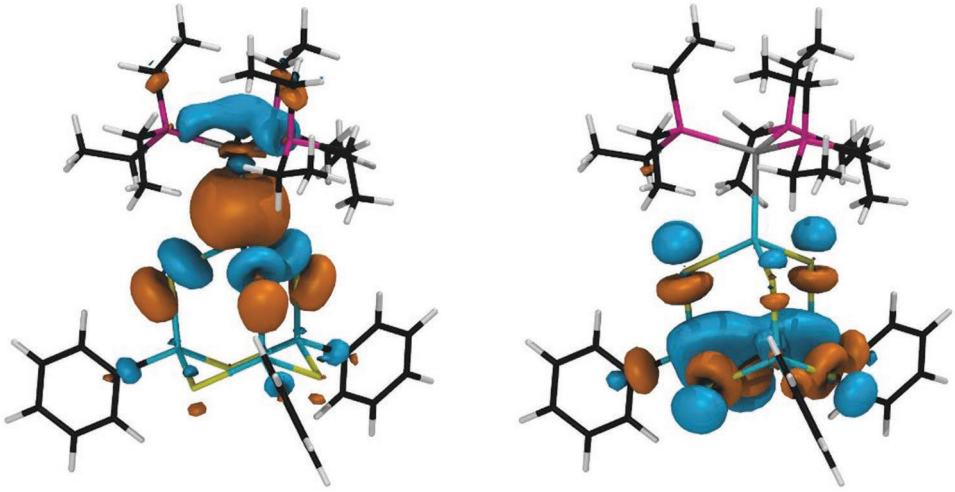

Figure 6. Orbitals of the lowest triplet (and singlet) excitation. The excitation takes place from the HOMO (left) to the LUMO (right). The orbitals are shown for the cluster $[\{(Et_3P)_3AgSn\}(PhSn)_3S_6]$ (4) as an example [color code: Sn (turquoise), S (yellow), C (black), P (pink), H (white), and Ag (grey)].

received. HR-ESI mass spectra (Figures S1–S8, Supporting Information) were acquired with an LTQ-FT ultra mass spectrometer (Thermo Fischer Scientific). The resolution was set to 100,000. Yields were based on the amount of Sn and refer to the amount of product isolated as single crystals. ^{1}H, ^{13}C, ^{31}P, and ^{119}Sn NMR spectroscopy was carried out at 25 °C using Bruker DRX 300 MHz and DRX 500 MHz spectrometers (Figures S9–S16, Supporting Information). The chemical shifts are given in ppm relative to the residual protons of deuterated solvents for ^{1}H spectra and relative to the solvent signal for ^{13}C spectra. ^{13}C, ^{31}P, and ^{119}Sn spectra were measured with ^{1}H decoupling. Me_4Sn was used as internal standard in ^{119}Sn NMR measurements. Infrared spectra (Figures S17–S21, Supporting Information) were measured on a Bruker Tensor 37 ATR spectrometer. The μ-XRF measurement was performed with a Bruker M4 Tornado, equipped with a Rh-target X-ray tube and a silicon drift detector. The data were collected through mapping of a freshly mounted crystal that was immersed in a thin protective coating of nondrying high viscosity oil (21 cSt). Mapping was performed with 5 μm spot sizes on a 5 μm x 5 μm grid and emitted fluorescence photons were detected with acquisition times of 5 ms per spot. All data points were averaged over three full cycles. Quantification of the elements was achieved through deconvolution of the spectra (see Figures S22–S26, Supporting Information). Raman spectra were recorded with a commercially available confocal Raman microscope (Renishaw inVia Qontor) using a HeNe Laser at 632.8 nm for excitation (see Figure S40, Supporting Information).

*Synthesis of $[(PhSn)_4S_6]$ (**A**)*: Compound **A** was prepared by a modified literature procedure.[10] Anhydrous sodium sulfide (3.56 g, 45.0 mmol) was suspended in THF (200 mL), phenyltin trichloride (5.00 mL, 30.4 mmol) was added and the resulting suspension stirred at room temperature for 24 h. The solvent was removed in vacuo and the off-white residue was taken up in water (40 mL), filtered, and washed five times with water (40 mL each). After drying in vacuum, **A** was obtained as a fine, colorless powder. Yield: 6.45 g, 6.61 mmol, 87%. All analytical data are in agreement with reported data.[10]

*Synthesis of $[\{(Me_3P)_3AuSn\}\{PhSn\}_3S_6]$ (**1**)*: **A** (30 mg, 31 μmol) and gold(I) chloride (7 mg, 30 μmol) were suspended in THF (3 mL) and trimethylphosphine (0.01 mL, 100 μmol) was added. After stirring the resulting yellow solution for 20 h at room temperature, it was filtered and layered with diethyl ether (1 mL) and n-pentane (3 mL). Colorless crystals of **1** formed within one day. Yield: 14 mg (10.6 μmol, 34%). ^{1}H-NMR (CD_2Cl_2, 300 MHz): δ = 1.54 (d, 27H, PMe_3, J = 6.0 Hz), 7.38–7.48 (m, 9H, C_{arom}), 7.63–7.68 (m, 6H, C_{arom}) ppm. IR: $\tilde{\nu}$ = 2962 (m), 1411 (w), 1260 (s), 1089 (s), 1017 (s), 942 (w), 865 (w), 797 (s), 691 (w), 442 (w) cm^{-1}. HRMS (ESI+): m/z calcd: 851.0133 $[Au_3P(PMe_3)_3H]^+$, found: 851.0032. HRMS (ESI–): m/z calcd: 1010.5665 $[(PhSn)_4S_6Cl]^-$; found: 1010.5677. CHN analysis (% calcd, % found for $C_{27}H_{42}Au_1P_3Sn_4S_6$ · 1 THF): C (26.68, 26.30), H (3.61, 3.63). μ-XRF data deviate from the calculated values owing to the very small crystal thickness that does not allow for the required penetration depth (see Figure S22, Supporting Information).

*Synthesis of $[(Me_3P)_4Au][(Me_3P)_2Au][(PhSnCl)_3S_4]$ (**2**)*: **A** (30 mg, 31 μmol) and gold(I) chloride (29 mg, 123 μmol) were suspended in THF (5 mL). After addition of trimethylphosphine (0.04 mL, 400 μmol), the resulting suspension was stirred at room temperature for 19 h. After filtration, the filtrate was layered with diethyl ether (2 mL) and n-pentane (5 mL). Colorless crystals of **2** formed within four days. Yield: 11 mg (6.6 μmol, 16%). ^{1}H-NMR (CD_2Cl_2, 300 MHz): δ = 1.49 (d, 54H, PMe_3, J = 6.0 Hz), 7.31–7.36 (m, 9H, C_{arom}), 8.07–8.11 (m, 6H, C_{arom}) ppm. ^{13}C-NMR (CD_2Cl_2, 75 MHz): δ = 19.0 (d, PMe_3), 128.3 (C_{arom}), 129.2 (C_{arom}), 135.6 (C_{arom}), 150.9 (C_{arom}) ppm. ^{31}P-NMR (CD_2Cl_2, 101 MHz): δ = –15.7 ppm (PMe_3). ^{119}Sn-NMR (CD_2Cl_2, 98 MHz): δ = –261 ppm. IR: $\tilde{\nu}$ = 2950 (s), 2926 (s), 1600 (w), 1471 (m), 1389 (m), 1366 (m), 1229 (m), 1101 (m), 962 (m), 806 (w), 752 (w), 697 (m), 440 (w) cm^{-1}. HRMS (ESI+): m/z calcd: 851.0133 $[Au_3P(PMe_3)_3H]^+$, found: 851.0032. HRMS (ESI–): m/z calcd: 786.6499 $[(PhSn)_3S_4Cl_2]^-$; found: 786.6493. CHN analysis (% calcd, % found for $C_{36}H_{69}Au_2P_6Sn_3S_4$ · 2 THF): C (29.09, 29.43), H (4.72, 4.71). μ-XRF data deviate from the calculated values owing to the very small crystal thickness that does not allow for the required penetration depth (see Figure S23, Supporting Information).

*Synthesis of $[(Me_3P)_3AgSnCl_3]$ (**3**)*: **A** (100 mg, 102 μmol) and silver(I) chloride (15 mg, 105 μmol) were suspended in dichloromethane (10 mL). After addition of trimethylphosphine (0.03 mL, 300 μmol), the resulting suspension was stirred at room temperature for 2 h. Subsequent removal of the solvent in vacuo afforded a colorless solid that was taken up in THF (10 mL) and filtered. The colorless filtrate was layered with n-hexane (10 mL). Colorless crystals of **3** were obtained after one week. Yield: 8 mg (14 μmol, 5%). ^{1}H-NMR (CD_2Cl_2, 300 MHz): δ = 1.64 (d, 9H, $^{2}J_{P\text{-}H}$ = 7.5 Hz, PMe_3) ppm. ^{13}C-NMR (CD_2Cl_2, 75 MHz): δ = 16.6 ppm. ^{31}P-NMR (CD_2Cl_2, 122 MHz): δ = 29.0 ppm. IR: $\tilde{\nu}$ = 3040 (w), 2960 (w), 2894 (w), 1570 (w), 1474 (w), 1429 (m), 1296 (w), 1281 (w), 1260 (w), 1060 (w), 1017 (w), 996 (w), 946 (s), 727 (s), 699 (s), 446 (s) cm^{-1}. CHN analysis (% calcd, % found for $C_9H_{27}Ag_1P_3Sn_1Cl_3$): C (19.26, 19.57), H (4.85, 4.77). μ-XRF data deviate from the calculated values owing to a surficial impurity upon isolation of the crystals (see Figure S24, Supporting Information).

*Synthesis of $[\{(Et_3P)_3AgSn\}\{PhSn\}_3S_6]$ (**4**)*: **A** (100 mg, 102 μmol) and silver(I) chloride (15 mg, 105 μmol) were suspended in THF (10 mL). After addition of triethylphosphine (0.05 mL, 337 μmol), the resulting suspension was stirred at room temperature for 15 h. After filtration and layering with n-pentane (10 mL), **4** was obtained as colorless needles within six days. Yield: 22 mg (16 μmol, 16%). IR: $\tilde{\nu}$ = 1305 (m), 1235 (s), 1208 (s), 1153 (s), 983 (m), 508 (m), 429 (m) cm^{-1}. HRMS (ESI+): m/z calcd: 1169.6286 $[\{(Et_3P)_2AgSn\}(PhSn)_2(ClSn)S_4O_2H]^+$, found 1169.6316; calcd: 1185.6063 $[\{(Et_3P)_2AgSn\}(PhSn)_2(ClSn)S_5OH]^+$, found 1185.6264. HRMS (ESI–): m/z calcd: 898.5588 $[Ph_3Sn_4S_6]^-$, found: 898.5608; calcd: 994.5966 $[(PhSn)_4S_6F]^-$, found: 994.5955. CHN analysis (% calcd, % found for $C_{36}H_{60}Ag_1P_3Sn_4S_6$): C (31.77, 31.88), H (4.44, 4.45). μ-XRF (% calcd, % found for Ag/P/Sn/S 1:3:4:6): Ag (7.14, 6.16), P (21.43, 24.10), Sn (28.57, 30.43), S (42.86, 40.43), see Figure S25 in the Supporting Information.

*Synthesis of $[\{(Me_3P)_3CuSn\}\{PhSn\}_3S_6]$ (**5**)*: **A** (100 mg, 102 μmol) and copper(I) chloride (10 mg, 101 μmol) were suspended in dichloromethane (10 mL). After addition of trimethylphosphine (0.03 mL, 300 μmol), the resulting suspension was stirred at room temperature for 2.5 h. After removal of the solvent in vacuo, the residue was taken up in THF (10 mL) and stirred for another 16 h at room temperature. Subsequently, the clear solution was layered with n-hexane (10 mL). Golden crystals of **5** formed within one day. Yield: 35 mg (29 μmol, 29%). ^{1}H-NMR (CD_2Cl, 300 MHz): δ = 1.35 (s, 27H, PMe_3), 7.42–7.46 (m, 9H, H_{arom}), 7.64–7.69 (m, 6H, H_{arom}) ppm. IR: $\tilde{\nu}$ = 2961 (m), 1428 (m), 1257 (s), 1069 (s), 1011 (s), 940 (m), 865 (w), 792 (s), 725 (m), 692 (m), 443 (m) cm^{-1}. HRMS (ESI+): m/z calcd: 962.4946 $[(CuSn)(PhSn)_3S_6{+}H]^+$; found: 962.4951; calcd: 1038.5388 $[\{(Me_3P)CuSn\}\{PhSn\}_3S_6{+}H]^+$ found: 1038.5394. HRMS (ESI–): m/z calcd: 898.5577 $[(PhSn)_3SnS_6]^-$; found: 898.5586. CHN analysis (% calcd, % found for $C_{27}H_{42}Cu_1P_3Sn_4S_6$): C (27.24, 27.08), H (3.56, 3.66). μ-XRF data deviate from the calculated values owing to the very small crystal thickness that does not allow for the required penetration depth (see Figure S26, Supporting Information).

X-Ray Diffraction and Structure Analyses: Data of the X-ray diffraction analyses were collected on a STOE IPDS 2 (**1**, **2**) or IPDS 2T (**3**, **4**, **5**) imaging plate diffractometer using $Mo_{K\alpha}$ radiation with graphite monochromatization (λ = 0.71073 Å) at 100 K. Reflection data were processed with X-Area 1.77.[21] Structure solution was performed by direct methods and full-matrix-least-squares refinement against F^2 using SHELXT[22] and SHELXL-2014[23] software. Powder diffraction data were collected on a STOE StadiMP diffractometer, equipped with a Mythen 1K silicon strip detector and a Cu-Kα X-ray source (λ = 1.54056 Å). Samples were measured in reflection mode between sheets of scotch tape. CCDC 1875435 – 1875439 contains the supporting crystallographic data for this paper. These data can be obtained free of charge from The Cambridge Crystallographic Data Centre via www.ccdc.cam.ac.uk/data_request/cif.

Computational Methods: Non periodic density functional theory calculations were carried out using the software package TURBOMOLE v6.6.[24] Structure optimizations were performed with the RIDFT program,[25] the BP86 density functional,[26,27] and grid size m4. The convergence criterion of the iteration cycle was set to 10^{-8} Hartree. Dispersion correction was utilized in Grimme's D3 scheme with zero-damping.[28] The elements Cu, S, P, C, and H were characterized in an all electron description using the correlation consistent (cc-pVTZ) Dunning-type basis set.[29] For the elements Au, Ag, and Sn the energy-consistent scalar-relativistic effective core potentials ECP60MWB, ECP28MWB, and ECP28MDF, respectively, in combination with the corresponding basis sets (cc-pVTZ-PP) were employed.[30] Frequency calculations were performed to confirm the presented stationary points as minima. In all cases low imaginary frequencies (in the range of 1.4 to 9.4 cm^{-1}) were found and identified as translational and rotational contributions. Electronic excitations were investigated by means of time-dependent density functional theory (TD-DFT)[31] using the ESCF program[32] employing different exchange-correlation functionals (BP86, B3PLYP,[27,33] and TPSS[34]).

Moreover, the Vienna ab initio simulation package[35] was used to evaluate the structural properties of the synthetized coinage metal complexes by periodic DFT. Isolated molecules were modeled within a box of 24 × 25 × 26 Å. Projected augmented wave pseudopotentials[36] were used to describe the ion–electron interaction. The generalized gradient approximation in the PBE formulation[37] was used to describe the electronic many-body interactions. The atomic positions were relaxed until the residual Hellmann–Feynman forces were lower than 0.001 eV $Å^{-1}$. The accurate modeling of (in particular, loosely) bonded adsorbate systems was a major challenge for DFT, as (semi)local exchange-correlation (XC) functionals did not properly describe the long-range van der Waals (vdW) interactions. Here, a semi-empirical DFT-D3 scheme with zero damping was applied,[28] which was sufficiently accurate to allow for valid conclusions concerning structural properties. Plane waves up to a cutoff of 400 eV were used as basis for the expansion of electron wave functions.

Optical Spectroscopy: Photoluminescence spectroscopy (PL) and steady-state white-light spectroscopy revealed the optical properties of those complexes. The same setup as in ref. [7] with a frequency-tripled excitation at 266 nm was used for PL measurements. Contrary to these previous studies, a 1450 nm semiconductor diode was used instead of an excitation source at 980 nm. Further details are provided in the Supporting Information.

Supporting Information

Supporting Information is available from the Wiley Online Library or from the author.

Acknowledgements

This work was supported by the Deutsche Forschungsgemeinschaft (DFG) within the framework of GRK 1782 (S.C., S.D.) and within the framework of FOR 2824 (S.S., D.M.). The authors thank Marius J. Müller for recording the Raman spectra. The Höchstleistungrechenzentrum Stuttgart (HLRS) is gratefully acknowledged for grants of high-performance computer time. The authors acknowledge computational resources provided by the HPC Core Facility and the HRZ of the Justus Liebig University Giessen.

Conflict of Interest

The authors declare no conflict of interest.

Keywords

amorphous molecular materials, DFT calculations, metal–tetrel chalcogenide clusters, supercontinuum generation, white-light emitters

Received: December 21, 2018
Revised: March 14, 2019
Published online:

[1] a) O. Fuhr, S. Dehnen, D. Fenske, *Chem. Soc. Rev.* **2013**, *42*, 1871; b) J. F. Corrigan, O. Fuhr, D. Fenske, *Adv. Mater.* **2009**, *21*, 1867; c) V. Chauhan, A. C. Reber, S. N. Khanna, *J. Am. Chem. Soc.* **2017**, *139*, 1871; d) J. L. Durham, W. B. Wilson, D. N. Hugh, R. McDonald, L. F. Szczepura, *Chem. Commun.* **2015**, *51*, 10536; e) A. M. Polgar, F. Weigend, A. Zhang, M. J. Stillman, J. F. Corrigan, *J. Am. Chem. Soc.* **2017**, *139*, 14045; f) V. Chauhan, A. C. Reber, S. N. Khanna, *J. Am. Chem. Soc.* **2017**, *139*, 1871; g) S. Li, X.-S. Du, B. Li, J.-Y. Wang, G.-P. Li, G.-G. Gao, S.-Q. Zang, *J. Am. Chem. Soc.* **2018**, *140*, 594; h) S. Li, Z.-Y. Wang, G.-G. Gao, B. Li, P. Luo, Y.-J. Kong, H. Liu, S.-Q. Zang, *Angew. Chem., Int. Ed.* **2018**, *57*, 12775; i) X.-Y. Dong, H.-L. Huang, J.-Y. Wang, H.-Y. Li, S.-Q. Zang, *Chem. Mater.* **2018**, *30*, 2160.

[2] a) X.-J. Wang, T. Langetepe, C. Persau, B.-S. Kang, G. M. Sheldrick, D. Fenske, *Angew. Chem., Int. Ed.* **2002**, *41*, 3818; b) A. M. Polgar, C. B. Khadka, M. A. Fard, B. Nikkel, T. O'Donnell, T. Neumann, K. Lahring, K. Thompson, C. Cadogan, F. Weigend, J. F. Corrigan, *Chem. - Eur. J.* **2016**, *22*, 18378; c) D. Fuhrmann, S. Dietrich, H. Krautscheid, *Chem. - Eur. J.* **2017**, *23*, 3338.

[3] a) D. Fenske, C. Persau, S. Dehnen, C. E. Anson, *Angew. Chem., Int. Ed.* **2004**, *43*, 305; b) A. I. Wallbank, A. Borecki, N. J. Taylor, J. F. Corrigan, *Organometallics* **2005**, *24*, 788.

[4] a) C. B. Khadka, B. K. Nafajabadi, M. Hesari, M. Workentin, J. F. Corrigan, *Inorg. Chem.* **2013**, *52*, 6798; b) E. G. Tulsky, J. R. Long, *Inorg. Chem.* **2001**, *40*, 6990; c) J. P. Eußner, S. Dehnen, *Chem. Commun.* **2014**, *50*, 11385.

[5] S. Dehnen, M. Mellulis, *Coord. Chem. Rev.* **2007**, *251*, 1259.

[6] a) S. V. Kershaw, A. S. Susha, A. L. Rogach, *Chem. Soc. Rev.* **2013**, *42*, 3033; b) L. Nicole, C. Laberty-Robert, L. Rozes, C. Sanchez, *Nanoscale* **2014**, *6*, 6267.

[7] a) N. W. Rosemann, J. P. Eußner, A. Beyer, S. W. Koch, K. Volz, S. Dehnen, S. Chatterjee, *Science* **2016**, *352*, 1301; b) N. W. Rosemann, J. P. Eußner, E. Dornsiepen, S. Chatterjee, S. Dehnen, *J. Am. Chem. Soc.* **2016**, *138*, 16224.

[8] a) X. He, V. W.-W. Yam, *Coord. Chem. Rev.* **2011**, *255*, 2111; b) T. Seki, N. Todokai, T. Omagari, T. Nakanishi, Y. Hasegawa, T. Iwasa, T. Taketsugu, H. Ito, *J. Am. Chem. Soc.* **2017**, *139*, 6514.

[9] R. Hauser, K. Merzweiler, *Z. Anorg. Allg. Chem.* **2002**, *628*, 905.

[10] H. Berwe, A. Haas, *Chem. Ber.* **1987**, *120*, 1175.

[11] R. Vilma Bojan, J. M. Lopez-de-Luzuriaga, M. Monge, M. E. Olmos, R. Echeverria, O. Lehtonen, D. Sundholm, *ChemPlusChem* **2014**, *79*, 67.

[12] a) J. P. Eußner, B. E. K. Barth, E. Leusmann, Z. You, N. Rinn, S. Dehnen, *Chem. - Eur. J.* **2013**, *19*, 13792; b) N. Rinn, J. P. Eußner, W. Kaschuba, X. Xie, S. Dehnen, *Chem. - Eur. J.* **2016**, *22*, 3094; c) J. P. Eußner, R. O. Kusche, S. Dehnen, *Chem. - Eur. J.* **2015**, *21*, 12376.

[13] P. Galez, J. L. Soubeyroux, T. Bertrand, T. Hopfinger, S. Beauquis, H. Nguyen Xuan, *J. Alloys Compd.* **2005**, *391*, 13.

[14] R. Garcia-Rodriguez, H. Liu, *J. Am. Chem. Soc.* **2012**, *134*, 1400.

[15] G. Kociok-Kohn, M. F. Mahon, K. C. Molloy, A. L. Sudlow, *Main Group Met. Chem.* **2014**, *37*, 11.

[16] C. A. Tolman, *J. Am. Chem. Soc.* **1970**, *92*, 2956.

[17] S. Hagen, H. Schubert, C. Maichle-Mössmer, I. Pantenburg, F. Weigend, L. Wesemann, *Inorg. Chem.* **2007**, *46*, 6775.
[18] a) S. Radenković, D. Danovich, S. Shaik, P. C. Hiberty, B. Brăda, *Comput. Theor. Chem* **2017**, *1116*, 195; b) J. Granatier, M. Urban, A. J. Sadlej, *Chem. Phys. Lett.* **2010**, *484*, 154.
[19] F. Canales, S. Canales, O. Crespo, M. Concepción Gimeno, P. G. Jones, A. Laguna, *Organometallics* **1998**, *17*, 1617.
[20] a) H. Zimmer, H. W. Sparmann, *Chem. Ber.* **1954**, *87*, 645; b) G. Brauer, *Handbuch der Präparativen Anorganischen Chemie*, 3rd Edition, Ferdinand Enke Verlag, Stuttgart **1975**; c) A. Kornath, F. Neumann, *Inorg. Chem.* **2003**, *42*, 2894; d) G. M. Whitesides, M. Hackett, R. L. Brainard, J. P. P. M. Lavalleye, A. F. Sowinski, A. N. Izumi, S. S. Moore, D. W. Brown, E. M. Staudt, *Organometallics* **1985**, *4*, 1819.
[21] Stoe and Cie GmbH, *X-Area*, *Version 1.77*, **2016**.
[22] G. M. Sheldrick, *Acta Crystallogr., Sect. A* **2015**, *71*, 3.
[23] C. B. Hübschle, G. M. Sheldrick, B. Dittrich, *J. Appl. Crystallogr.* **2011**, *44*, 1281.
[24] TURBOMOLE v6.6 2014. A development of University of Karlsruhe and Forschungeszentrum Karlsruhe GmbH, **1989–2007**, TURBOMOLE GmbH, http://www.turbomole.com, (accessed: 2014).
[25] a) K. Eichkorn, O. Treutler, H. Öhm, M. Häser, R. Ahlrichs, *Chem. Phys. Lett.* **1995**, *240*, 283; b) K. Eichkorn, O. Treutler, H. Öhm, M. Häser, R. Ahlrichs, *Chem. Phys. Lett.* **1995**, *242*, 652; c) K. Eichkorn, F. Weigend, O. Treutler, R. Ahlrichs, *Theor. Chem. Acc.* **1997**, *97*, 119.
[26] S. Vosko, L. Wilk, M. Nusair, *Can. J. Phys.* **1980**, *58*, 1200.
[27] a) A. Becke, *Phys. Rev. A* **1988**, *38*, 3098; b) J. Perdew, *Phys. Rev. B* **1986**, *33*, 8822.
[28] a) S. Grimme, J. Antony, S. Ehrlich, H. Krieg, *J. Chem. Phys.* **2010**, *132*, 154104; b) S. Grimme, *J. Comput. Chem.* **2006**, *27*, 1787.
[29] T. Dunning, *J. Chem. Phys.* **1989**, *90*, 1007.
[30] a) K. Peterson, *J. Chem. Phys.* **2003**, *119*, 11099; b) B. Metz, H. Stoll, M. Dolg, *J. Chem. Phys.* **2000**, *113*, 2563; c) K. Peterson, C. Puzzarini, *Theor. Chem. Acc.* **2005**, *114*, 283; d) D. Figgen, G. Rauhut, M. Dolg, H. Stoll, *Chem. Phys.* **2005**, *311*, 227; e) D. Andrae, U. Haeussermann, M. Dolg, H. Stoll, H. Preuss, *Theor. Chim. Acta* **1990**, *77*, 123.
[31] a) E. Runge, E. Gross, *Phys. Rev. Lett.* **1984**, *52*, 997; b) E. Gross, W. Kohn, *Adv. Quantum Chem.* **1990**, *21*, 255.
[32] a) R. Bauernschmitt, R. Ahlrichs, *J. Chem. Phys.* **1996**, *104*, 9047; b) R. Bauernschmitt, R. Ahlrichs, *Chem. Phys. Lett.* **1996**, *256*, 454.
[33] a) C. Lee, W. Yang, R. Parr, *Phys. Rev. B* **1988**, *37*, 785; b) A. Becke, *J. Chem. Phys.* **1993**, *98*, 5648.
[34] a) J. Perdew, Y. Wang, *Phys. Rev. B* **1992**, *45*, 13244; b) J. Tao, J. Perdew, V. Staroverov, G. Scuseria, *Phys. Rev. Lett.* **2003**, *91*, 146401.
[35] a) G. Kresse, J. Furthmüller, *Phys. Rev. B* **1996**, *54*, 11169; b) G. Kresse, J. Furthmüller, *Comput. Mater. Sci.* **1996**, *6*, 15; c) G. Kresse, J. Joubert, *Phys. Rev. B* **1999**, *59*, 1758.
[36] P. E. Blöchl, *Phys. Rev. B* **1994**, *50*, 17953.
[37] a) J. Perdew, K. Burke, M. Ernzerhof, *Phys. Rev. Lett.* **1996**, *77*, 3865; b) J. Perdew, K. Burke, M. Ernzerhof, *Phys. Rev. Lett.* **1997**, *78*, 1396.

ADVANCED OPTICAL MATERIALS

Supporting Information

for *Advanced Optical Materials,* DOI: 10.1002/adom.201801793

White-Light Generation Upon In-Situ Amorphization of Single Crystals of $[\{(Me_3P)_3AuSn\}(PhSn)_3S_6]$ and $[\{(Et_3P)_3AgSn\}(PhSn)_3S_6]$

*Eike Dornsiepen, Florian Dobener, Nils Mengel, Olena Lenchuk, Christof Dues, Simone Sanna, Doreen Mollenhauer, Sangam Chatterjee, and Stefanie Dehnen**

Supporting Information

White-Light Generation Upon In-Situ Amorphization of Single Crystals of [{(Me$_3$P)$_3$AuSn}(PhSn)$_3$S$_6$] and [{(Et$_3$P)$_3$AgSn}(PhSn)$_3$S$_6$]

Eike Dornsiepen,[†] Florian Dobener,[‡] Nils Mengel,[‡] Olena Lenchuk,[§] Christof Dues,[◊] Simone Sanna,[◊] Doreen Mollenhauer,[§] Sangam Chatterjee,[‡] and Stefanie Dehnen[†]*

Content

1. Mass Spectra of Compounds 1-5

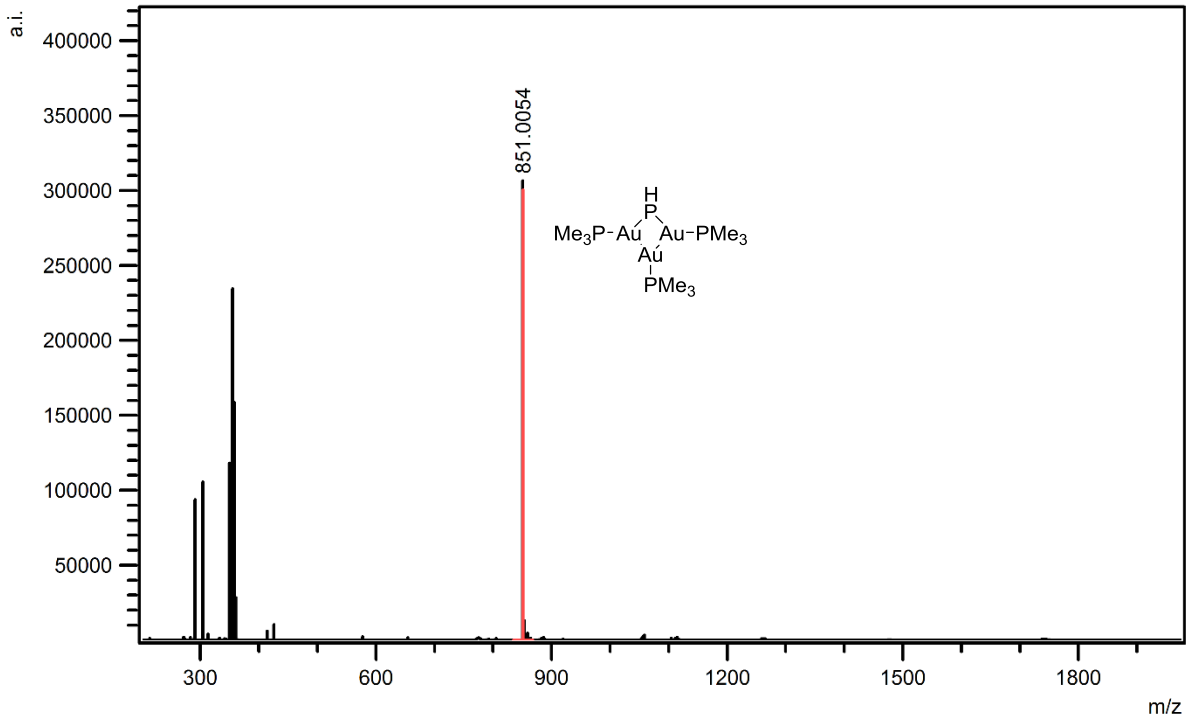

Figure S1. ESI(+) mass spectrum of **1**.

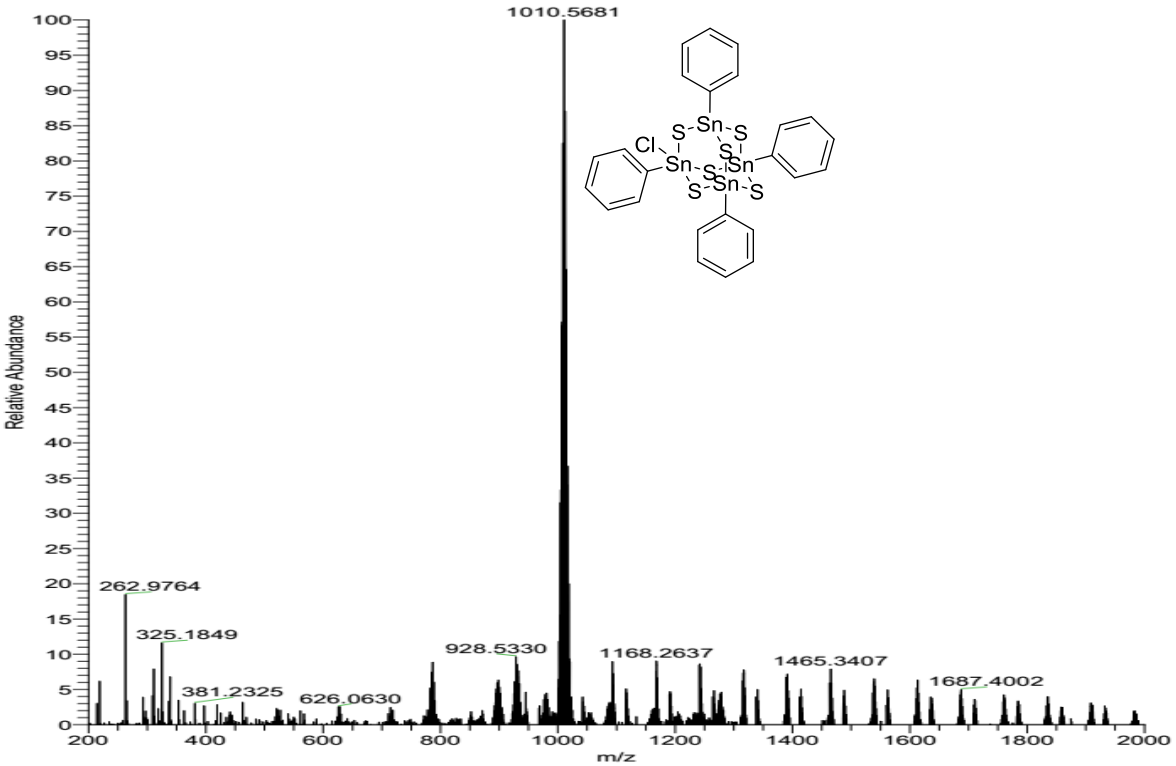

Figure S2. ESI(-) mass spectrum of **1**.

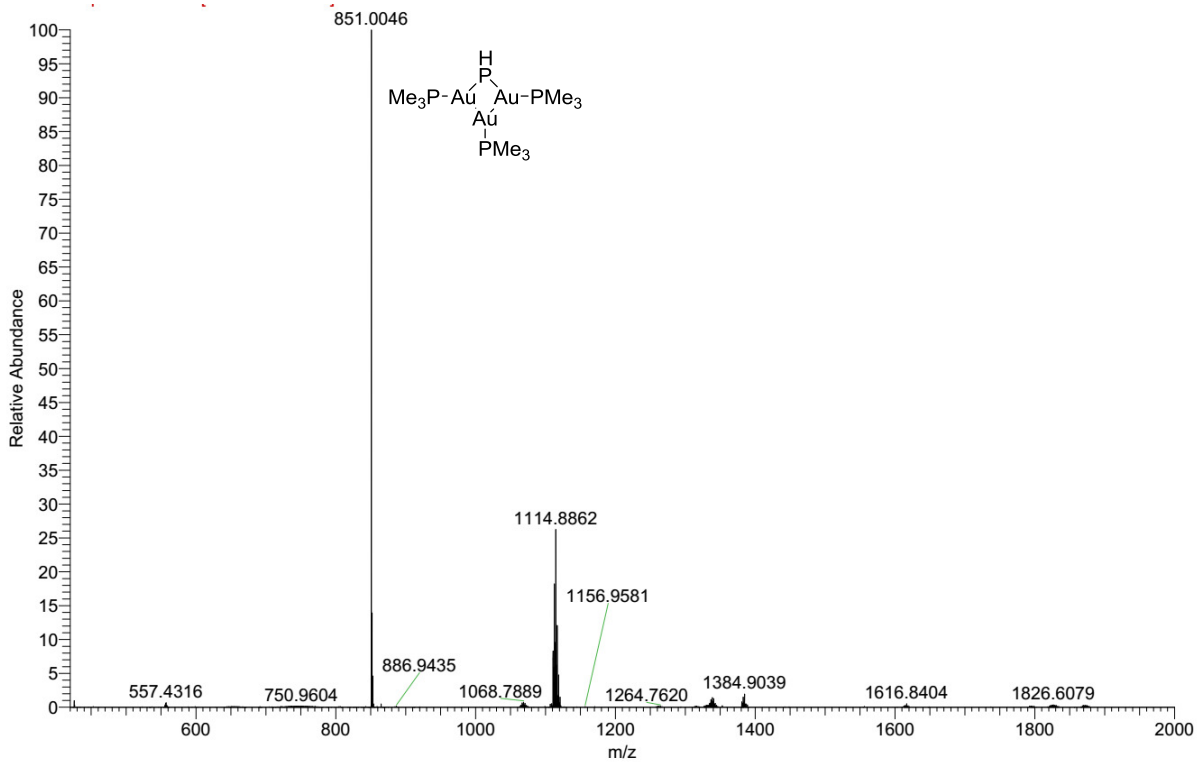

Figure S3: ESI(+) mass spectrum of **2**.

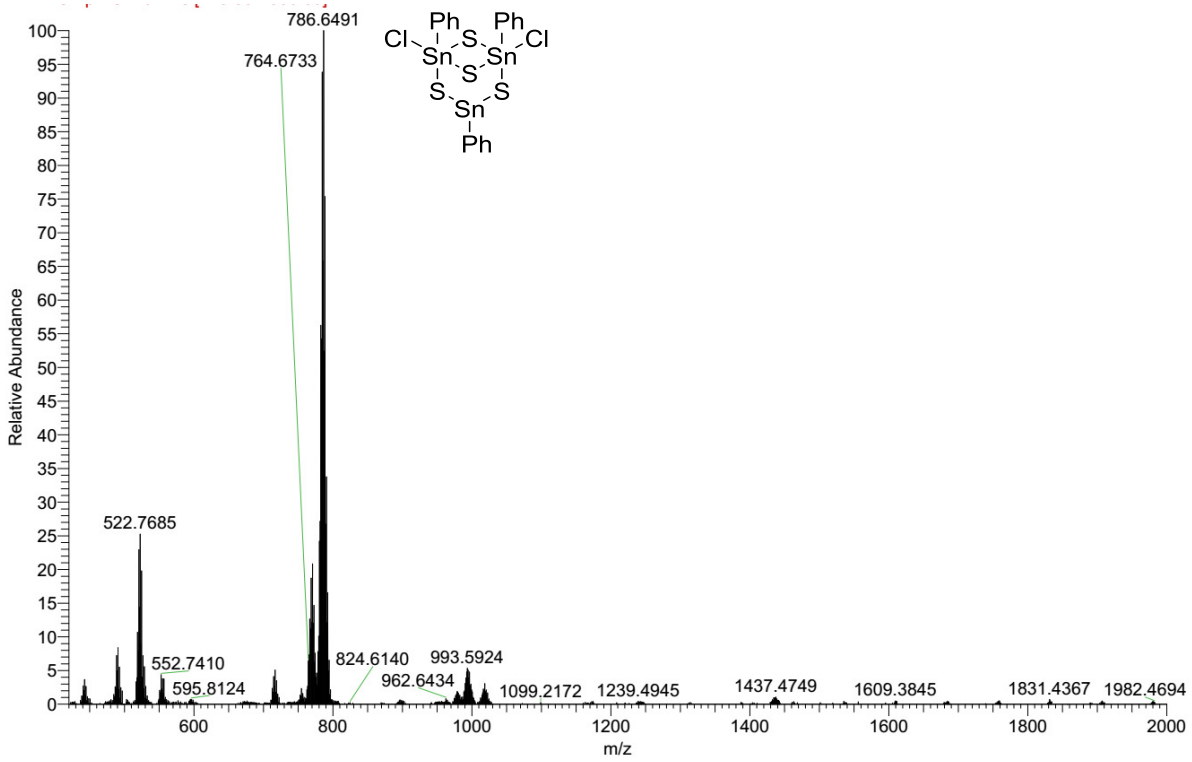

Figure S4: ESI(-) mass spectrum of **2**.

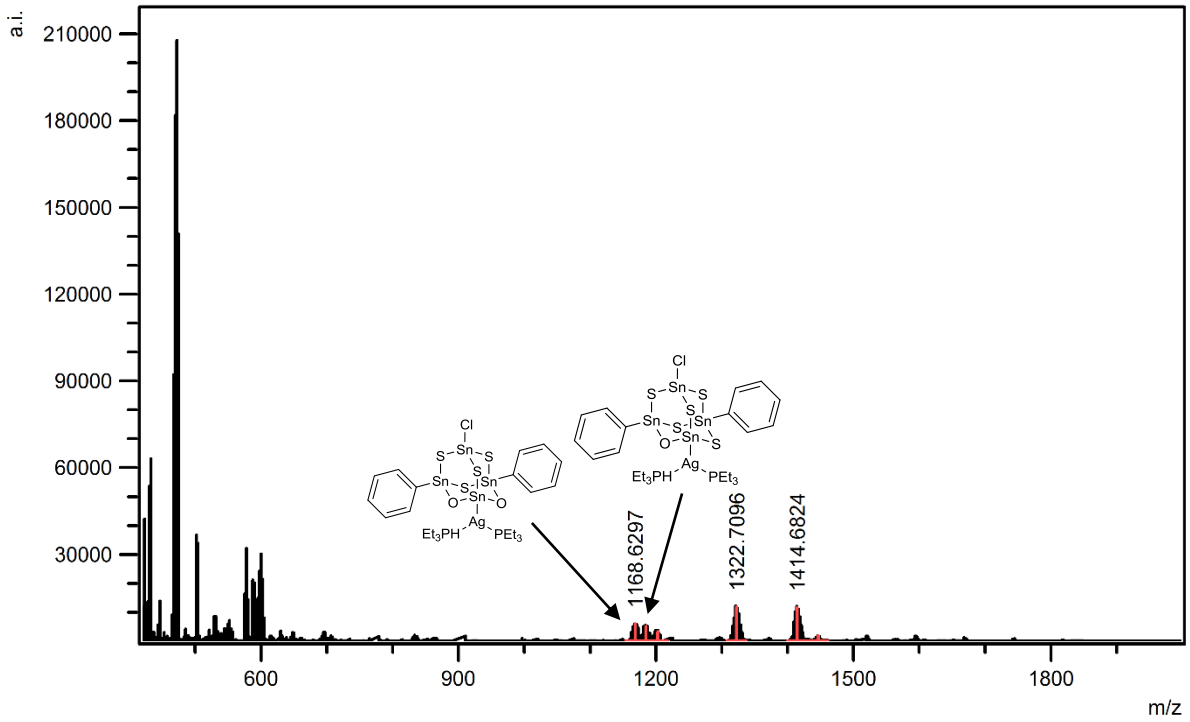

Figure S5: ESI(+) mass spectrum of **4**.

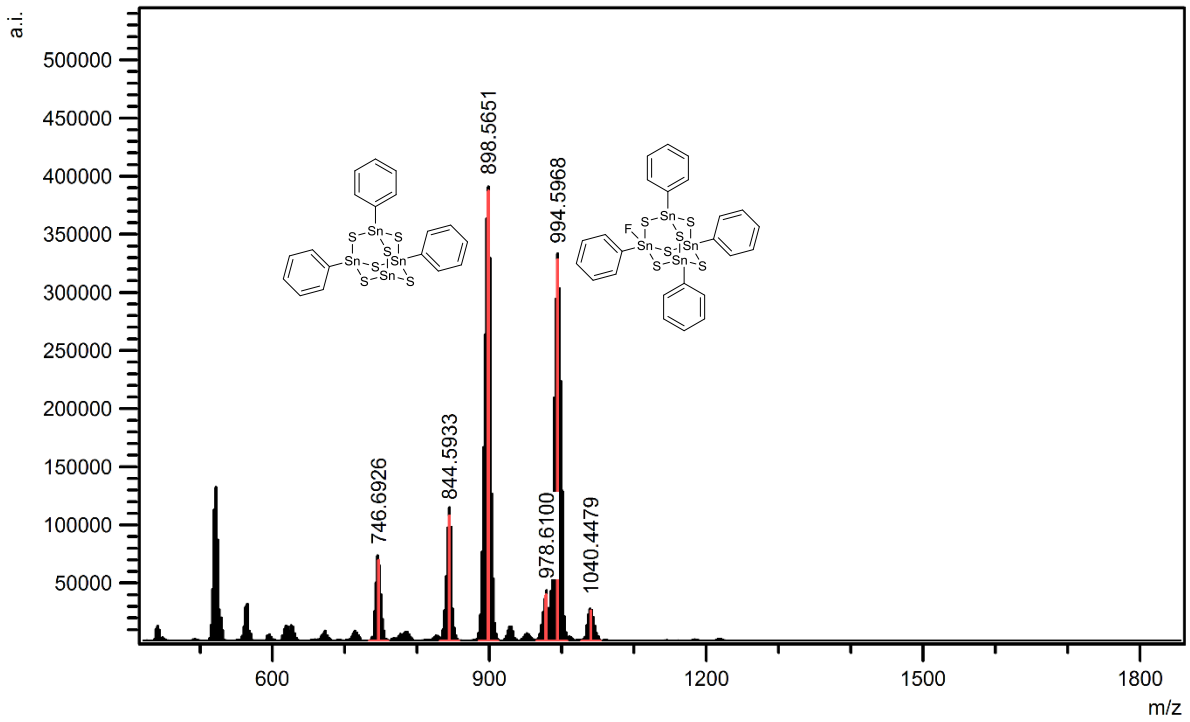

Figure S6: ESI(-) mass spectrum of **4**.

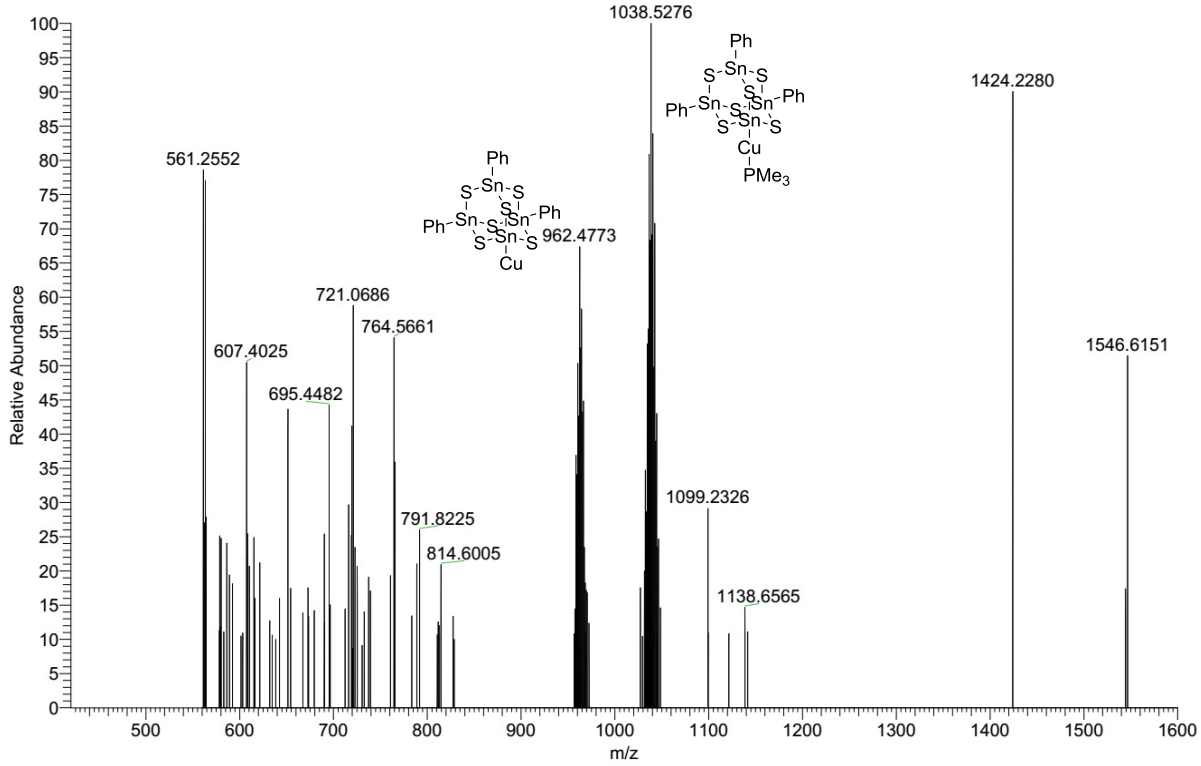

Figure S7: ESI(+) mass spectrum of **5**.

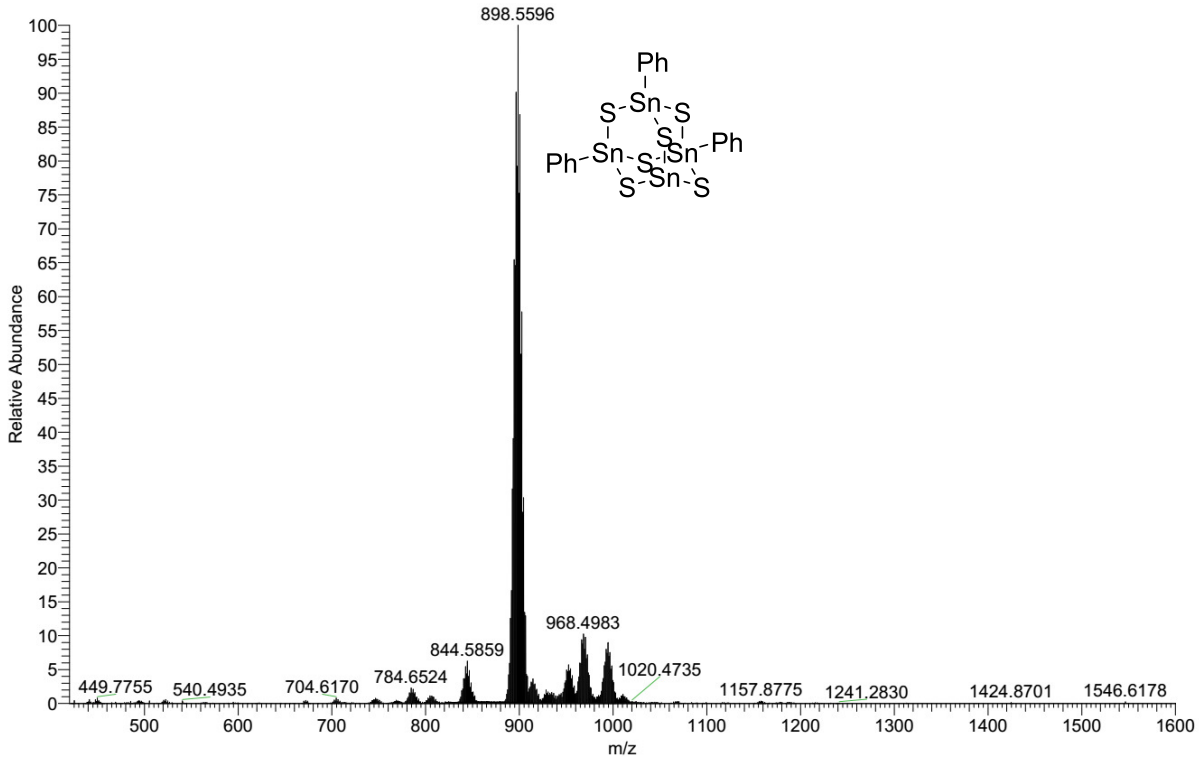

Figure S8: ESI(-) mass spectrum of **5**.

2. NMR Spectra of Compounds 1-5

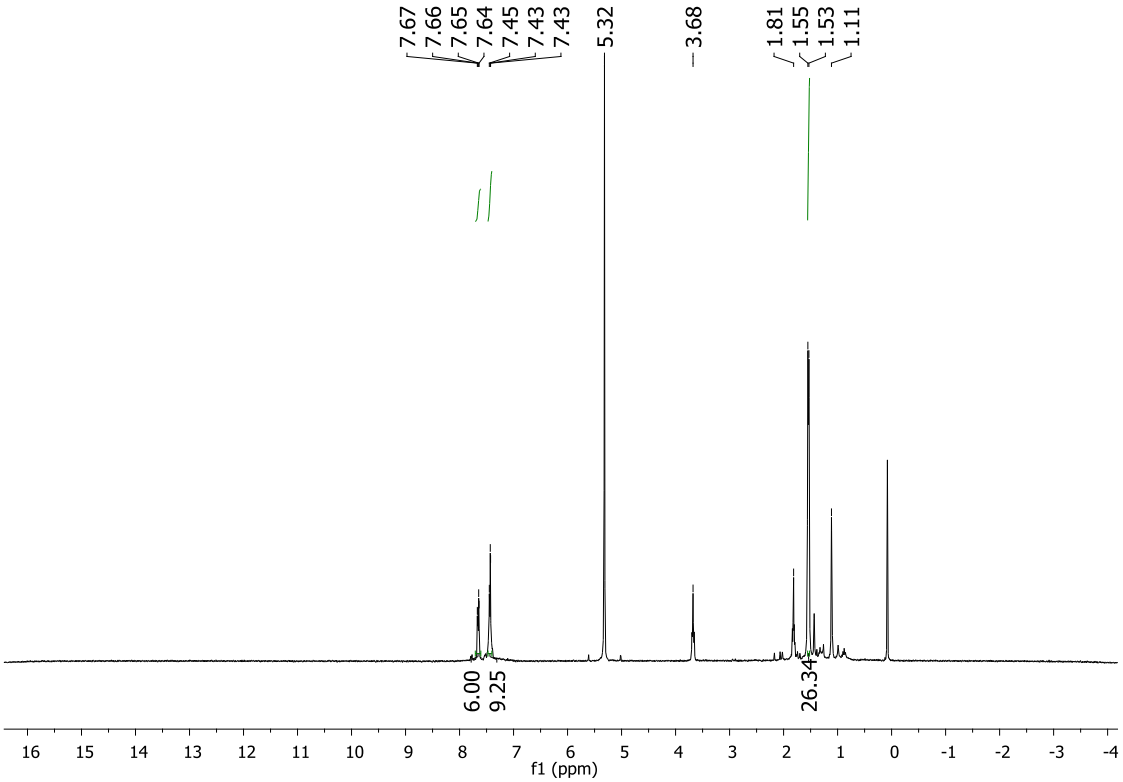

Figure S9: ^{1}H-NMR spectrum of **1** (300 MHz, 298 K, CD_2Cl_2).

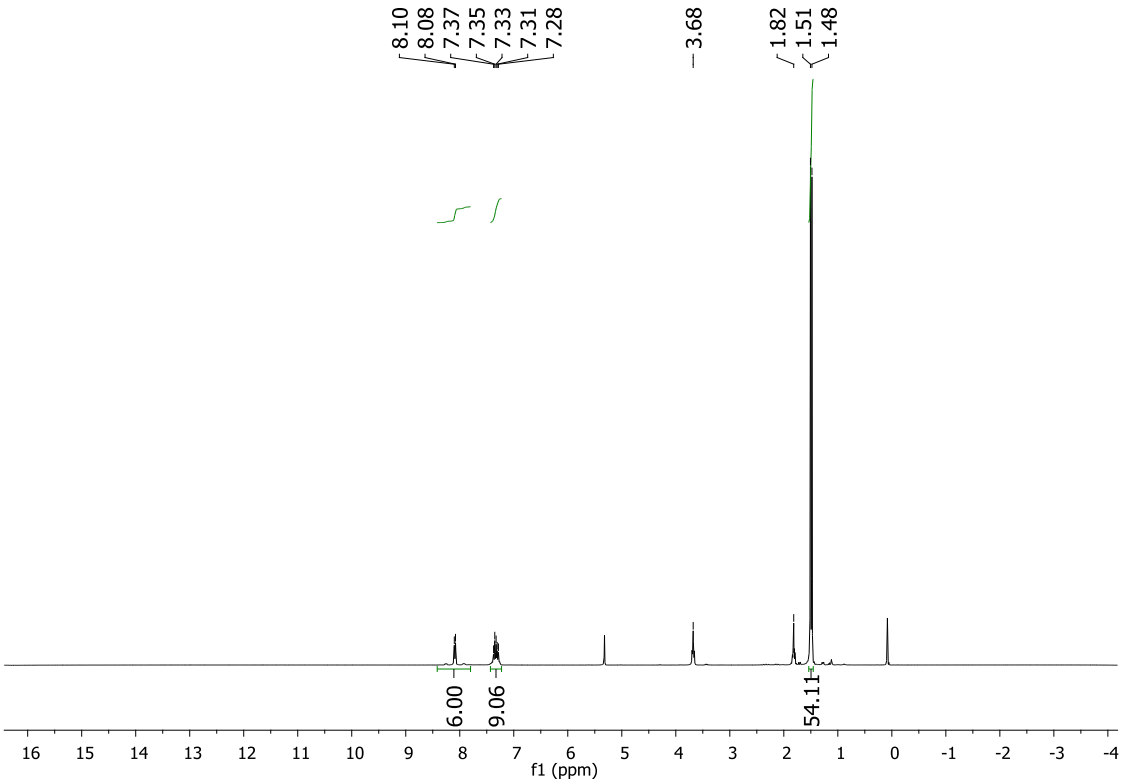

Figure S10: ^{1}H-NMR spectrum of **2** (300 MHz, 298 K, CD_2Cl_2).

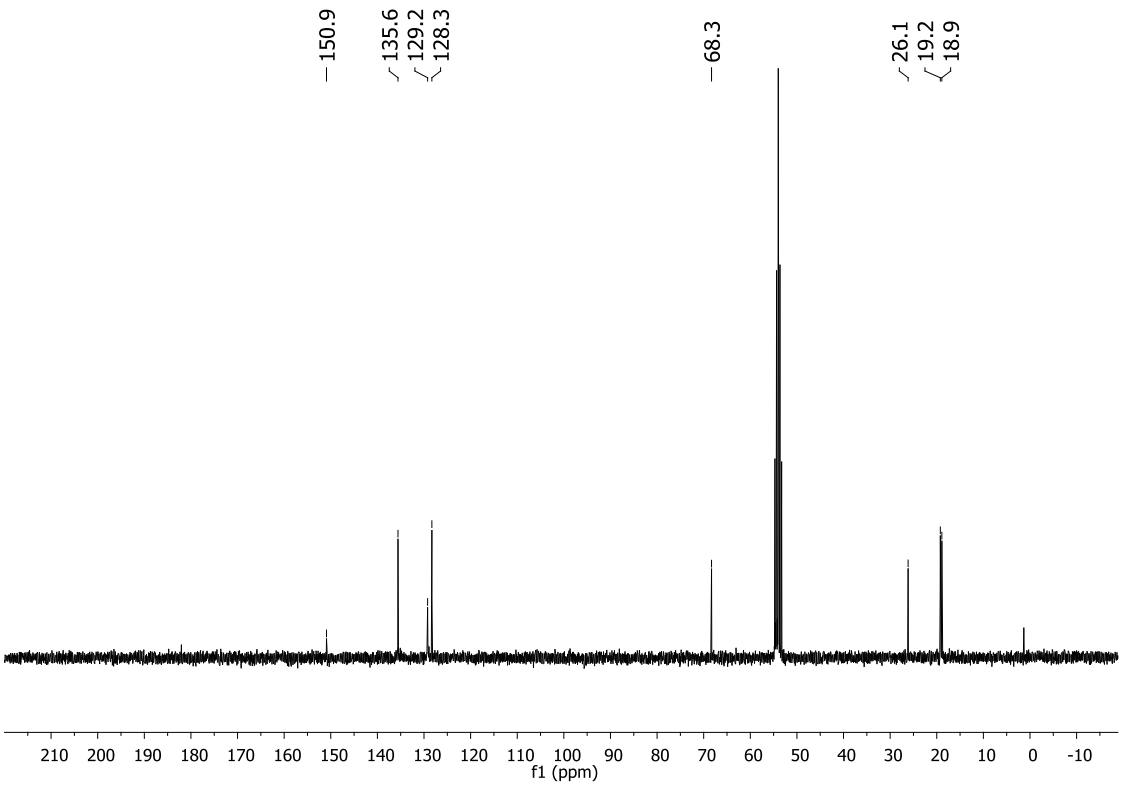

Figure S11: ^{13}C-NMR spectrum of **2** (75 MHz, 298 K, CD_2Cl_2).

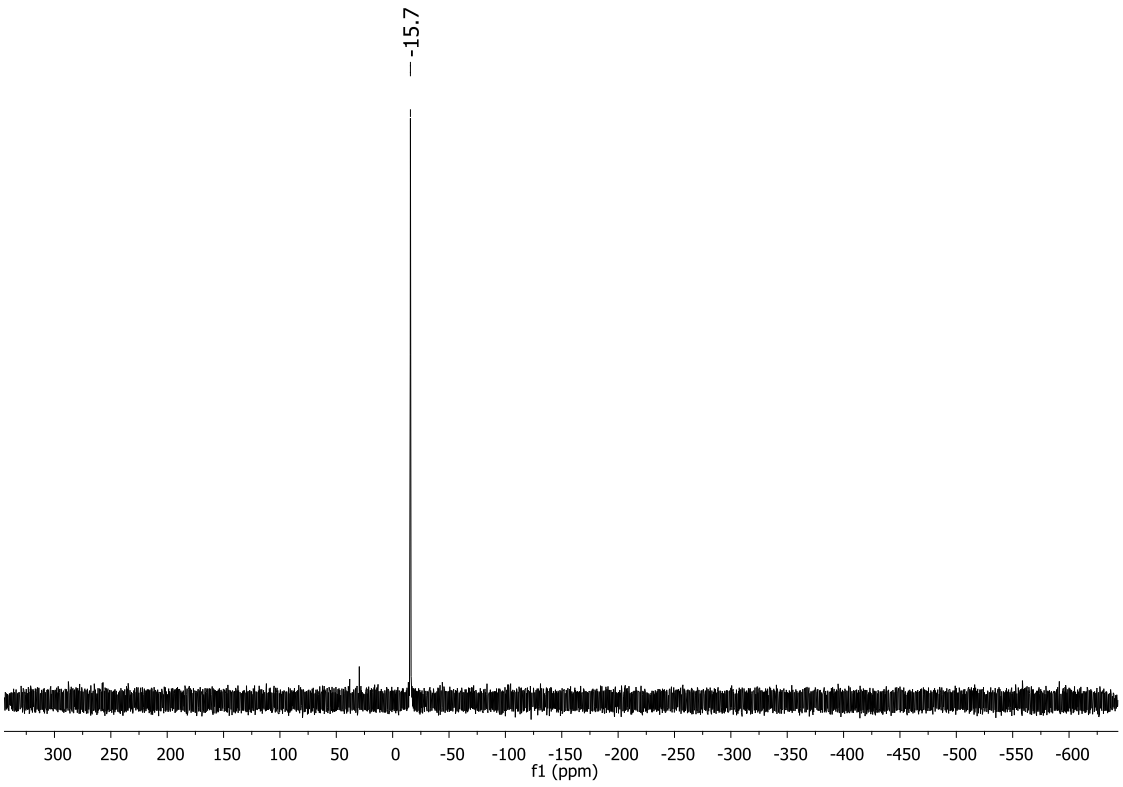

Figure S12: ^{31}P-NMR spectrum of **2** (101 MHz, 298 K, CD_2Cl_2).

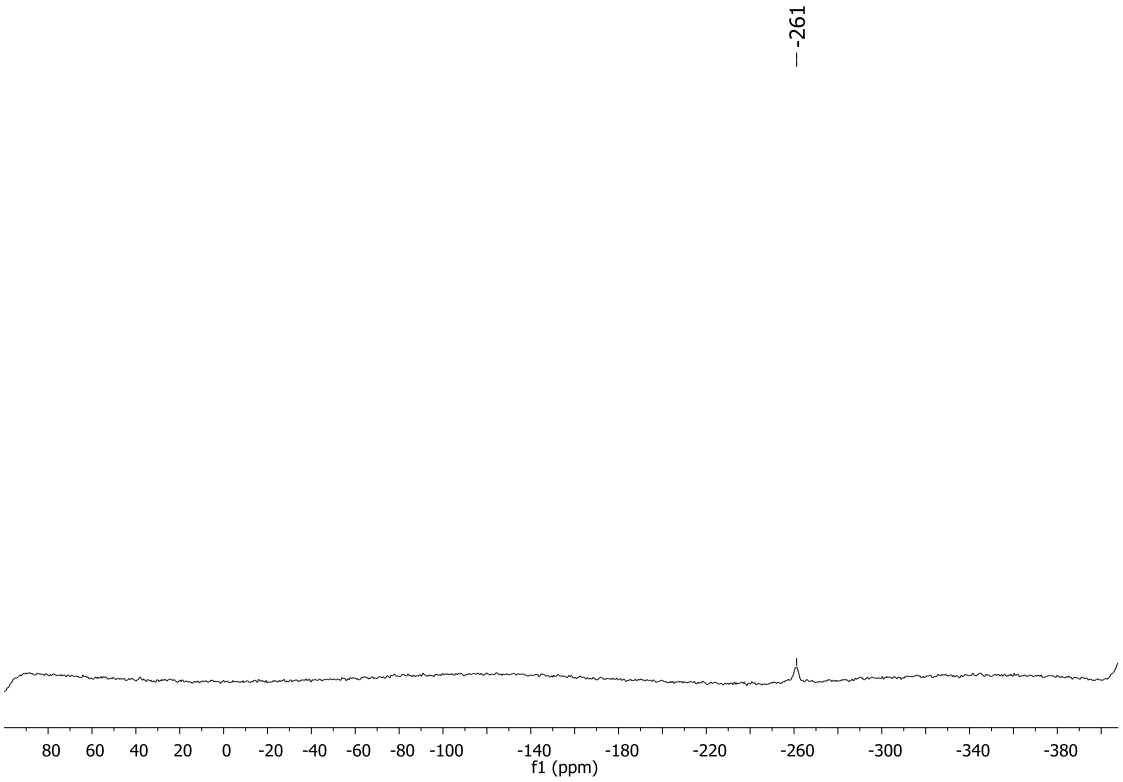

Figure S13: ^{119}Sn-NMR spectrum of **2** (98 MHz, 298 K, CD_2Cl_2).

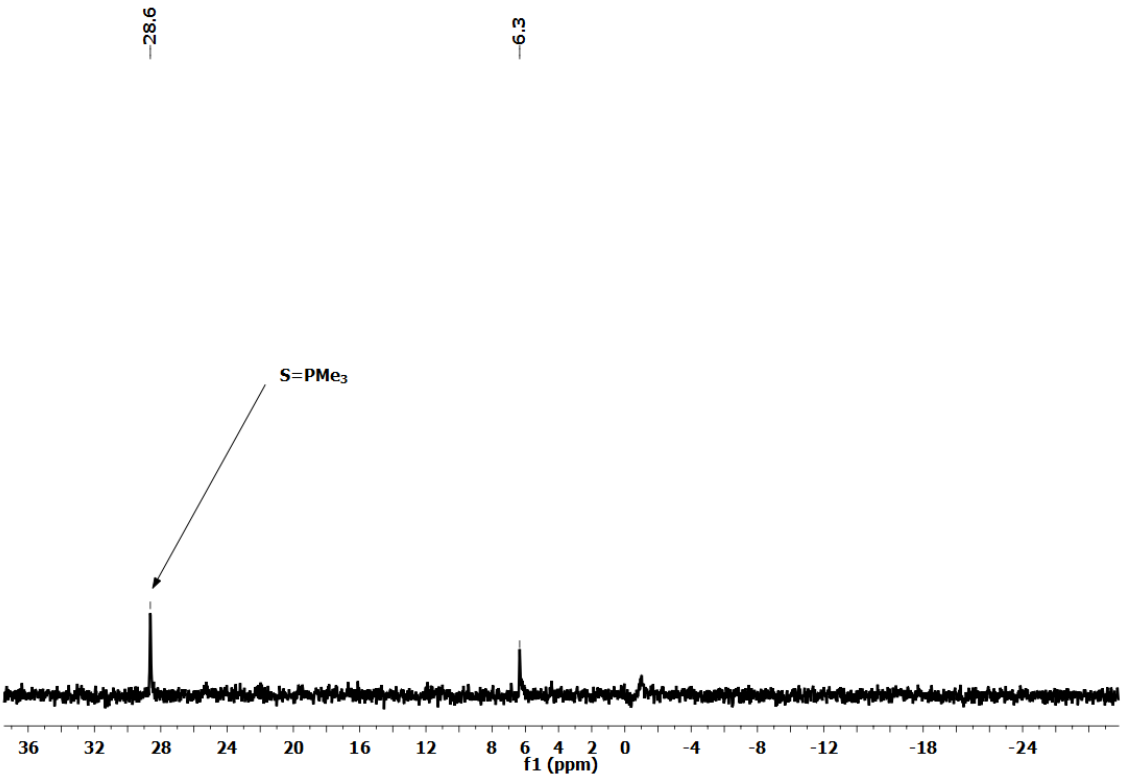

Figure S14: ^{31}P-NMR spectrum of the reaction solution of **2** (101 MHz, 298 K, THF).

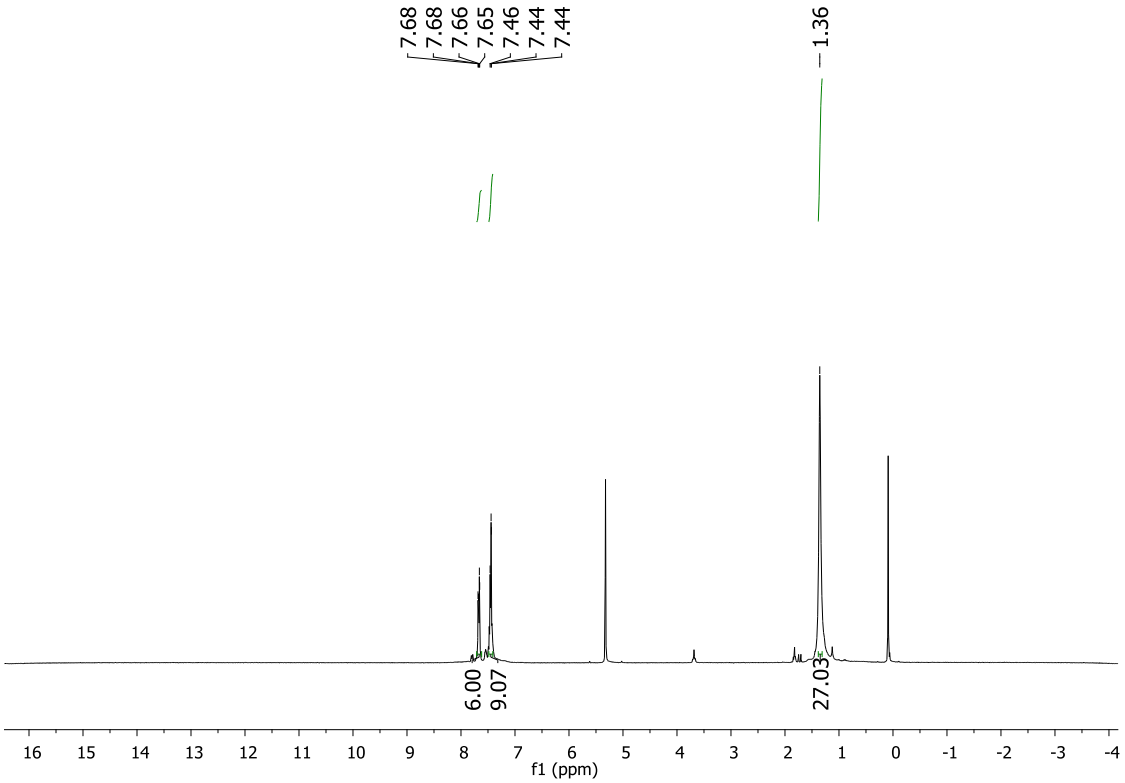

Figure S15: ^{1}H-NMR spectrum of **5** (300 MHz, 298 K, CD_2Cl_2).

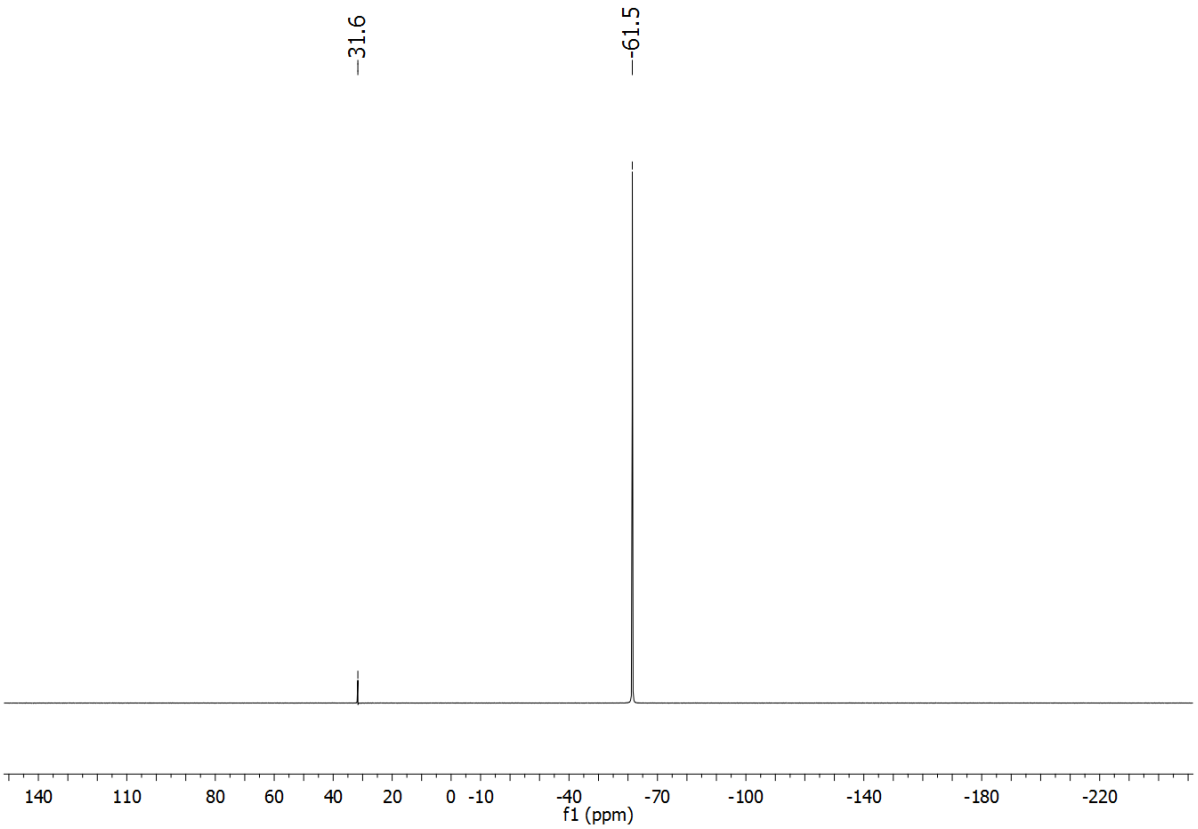

Figure S16: ^{31}P-NMR spectrum of the reaction solution of **5** (300 MHz, 298 K, CD_2Cl_2).

3. IR spectra of compounds 1-5

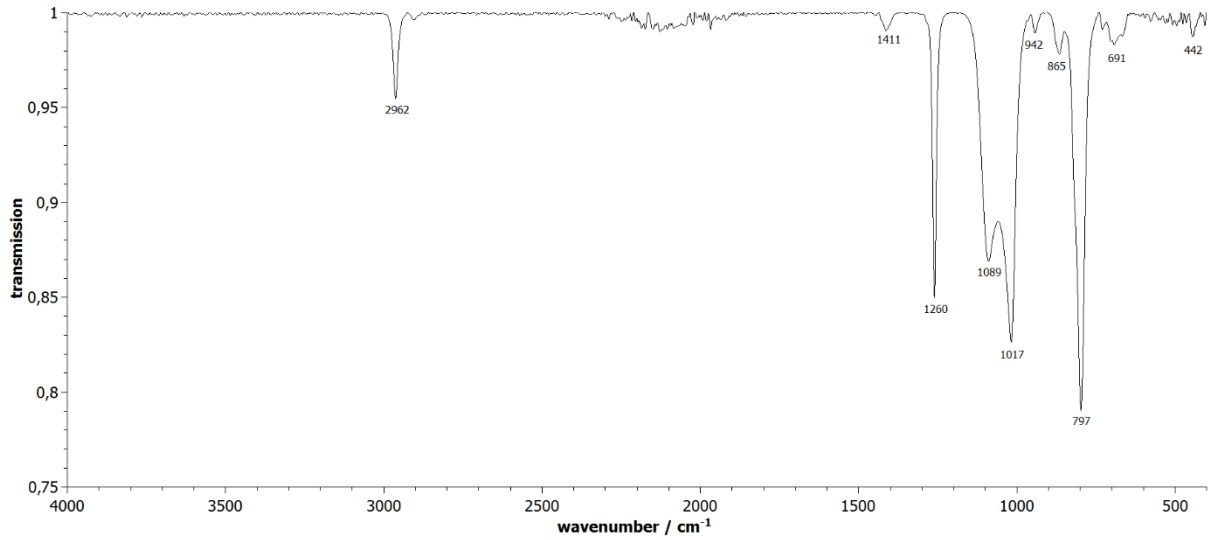

Figure S17: IR spectrum of **1**.

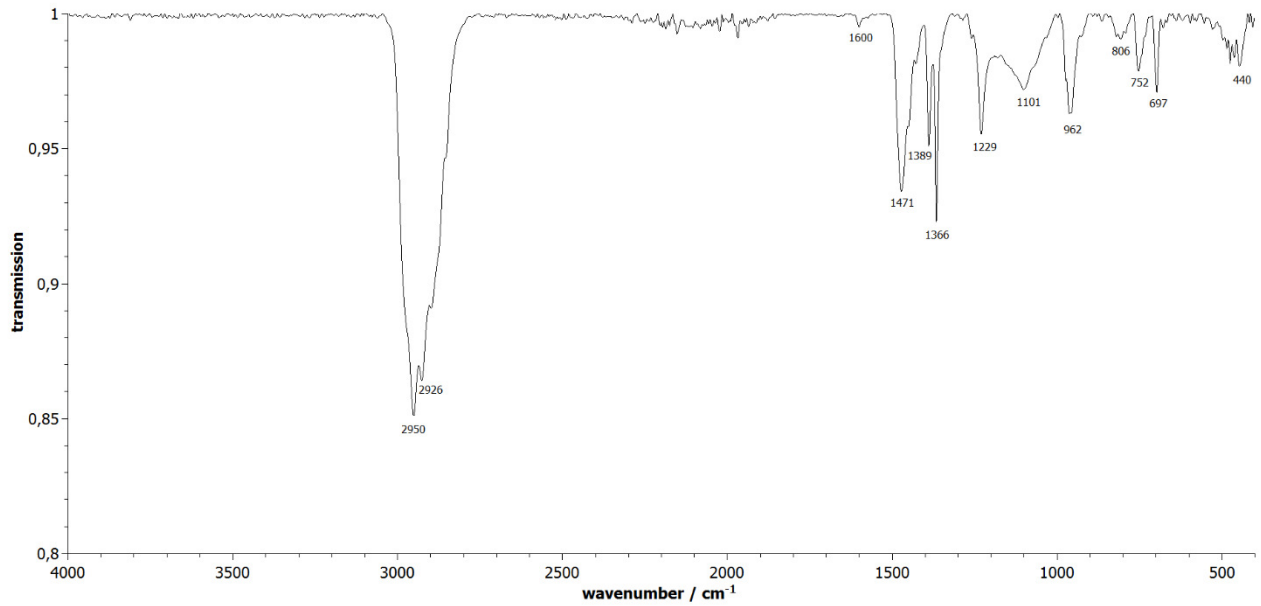

Figure S18: IR spectrum of **2**.

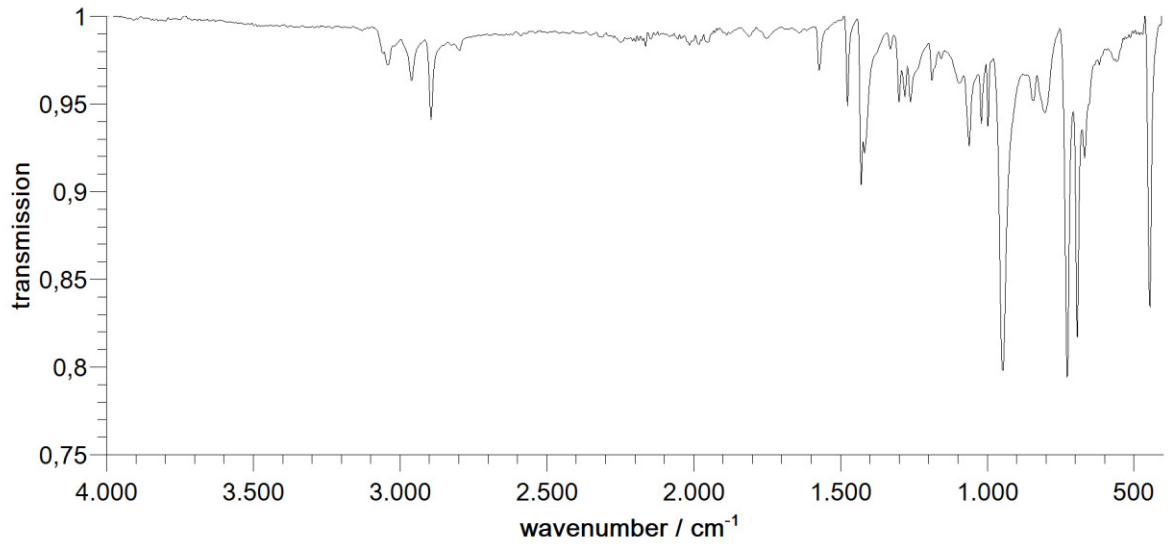

Figure S19: IR spectrum of **3**.

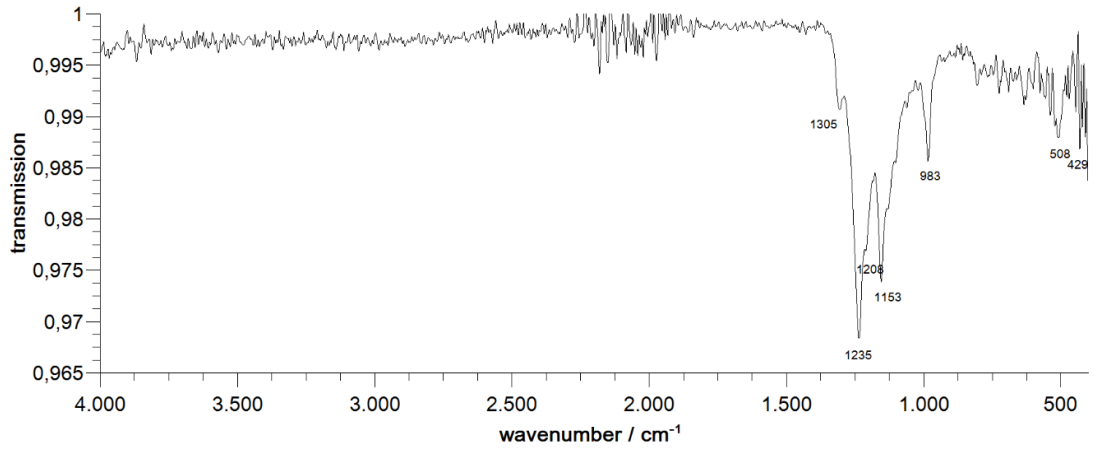

Figure S20: IR spectrum of **4**.

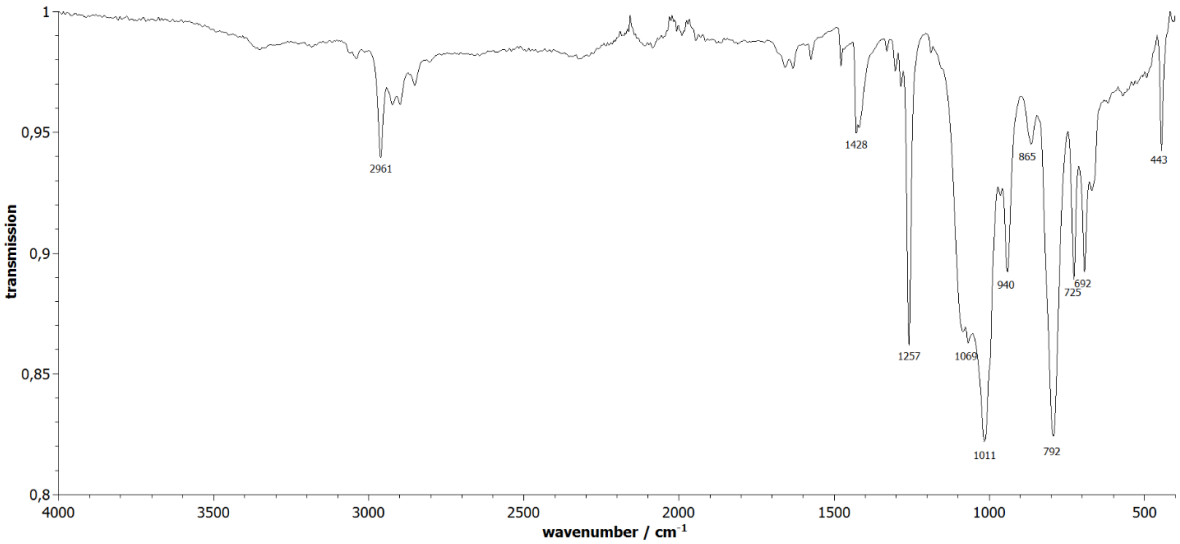

Figure S21: IR spectrum of **5**.

4. Micro X-Ray Fluorescence (µ-XRF) Spectra of Compounds 1-5

We note that the very small thickness of the crystals leads to systematic errors for the Cu and Au compounds owing to the applied energies that require larger penetration depths than provided. For compound **3**, the accuracy is lowered by a systematic surface impurity upon isolation.

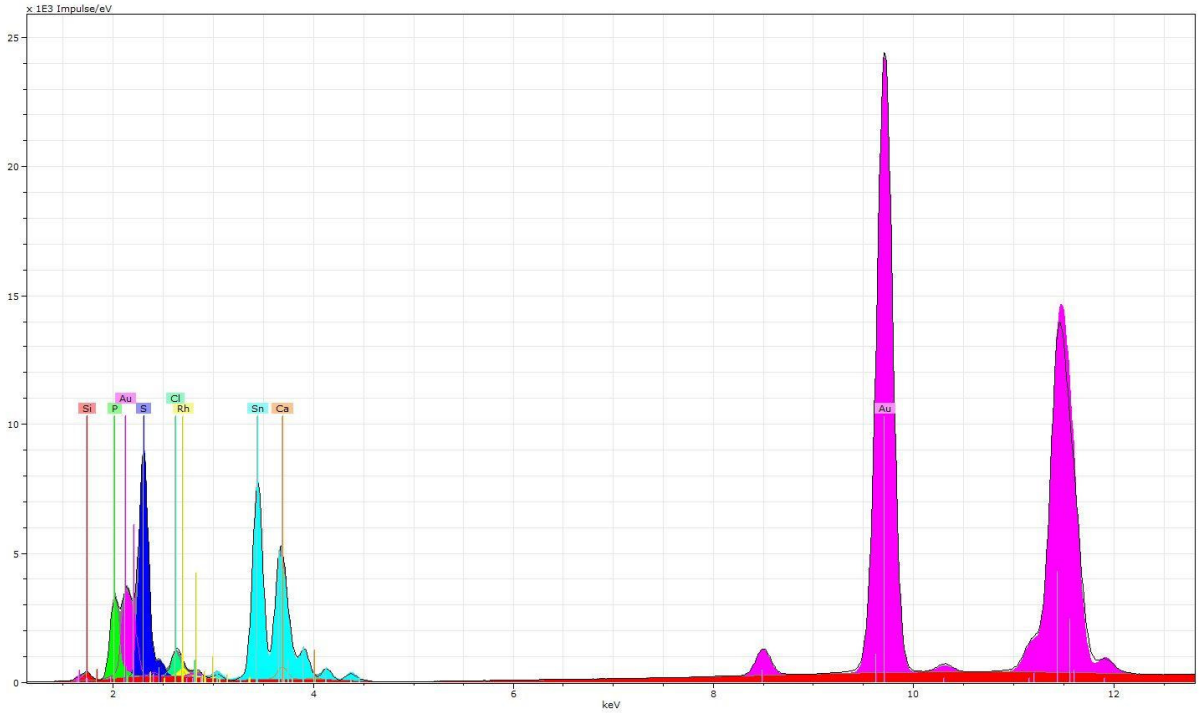

Figure S22: XRF spectrum of **1**, (% calcd, % found) for Au/P/Sn/S 1:3:4:6: Au (7.14, 9.60), P (21.43, 16.62), Sn (28.57, 28.98), S (42.86, 36.07).

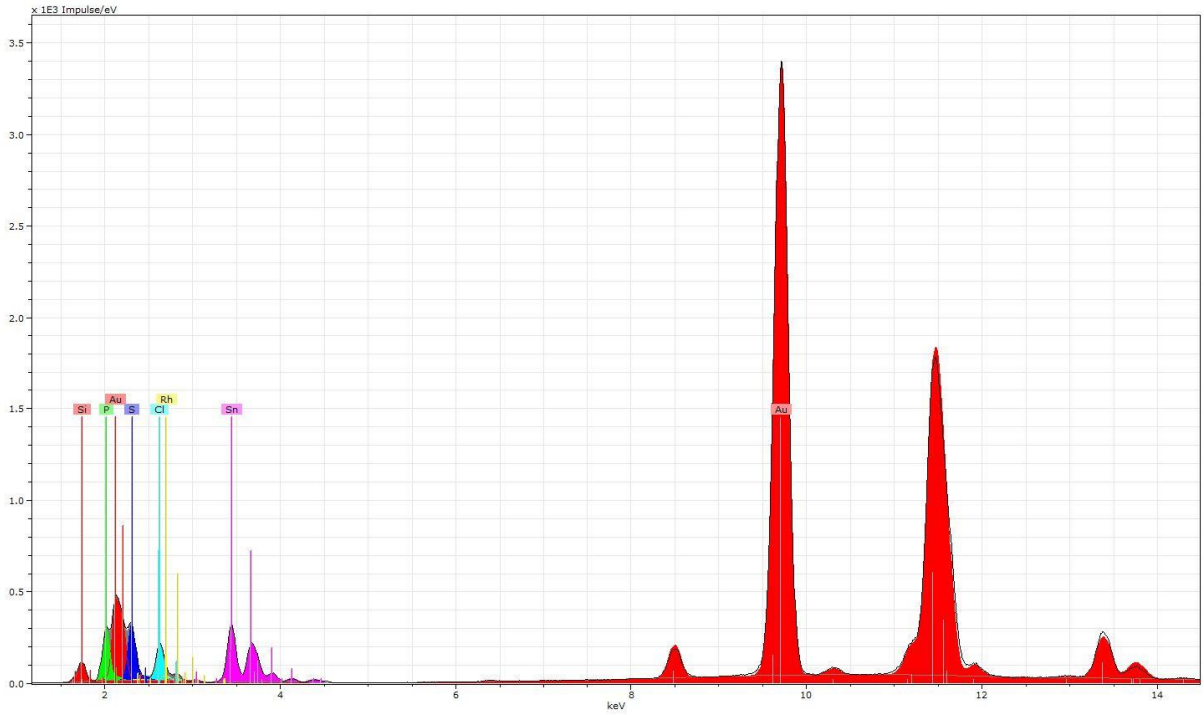

Figure S23: XRF spectrum of **2**, (% calcd, % found) for Au/P/Sn/S 2:6:3:4: Au (13.33, 16.71), P (40.00, 19.87), Sn (20.00, 17.55), S (26.67, 18.76).

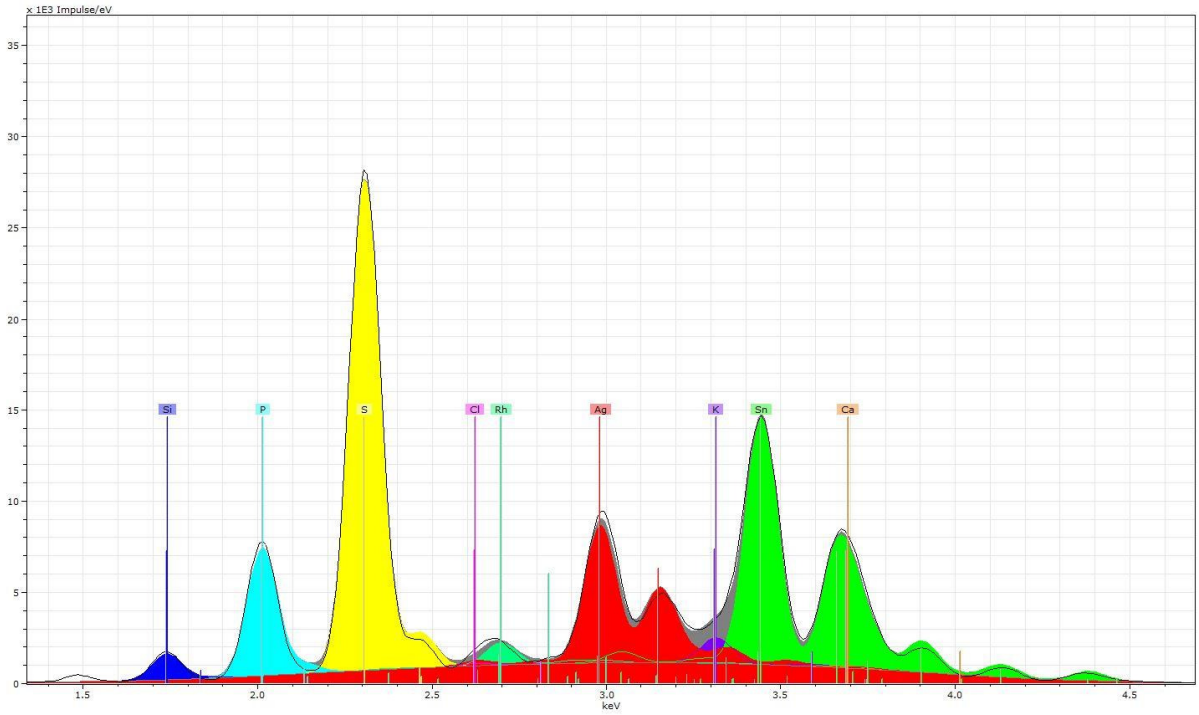

Figure S24: XRF spectrum of **3**, (% calcd, % found) for Ag/P/Sn/Cl 1:3:1:3: Ag (12.50, 17.37), P (37.50, 15.40), Sn (12.50, 20.34), Cl (37.50, 37.38).

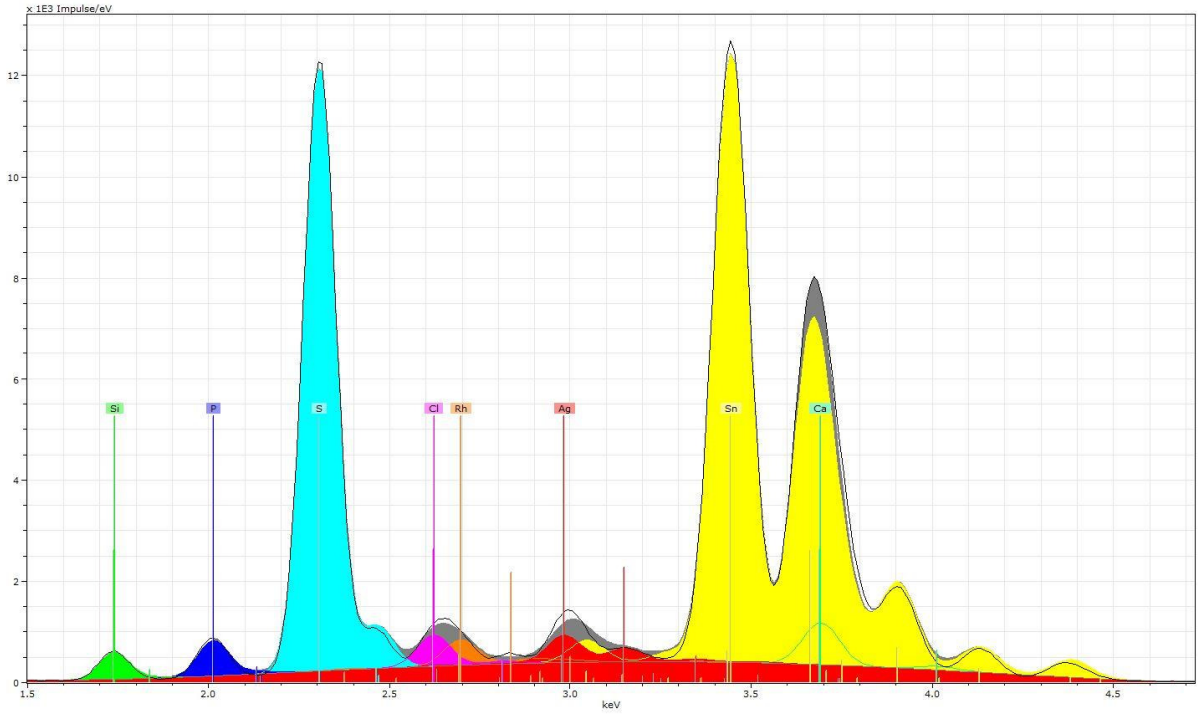

Figure S25: XRF spectrum of **4**, (% calcd, % found) for Ag/P/Sn/S 1:3:4:6: Ag (7.14, 6.16), P (21.43, 24.10), Sn (28.57, 30.43), S (42.86, 40.43).

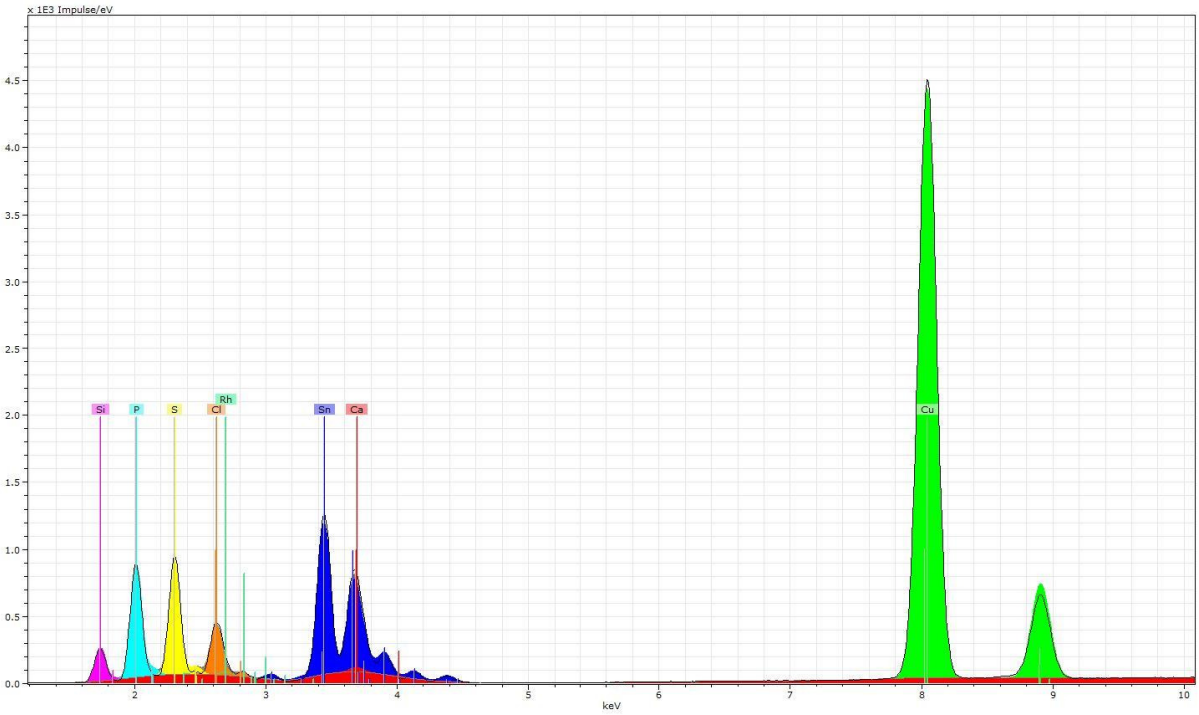

Figure S26: XRF spectrum of **5**, (% calcd, % found) for Cu/P/Sn/S 1:3:4:6: Cu (7.14, 12.01), P (21.43, 23.17), Sn (28.57, 28.14), S (42.86, 40.32).

5. Powder X-Ray Diffraction Data

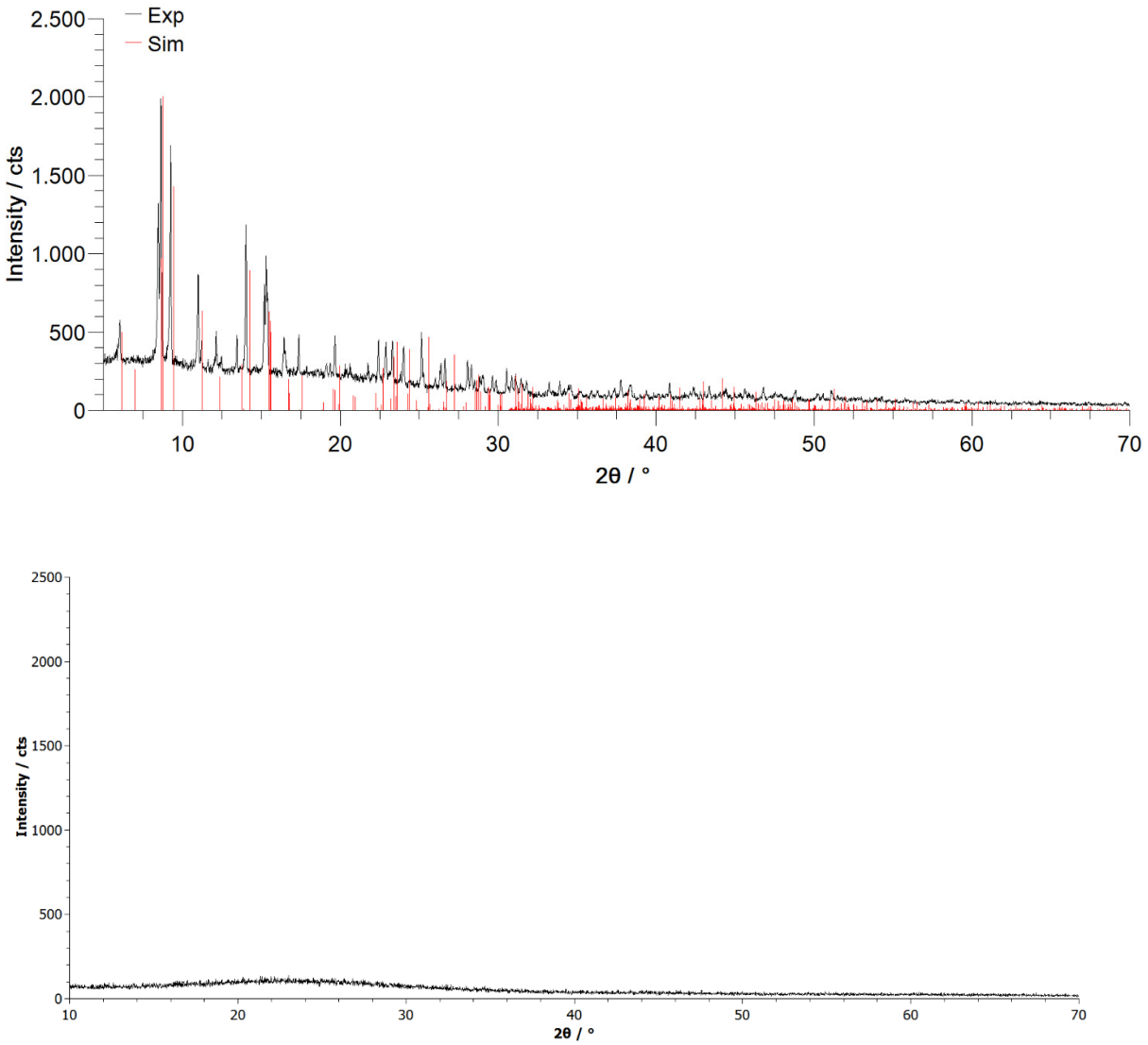

Figure S27: Powder X-ray diffractograms of a sample of compound **1** before (top) and after (bottom) irradiation with a titan-sapphire laser oscillator (emission wavelength 800 nm). Black: measured diffractograms. Red: reflex positions simulated from the single crystal structure; the shift of reflections in the simulated diagram to higher 2theta values with increasing 2theta range in comparison with the measured reflections is due to different temperatures during the SCXRD measurement (100 K) and the PXRD measurement (295 K).

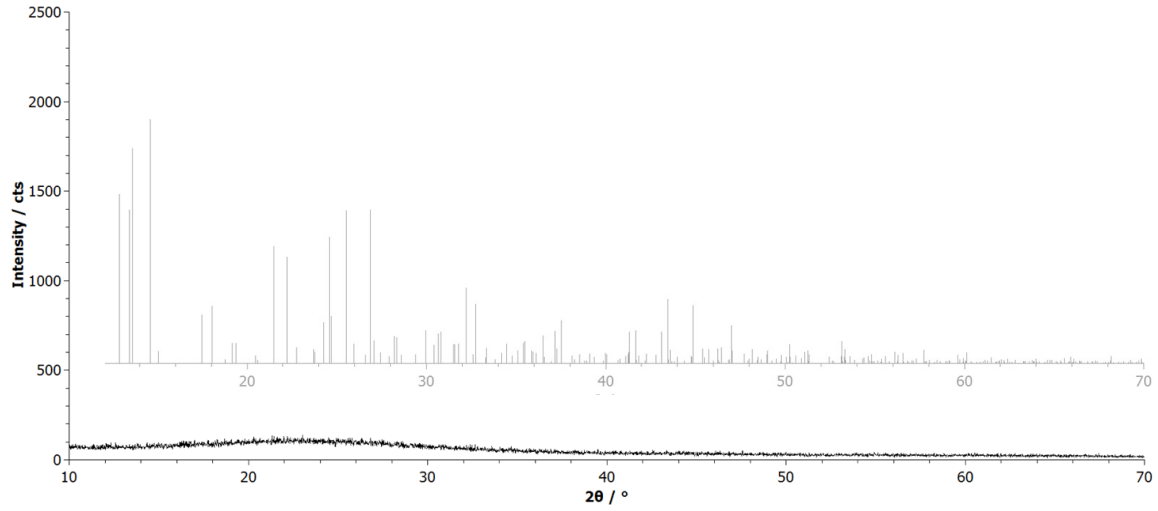

Figure S28: Powder X-ray diffractogram of a sample of compound **4** after irradiation. The powder X-ray diffractogram of compound **4** before irradiation, simulated from the single crystal structure, is shown as inset for comparison. Experimental PXRD data before irradiation cannot be recorded, as the compound gets a creamy consistence during pulverization owing to the crystal solvent.

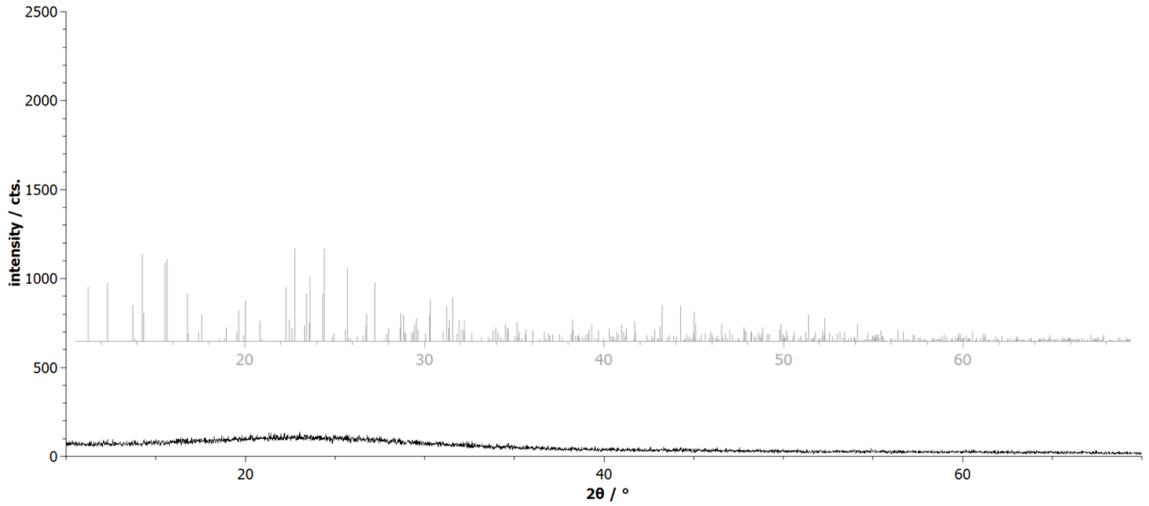

Figure S29: Powder X-ray diffractogram of a sample of compound **5** after irradiation. The powder X-ray diffractogram of compound **5** before irradiation, simulated from the single crystal structure, is shown as inset for comparison. Experimental PXRD data before irradiation cannot be recorded, as the compound gets a creamy consistence during pulverization owing to the crystal solvent.

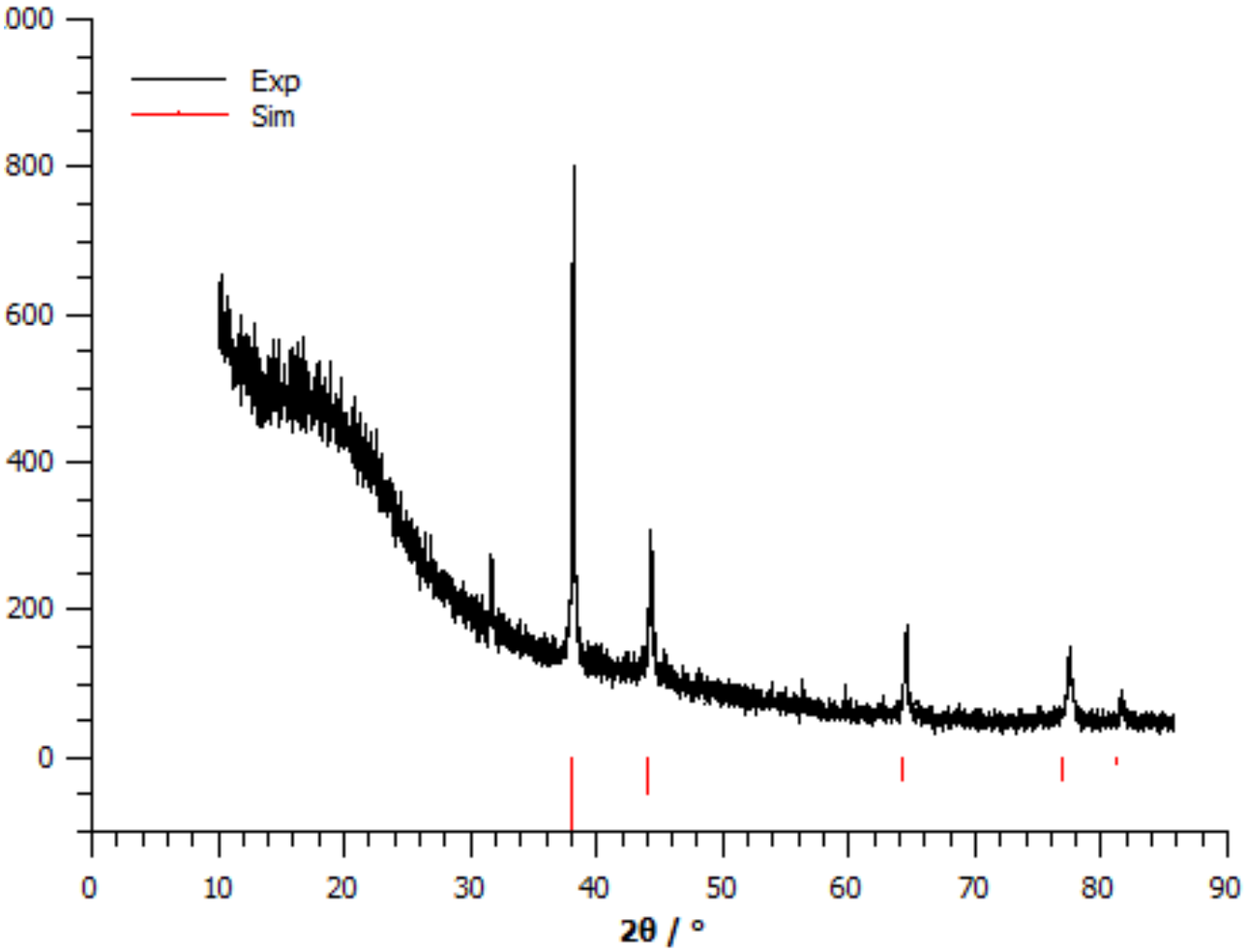

Figure S30: Powder X-ray diffractogram of the gold precipitate during formation of **2**. Black: measured diffractogram. Red: reflex positions simulated from the single crystal structure.[1]

6. Single-Crystal X-Ray Crystallography of Compound 1

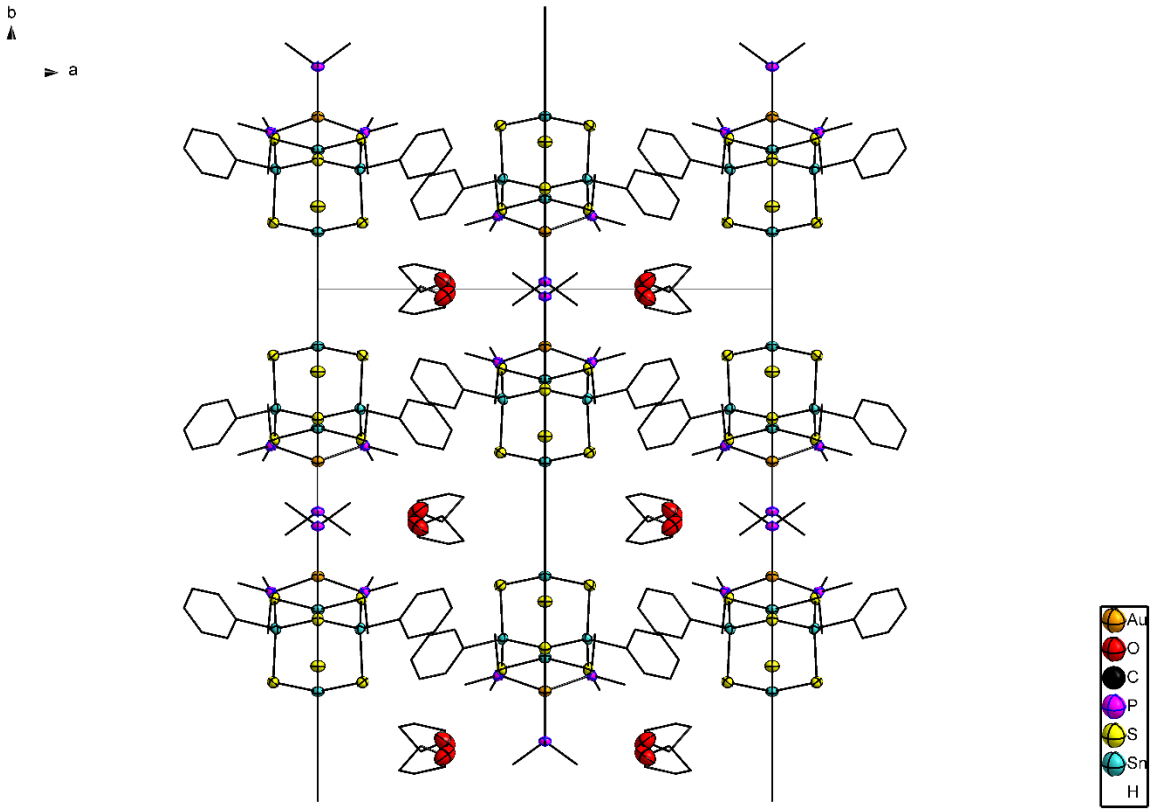

Figure S31: Crystal structure of **1** · 2 THF, viewed along the crystallographic c axis. Ellipsoids are shown at 50% probability, hydrogen atoms and the disorder of the solvent molecules are omitted for clarity.

Table S1: Crystal data and structure refinement for **1**·2 THF (CCDC 1875435)

Empirical formula	$C_{35}H_{58}Au_1O_2P_3S_6Sn_4$	
Formula weight	1467.81	
Temperature	100(2) K	
Wavelength	0.71073 Å	
Crystal system	Orthorhombic	
Space group	$Cmc2_1$	
Unit cell dimensions	a = 20.1590(9) Å	α= 90°.
	b = 20.3549(6) Å	β= 90°.
	c = 12.3998(4) Å	γ = 90°.
Volume	5088.1(3) $Å^3$	
Z	4	
Density (calculated)	1.916 Mg/m^3	
Absorption coefficient	5.178 mm^{-1}	
F(000)	2816	
Crystal size	0.2 x 0.14 x 0.09 mm^3	
Theta range for data collection	1.422 to 27.918°.	
Index ranges	-26<=h<=26, -26<=k<=26, -16<=l<=15	
Reflections collected	25525	
Independent reflections	5946 [R(int) = 0.0476]	
Completeness to theta = 25.242°	100.0 %	
Absorption correction	Integration	
Max. and min. transmission	0.6028 and 0.4232	
Refinement method	Full-matrix least-squares on F^2	
Data / restraints / parameters	5946 / 1 / 292	
Goodness-of-fit on F^2	0.954	
Final R indices [I>2sigma(I)]	R1 = 0.0234, wR2 = 0.0446	
R indices (all data)	R1 = 0.0279, wR2 = 0.0455	
Absolute structure parameter	-0.006(3)	
Extinction coefficient	n/a	
Largest diff. peak and hole	0.800 and -0.465 e.$Å^{-3}$	

Table S2: Atomic coordinates (x 10^4) and equivalent isotropic displacement parameters ($Å^2$x 10^3) for **1**. U(eq) is defined as one third of the trace of the orthogonalized U^{ij} tensor.

	x	y	z	U(eq)
Au(1)	5000	1251(1)	2541(1)	24(1)
O(1)	7206(4)	154(4)	6096(7)	82(2)
C(1)	6798(3)	2184(3)	8093(5)	28(1)
P(1)	5000	163(1)	3209(2)	24(1)
S(1)	5951(1)	1740(1)	5621(1)	26(1)
Sn(1)	5930(1)	2391(1)	7187(1)	23(1)
Sn(3)	5000	1976(1)	4380(1)	24(1)
C(3)	7759(3)	1518(5)	8442(7)	46(2)
S(3)	5000	3203(1)	4141(2)	28(1)
Sn(2)	5000	3756(1)	5812(1)	23(1)
C(2)	7189(3)	1640(4)	7849(5)	35(2)
P(2)	3986(1)	1602(1)	1771(1)	26(1)
S(2)	5983(1)	3554(1)	6867(1)	27(1)
S(4)	5000	2187(1)	8368(2)	24(1)
C(4)	7946(4)	1936(4)	9275(6)	47(2)
C(7)	5000	4786(5)	5554(7)	26(2)
C(6)	6988(3)	2593(4)	8930(6)	34(2)
C(5)	7553(3)	2467(4)	9525(6)	40(2)
C(9)	5000	5889(6)	6212(11)	76(5)
C(8)	5000	5220(6)	6392(10)	67(4)
C(10)	5000	6131(5)	5206(9)	41(2)
C(11)	5000	5716(5)	4372(10)	63(4)
C(12)	5000	5045(6)	4540(10)	63(4)
C(14)	5000	91(5)	4664(8)	34(2)
C(15)	3901(4)	2484(3)	1589(6)	43(2)
C(16)	3251(3)	1396(4)	2534(7)	43(2)
C(17)	3796(3)	1276(3)	448(5)	34(1)
C(18)	7734(15)	-60(30)	6330(40)	101(17)
C(19)	8208(11)	474(16)	5880(20)	90(9)
C(20)	7879(15)	544(17)	4840(20)	117(14)
C(21)	7203(11)	393(17)	5030(30)	70(11)
C(18B)	7980(20)	80(20)	6290(40)	120(20)
C(19B)	8251(9)	17(14)	5070(20)	67(7)
C(20B)	7680(14)	253(19)	4340(20)	84(10)
C(21B)	7190(30)	320(30)	5050(50)	120(20)
C(13)	4295(3)	-344(3)	2812(6)	37(2)

Table S3: Bond lengths [Å] and angles [°] for **1**.

Au(1)-P(1)	2.365(2)	C(9)-C(8)	1.381(16)
Au(1)-P(2)	2.3671(16)	C(9)-H(9)	0.9300
Au(1)-P(2)#1	2.3672(16)	C(8)-H(8)	0.9300
Au(1)-Sn(3)	2.7162(7)	C(10)-C(11)	1.335(16)
O(1)-C(18)	1.19(4)	C(10)-H(10)	0.9300
O(1)-C(21B)	1.34(6)	C(11)-C(12)	1.381(17)
O(1)-C(21)	1.41(3)	C(11)-H(11)	0.9300
O(1)-C(18B)	1.58(4)	C(12)-H(12)	0.9300
C(1)-C(6)	1.384(10)	C(14)-H(14A)	0.9600
C(1)-C(2)	1.391(9)	C(14)-H(14B)	0.9600
C(1)-Sn(1)	2.122(6)	C(14)-H(14C)	0.9600
P(1)-C(14)	1.810(10)	C(14)-H(14A)#1	0.96(4)
P(1)-C(13)#1	1.823(6)	C(14)-H(14B)#1	0.96(7)
P(1)-C(13)	1.823(6)	C(14)-H(14C)#1	0.96(11)
S(1)-Sn(1)	2.3523(16)	C(15)-H(15A)	0.9600
S(1)-Sn(3)	2.5049(15)	C(15)-H(15B)	0.9600
Sn(1)-S(2)	2.4024(17)	C(15)-H(15C)	0.9600
Sn(1)-S(4)	2.4140(14)	C(16)-H(16A)	0.9600
Sn(3)-S(3)	2.514(2)	C(16)-H(16B)	0.9600
C(3)-C(2)	1.386(9)	C(16)-H(16C)	0.9600
C(3)-C(4)	1.390(12)	C(17)-H(17A)	0.9600
C(3)-H(3)	0.9300	C(17)-H(17B)	0.9600
S(3)-Sn(2)	2.357(2)	C(17)-H(17C)	0.9600
Sn(2)-C(7)	2.122(9)	C(18)-C(19)	1.55(4)
Sn(2)-S(2)	2.4092(16)	C(18)-H(18A)	0.9700
Sn(2)-S(2)#1	2.4092(16)	C(18)-H(18B)	0.9700
C(2)-H(2)	0.9300	C(19)-C(20)	1.46(4)
P(2)-C(16)	1.808(7)	C(19)-H(19A)	0.9700
P(2)-C(17)	1.811(7)	C(19)-H(19B)	0.9700
P(2)-C(15)	1.816(7)	C(20)-C(21)	1.42(4)
C(4)-C(5)	1.374(12)	C(20)-H(20A)	0.9700
C(4)-H(4)	0.9300	C(20)-H(20B)	0.9700
C(7)-C(8)	1.364(14)	C(21)-H(21A)	0.9700
C(7)-C(12)	1.364(14)	C(21)-H(21B)	0.9700
C(6)-C(5)	1.382(9)	C(18B)-C(19B)	1.62(6)
C(6)-H(6)	0.9300	C(18B)-H(18C)	0.9700
C(5)-H(5)	0.9300	C(18B)-H(18D)	0.9700
C(9)-C(10)	1.342(17)	C(19B)-C(20B)	1.54(3)

C(19B)-H(19C)	0.9700	S(3)-Sn(3)-Au(1)	116.15(5)
C(19B)-H(19D)	0.9700	C(2)-C(3)-C(4)	120.6(7)
C(20B)-C(21B)	1.32(6)	C(2)-C(3)-H(3)	119.7
C(20B)-H(20C)	0.9700	C(4)-C(3)-H(3)	119.7
C(20B)-H(20D)	0.9700	Sn(2)-S(3)-Sn(3)	111.74(9)
C(21B)-H(21C)	0.9700	C(7)-Sn(2)-S(3)	109.9(3)
C(21B)-H(21D)	0.9700	C(7)-Sn(2)-S(2)	104.48(14)
C(13)-H(13A)	0.9600	S(3)-Sn(2)-S(2)	113.34(5)
C(13)-H(13B)	0.9600	C(7)-Sn(2)-S(2)#1	104.48(14)
C(13)-H(13C)	0.9600	S(3)-Sn(2)-S(2)#1	113.33(5)
P(1)-Au(1)-P(2)	115.10(5)	S(2)-Sn(2)-S(2)#1	110.61(8)
P(1)-Au(1)-P(2)#1	115.10(5)	C(3)-C(2)-C(1)	119.8(7)
P(2)-Au(1)-P(2)#1	119.45(8)	C(3)-C(2)-H(2)	120.1
P(1)-Au(1)-Sn(3)	102.43(6)	C(1)-C(2)-H(2)	120.1
P(2)-Au(1)-Sn(3)	100.07(4)	C(16)-P(2)-C(17)	102.5(4)
P(2)#1-Au(1)-Sn(3)	100.07(4)	C(16)-P(2)-C(15)	102.5(4)
C(18)-O(1)-C(21)	111(2)	C(17)-P(2)-C(15)	103.3(3)
C(21B)-O(1)-C(18B)	101(3)	C(16)-P(2)-Au(1)	115.3(3)
C(6)-C(1)-C(2)	118.9(6)	C(17)-P(2)-Au(1)	115.9(2)
C(6)-C(1)-Sn(1)	120.3(5)	C(15)-P(2)-Au(1)	115.4(2)
C(2)-C(1)-Sn(1)	120.7(5)	Sn(1)-S(2)-Sn(2)	102.77(6)
C(14)-P(1)-C(13)#1	102.9(3)	Sn(1)#1-S(4)-Sn(1)	101.86(8)
C(14)-P(1)-C(13)	102.9(3)	C(5)-C(4)-C(3)	119.5(6)
C(13)#1-P(1)-C(13)	102.4(4)	C(5)-C(4)-H(4)	120.2
C(14)-P(1)-Au(1)	115.1(3)	C(3)-C(4)-H(4)	120.2
C(13)#1-P(1)-Au(1)	115.8(2)	C(8)-C(7)-C(12)	116.9(10)
C(13)-P(1)-Au(1)	115.8(2)	C(8)-C(7)-Sn(2)	121.7(8)
Sn(1)-S(1)-Sn(3)	112.63(6)	C(12)-C(7)-Sn(2)	121.4(8)
C(1)-Sn(1)-S(1)	108.02(19)	C(5)-C(6)-C(1)	121.2(7)
C(1)-Sn(1)-S(2)	104.32(18)	C(5)-C(6)-H(6)	119.4
S(1)-Sn(1)-S(2)	114.70(6)	C(1)-C(6)-H(6)	119.4
C(1)-Sn(1)-S(4)	106.58(17)	C(4)-C(5)-C(6)	120.0(7)
S(1)-Sn(1)-S(4)	114.70(6)	C(4)-C(5)-H(5)	120.0
S(2)-Sn(1)-S(4)	107.73(7)	C(6)-C(5)-H(5)	120.0
S(1)-Sn(3)-S(1)#1	99.93(7)	C(10)-C(9)-C(8)	120.8(12)
S(1)-Sn(3)-S(3)	105.24(5)	C(10)-C(9)-H(9)	119.6
S(1)#1-Sn(3)-S(3)	105.24(5)	C(8)-C(9)-H(9)	119.6
S(1)-Sn(3)-Au(1)	114.28(4)	C(7)-C(8)-C(9)	121.0(11)
S(1)#1-Sn(3)-Au(1)	114.28(4)	C(7)-C(8)-H(8)	119.5

C(9)-C(8)-H(8)	119.5	H(16A)-C(16)-H(16B)	109.5
C(11)-C(10)-C(9)	119.2(10)	P(2)-C(16)-H(16C)	109.5
C(11)-C(10)-H(10)	120.4	H(16A)-C(16)-H(16C)	109.5
C(9)-C(10)-H(10)	120.4	H(16B)-C(16)-H(16C)	109.5
C(10)-C(11)-C(12)	120.5(11)	P(2)-C(17)-H(17A)	109.5
C(10)-C(11)-H(11)	119.7	P(2)-C(17)-H(17B)	109.5
C(12)-C(11)-H(11)	119.7	H(17A)-C(17)-H(17B)	109.5
C(7)-C(12)-C(11)	121.5(11)	P(2)-C(17)-H(17C)	109.5
C(7)-C(12)-H(12)	119.3	H(17A)-C(17)-H(17C)	109.5
C(11)-C(12)-H(12)	119.3	H(17B)-C(17)-H(17C)	109.5
P(1)-C(14)-H(14A)	109.5	O(1)-C(18)-C(19)	102(3)
P(1)-C(14)-H(14B)	109.5	O(1)-C(18)-H(18A)	111.4
H(14A)-C(14)-H(14B)	109.5	C(19)-C(18)-H(18A)	111.4
P(1)-C(14)-H(14C)	109.5	O(1)-C(18)-H(18B)	111.4
H(14A)-C(14)-H(14C)	109.5	C(19)-C(18)-H(18B)	111.4
H(14B)-C(14)-H(14C)	109.5	H(18A)-C(18)-H(18B)	109.3
P(1)-C(14)-H(14A)#1	109.5(10)	C(20)-C(19)-C(18)	96(2)
H(14A)-C(14)-H(14A)#1	21.6	C(20)-C(19)-H(19A)	112.5
H(14B)-C(14)-H(14A)#1	89.9	C(18)-C(19)-H(19A)	112.5
H(14C)-C(14)-H(14A)#1	126.7	C(20)-C(19)-H(19B)	112.5
P(1)-C(14)-H(14B)#1	109.5(14)	C(18)-C(19)-H(19B)	112.5
H(14A)-C(14)-H(14B)#1	89.9	H(19A)-C(19)-H(19B)	110.0
H(14B)-C(14)-H(14B)#1	126.7	C(21)-C(20)-C(19)	106(2)
H(14C)-C(14)-H(14B)#1	21.6	C(21)-C(20)-H(20A)	110.6
H(14A)#1-C(14)-H(14B)#1	109.5	C(19)-C(20)-H(20A)	110.6
P(1)-C(14)-H(14C)#1	109(2)	C(21)-C(20)-H(20B)	110.6
H(14A)-C(14)-H(14C)#1	126.7	C(19)-C(20)-H(20B)	110.6
H(14B)-C(14)-H(14C)#1	21.6	H(20A)-C(20)-H(20B)	108.8
H(14C)-C(14)-H(14C)#1	89.9	O(1)-C(21)-C(20)	103(2)
H(14A)#1-C(14)-H(14C)#1	109.5	O(1)-C(21)-H(21A)	111.1
H(14B)#1-C(14)-H(14C)#1	109.5	C(20)-C(21)-H(21A)	111.1
P(2)-C(15)-H(15A)	109.5	O(1)-C(21)-H(21B)	111.1
P(2)-C(15)-H(15B)	109.5	C(20)-C(21)-H(21B)	111.1
H(15A)-C(15)-H(15B)	109.5	H(21A)-C(21)-H(21B)	109.1
P(2)-C(15)-H(15C)	109.5	O(1)-C(18B)-C(19B)	102(2)
H(15A)-C(15)-H(15C)	109.5	O(1)-C(18B)-H(18C)	111.5
H(15B)-C(15)-H(15C)	109.5	C(19B)-C(18B)-H(18C)	111.5
P(2)-C(16)-H(16A)	109.5	O(1)-C(18B)-H(18D)	111.5
P(2)-C(16)-H(16B)	109.5	C(19B)-C(18B)-H(18D)	111.5

H(18C)-C(18B)-H(18D)	109.3	O(1)-C(21B)-H(21C)	105.5
C(20B)-C(19B)-C(18B)	105.4(19)	C(20B)-C(21B)-H(21D)	105.5
C(20B)-C(19B)-H(19C)	110.7	O(1)-C(21B)-H(21D)	105.5
C(18B)-C(19B)-H(19C)	110.7	H(21C)-C(21B)-H(21D)	106.1
C(20B)-C(19B)-H(19D)	110.7	P(1)-C(13)-H(13A)	109.5
C(18B)-C(19B)-H(19D)	110.7	P(1)-C(13)-H(13B)	109.5
H(19C)-C(19B)-H(19D)	108.8	H(13A)-C(13)-H(13B)	109.5
C(21B)-C(20B)-C(19B)	102(3)	P(1)-C(13)-H(13C)	109.5
C(21B)-C(20B)-H(20C)	111.4	H(13A)-C(13)-H(13C)	109.5
C(19B)-C(20B)-H(20C)	111.4	H(13B)-C(13)-H(13C)	109.5
C(21B)-C(20B)-H(20D)	111.4		
C(19B)-C(20B)-H(20D)	111.4		
H(20C)-C(20B)-H(20D)	109.3		
C(20B)-C(21B)-O(1)	127(5)		
C(20B)-C(21B)-H(21C)	105.5		

Symmetry transformations used to generate equivalent atoms:
#1 -x+1,y,z

The inorganic core of **1** shows a slightly distorted adamantane-type structure (Figure 1 of the manuscript, top left). The Sn3–S1 (2.5049(15) Å) and Sn3–S3 (2.514(2) Å) bond lengths involving the tin atom with the gold-substituent are longer than the other Sn–S bonds (2.3523(16) - 2.4140(14) Å), which are in the range for reported single-crystalline adamantane-type tin sulfide clusters such as $[(C_6F_5Sn)_4S_6]$ (2.38 – 2.41 Å).[2] The bond angles are all in the usual range for adamantane-type structures, varying from 99.93(7)° to 114.70(6)° (reported: 102.7° - 114.8°).[2] The Sn–Au bond has a length of 2.7162(7) Å, which is close to the respective bond length in $[(Me_3P)_3AuSnCl_3]$ (2.724 Å).[3] The same holds true for the Au–P bond lengths (2.365(2) – 2.3672(16) Å in 1 vs. 2.364 – 2.371 Å in $[(Me_3P)_3AuSnCl_3]$) and the Sn–Au–P bond angles (100.07(4) – 102.43(6)° in 1 vs. 101.64 – 104.60° in $[(Me_3P)_3AuSnCl_3]$).

7. Single-Crystal X-Ray Crystallography of Compound 2

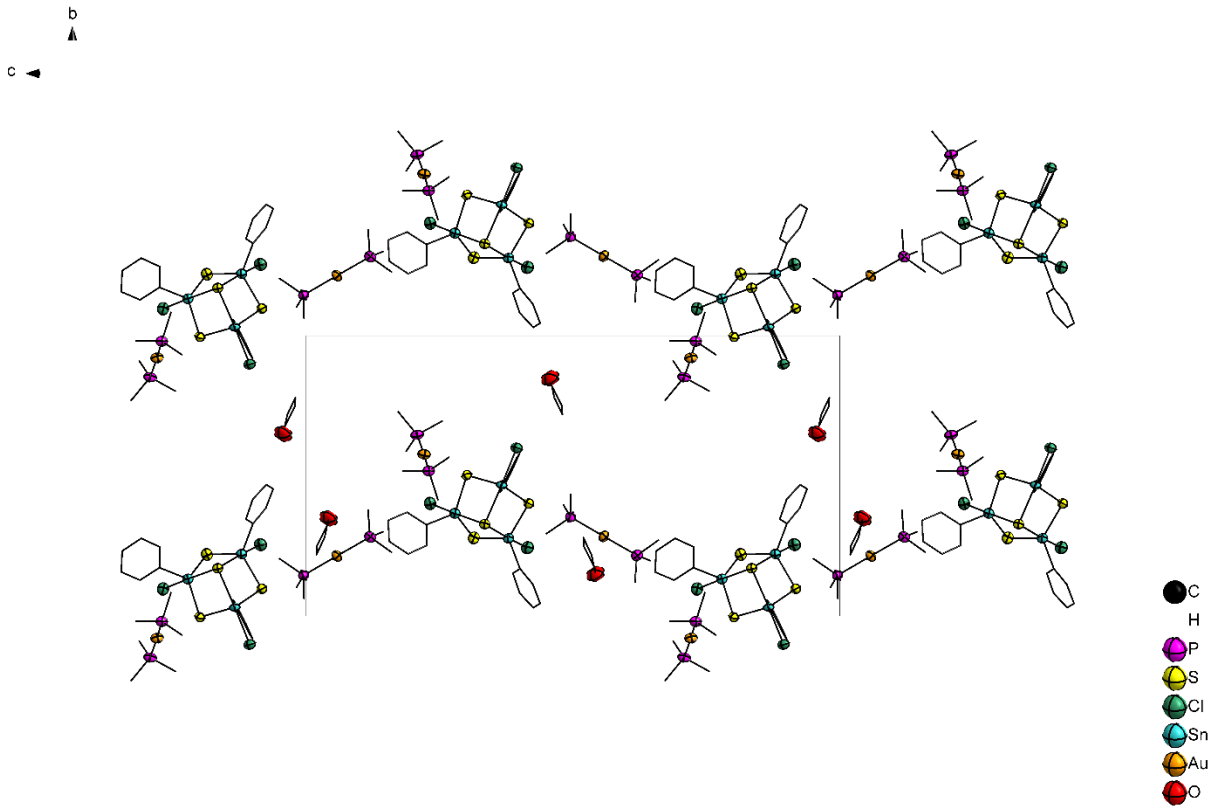

Figure S32: Crystal structure of **2** · 2 THF, viewed along the crystallographic a axis. Ellipsoids are shown at 50% probability, hydrogen atoms are omitted for clarity.

Table S4: Crystal data and structure refinement for **2**·2 THF (CCDC 1875437).

Empirical formula	$C_{44}H_{85}Au_2Cl_3O_2P_6S_4Sn_3$	
Formula weight	1816.53	
Temperature	100(2) K	
Wavelength	0.71073 Å	
Crystal system	Monoclinic	
Space group	$P2_1/c$	
Unit cell dimensions	a = 13.7234(4) Å	α= 90°.
	b = 18.3634(4) Å	β= 96.048(2)°.
	c = 26.0465(8) Å	γ = 90°.
Volume	6527.4(3) $Å^3$	
Z	4	
Density (calculated)	1.848 Mg/m^3	
Absorption coefficient	6.041 mm^{-1}	
F(000)	3512	
Crystal size	0.30 x 0.25 x 0.20 mm^3	
Theta range for data collection	1.359 to 26.775°.	
Index ranges	-17<=h<=17, -23<=k<=23, -27<=l<=32	
Reflections collected	46854	
Independent reflections	13805 [R(int) = 0.0476]	
Completeness to theta = 25.242°	100.0 %	
Absorption correction	Integration	
Max. and min. transmission	0.4186 and 0.2191	
Refinement method	Full-matrix least-squares on F^2	
Data / restraints / parameters	13805 / 0 / 626	
Goodness-of-fit on F^2	0.808	
Final R indices [I>2sigma(I)]	R1 = 0.0292, wR2 = 0.0470	
R indices (all data)	R1 = 0.0627, wR2 = 0.0523	
Extinction coefficient	n/a	
Largest diff. peak and hole	0.950 and -0.749 $e.Å^{-3}$	

Table S5: Atomic coordinates (x 10^4) and equivalent isotropic displacement parameters ($Å^2$x 10^3) for **2**. U(eq) is defined as one third of the trace of the orthogonalized U^{ij} tensor.

	x	y	z	U(eq)
Au(1)	-377(1)	3287(1)	7591(1)	30(1)
C(1)	4528(3)	6168(3)	7460(2)	29(1)
P(1)	1074(1)	2703(1)	7488(1)	29(1)
Cl(1)	4785(1)	4345(1)	7466(1)	41(1)
Sn(1)	3468(1)	5305(1)	7388(1)	27(1)
O(1)	3136(4)	5160(3)	3862(3)	92(2)
S(1)	2884(1)	4807(1)	8161(1)	29(1)
Au(2)	4880(1)	7529(1)	4907(1)	32(1)
C(2)	5450(3)	6075(3)	7729(2)	32(1)
P(2)	-1913(1)	3719(1)	7701(1)	31(1)
Cl(2)	462(1)	4330(1)	6027(1)	39(1)
Sn(2)	1153(1)	5326(1)	6617(1)	27(1)
O(2)	8180(6)	8941(4)	4708(3)	121(2)
S(2)	2772(1)	4814(1)	6573(1)	33(1)
Sn(3)	1282(1)	5359(1)	8005(1)	25(1)
C(3)	6080(4)	6662(3)	7828(2)	39(1)
P(3)	5820(1)	8204(1)	5560(1)	35(1)
Cl(3)	590(1)	4387(1)	8566(1)	34(1)
S(3)	1976(1)	6197(1)	7331(1)	26(1)
S(4)	241(1)	4839(1)	7288(1)	29(1)
C(4)	5792(4)	7351(3)	7651(2)	35(1)
P(4)	3555(1)	6902(1)	5242(1)	44(1)
P(6)	4185(1)	8370(1)	4263(1)	33(1)
C(6)	4266(4)	6859(3)	7281(2)	31(1)
P(5)	5836(1)	6673(1)	4483(1)	38(1)
C(5)	4891(4)	7448(3)	7372(2)	33(1)
C(9)	-32(4)	7422(3)	6008(2)	34(1)
C(8)	424(3)	6879(3)	6310(2)	29(1)
C(7)	521(3)	6176(3)	6121(2)	27(1)
C(10)	-405(4)	7271(3)	5500(2)	37(1)
C(13)	936(3)	6229(3)	8513(2)	28(1)
C(12)	144(4)	6033(3)	5616(2)	34(1)
C(11)	-312(4)	6580(3)	5305(2)	38(1)
C(14)	536(4)	6093(3)	8971(2)	42(1)
C(15)	355(5)	6660(3)	9301(3)	53(2)
C(16)	546(4)	7371(3)	9170(2)	45(2)

C(17)	933(3)	7512(3)	8714(2)	33(1)
C(18)	1126(3)	6948(3)	8392(2)	29(1)
C(19)	1985(4)	2843(3)	8024(2)	38(1)
C(20)	1626(4)	2994(3)	6928(2)	43(2)
C(21)	1010(4)	1725(3)	7429(3)	40(1)
C(22)	-2816(4)	3491(3)	7171(2)	42(2)
C(23)	-2382(4)	3346(3)	8262(2)	45(2)
C(24)	-2018(4)	4688(3)	7785(3)	46(2)
C(25)	7124(4)	8036(4)	5641(2)	47(2)
C(26)	5802(5)	9187(3)	5470(3)	61(2)
C(27)	5492(4)	8118(4)	6211(2)	49(2)
C(28)	2765(5)	6370(4)	4788(3)	74(2)
C(29)	3888(7)	6317(6)	5758(4)	130(5)
C(30)	2626(6)	7476(5)	5492(4)	102(3)
C(31A)	6751(14)	7099(9)	4112(8)	55(5)
C(32A)	5210(13)	6095(13)	4039(10)	77(8)
C(33A)	6659(15)	6051(10)	4890(6)	66(7)
C(31B)	7082(11)	6816(10)	4484(11)	100(9)
C(32B)	5331(18)	6530(11)	3816(7)	104(9)
C(33B)	5770(12)	5738(6)	4699(6)	70(6)
C(34)	3169(4)	8911(3)	4444(3)	46(2)
C(35)	4999(4)	9058(3)	4046(2)	40(1)
C(36)	3677(4)	7990(3)	3655(2)	44(2)
C(37)	3669(5)	4699(4)	3569(3)	63(2)
C(38)	3256(5)	3960(4)	3618(3)	69(2)
C(39)	2196(5)	4111(4)	3703(3)	70(2)
C(40)	2213(5)	4850(4)	3926(4)	74(2)
C(41)	8524(7)	9586(6)	4972(4)	98(3)
C(42)	8468(8)	10213(6)	4594(6)	124(5)
C(43)	7607(9)	9954(7)	4255(5)	118(4)
C(44)	7828(7)	9193(8)	4197(5)	120(4)

Table S6: Bond lengths [Å] and angles [°] for **2**.

Au(1)-P(2)	2.2985(13)	P(3)-C(27)	1.806(6)
Au(1)-P(1)	2.3016(13)	P(3)-C(26)	1.819(6)
C(1)-C(6)	1.386(7)	C(4)-C(5)	1.378(7)
C(1)-C(2)	1.392(7)	C(4)-H(4)	0.9300
C(1)-Sn(1)	2.146(5)	P(4)-C(29)	1.741(9)
P(1)-C(19)	1.793(6)	P(4)-C(28)	1.805(7)
P(1)-C(20)	1.793(6)	P(4)-C(30)	1.826(8)
P(1)-C(21)	1.805(5)	P(6)-C(36)	1.802(6)
Cl(1)-Sn(1)	2.5186(12)	P(6)-C(34)	1.814(5)
Sn(1)-S(2)	2.4083(15)	P(6)-C(35)	1.817(6)
Sn(1)-S(1)	2.4236(14)	C(6)-C(5)	1.384(7)
Sn(1)-S(3)	2.6136(12)	C(6)-H(6)	0.9300
O(1)-C(37)	1.397(8)	P(5)-C(31B)	1.729(14)
O(1)-C(40)	1.415(8)	P(5)-C(32A)	1.729(18)
S(1)-Sn(3)	2.4165(12)	P(5)-C(33B)	1.812(13)
Au(2)-P(3)	2.3743(15)	P(5)-C(32B)	1.820(19)
Au(2)-P(5)	2.3908(14)	P(5)-C(31A)	1.837(16)
Au(2)-P(4)	2.3943(15)	P(5)-C(33A)	1.860(15)
Au(2)-P(6)	2.4026(15)	C(5)-H(5)	0.9300
C(2)-C(3)	1.389(7)	C(9)-C(8)	1.379(7)
C(2)-H(2)	0.9300	C(9)-C(10)	1.395(8)
P(2)-C(23)	1.793(6)	C(9)-H(9)	0.9300
P(2)-C(24)	1.801(6)	C(8)-C(7)	1.393(7)
P(2)-C(22)	1.805(6)	C(8)-H(8)	0.9300
Cl(2)-Sn(2)	2.5081(14)	C(7)-C(12)	1.389(7)
Sn(2)-C(7)	2.149(5)	C(10)-C(11)	1.377(8)
Sn(2)-S(4)	2.4245(13)	C(10)-H(10)	0.9300
Sn(2)-S(2)	2.4255(13)	C(13)-C(14)	1.386(8)
Sn(2)-S(3)	2.6180(13)	C(13)-C(18)	1.388(7)
O(2)-C(41)	1.424(11)	C(12)-C(11)	1.395(8)
O(2)-C(44)	1.441(12)	C(12)-H(12)	0.9300
Sn(3)-C(13)	2.160(5)	C(11)-H(11)	0.9300
Sn(3)-S(4)	2.4259(14)	C(14)-C(15)	1.388(8)
Sn(3)-Cl(3)	2.5528(13)	C(14)-H(14)	0.9300
Sn(3)-S(3)	2.5910(13)	C(15)-C(16)	1.381(8)
C(3)-C(4)	1.389(8)	C(15)-H(15)	0.9300
C(3)-H(3)	0.9300	C(16)-C(17)	1.377(8)
P(3)-C(25)	1.806(6)	C(16)-H(16)	0.9300

C(17)-C(18)	1.374(7)	C(31A)-H(31A)	0.9600
C(17)-H(17)	0.9300	C(31A)-H(31B)	0.9600
C(18)-H(18)	0.9300	C(31A)-H(31C)	0.9600
C(19)-H(19A)	0.9600	C(32A)-H(32A)	0.9600
C(19)-H(19B)	0.9600	C(32A)-H(32B)	0.9600
C(19)-H(19C)	0.9600	C(32A)-H(32C)	0.9600
C(20)-H(20A)	0.9600	C(33A)-H(33A)	0.9600
C(20)-H(20B)	0.9600	C(33A)-H(33B)	0.9600
C(20)-H(20C)	0.9600	C(33A)-H(33C)	0.9600
C(21)-H(21A)	0.9600	C(31B)-H(31D)	0.9600
C(21)-H(21B)	0.9600	C(31B)-H(31E)	0.9600
C(21)-H(21C)	0.9600	C(31B)-H(31F)	0.9600
C(22)-H(22A)	0.9600	C(32B)-H(32D)	0.9600
C(22)-H(22B)	0.9600	C(32B)-H(32E)	0.9600
C(22)-H(22C)	0.9600	C(32B)-H(32F)	0.9600
C(23)-H(23A)	0.9600	C(33B)-H(33D)	0.9600
C(23)-H(23B)	0.9600	C(33B)-H(33E)	0.9600
C(23)-H(23C)	0.9600	C(33B)-H(33F)	0.9600
C(24)-H(24A)	0.9600	C(34)-H(34A)	0.9600
C(24)-H(24B)	0.9600	C(34)-H(34B)	0.9600
C(24)-H(24C)	0.9600	C(34)-H(34C)	0.9600
C(25)-H(25A)	0.9600	C(35)-H(35A)	0.9600
C(25)-H(25B)	0.9600	C(35)-H(35B)	0.9600
C(25)-H(25C)	0.9600	C(35)-H(35C)	0.9600
C(26)-H(26A)	0.9600	C(36)-H(36A)	0.9600
C(26)-H(26B)	0.9600	C(36)-H(36B)	0.9600
C(26)-H(26C)	0.9600	C(36)-H(36C)	0.9600
C(27)-H(27A)	0.9600	C(37)-C(38)	1.480(9)
C(27)-H(27B)	0.9600	C(37)-H(37A)	0.9700
C(27)-H(27C)	0.9600	C(37)-H(37B)	0.9700
C(28)-H(28A)	0.9600	C(38)-C(39)	1.520(9)
C(28)-H(28B)	0.9600	C(38)-H(38A)	0.9700
C(28)-H(28C)	0.9600	C(38)-H(38B)	0.9700
C(29)-H(29A)	0.9600	C(39)-C(40)	1.476(10)
C(29)-H(29B)	0.9600	C(39)-H(39A)	0.9700
C(29)-H(29C)	0.9600	C(39)-H(39B)	0.9700
C(30)-H(30A)	0.9600	C(40)-H(40A)	0.9700
C(30)-H(30B)	0.9600	C(40)-H(40B)	0.9700
C(30)-H(30C)	0.9600	C(41)-C(42)	1.511(14)

C(41)-H(41A)	0.9700	C(3)-C(2)-H(2)	119.6
C(41)-H(41B)	0.9700	C(1)-C(2)-H(2)	119.6
C(42)-C(43)	1.477(14)	C(23)-P(2)-C(24)	103.8(3)
C(42)-H(42A)	0.9700	C(23)-P(2)-C(22)	105.0(3)
C(42)-H(42B)	0.9700	C(24)-P(2)-C(22)	105.4(3)
C(43)-C(44)	1.440(14)	C(23)-P(2)-Au(1)	112.5(2)
C(43)-H(43A)	0.9700	C(24)-P(2)-Au(1)	116.26(18)
C(43)-H(43B)	0.9700	C(22)-P(2)-Au(1)	112.90(18)
C(44)-H(44A)	0.9700	C(7)-Sn(2)-S(4)	119.62(13)
C(44)-H(44B)	0.9700	C(7)-Sn(2)-S(2)	124.53(13)
P(2)-Au(1)-P(1)	172.41(5)	S(4)-Sn(2)-S(2)	115.84(5)
C(6)-C(1)-C(2)	118.2(5)	C(7)-Sn(2)-Cl(2)	93.39(14)
C(6)-C(1)-Sn(1)	119.8(4)	S(4)-Sn(2)-Cl(2)	88.97(5)
C(2)-C(1)-Sn(1)	121.7(4)	S(2)-Sn(2)-Cl(2)	88.74(5)
C(19)-P(1)-C(20)	105.7(3)	C(7)-Sn(2)-S(3)	95.69(14)
C(19)-P(1)-C(21)	103.4(3)	S(4)-Sn(2)-S(3)	86.02(4)
C(20)-P(1)-C(21)	104.4(3)	S(2)-Sn(2)-S(3)	86.62(4)
C(19)-P(1)-Au(1)	112.52(19)	Cl(2)-Sn(2)-S(3)	170.90(4)
C(20)-P(1)-Au(1)	113.64(19)	C(41)-O(2)-C(44)	103.9(8)
C(21)-P(1)-Au(1)	116.04(17)	Sn(1)-S(2)-Sn(2)	95.40(5)
C(1)-Sn(1)-S(2)	123.79(14)	C(13)-Sn(3)-S(1)	117.57(13)
C(1)-Sn(1)-S(1)	119.10(14)	C(13)-Sn(3)-S(4)	127.88(13)
S(2)-Sn(1)-S(1)	117.09(5)	S(1)-Sn(3)-S(4)	114.55(5)
C(1)-Sn(1)-Cl(1)	92.06(13)	C(13)-Sn(3)-Cl(3)	92.69(14)
S(2)-Sn(1)-Cl(1)	91.36(5)	S(1)-Sn(3)-Cl(3)	89.85(4)
S(1)-Sn(1)-Cl(1)	88.04(5)	S(4)-Sn(3)-Cl(3)	86.62(4)
C(1)-Sn(1)-S(3)	93.54(13)	C(13)-Sn(3)-S(3)	95.55(14)
S(2)-Sn(1)-S(3)	87.08(4)	S(1)-Sn(3)-S(3)	88.28(4)
S(1)-Sn(1)-S(3)	87.61(4)	S(4)-Sn(3)-S(3)	86.59(4)
Cl(1)-Sn(1)-S(3)	174.10(4)	Cl(3)-Sn(3)-S(3)	171.47(4)
C(37)-O(1)-C(40)	110.4(5)	C(2)-C(3)-C(4)	119.7(5)
Sn(3)-S(1)-Sn(1)	94.40(5)	C(2)-C(3)-H(3)	120.1
P(3)-Au(2)-P(5)	113.00(5)	C(4)-C(3)-H(3)	120.1
P(3)-Au(2)-P(4)	111.47(6)	C(25)-P(3)-C(27)	102.6(3)
P(5)-Au(2)-P(4)	109.12(6)	C(25)-P(3)-C(26)	100.7(3)
P(3)-Au(2)-P(6)	108.07(5)	C(27)-P(3)-C(26)	101.9(3)
P(5)-Au(2)-P(6)	107.29(5)	C(25)-P(3)-Au(2)	116.8(2)
P(4)-Au(2)-P(6)	107.66(5)	C(27)-P(3)-Au(2)	117.1(2)
C(3)-C(2)-C(1)	120.8(5)	C(26)-P(3)-Au(2)	115.3(2)

Sn(3)-S(3)-Sn(1)	86.05(4)	C(10)-C(9)-H(9)	120.1
Sn(3)-S(3)-Sn(2)	87.50(4)	C(9)-C(8)-C(7)	121.5(5)
Sn(1)-S(3)-Sn(2)	86.22(4)	C(9)-C(8)-H(8)	119.2
Sn(2)-S(4)-Sn(3)	95.91(4)	C(7)-C(8)-H(8)	119.2
C(5)-C(4)-C(3)	120.0(5)	C(12)-C(7)-C(8)	118.0(5)
C(5)-C(4)-H(4)	120.0	C(12)-C(7)-Sn(2)	121.3(4)
C(3)-C(4)-H(4)	120.0	C(8)-C(7)-Sn(2)	120.6(4)
C(29)-P(4)-C(28)	105.2(5)	C(11)-C(10)-C(9)	119.6(5)
C(29)-P(4)-C(30)	102.6(6)	C(11)-C(10)-H(10)	120.2
C(28)-P(4)-C(30)	98.8(4)	C(9)-C(10)-H(10)	120.2
C(29)-P(4)-Au(2)	115.5(3)	C(14)-C(13)-C(18)	117.9(5)
C(28)-P(4)-Au(2)	116.6(3)	C(14)-C(13)-Sn(3)	121.8(4)
C(30)-P(4)-Au(2)	115.9(3)	C(18)-C(13)-Sn(3)	120.3(4)
C(36)-P(6)-C(34)	101.8(3)	C(7)-C(12)-C(11)	120.9(5)
C(36)-P(6)-C(35)	101.0(3)	C(7)-C(12)-H(12)	119.6
C(34)-P(6)-C(35)	102.4(3)	C(11)-C(12)-H(12)	119.6
C(36)-P(6)-Au(2)	116.9(2)	C(10)-C(11)-C(12)	120.2(5)
C(34)-P(6)-Au(2)	115.4(2)	C(10)-C(11)-H(11)	119.9
C(35)-P(6)-Au(2)	116.90(19)	C(12)-C(11)-H(11)	119.9
C(5)-C(6)-C(1)	121.5(5)	C(13)-C(14)-C(15)	120.6(5)
C(5)-C(6)-H(6)	119.3	C(13)-C(14)-H(14)	119.7
C(1)-C(6)-H(6)	119.3	C(15)-C(14)-H(14)	119.7
C(31B)-P(5)-C(33B)	103.0(9)	C(16)-C(15)-C(14)	120.3(6)
C(31B)-P(5)-C(32B)	107.5(11)	C(16)-C(15)-H(15)	119.8
C(33B)-P(5)-C(32B)	97.7(8)	C(14)-C(15)-H(15)	119.8
C(32A)-P(5)-C(31A)	103.2(11)	C(17)-C(16)-C(15)	119.4(5)
C(32A)-P(5)-C(33A)	103.5(10)	C(17)-C(16)-H(16)	120.3
C(31A)-P(5)-C(33A)	98.8(8)	C(15)-C(16)-H(16)	120.3
C(31B)-P(5)-Au(2)	119.4(5)	C(18)-C(17)-C(16)	120.1(5)
C(32A)-P(5)-Au(2)	117.0(6)	C(18)-C(17)-H(17)	120.0
C(33B)-P(5)-Au(2)	115.6(4)	C(16)-C(17)-H(17)	120.0
C(32B)-P(5)-Au(2)	111.3(5)	C(17)-C(18)-C(13)	121.7(5)
C(31A)-P(5)-Au(2)	113.7(5)	C(17)-C(18)-H(18)	119.2
C(33A)-P(5)-Au(2)	118.0(5)	C(13)-C(18)-H(18)	119.2
C(4)-C(5)-C(6)	119.7(5)	P(1)-C(19)-H(19A)	109.5
C(4)-C(5)-H(5)	120.1	P(1)-C(19)-H(19B)	109.5
C(6)-C(5)-H(5)	120.1	H(19A)-C(19)-H(19B)	109.5
C(8)-C(9)-C(10)	119.8(5)	P(1)-C(19)-H(19C)	109.5
C(8)-C(9)-H(9)	120.1	H(19A)-C(19)-H(19C)	109.5

H(19B)-C(19)-H(19C)	109.5	H(26A)-C(26)-H(26B)	109.5
P(1)-C(20)-H(20A)	109.5	P(3)-C(26)-H(26C)	109.5
P(1)-C(20)-H(20B)	109.5	H(26A)-C(26)-H(26C)	109.5
H(20A)-C(20)-H(20B)	109.5	H(26B)-C(26)-H(26C)	109.5
P(1)-C(20)-H(20C)	109.5	P(3)-C(27)-H(27A)	109.5
H(20A)-C(20)-H(20C)	109.5	P(3)-C(27)-H(27B)	109.5
H(20B)-C(20)-H(20C)	109.5	H(27A)-C(27)-H(27B)	109.5
P(1)-C(21)-H(21A)	109.5	P(3)-C(27)-H(27C)	109.5
P(1)-C(21)-H(21B)	109.5	H(27A)-C(27)-H(27C)	109.5
H(21A)-C(21)-H(21B)	109.5	H(27B)-C(27)-H(27C)	109.5
P(1)-C(21)-H(21C)	109.5	P(4)-C(28)-H(28A)	109.5
H(21A)-C(21)-H(21C)	109.5	P(4)-C(28)-H(28B)	109.5
H(21B)-C(21)-H(21C)	109.5	H(28A)-C(28)-H(28B)	109.5
P(2)-C(22)-H(22A)	109.5	P(4)-C(28)-H(28C)	109.5
P(2)-C(22)-H(22B)	109.5	H(28A)-C(28)-H(28C)	109.5
H(22A)-C(22)-H(22B)	109.5	H(28B)-C(28)-H(28C)	109.5
P(2)-C(22)-H(22C)	109.5	P(4)-C(29)-H(29A)	109.5
H(22A)-C(22)-H(22C)	109.5	P(4)-C(29)-H(29B)	109.5
H(22B)-C(22)-H(22C)	109.5	H(29A)-C(29)-H(29B)	109.5
P(2)-C(23)-H(23A)	109.5	P(4)-C(29)-H(29C)	109.5
P(2)-C(23)-H(23B)	109.5	H(29A)-C(29)-H(29C)	109.5
H(23A)-C(23)-H(23B)	109.5	H(29B)-C(29)-H(29C)	109.5
P(2)-C(23)-H(23C)	109.5	P(4)-C(30)-H(30A)	109.5
H(23A)-C(23)-H(23C)	109.5	P(4)-C(30)-H(30B)	109.5
H(23B)-C(23)-H(23C)	109.5	H(30A)-C(30)-H(30B)	109.5
P(2)-C(24)-H(24A)	109.5	P(4)-C(30)-H(30C)	109.5
P(2)-C(24)-H(24B)	109.5	H(30A)-C(30)-H(30C)	109.5
H(24A)-C(24)-H(24B)	109.5	H(30B)-C(30)-H(30C)	109.5
P(2)-C(24)-H(24C)	109.5	P(5)-C(31A)-H(31A)	109.5
H(24A)-C(24)-H(24C)	109.5	P(5)-C(31A)-H(31B)	109.5
H(24B)-C(24)-H(24C)	109.5	H(31A)-C(31A)-H(31B)	109.5
P(3)-C(25)-H(25A)	109.5	P(5)-C(31A)-H(31C)	109.5
P(3)-C(25)-H(25B)	109.5	H(31A)-C(31A)-H(31C)	109.5
H(25A)-C(25)-H(25B)	109.5	H(31B)-C(31A)-H(31C)	109.5
P(3)-C(25)-H(25C)	109.5	P(5)-C(32A)-H(32A)	109.5
H(25A)-C(25)-H(25C)	109.5	P(5)-C(32A)-H(32B)	109.5
H(25B)-C(25)-H(25C)	109.5	H(32A)-C(32A)-H(32B)	109.5
P(3)-C(26)-H(26A)	109.5	P(5)-C(32A)-H(32C)	109.5
P(3)-C(26)-H(26B)	109.5	H(32A)-C(32A)-H(32C)	109.5

H(32B)-C(32A)-H(32C) 109.5
P(5)-C(33A)-H(33A) 109.5
P(5)-C(33A)-H(33B) 109.5
H(33A)-C(33A)-H(33B) 109.5
P(5)-C(33A)-H(33C) 109.5
H(33A)-C(33A)-H(33C) 109.5
H(33B)-C(33A)-H(33C) 109.5
P(5)-C(31B)-H(31D) 109.5
P(5)-C(31B)-H(31E) 109.5
H(31D)-C(31B)-H(31E) 109.5
P(5)-C(31B)-H(31F) 109.5
H(31D)-C(31B)-H(31F) 109.5
H(31E)-C(31B)-H(31F) 109.5
P(5)-C(32B)-H(32D) 109.5
P(5)-C(32B)-H(32E) 109.5
H(32D)-C(32B)-H(32E) 109.5
P(5)-C(32B)-H(32F) 109.5
H(32D)-C(32B)-H(32F) 109.5
H(32E)-C(32B)-H(32F) 109.5
P(5)-C(33B)-H(33D) 109.5
P(5)-C(33B)-H(33E) 109.5
H(33D)-C(33B)-H(33E) 109.5
P(5)-C(33B)-H(33F) 109.5
H(33D)-C(33B)-H(33F) 109.5
H(33E)-C(33B)-H(33F) 109.5
P(6)-C(34)-H(34A) 109.5
P(6)-C(34)-H(34B) 109.5
H(34A)-C(34)-H(34B) 109.5
P(6)-C(34)-H(34C) 109.5
H(34A)-C(34)-H(34C) 109.5
H(34B)-C(34)-H(34C) 109.5
P(6)-C(35)-H(35A) 109.5
P(6)-C(35)-H(35B) 109.5
H(35A)-C(35)-H(35B) 109.5
P(6)-C(35)-H(35C) 109.5
H(35A)-C(35)-H(35C) 109.5
H(35B)-C(35)-H(35C) 109.5
P(6)-C(36)-H(36A) 109.5
P(6)-C(36)-H(36B) 109.5
H(36A)-C(36)-H(36B) 109.5
P(6)-C(36)-H(36C) 109.5
H(36A)-C(36)-H(36C) 109.5
H(36B)-C(36)-H(36C) 109.5
O(1)-C(37)-C(38) 106.3(6)
O(1)-C(37)-H(37A) 110.5
C(38)-C(37)-H(37A) 110.5
O(1)-C(37)-H(37B) 110.5
C(38)-C(37)-H(37B) 110.5
H(37A)-C(37)-H(37B) 108.7
C(37)-C(38)-C(39) 103.1(6)
C(37)-C(38)-H(38A) 111.1
C(39)-C(38)-H(38A) 111.1
C(37)-C(38)-H(38B) 111.1
C(39)-C(38)-H(38B) 111.1
H(38A)-C(38)-H(38B) 109.1
C(40)-C(39)-C(38) 104.4(6)
C(40)-C(39)-H(39A) 110.9
C(38)-C(39)-H(39A) 110.9
C(40)-C(39)-H(39B) 110.9
C(38)-C(39)-H(39B) 110.9
H(39A)-C(39)-H(39B) 108.9
O(1)-C(40)-C(39) 107.4(6)
O(1)-C(40)-H(40A) 110.2
C(39)-C(40)-H(40A) 110.2
O(1)-C(40)-H(40B) 110.2
C(39)-C(40)-H(40B) 110.2
H(40A)-C(40)-H(40B) 108.5
O(2)-C(41)-C(42) 109.1(8)
O(2)-C(41)-H(41A) 109.9
C(42)-C(41)-H(41A) 109.9
O(2)-C(41)-H(41B) 109.9
C(42)-C(41)-H(41B) 109.9
H(41A)-C(41)-H(41B) 108.3
C(43)-C(42)-C(41) 97.2(8)
C(43)-C(42)-H(42A) 112.3
C(41)-C(42)-H(42A) 112.3
C(43)-C(42)-H(42B) 112.3
C(41)-C(42)-H(42B) 112.3

H(42A)-C(42)-H(42B)	109.9	C(43)-C(44)-O(2)	105.6(10)
C(44)-C(43)-C(42)	102.2(10)	C(43)-C(44)-H(44A)	110.6
C(44)-C(43)-H(43A)	111.3	O(2)-C(44)-H(44A)	110.6
C(42)-C(43)-H(43A)	111.3	C(43)-C(44)-H(44B)	110.6
C(44)-C(43)-H(43B)	111.3	O(2)-C(44)-H(44B)	110.6
C(42)-C(43)-H(43B)	111.3	H(44A)-C(44)-H(44B)	108.8
H(43A)-C(43)-H(43B)	109.2		

Figure 1 (bottom left) in the manuscript illustrates the asymmetric unit of **2.** The $[(PhSnCl)_3S_4]^{2-}$ anion features pseudo-C_3 symmetry along an axis perpendicular to a Sn_3S_3 six-membered ring (Sn1, S3, Sn2, S2, Sn3, and S4), which runs through S3.

The Sn–S bond lengths within the ring are of similar lengths, ranging from 2.401(3) Å to 2.432(3) Å, while the bonds to S4 are significantly elongated (2.564(4) Å - 2.612(3) Å). The Sn–S–Sn bond angles within the ring are all slightly above 90° (93.58(9)° to 95.48(9)°), while the Sn–S–Sn angles involving S4 (86.17(8)° - 87.06(8)°) are below 90°. The gold atom within the $[Au(PMe_3)_2]^+$ cation is coordinated in an almost linear fashion (P1–Au1–P2: 172.41(5)°), while the $[Au(PMe_3)_4]^+$ cation features a tetrahedrally coordinated gold atom with P–Au–P bond angles ranging from 107.66(5)° to 113.00(5)°.

8. Single-Crystal X-Ray Crystallography of Compound 3

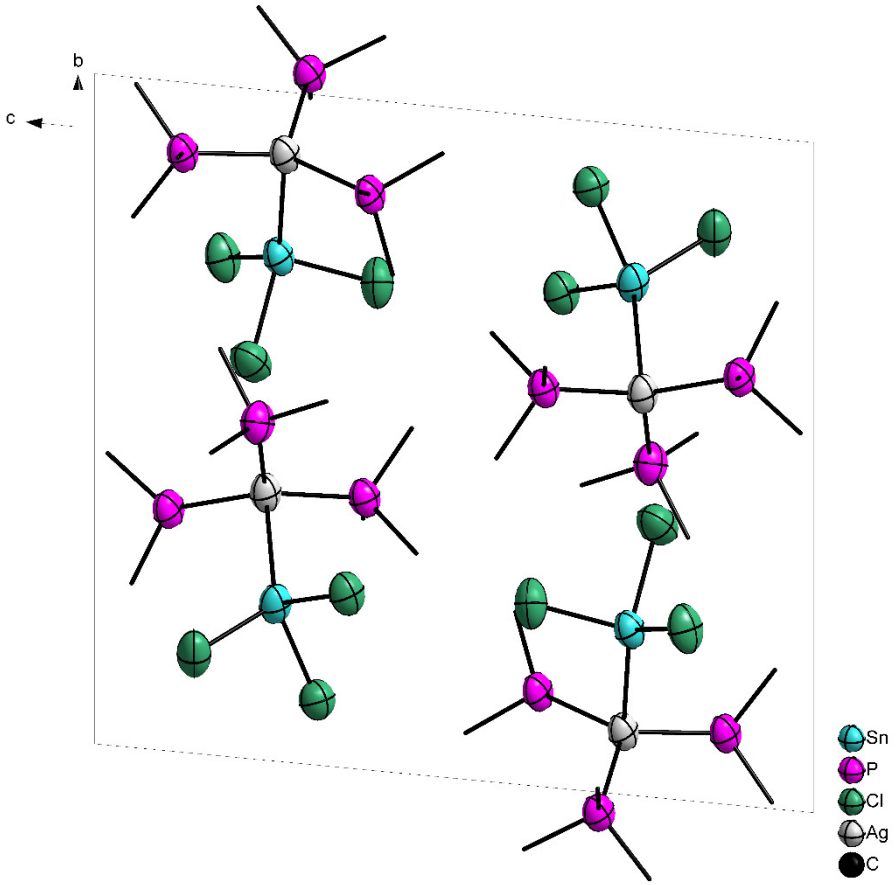

Figure S33: Crystal structure of **3**, viewed along the crystallographic a axis. Ellipsoids are shown at 50% probability, hydrogen atoms are omitted for clarity.

Table S7: Crystal data and structure refinement for **3** (CCDC 1875436).

Empirical formula	$C_9H_{27}Ag_1Cl_3P_3Sn_1$	
Formula weight	561.12	
Temperature	100(2) K	
Wavelength	0.71073 Å	
Crystal system	Triclinic	
Space group	$P\bar{1}$	
Unit cell dimensions	a = 9.4893(5) Å	α= 84.355(5)°.
	b = 14.6007(8) Å	β= 85.266(4)°.
	c = 15.7706(9) Å	γ = 87.718(4)°.
Volume	2165.9(2) $Å^3$	
Z	4	
Density (calculated)	1.721 Mg/m^3	
Absorption coefficient	2.633 mm^{-1}	
F(000)	1096	
Crystal size	0.70 x 0.50 x 0.30 mm^3	
Theta range for data collection	2.428 to 26.794°.	
Index ranges	-11<=h<=12, -18<=k<=18, -19<=l<=19	
Reflections collected	9151	
Independent reflections	9151	
Completeness to theta = 25.242°	99.8 %	
Absorption correction	Integration	
Max. and min. transmission	0.2312 and 0.1525	
Refinement method	Full-matrix least-squares on F^2	
Data / restraints / parameters	9151 / 0 / 326	
Goodness-of-fit on F^2	1.202	
Final R indices [I>2sigma(I)]	R1 = 0.0790, wR2 = 0.2048	
R indices (all data)	R1 = 0.1135, wR2 = 0.2239	
Extinction coefficient	n/a	
Largest diff. peak and hole	1.954 and -1.975 $e.Å^{-3}$	

Table S8: Atomic coordinates (x 10^4) and equivalent isotropic displacement parameters ($Å^2$x 10^3) for **3**. U(eq) is defined as one third of the trace of the orthogonalized U^{ij} tensor.

	x	y	z	U(eq)
Sn(1)	9876(1)	2347(1)	7484(1)	62(1)
P(1)	10151(3)	5026(2)	7731(2)	70(1)
Cl(1)	11961(3)	2602(2)	6490(2)	71(1)
Ag(1)	8204(1)	3992(1)	7620(1)	59(1)
Cl(2)	11117(3)	1486(2)	8616(2)	85(1)
P(2)	6790(3)	3608(2)	8968(2)	62(1)
Ag(2)	6879(1)	9062(1)	7352(1)	57(1)
Sn(2)	5080(1)	7532(1)	7439(1)	59(1)
P(6)	5135(3)	10305(2)	7010(2)	60(1)
Cl(6)	4247(3)	7284(3)	6069(2)	85(1)
P(5)	8511(3)	8591(2)	6167(2)	59(1)
Cl(5)	5769(4)	5925(2)	7825(2)	87(1)
P(4)	7760(3)	8944(2)	8773(2)	59(1)
Cl(4)	2765(3)	7438(2)	8215(2)	81(1)
P(3)	7170(3)	4056(2)	6243(2)	59(1)
Cl(3)	9080(3)	975(2)	6904(2)	69(1)
C(00H)	4966(11)	11223(8)	7716(7)	68(3)
C(00I)	8301(11)	7429(7)	5855(7)	70(3)
C(00J)	8076(11)	3303(8)	5526(6)	66(3)
C(00K)	8353(11)	9306(8)	5162(6)	66(3)
C(00L)	10365(10)	8616(8)	6305(7)	68(3)
C(00M)	3289(11)	9950(8)	6997(7)	66(3)
C(00N)	7130(13)	2451(8)	9482(7)	74(3)
C(00O)	5385(11)	10958(8)	5973(7)	70(3)
C(00P)	7176(15)	5162(8)	5589(8)	85(4)
C(00Q)	7209(17)	7927(10)	9458(8)	106(5)
C(00R)	7041(15)	4354(9)	9813(7)	85(4)
C(00S)	5317(11)	3748(9)	6264(8)	84(4)
C(00T)	9590(14)	6072(10)	8251(8)	90(4)
C(00U)	11120(13)	5442(10)	6777(8)	88(4)
C(00V)	4867(11)	3635(8)	8938(9)	87(4)
C(00W)	9656(11)	8869(11)	8839(8)	91(4)
C(00X)	11597(14)	4512(11)	8374(9)	103(5)
C(00Y)	7307(19)	9904(11)	9417(9)	116(6)

Table S9: Bond lengths [Å] and angles [°] for **3**.

Sn(1)-Cl(2)	2.437(3)	C(00J)-H(00G)	0.9600
Sn(1)-Cl(1)	2.437(3)	C(00J)-H(00H)	0.9600
Sn(1)-Cl(3)	2.453(3)	C(00J)-H(00I)	0.9600
Sn(1)-Ag(1)	2.8411(10)	C(00K)-H(00J)	0.9600
P(1)-C(00U)	1.765(12)	C(00K)-H(00K)	0.9600
P(1)-C(00X)	1.863(12)	C(00K)-H(00L)	0.9600
P(1)-C(00T)	1.844(14)	C(00L)-H(00M)	0.9600
P(1)-Ag(1)	2.460(3)	C(00L)-H(00N)	0.9600
Ag(1)-P(3)	2.448(3)	C(00L)-H(00O)	0.9600
Ag(1)-P(2)	2.448(3)	C(00M)-H(00P)	0.9600
P(2)-C(00R)	1.837(11)	C(00M)-H(00Q)	0.9600
P(2)-C(00V)	1.828(11)	C(00M)-H(00R)	0.9600
P(2)-C(00N)	1.829(11)	C(00N)-H(00S)	0.9600
Ag(2)-P(4)	2.444(3)	C(00N)-H(00T)	0.9600
Ag(2)-P(6)	2.457(3)	C(00N)-H(00U)	0.9600
Ag(2)-P(5)	2.461(3)	C(00O)-H(00V)	0.9600
Ag(2)-Sn(2)	2.8521(11)	C(00O)-H(00W)	0.9600
Sn(2)-Cl(6)	2.426(3)	C(00O)-H(00X)	0.9600
Sn(2)-Cl(4)	2.426(3)	C(00P)-H(00Y)	0.9600
Sn(2)-Cl(5)	2.442(3)	C(00P)-H(00Z)	0.9600
P(6)-C(00H)	1.819(11)	C(00P)-H(010)	0.9600
P(6)-C(00O)	1.813(10)	C(00Q)-H(011)	0.9600
P(6)-C(00M)	1.850(11)	C(00Q)-H(012)	0.9600
P(5)-C(00L)	1.792(10)	C(00Q)-H(013)	0.9600
P(5)-C(00K)	1.823(10)	C(00R)-H(014)	0.9600
P(5)-C(00I)	1.835(11)	C(00R)-H(015)	0.9600
P(4)-C(00Q)	1.816(12)	C(00R)-H(016)	0.9600
P(4)-C(00W)	1.809(11)	C(00S)-H(017)	0.9600
P(4)-C(00Y)	1.827(14)	C(00S)-H(018)	0.9600
P(3)-C(00J)	1.799(10)	C(00S)-H(019)	0.9600
P(3)-C(00S)	1.830(11)	C(00T)-H(01A)	0.9600
P(3)-C(00P)	1.829(11)	C(00T)-H(01B)	0.9600
C(00H)-H(00A)	0.9600	C(00T)-H(01C)	0.9600
C(00H)-H(00B)	0.9600	C(00U)-H(01D)	0.9600
C(00H)-H(00C)	0.9600	C(00U)-H(01E)	0.9600
C(00I)-H(00D)	0.9600	C(00U)-H(01F)	0.9600
C(00I)-H(00E)	0.9600	C(00V)-H(01G)	0.9600
C(00I)-H(00F)	0.9600	C(00V)-H(01H)	0.9600

C(00V)-H(01I)	0.9600	P(5)-Ag(2)-Sn(2)	96.30(7)
C(00W)-H(01J)	0.9600	Cl(6)-Sn(2)-Cl(4)	95.13(11)
C(00W)-H(01K)	0.9600	Cl(6)-Sn(2)-Cl(5)	95.80(13)
C(00W)-H(01L)	0.9600	Cl(4)-Sn(2)-Cl(5)	94.88(11)
C(00X)-H(01M)	0.9600	Cl(6)-Sn(2)-Ag(2)	113.20(9)
C(00X)-H(01N)	0.9600	Cl(4)-Sn(2)-Ag(2)	124.90(9)
C(00X)-H(01O)	0.9600	Cl(5)-Sn(2)-Ag(2)	125.71(9)
C(00Y)-H(01P)	0.9600	C(00H)-P(6)-C(00O)	101.3(5)
C(00Y)-H(01Q)	0.9600	C(00H)-P(6)-C(00M)	102.8(5)
C(00Y)-H(01R)	0.9600	C(00O)-P(6)-C(00M)	100.8(5)
Cl(2)-Sn(1)-Cl(1)	95.99(10)	C(00H)-P(6)-Ag(2)	116.3(3)
Cl(2)-Sn(1)-Cl(3)	94.78(11)	C(00O)-P(6)-Ag(2)	117.3(3)
Cl(1)-Sn(1)-Cl(3)	97.22(10)	C(00M)-P(6)-Ag(2)	115.9(4)
Cl(2)-Sn(1)-Ag(1)	126.63(8)	C(00L)-P(5)-C(00K)	102.6(5)
Cl(1)-Sn(1)-Ag(1)	111.50(7)	C(00L)-P(5)-C(00I)	103.2(5)
Cl(3)-Sn(1)-Ag(1)	124.08(7)	C(00K)-P(5)-C(00I)	102.3(5)
C(00U)-P(1)-C(00X)	101.1(7)	C(00L)-P(5)-Ag(2)	116.7(4)
C(00U)-P(1)-C(00T)	104.2(7)	C(00K)-P(5)-Ag(2)	113.9(4)
C(00X)-P(1)-C(00T)	103.6(6)	C(00I)-P(5)-Ag(2)	116.2(3)
C(00U)-P(1)-Ag(1)	117.8(5)	C(00Q)-P(4)-C(00W)	101.2(7)
C(00X)-P(1)-Ag(1)	114.8(5)	C(00Q)-P(4)-C(00Y)	104.7(7)
C(00T)-P(1)-Ag(1)	113.6(4)	C(00W)-P(4)-C(00Y)	99.9(8)
P(3)-Ag(1)-P(2)	121.50(10)	C(00Q)-P(4)-Ag(2)	114.3(5)
P(3)-Ag(1)-P(1)	117.39(10)	C(00W)-P(4)-Ag(2)	117.7(4)
P(2)-Ag(1)-P(1)	114.14(11)	C(00Y)-P(4)-Ag(2)	116.7(5)
P(3)-Ag(1)-Sn(1)	98.06(7)	C(00J)-P(3)-C(00S)	103.7(6)
P(2)-Ag(1)-Sn(1)	101.06(7)	C(00J)-P(3)-C(00P)	102.1(5)
P(1)-Ag(1)-Sn(1)	97.36(8)	C(00S)-P(3)-C(00P)	101.8(6)
C(00R)-P(2)-C(00V)	102.7(6)	C(00J)-P(3)-Ag(1)	112.9(4)
C(00R)-P(2)-C(00N)	103.2(6)	C(00S)-P(3)-Ag(1)	117.0(4)
C(00V)-P(2)-C(00N)	101.8(6)	C(00P)-P(3)-Ag(1)	117.3(5)
C(00R)-P(2)-Ag(1)	114.8(4)	P(6)-C(00H)-H(00A)	109.5
C(00V)-P(2)-Ag(1)	117.4(4)	P(6)-C(00H)-H(00B)	109.5
C(00N)-P(2)-Ag(1)	115.0(4)	H(00A)-C(00H)-H(00B)	109.5
P(4)-Ag(2)-P(6)	117.46(10)	P(6)-C(00H)-H(00C)	109.5
P(4)-Ag(2)-P(5)	117.44(9)	H(00A)-C(00H)-H(00C)	109.5
P(6)-Ag(2)-P(5)	117.11(9)	H(00B)-C(00H)-H(00C)	109.5
P(4)-Ag(2)-Sn(2)	103.28(7)	P(5)-C(00I)-H(00D)	109.5
P(6)-Ag(2)-Sn(2)	98.85(7)	P(5)-C(00I)-H(00E)	109.5

H(00D)-C(00I)-H(00E) 109.5
P(5)-C(00I)-H(00F) 109.5
H(00D)-C(00I)-H(00F) 109.5
H(00E)-C(00I)-H(00F) 109.5
P(3)-C(00J)-H(00G) 109.5
P(3)-C(00J)-H(00H) 109.5
H(00G)-C(00J)-H(00H) 109.5
P(3)-C(00J)-H(00I) 109.5
H(00G)-C(00J)-H(00I) 109.5
H(00H)-C(00J)-H(00I) 109.5
P(5)-C(00K)-H(00J) 109.5
P(5)-C(00K)-H(00K) 109.5
H(00J)-C(00K)-H(00K) 109.5
P(5)-C(00K)-H(00L) 109.5
H(00J)-C(00K)-H(00L) 109.5
H(00K)-C(00K)-H(00L) 109.5
P(5)-C(00L)-H(00M) 109.5
P(5)-C(00L)-H(00N) 109.5
H(00M)-C(00L)-H(00N) 109.5
P(5)-C(00L)-H(00O) 109.5
H(00M)-C(00L)-H(00O) 109.5
H(00N)-C(00L)-H(00O) 109.5
P(6)-C(00M)-H(00P) 109.5
P(6)-C(00M)-H(00Q) 109.5
H(00P)-C(00M)-H(00Q) 109.5
P(6)-C(00M)-H(00R) 109.5
H(00P)-C(00M)-H(00R) 109.5
H(00Q)-C(00M)-H(00R) 109.5
P(2)-C(00N)-H(00S) 109.5
P(2)-C(00N)-H(00T) 109.5
H(00S)-C(00N)-H(00T) 109.5
P(2)-C(00N)-H(00U) 109.5
H(00S)-C(00N)-H(00U) 109.5
H(00T)-C(00N)-H(00U) 109.5
P(6)-C(00O)-H(00V) 109.5
P(6)-C(00O)-H(00W) 109.5
H(00V)-C(00O)-H(00W) 109.5
P(6)-C(00O)-H(00X) 109.5
H(00V)-C(00O)-H(00X) 109.5
H(00W)-C(00O)-H(00X) 109.5
P(3)-C(00P)-H(00Y) 109.5
P(3)-C(00P)-H(00Z) 109.5
H(00Y)-C(00P)-H(00Z) 109.5
P(3)-C(00P)-H(010) 109.5
H(00Y)-C(00P)-H(010) 109.5
H(00Z)-C(00P)-H(010) 109.5
P(4)-C(00Q)-H(011) 109.5
P(4)-C(00Q)-H(012) 109.5
H(011)-C(00Q)-H(012) 109.5
P(4)-C(00Q)-H(013) 109.5
H(011)-C(00Q)-H(013) 109.5
H(012)-C(00Q)-H(013) 109.5
P(2)-C(00R)-H(014) 109.5
P(2)-C(00R)-H(015) 109.5
H(014)-C(00R)-H(015) 109.5
P(2)-C(00R)-H(016) 109.5
H(014)-C(00R)-H(016) 109.5
H(015)-C(00R)-H(016) 109.5
P(3)-C(00S)-H(017) 109.5
P(3)-C(00S)-H(018) 109.5
H(017)-C(00S)-H(018) 109.5
P(3)-C(00S)-H(019) 109.5
H(017)-C(00S)-H(019) 109.5
H(018)-C(00S)-H(019) 109.5
P(1)-C(00T)-H(01A) 109.5
P(1)-C(00T)-H(01B) 109.5
H(01A)-C(00T)-H(01B) 109.5
P(1)-C(00T)-H(01C) 109.5
H(01A)-C(00T)-H(01C) 109.5
H(01B)-C(00T)-H(01C) 109.5
P(1)-C(00U)-H(01D) 109.5
P(1)-C(00U)-H(01E) 109.5
H(01D)-C(00U)-H(01E) 109.5
P(1)-C(00U)-H(01F) 109.5
H(01D)-C(00U)-H(01F) 109.5
H(01E)-C(00U)-H(01F) 109.5
P(2)-C(00V)-H(01G) 109.5
P(2)-C(00V)-H(01H) 109.5

H(01G)-C(00V)-H(01H)	109.5	P(1)-C(00X)-H(01N)	109.5
P(2)-C(00V)-H(01I)	109.5	H(01M)-C(00X)-H(01N)	109.5
H(01G)-C(00V)-H(01I)	109.5	P(1)-C(00X)-H(01O)	109.5
H(01H)-C(00V)-H(01I)	109.5	H(01M)-C(00X)-H(01O)	109.5
P(4)-C(00W)-H(01J)	109.5	H(01N)-C(00X)-H(01O)	109.5
P(4)-C(00W)-H(01K)	109.5	P(4)-C(00Y)-H(01P)	109.5
H(01J)-C(00W)-H(01K)	109.5	P(4)-C(00Y)-H(01Q)	109.5
P(4)-C(00W)-H(01L)	109.5	H(01P)-C(00Y)-H(01Q)	109.5
H(01J)-C(00W)-H(01L)	109.5	P(4)-C(00Y)-H(01R)	109.5
H(01K)-C(00W)-H(01L)	109.5	H(01P)-C(00Y)-H(01R)	109.5
P(1)-C(00X)-H(01M)	109.5	H(01Q)-C(00Y)-H(01R)	109.5

The molecular structure of **3** is shown in Figure 1, bottom right. It crystallizes in the triclinic crystal system in the space group $P\bar{1}$ with four formula units per unit cell. The Ag–P bond lengths range from 2.448(3) to 2.460(3) Å, being naturally longer than in the copper complex (2.247 to 2.253 Å), but also slightly longer than in the gold complex (2.364 to 2.371 Å). Also, the Ag–Sn bond (2.8411(10) Å) is longer than the M-Sn bonds in the literature-known complexes (2.258 Å for M = Cu, 2.724 Å for M = Au), showcasing the notably weaker metal–metal bond for M = Ag. The coordination geometry of the silver atom is distorted from an ideal tetrahedron more than in the copper and gold homologues regarding the angles, Sn–Ag–P angles, which range from 97.36(8) to 101.06(7)° (Cu: 100.23 to 102.29°; Au: 101.64 to 104.6°) and thus render it a trigonal pyramidal rather than a pseudo-tetrahedral coordination.

9. Single-Crystal X-Ray Crystallography of Compound 4

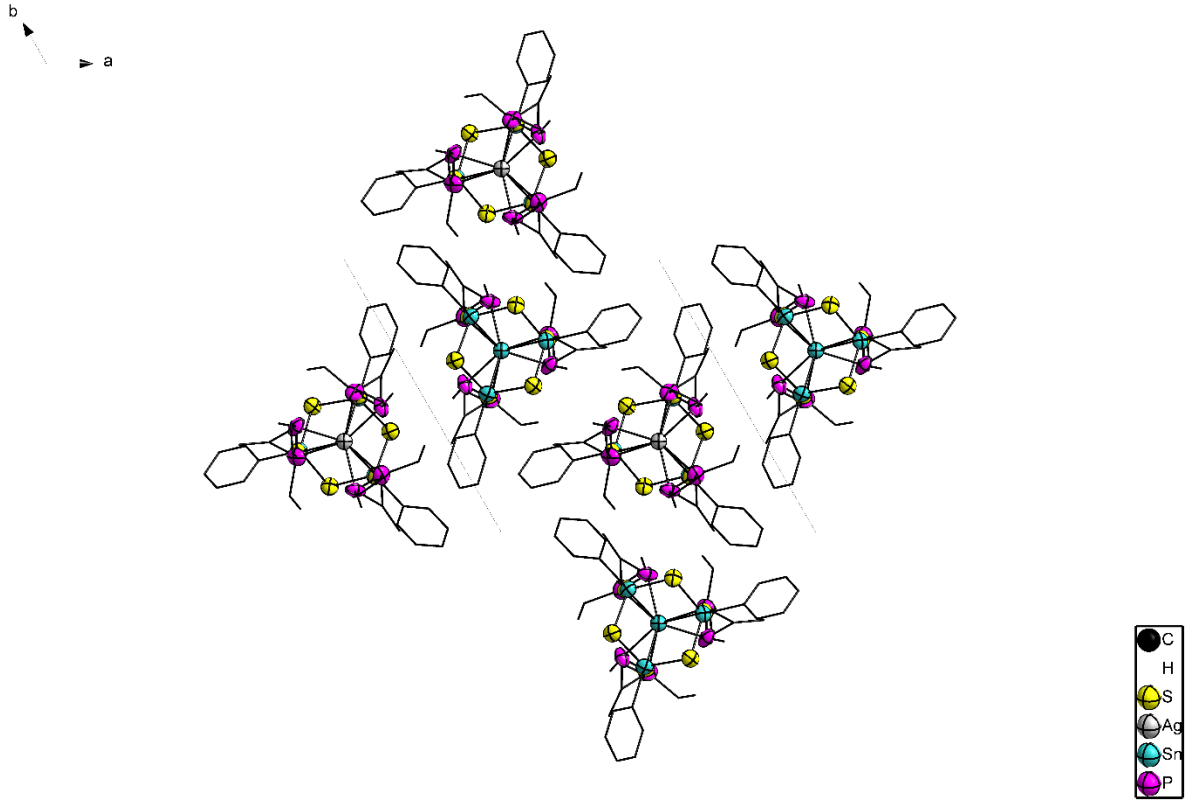

Figure S34: Crystal structure of **4**, viewed along the crystallographic c axis. Ellipsoids are shown at 50% probability, hydrogen are omitted for clarity.

Table S10: Crystal data and structure refinement for **4** (CCDC 1875439).

Empirical formula	$C_{36}H_{60}Ag_1P_3S_6Sn_4$	
Formula weight	1360.74	
Temperature	100(2) K	
Wavelength	0.71073 Å	
Crystal system	Trigonal	
Space group	P-3	
Unit cell dimensions	a = 15.0052(2) Å	α= 90°.
	b = 15.0052(2) Å	β= 90°.
	c = 13.7225(3) Å	γ= 120°.
Volume	2675.76(9) $Å^3$	
Z	2	
Density (calculated)	1.689 Mg/m^3	
Absorption coefficient	2.547 mm^{-1}	
F(000)	1328	
Crystal size	0.20 x 0.07 x 0.05 mm^3	
Theta range for data collection	1.484 to 27.905°.	
Index ranges	-19<=h<=19, -19<=k<=19, -17<=l<=18	
Reflections collected	34608	
Independent reflections	4287 [R(int) = 0.0387]	
Completeness to theta = 25.242°	100.0 %	
Absorption correction	Integration	
Max. and min. transmission	0.5207 and 0.3126	
Refinement method	Full-matrix least-squares on F^2	
Data / restraints / parameters	4287 / 0 / 135	
Goodness-of-fit on F^2	0.998	
Final R indices [I>2sigma(I)]	R1 = 0.0494, wR2 = 0.1562	
R indices (all data)	R1 = 0.0567, wR2 = 0.1604	
Extinction coefficient	n/a	
Largest diff. peak and hole	1.674 and -1.138 $e.Å^{-3}$	

Table S11: Atomic coordinates (x 10^4) and equivalent isotropic displacement parameters (Å^{2}x 10^3) for **4**. U(eq) is defined as one third of the trace of the orthogonalized U^{ij} tensor.

	x	y	z	U(eq)
C(1)	3600(4)	2637(5)	1503(4)	55(1)
C(2)	2744(5)	1871(5)	1968(5)	67(2)
C(3)	1768(5)	1633(6)	1673(6)	78(2)
C(4)	1624(7)	2136(7)	911(7)	91(3)
C(5)	2498(7)	2941(7)	441(6)	79(2)
C(6)	3455(6)	3170(5)	743(5)	67(2)
C(7)	9040(12)	5736(11)	6391(12)	173(3)
C(8)	9940(12)	6727(11)	6715(12)	173(3)
C(9)	8695(13)	4708(12)	8406(12)	173(3)
C(11)	7401(12)	6065(11)	6821(12)	173(3)
C(10)	8083(12)	5187(12)	8594(12)	173(3)
C(12)	6825(12)	5966(11)	5857(12)	173(3)
S(004)	5000(1)	2925(1)	3714(1)	58(1)
S(005)	6300(1)	4622(1)	1311(1)	63(1)
Ag(1)	6667	3333	6518(1)	51(1)
Sn(01)	6667	3333	4499(1)	48(1)
Sn(02)	5082(1)	2988(1)	1998(1)	54(1)
P(1)	7899(3)	5129(3)	6926(3)	70(1)
P(2)	8461(2)	4590(3)	6989(2)	65(1)

Table S12: Bond lengths [Å] and angles [°] for **4**.

C(1)-C(2)	1.379(10)
C(1)-C(6)	1.397(9)
C(1)-Sn(02)	2.125(5)
C(2)-C(3)	1.383(9)
C(2)-H(2)	0.9300
C(3)-C(4)	1.368(12)
C(3)-H(3)	0.9300
C(4)-C(5)	1.417(13)
C(4)-H(4)	0.9300
C(5)-C(6)	1.363(10)
C(5)-H(5)	0.9300
C(6)-H(6)	0.9300
C(7)-C(8)	1.491(17)
C(7)-P(1)	1.656(18)
C(7)-P(2)	1.701(16)
C(7)-H(7A)	0.9700
C(7)-H(7B)	0.9700
C(8)-H(8A)	0.9600
C(8)-H(8B)	0.9600
C(8)-H(8C)	0.9600
C(9)-C(10)	1.44(2)
C(9)-P(2)	1.969(16)
C(9)-H(9A)	0.9700
C(9)-H(9B)	0.9700
C(11)-C(12)	1.547(18)
C(11)-P(1)	1.897(18)
C(11)-H(11A)	0.9700
C(11)-H(11B)	0.9700
C(10)-P(1)	2.301(17)
C(10)-H(10A)	0.9600
C(10)-H(10B)	0.9600
C(10)-H(10C)	0.9600
C(12)-H(12A)	0.9600
C(12)-H(12B)	0.9600
C(12)-H(12C)	0.9600
S(004)-Sn(02)	2.3579(15)
S(004)-Sn(01)	2.5012(15)
S(005)-Sn(02)	2.4001(16)
S(005)-Sn(02)#1	2.4128(16)
Ag(1)-P(1)#2	2.451(4)
Ag(1)-P(1)	2.452(4)
Ag(1)-P(1)#1	2.452(4)
Ag(1)-P(2)#1	2.478(3)
Ag(1)-P(2)#2	2.478(3)
Ag(1)-P(2)	2.478(3)
Ag(1)-Sn(01)	2.7703(9)
C(2)-C(1)-C(6)	118.4(6)
C(2)-C(1)-Sn(02)	118.8(5)
C(6)-C(1)-Sn(02)	122.7(5)
C(1)-C(2)-C(3)	120.3(7)
C(1)-C(2)-H(2)	119.9
C(3)-C(2)-H(2)	119.9
C(4)-C(3)-C(2)	121.3(8)
C(4)-C(3)-H(3)	119.3
C(2)-C(3)-H(3)	119.3
C(3)-C(4)-C(5)	119.0(7)
C(3)-C(4)-H(4)	120.5
C(5)-C(4)-H(4)	120.5
C(6)-C(5)-C(4)	119.0(7)
C(6)-C(5)-H(5)	120.5
C(4)-C(5)-H(5)	120.5
C(5)-C(6)-C(1)	122.0(7)
C(5)-C(6)-H(6)	119.0
C(1)-C(6)-H(6)	119.0
C(8)-C(7)-P(1)	126.0(14)
C(8)-C(7)-P(2)	127.9(11)
C(8)-C(7)-H(7A)	105.8
P(1)-C(7)-H(7A)	105.8
C(8)-C(7)-H(7B)	105.8
P(1)-C(7)-H(7B)	105.8
H(7A)-C(7)-H(7B)	106.2
C(7)-C(8)-H(8A)	109.5
C(7)-C(8)-H(8B)	109.5
H(8A)-C(8)-H(8B)	109.5
C(7)-C(8)-H(8C)	109.5

H(8A)-C(8)-H(8C)	109.5
H(8B)-C(8)-H(8C)	109.5
C(10)-C(9)-P(2)	95.2(11)
C(10)-C(9)-H(9A)	112.7
P(2)-C(9)-H(9A)	112.7
C(10)-C(9)-H(9B)	112.7
P(2)-C(9)-H(9B)	112.7
H(9A)-C(9)-H(9B)	110.2
C(12)-C(11)-P(1)	113.7(12)
C(12)-C(11)-H(11A)	108.8
P(1)-C(11)-H(11A)	108.8
C(12)-C(11)-H(11B)	108.8
P(1)-C(11)-H(11B)	108.8
H(11A)-C(11)-H(11B)	107.7
C(9)-C(10)-P(1)	84.2(11)
C(9)-C(10)-H(10A)	109.5
P(1)-C(10)-H(10A)	55.2
C(9)-C(10)-H(10B)	109.5
P(1)-C(10)-H(10B)	163.2
H(10A)-C(10)-H(10B)	109.5
C(9)-C(10)-H(10C)	109.5
P(1)-C(10)-H(10C)	73.4
H(10A)-C(10)-H(10C)	109.5
H(10B)-C(10)-H(10C)	109.5
C(11)-C(12)-H(12A)	109.5
C(11)-C(12)-H(12B)	109.5
H(12A)-C(12)-H(12B)	109.5
C(11)-C(12)-H(12C)	109.5
H(12A)-C(12)-H(12C)	109.5
H(12B)-C(12)-H(12C)	109.5
Sn(02)-S(004)-Sn(01)	113.22(6)
Sn(02)-S(005)-Sn(02)#1	102.38(6)
P(1)#2-Ag(1)-P(1)	114.94(7)
P(1)#2-Ag(1)-P(1)#1	114.94(7)
P(1)-Ag(1)-P(1)#1	114.94(7)
P(1)#2-Ag(1)-P(2)#1	82.02(13)
P(1)-Ag(1)-P(2)#1	142.28(12)
P(1)#1-Ag(1)-P(2)#1	33.79(13)
P(1)#2-Ag(1)-P(2)#2	33.79(13)
P(1)-Ag(1)-P(2)#2	82.03(13)
P(1)#1-Ag(1)-P(2)#2	142.28(12)
P(2)#1-Ag(1)-P(2)#2	113.46(7)
P(2)#1-Ag(1)-P(2)	113.46(7)
P(2)#2-Ag(1)-P(2)	113.46(7)
P(1)#2-Ag(1)-Sn(01)	103.22(9)
P(1)-Ag(1)-Sn(01)	103.22(9)
P(1)#1-Ag(1)-Sn(01)	103.21(9)
P(2)#1-Ag(1)-Sn(01)	105.11(8)
P(2)#2-Ag(1)-Sn(01)	105.11(8)
P(2)-Ag(1)-Sn(01)	105.11(8)
S(004)#2-Sn(01)-S(004)#1	102.83(4)
S(004)#2-Sn(01)-S(004)	102.83(4)
S(004)#1-Sn(01)-S(004)	102.83(4)
S(004)#2-Sn(01)-Ag(1)	115.50(4)
S(004)#1-Sn(01)-Ag(1)	115.50(4)
S(004)-Sn(01)-Ag(1)	115.50(4)
C(1)-Sn(02)-S(004)	106.38(17)
C(1)-Sn(02)-S(005)	107.20(17)
S(004)-Sn(02)-S(005)	115.55(6)
C(1)-Sn(02)-S(005)#2	105.61(16)
S(004)-Sn(02)-S(005)#2	112.65(6)
S(005)-Sn(02)-S(005)#2	108.81(9)
C(7)-P(1)-C(11)	103.9(8)
C(7)-P(1)-C(10)	110.4(7)
C(11)-P(1)-C(10)	97.6(7)
C(7)-P(1)-Ag(1)	120.5(6)
C(11)-P(1)-Ag(1)	115.9(4)
C(10)-P(1)-Ag(1)	106.2(4)
C(7)-P(2)-C(9)	114.1(7)
C(7)-P(2)-Ag(1)	117.1(5)
C(9)-P(2)-Ag(1)	113.8(5)

Symmetry transformations used to generate equivalent atoms:

#1 -x+y+1,-x+1,z #2 -y+1,x-y,z

Compound **4** (Figure 1 of the manuscript, top center) was obtained upon changing the phosphine ligand to triethylphosphine. The $[\{(Et_3P)_3AgSn\}(PhSn)_3S_6]$ cluster in **4** is analogous, yet not homologous, to compound **1**. Compound **4** crystallizes in the trigonal crystal system in the space group $P\bar{3}$ with two formula units per unit cell. The adamantane-type cage shows the same slight distortion as in **1**, as indicated by the elongated Sn1–S4 bonds (2.5012(15) Å vs. 2.3579(15)-2.4128(16) Å for the other Sn–S bonds). The Sn–Ag bond has a length of 2.7703(9) Å, which is by 5.5 pm longer than the Sn–Au bond in **1**. There are only few literature-known compounds with tin-silver bonds. In the cluster $[(RSn)_4(AgPPh_3)_2(SnCl)_2S_8]$ (R = $CMe_2CH_2C(O)Me$), the Sn–Ag bond is slightly shorter (2.7100(4) Å),[4] while in the stannaborate-decorated silver clusters reported by the Wesemann group, they range from 2.56226(10) to 3.1424(6) Å.[5]

10. Single-Crystal X-Ray Crystallography of Compound 5

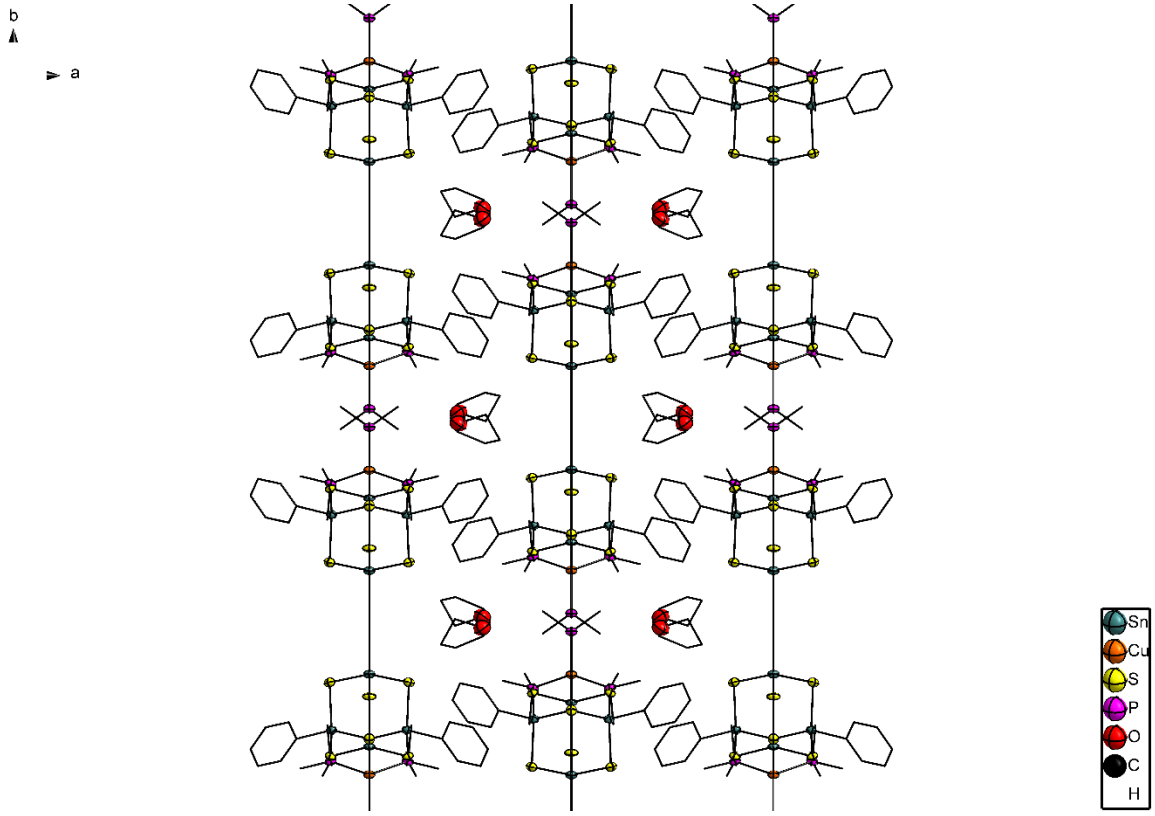

Figure S35: Crystal structure of **5** · 2 THF, viewed along the crystallographic c axis. Ellipsoids are shown at 50% probability, hydrogen atoms and the disorder of the solvent molecules are omitted for clarity.

Table S13: Crystal data and structure refinement for **5** · 2 THF (CCDC 1875438).

Empirical formula	$C_{35}H_{58}Cu_1O_2P_3S_6Sn_4$	
Formula weight	1334.38	
Temperature	100(2) K	
Wavelength	0.71073 Å	
Crystal system	Orthorhombic	
Space group	$Cmc2_1$	
Unit cell dimensions	a = 20.1274(9) Å	α= 90°.
	b = 20.3455(9) Å	β= 90°.
	c = 12.3261(4) Å	γ = 90°.
Volume	5047.6(4) $Å^3$	
Z	4	
Density (calculated)	1.756 Mg/m^3	
Absorption coefficient	2.738 mm^{-1}	
F(000)	2616	
Crystal size	0.20 x 0.15 x 0.10 mm^3	
Theta range for data collection	2.596 to 26.499°.	
Index ranges	-25<=h<=25, -25<=k<=16, -15<=l<=15	
Reflections collected	11625	
Independent reflections	5114 [R(int) = 0.0433]	
Completeness to theta = 25.242°	98.1 %	
Absorption correction	Integration	
Max. and min. transmission	0.6927 and 0.5485	
Refinement method	Full-matrix least-squares on F^2	
Data / restraints / parameters	5114 / 1 / 193	
Goodness-of-fit on F^2	1.034	
Final R indices [I>2sigma(I)]	R1 = 0.0383, wR2 = 0.0966	
R indices (all data)	R1 = 0.0462, wR2 = 0.1005	
Absolute structure parameter	-0.05(2)	
Extinction coefficient	n/a	
Largest diff. peak and hole	1.515 and -2.184 e.$Å^{-3}$	

Table S14: Atomic coordinates (x 10^4) and equivalent isotropic displacement parameters ($Å^2$x 10^3) for **5**. U(eq) is defined as one third of the trace of the orthogonalized U^{ij} tensor.

	x	y	z	U(eq)
Sn(1)	5931(1)	7633(1)	2791(1)	19(1)
Cu(1)	5000	8723(1)	-1801(1)	20(1)
S(1)	5000	7849(2)	3969(2)	22(1)
P(1)	5000	9774(2)	-1226(3)	20(1)
O(1)	2793(6)	10130(7)	-3280(10)	78(3)
C(1)	6800(5)	7845(7)	3700(9)	37(1)
Sn(2)	5000	6267(1)	1423(1)	20(1)
S(2)	5955(1)	8275(1)	1202(2)	22(1)
P(2)	4043(1)	8397(1)	-2582(2)	22(1)
C(2)	7188(5)	8389(7)	3464(9)	37(1)
Sn(3)	5000	8040(1)	-36(1)	20(1)
S(3)	5000	6811(2)	-263(2)	25(1)
C(3)	7755(5)	8519(7)	4062(9)	37(1)
S(4)	4020(1)	6467(1)	2482(2)	24(1)
C(4)	7938(5)	8100(7)	4886(9)	37(1)
C(5)	7559(6)	7564(7)	5158(9)	37(1)
C(6)	6988(6)	7439(6)	4552(9)	37(1)
C(7)	5000	5243(9)	1158(13)	55(2)
C(8)	5000	4796(9)	2002(14)	55(2)
C(9)	5000	4126(10)	1805(13)	55(2)
C(10)	5000	3887(9)	780(13)	55(2)
C(11)	5000	4326(9)	-61(14)	55(2)
C(12)	5000	4991(10)	108(12)	55(2)
C(13)	3961(7)	7512(6)	-2824(10)	42(3)
C(14)	3300(5)	8575(7)	-1813(9)	38(3)
C(15)	3844(5)	8748(6)	-3904(7)	29(2)
C(16)	4298(6)	10271(6)	-1630(9)	33(2)
C(17)	5000	9881(8)	235(11)	28(3)
C(18)	2799(9)	10328(13)	-4340(16)	95(4)
C(19)	2131(15)	10590(20)	-4500(30)	95(4)
C(20)	1797(15)	10390(20)	-3480(30)	95(4)
C(19B)	2330(20)	10270(30)	-5150(50)	95(4)
C(20B)	1720(20)	10070(30)	-4400(40)	95(4)
C(21)	2133(9)	9963(14)	-3036(19)	95(4)

Table S15: Bond lengths [Å] and angles [°] for **5**.

Sn(1)-C(1)	2.121(11)	C(9)-H(9)	0.9300
Sn(1)-S(2)	2.355(2)	C(10)-C(11)	1.37(2)
Sn(1)-S(4)#1	2.404(3)	C(10)-H(10)	0.9300
Sn(1)-S(1)	2.411(2)	C(11)-C(12)	1.37(3)
Cu(1)-P(1)	2.253(4)	C(11)-H(11)	0.9300
Cu(1)-P(2)#1	2.253(3)	C(12)-H(12)	0.9300
Cu(1)-P(2)	2.253(3)	C(13)-H(13A)	0.9600
Cu(1)-Sn(3)	2.5818(18)	C(13)-H(13B)	0.9600
P(1)-C(16)	1.809(10)	C(13)-H(13C)	0.9600
P(1)-C(16)#1	1.809(10)	C(14)-H(14A)	0.9600
P(1)-C(17)	1.813(14)	C(14)-H(14B)	0.9600
O(1)-C(18)	1.37(2)	C(14)-H(14C)	0.9600
O(1)-C(21)	1.40(2)	C(15)-H(15A)	0.9600
C(1)-C(2)	1.385(18)	C(15)-H(15B)	0.9600
C(1)-C(6)	1.389(17)	C(15)-H(15C)	0.9600
Sn(2)-C(7)	2.109(18)	C(16)-H(16A)	0.9600
Sn(2)-S(3)	2.355(3)	C(16)-H(16B)	0.9600
Sn(2)-S(4)#1	2.401(2)	C(16)-H(16C)	0.9600
Sn(2)-S(4)	2.401(2)	C(17)-H(17A)	0.9600
S(2)-Sn(3)	2.500(2)	C(17)-H(17B)	0.9600
P(2)-C(14)	1.807(11)	C(17)-H(17C)	0.9600
P(2)-C(15)	1.824(10)	C(17)-H(17A)#1	0.9601
P(2)-C(13)	1.834(12)	C(17)-H(17B)#1	0.9600
C(2)-C(3)	1.383(15)	C(17)-H(17C)#1	0.9600
C(2)-H(2)	0.9300	C(18)-C(19B)	1.37(5)
Sn(3)-S(3)	2.516(4)	C(18)-C(19)	1.46(4)
C(3)-C(4)	1.376(17)	C(18)-H(18A)	0.9700
C(3)-H(3)	0.9300	C(18)-H(18B)	0.9700
C(4)-C(5)	1.372(18)	C(18)-H(18C)	0.9700
C(4)-H(4)	0.9300	C(18)-H(18D)	0.9700
C(5)-C(6)	1.394(16)	C(19)-C(20)	1.49(5)
C(5)-H(5)	0.9300	C(19)-H(19A)	0.9700
C(6)-H(6)	0.9300	C(19)-H(19B)	0.9700
C(7)-C(8)	1.38(2)	C(20)-C(21)	1.23(4)
C(7)-C(12)	1.39(2)	C(20)-H(20A)	0.9700
C(8)-C(9)	1.38(3)	C(20)-H(20B)	0.9700
C(8)-H(8)	0.9300	C(19B)-C(20B)	1.60(6)
C(9)-C(10)	1.35(2)	C(19B)-H(19C)	0.9700

C(19B)-H(19D)	0.9700	C(14)-P(2)-Cu(1)	115.1(4)
C(20B)-C(21)	1.90(5)	C(15)-P(2)-Cu(1)	117.0(4)
C(20B)-H(20C)	0.9700	C(13)-P(2)-Cu(1)	115.8(4)
C(20B)-H(20D)	0.9700	C(3)-C(2)-C(1)	120.4(11)
C(21)-H(21A)	0.9700	C(3)-C(2)-H(2)	119.8
C(21)-H(21B)	0.9700	C(1)-C(2)-H(2)	119.8
C(1)-Sn(1)-S(2)	108.0(4)	S(2)-Sn(3)-S(2)#1	100.55(11)
C(1)-Sn(1)-S(4)#1	104.5(4)	S(2)-Sn(3)-S(3)	104.92(8)
S(2)-Sn(1)-S(4)#1	114.47(9)	S(2)#1-Sn(3)-S(3)	104.93(8)
C(1)-Sn(1)-S(1)	106.6(3)	S(2)-Sn(3)-Cu(1)	114.30(6)
S(2)-Sn(1)-S(1)	114.56(10)	S(2)#1-Sn(3)-Cu(1)	114.30(6)
S(4)#1-Sn(1)-S(1)	107.90(11)	S(3)-Sn(3)-Cu(1)	116.15(8)
P(1)-Cu(1)-P(2)#1	114.43(9)	Sn(2)-S(3)-Sn(3)	111.67(13)
P(1)-Cu(1)-P(2)	114.43(9)	C(4)-C(3)-C(2)	119.7(12)
P(2)#1-Cu(1)-P(2)	117.52(15)	C(4)-C(3)-H(3)	120.2
P(1)-Cu(1)-Sn(3)	104.19(10)	C(2)-C(3)-H(3)	120.2
P(2)#1-Cu(1)-Sn(3)	101.65(8)	Sn(2)-S(4)-Sn(1)#1	102.69(10)
P(2)-Cu(1)-Sn(3)	101.65(8)	C(5)-C(4)-C(3)	121.6(10)
Sn(1)#1-S(1)-Sn(1)	102.06(12)	C(5)-C(4)-H(4)	119.2
C(16)-P(1)-C(16)#1	102.8(8)	C(3)-C(4)-H(4)	119.2
C(16)-P(1)-C(17)	101.9(5)	C(4)-C(5)-C(6)	118.1(11)
C(16)#1-P(1)-C(17)	101.9(5)	C(4)-C(5)-H(5)	120.9
C(16)-P(1)-Cu(1)	116.4(4)	C(6)-C(5)-H(5)	120.9
C(16)#1-P(1)-Cu(1)	116.4(4)	C(1)-C(6)-C(5)	121.5(12)
C(17)-P(1)-Cu(1)	115.3(5)	C(1)-C(6)-H(6)	119.3
C(18)-O(1)-C(21)	106.5(15)	C(5)-C(6)-H(6)	119.3
C(2)-C(1)-C(6)	118.7(10)	C(8)-C(7)-C(12)	117.3(17)
C(2)-C(1)-Sn(1)	121.2(9)	C(8)-C(7)-Sn(2)	122.2(12)
C(6)-C(1)-Sn(1)	120.2(9)	C(12)-C(7)-Sn(2)	120.5(13)
C(7)-Sn(2)-S(3)	109.1(4)	C(7)-C(8)-C(9)	121.0(16)
C(7)-Sn(2)-S(4)#1	104.6(2)	C(7)-C(8)-H(8)	119.5
S(3)-Sn(2)-S(4)#1	113.57(8)	C(9)-C(8)-H(8)	119.5
C(7)-Sn(2)-S(4)	104.6(2)	C(10)-C(9)-C(8)	121.2(17)
S(3)-Sn(2)-S(4)	113.57(8)	C(10)-C(9)-H(9)	119.4
S(4)#1-Sn(2)-S(4)	110.56(12)	C(8)-C(9)-H(9)	119.4
Sn(1)-S(2)-Sn(3)	112.69(10)	C(9)-C(10)-C(11)	118.2(17)
C(14)-P(2)-C(15)	102.1(5)	C(9)-C(10)-H(10)	120.9
C(14)-P(2)-C(13)	102.0(6)	C(11)-C(10)-H(10)	120.9
C(15)-P(2)-C(13)	102.7(5)	C(12)-C(11)-C(10)	122.0(16)

C(12)-C(11)-H(11)	119.0	P(1)-C(17)-H(17B)#1	109.5(5)
C(10)-C(11)-H(11)	119.0	H(17A)-C(17)-H(17B)#1	120.4
C(11)-C(12)-C(7)	120.4(17)	H(17B)-C(17)-H(17B)#1	13.2
C(11)-C(12)-H(12)	119.8	H(17C)-C(17)-H(17B)#1	97.7
C(7)-C(12)-H(12)	119.8	H(17A)#1-C(17)-H(17B)#1	109.5
P(2)-C(13)-H(13A)	109.5	P(1)-C(17)-H(17C)#1	109.5(2)
P(2)-C(13)-H(13B)	109.5	H(17A)-C(17)-H(17C)#1	13.2
H(13A)-C(13)-H(13B)	109.5	H(17B)-C(17)-H(17C)#1	97.7
P(2)-C(13)-H(13C)	109.5	H(17C)-C(17)-H(17C)#1	120.4
H(13A)-C(13)-H(13C)	109.5	H(17A)#1-C(17)-H(17C)#1	109.5
H(13B)-C(13)-H(13C)	109.5	H(17B)#1-C(17)-H(17C)#1	109.5
P(2)-C(14)-H(14A)	109.5	C(19B)-C(18)-O(1)	131(3)
P(2)-C(14)-H(14B)	109.5	O(1)-C(18)-C(19)	103(2)
H(14A)-C(14)-H(14B)	109.5	O(1)-C(18)-H(18A)	111.1
P(2)-C(14)-H(14C)	109.5	C(19)-C(18)-H(18A)	111.1
H(14A)-C(14)-H(14C)	109.5	O(1)-C(18)-H(18B)	111.1
H(14B)-C(14)-H(14C)	109.5	C(19)-C(18)-H(18B)	111.1
P(2)-C(15)-H(15A)	109.5	H(18A)-C(18)-H(18B)	109.1
P(2)-C(15)-H(15B)	109.5	C(19B)-C(18)-H(18C)	104.4
H(15A)-C(15)-H(15B)	109.5	O(1)-C(18)-H(18C)	104.4
P(2)-C(15)-H(15C)	109.5	C(19B)-C(18)-H(18D)	104.4
H(15A)-C(15)-H(15C)	109.5	O(1)-C(18)-H(18D)	104.4
H(15B)-C(15)-H(15C)	109.5	H(18C)-C(18)-H(18D)	105.6
P(1)-C(16)-H(16A)	109.5	C(18)-C(19)-C(20)	101(3)
P(1)-C(16)-H(16B)	109.5	C(18)-C(19)-H(19A)	111.5
H(16A)-C(16)-H(16B)	109.5	C(20)-C(19)-H(19A)	111.5
P(1)-C(16)-H(16C)	109.5	C(18)-C(19)-H(19B)	111.5
H(16A)-C(16)-H(16C)	109.5	C(20)-C(19)-H(19B)	111.5
H(16B)-C(16)-H(16C)	109.5	H(19A)-C(19)-H(19B)	109.3
P(1)-C(17)-H(17A)	109.5	C(21)-C(20)-C(19)	109(3)
P(1)-C(17)-H(17B)	109.5	C(21)-C(20)-H(20A)	109.9
H(17A)-C(17)-H(17B)	109.5	C(19)-C(20)-H(20A)	109.9
P(1)-C(17)-H(17C)	109.5	C(21)-C(20)-H(20B)	109.9
H(17A)-C(17)-H(17C)	109.5	C(19)-C(20)-H(20B)	109.9
H(17B)-C(17)-H(17C)	109.5	H(20A)-C(20)-H(20B)	108.3
P(1)-C(17)-H(17A)#1	109.5(3)	C(18)-C(19B)-C(20B)	98(4)
H(17A)-C(17)-H(17A)#1	97.7	C(18)-C(19B)-H(19C)	112.2
H(17B)-C(17)-H(17A)#1	120.4	C(20B)-C(19B)-H(19C)	112.2
H(17C)-C(17)-H(17A)#1	13.2	C(18)-C(19B)-H(19D)	112.2

C(20B)-C(19B)-H(19D)	112.2
H(19C)-C(19B)-H(19D)	109.8
C(19B)-C(20B)-C(21)	101(3)
C(19B)-C(20B)-H(20C)	111.5
C(21)-C(20B)-H(20C)	111.5
C(19B)-C(20B)-H(20D)	111.5
C(21)-C(20B)-H(20D)	111.5
H(20C)-C(20B)-H(20D)	109.3
C(20)-C(21)-O(1)	105(2)
O(1)-C(21)-C(20B)	101.7(18)
C(20)-C(21)-H(21A)	110.8
O(1)-C(21)-H(21A)	110.8
C(20)-C(21)-H(21B)	110.8
O(1)-C(21)-H(21B)	110.8
H(21A)-C(21)-H(21B)	108.8

Symmetry transformations used to generate equivalent atoms:

#1 -x+1,y,z

11. Optical Spectroscopy

Photoluminescence spectroscopy (PL) is performed using a confocal microscopy setup (Figure S26). For excitation, we used 100-fs pulses from a titan-sapphire laser oscillator with a repetition rate of 78 MHz. The emission wavelength of the oscillator was 800 nm. The light can be frequency doubled and tripled to extend the intrinsic operating range, generating an excitation wavelength of 266 nm for the experiment. A 0.5 NA Schwarzschild objective focuses the beam onto the sample at room temperature (293K). The light reflects back from the sample through the same objective. A lens collects the back reflected light and focuses it into an imaging camera and the entrance slit of a quarter meter Czechy-Turner monochromator. The grating has a blaze angle of 410 nm and 122 gratings / mm. A silicon deep-depletion charge-coupled-device array sensor thermoelectrically cooled to -60 °C detects the dispersed light.
The steady-state white-light measurements is performed with the same setup. Yet, the excitation wavelength was 1450 nm, supplied by a continuous wave laser diode.

12. DFT Calculations

12.1. Non-periodic DFT Calculations of Compounds 1, 4 and 5 without dispersion correction

Table S16: Calculated structural parameters (DFT) at BP86/cc-pVTZ(-PP) level of theory of the cluster $[\{(R_3P)_3MSn\}\{PhSn\}_3S_6]$ with R/M = Me/Au (**1**), Et/Ag (**4**), or Me/Cu (**5**). Experimental values are given in parentheses for comparison.

	1 [Å, deg]	**4** [Å, deg]	**5** [Å, deg]
Sn–S	2.42 - 2.45; (2.35 - 2.41)	2.41 - 2.46; (2.36 - 2.41)	2.42 - 2.45; (2.36 - 2.41)
Sn–S (close to M)	2.54 - 2.55; (2.50 - 2.51)	2.54 - 2.55; (2.50)	2.54; (2.52)
Sn–C	2.16; (2.11 - 2.12)	2.16 - 2.17; (2.12)	2.16; (2.11 - 2.12)
M–Sn	2.80; (2.72)	2.84; (2.77)	2.63; (2.58)
M–P	2.41 - 2.43; (2.36 - 2.37)	2.51 - 2.53; (2.45 - 2.48)	2.29 - 2.29; (2.25)
Sn–S–Sn	103.5 - 110.1; (101.9 - 112.6)	102.8 - 111.6; (102.4 - 113.2)	103.5 - 110.1; (102.0 - 112.7)
S–Sn–S	105.7 - 113.3; (104.3 - 114.7)	103.8 - 114.2; (102.8 - 115.6)	105.7 - 113.8; (100.5 - 114.6)
Sn-Me-P	98.6 - 101.3	102.9 – 106.0	101.5-101.8

12.2. Non-periodic DFT Calculations with and without Dispersion Correction of Compound 4a

Table S17: Calculated structural parameters (DFT) at BP86/cc-pVTZ(-PP) and BP86-D3/cc-pVTZ(-PP) level of theory of the cluster [{$(Me_3P)_3AgSn$}{$PhSn$}$_3S_6$] (**4a**).

	BP86-D3 [Å, deg]	**BP86** [Å, deg]
Sn–S	2.41 - 2.53	2.42 - 2.54
Sn–S (close to Ag)	2.52 - 2.53	2.54 - 2.54
Ag–Sn	2.74	2.80
Ag–P	2.44 - 2.45	2.49 - 2.49
S–Sn–S, S–Sn–S	103.0 - 113.9	103.4 - 113.3
Sn–Ag–P	98.0 - 100.5	99.2 - 101.9

12.3. DFT-calculated molecular orbitals

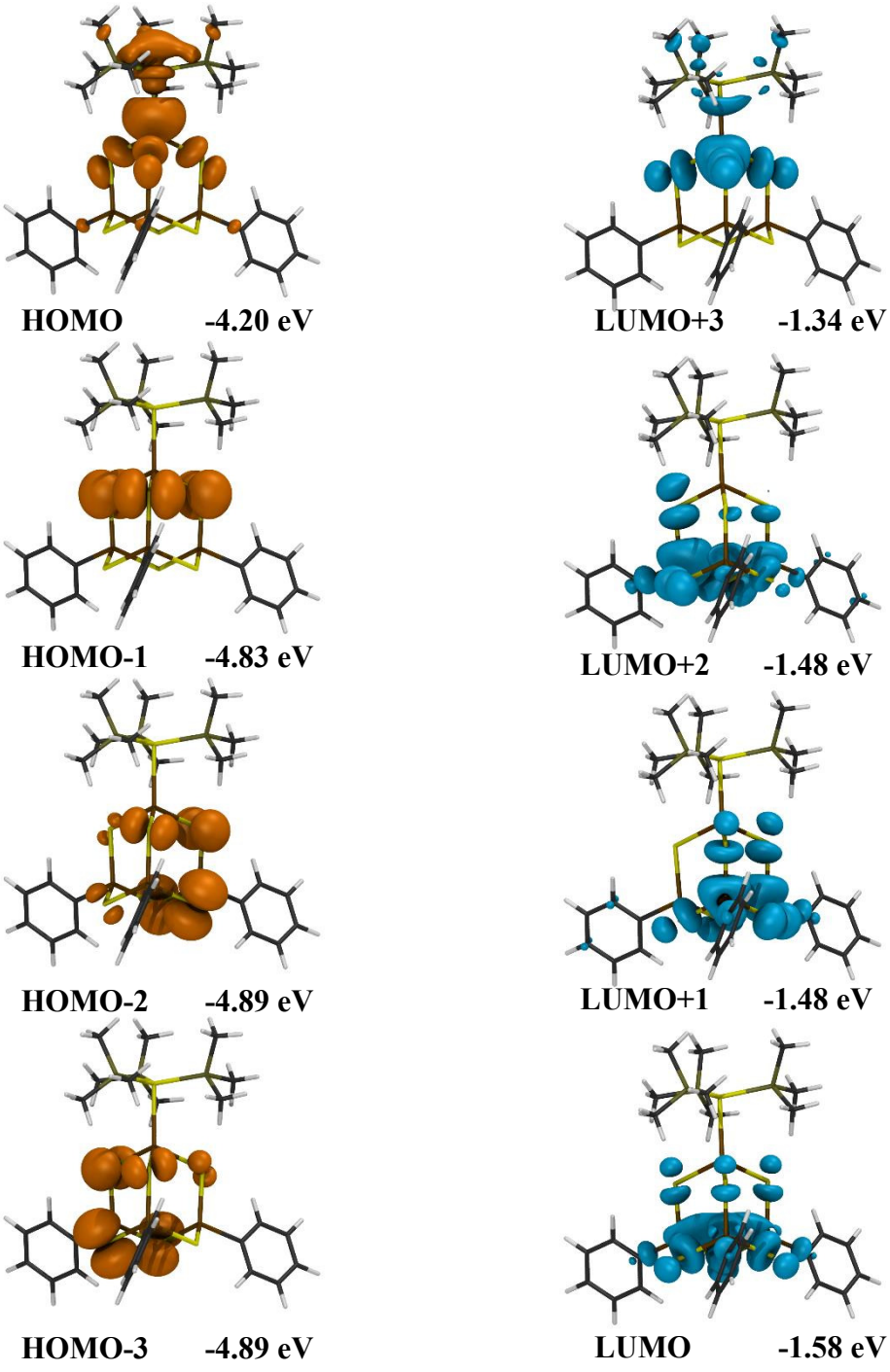

Figure S36: DFT calculated HOMO and LUMO (charge isosurfaces for 0.1 e/Å^3) for compound **1**.

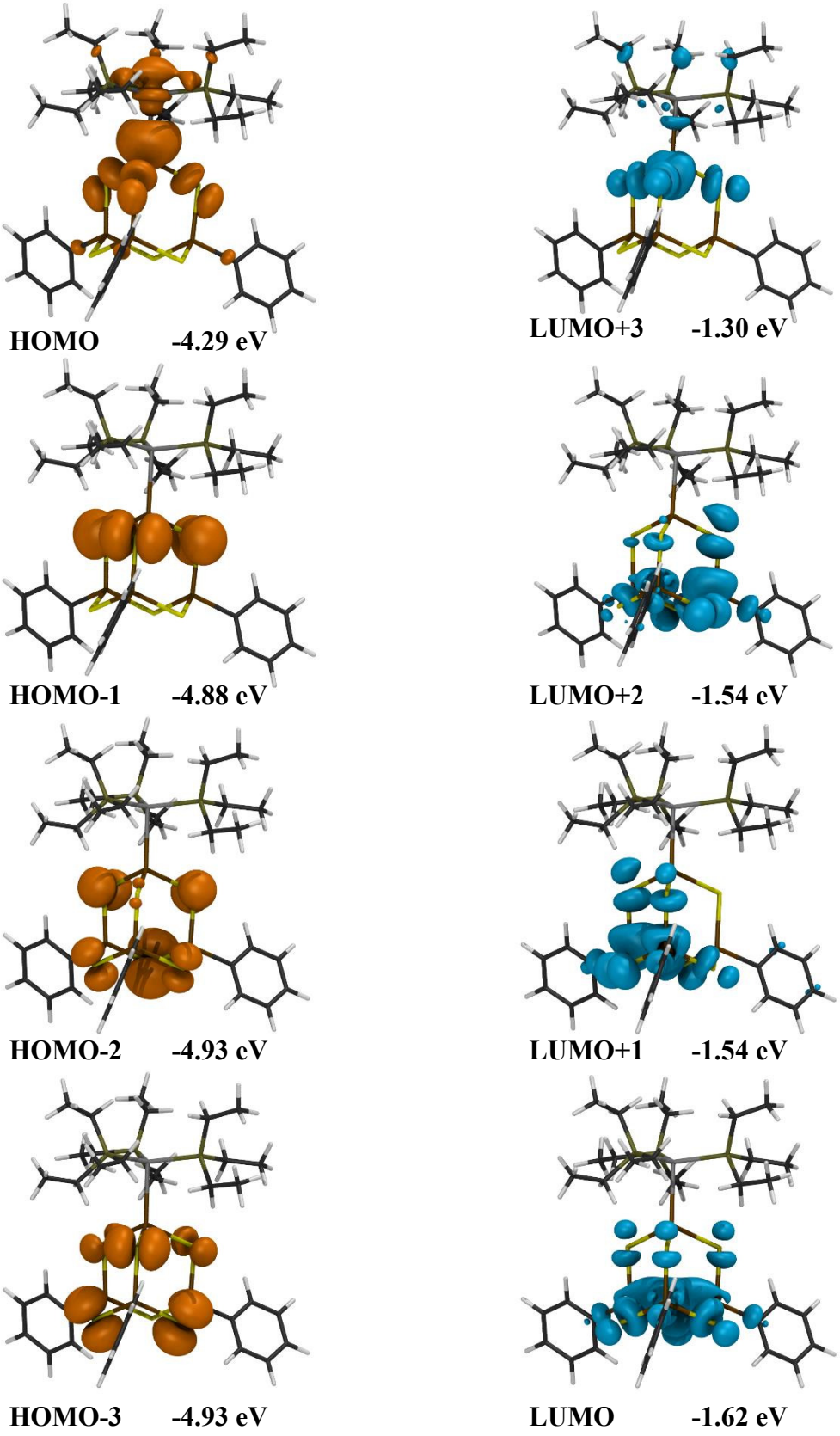

Figure S37: DFT calculated HOMO and LUMO (charge isosurfaces for 0.1 e/Å^3) for compound **4**.

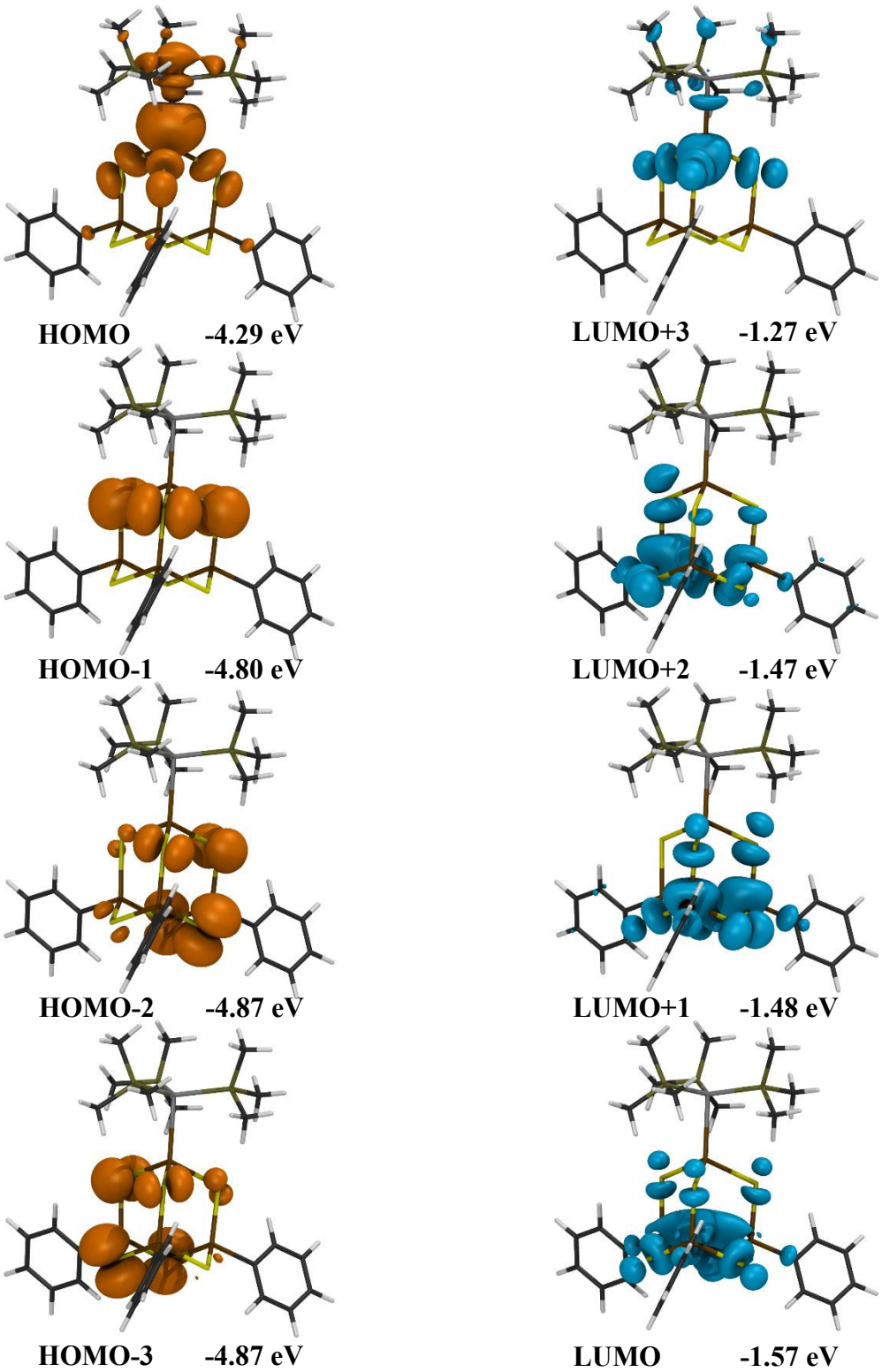

Figure S38: DFT calculated HOMO and LUMO (charge isosurfaces for 0.1 e/Å^3) for the hypothetical compound **4a**.

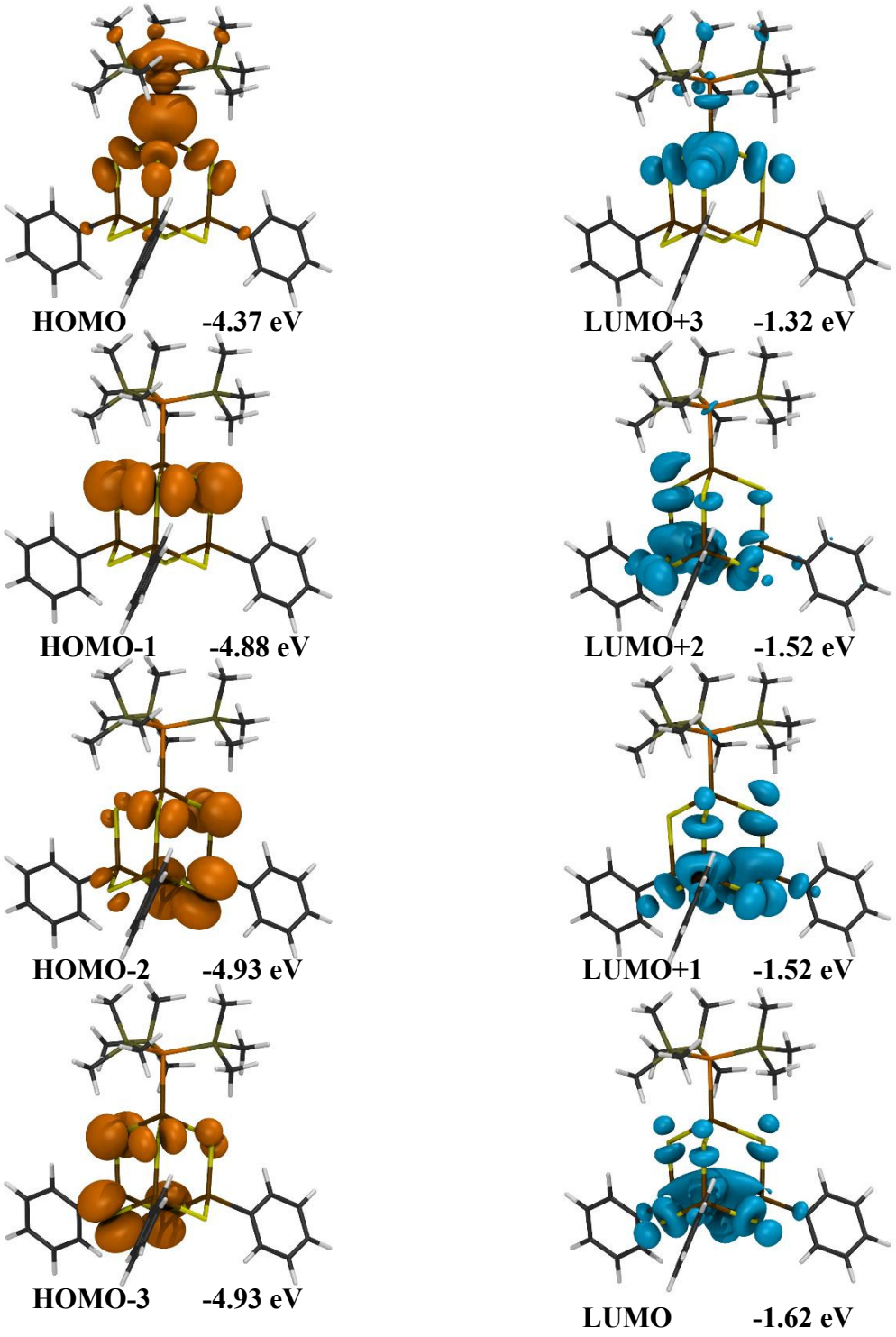

Figure S39: DFT calculated HOMO and LUMO (charge isosurfaces for 0.1 e/Å^3) for compound **5**.

13. Raman Spectroscopy

Raman spectra of compounds **1**, **4** and **5** before irradiation with light (Figure S40). Measurements were performed by a commercially available confocal Raman microscope (Renishaw inVia Qontor) using a HeNe Laser at 632.8 nm for excitation.

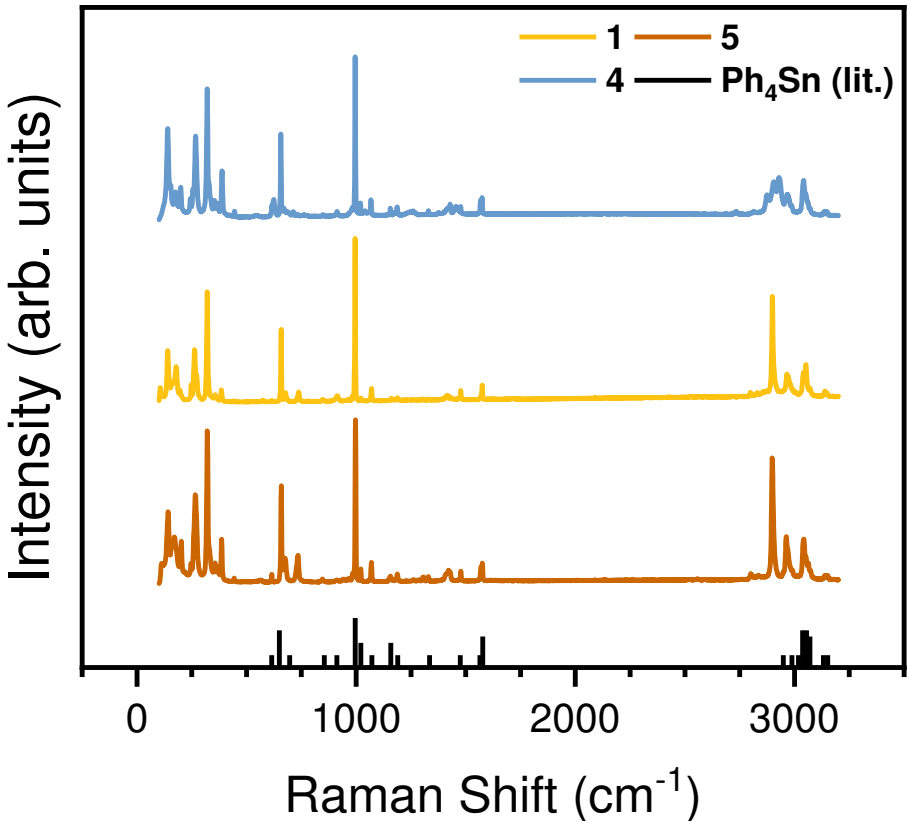

Figure S40: Raman spectra of compounds 1, 4 and 5. The spectra are shifted vertically for clarity. The black lines indicate the literature values for the vibrational modes of [$SnPh_4$] without Sn modes (> 400 cm^{-1}).[6] The lower-frequency modes can thus be assigned to the vibrational modes involving the inorganic core of the cluster.

14. ^{1}H NMR Spectra of the Irradiated Samples

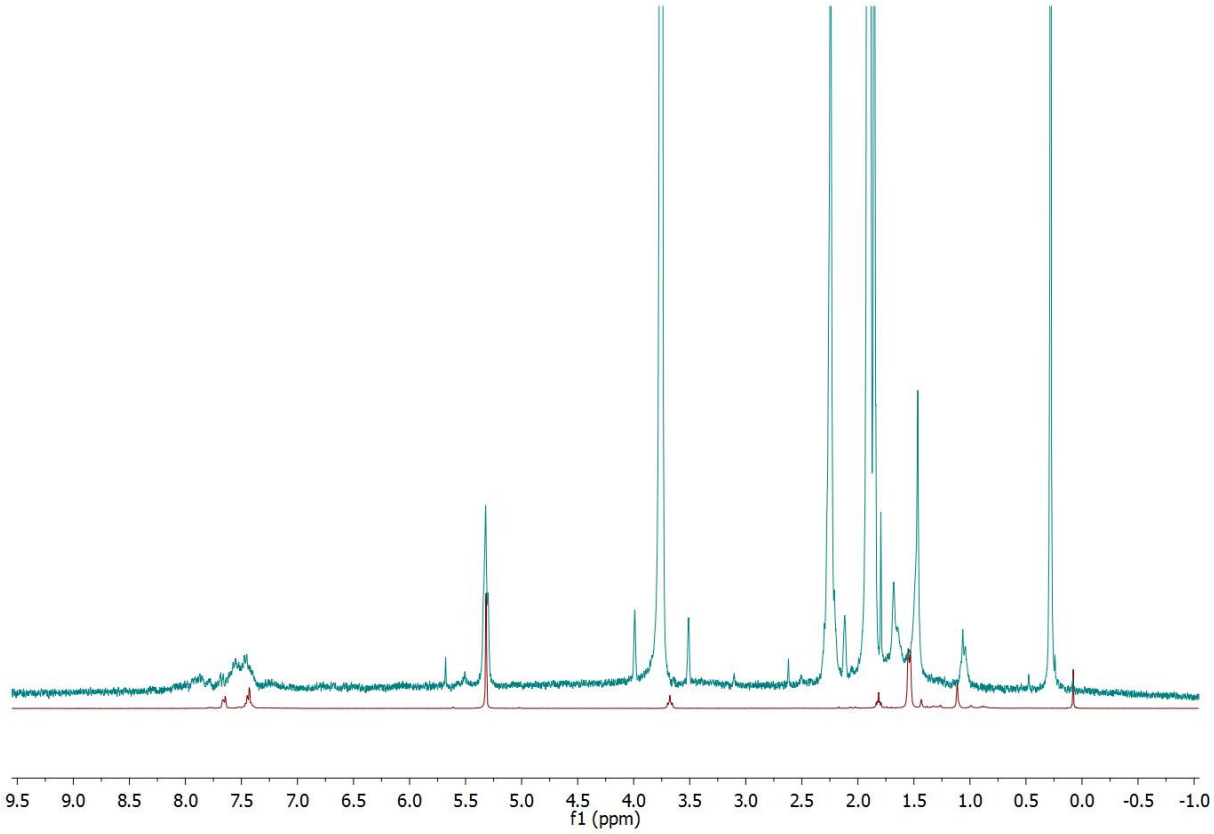

Figure S41: ^{1}H NMR spectra of **1** before (red, measured in CD_2Cl_2) and after irradiation (blue, measured in THF-d8, scaled by factor 10 due to the low solubility and the limited amount of the irradiated sample). The spectra indicate that **1** is still present after irradiation, beside minor decomposition products.

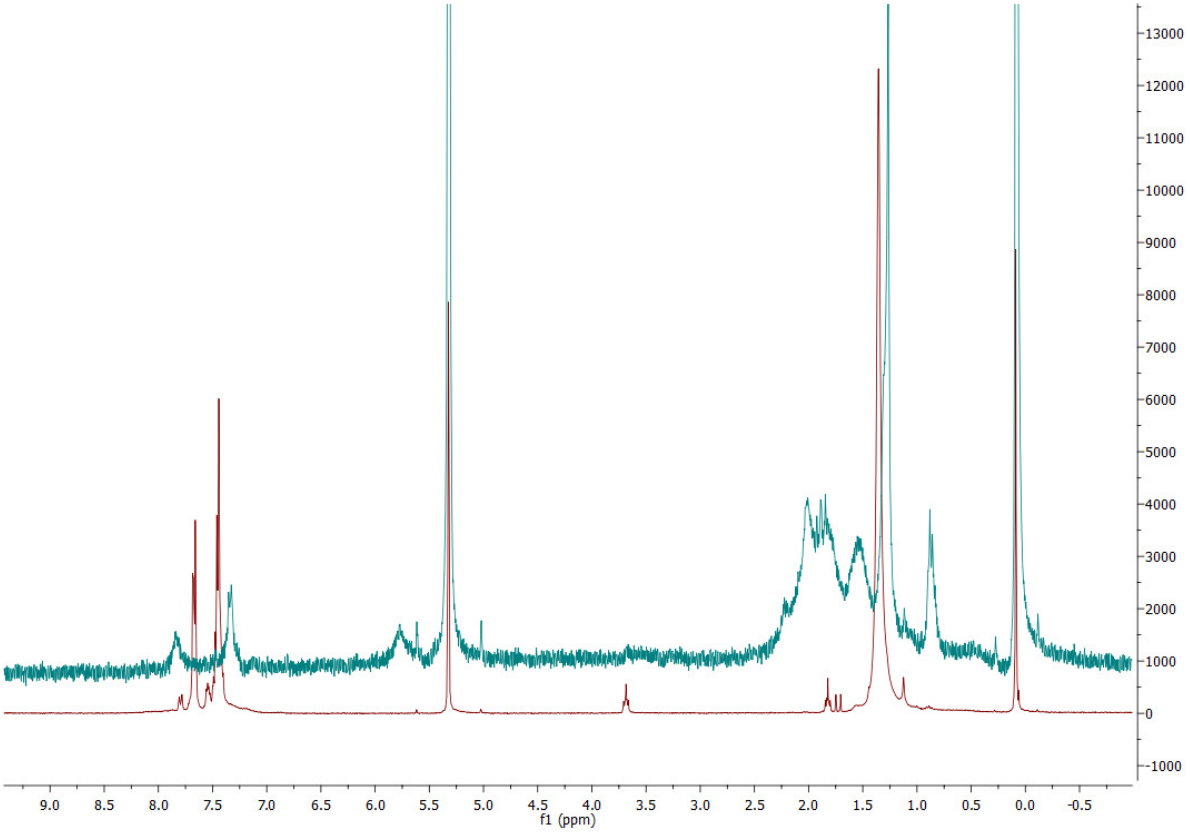

Figure S42: ^{1}H NMR spectra of **5** before (red, measured in CD_2Cl_2) and after irradiation (blue, measured in THF-d8, scaled by factor 10 due to the low solubility and the limited amount of the irradiated sample). The spectra indicate that **5** is still present after irradiation, beside minor decomposition products.

15. References for the Supporting Information

[1] P. Galez, J.L. Soubeyroux, T. Bertrand, T. Hopfinger, S. Beauquis, H. Nguyen Xuan, J. Alloys Compd. **2005**, 391, 13.

[2] H. Berwe, A. Haas, Chem. Ber. **1987**, 120, 1175.

[3] R. Vilma Bojan, J.M. Lopez-de-Luzuriaga, M. Monge, M. Elena Olmos, R. Echeverria, O. Lehtonen, D. Sundholm, ChemPLusChem **2014**, 79, 67.

[4] J.P. Eußner, S. Dehnen, Chem. Commun. **2014**, 50, 11385.

[5] S. Hagen, H. Schubert, C. Maichle-Mössmer, I. Pantenburg, F. Weigend, L. Wesemann, Inorg. Chem. **2007**, 46(16), 6775.

[6] N.E. Schlotter, B. Hudson, J. Chem. Phys, **1982**, 76, 4844.

4.4 Transition-Metal-Induced Rearrangement of $[(PhSn)_4S_6]$ Towards Ternary $Cu^{I}/Sn/S$ or $Cu^{II}/Sn/S$ Clusters

Zitat: E. Dornsiepen, F. Weigend, S. Dehnen, *Chem. Eur. J.* **2019**, *25*, 2486-2490.

Abstract

Direct access of ternary copper-tin sulfide clusters by reactions of a binary organotin sulfide cluster, $[(PhSn)_4S_6]$ (**A**), with transition metal complexes was achieved for the first time without extra addition of further chalcogenide sources. This indicates that an in situ rearrangement of the inorganic core takes place even without initial formation of anionic fragments. The use of $[Cu(PPh_3)_3Cl]$ or $[Cu(PPh_3)_2Cl_2]$ as reactants yielded the ternary clusters $[(CuPPh_3)_4(PhSn)_{18}Cu_6S_{31}Cl_2]$ (**1**) and $[\{Cu(PPh_3)_2\}_2(PhSn)_3(SnCl)S_8]$ (**2**), respectively. Whereas **1** represents the largest neutral Cu/Sn/S cluster known to date, compound **2**, which is the first example of a ternary Cu/Sn/E (E = S, Se) cluster containing copper in the +II oxidation state, may be viewed as a very early stage of cluster formation. Apparently, the presence of Cu^{II} inhibits effective cluster growth, which rationalizes the lack of such species so far. The two ternary clusters exhibit very similar optical absorption energies despite their markedly different cluster sizes. According to time-dependent DFT calculations, this is due to different characters of the electronic excitation in the triplet compound **2**, as compared to the excitation of the closed shell cluster **1**, which serve to compensate for the different extensions of the clusters.

Eigener Anteil

Alle Synthesen wurden von mir geplant und durchgeführt, alle analytischen Daten wurden von mir ausgewertet. Die röntgenographischen Daten wurden von mir selbst aufgenommen. ^{1}H- und ^{13}C-NMR-Experimente wurden von mir, ^{31}P- und ^{119}Sn-NMR-Experimente von der zentralen NMR-Abteilung des Fachbereichs Chemie an der Philipps-Universität unter Leitung von Dr. Xiulan Xie durchgeführt. Infrarot- und UV/Vis-Spektren wurden von mir gemessen. Die quantenchemischen Rechnungen wurden von PD Dr. Florian Weigend am Karlsruhe Institute of Technology (KIT) durchgeführt und ausgewertet. Das Manuskript habe ich in Kooperation mit Prof. Dr. Stefanie Dehnen verfasst. Die Co-Autoren haben jeweils kurze Abschnitte über ihre Beiträge eingefügt.

ChemPubSoc Europe

DOI: 10.1002/chem.201806407

CHEMISTRY
A European Journal
Communication

Cluster compounds

Transition-Metal-Induced Rearrangement of $[(PhSn)_4S_6]$ Towards Ternary $Cu^I/Sn/S$ or $Cu^{II}/Sn/S$ Clusters

Eike Dornsiepen,[a] Florian Weigend,[b] and Stefanie Dehnen*[a]

Abstract: Direct access of ternary copper-tin sulfide clusters by reactions of a binary organotin sulfide cluster, $[(PhSn)_4S_6]$ (**A**), with transition metal complexes was achieved for the first time without extra addition of further chalcogenide sources. This indicates that an in situ rearrangement of the inorganic core takes place even without initial formation of anionic fragments. The use of $[Cu(PPh_3)_3Cl]$ or $[Cu(PPh_3)_2Cl_2]$ as reactants yielded the ternary clusters $[(CuPPh_3)_4(PhSn)_{18}Cu_6S_{31}Cl_2]$ (**1**) and $[\{Cu(PPh_3)_2\}_2(PhSn)_3(SnCl)S_8]$ (**2**), respectively. Whereas **1** represents the largest neutral Cu/Sn/S cluster known to date, compound **2**, which is the first example of a ternary Cu/Sn/E (E = S, Se) cluster containing copper in the +II oxidation state, may be viewed as a very early stage of cluster formation. Apparently, the presence of Cu^{II} inhibits effective cluster growth, which rationalizes the lack of such species so far. The two ternary clusters exhibit very similar optical absorption energies despite their markedly different cluster sizes. According to time-dependent DFT calculations, this is due to different characters of the electronic excitation in the triplet compound **2**, as compared to the excitation of the closed shell cluster **1**, which serve to compensate for the different extensions of the clusters.

A large variety of metal chalcogenide clusters have been prepared during the last decades;[1] a significant share of them comprising the group 11 elements.[2] In the case of binary clusters, molecules with inorganic cores of considerable sizes with more than 500 atoms have been reported.[3] Clusters with ternary inorganic cores have also been reported, though their cores are usually smaller.[4]

The elemental combination Cu/Sn/S has attracted attention, as compounds with ternary ions containing these elements are semiconductors with band gaps of 1.5–2.5 eV.[5] Some of them have been shown to exhibit photoconductivity,[5b] making them potential precursor materials for thin-film solar cells, like copper zinc tin sulfide (CZTS) cells.[6]

Our work focuses on the reactivity of binary organotin chalcogenide clusters as effective starting materials in the generation of ternary clusters with organic decoration, by reaction with transition metal complexes. Organo-functionalized clusters with the elemental combination Cu/Sn/S have already been reported by our group,[7] as well as others.[5a,8] In all of these cases however, an additional sulfide source, usually an alkali metal sulfide or $(Me_3Si)_2S$, was added to the reaction solution, to induce fragmentation of the binary cluster under formation of anionic, nucleophilic chalcogenide sites for subsequent attack of the metal centres, and eventually formation of a ternary cluster.

Herein, we report on the formation of a ligand-protected Cu/Sn/S cluster by reaction of the binary organotin sulfide cluster $[(PhSn)_4S_6]$ (**A**) with $[Cu(PPh_3)_3Cl]$ (Scheme 1), yet without preceding addition of a sulfide source. The single-crystalline product of the reaction, $[(CuPPh_3)_4(PhSn)_{18}Cu_6S_{31}Cl_2]$ (**1**), represents the largest neutral cluster of this elemental combination. Repeating the reaction with the corresponding Cu^{II} complex $[Cu(PPh_3)_2Cl_2]$ leads to the formation of another ternary cluster with the composition $[\{Cu(PPh_3)_2\}_2(PhSn)_3(SnCl)S_8]$ (**2**) as the only single-crystalline product, which can also be obtained by treating the reaction solution of compound **1** with oxygen (air).

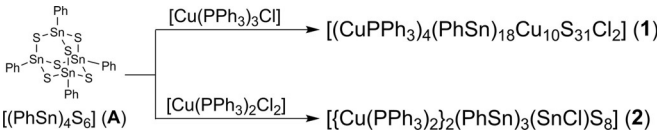

Scheme 1. Reaction scheme for the synthesis of compounds **1** and **2** from **A**.

The reaction of **A** with $[Cu(PPh_3)_3Cl]$ in THF affords a yellow solid upon solvent removal. Re-dissolving the solid in toluene and layering with *n*-hexane affords single crystals of **1** as yellow blocks. **1** crystallizes in the triclinic space group $P\bar{1}$ with two formula units per unit cell. The cluster consists of an inorganic core with the composition $[Sn_{18}Cu_{10}S_{31}]$ that is shielded by phenyl groups (one at each of the tin atoms), PPh_3 substituents (one at four of the copper atoms), and chlorine ligands (one at two of the tin atoms). The inorganic core is separated in two identical parts that are connected by a single sulfur

[a] E. Dornsiepen, Prof. Dr. S. Dehnen
Fachbereich Chemie und
Wissenschaftliches Zentrum für Materialwissenschaften
Philipps-Universität Marburg
Hans-Meerwein-Strasse 4, 35043 Marburg (Germany)
E-mail: dehnen@chemie.uni-marburg.de

[b] Dr. F. Weigend
Institute of Nanotechnology (INT), Karlsruhe Institute of Technology (KIT)
Hermann-von-Helmholtz-Platz 1
76344 Eggenstein-Leopoldshafen (Germany)

Supporting information and the ORCID identification number(s) for the author(s) of this article can be found under:
https://doi.org/10.1002/chem.201806407.

atom. Figure 1 depicts the molecular structure of the cluster. The relatively complicated composition of subunits within the inorganic cluster core of **1** is illustrated in Figure 2.

Each part is formed around a central (distorted) 2.2.2-propellane unit with the composition $[Cu_4S_4]$ (Figure 2, red fragment), with two of the open faces being capped by $[Sn_3S_3]$ six-membered rings (Figure 2, blue fragment). The third face, on the other hand, is capped by an $[Sn_2CuS_3]$ six-membered ring (Figure 2, yellow fragment). Such six-membered rings are also found as structural motifs in ternary copper tin sulfides, such as Cu_2SnS_3,[9] $Cu_{2.67}Sn_{1.33}S_4$,[10] or $Cu_{1.33}Sn_{0.67}S_2$.[11] Additionally, the

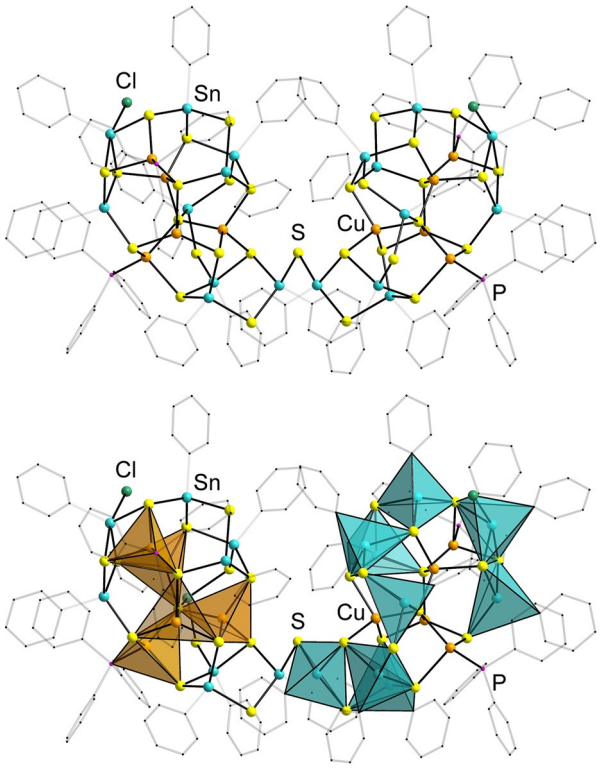

Figure 1. Molecular structure of **1** in ball-stick representation (top) and with coordination polyhedra (bottom) around the Sn (blue) and Cu (orange) atoms. Organic groups are shown as transparent wires, thereby omitting H atoms and the disorder of two of the organic substituents for clarity. Selected bond lengths [Å]: Cu–S 2.224(4)–2.520(5) (shortest values within central Cu_2S_4 unit, longest values at PPh_3-bearing copper atoms), Sn–S 2.337(5)–2.466(4) (generally), 2.605(6) and 2.607(4) at the chloride-bearing tin atoms in *trans*-position to the chloride substituent. Further details are provided in the Supporting Information.

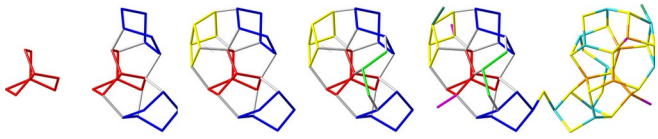

Figure 2. Illustration of the composition and connection of subunits in the inorganic cluster core of **1** (from left): In each of the cluster halves, an inner 2.2.2-propellane-like $[Cu_4S_4]$ unit (red) is linked to two $[Sn_3S_3]$ six-membered rings (blue) and one $[Sn_2CuS_3]$ six-membered ring (yellow). An $[SnS_2]$ group (green) connects the two $[Sn_3S_3]$ fragments. A μ-S ligand connects the two cluster halves.

two Sn_3S_3 rings are connected by an $[SnS_2]$ group (Figure 2, green fragment). Doubling of the building unit and addition of the single bridging sulfur atom gives the complete inorganic core of **1**.

As can be anticipated from the individual fragments of the molecular structure shown in Figure 2, the cluster **1** formally results from complete decomposition of the initial binary cluster into $[PhSn]^{3+}$ and S^{2-} fragments, which then rearrange together with copper and chlorine atoms from $[Cu(PPh_3)_3Cl]$. As we did not supply any S^{2-} anions during the reaction, this indicates that the precursor cluster **A** is nucleophilic enough to interact with the copper ions. The result is a nucleophilic replacement of chloride ligands within the complex by formerly bridging sulfide ligands and the concomitant in situ fragmentation of the tin-sulfur substructure.

As **1** is a pseudo-dimer of two smaller clusters, it seems to have crystallized while the cluster growth process was still in progress–that might have led to a macrocyclic arrangement, for instance. Furthermore, the rather asymmetric structure of the two cluster halves indicates the immaturity of the inorganic structure. Most of the known cluster structures, including a monoanionic cluster with a core comprising 59 atoms as in **1**,[8b] are much more symmetric, hence seem to be closer to a global minimum structure. The reason for the observation of the intermediate-type cluster **1** could be a lower reaction rate that occurs in the present case owing to the absence of free S^{2-} reactants. So, the crystallization of an intermediate can occur with higher probability. Generally speaking, this approach may be useful for trapping further cluster intermediates, and thus is suitable to learn more about the still widely unknown growth mechanism of metal chalcogenide clusters, in particular ternary ones.

By use of $[Cu(PPh_3)_2Cl_2]$, with copper in a +II oxidation state, or upon treatment of the mother liquor at the synthesis of **1** with oxygen (air), another ternary cluster was obtained. $[\{Cu(PPh_3)_2\}_2(PhSn)_3(SnCl)S_8]$ (**2**) crystallizes in the orthorhombic space group *Pnma* with four formula units per unit cell. The extremely low yield clearly indicates that **2** is not an efficient reaction product, yet, no other products could be isolated as single crystals, and the NMR spectrum of the reaction solution does not give any distinct information about any other clusters forming. Figure 3 illustrates the molecular structure in different views.

The molecular structure is related to the adamantane-type topology of $[(PhSn)_4S_6]$ (Figure 3, bottom right), but also shows notable deviations that may indicate its snapshot character at the outset of a ternary cluster formation reaction. One of the four phenyl groups is replaced with a chlorine atom at Sn3. Two further tin atoms, Sn2 and its symmetry equivalent Sn2′, bear an additional $[SCu(PPh_3)_2]$ substituent each, which forms a four-membered $[SnCuS_2]$ ring together with one of the sulfur atoms from the parent adamantane-type cage, S1 (and its symmetry equivalent S1′). As a consequence of the coordination by the additional sulfur atom S3, which increases the coordination number at Sn2 to five, the cage undergoes a distortion, so that S2 (located between the said tin atoms) is shifted inside the cage (Figure 3, center right).

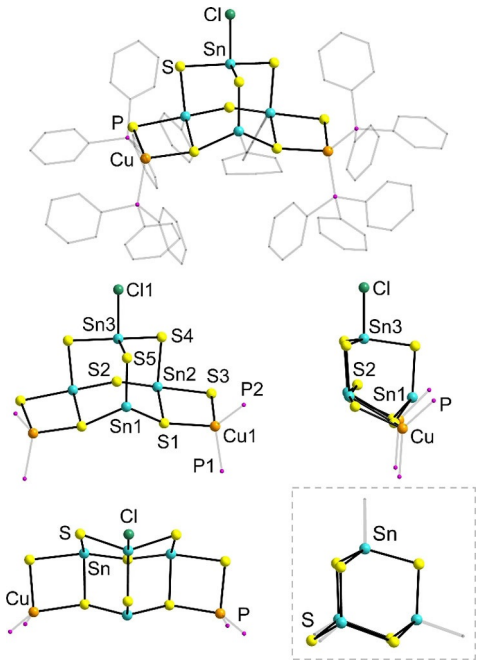

Figure 3. Molecular structure of **2** (top). Organic groups are shown as transparent wires, thereby omitting H atoms and the disorder of two of the organic substituents per asymmetric unit for clarity. Illustration of the inorganic core of **2** (centre and bottom) in three different orientations, to illustrate its relation with and the unprecedented deviation from the adamantane-type precursor cluster topology; the latter is shown in the inset that illustrates the calculated structure of the $[(RSn)_4S_6]$ core.[12] Selected bond lengths [Å]: Sn–S 2.381(3)–2.576(3) (longest values in the $CuSnS_2$ rings), Cu–S 2.408(3), 2.457(4). Further details are provided in the Supporting Information.

2 is a rare example of a ternary Cu/Sn/E (E = chalcogenide) cluster featuring Cu^{II}, and actually the first one for E = S, Se. In similar reactions employing $[Cu(PPh_3)_2Cl_2]$, reduction of the copper ions to the +I oxidation state was always observed,[4e] although there are examples for mixed-valent copper chalcogenide clusters, predominantly with tellurium atoms acting as bridging ligands.[13] The observation of the copper ions in their original oxidation state, despite the reductive environment of sulfide ions and phosphine molecules, may be due to the immatureness of the cluster; apparently, it has just passed the first step of cluster growth, such that reduction has not yet occurred, but would be the next step. Further incorporation of Cu^{II}–hence further cluster growth without reduction–seems unlikely, as this would cause an accumulation of positive charges that clearly reduces the overall nucleophilicity of the growing cluster.

Density functional theory (DFT) calculations were performed for both compounds to gain insight into their optical properties. A singlet state was found for **1** and a triplet state for **2**. After optimization of structure parameters (for Cartesian coordinates, see Supporting Information, Tables S7 and S8), the lowest 10 (40) spin-conserving excitations for **1** (**2**) were calculated by means of time-dependent DFT. In Figure 4, their energies and oscillator strengths are shown, together with modelled spectra and non-relaxed difference densities with respect to the ground state for the entire bands.

For **1**, the onset of excitations is calculated at ca. 2 eV. The two lowest excitations, which dominate the first band, mainly involve HOMO to HOMO−3 as well as LUMO to LUMO+2 (see Figure S12). This yields transitions from the Cu(d) orbitals mainly to the Sn(s) orbitals (see contour plot in Figure 4).

For **2**, the main onset is also calculated at ca. 2 eV. However, between 1.5 and 2 eV, transitions with similar intensities (and at smaller energies, transitions with lower intensities) are observed. In **2**, all calculated transitions take place only within the minority spin component from energetically high occupied orbitals to solely the two lowest unoccupied orbitals (their counterparts of the majority spin component are occupied and lower in energy). These two unoccupied orbitals are energeti-

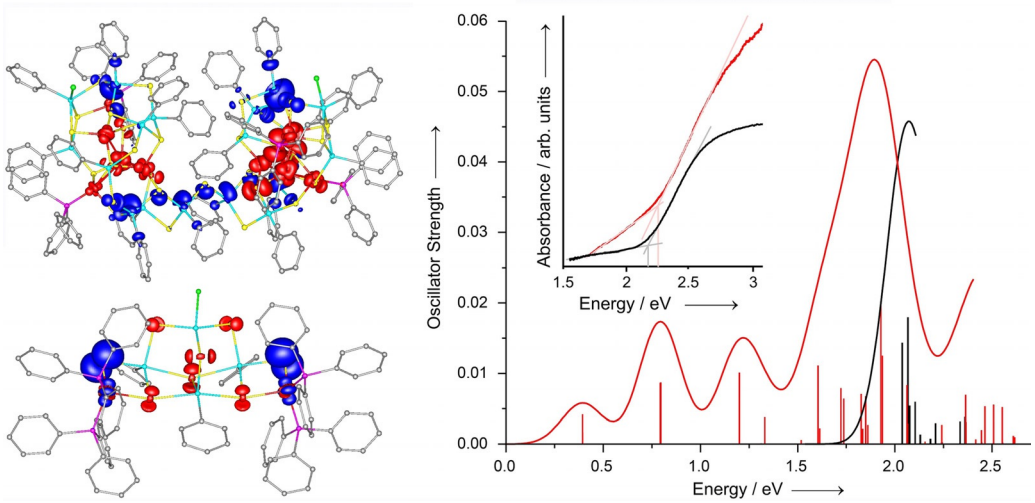

Figure 4. Calculated excitation energies (vertical lines) for compounds **1** (black) and **2** (red), and non-relaxed electronic difference densities (left) for the entire bands with respect to the ground state. Contours are drawn at 0.001 a.u. The contributions of occupied orbitals are plotted in red and those of the unoccupied orbitals in blue. From the excitations, the experimental spectrum was modelled by superposition of Gaussians with a FWHM of 0.25 eV. The inset shows the measured UV/Vis spectra (see Figures S11 and S12 for full spectra).

cally well separated from the highest occupied orbitals by 1.6 eV, and from the next unoccupied orbitals by 2.1 eV (see Figure S13). Their main contributions stem from the p-orbitals of S3 (see contour plot in Figure 4) and its counterpart, whereas the energetically high occupied MOs have contributions dominantly from the other sulfur atoms. Consequently, charge is transferred mainly from the latter to the former upon excitation.

In order to validate the optoelectronic behaviour that is to be expected from the electronic structure of the clusters, we investigated optical absorption properties. The UV/Vis spectra of **1** and **2** in the solid state are shown in the inset in Figure 4. For compound **1** (red curve), an absorption edge is observed between ca. 590 to 470 nm; determination of the band gap by a tangential fit (giving the onset of absorption energy) indicates a value of 578 nm (2.14 eV), which is in accordance with the visual appearance of the crystals (yellow). Compound **2** shows a much smoother increase of absorption, setting in at 550 nm and reaching saturation at around 400 nm. Here, the tangential fit reveals a band gap of 590 nm (2.10 eV). Both results are in excellent agreement with the calculations, which rationalize similar excitation energies despite notably different cluster sizes, as a result of their fundamentally different electronic structures.

In summary, we isolated a large copper organotin sulfide cluster that was obtained upon copper ion-induced in situ rearrangement of a binary organotin sulfide cluster–for the first time without addition of an additional sulfide source. The reduced reaction rate in the absence of free S^{2-} ions apparently allowed for the isolation of very unusual reaction intermediates that resemble immature clusters on the way towards potentially more symmetric, larger ones. Oxidation of the reaction solution, or use of a corresponding copper(II) complex, results in the isolation of another snapshot of the ternary metal chalcogenide cluster formation process, with the unusual finding of copper atoms that are retained in the +II oxidation state, which at the same time indicates that the growth of cluster architectures does not seem to proceed efficiently under incorporation of Cu^{2+} ions. This may be ascribed to the accumulation of positive charges, which reduces the nucleophilicity of the growing cluster. Despite their very different cluster sizes, the title compounds exhibit similar absorption energies, which was rationalized by (TD-)DFT calculations. The latter indicate not only different electronic structures of the clusters, but also different excitation characters to be present for the closed-shell compound **1** and the open-shell compound **2**, which explains the finding.

Experimental Section

General: All synthetic steps, unless stated otherwise, were carried out under exclusion of oxygen and moisture by use of standard Schlenk procedures. $[(PhSn)_4S_6]$,[14] $[Cu(PPh_3)_3Cl]$,[15] and $[Cu(PPh_3)_2Cl_2]$[16] were prepared according to literature procedures. ^{1}H NMR and ^{13}C spectroscopy was carried out at 25 °C using a Bruker DRX 300 MHz spectrometer. The chemical shifts are given in ppm relative to the residual protons of deuterated solvent for ^{1}H and the solvent signal in ^{13}C NMR. Yields are based on the amount of Sn and refer to the amount of product isolated as single crystals.

Synthesis of $[(CuPPh_3)_4(PhSn)_{18}Cu_6S_{31}Cl_2]$ (1): $[(PhSn)_4S_6]$ (50 mg, 51 μmol) and $[Cu(PPh_3)_3Cl]$ (90 mg, 102 μmol) were dissolved in THF (5 mL) and the resulting yellow solution stirred at RT for 24 hours. Volatiles were removed under vacuum; the yellow residue re-dissolved in toluene (10 mL) and layered with *n*-hexane (10 mL). Crystals of **1** were obtained within ten days as yellow blocks. Yield: 18 mg (2.9 μmol, 26%); IR: $\tilde{\nu}$ = 403 (w), 440 (s), 485 (m), 502 (m), 519 (s), 686 (s), 720 (s), 803 (m), 990 (m), 1018 (m), 1062 (m), 1095 (m), 1155 (w), 1186 (w), 1259 (m), 1296 (w), 1326 (w), 1428 (m), 1474 (m), 1569 (w), 2960 (w), 3044 cm^{-1} (w). Due to the insolubility of **1** once formed, NMR and mass spectra of the compound could not be obtained. ^{1}H, ^{13}C, ^{31}P and ^{119}Sn NMR spectra of the reaction solutions are shown as Figures S5–S8, showing $Cu[(PPh_3)_3Cl]$ and one further phosphorus species, as well as a single tin species, indicating formation of the cluster during crystallization.

Synthesis of $[\{Cu(PPh_3)_2\}_2(PhSn)_3(SnCl)S_8]$ (2): $[(PhSn)_4S_6]$ (50 mg, 51 μmol) and $[Cu(PPh_3)_2Cl_2]$ (33 mg, 51 μmol) were dissolved in THF (5 mL) and the resulting yellow solution stirred at RT for 16 hours. Volatiles were removed under vacuum and the yellow residue was re-dissolved in dichloromethane (5 mL). After layering with *n*-pentane (5 mL), crystals of **2** were obtained within two week as yellow rods. Yield: 3 mg (1.4 μmol, 3%); IR: $\tilde{\nu}$ = 442 (s), 487 (m), 501 (s), 513 (s), 616 (w), 642 (w), 690 (s), 726 (m), 739 (m), 838 (m), 912 (m), 997 (m), 1021 (m), 1041 (m), 1066 (m), 1093 (m), 1154 (w), 1186 (w), 1259 (w), 1305 (w), 1329 (w), 1439 (s), 1476 (m), 1573 (w), 1583 (w), 1815 (w), 1882 (w), 1956 (w), 2080 (w), 2231 (w), 3048 cm^{-1} (w). ^{1}H, ^{13}C and ^{31}P NMR spectra of the reaction solutions are shown as Figures S9 and S10, reflecting a broad range of aromatic signals which could not be assigned, and a mixture of three unassignable phosphorus species in the ^{31}P NMR spectrum.

Synthesis of 2 by in situ oxidation: $[(PhSn)_4S_6]$ (50 mg, 51 μmol) and $[Cu(PPh_3)_3Cl]$ (90 mg, 102 μmol) were dissolved in THF (10 mL) and the resulting yellow solution stirred at RT for 16 hours. Volatiles were removed under vacuum and the yellow residue was re-dissolved in dichloromethane (15 mL). After layering with *n*-pentane (15 mL) and exposing the solution to air, crystals of **2** were obtained within one week as yellow rods. Yield: 2 mg (0.9 μmol, 2%).

Single-crystal structure analyses: Details on the single-crystal X-ray diffraction measurements, structure solution, and refinement are given in the Supporting Information. CCDC 18757559 (**1**) and 1875756 (**2**), contain the supplementary crystallographic data for this paper. These data are provided free of charge by The Cambridge Crystallographic Data Centre.

UV/visible spectroscopy: UV/Visible absorption spectroscopy was performed by analyses of the diffuse reflection of powdered samples. The measurements were carried out using a Varian Cary 5000 dual-beam spectrometer with a Praying Mantis sample holder from Harrick.

Quantum chemical investigations: Density functional theory calculations were carried out with TURBOMOLE[17] using def2-SVP basis sets[18] and taking advantage of the multipole-accelerated resolution-of the-identity method.[19] Structures were optimized with the functional BP86;[20] the B3-LYP functional[21] was employed for the calculation of the excitations. Non-relaxed electronic difference densities of the excited states weighted with the respective oscillator strengths are obtained in the way described in reference [22].

Acknowledgements

This work was funded by the Deutsche Forschungsgemeinschaft (DFG) within the framework of GRK 1782.

Conflict of interest

The authors declare no conflict of interest.

Keywords: DFT calculations · intermediates · ternary chalcogenide clusters · tin · X-ray diffraction

[1] a) S. Schulz, H. W. Roesky, H. J. Koch, G. M. Sheldrick, D. Stalke, A. Kuhn, *Angew. Chem. Int. Ed. Engl.* **1993**, *32*, 1729 – 1731; *Angew. Chem.* **1993**, *105*, 1828 – 1830; b) J. M. McConnachie, M. A. Ansari, J. A. Ibers, *J. Am. Chem. Soc.* **1991**, *113*, 7078 – 7079; c) A. Lorenz, D. Fenske, *Angew. Chem. Int. Ed.* **2001**, *40*, 4402 – 4406; *Angew. Chem.* **2001**, *113*, 4537 – 4541; d) C. Zimmermann, M. Melullis, S. Dehnen, *Angew. Chem. Int. Ed.* **2002**, *41*, 4269 – 4272; *Angew. Chem.* **2002**, *114*, 4444 – 4447; e) A. Kornienko, S. Banerjee, G. A. Kumar, R. E. Riman, T. J. Emge, J. G. Brennan, *J. Am. Chem. Soc.* **2005**, *127*, 3501 – 3505; f) T. Wu, L. Wang, X. Bu, V. Chau, P. Feng, *J. Am. Chem. Soc.* **2010**, *132*, 10823 – 10831; g) D. Fuhrmann, S. Dietrich, H. Krautscheid, *Chem. Eur. J.* **2017**, *23*, 3338 – 3346.

[2] a) O. Fuhr, S. Dehnen, D. Fenske, *Chem. Soc. Rev.* **2013**, *42*, 1871 – 1906; b) D. Ohlmann, H. Pritzkow, H. Grützmacher, M. Anthamatten, P. Glaser, *J. Chem. Soc., Chem. Commun.* **1995**, 1011 – 1012; c) D. Fenske, T. Langetepe, M. M. Kappes, O. Hampe, P. Weis, *Angew. Chem. Int. Ed.* **2000**, *39*, 1857 – 1860; *Angew. Chem.* **2000**, *112*, 1925 – 1928; d) S. Schneider, J. A. S. Roberts, M. R. Salata, T. J. Marks, *Angew. Chem. Int. Ed.* **2006**, *45*, 1733 – 1736; *Angew. Chem.* **2006**, *118*, 1765 – 1768; e) M. T. Aroz, M. C. Gimeno, M. Kulcsar, A. Laguna, V. Lippolis, *Eur. J. Inorg. Chem.* **2011**, 2884 – 22894; f) A. Castiñeiras, I. García-Santos, S. Dehnen, P. Sevillano, *Polyhedron* **2006**, *25*, 3653 – 3660.

[3] a) B. H. Krautscheid, D. Fenske, G. Baum, M. Semmelmann, *Angew. Chem. Int. Ed. Engl.* **1993**, *32*, 1303 – 1305; *Angew. Chem.* **1993**, *105*, 1364 – 1367; b) D. Fenske, C. E. Anson, A. Eichhöfer, O. Fuhr, A. Ingendoh, C. Persau, C. Richert, *Angew. Chem. Int. Ed.* **2005**, *44*, 5242 – 5246; *Angew. Chem.* **2005**, *117*, 5376 – 5381; c) C. E. Anson, A. Eichöfer, I. Issac, D. Fenske, O. Fuhr, P. Sevillano, C. Persau, D. Stalke, J. Zhang, *Angew. Chem. Int. Ed.* **2008**, *47*, 1326 – 1331; *Angew. Chem.* **2008**, *120*, 1346 – 1351.

[4] a) T. Zell, W. Shi, R. Langer, L. Ponikiewski, A. Rothenberger, *Dalton Trans.* **2008**, 932 – 937; b) C. B. Khadka, A. Eichhöfer, F. Weigend, J. F. Corrigan, *Inorg. Chem.* **2012**, *51*, 2747 – 2756; c) B. E. K. Barth, E. Leusmann, K. Harms, S. Dehnen, *Chem. Commun.* **2013**, *49*, 6590 – 6592; d) E. Dornsiepen, J. P. Eußner, N. W. Rosemann, S. Chatterjee, S. Dehnen, *Inorg. Chem.* **2017**, *56*, 11326 – 11335; e) N. Rinn, L. Guggolz, J. Lange, S. Chatterjee, T. Block, R. Pöttgen, S. Dehnen, *Chem. Eur. J.* **2018**, *24*, 5840 – 5848; f) E. Dornsiepen, E. Geringer, N. Rinn, S. Dehnen, *Coord. Chem. Rev.* **2019**, *380*, 136 – 169.

[5] a) X. Wang, T.-L. Sheng, R.-B. Fu, S.-M. Hu, S.-C. Xiang, L.-S. Wang, X.-T. Wu, *Inorg. Chem.* **2006**, *45*, 5236 – 5238; b) N. Pienack, A. Puls, C Näther, W. Bensch, *Inorg. Chem.* **2008**, *47*, 9606 – 9611; c) Y.-G. Han, C. Xu, T. Duan, F.-H. Wu, Q.-F. Zhang, W.-H. Leung, *Inorg. Chem.* **2009**, *48*, 8796 – 8802; d) R. Chen, F. Wang, C. Tang, Y. Zhang, D. Jia, *Chem. Eur. J.* **2013**, *19*, 8199 – 8206; e) X.-F. Tan, X. Liu, J. Zhou, L. Zhu, R. Zhao, Q. Huang, *J. Cluster Sci.* **2016**, *27*, 257 – 265.

[6] a) K. Ito, *Copper Zinc Tin Sulfide-Based Thin Film Solar Cells*, Wiley, Hoboken, **2015**; b) C. Steinhagen, M. G. Panthani, V. Akhavan, B. Goodfellow, B. Koo, B. A. Korgel, *J. Am. Chem. Soc.* **2009**, *131*, 12554 – 12555; c) W. Wang, M. T. Winkler, O. Gunawan, T. Gokmen, T. K. Todorov, Y. Zhu, D. B. Mitzi, *Adv. Energy Mater.* **2014**, *4*, 1301465; d) Y. Feng, T.-K. Lau, G. Cheng, L. Yin, Z. Li, H. Luo, Z. Liu, X. Lu, C. Yang, X. Xiao, *CrystEngComm* **2016**, *18*, 1070 – 1077.

[7] a) H. P. Nayek, W. Massa, S. Dehnen, *Inorg. Chem.* **2008**, *47*, 9146 – 9148; b) Z. Hassanzahdeh Fard, L. Xiong, C. Müller, M. Holynska, S. Dehnen, *Chem. Eur. J.* **2009**, *15*, 6595 – 6604; c) M. R. Halvagar, Z. Hassanzahdeh Fard, S. Dehnen, *Chem. Commun.* **2010**, *46*, 4716 – 4718; d) J. P. Eußner, S. Dehnen, *Chem. Commun.* **2014**, *50*, 11385 – 11388.

[8] a) R. Hauser, K. Merzweiler, *Z. Anorg. Allg. Chem.* **2002**, *628*, 905 – 906; b) A. Eichhöfer, J. Jiang, S. Lebedkin, D. Fenske, D. G. McDonald, J. F. Corrigan, C.-Y. Su, *Dalton Trans.* **2012**, *41*, 3321 – 3327; c) A. Eichhöfer, M. Kuhn, S. Lebedkin, M. Kehry, M. M. Kappes, F. Weigend, *Inorg. Chem.* **2017**, *56*, 9330 – 9336.

[9] T. Nomura, T. Maeda, K. Takei, M. Morihama, T. Wada, *Phys. Status Solidi C* **2013**, *10*, 1093 – 1097.

[10] X. Chen, H. Wada, A. Sato, M. Mieno, *J. Solid State Chem.* **1998**, *139*, 144 – 151.

[11] H. Hahn, W. Klingen, P. Ness, H. Schulze, *Naturwissenschaften* **1966**, *53*, 18.

[12] N. W. Rosemann, J. P. Eußner, A. Beyer, S. W. Koch, K. Volz, S. Dehnen, S. Chatterjee, *Science* **2016**, *352*, 1301 – 1304.

[13] a) D. Fenske, J. C. Steck, *Angew. Chem. Int. Ed. Engl.* **1993**, *32*, 238; *Angew. Chem.* **1993**, *105*, 254; b) A. Eichhöfer, J. F. Corrigan, D. Fenske, E. Tröster, *Z. Anorg. Allg. Chem.* **2000**, *626*, 338.

[14] H. Berwe, A. Haas, *Chem. Ber.* **1987**, *120*, 1175 – 1182.

[15] J. V. Hanna, S. E. Boyd, P. C. Healy, G. A. Bowmaker, B. W. Skelton, A. H. White, *Dalton Trans.* **2005**, 2547 – 2556.

[16] D. Ramakrishna, B. R. Bhat, *Inorg. Chem. Commun.* **2011**, *14*, 690 – 693.

[17] TURBOMOLE Version 7.3, TURBOMOLE GmbH 2018. TURBOMOLE is a development of University of Karlsruhe and Forschungszentrum Karlsruhe **1989 – 2007**, TURBOMOLE GmbH since 2007.

[18] F. Weigend, R. Ahlrichs, *Phys. Chem. Chem. Phys.* **2005**, *7*, 3297.

[19] M. Sierka, A. Hogekamp, R. Ahlrichs, *J. Chem. Phys.* **2003**, *118*, 9136 – 9148.

[20] a) A. Becke, *Phys. Rev. A* **1988**, *38*, 3098 – 3100; b) J. Perdew, *Phys. Rev. B* **1986**, *33*, 8822 – 8824.

[21] C. Lee, W. Yang, R. G. Parr, *Phys. Rev. B.* **1988**, *37*, 785 – 789.

[22] M. Kühn, F. Weigend, *J. Chem. Phys.* **2014**, *141*, 224302.

Manuscript received: December 22, 2018
Accepted manuscript online: January 2, 2019
Version of record online: January 25, 2019

CHEMISTRY
A European Journal

Supporting Information

Transition-Metal-Induced Rearrangement of $[(PhSn)_4S_6]$ Towards Ternary $Cu^I/Sn/S$ or $Cu^{II}/Sn/S$ Clusters

Eike Dornsiepen,[a] Florian Weigend,[b] and Stefanie Dehnen*[a]

chem_201806407_sm_miscellaneous_information.pdf

Table of Contents

1. Single-Crystal X-Ray Crystallography of Compound 1

Compound **1** crystallizes in the shape of yellow blocks. Data of the X-Ray diffraction analysis was collected on a STOE STADIVARI diffractometer using Cu K_α radiation (λ = 1.54186 Å) from an X-ray micro source with X-ray optics and a Pilatus 300K Si hybrid pixel array detector at 100 K. Reflection data were processed with X-Area 1.77.[1] Structure solution was performed by direct methods and full-matrix-least-squares refinement against F^2 using SHELXT[2] and SHELXL-2014[3] software. All non-hydrogen atoms were refined anisotropically, though the carbon atoms had to be constrained by EADP due to severe rotational disorder of the phenyl groups. Hydrogen atom positions were calculated. The cocrystallized solvent molecules could not be refined due to their disorder and were thus removed from the reflection data using the SQUEEZE routine. The void is located at -0.005, -0.005, 0.000, has a volume of 3733 $Å^3$ and contains 853 electrons, which amounts to 17 molecules of either toluene or hexane per unit cell.

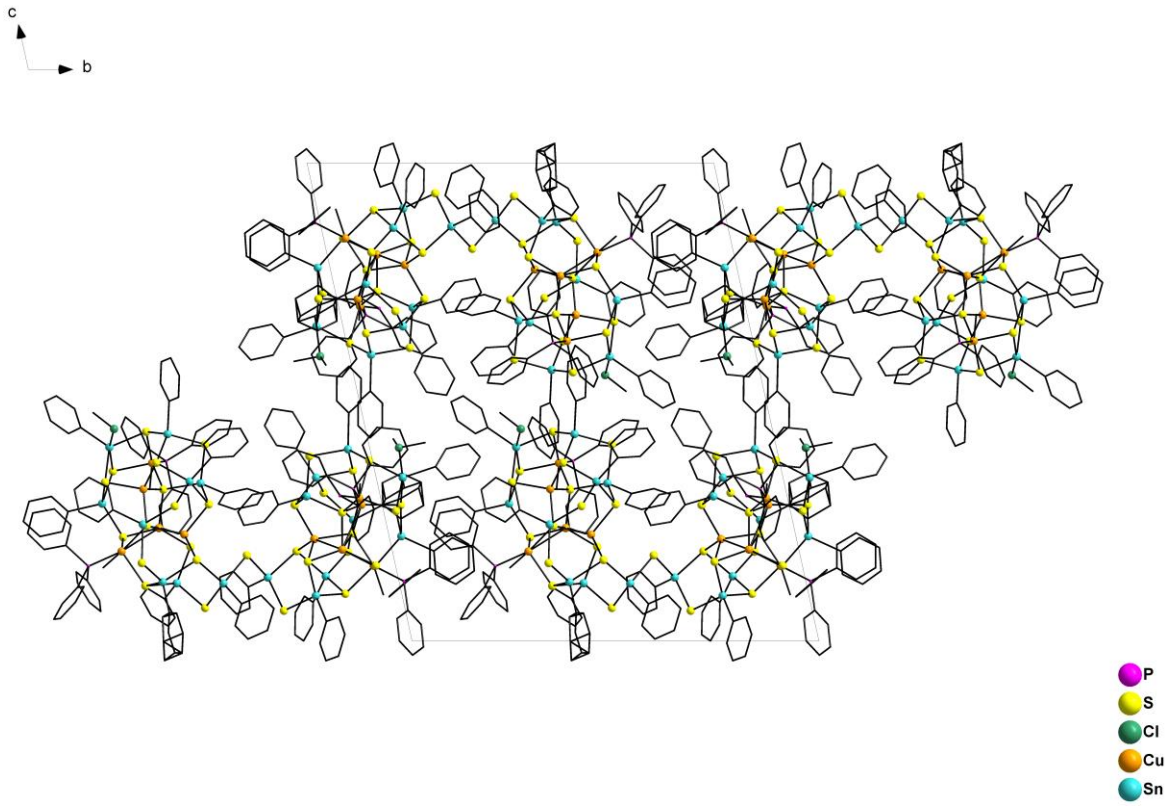

Figure S1: Crystal structure of **1**, viewed along the crystallographic *a* axis. Hydrogen atoms and the disorder of the organic substituents are omitted for clarity.

Table S1: Crystal data and structure refinement for **1** (CCDC 1875756).

Empirical formula	$C_{180}H_{150}Cl_2Cu_{10}P_4S_{31}Sn_{18}$	
Formula weight	6274.00	
Temperature	100(2) K	
Wavelength	1.54178 Å	
Crystal system	Triclinic	
Space group	$P\bar{1}$	
Unit cell dimensions	*a* = 18.7997(3) Å	*α*= 97.7650(10)°.
	b = 25.7334(4) Å	*β*= 101.2790(10)°.
	c = 29.7701(6) Å	*γ* = 109.1630(10)°.
Volume	13028.9(4) $Å^3$	
Z	2	
Density (calculated)	1.599 Mg/m^3	
Absorption coefficient	17.313 mm^{-1}	
F(000)	6021	
Crystal size	0.15 x 0.06 x 0.04 mm^3	
Theta range for data collection	2.574 to 73.989°.	
Index ranges	-23<=h<=22, -18<=k<=31, -34<=l<=36	
Reflections collected	144382	
Independent reflections	49786 [R(int) = 0.0827]	
Completeness to theta = 67.679°	98.2 %	
Absorption correction	Sphere	
Max. and min. transmission	0.0157 and 0.0000	
Refinement method	Full-matrix least-squares on F^2	
Data / restraints / parameters	49786 / 0 / 805	
Goodness-of-fit on F^2	1.275	
Final R indices [I>2sigma(I)]	R1 = 0.1077, wR2 = 0.2661	
R indices (all data)	R1 = 0.1458, wR2 = 0.2759	
Largest diff. peak and hole	2.251 and -1.358 e.$Å^{-3}$	

Table S2: Atomic coordinates (x 10^4) and equivalent isotropic displacement parameters ($Å^2$x 10^3) for **1**. U(eq) is defined as one third of the trace of the orthogonalized U^{ij} tensor.

	x	y	z	U(eq)
C(1)	3590(8)	10064(6)	641(4)	138(1)
C(2)	3199(7)	10312(5)	345(5)	138(1)
C(3)	3214(7)	10248(5)	-124(5)	138(1)
C(4)	3619(8)	9936(5)	-296(4)	138(1)
C(5)	4009(7)	9688(5)	0(5)	138(1)
C(6)	3995(7)	9752(5)	469(5)	138(1)
C(7)	4186(8)	10834(4)	1529(5)	138(1)
C(8)	4379(8)	10961(5)	2017(5)	138(1)
C(9)	4864(8)	11502(6)	2262(4)	138(1)
C(10)	5155(8)	11916(4)	2019(5)	138(1)
C(11)	4962(8)	11788(5)	1532(5)	138(1)
C(12)	4477(8)	11248(6)	1287(4)	138(1)
C(13)	7447(8)	11518(4)	3647(5)	138(1)
C(14)	7381(7)	11872(6)	4019(5)	138(1)
C(15)	7818(8)	12446(5)	4121(4)	138(1)
C(16)	8321(7)	12665(4)	3851(5)	138(1)
C(17)	8388(7)	12310(6)	3478(5)	138(1)
C(18)	7951(9)	11737(5)	3376(4)	138(1)
C(19)	6017(9)	9676(6)	4772(4)	138(1)
C(20)	5489(6)	9445(5)	5025(5)	138(1)
C(21)	5715(8)	9574(5)	5512(5)	138(1)
C(22)	6469(9)	9934(5)	5747(4)	138(1)
C(23)	6997(6)	10165(5)	5494(5)	138(1)
C(24)	6772(8)	10036(6)	5006(5)	138(1)
C(25)	3524(8)	8201(5)	4028(4)	138(1)
C(26)	3697(8)	7727(5)	4092(5)	138(1)
C(27)	3660(8)	7539(4)	4506(5)	138(1)
C(28)	3451(8)	7826(5)	4857(4)	138(1)
C(29)	3279(8)	8300(5)	4793(5)	138(1)
C(30)	3316(8)	8488(4)	4379(5)	138(1)
C(31)	3720(8)	5323(5)	5017(4)	138(1)
C(32)	3390(6)	5207(5)	5388(6)	138(1)
C(33)	3864(8)	5343(5)	5841(5)	138(1)
C(34)	4667(8)	5595(5)	5923(4)	138(1)
C(35)	4997(6)	5711(5)	5552(6)	138(1)
C(36)	4523(9)	5575(5)	5099(5)	138(1)
C(37)	4962(8)	6049(4)	3834(5)	138(1)

C(38)	5552(8)	5934(4)	4113(5)	138(1)
C(39)	6183(7)	6372(5)	4420(5)	138(1)
C(40)	6223(7)	6925(4)	4449(5)	138(1)
C(41)	5633(8)	7040(4)	4170(5)	138(1)
C(42)	5002(7)	6603(5)	3863(5)	138(1)
C(43)	970(8)	3008(5)	4465(5)	138(1)
C(44)	181(7)	2679(6)	4340(4)	138(1)
C(45)	-120(6)	2300(5)	4608(5)	138(1)
C(46)	369(8)	2250(5)	5002(5)	138(1)
C(47)	1159(7)	2579(5)	5127(4)	138(1)
C(48)	1459(6)	2958(5)	4859(5)	138(1)
C(54)	2069(6)	6768(5)	3187(6)	138(1)
C(53)	1697(7)	7136(4)	3072(5)	138(1)
C(52)	904(7)	6928(5)	2855(6)	138(1)
C(51)	483(6)	6351(5)	2753(6)	138(1)
C(50)	855(8)	5983(4)	2868(6)	138(1)
C(49)	1648(8)	6192(5)	3085(6)	138(1)
C(55)	1128(9)	2005(5)	2000(5)	138(1)
C(56)	614(8)	1451(5)	1914(4)	138(1)
C(57)	662(8)	1132(4)	2252(5)	138(1)
C(58)	1224(9)	1367(5)	2677(5)	138(1)
C(59)	1738(8)	1922(5)	2763(4)	138(1)
C(60)	1690(8)	2240(4)	2425(5)	138(1)
C(61)	-261(8)	2242(4)	2708(5)	138(1)
C(62)	-115(8)	1914(5)	3023(4)	138(1)
C(63)	-542(9)	1339(5)	2919(5)	138(1)
C(64)	-1115(8)	1091(4)	2500(5)	138(1)
C(65)	-1261(8)	1418(5)	2185(4)	138(1)
C(66)	-834(9)	1994(5)	2289(5)	138(1)
C(67)	207(6)	2063(5)	1120(5)	138(1)
C(68)	-424(9)	2226(5)	1136(4)	138(1)
C(69)	-1137(7)	1932(6)	811(5)	138(1)
C(70)	-1219(6)	1475(5)	471(5)	138(1)
C(71)	-587(9)	1312(5)	455(4)	138(1)
C(72)	126(7)	1605(6)	780(5)	138(1)
C(73)	1844(7)	2339(6)	1261(5)	138(1)
C(74)	1865(7)	2533(5)	848(5)	138(1)
C(75)	2432(8)	2505(5)	619(4)	138(1)
C(76)	2979(7)	2282(5)	802(5)	138(1)

C(77)	2958(7)	2089(5)	1215(5)	138(1)
C(78)	2390(9)	2117(5)	1444(4)	138(1)
C(79)	5409(8)	7447(4)	2850(5)	138(1)
C(80)	4881(7)	7004(5)	2492(5)	138(1)
C(81)	4979(8)	6490(5)	2420(5)	138(1)
C(82)	5605(8)	6418(4)	2705(5)	138(1)
C(83)	6133(7)	6861(5)	3062(5)	138(1)
C(84)	6035(8)	7375(4)	3135(5)	138(1)
C(85)	757(6)	6265(5)	1130(5)	138(1)
C(86)	288(8)	6188(5)	685(5)	138(1)
C(87)	-488(8)	5828(5)	564(4)	138(1)
C(88)	-794(6)	5544(5)	889(5)	138(1)
C(89)	-325(8)	5620(5)	1334(5)	138(1)
C(90)	451(8)	5981(5)	1455(4)	138(1)
C(91)	-311(6)	4143(6)	881(5)	138(1)
C(92)	-646(7)	4297(5)	486(5)	138(1)
C(93)	-1451(8)	4086(5)	311(4)	138(1)
C(94)	-1921(6)	3722(5)	530(5)	138(1)
C(95)	-1586(7)	3568(5)	924(5)	138(1)
C(96)	-781(8)	3779(5)	1100(4)	138(1)
C(97)	3720(8)	3353(5)	2743(5)	138(1)
C(98)	3700(8)	3359(5)	3208(5)	138(1)
C(99)	3842(8)	2941(6)	3420(4)	138(1)
C(100)	4004(8)	2518(5)	3167(5)	138(1)
C(101)	4024(8)	2512(5)	2702(5)	138(1)
C(102)	3882(8)	2930(6)	2490(4)	138(1)
C(103)	3486(8)	6011(6)	777(5)	138(1)
C(104)	4081(9)	6534(6)	957(4)	138(1)
C(105)	4555(7)	6778(4)	680(5)	138(1)
C(106)	4433(7)	6500(6)	222(5)	138(1)
C(107)	3838(9)	5977(5)	41(4)	138(1)
C(108)	3365(7)	5733(4)	319(5)	138(1)
C(109)	6387(8)	11022(5)	1881(5)	138(1)
C(110)	6862(8)	11548(6)	2160(4)	138(1)
C(111)	7192(8)	11991(4)	1953(5)	138(1)
C(112)	7046(8)	11907(5)	1468(5)	138(1)
C(113)	6570(8)	11381(6)	1189(4)	138(1)
C(114)	6241(8)	10939(4)	1395(5)	138(1)
C(115)	2606(6)	10144(6)	1223(5)	138(1)

C(116)	2494(7)	10582(5)	1491(5)	138(1)
C(117)	1744(9)	10567(5)	1476(5)	138(1)
C(118)	1105(6)	10114(6)	1193(5)	138(1)
C(119)	1217(7)	9675(5)	925(5)	138(1)
C(120)	1967(9)	9690(5)	940(5)	138(1)
C(121)	2781(13)	10021(6)	2849(7)	138(1)
C(122)	3498(11)	10462(9)	2969(9)	138(1)
C(123)	3576(10)	10990(7)	3204(9)	138(1)
C(124)	2936(13)	11077(6)	3320(7)	138(1)
C(125)	2219(11)	10635(9)	3201(9)	138(1)
C(126)	2141(10)	10107(7)	2965(9)	138(1)
C(181)	2700(20)	10385(15)	2556(17)	138(1)
C(182)	2860(20)	11014(16)	2835(17)	138(1)
C(183)	2540(20)	10122(16)	3308(17)	138(1)
C(184)	2510(20)	10649(14)	3508(16)	138(1)
C(127)	-739(8)	4918(6)	3173(4)	138(1)
C(128)	-1124(8)	5279(5)	3061(5)	138(1)
C(129)	-1487(7)	5237(5)	2596(5)	138(1)
C(130)	-1465(8)	4834(6)	2243(4)	138(1)
C(131)	-1079(8)	4473(5)	2356(5)	138(1)
C(132)	-716(8)	4515(5)	2820(5)	138(1)
C(133)	4013(9)	7999(6)	410(5)	138(1)
C(134)	3591(6)	7722(5)	-47(6)	138(1)
C(135)	3955(8)	7775(5)	-412(4)	138(1)
C(136)	4740(8)	8105(6)	-319(5)	138(1)
C(137)	5162(6)	8382(5)	138(6)	138(1)
C(138)	4798(8)	8329(5)	502(4)	138(1)
C(139)	8122(8)	8794(4)	3461(5)	138(1)
C(140)	8348(8)	8387(6)	3238(4)	138(1)
C(141)	8248(8)	7887(5)	3390(5)	138(1)
C(142)	7922(8)	7793(4)	3766(5)	138(1)
C(143)	7696(8)	8199(6)	3990(4)	138(1)
C(144)	7796(8)	8700(5)	3837(5)	138(1)
C(145)	2996(11)	4185(6)	588(5)	138(1)
C(146)	2420(8)	4055(6)	174(6)	138(1)
C(147)	2623(10)	4103(6)	-247(5)	138(1)
C(148)	3402(12)	4279(9)	-255(7)	138(1)
C(149)	3978(8)	4408(10)	159(9)	138(1)
C(150)	3775(9)	4361(9)	581(7)	138(1)

C(186)	3590(30)	3998(18)	502(19)	138(1)
C(187)	3700(30)	3887(17)	-13(18)	138(1)
C(188)	3110(30)	3808(17)	-410(18)	138(1)
C(151)	8764(8)	9402(6)	2832(5)	138(1)
C(152)	9549(9)	9719(5)	3031(4)	138(1)
C(153)	10079(6)	9774(5)	2757(6)	138(1)
C(154)	9823(8)	9512(6)	2285(5)	138(1)
C(155)	9038(9)	9194(5)	2086(4)	138(1)
C(156)	8508(6)	9139(5)	2360(6)	138(1)
C(157)	8825(8)	9927(4)	3678(4)	138(1)
C(158)	9194(9)	9840(4)	4098(5)	138(1)
C(159)	9623(8)	10295(5)	4470(4)	138(1)
C(160)	9683(8)	10837(4)	4423(4)	138(1)
C(161)	9314(9)	10924(4)	4003(5)	138(1)
C(162)	8885(9)	10468(5)	3630(4)	138(1)
C(163)	805(7)	7775(5)	808(5)	138(1)
C(164)	812(7)	7644(5)	341(6)	138(1)
C(165)	120(9)	7333(5)	3(4)	138(1)
C(166)	-578(7)	7154(5)	131(5)	138(1)
C(167)	-585(7)	7285(5)	599(6)	138(1)
C(168)	106(9)	7596(5)	937(4)	138(1)
C(169)	-978(7)	4548(5)	4023(5)	138(1)
C(170)	-734(6)	4433(5)	4457(5)	138(1)
C(171)	-1281(8)	4164(5)	4686(4)	138(1)
C(172)	-2071(7)	4010(5)	4480(5)	138(1)
C(173)	-2315(6)	4125(5)	4045(5)	138(1)
C(174)	-1768(8)	4394(6)	3817(4)	138(1)
C(175)	-341(6)	5822(5)	4374(5)	138(1)
C(176)	86(9)	5645(4)	4096(5)	138(1)
C(177)	795(8)	6022(6)	4072(5)	138(1)
C(178)	1077(6)	6575(5)	4325(5)	138(1)
C(179)	650(8)	6751(4)	4602(5)	138(1)
C(180)	-59(8)	6375(6)	4627(5)	138(1)
P(1)	3557(3)	10122(2)	1252(2)	102(1)
P(2)	1130(3)	2447(2)	1563(2)	106(2)
P(3)	-230(3)	4923(2)	3762(2)	96(1)
P(4)	8194(8)	9380(7)	3179(4)	92(5)
P(4B)	7754(10)	9014(7)	3041(5)	117(6)
S(1)	3613(3)	3777(2)	1630(2)	107(2)

S(2)	1390(2)	3741(1)	1151(2)	90(1)
S(3)	2330(3)	7012(2)	633(2)	110(2)
S(4)	5645(3)	8474(2)	3866(2)	122(2)
S(5)	2331(2)	4094(1)	2406(2)	88(1)
S(6)	234(2)	3458(1)	2170(2)	95(1)
S(7)	1736(2)	3310(1)	3320(2)	90(1)
S(8)	107(2)	3561(2)	3551(2)	92(1)
S(9)	1647(2)	4595(2)	4377(2)	95(1)
S(10)	1380(2)	4703(1)	3169(2)	93(1)
S(11)	3430(2)	4676(1)	3730(2)	96(1)
S(12)	1268(2)	5060(1)	1970(2)	94(1)
S(13)	3218(2)	5743(1)	2860(2)	94(1)
S(14)	2942(3)	5973(2)	4115(2)	104(2)
S(15)	1506(2)	5089(2)	692(2)	103(2)
S(16)	3267(2)	5142(1)	1695(2)	96(1)
S(17)	4599(2)	4892(2)	2823(2)	105(2)
S(18)	2736(2)	6403(2)	1794(2)	96(1)
S(19)	2889(3)	8612(2)	988(2)	116(2)
S(20)	4230(3)	7863(2)	1658(2)	109(2)
S(21)	2146(2)	7646(2)	1878(2)	96(1)
S(22)	1573(3)	8901(2)	1868(2)	114(2)
S(23)	5179(3)	9518(2)	1578(2)	105(1)
S(24)	7146(2)	10308(2)	2719(2)	106(2)
S(25)	5421(3)	10455(2)	2845(2)	101(1)
S(26)	5668(2)	8972(2)	2687(2)	114(2)
S(27)	4564(3)	9467(2)	3564(2)	116(2)
S(28)	2408(2)	8627(2)	3099(2)	108(2)
S(29)	6950(2)	9924(2)	3776(2)	98(1)
S(30)	3749(3)	9115(2)	2251(2)	111(2)
S(31)	3795(2)	7850(2)	2844(2)	99(1)
Cl(1)	5923(3)	10722(2)	4043(2)	110(1)
Cl(2)	2842(2)	3819(2)	4436(2)	101(1)
Cu(1)	2244(1)	4216(1)	3179(1)	93(1)
Cu(2)	1283(1)	3344(1)	1874(1)	95(1)
Cu(3)	2463(1)	4975(1)	2227(1)	96(1)
Cu(4)	689(1)	4571(1)	3722(1)	95(1)
Cu(5)	892(1)	4385(1)	2363(1)	93(1)
Cu(6)	4983(1)	8775(1)	1913(1)	111(1)
Cu(7)	6985(1)	9471(1)	2994(1)	105(1)

Cu(8)	3887(2)	9463(1)	1574(1)	107(1)
Cu(9)	4882(1)	9491(1)	2851(1)	111(1)
Cu(10)	3517(1)	8145(1)	2132(1)	105(1)
Sn(1)	2226(1)	5652(1)	3301(1)	93(1)
Sn(2)	5986(1)	10302(1)	2192(1)	101(1)
Sn(3)	2694(1)	9206(1)	2530(1)	104(1)
Sn(4)	1948(1)	6795(1)	1329(1)	98(1)
Sn(5)	5794(1)	9460(1)	4010(1)	107(1)
Sn(6)	3617(1)	8523(1)	3418(1)	102(1)
Sn(7)	1839(1)	8229(1)	1355(1)	106(1)
Sn(8)	3449(1)	7878(1)	947(1)	107(1)
Sn(9)	6649(1)	10652(1)	3418(1)	101(1)
Sn(10)	5213(1)	8186(1)	3027(1)	110(1)
Sn(11)	2955(1)	5106(1)	4329(1)	95(1)
Sn(12)	920(1)	4526(1)	1208(1)	90(1)
Sn(13)	404(1)	3124(1)	2874(1)	90(1)
Sn(14)	3548(1)	4011(1)	2438(1)	94(1)
Sn(15)	2738(1)	5672(1)	1202(1)	97(1)
Sn(16)	1436(1)	3606(1)	4054(1)	93(1)
Sn(17)	2769(1)	4187(1)	1232(1)	98(1)
Sn(18)	4074(1)	5392(1)	3336(1)	96(1)

Table S3: Bond lengths [Å] and angles [°] for **1**.

C(1)-P(1)	1.817(13)	C(151)-P(4)	1.619(17)	S(10)-Cu(5)	2.320(5)
C(7)-P(1)	1.796(10)	C(151)-P(4B)	2.09(2)	S(10)-Cu(1)	2.353(5)
C(13)-Sn(9)	2.161(9)	C(157)-P(4)	1.800(18)	S(10)-Sn(1)	2.365(3)
C(19)-Sn(5)	2.183(11)	C(163)-Sn(7)	2.133(10)	S(11)-Cu(1)	2.319(4)
C(25)-Sn(6)	2.111(10)	C(169)-P(3)	1.802(12)	S(11)-Sn(11)	2.436(5)
C(31)-Sn(11)	2.142(10)	C(176)-P(3)	1.828(11)	S(11)-Sn(18)	2.432(4)
C(37)-Sn(18)	2.085(10)	P(1)-Cu(8)	2.255(4)	S(12)-Cu(5)	2.224(4)
C(43)-Sn(16)	2.163(9)	P(2)-Cu(2)	2.272(5)	S(12)-Cu(3)	2.318(4)
C(49)-Sn(1)	2.117(9)	P(3)-Cu(4)	2.213(5)	S(12)-Sn(12)	2.337(5)
C(55)-P(2)	1.841(10)	P(4)-Cu(7)	2.328(11)	S(13)-Cu(3)	2.363(5)
C(61)-Sn(13)	2.134(8)	P(4B)-Cu(7)	2.138(9)	S(13)-Sn(18)	2.411(3)
C(67)-P(2)	1.830(10)	S(1)-Sn(17)	2.394(4)	S(13)-Sn(1)	2.450(5)
C(73)-P(2)	1.826(13)	S(1)-Sn(14)	2.436(6)	S(14)-Sn(11)	2.406(3)
C(79)-Sn(10)	2.074(10)	S(2)-Sn(17)	2.413(4)	S(14)-Sn(1)	2.413(4)
C(85)-Sn(4)	2.118(10)	S(2)-Sn(12)	2.454(4)	S(15)-Sn(15)	2.376(4)
C(91)-Sn(12)	2.153(10)	S(2)-Cu(2)	2.518(5)	S(15)-Sn(12)	2.427(4)
C(97)-Sn(14)	2.109(8)	S(3)-Sn(4)	2.396(5)	S(16)-Cu(3)	2.380(6)
C(98)-C(99)	1.3900	S(3)-Sn(8)	2.419(4)	S(16)-Sn(15)	2.423(3)
C(103)-Sn(15)	2.130(11)	S(4)-Sn(10)	2.400(6)	S(16)-Sn(17)	2.427(4)
C(109)-Sn(2)	2.163(9)	S(4)-Sn(5)	2.428(4)	S(17)-Sn(18)	2.419(6)
C(115)-P(1)	1.792(11)	S(5)-Cu(1)	2.324(5)	S(17)-Sn(14)	2.415(4)
C(121)-C(183)	1.53(5)	S(5)-Cu(3)	2.344(3)	S(18)-Sn(4)	2.387(3)
C(121)-C(181)	1.39(4)	S(5)-Sn(14)	2.352(4)	S(18)-Sn(15)	2.398(5)
C(121)-Sn(3)	2.122(14)	S(5)-Cu(2)	2.360(4)	S(19)-Sn(7)	2.432(6)
C(124)-C(184)	1.39(4)	S(6)-Cu(5)	2.229(4)	S(19)-Sn(8)	2.446(5)
C(124)-C(182)	1.41(5)	S(6)-Sn(13)	2.373(4)	S(19)-Cu(8)	2.520(5)
C(181)-C(182)	1.62(6)	S(6)-Cu(2)	2.395(6)	S(20)-Cu(6)	2.237(4)
C(183)-C(184)	1.43(6)	S(7)-Cu(1)	2.341(4)	S(20)-Cu(10)	2.328(7)
C(127)-P(3)	1.824(10)	S(7)-Sn(16)	2.446(5)	S(20)-Sn(8)	2.340(4)
C(133)-Sn(8)	2.088(12)	S(7)-Sn(13)	2.451(4)	S(21)-Cu(10)	2.379(4)
C(139)-P(4B)	1.574(14)	S(8)-Cu(4)	2.403(4)	S(21)-Sn(7)	2.420(3)
C(139)-P(4)	1.804(15)	S(8)-Sn(13)	2.425(5)	S(21)-Sn(4)	2.424(5)
C(145)-C(186)	1.41(5)	S(8)-Sn(16)	2.607(4)	S(22)-Sn(7)	2.393(6)
C(145)-Sn(17)	2.044(16)	S(9)-Cu(4)	2.362(4)	S(22)-Sn(3)	2.410(4)
C(147)-C(188)	1.47(5)	S(9)-Sn(11)	2.422(4)	S(23)-Cu(6)	2.232(4)
C(186)-C(187)	1.59(7)	S(9)-Sn(16)	2.466(4)	S(23)-Sn(2)	2.371(5)
C(187)-C(188)	1.40(6)	S(10)-Cu(4)	2.284(6)	S(23)-Cu(8)	2.384(5)

S(24)-Cu(7)	2.353(4)	C(30)-C(25)-Sn(6)	118.5(8)	C(121)-C(183)-C(184)	123(3)
S(24)-Sn(2)	2.420(4)	C(32)-C(31)-Sn(11)	118.0(9)	C(124)-C(184)-C(183)	111(4)
S(24)-Sn(9)	2.605(6)	C(36)-C(31)-Sn(11)	122.0(9)	C(128)-C(127)-P(3)	125.3(9)
S(25)-Cu(9)	2.356(4)	C(38)-C(37)-Sn(18)	119.0(7)	C(132)-C(127)-P(3)	114.7(9)
S(25)-Sn(2)	2.437(6)	C(42)-C(37)-Sn(18)	120.8(7)	C(134)-C(133)-Sn(8)	118.4(9)
S(25)-Sn(9)	2.439(4)	C(44)-C(43)-Sn(16)	120.0(7)	C(138)-C(133)-Sn(8)	121.6(9)
S(26)-Cu(7)	2.309(4)	C(48)-C(43)-Sn(16)	120.0(7)	C(140)-C(139)-P(4B)	102.8(10)
S(26)-Cu(6)	2.307(5)	C(50)-C(49)-Sn(1)	121.3(7)	C(144)-C(139)-P(4B)	122.6(10)
S(26)-Cu(9)	2.366(6)	C(54)-C(49)-Sn(1)	118.6(7)	C(140)-C(139)-P(4)	114.0(10)
S(26)-Sn(10)	2.365(4)	C(56)-C(55)-P(2)	122.7(8)	C(144)-C(139)-P(4)	125.7(10)
S(27)-Cu(9)	2.319(7)	C(60)-C(55)-P(2)	117.2(8)	C(186)-C(145)-C(146)	110(2)
S(27)-Sn(6)	2.414(4)	C(62)-C(61)-Sn(13)	119.3(7)	C(186)-C(145)-Sn(17)	118(2)
S(27)-Sn(5)	2.437(4)	C(66)-C(61)-Sn(13)	120.7(7)	C(146)-C(145)-Sn(17)	123.2(11)
S(28)-Sn(6)	2.401(4)	C(68)-C(67)-P(2)	118.8(9)	C(150)-C(145)-Sn(17)	116.6(11)
S(28)-Sn(3)	2.427(4)	C(72)-C(67)-P(2)	121.2(9)	C(146)-C(147)-C(188)	121(2)
S(29)-Sn(5)	2.396(5)	C(74)-C(73)-P(2)	116.8(9)	C(145)-C(186)-C(187)	121(4)
S(29)-Sn(9)	2.444(4)	C(78)-C(73)-P(2)	123.0(9)	C(186)-C(187)-C(188)	122(5)
S(29)-Cu(7)	2.482(6)	C(80)-C(79)-Sn(10)	121.4(7)	C(147)-C(188)-C(187)	105(4)
S(30)-Cu(9)	2.315(5)	C(84)-C(79)-Sn(10)	118.2(7)	C(152)-C(151)-P(4)	116.0(12)
S(30)-Cu(8)	2.338(5)	C(86)-C(85)-Sn(4)	121.6(8)	C(156)-C(151)-P(4)	124.0(12)
S(30)-Cu(10)	2.351(4)	C(90)-C(85)-Sn(4)	118.4(8)	C(152)-C(151)-P(4B)	139.4(10)
S(30)-Sn(3)	2.362(6)	C(92)-C(91)-Sn(12)	121.3(7)	C(156)-C(151)-P(4B)	99.2(10)
S(31)-Cu(10)	2.369(4)	C(96)-C(91)-Sn(12)	118.4(7)	C(158)-C(157)-P(4)	125.4(8)
S(31)-Sn(6)	2.415(5)	C(98)-C(97)-Sn(14)	119.2(8)	C(162)-C(157)-P(4)	114.5(8)
S(31)-Sn(10)	2.438(4)	C(102)-C(97)-Sn(14)	120.7(8)	C(164)-C(163)-Sn(7)	122.7(9)
Cl(1)-Sn(9)	2.536(6)	C(104)-C(103)-Sn(15)	118.7(9)	C(168)-C(163)-Sn(7)	117.2(9)
Cl(2)-Sn(16)	2.508(4)	C(108)-C(103)-Sn(15)	121.2(9)	C(170)-C(169)-P(3)	117.1(9)
Cu(3)-Cu(5)	2.980(3)	C(110)-C(109)-Sn(2)	120.7(8)	C(174)-C(169)-P(3)	122.9(8)
Cu(6)-Cu(10)	2.950(4)	C(114)-C(109)-Sn(2)	118.8(8)	C(177)-C(176)-P(3)	117.0(9)
		C(116)-C(115)-P(1)	122.0(9)	C(175)-C(176)-P(3)	123.0(9)
C(2)-C(1)-P(1)	121.0(9)	C(120)-C(115)-P(1)	117.9(9)	C(115)-P(1)-C(7)	102.6(7)
C(6)-C(1)-P(1)	118.9(9)	C(183)-C(121)-C(181)	115(3)	C(115)-P(1)-C(1)	102.0(7)
C(8)-C(7)-P(1)	116.0(9)	C(183)-C(121)-Sn(3)	121.1(18)	C(7)-P(1)-C(1)	104.2(7)
C(12)-C(7)-P(1)	124.0(9)	C(181)-C(121)-Sn(3)	117(2)	C(115)-P(1)-Cu(8)	119.3(5)
C(14)-C(13)-Sn(9)	120.3(9)	C(122)-C(121)-Sn(3)	119.3(12)	C(7)-P(1)-Cu(8)	114.3(5)
C(18)-C(13)-Sn(9)	119.0(9)	C(126)-C(121)-Sn(3)	120.6(12)	C(1)-P(1)-Cu(8)	112.6(5)
C(20)-C(19)-Sn(5)	124.7(8)	C(184)-C(124)-C(182)	122(3)	C(73)-P(2)-C(67)	102.5(7)
C(24)-C(19)-Sn(5)	115.0(9)	C(121)-C(181)-C(182)	113(4)	C(73)-P(2)-C(55)	103.6(7)
C(26)-C(25)-Sn(6)	121.4(8)	C(124)-C(182)-C(181)	115(3)	C(67)-P(2)-C(55)	104.1(6)

C(73)-P(2)-Cu(2)	118.2(5)	Cu(4)-S(9)-Sn(11)	112.21(19)	Cu(7)-S(24)-Sn(9)	87.38(19)
C(67)-P(2)-Cu(2)	113.7(5)	Cu(4)-S(9)-Sn(16)	89.34(14)	Sn(2)-S(24)-Sn(9)	88.34(16)
C(55)-P(2)-Cu(2)	113.1(6)	Sn(11)-S(9)-Sn(16)	103.44(18)	Cu(9)-S(25)-Sn(2)	94.42(18)
C(169)-P(3)-C(127)	105.5(7)	Cu(4)-S(10)-Cu(5)	126.80(18)	Cu(9)-S(25)-Sn(9)	96.21(14)
C(169)-P(3)-C(176)	102.1(7)	Cu(4)-S(10)-Cu(1)	114.44(16)	Sn(2)-S(25)-Sn(9)	91.85(17)
C(127)-P(3)-C(176)	106.0(6)	Cu(5)-S(10)-Cu(1)	91.20(19)	Cu(7)-S(26)-Cu(6)	126.7(3)
C(169)-P(3)-Cu(4)	115.8(5)	Cu(4)-S(10)-Sn(1)	111.35(19)	Cu(7)-S(26)-Cu(9)	113.56(19)
C(127)-P(3)-Cu(4)	109.5(6)	Cu(5)-S(10)-Sn(1)	106.80(17)	Cu(6)-S(26)-Cu(9)	86.64(16)
C(176)-P(3)-Cu(4)	116.9(5)	Cu(1)-S(10)-Sn(1)	102.39(16)	Cu(7)-S(26)-Sn(10)	112.06(16)
C(151)-P(4)-C(157)	101.6(11)	Cu(1)-S(11)-Sn(11)	97.77(18)	Cu(6)-S(26)-Sn(10)	110.25(15)
C(151)-P(4)-C(139)	109.7(9)	Cu(1)-S(11)-Sn(18)	100.58(15)	Cu(9)-S(26)-Sn(10)	102.6(2)
C(157)-P(4)-C(139)	97.0(8)	Sn(11)-S(11)-Sn(18)	108.97(14)	Cu(9)-S(27)-Sn(6)	101.9(2)
C(151)-P(4)-Cu(7)	125.7(7)	Cu(5)-S(12)-Cu(3)	81.97(13)	Cu(9)-S(27)-Sn(5)	97.0(2)
C(157)-P(4)-Cu(7)	109.2(8)	Cu(5)-S(12)-Sn(12)	100.76(15)	Sn(6)-S(27)-Sn(5)	107.13(13)
C(139)-P(4)-Cu(7)	109.5(8)	Cu(3)-S(12)-Sn(12)	98.1(2)	Sn(6)-S(28)-Sn(3)	104.34(19)
C(139)-P(4B)-C(151)	98.7(10)	Cu(3)-S(13)-Sn(18)	104.37(15)	Sn(5)-S(29)-Sn(9)	103.40(16)
C(139)-P(4B)-Cu(7)	131.2(9)	Cu(3)-S(13)-Sn(1)	97.10(15)	Sn(5)-S(29)-Cu(7)	114.25(16)
C(151)-P(4B)-Cu(7)	113.0(7)	Sn(18)-S(13)-Sn(1)	100.26(16)	Sn(9)-S(29)-Cu(7)	88.23(16)
Sn(17)-S(1)-Sn(14)	101.81(19)	Sn(11)-S(14)-Sn(1)	101.84(15)	Cu(9)-S(30)-Cu(8)	112.8(2)
Sn(17)-S(2)-Sn(12)	104.24(12)	Sn(15)-S(15)-Sn(12)	101.31(16)	Cu(9)-S(30)-Cu(10)	102.14(16)
Sn(17)-S(2)-Cu(2)	105.37(14)	Cu(3)-S(16)-Sn(15)	103.72(17)	Cu(8)-S(30)-Cu(10)	112.3(3)
Sn(12)-S(2)-Cu(2)	107.6(2)	Cu(3)-S(16)-Sn(17)	97.31(14)	Cu(9)-S(30)-Sn(3)	109.9(3)
Sn(4)-S(3)-Sn(8)	101.76(18)	Sn(15)-S(16)-Sn(17)	105.32(16)	Cu(8)-S(30)-Sn(3)	114.37(17)
Sn(10)-S(4)-Sn(5)	103.21(15)	Sn(18)-S(17)-Sn(14)	105.74(18)	Cu(10)-S(30)-Sn(3)	104.35(18)
Cu(1)-S(5)-Cu(3)	103.54(18)	Sn(4)-S(18)-Sn(15)	100.01(16)	Cu(10)-S(31)-Sn(6)	104.05(15)
Cu(1)-S(5)-Sn(14)	105.16(14)	Sn(7)-S(19)-Sn(8)	102.08(13)	Cu(10)-S(31)-Sn(10)	100.48(18)
Cu(3)-S(5)-Sn(14)	105.44(16)	Sn(7)-S(19)-Cu(8)	106.6(2)	Sn(6)-S(31)-Sn(10)	100.43(14)
Cu(1)-S(5)-Cu(2)	115.01(19)	Sn(8)-S(19)-Cu(8)	106.95(18)	S(11)-Cu(1)-S(5)	114.45(19)
Cu(3)-S(5)-Cu(2)	113.20(15)	Cu(6)-S(20)-Cu(10)	80.49(19)	S(11)-Cu(1)-S(7)	106.54(14)
Sn(14)-S(5)-Cu(2)	113.45(19)	Cu(6)-S(20)-Sn(8)	101.15(15)	S(5)-Cu(1)-S(7)	106.25(17)
Cu(5)-S(6)-Sn(13)	106.58(17)	Cu(10)-S(20)-Sn(8)	96.02(18)	S(11)-Cu(1)-S(10)	113.86(17)
Cu(5)-S(6)-Cu(2)	88.81(17)	Cu(10)-S(21)-Sn(7)	97.75(14)	S(5)-Cu(1)-S(10)	102.27(15)
Sn(13)-S(6)-Cu(2)	101.70(14)	Cu(10)-S(21)-Sn(4)	106.2(2)	S(7)-Cu(1)-S(10)	113.38(17)
Cu(1)-S(7)-Sn(16)	95.94(16)	Sn(7)-S(21)-Sn(4)	101.59(17)	P(2)-Cu(2)-S(5)	132.68(17)
Cu(1)-S(7)-Sn(13)	94.46(12)	Sn(7)-S(22)-Sn(3)	101.88(18)	P(2)-Cu(2)-S(6)	116.05(18)
Sn(16)-S(7)-Sn(13)	91.10(16)	Cu(6)-S(23)-Sn(2)	105.0(2)	S(5)-Cu(2)-S(6)	99.04(17)
Cu(4)-S(8)-Sn(13)	112.66(19)	Cu(6)-S(23)-Cu(8)	88.94(18)	P(2)-Cu(2)-S(2)	98.01(19)
Cu(4)-S(8)-Sn(16)	85.23(12)	Sn(2)-S(23)-Cu(8)	104.3(2)	S(5)-Cu(2)-S(2)	96.93(14)
Sn(13)-S(8)-Sn(16)	87.96(15)	Cu(7)-S(24)-Sn(2)	114.23(16)	S(6)-Cu(2)-S(2)	111.98(15)

S(12)-Cu(3)-S(5)	112.18(15)	S(30)-Cu(8)-S(23)	100.31(18)	C(85)-Sn(4)-S(3)	108.1(4)
S(12)-Cu(3)-S(13)	107.55(17)	P(1)-Cu(8)-S(19)	97.33(18)	S(18)-Sn(4)-S(3)	114.68(18)
S(5)-Cu(3)-S(13)	113.73(15)	S(30)-Cu(8)-S(19)	97.48(16)	C(85)-Sn(4)-S(21)	110.2(4)
S(12)-Cu(3)-S(16)	114.26(17)	S(23)-Cu(8)-S(19)	111.4(2)	S(18)-Sn(4)-S(21)	100.93(14)
S(5)-Cu(3)-S(16)	108.62(17)	S(30)-Cu(9)-S(27)	109.1(2)	S(3)-Sn(4)-S(21)	110.90(15)
S(13)-Cu(3)-S(16)	100.00(17)	S(30)-Cu(9)-S(25)	106.23(15)	C(19)-Sn(5)-S(29)	110.0(4)
S(12)-Cu(3)-Cu(5)	47.64(11)	S(27)-Cu(9)-S(25)	105.1(2)	C(19)-Sn(5)-S(4)	102.3(4)
S(5)-Cu(3)-Cu(5)	67.87(12)	S(30)-Cu(9)-S(26)	106.1(2)	S(29)-Sn(5)-S(4)	104.37(18)
S(13)-Cu(3)-Cu(5)	111.24(17)	S(27)-Cu(9)-S(26)	115.47(18)	C(19)-Sn(5)-S(27)	115.9(4)
S(16)-Cu(3)-Cu(5)	147.30(14)	S(25)-Cu(9)-S(26)	114.40(19)	S(29)-Sn(5)-S(27)	117.84(16)
P(3)-Cu(4)-S(10)	122.57(17)	S(20)-Cu(10)-S(30)	113.5(2)	S(4)-Sn(5)-S(27)	104.35(14)
P(3)-Cu(4)-S(9)	124.3(2)	S(20)-Cu(10)-S(31)	107.16(18)	C(25)-Sn(6)-S(28)	107.8(4)
S(10)-Cu(4)-S(9)	101.47(17)	S(30)-Cu(10)-S(31)	112.53(19)	C(25)-Sn(6)-S(31)	109.2(4)
P(3)-Cu(4)-S(8)	108.85(18)	S(20)-Cu(10)-S(21)	114.96(19)	S(28)-Sn(6)-S(31)	107.93(16)
S(10)-Cu(4)-S(8)	100.69(18)	S(30)-Cu(10)-S(21)	108.17(17)	C(25)-Sn(6)-S(27)	113.9(4)
S(9)-Cu(4)-S(8)	92.77(13)	S(31)-Cu(10)-S(21)	99.79(16)	S(28)-Sn(6)-S(27)	103.34(14)
S(6)-Cu(5)-S(12)	135.6(2)	S(20)-Cu(10)-Cu(6)	48.40(12)	S(31)-Sn(6)-S(27)	114.13(19)
S(6)-Cu(5)-S(10)	111.41(16)	S(30)-Cu(10)-Cu(6)	68.58(15)	C(163)-Sn(7)-S(22)	108.0(4)
S(12)-Cu(5)-S(10)	112.82(16)	S(31)-Cu(10)-Cu(6)	109.80(13)	C(163)-Sn(7)-S(21)	112.2(4)
S(6)-Cu(5)-Cu(3)	125.90(17)	S(21)-Cu(10)-Cu(6)	149.18(16)	S(22)-Sn(7)-S(21)	101.42(17)
S(12)-Cu(5)-Cu(3)	50.39(11)	C(49)-Sn(1)-S(10)	113.3(4)	C(163)-Sn(7)-S(19)	107.6(5)
S(10)-Cu(5)-Cu(3)	90.25(13)	C(49)-Sn(1)-S(14)	111.7(4)	S(22)-Sn(7)-S(19)	116.05(17)
S(23)-Cu(6)-S(20)	133.2(2)	S(10)-Sn(1)-S(14)	109.44(14)	S(21)-Sn(7)-S(19)	111.53(16)
S(23)-Cu(6)-S(26)	114.84(17)	C(49)-Sn(1)-S(13)	105.7(5)	C(133)-Sn(8)-S(20)	114.9(4)
S(20)-Cu(6)-S(26)	111.94(17)	S(10)-Sn(1)-S(13)	111.11(16)	C(133)-Sn(8)-S(3)	105.4(4)
S(23)-Cu(6)-Cu(10)	125.31(16)	S(14)-Sn(1)-S(13)	105.22(16)	S(20)-Sn(8)-S(3)	112.43(13)
S(20)-Cu(6)-Cu(10)	51.11(17)	C(109)-Sn(2)-S(23)	107.9(4)	C(133)-Sn(8)-S(19)	103.9(4)
S(26)-Cu(6)-Cu(10)	91.57(17)	C(109)-Sn(2)-S(24)	104.9(4)	S(20)-Sn(8)-S(19)	115.05(18)
P(4B)-Cu(7)-S(26)	118.3(6)	S(23)-Sn(2)-S(24)	122.38(15)	S(3)-Sn(8)-S(19)	104.07(17)
S(26)-Cu(7)-P(4)	143.6(4)	C(109)-Sn(2)-S(25)	115.2(4)	C(13)-Sn(9)-S(25)	117.7(4)
P(4B)-Cu(7)-S(24)	127.5(5)	S(23)-Sn(2)-S(25)	114.75(16)	C(13)-Sn(9)-S(29)	119.8(4)
S(26)-Cu(7)-S(24)	101.76(15)	S(24)-Sn(2)-S(25)	91.19(17)	S(25)-Sn(9)-S(29)	122.31(12)
P(4)-Cu(7)-S(24)	108.1(4)	C(121)-Sn(3)-S(30)	118.4(6)	C(13)-Sn(9)-Cl(1)	94.3(5)
P(4B)-Cu(7)-S(29)	112.4(4)	C(121)-Sn(3)-S(22)	104.2(5)	S(25)-Sn(9)-Cl(1)	86.72(17)
S(26)-Cu(7)-S(29)	98.8(2)	S(30)-Sn(3)-S(22)	107.8(2)	S(29)-Sn(9)-Cl(1)	85.07(16)
P(4)-Cu(7)-S(29)	100.5(3)	C(121)-Sn(3)-S(28)	105.7(6)	C(13)-Sn(9)-S(24)	100.7(5)
S(24)-Cu(7)-S(29)	91.80(18)	S(30)-Sn(3)-S(28)	111.06(15)	S(25)-Sn(9)-S(24)	86.89(16)
P(1)-Cu(8)-S(30)	134.7(2)	S(22)-Sn(3)-S(28)	109.23(16)	S(29)-Sn(9)-S(24)	86.88(16)
P(1)-Cu(8)-S(23)	113.41(19)	C(85)-Sn(4)-S(18)	111.9(4)	Cl(1)-Sn(9)-S(24)	164.96(13)

C(79)-Sn(10)-S(26)	122.9(5)	S(6)-Sn(13)-S(8)	119.39(14)	S(7)-Sn(16)-Cl(2)	85.96(15)
C(79)-Sn(10)-S(4)	106.4(4)	C(61)-Sn(13)-S(7)	110.2(4)	S(9)-Sn(16)-Cl(2)	88.07(13)
S(26)-Sn(10)-S(4)	109.73(15)	S(6)-Sn(13)-S(7)	118.08(15)	C(43)-Sn(16)-S(8)	97.3(4)
C(79)-Sn(10)-S(31)	101.9(4)	S(8)-Sn(13)-S(7)	91.84(15)	S(7)-Sn(16)-S(8)	87.70(14)
S(26)-Sn(10)-S(31)	108.98(13)	C(97)-Sn(14)-S(5)	115.3(4)	S(9)-Sn(16)-S(8)	85.65(12)
S(4)-Sn(10)-S(31)	105.35(19)	C(97)-Sn(14)-S(17)	110.0(4)	Cl(2)-Sn(16)-S(8)	166.78(13)
C(31)-Sn(11)-S(14)	107.2(3)	S(5)-Sn(14)-S(17)	110.94(15)	C(145)-Sn(17)-S(1)	104.4(5)
C(31)-Sn(11)-S(9)	108.0(5)	C(97)-Sn(14)-S(1)	105.1(5)	C(145)-Sn(17)-S(2)	110.5(5)
S(14)-Sn(11)-S(9)	106.39(15)	S(5)-Sn(14)-S(1)	106.75(15)	S(1)-Sn(17)-S(2)	117.48(14)
C(31)-Sn(11)-S(11)	113.0(4)	S(17)-Sn(14)-S(1)	108.33(17)	C(145)-Sn(17)-S(16)	110.3(5)
S(14)-Sn(11)-S(11)	104.57(16)	C(103)-Sn(15)-S(15)	107.5(4)	S(1)-Sn(17)-S(16)	102.64(15)
S(9)-Sn(11)-S(11)	117.02(14)	C(103)-Sn(15)-S(18)	111.1(4)	S(2)-Sn(17)-S(16)	110.98(16)
C(91)-Sn(12)-S(12)	115.7(5)	S(15)-Sn(15)-S(18)	116.29(17)	C(37)-Sn(18)-S(17)	111.1(5)
C(91)-Sn(12)-S(15)	106.9(4)	C(103)-Sn(15)-S(16)	111.2(4)	C(37)-Sn(18)-S(13)	110.8(4)
S(12)-Sn(12)-S(15)	110.96(15)	S(15)-Sn(15)-S(16)	110.95(12)	S(17)-Sn(18)-S(13)	108.26(16)
C(91)-Sn(12)-S(2)	104.7(4)	S(18)-Sn(15)-S(16)	99.77(15)	C(37)-Sn(18)-S(11)	109.0(5)
S(12)-Sn(12)-S(2)	113.28(13)	C(43)-Sn(16)-S(7)	121.5(4)	S(17)-Sn(18)-S(11)	102.69(15)
S(15)-Sn(12)-S(2)	104.33(17)	C(43)-Sn(16)-S(9)	115.6(4)	S(13)-Sn(18)-S(11)	114.76(13)
C(61)-Sn(13)-S(6)	107.6(4)	S(7)-Sn(16)-S(9)	122.88(14)		
C(61)-Sn(13)-S(8)	108.9(5)	C(43)-Sn(16)-Cl(2)	95.9(4)		

2. Single-Crystal X-Ray Crystallography of Compound 2

Compound **2** crystallizes in the shape of yellow rods. Data of the X-Ray diffraction analysis was collected on a STOE STADIVARI diffractometer using Cu K_α radiation (λ = 1.54186 Å) from an X-ray micro source with X-ray optics and a Pilatus 300K Si hybrid pixel array detector at 100 K. Reflection data were processed with X-Area 1.77.[1] Structure solution was performed by direct methods and full-matrix-least-squares refinement against F^2 using SHELXT[2] and SHELXL-2014[3] software. All non-hydrogen atoms were refined anisotropically, though the carbon atoms had to be constrained by EADP due to severe rotational disorder of the phenyl groups. Hydrogen atom positions were calculated.

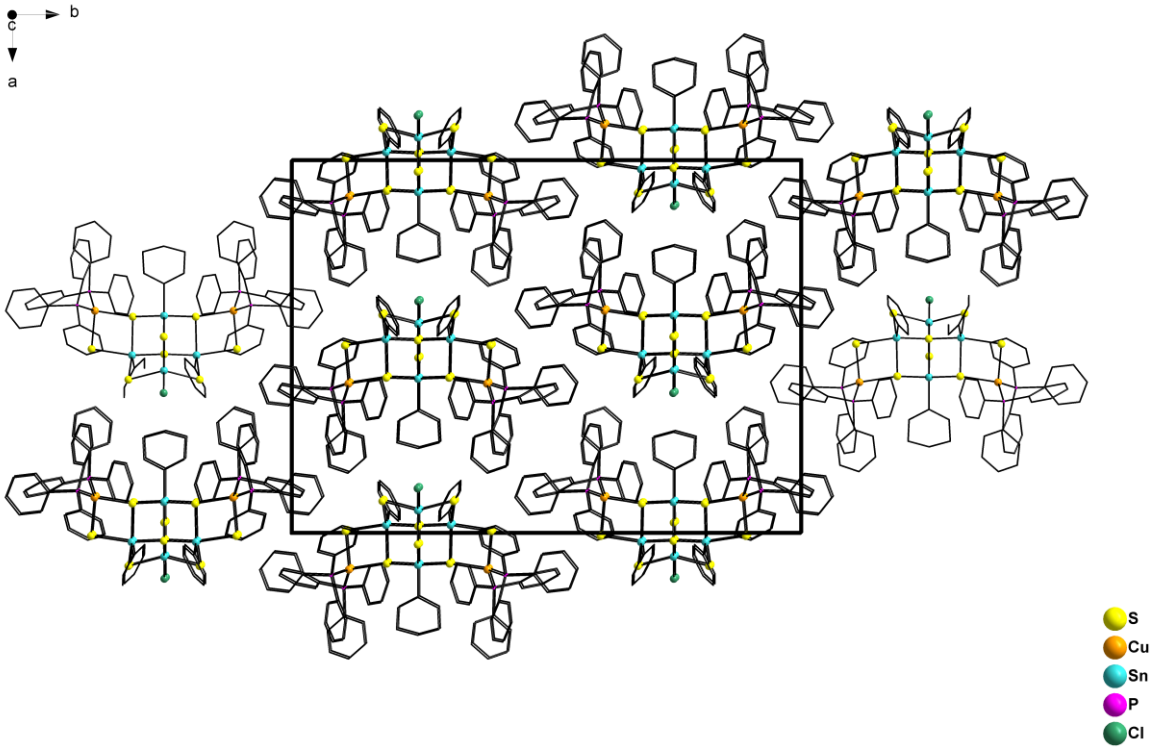

Figure S4: Crystal structure of **2**, viewed along the crystallographic *c* axis. Hydrogen atoms and the disorder of the organic substituents are omitted for clarity.

Table S4: Crystal data and structure refinement for **2** (CCDC 1875755).

Empirical formula	$C_{90}H_{75}Cl_1Cu_2P_4S_8Sn_4$	
Formula weight	2174.35	
Temperature	100(2) K	
Wavelength	1.54178 Å	
Crystal system	Orthorhombic	
Space group	*Pnma*	
Unit cell dimensions	*a* = 23.3984(3) Å	*α*= 90°.
	b = 31.9765(4) Å	*β*= 90°.
	c = 11.6160(2) Å	*γ* = 90°.
Volume	8691.1(2) $Å^3$	
Z	8	
Density (calculated)	1.662 Mg/m^3	
Absorption coefficient	12.657 mm^{-1}	
F(000)	4312	
Crystal size	0.12 x 0.05 x 0.03 mm^3	
Theta range for data collection	2.764 to 73.958°.	
Index ranges	-29<=h<=21, -37<=k<=39, -14<=l<=14	
Reflections collected	152483	
Independent reflections	8919 [R(int) = 0.1622]	
Completeness to theta = 67.679°	99.8 %	
Refinement method	Full-matrix least-squares on F^2	
Data / restraints / parameters	8919 / 3 / 166	
Goodness-of-fit on F^2	1.433	
Final R indices [I>2sigma(I)]	R1 = 0.0880, wR2 = 0.2299	
R indices (all data)	R1 = 0.1326, wR2 = 0.2483	
Largest diff. peak and hole	1.875 and -1.605 $e.Å^{-3}$	

Table S5: Atomic coordinates (x 10^4) and equivalent isotropic displacement parameters ($Å^2$x 10^3) for **2**. U(eq) is defined as one third of the trace of the orthogonalized U^{ij} tensor.

	x	y	z	U(eq)
C(1)	3669(6)	5527(3)	3643(9)	109(1)
C(2)	3919(5)	5201(4)	4253(7)	109(1)
C(3)	4019(5)	4820(3)	3715(9)	109(1)
C(4)	3868(5)	4764(3)	2567(9)	109(1)
C(5)	3618(5)	5090(4)	1958(7)	109(1)
C(6)	3518(5)	5472(3)	2496(9)	109(1)
C(7)	3567(6)	6398(4)	3130(8)	109(1)
C(8)	4104(5)	6529(4)	2764(9)	109(1)
C(9)	4157(4)	6770(4)	1773(10)	109(1)
C(10)	3673(6)	6880(4)	1149(8)	109(1)
C(11)	3136(5)	6750(4)	1516(9)	109(1)
C(12)	3083(4)	6509(4)	2506(10)	109(1)
C(13)	2770(4)	6038(4)	4714(10)	109(1)
C(14)	2382(6)	5714(3)	4553(9)	109(1)
C(15)	1818(5)	5760(3)	4909(10)	109(1)
C(16)	1643(4)	6131(4)	5427(9)	109(1)
C(17)	2031(6)	6455(3)	5588(9)	109(1)
C(18)	2594(5)	6408(4)	5231(10)	109(1)
C(19)	5585(9)	6907(7)	4107(12)	109(1)
C(20)	5328(8)	7104(6)	3174(17)	109(1)
C(21)	5593(9)	7100(6)	2104(14)	109(1)
C(22)	6117(9)	6901(7)	1966(13)	109(1)
C(23)	6374(8)	6704(6)	2899(17)	109(1)
C(24)	6109(9)	6708(6)	3970(14)	109(1)
C(19B)	5798(12)	6933(10)	4210(20)	109(1)
C(20B)	5708(12)	6710(9)	3190(30)	109(1)
C(21B)	6100(14)	6739(9)	2300(20)	109(1)
C(22B)	6581(12)	6990(10)	2410(20)	109(1)
C(23B)	6671(12)	7213(9)	3430(20)	109(1)
C(24B)	6279(14)	7184(9)	4320(20)	109(1)
C(25)	3904(6)	5229(3)	7359(10)	109(1)
C(26)	3437(4)	4960(4)	7389(9)	109(1)
C(27)	3504(5)	4542(4)	7086(10)	109(1)
C(28)	4037(6)	4393(3)	6753(9)	109(1)
C(29)	4503(4)	4662(4)	6722(9)	109(1)
C(30)	4437(5)	5080(4)	7025(9)	109(1)
C(31)	4411(5)	5849(4)	8771(8)	109(1)

C(32)	4687(5)	6233(3)	8849(9)	109(1)
C(33)	5080(5)	6304(3)	9726(10)	109(1)
C(34)	5196(5)	5992(4)	10524(8)	109(1)
C(35)	4920(5)	5608(3)	10445(8)	109(1)
C(36)	4528(5)	5537(3)	9569(10)	109(1)
C(37)	3303(12)	7500	7770(20)	109(1)
C(38)	3025(8)	7107(6)	8005(14)	109(1)
C(40)	2293(12)	7500	8750(20)	109(1)
C(39)	2447(8)	7086(5)	8463(15)	109(1)
C(43)	3179(8)	5921(7)	8443(17)	109(1)
C(44)	2692(10)	6071(7)	7894(14)	109(1)
C(45)	2160(9)	6025(7)	8410(17)	109(1)
C(46)	2114(8)	5830(7)	9475(17)	109(1)
C(47)	2601(10)	5680(7)	10024(14)	109(1)
C(48)	3133(8)	5726(7)	9508(17)	109(1)
C(43B)	3225(12)	5836(9)	8420(20)	109(1)
C(44B)	2711(15)	5740(9)	7880(19)	109(1)
C(45B)	2196(12)	5853(9)	8390(20)	109(1)
C(46B)	2195(11)	6062(9)	9440(20)	109(1)
C(47B)	2709(14)	6158(9)	9979(19)	109(1)
C(48B)	3224(11)	6045(9)	9470(20)	109(1)
S(1)	4198(1)	6883(1)	5909(2)	54(1)
S(2)	5200(5)	7500	6242(11)	175(4)
S(3)	5066(1)	6073(1)	5576(3)	64(1)
S(4)	5880(1)	6801(1)	7300(3)	63(1)
S(5)	4722(2)	7500	8859(4)	61(1)
Cu(1)	4039(1)	6140(1)	5974(1)	55(1)
Sn(1)	4165(1)	7500	7120(1)	50(1)
Sn(2)	5233(1)	6868(1)	5719(1)	51(1)
Sn(3)	5634(1)	7500	7895(1)	61(1)
P(1)	3532(1)	6025(1)	4338(2)	51(1)
P(2)	3880(2)	5794(1)	7642(3)	66(1)
Cl(1)	6231(3)	7500	9560(5)	121(3)

Table S6: Bond lengths [Å] and angles [°] for **2**.

(1)-P(1)	1.813(9)	C(24)-C(19)-Sn(2)	115.5(11)	S(5)-Sn(1)-S(1)#1	118.09(9)
C(7)-P(1)	1.845(8)	C(20B)-C(19B)-Sn(2)	122.3(16)	S(1)-Sn(1)-S(1)#1	108.90(14)
C(13)-P(1)	1.836(10)	C(24B)-C(19B)-Sn(2)	117.5(16)	C(37)-Sn(1)-S(2)	177.6(7)
C(19)-Sn(2)	2.050(14)	C(26)-C(25)-P(2)	125.4(8)	S(5)-Sn(1)-S(2)	80.0(3)
C(19B)-Sn(2)	2.21(2)	C(30)-C(25)-P(2)	114.4(8)	S(1)-Sn(1)-S(2)	75.25(16)
C(25)-P(2)	1.836(10)	C(32)-C(31)-P(2)	116.9(7)	S(1)#1-Sn(1)-S(2)	75.25(16)
C(31)-P(2)	1.815(9)	C(36)-C(31)-P(2)	123.1(7)	C(19)-Sn(2)-S(2)	102.6(7)
C(37)-C(38)	1.443(15)	C(38)-C(37)-C(38)#1	121(3)	S(2)-Sn(2)-C(19B)	99.3(9)
C(37)-C(38)#1	1.443(15)	C(38)-C(37)-Sn(1)	119.3(13)	C(19)-Sn(2)-S(4)	116.9(6)
C(37)-Sn(1)	2.15(3)	C(38)#1-C(37)-Sn(1)	119.3(13)	S(2)-Sn(2)-S(4)	83.6(3)
C(38)-C(39)	1.455(15)	C(37)-C(38)-C(39)	122(2)	C(19B)-Sn(2)-S(4)	103.9(8)
C(40)-C(39)#1	1.411(15)	C(39)#1-C(40)-C(39)	139(3)	C(19)-Sn(2)-S(1)	118.8(6)
C(40)-C(39)	1.411(15)	C(40)-C(39)-C(38)	106(2)	S(2)-Sn(2)-S(1)	85.3(4)
C(43)-P(2)	1.930(19)	C(44)-C(43)-P(2)	123.2(12)	C(19B)-Sn(2)-S(1)	131.8(8)
C(43B)-P(2)	1.79(2)	C(48)-C(43)-P(2)	113.6(12)	S(4)-Sn(2)-S(1)	124.28(11)
S(1)-Cu(1)	2.408(3)	C(44B)-C(43B)-P(2)	119.9(19)	C(19)-Sn(2)-S(3)	93.6(6)
S(1)-Sn(1)	2.423(3)	C(48B)-C(43B)-P(2)	118.7(19)	S(2)-Sn(2)-S(3)	163.1(4)
S(1)-Sn(2)	2.431(3)	Cu(1)-S(1)-Sn(1)	141.29(14)	C(19B)-Sn(2)-S(3)	97.6(8)
S(2)-Sn(2)	2.113(4)	Cu(1)-S(1)-Sn(2)	97.85(11)	S(4)-Sn(2)-S(3)	93.26(11)
S(2)-Sn(2)#1	2.113(4)	Sn(1)-S(1)-Sn(2)	95.80(10)	S(1)-Sn(2)-S(3)	82.87(10)
S(2)-Sn(3)	2.172(12)	Sn(2)-S(2)-Sn(2)#1	146.3(7)	S(2)-Sn(3)-Cl(1)	172.0(4)
S(2)-Sn(1)	2.626(13)	Sn(2)-S(2)-Sn(3)	103.7(3)	S(2)-Sn(3)-S(5)	89.8(4)
S(3)-Cu(1)	2.457(4)	Sn(2)#1-S(2)-Sn(3)	103.7(3)	Cl(1)-Sn(3)-S(5)	98.16(19)
S(3)-Sn(2)	2.576(3)	Sn(2)-S(2)-Sn(1)	98.4(4)	S(2)-Sn(3)-S(4)#1	81.87(15)
S(4)-Sn(2)	2.391(3)	Sn(2)#1-S(2)-Sn(1)	98.4(4)	Cl(1)-Sn(3)-S(4)#1	95.28(10)
S(4)-Sn(3)	2.410(3)	Sn(3)-S(2)-Sn(1)	95.0(5)	S(5)-Sn(3)-S(4)#1	110.20(8)
S(5)-Sn(1)	2.403(4)	Cu(1)-S(3)-Sn(2)	92.86(10)	S(2)-Sn(3)-S(4)	81.87(15)
S(5)-Sn(3)	2.410(5)	Sn(2)-S(4)-Sn(3)	89.16(10)	Cl(1)-Sn(3)-S(4)	95.28(10)
Cu(1)-P(2)	2.262(3)	Sn(1)-S(5)-Sn(3)	95.12(15)	S(5)-Sn(3)-S(4)	110.20(8)
Cu(1)-P(1)	2.270(3)	P(2)-Cu(1)-P(1)	123.50(13)	S(4)#1-Sn(3)-S(4)	136.13(16)
Sn(3)-Cl(1)	2.385(5)	P(2)-Cu(1)-S(1)	122.38(13)	C(1)-P(1)-C(13)	107.3(6)
		P(1)-Cu(1)-S(1)	102.41(11)	C(1)-P(1)-C(7)	102.8(6)
C(2)-C(1)-P(1)	120.4(7)	P(2)-Cu(1)-S(3)	106.18(14)	C(13)-P(1)-C(7)	102.0(6)
C(6)-C(1)-P(1)	119.6(7)	P(1)-Cu(1)-S(3)	109.86(13)	C(1)-P(1)-Cu(1)	115.0(4)
C(8)-C(7)-P(1)	117.9(7)	S(1)-Cu(1)-S(3)	85.90(11)	C(13)-P(1)-Cu(1)	107.7(4)
C(12)-C(7)-P(1)	121.6(7)	C(37)-Sn(1)-S(5)	102.4(7)	C(7)-P(1)-Cu(1)	120.5(4)
C(14)-C(13)-P(1)	125.8(8)	C(37)-Sn(1)-S(1)	103.4(4)	C(43B)-P(2)-C(31)	102.4(11)
C(18)-C(13)-P(1)	114.2(8)	S(5)-Sn(1)-S(1)	118.09(8)	C(43B)-P(2)-C(25)	101.0(11)
C(20)-C(19)-Sn(2)	124.4(11)	C(37)-Sn(1)-S(1)#1	103.4(4)	C(31)-P(2)-C(25)	101.9(6)

C(31)-P(2)-C(43)	102.3(8)	C(43B)-P(2)-Cu(1)	122.5(10)	C(25)-P(2)-Cu(1)	108.8(4)
C(25)-P(2)-C(43)	108.6(8)	C(31)-P(2)-Cu(1)	117.3(4)	C(43)-P(2)-Cu(1)	116.7

Symmetry transformations used to generate equivalent atoms:
#1 x,-y+3/2,z

3. Infrared Spectra of Compounds 1 and 2

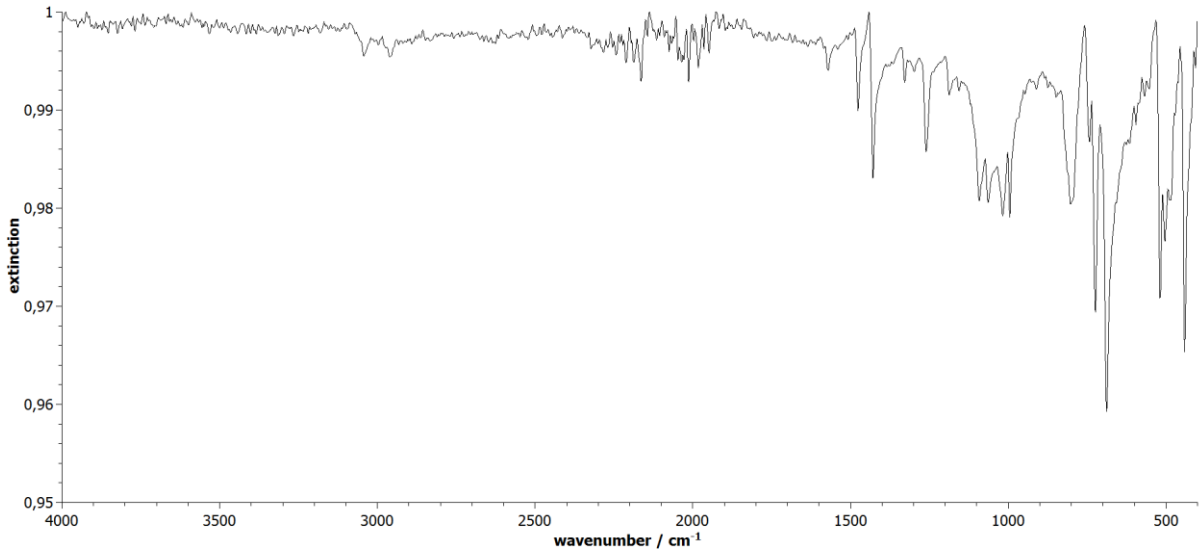

Figure S3: IR spectrum of **1**.

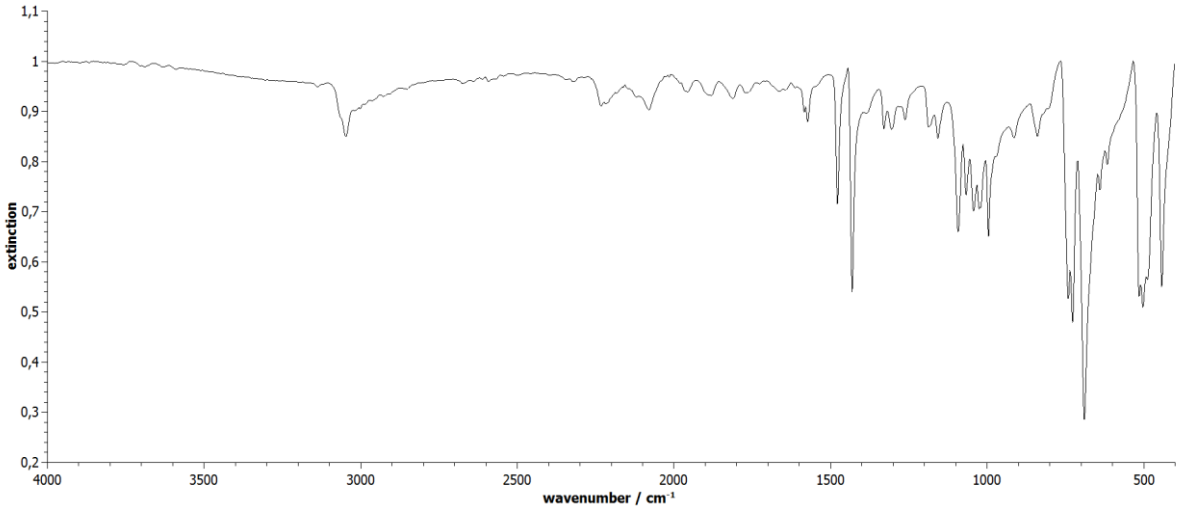

Figure S4: IR spectrum of **2**.

4. NMR Spectra of the Reaction Solutions

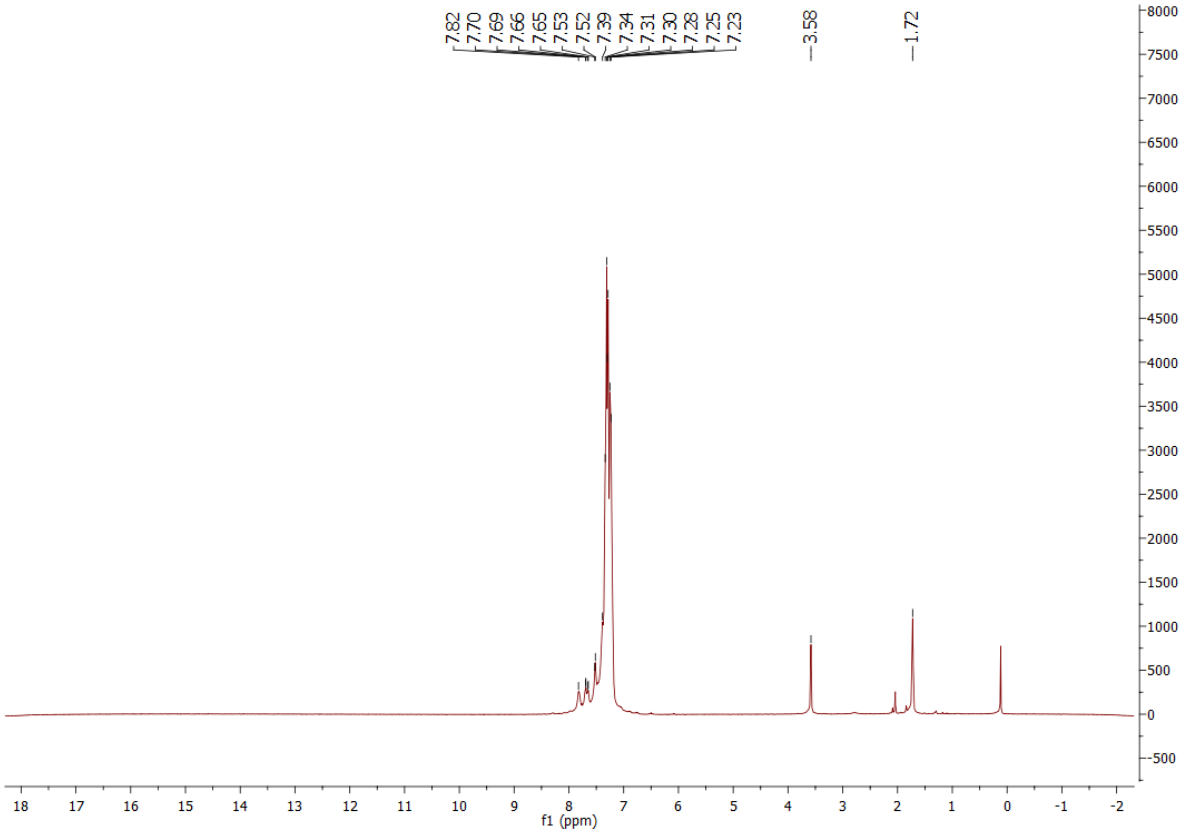

Figure S5: ^{1}H-NMR spectrum of the reaction solution of **1** after 12 hours (300 MHz, THF-d8, room temperature).

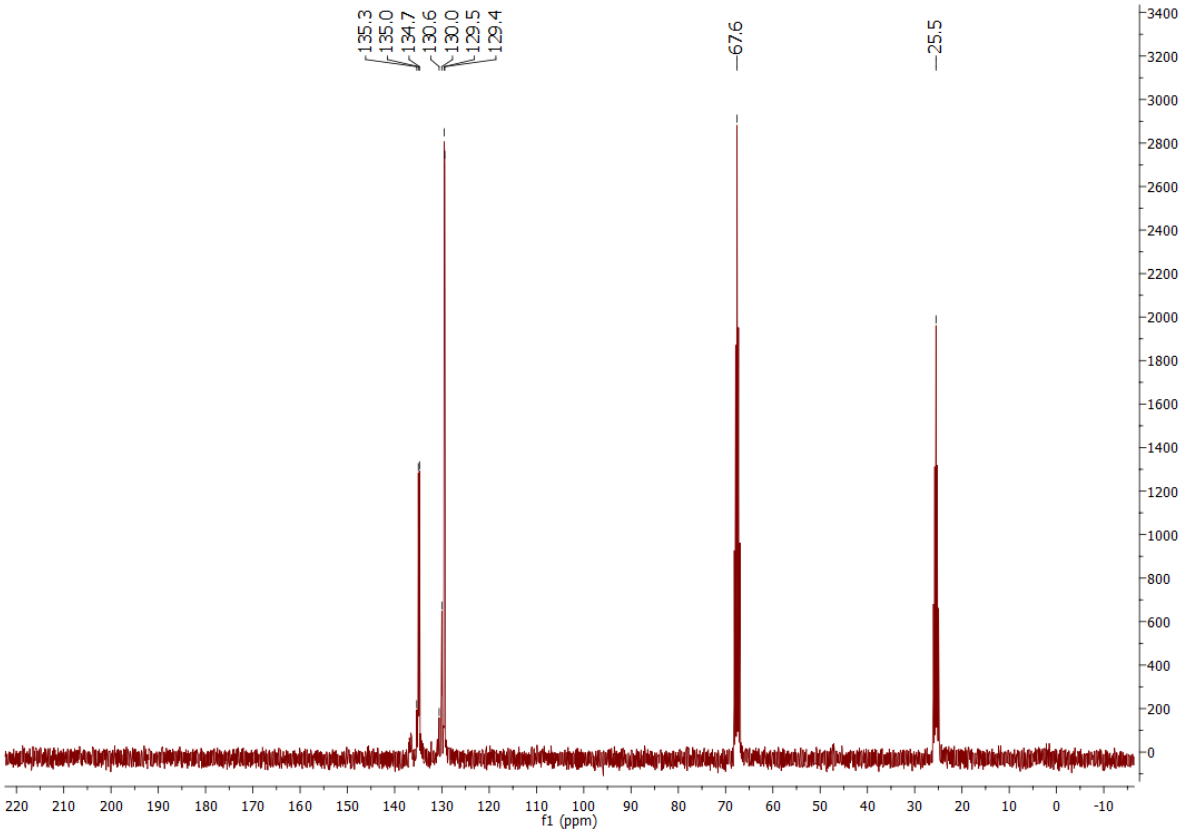

Figure S6: ^{13}C-NMR spectrum of the reaction solution of **1** after 12 hours (75 MHz, THF-d8, room temperature).

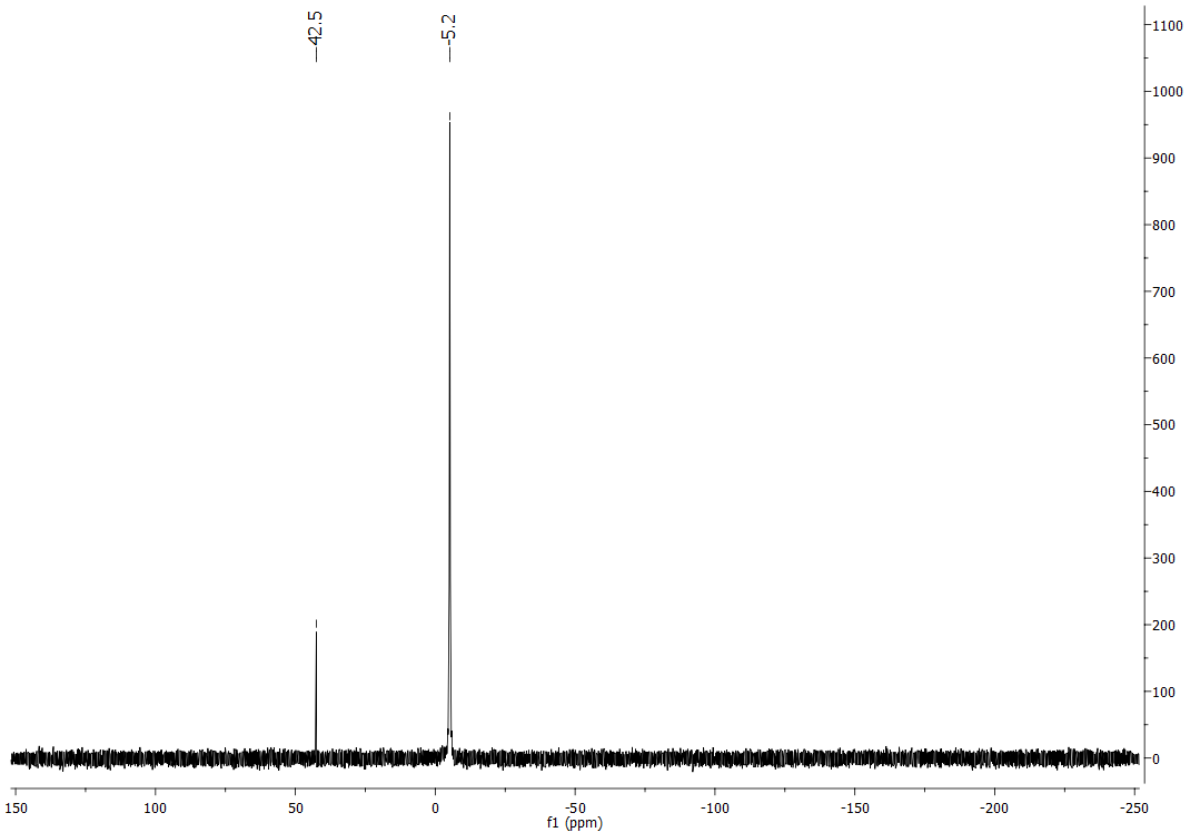

Figure S7: ^{31}**P**-NMR spectrum of the reaction solution of **1** after 12 hours (121 MHz, THF-d8, room temperature).

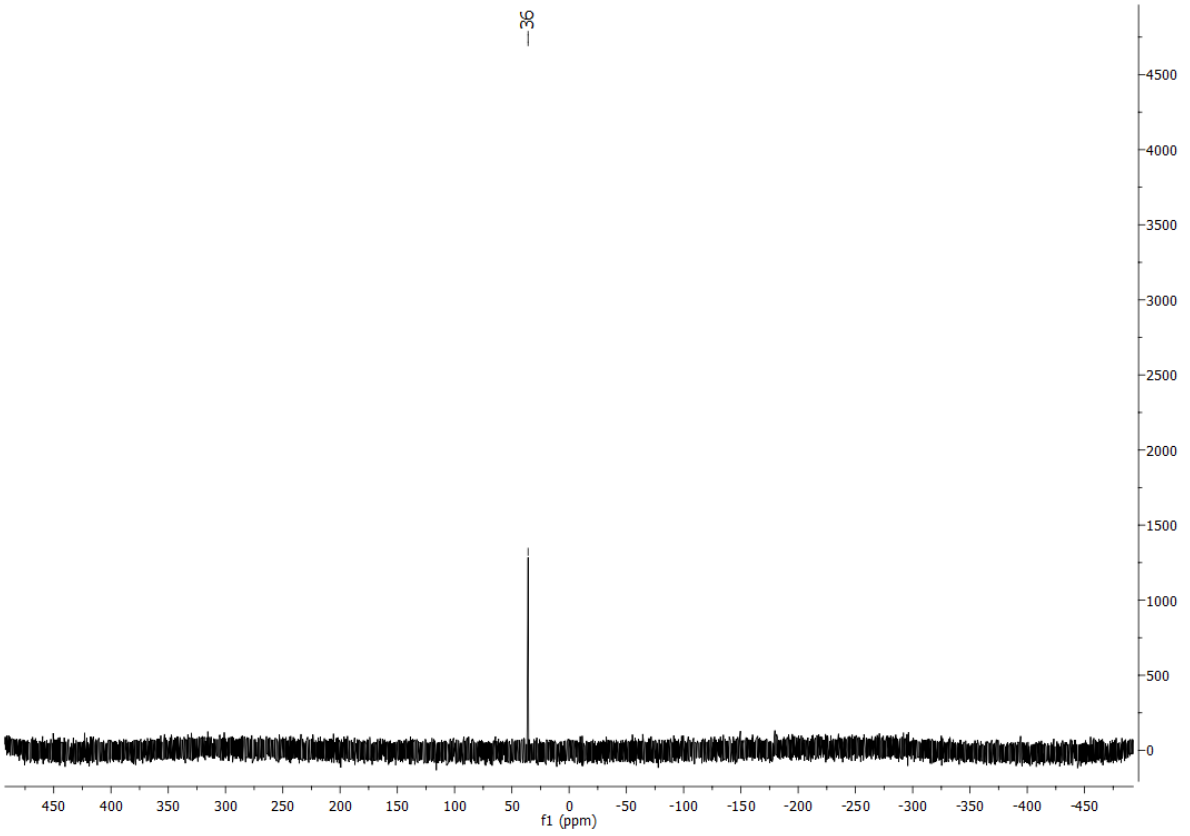

Figure S8: ^{119}Sn-NMR spectrum of the reaction solution of **1** after 12 hours (112 MHz, THF-d8, room temperature).

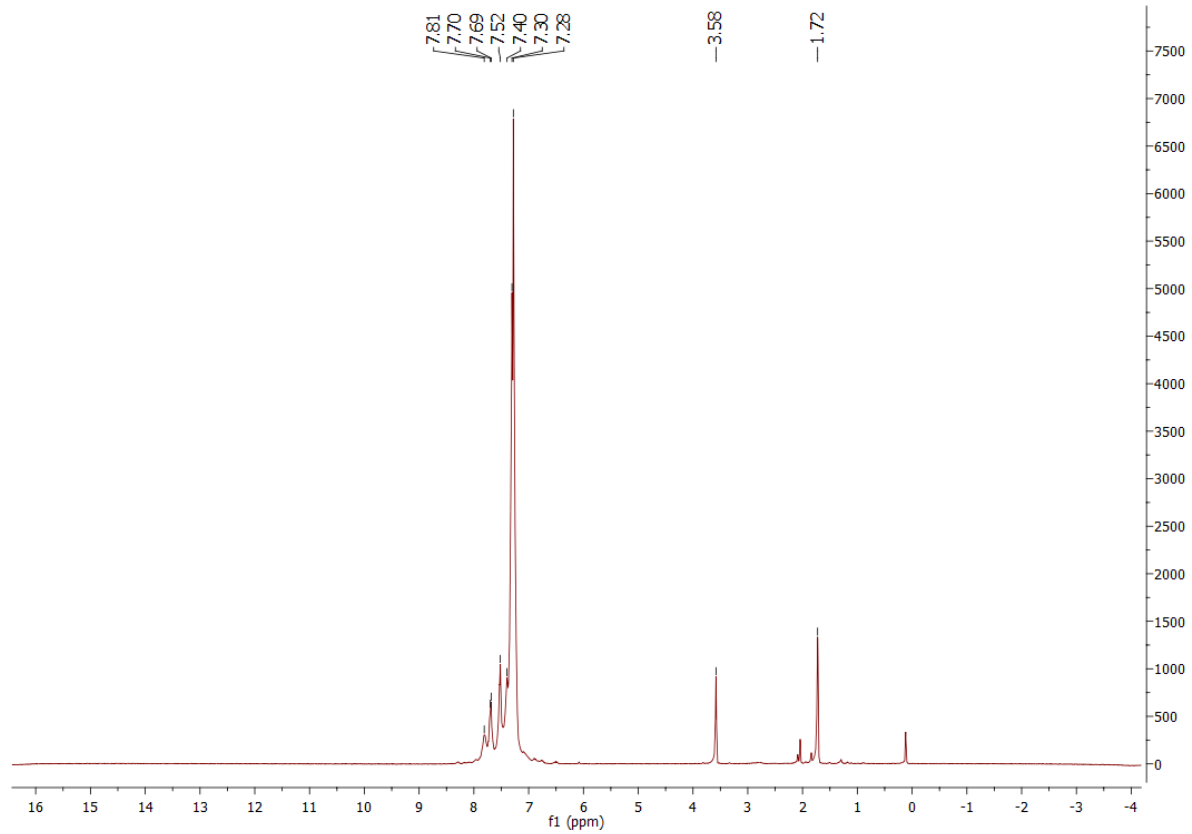

Figure S9: ^{1}H-NMR spectrum of the reaction solution of **2** after 12 hours (300 MHz, THF-d8, room temperature).

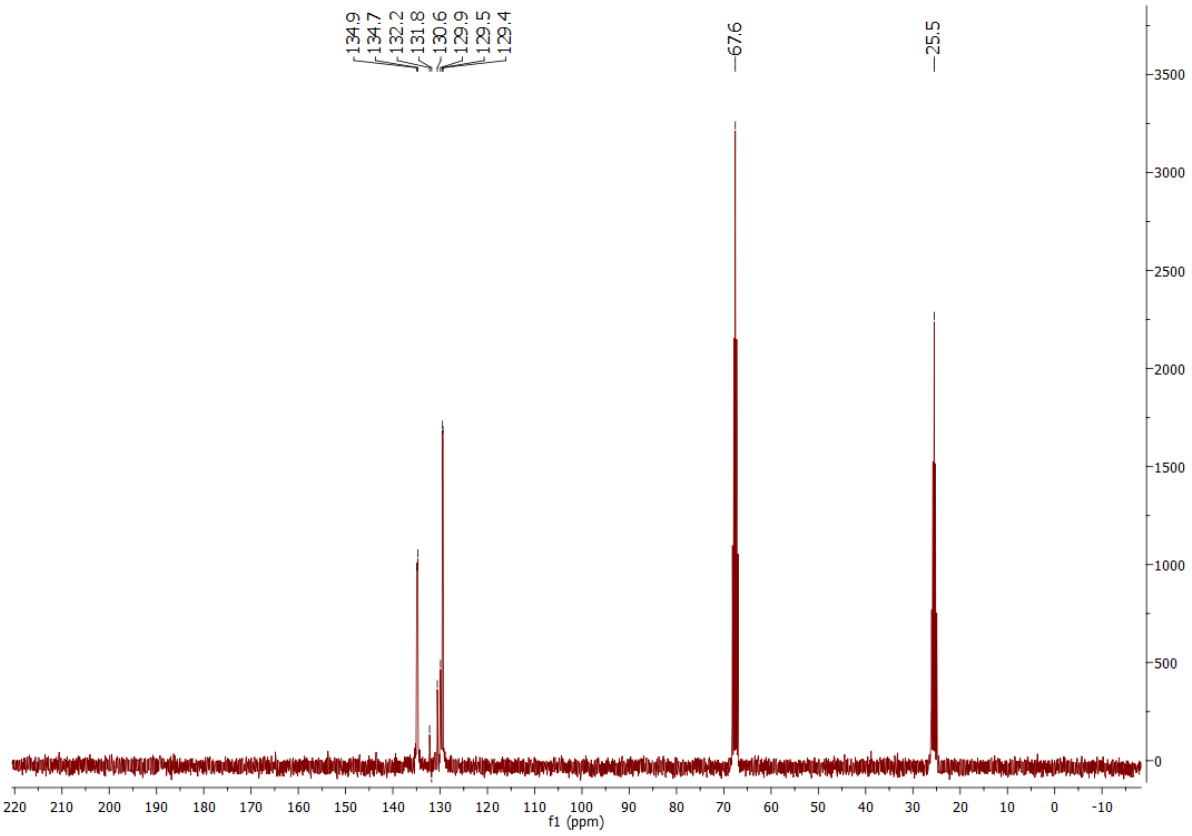

Figure S10: ^{13}C-NMR spectrum of the reaction solution of **2** after 12 hours (75 MHz, THF-d8, room temperature).

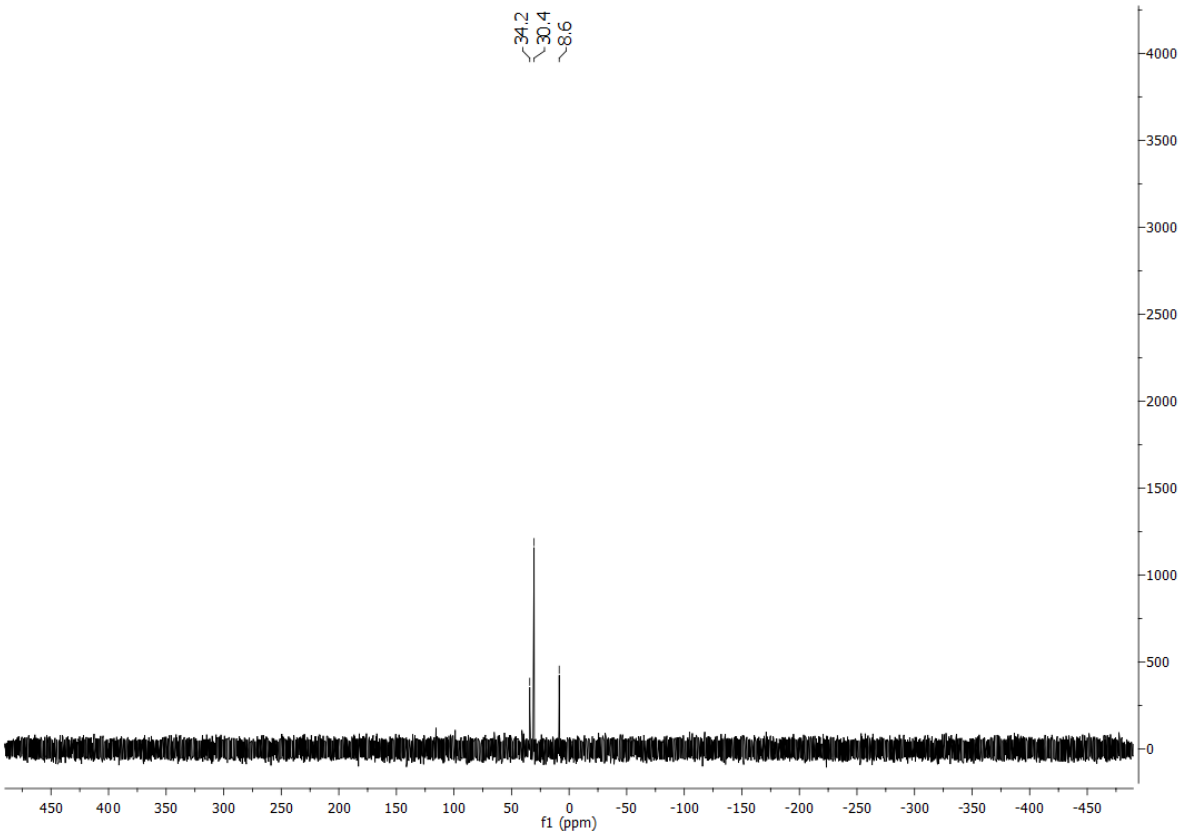

Figure S11: ^{31}P-NMR spectrum of the reaction solution of **2** after 12 hours (121 MHz, THF-d8, room temperature).

5. Density Functional Theory Calculations

DFT calculations were carried out with TURBOMOLE[4] using def2-SVP basis sets[5] and taking advantage from the multipole-accelerated resolution-of the-identity method[6] Structures were optimized with the functional BP86[7]. Cartesian coordinates of compounds **1** and **2** are listed in Tables S7 and S8. The B3-LYP functional[8] was employed for the calculation of the excitations. The frontier MOs contributing to the transitions are shown in Figures S9 for **1** and S10 for **2**.

Table S7. Cartesian coordinates of **1** optimized with BP86/def2-SVP in Å.

Number of atoms: 395			
E_{total} (Hartree): −41825.37320449			
C	-0.8402601	9.9368481	-5.2258596
C	-1.5713615	10.7517387	-6.1198365
H	-2.5435125	11.1680096	-5.8142706
C	-1.0722218	11.0178066	-7.4052531
H	-1.6499912	11.6543447	-8.0935001
C	0.1545768	10.4667143	-7.8155994
H	0.5383189	10.6694955	-8.8275698
C	0.8806903	9.6461924	-6.9369247
H	1.8318880	9.1937212	-7.2562375
C	0.3862286	9.3812039	-5.6485689
H	0.9462934	8.7263258	-4.9616462
C	-1.1856133	11.1023673	-2.5498865
C	-1.1917283	10.9929448	-1.1418971
H	-1.3011386	10.0039907	-0.6683618
C	-1.0477680	12.1344158	-0.3364993
H	-1.0538559	12.0254155	0.7580959
C	-0.8748629	13.3951185	-0.9299397
H	-0.7501469	14.2894476	-0.3003680
C	-0.8451994	13.5093709	-2.3303181
H	-0.6933077	14.4929374	-2.8010317
C	-1.0019151	12.3717508	-3.1383879
H	-0.9713369	12.4743588	-4.2329189
C	3.6745841	11.2601348	3.4321275
C	3.1433156	11.8736315	4.5829367
H	2.3317803	11.3819905	5.1419390
C	3.6552112	13.1117526	5.0111525
H	3.2393617	13.5898992	5.9120000
C	4.6912139	13.7358621	4.2948816
H	5.0886310	14.7054005	4.6335962
C	5.2201890	13.1210666	3.1472037
H	6.0323943	13.6066907	2.5836156
C	4.7150891	11.8809257	2.7139431
H	5.1315125	11.3950332	1.8161436
C	1.5754863	6.1657347	6.6655388
C	0.6391121	5.3211959	7.2925252
H	0.0113103	4.6325118	6.7054997
C	0.5030028	5.3541357	8.6922217
H	-0.2316227	4.6963832	9.1821129
C	1.3007142	6.2195697	9.4596622
H	1.1925356	6.2410730	10.5552947
C	2.2356495	7.0589099	8.8294761
H	2.8617362	7.7385668	9.4285959
C	2.3734604	7.0374017	7.4305267
H	3.0993752	7.7045539	6.9399610
C	-1.6879422	3.0350380	4.5582418
C	-1.0619128	1.7946880	4.7854283
H	-0.3265874	1.4003746	4.0672764
C	-1.3781867	1.0486666	5.9344861
H	-0.8991606	0.0710195	6.0969736
C	-2.3118924	1.5460003	6.8598824
H	-2.5571674	0.9599675	7.7592455
C	-2.9359817	2.7853117	6.6349319
H	-3.6728103	3.1737489	7.3555109
C	-2.6298401	3.5315490	5.4826809
H	-3.1385291	4.4930220	5.3085431
C	0.1866666	-4.8615961	7.2959482
C	-0.4428530	-5.5258487	8.3656121
H	-1.2795319	-6.2166853	8.1779043
C	0.0047943	-5.3068644	9.6802032
H	-0.4896055	-5.8236446	10.5177071
C	1.0803307	-4.4354883	9.9242018
H	1.4313454	-4.2695115	10.9546433
C	1.7082109	-3.7771730	8.8535052
H	2.5517265	-3.0943018	9.0392453
C	1.2619700	-3.9849920	7.5355990
H	1.7621311	-3.4573937	6.7081065
C	2.8179235	-2.3113116	3.9596342
C	3.8576748	-2.7671220	4.7956855
H	4.2544801	-3.7903037	4.6972088
C	4.4016246	-1.9053129	5.7652834
H	5.2140793	-2.2624609	6.4178506
C	3.9117123	-0.5944661	5.8971169
H	4.3377384	0.0790266	6.6570150
C	2.8816732	-0.1381671	5.0569114
H	2.5095265	0.8946473	5.1466869
C	2.3319182	-0.9967232	4.0885266
H	1.5286457	-0.6336715	3.4287087
C	-2.4130897	-10.4367745	5.6453241
C	-3.5898644	-11.1494946	5.3444360
H	-4.2418759	-10.8195854	4.5181709
C	-3.9333278	-12.2823844	6.1049266
H	-4.8537325	-12.8390015	5.8675775
C	-3.1074777	-12.6997100	7.1621183
H	-3.3788910	-13.5858355	7.7572273
C	-1.9351380	-11.9844908	7.4610890
H	-1.2860629	-12.3076526	8.2903515
C	-1.5839010	-10.8521696	6.7049189
H	-0.6669564	-10.2880646	6.9391810
C	-2.9252212	-0.2982513	1.4729349
H	-1.9414054	0.0777228	1.7938783
C	-3.8841505	0.6121725	0.9936755
H	-3.6509335	1.6877083	0.9544834
C	-5.1375178	0.1491683	0.5562587
H	-5.8824833	0.8671612	0.1802977
C	-5.4350338	-1.2230617	0.5891377
H	-6.4119384	-1.5917435	0.2406160
C	-4.4801586	-2.1394018	1.0651133
H	-4.7166055	-3.2150944	1.0764947
C	-3.2276033	-1.6740013	1.5125930
C	0.7831197	-11.2692503	-1.3931346
C	0.5311314	-12.6391482	-1.6205035
H	0.1655703	-12.9791735	-2.6005177
C	0.7361393	-13.5743255	-0.5934709
H	0.5278039	-14.6393002	-0.7791778
C	1.1982800	-13.1552916	0.6660089
H	1.3583703	-13.8923807	1.4680744
C	1.4392793	-11.7926304	0.9040748
H	1.7816793	-11.4454308	1.8897824
C	1.2216911	-10.8534895	-0.1169161
H	1.3871611	-9.7831697	0.0840070
C	-2.8092320	-11.3861149	0.5804769
C	-2.6105989	-12.3508035	1.5882022
H	-2.2244102	-12.0604341	2.5782794
C	-2.9080079	-13.7017767	1.3372986
H	-2.7511600	-14.4505420	2.1296003
C	-3.4055661	-14.0939743	0.0825408
H	-3.6418078	-15.1522709	-0.1102993
C	-3.6003113	-13.1347021	-0.9251039
H	-3.9853369	-13.4374395	-1.9114962
C	-3.3018770	-11.7825608	-0.6783687
H	-3.4537804	-11.0364708	-1.4746256
C	-0.4741367	-10.7189408	-3.9929164
C	-1.8182950	-10.3004733	-4.0852088
H	-2.1911128	-9.5319470	-3.3888823
C	-2.6674633	-10.8482118	-5.0612721
H	-3.7102002	-10.5024321	-5.1296679
C	-2.1832599	-11.8169917	-5.9552571
H	-2.8474314	-12.2421024	-6.7238534

C	-0.8426925	-12.2329442	-5.8753429	H	3.5295155	14.7626329	-3.3328319
H	-0.4548780	-12.9851827	-6.5799952	C	3.0837652	12.6620880	-3.6860673
C	0.0101947	-11.6849579	-4.9036428	H	3.0778871	12.7628639	-4.7826589
H	1.0639327	-12.0002985	-4.8622090	C	2.8380694	11.4067829	-3.1008536
C	2.2530548	-9.9523722	-3.5178896	H	2.6425113	10.5338326	-3.7440360
C	2.3861528	-9.2663818	-4.7481001	C	-3.2731225	9.4802900	-3.7479147
H	1.5063715	-8.7889929	-5.2080627	C	-4.1632424	10.1771259	-2.9047749
C	3.6296086	-9.1937548	-5.3934227	H	-3.7741691	10.8351938	-2.1136521
H	3.7141731	-8.6552751	-6.3496201	C	-5.5523606	10.0414090	-3.0710778
C	4.7609396	-9.7994293	-4.8191684	H	-6.2322383	10.5953328	-2.4053434
H	5.7372413	-9.7398112	-5.3242086	C	-6.0700926	9.2113363	-4.0771854
C	4.6369855	-10.4794470	-3.5977234	H	-7.1584576	9.1059694	-4.2041601
H	5.5161710	-10.9621752	-3.1429550	C	-5.1894238	8.5117956	-4.9202948
C	3.3923084	-10.5566995	-2.9478654	H	-5.5832383	7.8545649	-5.7106903
H	3.3104618	-11.0954686	-1.9923164	C	-3.8020863	8.6405377	-4.7560256
C	3.4249029	1.6842282	1.1051700	H	-3.1227854	8.0865798	-5.4232400
C	2.9215704	0.8429832	0.0930799	C	-3.7281997	8.3578007	1.1802893
H	1.9965876	1.0936560	-0.4515101	C	-2.8501201	9.0791759	2.0136011
C	3.6012073	-0.3471034	-0.2201448	H	-1.8038778	8.7619617	2.1474032
H	3.2003787	-1.0205439	-0.9932650	C	-3.3106628	10.2206690	2.6944282
C	4.7778097	-0.6917363	0.4666222	H	-2.6189778	10.7720111	3.3502818
H	5.2923430	-1.6345491	0.2270191	C	-4.6428758	10.6420597	2.5468233
C	5.2792967	0.1540039	1.4693096	H	-5.0029149	11.5322710	3.0858546
H	6.1964133	-0.1140271	2.0156852	C	-5.5176442	9.9243059	1.7130125
C	4.6039646	1.3429625	1.7959204	H	-6.5632158	10.2506249	1.5966085
H	5.0002210	1.9874809	2.5956076	C	-5.0627948	8.7839208	1.0267726
C	-3.5080011	0.1172981	-4.2179762	H	-5.7564727	8.2335486	0.3708461
C	-4.2568701	0.5055366	-5.3458276	C	-7.0110704	-5.1720993	1.9374950
H	-3.9823379	1.3997885	-5.9275203	C	-8.1509776	-4.3427493	1.8605049
C	-5.3696178	-0.2604319	-5.7359937	H	-8.5785459	-3.9071068	2.7768575
H	-5.9532420	0.0415145	-6.6196100	C	-8.7373008	-4.0622745	0.6145552
C	-5.7328532	-1.4033951	-5.0039299	H	-9.6257202	-3.4135998	0.5639333
H	-6.6030905	-2.0025684	-5.3143425	C	-8.1906702	-4.6027850	-0.5628027
C	-4.9825894	-1.7865561	-3.8794816	H	-8.6503003	-4.3780346	-1.5376557
H	-5.2547339	-2.6844044	-3.3036524	C	-7.0493036	-5.4199733	-0.4938052
C	-3.8664582	-1.0295950	-3.4832528	H	-6.6036706	-5.8335392	-1.4112947
H	-3.2749289	-1.3586123	-2.6134973	C	-6.4580050	-5.6987431	0.7491197
C	-3.3452481	-5.6194195	-4.9726227	H	-5.5471055	-6.3166697	0.8032123
C	-3.6932391	-5.1797485	-6.2653740	C	1.8094513	4.9288380	-6.0543004
H	-3.1002782	-4.3992930	-6.7686992	C	1.6345496	4.5414372	-7.3979057
C	-4.8121559	-5.7296815	-6.9170333	H	0.8115888	3.8668648	-7.6836176
H	-5.0812820	-5.3822617	-7.9269440	C	2.5226584	5.0073645	-8.3837238
C	-5.5854254	-6.7152742	-6.2802336	H	2.3833082	4.7019057	-9.4326918
H	-6.4616943	-7.1438979	-6.7911972	C	3.5861680	5.8561976	-8.0307013
C	-5.2410763	-7.1510510	-4.9888698	H	4.2811559	6.2183658	-8.8043970
H	-5.8468361	-7.9196767	-4.4832575	C	3.7631353	6.2398408	-6.6899399
C	-4.1230525	-6.6059918	-4.3314575	H	4.5956952	6.9033017	-6.4076133
H	-3.8688176	-6.9549962	-3.3163354	C	2.8776946	5.7776704	-5.6988265
C	4.0385825	-8.1716679	0.9253735	H	3.0221044	6.0909357	-4.6515505
C	3.7606799	-8.4619636	2.2770250	C	7.1813326	4.3501383	2.4670238
H	3.0443495	-7.8551565	2.8542059	C	8.0580288	3.3482518	1.9995734
C	4.4024133	-9.5440971	2.9061139	H	8.5456717	3.4571398	1.0188249
H	4.1782958	-9.7665602	3.9610856	C	8.3156148	2.2107404	2.7843752
C	5.3231263	-10.3319507	2.1934915	H	9.0030884	1.4363826	2.4102059
H	5.8268924	-11.1757793	2.6901681	C	7.7000546	2.0616205	4.0385077
C	5.5993096	-10.0425264	0.8465126	H	7.9029852	1.1702301	4.6516966
H	6.3199200	-10.6578450	0.2851679	C	6.8113308	3.0483946	4.5017384
C	4.9558417	-8.9660183	0.2087445	H	6.3079662	2.9304804	5.4731307
H	5.1691771	-8.7528503	-0.8512376	C	6.5469955	4.1833383	3.7190234
C	2.1659150	-0.6743658	-5.1309101	H	5.8366380	4.9446763	4.0769024
C	2.6966302	0.5395590	-4.6514784	C	3.0667654	-5.0427568	-5.5849147
H	2.3528410	0.9729447	-3.6981490	C	2.3020601	-5.2601867	-6.7482043
C	3.6653795	1.2211435	-5.4088499	H	1.2489111	-5.5717064	-6.6707562
H	4.0738894	2.1718615	-5.0337694	C	2.8883897	-5.0794875	-8.0140866
C	4.0975169	0.6966165	-6.6390768	H	2.2895416	-5.2514589	-8.9221026
H	4.8523310	1.2366625	-7.2313960	C	4.2335267	-4.6842723	-8.1191562
C	3.5625774	-0.5122361	-7.1159569	H	4.6906567	-4.5463930	-9.1114510
H	3.8969819	-0.9245152	-8.0805293	C	4.9959180	-4.4680801	-6.9580869
C	2.5956079	-1.2033932	-6.3639802	H	6.0497940	-4.1588822	-7.0369837
H	2.1841097	-2.1507254	-6.7462586	C	4.4161413	-4.6477448	-5.6897045
C	2.8439824	11.2681954	-1.6987962	H	5.0250657	-4.4858302	-4.7861100
C	3.0920085	12.3924525	-0.8860848	C	7.5209420	5.6117981	-0.1476622
H	3.1015742	12.3040691	0.2118194	C	8.8699219	5.8404200	-0.4947807
C	3.3350001	13.6457667	-1.4747866	H	9.5744023	6.2234252	0.2592807
H	3.5275956	14.5207236	-0.8342335	C	9.3140320	5.5894815	-1.8042074
C	3.3344704	13.7806719	-2.8740321	H	10.3668807	5.7755153	-2.0674322

C	8.4188049	5.1068277	-2.7740200
H	8.7692935	4.9126512	-3.7994941
C	7.0732125	4.8819528	-2.4350546
H	6.3628134	4.5144585	-3.1910801
C	6.6224004	5.1413379	-1.1310960
H	5.5614464	4.9915066	-0.8727389
C	8.0633904	7.0847977	2.3128962
C	9.1532096	6.6447362	3.0957216
H	9.3084211	5.5692665	3.2681725
C	10.0393342	7.5744751	3.6661878
H	10.8824607	7.2173962	4.2778687
C	9.8482352	8.9509103	3.4626084
H	10.5393581	9.6781478	3.9161308
C	8.7656655	9.3955802	2.6843213
H	8.6035598	10.4728410	2.5263259
C	7.8749418	8.4711312	2.1166462
H	7.0203112	8.8282170	1.5194255
C	-4.5468752	4.3282272	-4.8385569
C	-4.1440336	4.4033545	-6.1864562
H	-3.1170875	4.7058749	-6.4429550
C	-5.0583498	4.0887237	-7.2080854
H	-4.7417266	4.1496939	-8.2610889
C	-6.3707772	3.7011235	-6.8862176
H	-7.0852616	3.4571742	-7.6879115
C	-6.7721151	3.6275236	-5.5411310
H	-7.7993377	3.3240341	-5.2855609
C	-5.8633850	3.9420109	-4.5154528
H	-6.1911051	3.8904635	-3.4650966
C	-7.2015310	-6.9887735	4.2190278
C	-6.7047384	-7.6477375	5.3666717
H	-5.7437517	-7.3321696	5.8039988
C	-7.4241023	-8.7018703	5.9483714
H	-7.0262224	-9.2031070	6.8440286
C	-8.6384107	-9.1259891	5.3792596
H	-9.1981894	-9.9598168	5.8304108
C	-9.1286188	-8.4883383	4.2283910
H	-10.0745157	-8.8210617	3.7732978
C	-8.4160852	-7.4228212	3.6495155
H	-8.8082958	-6.9304655	2.7470007
C	-7.7330411	-4.1528227	5.4486902
H	-8.4490749	-4.9885550	5.4223035
C	-6.5638040	-4.2019911	4.6581872
C	-5.6392799	-3.1375144	4.7309613
H	-4.7065005	-3.1789879	4.1482354
C	-5.8932482	-2.0295873	5.5543670
H	-5.1624187	-1.2081116	5.5975189
C	-7.0653565	-1.9811228	6.3277307
H	-7.2617764	-1.1152457	6.9788427
C	-7.9808994	-3.0460719	6.2776621
H	-8.8950910	-3.0190867	6.8910153
P	-1.4340376	9.5439240	-3.5151556
P	0.5953529	-9.9577614	-2.6840389
P	-6.1730571	-5.6135265	3.5276591
P	6.8415167	5.9183821	1.5440135
S	3.9755511	-6.4740726	-2.3607438
S	0.0701443	-6.6134138	-3.9413305
S	-0.8086674	2.3338699	-5.5612024
S	2.3851124	3.6892086	4.1177266
S	0.6341440	-6.4409662	-0.2717533
S	-2.5131217	-8.0379759	-1.1220511
S	-0.4500643	-8.8661595	2.4103353
S	-4.0041617	-8.6335333	2.8297875
S	-2.7056681	-6.4223706	5.2654475
S	-2.4428483	-5.4260629	1.7418058
S	1.1587292	-5.7730540	3.5444464
S	-2.0854403	-3.9411481	-1.7144860
S	0.3378433	-2.6214983	0.9706195
S	-1.2366719	-2.8591267	4.6023313
S	-0.7341304	-3.0043016	-5.4571737
S	1.7767492	-3.2930371	-2.3041229
S	3.8939649	-4.4343710	1.1517024
S	-0.2936325	-0.2040583	-2.2696070
S	-1.2552249	6.0538650	-4.3080531
S	1.5043520	3.6447849	-2.4163867
S	-2.3324077	2.9877947	-1.8584804
S	-4.5633817	6.1964452	-1.7296989
S	1.9929256	7.7175544	-2.5902290
S	4.5218036	8.9062714	0.6794817
S	0.9957159	9.2153093	1.1175935
S	2.7890515	5.6226480	0.6173430
S	-0.2609773	6.4219114	3.1684744
S	-3.4820202	4.6652893	1.8218344
S	3.8979001	7.2435559	3.7427752
S	-0.7672934	6.4159264	-0.6668678
S	-0.0537633	2.8745768	1.0491336
Cl	1.1063477	9.1059116	4.5783644
Cl	0.2686697	-8.1269846	5.7340802
Cu	-0.3520884	-6.5269635	1.8510640
Cu	-0.2361446	-7.9614832	-1.8922632
Cu	0.0734928	-4.2108931	-0.8189068
Cu	-4.0330338	-6.2492930	3.2299899
Cu	-2.0643097	-5.8914300	-0.5107446
Cu	1.8123871	5.7247418	-1.4917079
Cu	4.7016627	6.6396387	1.4996547
Cu	-0.4087181	7.6737490	-2.6599466
Cu	0.7834614	6.8124397	1.0446502
Cu	-0.3211239	4.1156417	-1.0017852
Sn	-1.7902024	-3.1315433	2.2111374
Sn	2.5732925	9.2897603	-0.8304557
Sn	-3.0483243	6.5278919	0.2149293
Sn	-1.7791929	1.2537452	-3.5849176
Sn	1.8304709	6.0890984	4.5137605
Sn	-1.2785956	4.1804422	2.7623772
Sn	-3.1778471	4.8766907	-3.2447337
Sn	0.4597867	4.2054788	-4.5130859
Sn	2.9026501	9.3357097	2.7462689
Sn	2.3249187	3.4636039	1.6589380
Sn	-0.5536048	-5.1623496	5.2796819
Sn	-1.6464176	-4.7533486	-3.9306624
Sn	-2.4666528	-9.2732209	0.9799896
Sn	3.0736609	-6.4700825	-0.0352843
Sn	0.7017704	-1.7276384	-3.9344901
Sn	-1.9000355	-8.6763762	4.4566590
Sn	2.2041016	-5.3634083	-3.6188020
Sn	1.9932585	-3.6699032	2.4872791

Table S8. Cartesian coordinates of **2** optimized with BP86/def2-SVP in Å.

Number of atoms: 184 E_{total} (Hartree): –12617.10388558			
C	0.9927843	2.3728775	-7.6563278
C	0.3779549	1.4374524	-8.5110630
H	-0.2466136	0.6388517	-8.0860430
C	0.5730752	1.5078285	-9.9016342
H	0.0859712	0.7665509	-10.5528237
C	1.3908397	2.5094053	-10.4470179
H	1.5494879	2.5619026	-11.5352705
C	2.0182369	3.4401131	-9.5986203
H	2.6701445	4.2206841	-10.0205324
C	1.8261034	3.3715717	-8.2106233
H	2.3354830	4.0921785	-7.5526386
C	2.4337181	2.5552060	-5.1877030
C	3.3549675	1.4869981	-5.2277540
H	3.0201259	0.4873394	-5.5494926
C	4.6896116	1.6875106	-4.8450094
H	5.3924496	0.8413956	-4.8705016
C	5.1153846	2.9530605	-4.4068188
H	6.1608222	3.1062865	-4.0976528
C	4.2005696	4.0171036	-4.3521735
H	4.5251259	5.0098737	-4.0035029
C	2.8642180	3.8233074	-4.7416590
H	2.1581756	4.6657607	-4.6959619
C	-0.1982536	3.7742061	-5.3890608
C	-0.7409308	4.6447541	-6.3595609
H	-0.5897326	4.4398166	-7.4297551
C	-1.4687033	5.7816464	-5.9657691
H	-1.8805388	6.4547710	-6.7337151
C	-1.6596344	6.0631688	-4.6031173
H	-2.2237193	6.9574461	-4.2964363
C	-1.1276492	5.1963728	-3.6316757
H	-1.2787664	5.4023985	-2.5612748
C	-0.4096961	4.0542071	-4.0182842
H	-0.0043295	3.3737744	-3.2520665
C	3.9603346	-1.3481046	-2.9383035
C	4.8111221	-0.6610251	-2.0542501
H	4.3847103	-0.0972313	-1.2099189
C	6.2040519	-0.6981204	-2.2462590
H	6.8656240	-0.1568187	-1.5516878
C	6.7516198	-1.4263228	-3.3165907
H	7.8430075	-1.4619421	-3.4596637
C	5.9024328	-2.1136090	-4.2012767
H	6.3251577	-2.6899061	-5.0394428
C	4.5081656	-2.0724454	-4.0158699
H	3.8478858	-2.6063653	-4.7189440
C	-2.2868743	-0.8973329	-7.6265451
C	-3.2053994	-0.3426326	-8.5420998
H	-3.9630155	0.3759722	-8.1954574
C	-3.1630407	-0.7117801	-9.8983431
H	-3.8874481	-0.2742705	-10.6027758
C	-2.2102314	-1.6388741	-10.3512013
H	-2.1843918	-1.9319423	-11.4121422
C	-1.2897082	-2.1927254	-9.4425626
H	-0.5383302	-2.9192443	-9.7883647
C	-1.3200613	-1.8214410	-8.0897580
H	-0.5871067	-2.2490574	-7.3854159
C	-2.8986561	-2.0412326	-5.0589446
C	-2.6131498	-2.3009602	-3.7021403
H	-1.9967952	-1.6021832	-3.1144547
C	-3.1122608	-3.4624050	-3.0898004
H	-2.8808184	-3.6631215	-2.0334123
C	-3.8860947	-4.3733819	-3.8263180
H	-4.2589876	-5.2895400	-3.3431658
C	-4.1711260	-4.1210242	-5.1790584
H	-4.7735140	-4.8345129	-5.7627442
C	-3.6825554	-2.9586636	-5.7955945
H	-3.9066896	-2.7689239	-6.8558491
C	-1.7798708	1.9618449	0.0000000
C	-2.3093066	2.4249069	-1.2175835
H	-1.9190413	2.0439688	-2.1752753
C	-3.8862486	3.8285210	0.0000000
H	-4.7151228	4.5538988	0.0000000
C	-3.3618184	3.3592783	-1.2162554
H	-3.7771589	3.7084809	-2.1743361
C	-3.6732727	0.7069653	-5.6178039
C	-3.4630697	2.0603596	-5.9638246
H	-2.4797417	2.3876818	-6.3345092
C	-4.4969216	2.9999680	-5.8291903
H	-4.3140570	4.0495402	-6.1060323
C	-5.7486021	2.6028917	-5.3268699
H	-6.5575928	3.3407827	-5.2119617
C	-5.9596444	1.2626240	-4.9631500
H	-6.9340422	0.9454773	-4.5606860
C	-4.9304109	0.3171102	-5.1076004
H	-5.1038324	-0.7299254	-4.8187451
S	0.2330262	0.5481760	-2.6256417
S	1.9472510	-0.7143004	0.0000000
S	1.1606476	-1.6697784	-5.1799847
S	0.9832522	-3.6921798	-2.1740950
S	-1.8290757	-1.6633897	0.0000000
Cu	-0.1261365	0.1713324	-5.0907015
Sn	-0.3269473	0.3098615	0.0000000
Sn	1.7853471	-1.3876154	-2.6912086
Sn	-0.0869187	-3.3848721	0.0000000
P	0.7253067	2.2349084	-5.8285078
P	-2.2706651	-0.4829314	-5.8209262
Cl	-1.5175416	-5.3402347	0.0000000
C	-2.3093066	2.4249069	1.2175835
H	-1.9190413	2.0439688	2.1752753
C	-3.3618184	3.3592783	1.2162554
H	-3.7771589	3.7084809	2.1743361
C	0.9927843	2.3728775	7.6563278
C	0.3779549	1.4374524	8.5110630
H	-0.2466136	0.6388517	8.0860430
C	0.5730752	1.5078285	9.9016342
H	0.0859712	0.7665509	10.5528237
C	1.3908397	2.5094053	10.4470179
H	1.5494879	2.5619026	11.5352705
C	2.0182369	3.4401131	9.5986203
H	2.6701445	4.2206841	10.0205324
C	1.8261034	3.3715717	8.2106233
H	2.3354830	4.0921785	7.5526386
C	2.4337181	2.5552060	5.1877030
C	3.3549675	1.4869981	5.2277540
H	3.0201259	0.4873394	5.5494926
C	4.6896116	1.6875106	4.8450094
H	5.3924496	0.8413956	4.8705016
C	5.1153846	2.9530605	4.4068188
H	6.1608222	3.1062865	4.0976528
C	4.2005696	4.0171036	4.3521735
H	4.5251259	5.0098737	4.0035029
C	2.8642180	3.8233074	4.7416590
H	2.1581756	4.6657607	4.6959619
C	-0.1982536	3.7742061	5.3890608
C	-0.7409308	4.6447541	6.3595609
H	-0.5897326	4.4398166	7.4297551
C	-1.4687033	5.7816464	5.9657691
H	-1.8805388	6.4547710	6.7337151
C	-1.6596344	6.0631688	4.6031173
H	-2.2237193	6.9574461	4.2964363
C	-1.1276492	5.1963728	3.6316757
H	-1.2787664	5.4023985	2.5612748
C	-0.4096961	4.0542071	4.0182842
H	-0.0043295	3.3737744	3.2520665
C	3.9603346	-1.3481046	2.9383035
C	4.8111221	-0.6610251	2.0542501
H	4.3847103	-0.0972313	1.2099189
C	6.2040519	-0.6981204	2.2462590
H	6.8656240	-0.1568187	1.5516878
C	6.7516198	-1.4263228	3.3165907
H	7.8430075	-1.4619421	3.4596637
C	5.9024328	-2.1136090	4.2012767
H	6.3251577	-2.6899061	5.0394428
C	4.5081656	-2.0724454	4.0158699
H	3.8478858	-2.6063653	4.7189440
C	-2.2868743	-0.8973329	7.6265451

C	-3.2053994	-0.3426326	8.5420998
H	-3.9630155	0.3759722	8.1954574
C	-3.1630407	-0.7117801	9.8983431
H	-3.8874481	-0.2742705	10.6027758
C	-2.2102314	-1.6388741	10.3512013
H	-2.1843918	-1.9319423	11.4121422
C	-1.2897082	-2.1927254	9.4425626
H	-0.5383302	-2.9192443	9.7883647
C	-1.3200613	-1.8214410	8.0897580
H	-0.5871067	-2.2490574	7.3854159
C	-2.8986561	-2.0412326	5.0589446
C	-2.6131498	-2.3009602	3.7021403
H	-1.9967952	-1.6021832	3.1144547
C	-3.1122608	-3.4624050	3.0898004
H	-2.8808184	-3.6631215	2.0334123
C	-3.8860947	-4.3733819	3.8263180
H	-4.2589876	-5.2895400	3.3431658
C	-4.1711260	-4.1210242	5.1790584
H	-4.7735140	-4.8345129	5.7627442
C	-3.6825554	-2.9586636	5.7955945
H	-3.9066896	-2.7689239	6.8558491
C	-3.6732727	0.7069653	5.6178039
C	-3.4630697	2.0603596	5.9638246
H	-2.4797417	2.3876818	6.3345092
C	-4.4969216	2.9999680	5.8291903
H	-4.3140570	4.0495402	6.1060323
C	-5.7486021	2.6028917	5.3268699
H	-6.5575928	3.3407827	5.2119617
C	-5.9596444	1.2626240	4.9631500
H	-6.9340422	0.9454773	4.5606860
C	-4.9304109	0.3171102	5.1076004
H	-5.1038324	-0.7299254	4.8187451
S	0.2330262	0.5481760	2.6256417
S	1.1606476	-1.6697784	5.1799847
S	0.9832522	-3.6921798	2.1740950
Cu	-0.1261365	0.1713324	5.0907015
Sn	1.7853471	-1.3876154	2.6912086
P	0.7253067	2.2349084	5.8285078
P	-2.2706651	-0.4829314	5.8209262

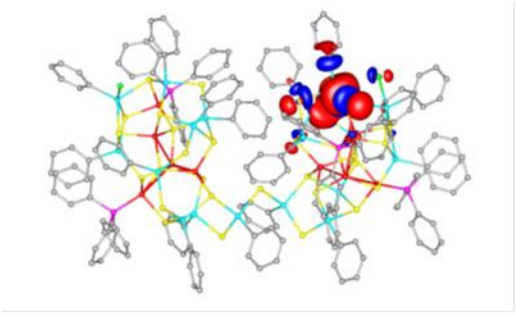

LUMO+1 (-2.09)

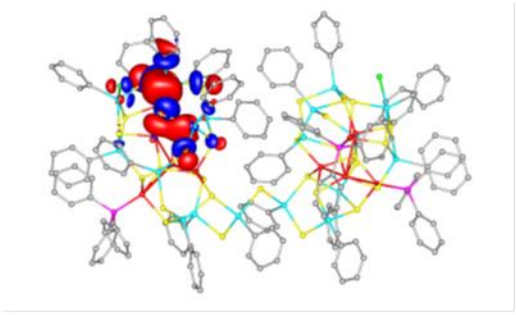

LUMO+2 (-2.06)

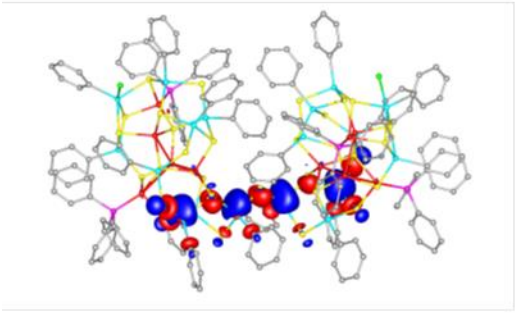

LUMO (-2.20)

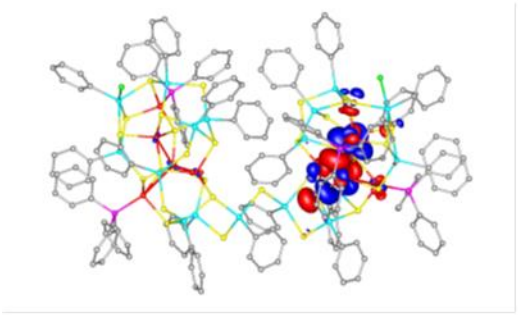

HOMO (-4.74)

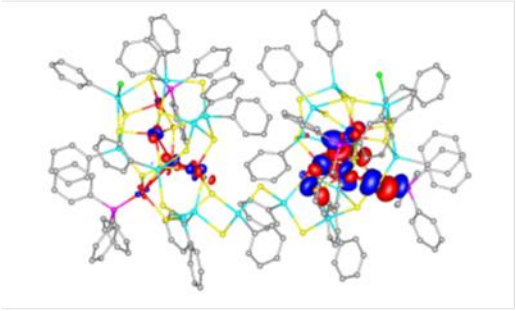

HOMO-1 (-4.78)

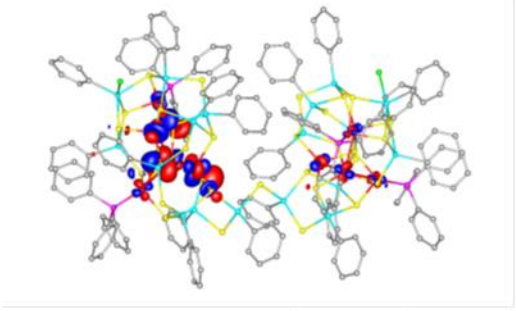

HOMO -2(-4.80)

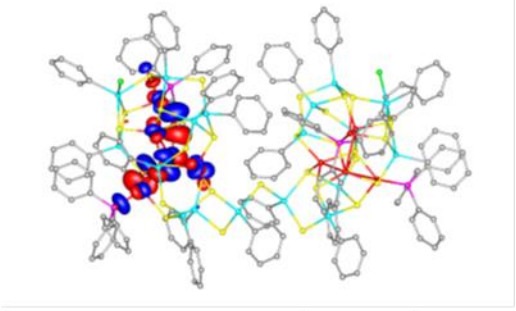

HOMO-3 (-4.88)

Figure S12: Frontier orbitals of **1**, calculated with B3-LYP/def2-SVP. Energies, in eV, are given in parentheses. Contours are plotted at ±0.03 a.u.

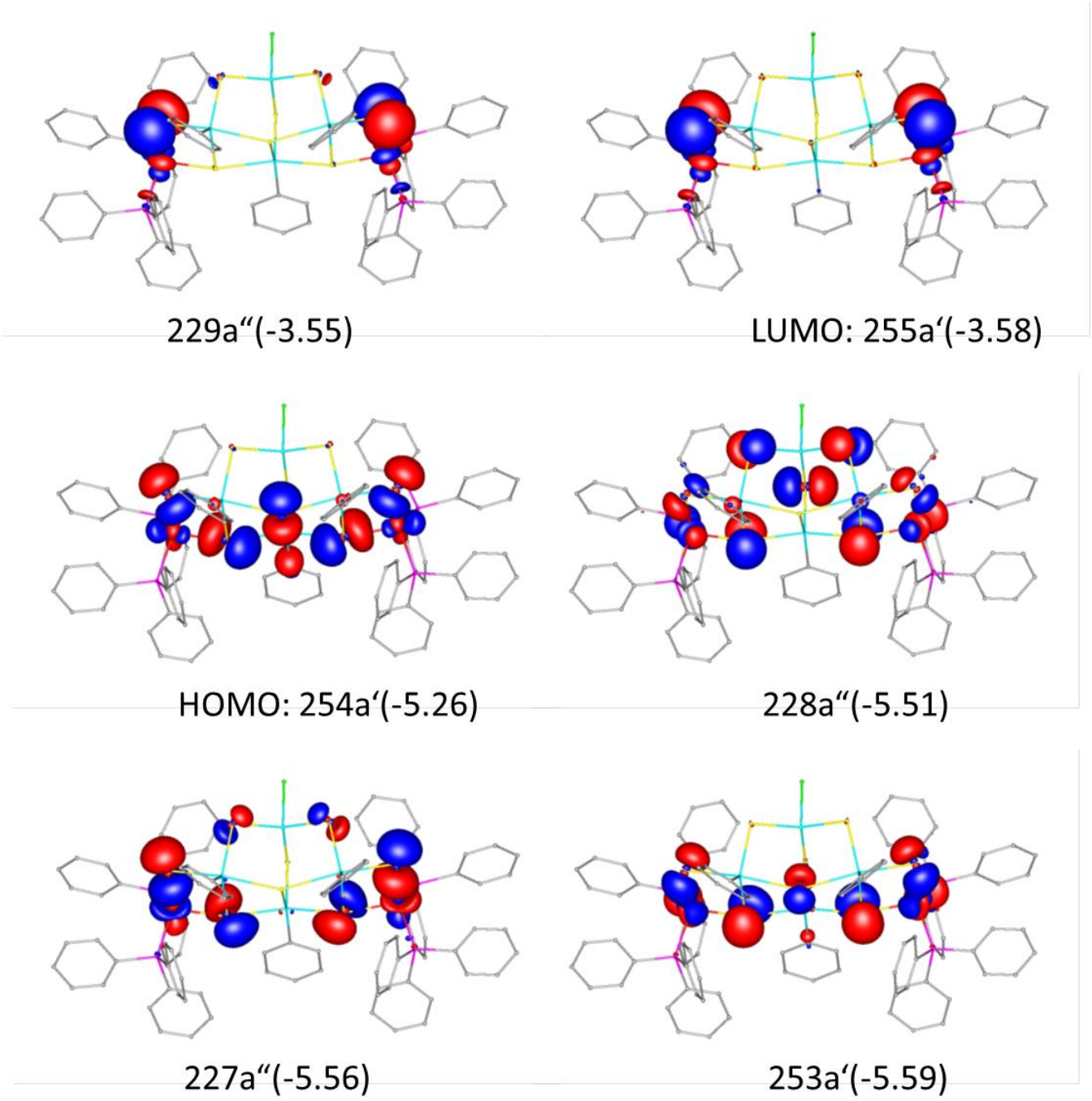

Figure S13: Minority spin component frontier orbitals of **2**, calculated with B3-LYP/def2-SVP. Energies, in eV, are given in parentheses. Contours are plotted at ±0.03 a.u.

6. UV-Vis spectroscopy

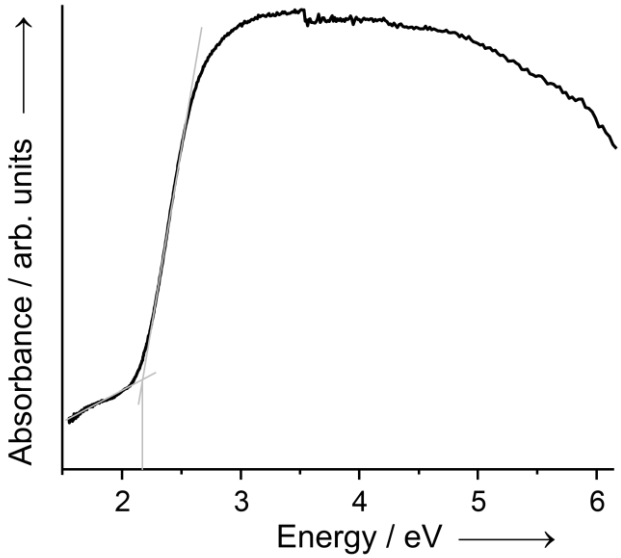

Figure S14: UV-Vis spectrum of **1**. The dent at 3.4 eV is caused by the change of the light source.

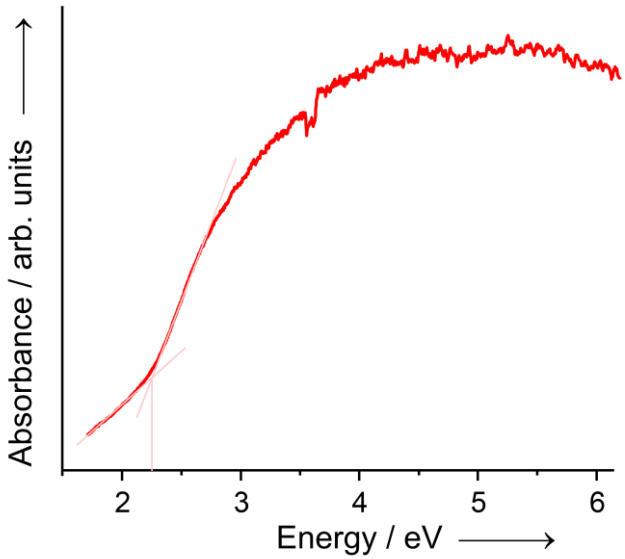

Figure S15: UV-Vis spectrum of **2**. The dent at 3.4 eV is caused by the change of the light source.

7. References for the Supporting Information

[1] Stoe and Cie GmbH, *X-Area*, *Version 1.77*, **2016**.
[2] Sheldrick, G. M., *Acta Crystallogr A* **2015**, *71*, 3-8.
[3] Hübschle, C. B., Sheldrick, G. M., Dittrich, B., *J. Appl. Cryst.* **2011**, 1281-1284.
[4] TURBOMOLE Version 7.3, TURBOMOLE GmbH 2018. TURBOMOLE is a development of University of Karlsruhe and Forschungszentrum Karlsruhe 1989–2007, TURBOMOLE GmbH since 2007
[5] F. Weigend, R. Ahlrichs, *Phys. Chem. Chem. Phys*. **2005**, *7*, 3297.
[6] M. Sierka, A. Hogekamp, R. Ahlrichs, *J. Chem. Phys.* **2003**, *118,* 9136-9148.
[7] a) A. Becke, *Phys. Rev. A* **1988**, *38(6)*, 3098-3100; b) J. Perdew, *Phys. Rev. B* **1986**, *33(12)*, 8822-8824
[8] C. Lee, W. Yang, R.G. Parr, *Phys. Rev. B.* **1988,** *37,* 785-789.

4.5 [{(PhSn)$_3$SnS$_6$}{(CpM)$_3$S$_4$}] (M = Mo, W): Minimal Molecular Models of Covalent Attachment of Metalchalcogenide Clusters on Layered Transition Metal Dichalcogenides (TMDCs)

Zitat: E. Dornsiepen, S. Dehnen, **2019**, *Manuskript in Vorbereitung.*

Abstract

With the aim to mimic the yet unknown covalent deposition of metal chalcogenide clusters on transition metal dichalcogenide (TMDC) MoS_2 or WS_2 layers, and thereby explore the interaction between the two systems and potential consequences on physical properties of the TMDC material, we synthesized heterobimetallic model systems. The heterocubane-type cluster $[(WCp)_3(SnCl_3)S_4]$ (**1**) and the organotin-sulfidotungstate cluster $[\{(PhSn)_3SnS_6\}\{(CpW)_3S_4\}]$ (**2**) and the corresponding molybdate $[\{(PhSn)_3SnS_6\}\{(CpMo)_3S_4\}]$ (**3**) were obtained in ligand exchange reactions from $[(PhSn)_4S_6]$ and $[M(CO)_3CpCl]$ (M = Mo, W). Indeed, the $\{M_3S_4\}$ cages in **1** – **3** resemble a section of the respective transition metal dichalcogenide monolayers, altogether representing minimal molecular model systems for the adsorption of organotin sulfide clusters on MoS_2 or WS_2. The interaction between the $\{(CpM)_3S_4\}$ and $\{(PhSn)_3SnS_6\}$ subunits are characterized by multicenter bonding, rendering the respective Sn atom as a Sn(II), hence driving the clusters into a mixed-valence Sn(IV)/Sn(II) situation, and the M atoms as M(IV) upon an in-situ redox process. The attachment is thus weaker than via regular covalent M–S bonds, but definitely stronger than via van-der-Waals interactions that have been characteristic for all known interactions of clusters on MS_2 surfaces.

Eigener Anteil

Alle Synthesen wurden von mir geplant und durchgeführt, alle analytischen Daten wurden von mir ausgewertet. Die Aufnahme der röntgenographischen Daten sowie der IR- und UV/Vis-Spektren wurde von mir durchgeführt. ^{1}H- und ^{13}C-NMR-Spektren wurden von mir, ^{31}P- und ^{119}Sn-NMR-Experimente von der NMR-Abteilung des Fachbereichs unter Leitung von Dr. Xiulan Xie gemessen. Massenspektren wurden von der entsprechenden Serviceabteilung des Fachbereichs unter Leitung von Dr. Uwe Linne aufgenommen. µ-RFA-Spektren wurden von Bertram Peters und Dr. Robert Wilson gemessen und zusammen mit mir ausgewertet. DFT-Rechnungen der erhaltenen Moleküle wurden von mir durchgeführt. Das Manuskript wurde gemeinsam von allen Autoren verfasst.

COMMUNICATION

[{(PhSn)$_3$SnS$_6$}{(CpM)$_3$S$_4$}] (M = W, Mo): Minimal Molecular Models of Covalent Attachment of Metalchalcogenide Clusters on Layered Transition Metal Dichalcogenides (TMDCs)

Eike Dornsiepen and Stefanie Dehnen*

Abstract: With the aim to mimic the yet unknown covalent deposition of metal chalcogenide clusters on transition metal dichalcogenide (TMDC) MoS_2 or WS_2 layers, and thereby explore the interaction between the two systems and potential consequences on physical properties of the TMDC material, we synthesized heterobimetallic model systems. The heterocubane-type cluster [(WCp)$_3$(SnCl$_3$)S$_4$] (**1**) and the organotin-sulfidotungstate cluster [{(PhSn)$_3$SnS$_6$}{(CpW)$_3$S$_4$}] (**2**) and the corresponding molybdate [(PhSn)$_3$SnS$_6${(CpMo)$_3$S$_4$}] (**3**) were obtained in ligand exchange reactions from [(PhSn)$_4$S$_6$] and [M(CO)$_3$CpCl]. Indeed, the {M$_3$S$_4$} cages in **1** – **3** resemble a section of the respective transition metal dichalcogenide monolayers, altogether representing minimal molecular model systems for the adsorption of organotin sulfide clusters on MoS_2 or WS_2. The interaction between the {(CpM)$_3$S$_4$} and {(PhSn)$_3$SnS$_6$} subunits are characterized by multicenter bonding, rendering the respective Sn atom as a Sn(II), hence driving the clusters into a mixed-valence Sn(IV)/Sn(II) situation, and the M atoms as M(IV) upon an *in-situ* redox process. The attachment is thus weaker than via regular covalent M–S bonds, but definitely stronger than via van-der-Waals interactions that have been characteristic for all known interactions of clusters on MS_2 surfaces.

Transition metal dichalcogenides (TMDCs) like MoS_2 or WS_2 have gained large interest in recent years. Their layered structures allow for the preparation of 2D materials whose electronic properties make them interesting for applications.[1] Combinations with other 2D materials in heterostructures have already been demonstrated in various devices such as tunneling transistors[2] or solar cells.[3] As an alternative to heterostructures made purely from 2D materials, hybrid systems combining 2D materials with layers of adsorbed molecules have proven to be successful for optoelectronic applications, due to the potential for tailoring electronic properties and advantages like high photo absorption of molecular materials as well as the easy preparation of thin films at low temperature.[4] In most of these studies, the adsorbed molecules were organic molecules like pentacene[5] or coordination compounds like phthalocyanines.[6] The interaction of larger organometallic systems with TMDCs, however, has not yet been studied.

[a] E. Dornsiepen, Prof. Dr. S. Dehnen
Fachbereich Chemie and Wissenschaftliches Zentrum für Materialwissenschaften (WZMW)
Philipps-Universität Marburg
Hans-Meerwein-Straße 4, D-35043 Marburg, Germany
E-mail: dehnen@chemie.uni-marburg.de

Supporting information for this article is given via a link at the end of the document.

In the course of our development of organotetrel chalcogenide clusters and their targeted extension by follow-up chemistry,[7,8] we recently identified extreme nonlinear optical properties of species of the general formula [(RT)$_4$E$_6$] (R = electron-rich organic substituent; T = Si, Ge, Sn; E = S, Se), which allows for a new and not yet fully understood way of supercontinuum generation.[9] It was also shown that such clusters can be deposited on semimetal surfaces (e.g., on Si or GaAs [110]), which is currently extended to other materials, including precious metals and TMDCs, with the purpose to generate functional devices of these new inexpensive white-light emitters.

To gain insight into the communication between organotetrel chalcogenide clusters and potential surface atoms, we develop molecular models and explore their electronic properties, which at the same time serves to modify the clusters themselves and study the photophysical response to it, such as reported recently for [{(R$_3$P)$_3$MSn}(PhSn)$_3$S$_6$] (R = Me, Et; M = Cu, Ag, Au).[10] The synthesis of these clusters was done by the replacement of one Ph ligand of the starting material [(PhSn)$_4$S$_6$] (**A**) with a [(PR$_3$)M] from the reactant [(PR$_3$)MCl]. For this, one tin-carbon bond is cleaved under release of chlorobenzene, and a Sn–M bond is formed under *in-situ* reduction of the involved Sn atom to Sn(II).

Here, we report our most recent work addressing TMDCs, for which we successfully transferred such ligand exchange reactions to group 6 metals. This yielded novel compounds [(WCp)$_3$(SnCl$_3$)S$_4$] (**1**), [{(PhSn)$_3$SnS$_6$}{(CpW)$_3$S$_4$}] (**2**), and [{(PhSn)$_3$SnS$_6$}{(CpMo)$_3$S$_4$}] (**3**), as shown in Scheme 1.

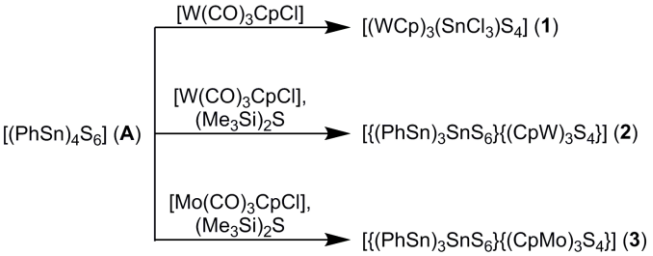

Scheme 1. Synthesis of compounds **1**–**3**. All reactions were carried out in THF (and CH_2Cl_2 for **2**), with subsequent layering by toluene (and n-pentane for **3**).

As a chloride ligand seems to be a necessary leaving group of the transition metal complex for the formation of chlorobenzene, we focused on reactions with chloro complexes, thus choosing the [M(CO)$_3$CpCl] (M = Mo, W) half-sandwich complexes as group 6 precursors. After first test reactions of [(PhSn)$_4$S$_6$] with [W(CO)$_3$CpCl], we obtained black crystals of [(WCp)$_3$(SnCl$_3$)S$_4$] (**1**). According to X-ray diffraction analyses and structure refinement (triclinic space group $P\bar{1}$), its molecular structure is

based on a trigonally distorted heterocubane-type topology, with four vertices occupied by sulfur atoms. Three of the remaining vertices are tungsten atoms (W–S 2.321(3) - 2.332(4) Å), each capped by a cyclopentadienyl ligand, while the remaining vertex is occupied by an $SnCl_3$ unit at significantly longer distances (Sn–S 2.780(4) - 2.812(4) Å). The molecular structure of **1** is shown in Figure 1.

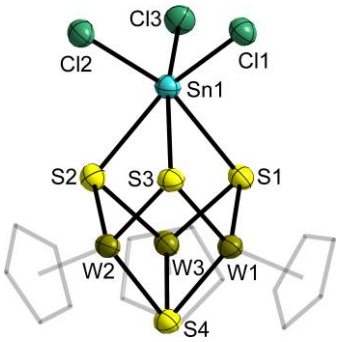

Figure 1. Molecular structure of **1**. Ellipsoids are drawn at 50% probability, hydrogen atoms are omitted for clarity. Selected interatomic distances (Å): Sn–S: 2.780(4) - 2.812(4), S–W: 2.321(3) - 2.332(4), W···W: 2.7379(10) - 2.7612(9).

The M_3S_4 (M = Mo, W) defect-heterocubane unit is a well-known structural motif that has been shown to be able to incorporate most elements of group 13-15 as eighth vertex to form heterobimetallic heterocubane-type clusters.[11] Usually, such clusters are prepared from compounds of the type $[(L_xM)_3S_4]$ (L = acac, py, SCN, etc.; M = transition metal atom), obtained by reduction of tetrathiometallate(IV) anions and subsequent addition of L, in reactions with the corresponding main group halides or aryls.[12] Compound **1**, in contrast, was formed from a mononuclear tungsten complex and reductive decomposition of the tinsulfide cluster **A**. The formation of $[Sn^{II}Cl_3]^-$ units from clusters of the type $[(RSn^{IV})_4S_6]$ is known to occur in the presence of Cl atoms from further reactants or even from the solvent. The subsequent incorporation of an $[SnX_3]^-$ unit (X = halide) into an $[(L_xM)_3E_4]$ defect-heterocubane unit (E = S, Se, Te) was observed in several cases, like $[(acacWpy)_3S_4SnCl_3]$,[12b] $[\{Mo(NCS)_3\}_3S_4SnCl_3]$[13] or $[(Cp^*Fe)_3Se_4SnCl_3]$.[14] At the formation of **1**, the three W atoms underwent oxidation to the +IV oxidation state, thereby compensating for the negative charges of one $[SnCl_3]^-$ group, four S^{2-} and three Cp^- ligands in the complex. With the $[W_3S_4]$ cage forming a trigonal antiprism that resembles a minimal cutout of a tungsten disulfide layer capped on one end by the fourth sulfur atom, the complex may be viewed as a minimal molecular model of an SnX_3 unit attached to a TMDC surface or layer. Attempts to transfer this reaction to the lighter homologue molybdenum were not successful, although a very similar, albeit salt-like complex with a tin(IV) anion is known to the literature, namely $[(CpMo)_3S_4][Me_3SnCl_2]$, prepared from $[Mo(CO)_3CpCl]$ and $[(Me_3Sn)_2S]$.[15]

We were interested to explore whether this concept might be transferred to corresponding molecular models incorporating entire tinsulfide clusters, and how such a linkage would influence electronic and magnetic properties

Since **1** was obtained by complete decomposition of **A** as a consequence of the thiophilicity of tungsten, we decided to add $(Me_3Si)_2S$ as additional, external sulfide source, such as reported for the synthesis of other clusters with M/Sn/S cores.[16] This way, we were able to isolate compound $[\{(PhSn)_3SnS_6\}\{(CpW)_3S_4\}]$ (**2**) as orange hexagonal plates. **2** crystallizes in the trigonal crystal system (space group $P\bar{3}c1$). The molecular structure, shown in Figure 2 (left), indicates that the molecules consist of a distorted adamantane-type $[Sn_4S_6]$ core in which three tin atoms (Sn1 and symmetry equivalents) still carry a phenyl moiety. The Ph group at the fourth tin atom (Sn2), however, is replaced with the $[(CpW)_3S_4]$ cage, such as observed in **1**. Similar to the situation in **1**, the Sn2–S3 bonds (2.814(3) Å) are significantly longer than the W1–S bonds (2.319(3) – 2.325(3) Å). Additionally, Sn2 is also set further apart from the adamantane core, with Sn2–S2 being 2.524(3) Å, while the distances at the phenyl-substituted tin atoms (Sn1–S 2.371(3) – 2.407(3) Å) are in the usual range for Sn–S bonds involving tetracoordinate Sn(IV) atoms.[17] Sn2 is therefore considered as Sn(II), like in **1** and as observed for some mixed-

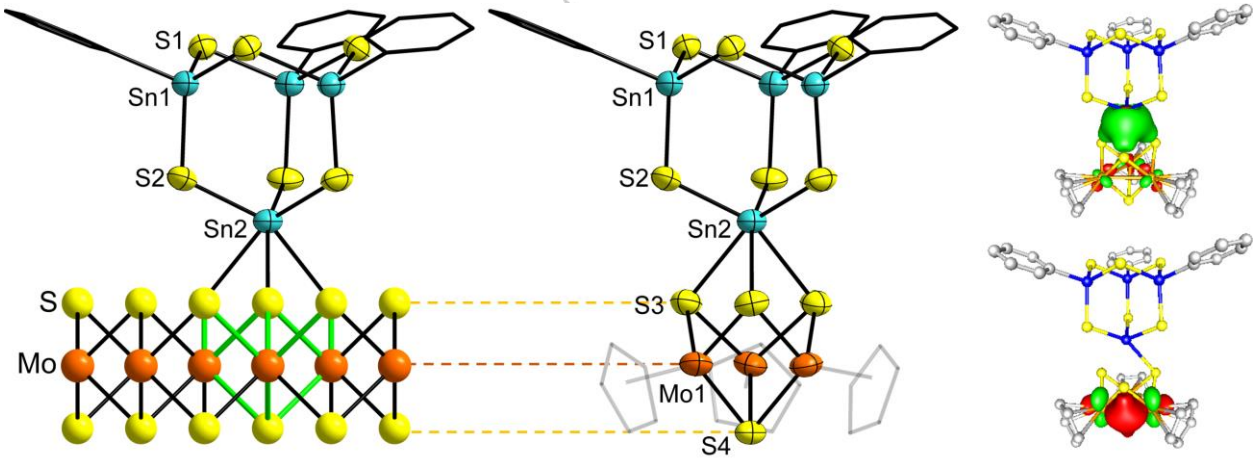

Figure 2. Hypothetical adsorption of an adamantane-type organotinsulfide cluster on a MoS_2 surface. Center; Molecular structure of **3**; ellipsoids are drawn at 50% probability; hydrogen atoms are omitted for clarity. Right: The two LMOs of **3** with the highest expectation values of the energy; amplitudes plotted at 0.05 a.u.; for the full set of frontier orbitals, see Figure S13. Corresponding figures including compound **3** are provided in the Supporting Information (Figures S3 and S14).

valence adamantane-type clusters substituted with coinage metal complexes. A sixfold coordination is highly unusual for Sn(II), and indeed, the coordination sphere of Sn2 is better described as *pseudo*-tetrahedral, in agreement with quantum chemical calculations (see below).

A transfer of the reaction to the corresponding molybdenum complex turned out to be successful as well, yielding compound $[\{(PhSn)_3SnS_6\}\{(CpW)_3S_4\}]$ (**3**) as deeply-red hexagonal plates. Compounds **2** and **3** are isomorphous and isostructural. As in **2**, the molecular structure features Sn–S bonds in the usual length range (Sn1–S 2.371(2)–2.407(2) Å) for the Sn(IV)–S bonds, while the Sn(II)–S bonds within the adamantane unit are elongated (Sn2–S2 2.505(2) Å). The Sn–S bonds that connect the $[Sn_4S_6]$ moiety to the $[Mo_3S_4]$ unit are significantly stretched (Sn2–S3 2.762(3) Å), similar to the observation made for **2**, and in agreement with the multicenter character of this linkage. The slightly smaller Sn–S bond length with regard to the respective bonds in **2** can be explained by XXX.

The composition of the clusters, $[\{(PhSn)_3SnS_6\}\{(CpM)_3S_4\}]$ (M = Mo, **2**; M = W, **3**), and the assignment of plausible oxidation states for Sn and S atoms as 3×Sn(IV) and 1×Sn(II), besides $10\times S^{2-}$, $3\times Ph^{-}$, and $3\times Cp^{-}$ as ligands, leaves a total charge of +12, consistent with three M(+IV) atoms to be present upon in-situ oxidation here, such as observed for compound **1**.

In the literature, the $[M_3S_4]$ cages are usually described as diamagnetic, with the six unpaired electrons of the M(IV) centers forming three covalent M–M bonds.[15,18] To check if this is also the case for our clusters **2** and **3**, we performed magnetic measurements of these two compounds (for **1**, this could not be carried out due to the low yields). The χT vs. T plots are shown in Figures S16 and S17, respectively. Compound **2** shows a temperature-independent paramagnetic contribution of $1.78\cdot10^{-3}$ $cm^3\cdot mol^{-1}$ that can be attributed to Van Vleck paramagnetism; no permanent magnetic moment that would lead to a Curie contribution was observed. This supports the bonding situation described in the literature. **3** also shows temperature-independent paramagnetism with a similar susceptibility of $1.93\cdot10^{-3}$ $cm^3\cdot mol^{-1}$. A small Curie contribution is seen as intercept in the χT vs. T plot, corresponding to an effective magnetic moment of 0.34 μ_B per molybdenum atom. This contribution probably arises from an impurity in the sample that contained small amounts of the reagent [Mo(CO)3CpCl].

To investigate the bonding situation between the adamantane cage and the thiotungstate unit, thereby modelling a yet not observed covalent interaction of a cluster with a MS_2 layer, we carried out quantum chemical studies using DFT methods. The geometry optimization of the clusters reproduced the molecular structure well, with maximum deviations of 0.10 Å (M = W) and 0.14 Å (M = Mo) at the relatively weak Sn1–S3 bonds. An inspection of the localized molecular orbitals revealed that the LMO with the highest expectation value of the energy corresponds to a 2e4c bond between Sn2 and S3 and its two symmetry-generated counterparts (see Figure 2, left). The three LMOs with next lower expectation values of the energy represent three 2e4c bonds between one M atom each and S3, S3', and S3'', while the next three ones following with decreasing expectation values of the energy are 2e3c bonds including one M atom and two of the three named S atoms (see Figure S13 and Figure S14). The coordination geometry around Sn2 should thus be the three S2 atoms, and one multicenter interaction with the three S3 atoms (similar to the *pseudo*-tetrahedral coordination of COD in $[NiCl_2COD]$), which is in agreement with the +II oxidation state of Sn2. The latter is also reflected in atomic charges obtained by a Mulliken population analysis, which reveals an atomic charge of 0.62 for Sn1, while the other three tin atoms have charges of 0.83 (see Table S10).

For comparison, we also checked the bonding situation in compound **1**, finding a very similar situation where the trichlorostannate group bonds to the thiotungstate cage via a 2e4c bond including Sn1 and the sulfur atoms S1, S2 and S3 that is represented by the LMO with the highest energy expectation value, while the next six LMOs correspond to multicenter bonds in the thiotungstate cage (see Figure S12). For a direct comparison of all three compounds, see also the MO diagram in Figure 3, including all bonding states within the cluster core.

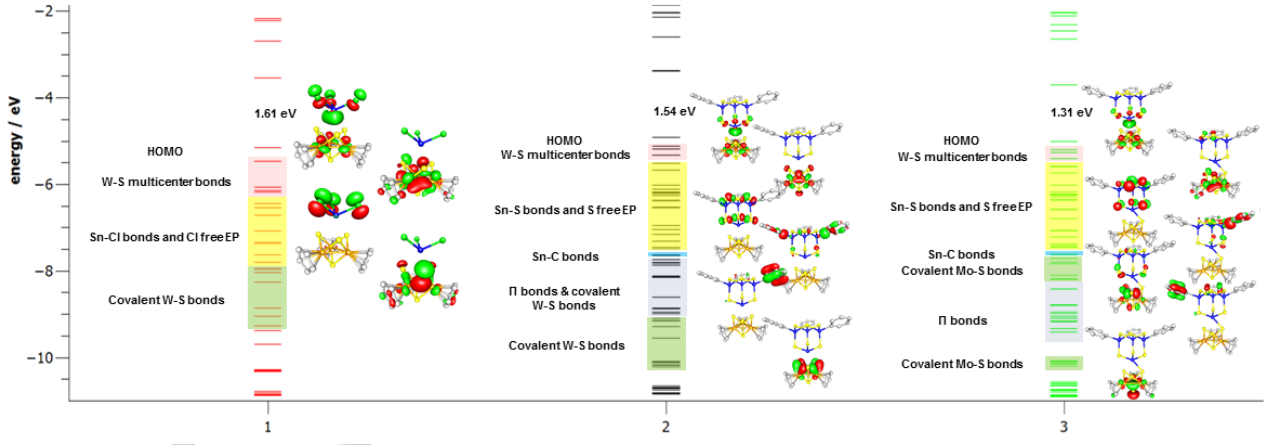

Figure 3. MO diagram of compounds **1**-**3**. Included are all canonical MOs that correspond to binding states within the cluster core.

The lesson we learn here is, that the covalent interaction of a tin complex or chalcogenide cluster with a TMDC surface is feasible, yet more weakly covalent than the attachment of, e.g., cyclooctyne on Si[19] or thiols on gold surfaces.[20] This noticeably influences the electronic absorption behavior. To probe the absorption properties and the result of the combination of the two underlying cluster units, we recorded UV-Vis absorption spectra of compounds **2** and **3**, which are shown in Figures S10 and S11, respectively, together with simulated absorption spectra calculated from the first 200 electronic excitations. Determinations of the excitation energy via the tangential method reveal values of 2.0 eV (620 nm) for **2** and 1.7 eV (730 nm) for **3**, in accordance with the orange or red appearance of the crystals, respectively. Figure 4 shows the calculated difference densities for both compounds, showing that the observed excitation is mainly a charge transfer from the sulfur atoms in the adamantane cage to the group 6 atoms

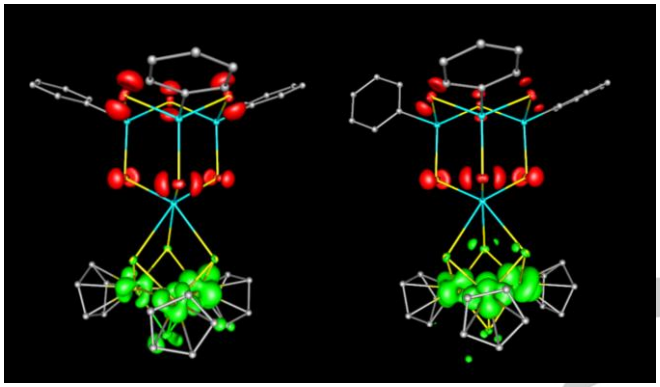

Figure 4. Non-relaxed electronic difference density for the entire bands of **2** (left) and **3** (right). The contour value was chosen to be 0.002.

In conclusion, the reaction of $[(PhSn)_4S_6]$ with $[M(CO)_3CpCl]$ complexes yielded three different new compounds, the heterocubane-type $[(CpW)_3(SnCl_3)S_4]$ (**1**) and the two isostructural clusters $[\{(PhSn)_3SnS_6\}\{(CpW)_3S_4\}]$ (**2**) and $[(PhSn)_3SnS_6\{(CpMo)_3S_4\}]$ (**3**), representing thiometallate-substituted adamantane-type clusters. The thiometallate cages resemble the structure of MoS_2 and WS_2 and show an interesting bonding situation with several multicenter bonds including the tin atom of the adamantane cage attached to the thiometallate. Optical absorption energies were determined and rationalized by TD-DFT calculations.

Experimental Section

General. All synthetic steps were carried out under exclusion of oxygen and moisture by use of standard Schlenk procedures. $[(PhSn)_4S_6]$,[17b] $[M(CO)_3CpCl]$ (M = Mo, W)[21] and $(Me_3Si)_2S$[22] were prepared according to literature procedures. Yields of the syntheses are calculated based on the Sn content and refer to the amount of product isolated as single crystals. IR spectra were reTrcorded on a Bruker Tensor 37 ATR spectrometer. ^{1}H NMR spectroscopy was carried out at 25°C using a Bruker DRX 300 MHz spectrometer. High-resolution ESI mass spectra were acquired with a LTQ-FT Ultra mass spectrometer (Thermo Fischer Scientific). The resolution was set to 100.000. UV-visible absorption spectroscopy was performed by analyses of the diffuse reflection of powdered samples. The measurements were carried out using a Varian Cary 5000 dual-beam spectrometer with a Praying Mantis sample holder from Harrick.

$[(WCp)_3(SnCl_3)S_4]$ (1): $[(PhSn)_4S_6]$ (100 mg, 102 µmol) and $[W(CO)_3CpCl]$ (38 mg, 102 µmol) were dissolved in THF (15 mL). The orange solution was stirred at room temperature for four days, after which the by now deep red suspension was filtered. The orange filtrate was layered with toluene (15 mL). Black crystals of **1** were obtained after three weeks. Yield: 2 mg (2 µmol, 2%). Elemental Analysis: % found (% calcd.): C 16.81 (16.38), H 1.42 (1.37), S 11.75 (11.66).

$[\{(PhSn)_3SnS_6\}\{(CpW)_3S_4\}]$ (2): $(Me_3Si)_2S$ (0.07 mL, 333 µmol) was added to a solution of $[(PhSn)_4S_6]$ (100 mg, 102 µmol) and $[W(CO)_3CpCl]$ (112 mg, 311 µmol) in THF (10 mL). The orange solution was stirred at room temperature for 15 hours. The solvent was removed *in vacuo*, the residue dissolved in dichloromethane (15 ml) and layered with toluene (15 mL). **2** was obtained as orange hexagonal plates within two weeks. Yield: 37 mg (21 µmol, 21%) IR: $\tilde{\nu}$ = 3097 (w), 3059 (w), 3034 (w), 2962 (w), 1994 (m), 1912 (m), 1571 (w), 1475 (m), 1427 (m), 1329 (w), 1297 (w), 1259 (m), 1187 (w), 1158 (w), 1064 (m), 1008 (m), 995 (m), 810 (s), 726 (s), 690 (s),624 (w), 577 (w), 557 (m), 480 (m), 442 (s) cm^{-1}. Elemental Analysis: % found (% calcd.): C 22.56 (22.35), H 1.72 (1.71), S 18.11 (18.08). µ-XRF: % found (% calcd) for Sn/W/S 4:3:10): Sn 31.8 (23.5), W 14.9 (17.6), S 53.3 (58.8).

$[\{(PhSn)_3SnS_6\}\{(CpMo)_3S_4\}]$ (3): $(Me_3Si)_2S$ (0.07 mL, 333 µmol) was added to a solution of $[(PhSn)_4S_6]$ (100 mg, 102 µmol) and $[Mo(CO)_3CpCl]$ (86 mg, 307 µmol) in THF (10 mL). The deep red solution was stirred at room temperature for 15 hours and then layered with toluene and *n*-pentane (5 ml each). **3** was obtained as red hexagonal plates within three weeks. Yield: 43 mg (28 µmol, 27%) IR: $\tilde{\nu}$ = 3091 (w), 3060 (w), 2963 (w), 2006 (m), 1944 (m), 1913 (m), 1575 (w), 1475 (m), 1426 (m), 1326 (w), 1293 (w), 1258 (m), 1187 (w), 1095 (w), 1063 (m), 1009 (m), 994 (m), 907 (m), 811 (s), 727 (s), 690 (s), 558 (m), 478 (m), 443 (s) cm^{-1}. HRMS (LIFDI): m/z calcd: 610.71969; found: 610.72107 for $[(C_5H_5)_3Mo_3S_4]^+$. Elemental Analysis: % found (% calcd.): C 26.03 (26.25), H 1.91 (2.00), S 20.77 (21.23). µ-XRF: % found (% calcd) for Sn/Mo/S 4:3:10): Sn 20.3 (23.5), Mo 18.3 (17.6), S 60.9 (58.9).

Quantum Chemical Investigations: Density functional theory calculations were carried out with TURBOMOLE[23] using def2-TZVP basis sets[24] and taking advantage of the multipole-accelerated resolution-of the-identity method.[25] Structures were optimized with the functional BP86.[26] Molecular orbitals were localized using the Boys method.[27] Non-relaxed electronic difference densities of the excited stated weighted with the respective oscillator strengths are obtained in the way described in reference [28].

Acknowledgements

This work was supported by the Deutsche Forschungsgemeinschaft within the framework of SFB 1083. We thank B. Peters and Dr. R. J. Wilson for the measurement of the XRF spectra and C. Pietzonka for the magnetic measurements.

Keywords: Organotinsulfide Clusters• Transition Metal Dichalcogenides • Molecular Model • X-Ray Crystallography • DFT calculations

[1] a) K. F. Mak, C. Lee, J. Hone, J. Shan, T. F. Heinz, *Phys. Rev. Lett.* **2010**, *105*, 136805; b) Q. H. Wang, K. Kalantar-Zadeh, A. Kis, J. N. Coleman, M. S. Strano, *Nature Nanotechnol.* **2012**, *7*, 699-712.

[2] L. Britnell, R. V. Gorbachev, R. Jalil, B. D. Belle, F. Schedin, A. Mishchenko, T. Georgiou, M. I. Katsnelson, L. Eaves, S. V. Morozov, N. M. R. Peres, J. Leist, A. K. Geim, K. S. Novoelov, L. A. Ponomarenko, *Science* **2012**, *335*, 947-950.

[3] M. M. Furchi, A. Pospischil, F. Libisch, J. Burgdörfer, T. Mueller, *Nano. Lett.* **2014**, *14*, 4785–4791.

[4] a) D. He, Y. Pan, H. Nan, S. Gu, Z. Yang, B. Wu, X. Luo, B. Xu, Y. Zhang, Y. Li, Z. Ni, B. Wang, J. Zhu, Y. Chai, Y. Shi, X. Wang, *Appl. Phys. Lett. 2015, 107*, 183103; b) D. Jariwala, S. L. Howell, K. S. Chen, J. Kang, V. K. Sangwan, S. A. Filippone, R. Turridi, T. J. Marks, L. J. Lauhorn, M. C. Hersam, *Nano Lett.* **2016**, *16*, 497–503.

[5] T. Breuer, T. Maßmeyer, A. Mänz, S. Zörb, B. Harbrecht, G. Witte, *Phys. Status Solidi RRL* **2016**, *10*, 905-910

[6] Y. Huang, F. Zhuge, J. Hou, L. Lv, P. Luo, N. Zhou, L. Gan, T. Zhai, *ACS Nano* **2018**, *12*, 4062-4073.

[7] a) Z. Hassanzahdeh Fard, C. Müller, T. Harmening, R. Pöttgen, S. Dehnen, *Angew. Chem. Int. Ed.* **2009**, *48*, 4441-4444; b) S. Heimann, M. Holynska, S. Dehnen, *Chem. Commun.* **2011**, *47*, 1881-1883; c) J.P. Eußner, B.E.K. Barth, E. Leusmann, Z. You, N. Rinn, S. Dehnen, *Chem. Eur. J.* **2013**, *19*, 13792–13802; d) N. Rinn, J.P. Eußner, W. Kaschuba, X. Xie, S. Dehnen, *Chem. Eur. J.* **2016**, *22*, 3094–3104.

[8] a) Z. Hassanzadeh Fard, M. R. Halvagar, S. Dehnen, *J. Am. Chem. Soc.* **2010**, *132*, 2848–2849; b) Z. You, S. Dehnen, *Inorg. Chem.* **2013**, *52*, 12332-12334; c) E. Leusmann, M. Wagner, N. W. Rosemann, S. Chatterjee, S. Dehnen, *Inorg. Chem.* **2014**, *53*, 4228-4233; d) J. P. Eußner, S. Dehnen, *Chem. Commun.* **2014**, *50*, 11385–11388; e) N. Rinn, L. Guggolz, K. Gries, K. Volz, J. Senker, S. Dehnen, *Chem. Eur. J.* **2017**, *23*, 15607–15611; f) E. Dornsiepen, E. Geringer, N. Rinn, S. Dehnen, *Coord. Chem. Rev.* **2019**, *380*, 136–169; g) J.-P. Berndt, A. Engel, R. Hrdina, S. Dehnen, P. R. Schreiner, *Organometallics* **2019**, **38**, 329–335.

[9] a) N.W. Rosemann, J.P. Eußner, A. Beyer, S.W. Koch, K. Volz, S. Dehnen, S. Chatterjee, *Science* **2016**, *352*, 1301–1304; b) N.W. Rosemann, J.P. Eußner, E. Dornsiepen, S. Chatterjee, S. Dehnen, *J. Am. Chem. Soc.* **2016**, *138*, 16224–16227.

[10] E. Dornsiepen, F. Dobener, N. Mengel, O. Lenchuk, C. Dues, S. Sanna, D. Mollenhauer, S. Chatterjee, and S. Dehnen, *Adv. Opt. Mater.* **2019**, DOI: 10.1002/adom.201801793.

[11] a) S.-F: Lu, J.-Q. Huang, Y.-H. Lin, J.-L. Huang, *Acta Chim. Sinica* **1987**, *3*, 191; b) R. Hernandez-Molina, V. Fedin, M. N. Sokolov, D. Saysell, A. G. Sykes, *Inorg. Chem.* **1998**, *37*, 4328; c) R. Hernandez-Molina, M. Sokolov, W. Clegg, P. Esparza, A. Mederos, *Inorg. Chimica Acta* **2002**, *331*, 52-58.

[12] a) A. Müller, V. P. Fedin, E. Diemann, H. Bögge, E. Krickemeyer, D. Sölter, A. M. Guiliani, R. Barbieri, P. Adler, *Inorg. Chem.* **1994**, *33*, 2243-2247; b) R. Hernandez-Molina, I. V. Kalinina, P. A. Abramov, M. Sokolov, A. V. Virovets, J. G. Platas, R. Llusar, V. Polo, C. Vincent, V. P. Fedin, *Inorg. Chem.* **2008**, *47*, 306-314.

[13] E. Varey, G. J. Lamprecht, V. P. Fedin, A. Holder, W. Clegg, M. R. J. Elsegood, A. G. Sykes, *Inorg. Chem.* **1996**, *35*, 5525-5530.

[14] C. Zimmermann, C.E. Anson, A.L. Eckermann, M. Wunder, G. Fischer, I. Keilhauer, E. Herrling, B. Pilawa, O. Hampe, F. Weigend, S. Dehnen, *Inorg. Chem.* **2004**, *43*, 4595–4603.

[15] P. J. Vergamini, H. Vahrenkamp, L. F. Dahl, *J. Am. Chem. Soc.* **1971**, *93*, 6327-6329.

[16] a) J. P. Eußner, S. Dehnen, *Chem Commun.* **2014**, *50*, 11385-11388; b) E. Dornsiepen, J. P. Eußner, N. W. Rosemann, S. Chatterjee, S. Dehnen, *Inorg. Chem.* **2017**, *56*, 11326–11335.

[17] a) D. Kobelt, E. F. Paulus, H. Scherer, *Acta Crystallogr.* **1972**, *B28*, 2323; b) H. Berwe, A. Haas, *Chem. Ber.* **1987**, *120*, 1175 – 1182; c) K. Wraage, T. Pape, R. Herbst-Irmer, M. Noltemeyer, H.-G. Schmidt, H. W. Roesky, *Eur. J. Inorg. Chem.* **1999**, 869; d) C. Wagner, C. Raschke, K. Merzweiler, *Appl. Organomet. Chem.* **2004**, *18*, 147; e) C. Pöhlker, I. Schellenberg, R. Pöttgen, S. Dehnen, *Chem. Commun.* **2010**, *2605*.

[18] a) P. A. Petrov, A. V. Virovets, A. Alberola, R. Llusar, S. N. Konchenko, *Dalton Trans.* **2010**, *39*, 8875-8877; b) P. A. Petrov, D. Yu. Naumov, R. Llusar, C. J. Gómez-García, V. Poloe, S. N. Konchenko, *Dalton Trans.* **2012**, *41*, 14031-14034.

[19] a) M. Reutzel, N. Münster, M. A. Lipponer, C. Länger, U. Höfer, U. Koert, M. Dürr, *J. Phys. Chem. C* **2016**, *120*, 26284–26289; b) C. Länger, J. Heep, P. Nikodemiak, T. Bohamud, P. Kirsten, U. Höfer, U. Koert, M. Dürr, *J. Phys.: Condens. Matter* **2019**, *31*, 034001.

[20] J. Ossowski, G. Nascimbeni, T. Żaba, E Verwüster, J. Rysz, A. Terfort, M. Zharnikov, E.t Zojer, P. Cyganik, *J. Phys. Chem. C* **2017**, *121*, 28031–28042.

[21] W.P. Fehlhammer, W.A. Herrmann, K. Öfele in *Handbuch der Präparativen Anorganischen Chemie, Vol 3* (Ed.: G. Brauer), Ferdinand Enke Verlag, Stuttgart, **1975**, pp. 1947-1948.

[22] J.-H. So, P. Boudjouk, *Synthesis* **1989**, 306-307.

[23] TURBOMOLE Version 7.3, TURBOMOLE GmbH 2018. TURBOMOLE is a development of University of Karlsruhe and Forschungszentrum Karlsruhe 1989 –2007, TURBOMOLE GmbH since 2007.

[24] K. Eichkorn, F. Weigend, O. Treutler, R. Ahlrichs, *Theor. Chem. Acc.* **1997**, *97*, 119.

[25] M. Sierka, A. Hogekamp, R. Ahlrichs, *J. Chem. Phys.* **2003**, *118*, 9136 – 9148.

[26] a) A. Becke, *Phys. Rev. A* **1988**, *38*, 3098 – 3100; b) J. Perdew, *Phys. Rev. B* **1986**, *33*, 8822 –8824.

[27] J. M. Foster, S. F. Boys, *Rev. Mod. Phys.* **1960**, *32*, 300-302.

[28] M. Kühn, F. Weigend, *J. Chem. Phys.* **2014**, *141*, 224302.

Supporting Information

69451 Weinheim, Germany

[{(PhSn)$_3$SnS$_6$}{(CpM)$_3$S$_4$}] (M = W, Mo): Minimal Molecular Models of Covalent Attachment of Metalchalcogenide Clusters on Layered Transition Metal Dichalcogenides (TMDCs)

Eike Dornsiepen and Stefanie Dehnen*

Abstract: The heterobimetallic heterocubane-type cluster [(WCp)$_3$(SnCl$_3$)S$_4$] (**1**) and the thiomolybdate- and thiotungstate-substituted organotinsulfide clusters [{(PhSn)$_3$SnS$_6$}{(CpW)$_3$S$_3$Cl}] (**2**) and [(PhSn)$_3$SnS$_6${(CpMo)$_3$S$_4$H}] (**3**) were obtained in ligand exchange reactions from [(PhSn)$_4$S$_6$] and [M(CO)$_3$CpCl]. The M$_3$S$_3$ cages in **2** and **3** resemble a section of the respective transition metal dichalcogenides, thus representing model systems for the adsorption of organotinsulfide clusters on MoS$_2$ or WS$_2$ surfaces.

Table of Contents

1. Single-Crystal X-Ray Crystallography of Compound 1

Compound **1** crystallizes in the shape of black blocks. Data of the X-Ray diffraction analysis was collected on a STOE STADIVARI diffractometer using Cu K_α radiation (λ = 1.54186 Å) from an X-ray micro source with X-ray optics and a Pilatus 300K Si hybrid pixel array detector at 100 K. Reflection data were processed with X-Area 1.77.[1] Structure solution was performed by direct methods and full-matrix-least-squares refinement against F^2 using SHELXT[2] and SHELXL-2014[3] software. All non-hydrogen atoms were refined anisotropically. Hydrogen atom positions were calculated.

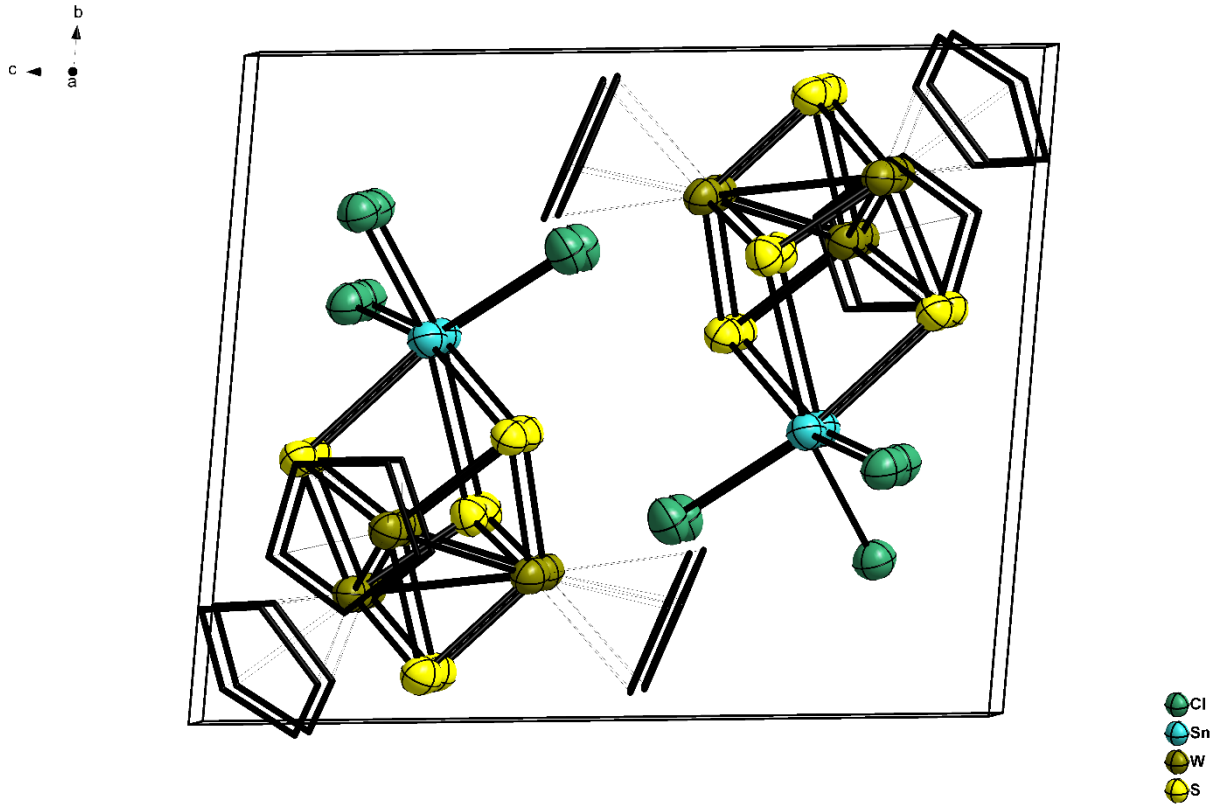

Figure S1: Crystal structure of **1**, viewed along the crystallographic *a* axis. Ellipsoids are drawn at 50% probability, hydrogen atoms are omitted for clarity.

Table S1: Crystal data and structure refinement for **1**.

Empirical formula	$C_{15}H_{15}Cl_3S_4Sn_1W_3$	
Formula weight	1100.10	
Temperature	100(2) K	
Wavelength	1.54178 Å	
Crystal system	Triclinic	
Space group	$P\bar{1}$	
Unit cell dimensions	a = 9.4238(4) Å	α = 94.067(3)°.
	b = 9.9348(4) Å	β = 97.043(3)°.
	c = 11.8329(5) Å	γ = 98.806(3)°.
Volume	1081.97(8) $Å^3$	
Z	2	
Density (calculated)	3.377 Mg/m^3	
Absorption coefficient	44.818 mm^{-1}	
F(000)	984	
Crystal size	0.7 x 0.04 x 0.02 mm^3	
Theta range for data collection	3.780 to 69.841°.	
Index ranges	-11<=h<=11, -12<=k<=7, -14<=l<=13	
Reflections collected	12229	
Independent reflections	4001 [R(int) = 0.0639]	
Completeness to theta = 67.679°	99.2 %	
Absorption correction	Sphere	
Max. and min. transmission	0.0231 and 0.0014	
Refinement method	Full-matrix least-squares on F^2	
Data / restraints / parameters	4001 / 6 / 208	
Goodness-of-fit on F^2	0.833	
Final R indices [I>2sigma(I)]	R1 = 0.0425, wR2 = 0.0979	
R indices (all data)	R1 = 0.0644, wR2 = 0.1020	
Largest diff. peak and hole	2.019 and -1.657 $e.Å^{-3}$	

Table S2: Atomic coordinates (x 10^4) and equivalent isotropic displacement parameters ($Å^2$x 10^3) for **1**. U(eq) is defined as one third of the trace of the orthogonalized U^{ij} tensor.

	x	y	z	U(eq)
C(1)	1710(12)	479(11)	4479(10)	50(4)
C(2)	3204(14)	430(11)	4454(10)	74(6)
C(3)	3846(10)	1677(12)	4075(10)	67(6)
C(4)	2748(14)	2496(9)	3866(9)	53(4)
C(5)	1428(10)	1756(13)	4116(10)	61(6)
C(6)	7415(13)	2543(11)	7183(7)	52(4)
C(7)	7039(12)	1686(8)	8047(9)	43(4)
C(8)	6985(12)	2535(11)	9053(7)	50(4)
C(9)	7329(13)	3918(9)	8810(9)	52(4)
C(10)	7594(12)	3923(9)	7655(10)	53(4)
C(11)	285(10)	583(10)	8418(8)	48(4)
C(12)	551(10)	1757(9)	9219(9)	35(3)
C(13)	1872(11)	1732(10)	9932(8)	42(4)
C(14)	2422(10)	543(11)	9573(9)	52(4)
C(15)	1442(12)	-167(8)	8637(10)	49(4)
Cl(1)	2047(4)	7039(4)	5749(3)	47(1)
Cl(2)	4561(4)	7665(3)	8327(3)	43(1)
Cl(3)	768(4)	6278(3)	8417(3)	45(1)
Sn(1)	2725(1)	5733(1)	7371(1)	35(1)
W(1)	2973(1)	2192(1)	5832(1)	37(1)
W(2)	2413(1)	1941(1)	8051(1)	35(1)
W(3)	5163(1)	2896(1)	7619(1)	35(1)
S(1)	4517(4)	4276(3)	6204(3)	36(1)
S(2)	1185(4)	3087(3)	6690(3)	37(1)
S(3)	3852(4)	3977(3)	8839(3)	35(1)
S(4)	3870(4)	713(3)	7075(3)	39(1)

Table S3: Bond lengths [Å] and angles [°] for **1**.

C(1)-C(2)	1.4200	W(1)-W(3)	2.7379(10)	Cl(3)-Sn(1)-Cl(1)	94.30(13)
C(1)-C(5)	1.4200	W(1)-W(2)	2.7612(9)	Cl(3)-Sn(1)-Cl(2)	95.40(12)
C(1)-W(1)	2.324(10)	W(2)-S(3)	2.320(3)	Cl(1)-Sn(1)-Cl(2)	92.70(13)
C(2)-C(3)	1.4200	W(2)-S(4)	2.325(3)	Cl(3)-Sn(1)-S(3)	98.57(12)
C(2)-W(1)	2.360(11)	W(2)-S(2)	2.332(4)	Cl(1)-Sn(1)-S(3)	166.52(12)
C(3)-C(4)	1.4200	W(2)-W(3)	2.7415(9)	Cl(2)-Sn(1)-S(3)	90.08(12)
C(3)-W(1)	2.379(11)	W(3)-S(1)	2.321(4)	Cl(3)-Sn(1)-S(1)	162.07(11)
C(4)-C(5)	1.4200	W(3)-S(3)	2.322(3)	Cl(1)-Sn(1)-S(1)	94.66(12)
C(4)-W(1)	2.355(11)	W(3)-S(4)	2.324(3)	Cl(2)-Sn(1)-S(1)	99.66(11)
C(5)-W(1)	2.321(10)	C(2)-C(1)-W(1)	73.7(4)	S(3)-Sn(1)-S(1)	71.87(10)
C(6)-C(7)	1.4200	C(5)-C(1)-W(1)	72.1(4)	Cl(3)-Sn(1)-S(2)	90.57(11)
C(6)-C(10)	1.4200	C(1)-C(2)-W(1)	71.0(4)	Cl(1)-Sn(1)-S(2)	103.26(12)
C(6)-W(3)	2.316(11)	C(3)-C(2)-W(1)	73.3(4)	Cl(2)-Sn(1)-S(2)	162.50(12)
C(7)-C(8)	1.4200	C(4)-C(3)-W(1)	71.6(4)	S(3)-Sn(1)-S(2)	72.74(10)
C(7)-W(3)	2.312(10)	C(2)-C(3)-W(1)	71.9(4)	S(1)-Sn(1)-S(2)	72.26(10)
C(8)-C(9)	1.4200	C(5)-C(4)-W(1)	71.0(4)	S(1)-W(1)-C(5)	118.8(3)
C(8)-W(3)	2.349(10)	C(3)-C(4)-W(1)	73.5(4)	S(1)-W(1)-C(1)	147.8(3)
C(9)-C(10)	1.4200	C(4)-C(5)-W(1)	73.6(4)	C(5)-W(1)-C(1)	35.60(14)
C(9)-W(3)	2.375(11)	C(1)-C(5)-W(1)	72.3(4)	S(1)-W(1)-S(2)	91.01(12)
C(10)-W(3)	2.355(11)	C(7)-C(6)-W(3)	72.0(4)	C(5)-W(1)-S(2)	89.9(2)
C(11)-C(12)	1.4200	C(10)-C(6)-W(3)	73.8(4)	C(1)-W(1)-S(2)	104.7(3)
C(11)-C(15)	1.4200	C(6)-C(7)-W(3)	72.3(4)	S(1)-W(1)-S(4)	107.05(13)
C(11)-W(2)	2.345(10)	C(8)-C(7)-W(3)	73.7(4)	C(5)-W(1)-S(4)	131.0(3)
C(12)-C(13)	1.4200	C(7)-C(8)-W(3)	70.8(4)	C(1)-W(1)-S(4)	95.5(3)
C(12)-W(2)	2.357(10)	C(9)-C(8)-W(3)	73.5(4)	S(2)-W(1)-S(4)	106.31(13)
C(13)-C(14)	1.4200	C(10)-C(9)-W(3)	71.8(4)	S(1)-W(1)-C(4)	89.5(3)
C(13)-W(2)	2.361(10)	C(8)-C(9)-W(3)	71.5(4)	C(5)-W(1)-C(4)	35.35(14)
C(14)-C(15)	1.4200	C(9)-C(10)-W(3)	73.3(4)	C(1)-W(1)-C(4)	58.81(17)
C(14)-W(2)	2.351(10)	C(6)-C(10)-W(3)	70.8(4)	S(2)-W(1)-C(4)	110.9(3)
C(15)-W(2)	2.341(10)	C(12)-C(11)-W(2)	72.9(4)	S(4)-W(1)-C(4)	138.8(3)
Cl(1)-Sn(1)	2.467(4)	C(15)-C(11)-W(2)	72.2(4)	S(1)-W(1)-C(2)	124.8(3)
Cl(2)-Sn(1)	2.481(3)	C(13)-C(12)-W(2)	72.6(4)	C(5)-W(1)-C(2)	58.78(17)
Cl(3)-Sn(1)	2.449(4)	C(11)-C(12)-W(2)	72.0(4)	C(1)-W(1)-C(2)	35.28(14)
Sn(1)-S(3)	2.780(4)	C(14)-C(13)-W(2)	72.1(4)	S(2)-W(1)-C(2)	139.8(3)
Sn(1)-S(1)	2.809(3)	C(12)-C(13)-W(2)	72.3(4)	S(4)-W(1)-C(2)	81.9(3)
Sn(1)-S(2)	2.812(4)	C(13)-C(14)-W(2)	72.8(4)	C(4)-W(1)-C(2)	58.33(17)
W(1)-S(1)	2.321(3)	C(15)-C(14)-W(2)	72.0(4)	S(1)-W(1)-C(3)	92.9(3)
W(1)-S(2)	2.326(3)	C(11)-C(15)-W(2)	72.5(4)	C(5)-W(1)-C(3)	58.52(17)
W(1)-S(4)	2.328(4)	C(14)-C(15)-W(2)	72.8(4)	C(1)-W(1)-C(3)	58.47(17)

S(2)-W(1)-C(3)	145.5(3)	C(11)-W(2)-C(12)	35.15(14)	S(4)-W(3)-C(8)	103.4(3)
S(4)-W(1)-C(3)	105.2(3)	C(14)-W(2)-C(12)	58.42(16)	C(7)-W(3)-C(10)	58.98(18)
C(4)-W(1)-C(3)	34.91(14)	S(3)-W(2)-C(13)	84.2(2)	C(6)-W(3)-C(10)	35.39(15)
C(2)-W(1)-C(3)	34.87(14)	S(4)-W(2)-C(13)	127.5(3)	S(1)-W(3)-C(10)	88.6(3)
S(1)-W(1)-W(3)	53.84(9)	S(2)-W(2)-C(13)	125.1(3)	S(3)-W(3)-C(10)	115.6(3)
C(5)-W(1)-W(3)	169.6(3)	C(15)-W(2)-C(13)	58.51(17)	S(4)-W(3)-C(10)	134.5(3)
C(1)-W(1)-W(3)	146.7(3)	C(11)-W(2)-C(13)	58.45(16)	C(8)-W(3)-C(10)	58.48(18)
S(2)-W(1)-W(3)	97.34(9)	C(14)-W(2)-C(13)	35.08(13)	C(7)-W(3)-C(9)	58.69(17)
S(4)-W(1)-W(3)	53.89(9)	C(12)-W(2)-C(13)	35.04(13)	C(6)-W(3)-C(9)	58.64(18)
C(4)-W(1)-W(3)	134.3(3)	S(3)-W(2)-W(3)	53.83(9)	S(1)-W(3)-C(9)	111.7(3)
C(2)-W(1)-W(3)	117.6(3)	S(4)-W(2)-W(3)	53.86(9)	S(3)-W(3)-C(9)	88.9(2)
C(3)-W(1)-W(3)	112.5(3)	S(2)-W(2)-W(3)	97.10(9)	S(4)-W(3)-C(9)	137.9(3)
S(1)-W(1)-W(2)	96.50(9)	C(15)-W(2)-W(3)	130.3(2)	C(8)-W(3)-C(9)	34.98(14)
C(5)-W(1)-W(2)	130.5(3)	C(11)-W(2)-W(3)	165.1(2)	C(10)-W(3)-C(9)	34.94(14)
C(1)-W(1)-W(2)	115.5(3)	C(14)-W(2)-W(3)	112.0(2)	C(7)-W(3)-W(1)	125.1(2)
S(2)-W(1)-W(2)	53.74(9)	C(12)-W(2)-W(3)	152.8(2)	C(6)-W(3)-W(1)	114.1(2)
S(4)-W(1)-W(2)	53.55(8)	C(13)-W(2)-W(3)	121.7(2)	S(1)-W(3)-W(1)	53.86(8)
C(4)-W(1)-W(2)	163.5(3)	S(3)-W(2)-W(1)	96.35(9)	S(3)-W(3)-W(1)	96.95(9)
C(2)-W(1)-W(2)	127.5(3)	S(4)-W(2)-W(1)	53.65(9)	S(4)-W(3)-W(1)	54.01(9)
C(3)-W(1)-W(2)	158.6(3)	S(2)-W(2)-W(1)	53.54(9)	C(8)-W(3)-W(1)	156.7(3)
W(3)-W(1)-W(2)	59.80(2)	C(15)-W(2)-W(1)	121.4(2)	C(10)-W(3)-W(1)	130.7(3)
S(3)-W(2)-S(4)	106.98(12)	C(11)-W(2)-W(1)	120.5(2)	C(9)-W(3)-W(1)	164.1(3)
S(3)-W(2)-S(2)	90.93(12)	C(14)-W(2)-W(1)	145.7(2)	C(7)-W(3)-W(2)	121.1(3)
S(4)-W(2)-S(2)	106.21(13)	C(12)-W(2)-W(1)	143.5(2)	C(6)-W(3)-W(2)	151.5(3)
S(3)-W(2)-C(15)	138.8(3)	C(13)-W(2)-W(1)	178.5(2)	S(1)-W(3)-W(2)	97.04(9)
S(4)-W(2)-C(15)	85.7(2)	W(3)-W(2)-W(1)	59.68(2)	S(3)-W(3)-W(2)	53.78(9)
S(2)-W(2)-C(15)	123.7(3)	C(7)-W(3)-C(6)	35.74(14)	S(4)-W(3)-W(2)	53.88(9)
S(3)-W(2)-C(11)	136.6(2)	C(7)-W(3)-S(1)	135.8(3)	C(8)-W(3)-W(2)	113.6(2)
S(4)-W(2)-C(11)	113.0(3)	C(6)-W(3)-S(1)	100.5(3)	C(10)-W(3)-W(2)	167.8(3)
S(2)-W(2)-C(11)	93.4(3)	C(7)-W(3)-S(3)	129.5(3)	C(9)-W(3)-W(2)	133.2(3)
C(15)-W(2)-C(11)	35.28(14)	C(6)-W(3)-S(3)	147.6(3)	W(1)-W(3)-W(2)	60.52(2)
S(3)-W(2)-C(14)	103.8(3)	S(1)-W(3)-S(3)	89.92(12)	W(3)-S(1)-W(1)	72.30(10)
S(4)-W(2)-C(14)	93.6(2)	C(7)-W(3)-S(4)	82.2(2)	W(3)-S(1)-Sn(1)	98.66(13)
S(2)-W(2)-C(14)	150.8(2)	C(6)-W(3)-S(4)	99.2(3)	W(1)-S(1)-Sn(1)	98.43(12)
C(15)-W(2)-C(14)	35.23(14)	S(1)-W(3)-S(4)	107.18(13)	W(1)-S(2)-W(2)	72.72(10)
C(11)-W(2)-C(14)	58.59(17)	S(3)-W(3)-S(4)	106.96(12)	W(1)-S(2)-Sn(1)	98.24(12)
S(3)-W(2)-C(12)	101.5(2)	C(7)-W(3)-C(8)	35.47(13)	W(2)-S(2)-Sn(1)	97.57(12)
S(4)-W(2)-C(12)	144.2(2)	C(6)-W(3)-C(8)	59.01(17)	W(2)-S(3)-W(3)	72.40(9)
S(2)-W(2)-C(12)	94.3(2)	S(1)-W(3)-C(8)	145.7(3)	W(2)-S(3)-Sn(1)	98.74(13)
C(15)-W(2)-C(12)	58.55(17)	S(3)-W(3)-C(8)	95.8(2)		

W(3)-S(3)-Sn(1)	99.46(13)	W(3)-S(4)-W(1)	72.10(10)	W(2)-S(4)-W(1)	72.80(10)
W(3)-S(4)-W(2)	72.26(9)				

2. Single-Crystal X-Ray Crystallography of Compound 2

Compound **2** crystallizes as orange hexagonal plates. Data of the X-Ray diffraction analysis was collected on a STOE STADIVARI diffractometer using Cu K_α radiation (λ = 1.54186 Å) from an X-ray micro source with X-ray optics and a Pilatus 300K Si hybrid pixel array detector at 100 K. Reflection data were processed with X-Area 1.77.[1] Structure solution was performed by direct methods and full-matrix-least-squares refinement against F^2 using SHELXT[2] and SHELXL-2014[3] software. All non-hydrogen atoms were refined anisotropically, although C7 – C11 were refined using an EADP restraint due to their disorder. Hydrogen atom positions were calculated. **2** reproducibly crystallizes as inversion twin and was refined accordingly. Cocrystallized toluene could not be refined and was thus removed using the SQUEEZE routine. The void is located at 0.0, 0.0, 0.5, has a volume of 236 $Å^3$ and contains 74 electrons, corresponding to 0.37 molecules of toluene per formula unit.

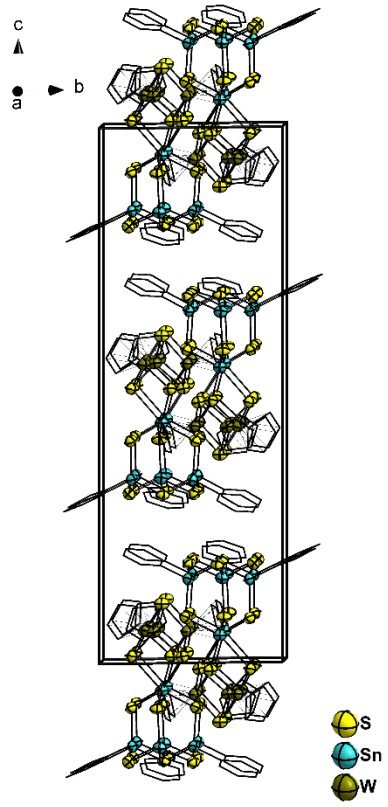

Figure S2: Crystal structure of **2**, viewed along the crystallographic *a* axis. Ellipsoids are drawn at 50% probability, hydrogen atoms are omitted for clarity.

Table S4: Crystal data and structure refinement for **2**.

Empirical formula	$C_{33}H_{30}S_{10}Sn_4W_3$	
Formula weight	1773.48	
Temperature	100(2) K	
Wavelength	154.178 pm	
Crystal system	Trigonal	
Space group	$P\bar{3}c1$	
Unit cell dimensions	a = 12.77920(10) Å	α = 90°.
	b = 12.77920(10) Å	β = 90°.
	c = 32.6497(4) Å	γ = 120°.
Volume	4.61761(9) nm^3	
Z	4	
Density (calculated)	2.551 Mg/m^3	
Absorption coefficient	34.735 mm^{-1}	
F(000)	3240	
Crystal size	0.15 x 0.10 x 0.03 mm^3	
Theta range for data collection	2.707 to 73.258°.	
Index ranges	-13<=h<=13, -15<=k<=15, 0<=l<=39	
Reflections collected	3104	
Independent reflections	3104 [R(int) = ?]	
Completeness to theta = 67.679°	100.0 %	
Absorption correction	Sphere	
Max. and min. transmission	0.0007 and 0.0000	
Refinement method	Full-matrix least-squares on F^2	
Data / restraints / parameters	3104 / 36 / 107	
Goodness-of-fit on F^2	1.066	
Final R indices [I>2sigma(I)]	R1 = 0.0592, wR2 = 0.1578	
R indices (all data)	R1 = 0.0604, wR2 = 0.1591	
Largest diff. peak and hole	2.984 and -1.793 e.$Å^{-3}$	

Table S5: Atomic coordinates (x 10^4) and equivalent isotropic displacement parameters ($Å^2$x 10^3) for **2**. U(eq) is defined as one third of the trace of the orthogonalized U^{ij} tensor.

	x	y	z	U(eq)
Sn(1)	5067(1)	-1684(1)	1593(1)	50(1)
S(1)	3415(3)	-1510(3)	1870(1)	53(1)
W(1)	2353(1)	-2918(1)	-565(1)	55(1)
C(1)	6570(7)	-126(7)	1847(2)	59(3)
C(2)	6398(8)	818(9)	1971(3)	71(4)
C(3)	7356(11)	1862(8)	2136(3)	100(7)
C(4)	8485(9)	1961(10)	2176(4)	87(5)
C(5)	8656(8)	1017(13)	2052(4)	109(8)
C(6)	7699(9)	-27(10)	1888(4)	95(6)
C(7)	323(13)	-3410(15)	-675(6)	119(4)
C(8)	862(17)	-2420(19)	-400(4)	119(4)
C(9)	1820(15)	-1428(14)	-608(6)	119(4)
C(10)	1873(15)	-1806(18)	-1013(5)	119(4)
C(11)	947(18)	-3031(18)	-1054(5)	119(4)
S(4)	3333	-3333	-1087(2)	60(1)
S(3)	1671(3)	-4497(3)	-99(1)	56(1)
Sn(2)	3333	-3333	540(1)	51(1)
S(2)	5207(3)	-1647(3)	869(1)	59(1)

Table S6: Bond lengths [Å] and angles [°] for **2**.

Sn(1)-C(1)	2.126(7)	Sn(2)-S(2)#1	2.524(3)	S(3)#1-W(1)-S(4)	106.83(10)
Sn(1)-S(2)	2.371(3)	C(1)-Sn(1)-S(2)	110.3(2)	S(3)-W(1)-C(8)	94.7(4)
Sn(1)-S(1)#1	2.395(3)	C(1)-Sn(1)-S(1)#1	107.4(3)	C(9)-W(1)-C(8)	35.3(2)
Sn(1)-S(1)	2.407(3)	S(2)-Sn(1)-S(1)#1	111.11(12)	C(10)-W(1)-C(8)	58.8(2)
W(1)-S(3)	2.321(3)	C(1)-Sn(1)-S(1)	101.0(3)	S(3)#1-W(1)-C(8)	98.9(5)
W(1)-C(9)	2.325(15)	S(2)-Sn(1)-S(1)	115.75(12)	S(4)-W(1)-C(8)	146.1(4)
W(1)-C(10)	2.325(13)	S(1)#1-Sn(1)-S(1)	110.65(14)	S(3)-W(1)-C(11)	116.6(5)
W(1)-S(3)#1	2.326(3)	Sn(1)#2-S(1)-Sn(1)	102.57(11)	C(9)-W(1)-C(11)	58.8(2)
W(1)-S(4)	2.330(4)	S(3)-W(1)-C(9)	128.0(5)	C(10)-W(1)-C(11)	35.32(18)
W(1)-C(8)	2.354(15)	S(3)-W(1)-C(10)	147.6(4)	S(3)#1-W(1)-C(11)	145.0(5)
W(1)-C(11)	2.355(15)	C(9)-W(1)-C(10)	35.56(19)	S(4)-W(1)-C(11)	88.2(4)
W(1)-C(7)	2.372(14)	S(3)-W(1)-S(3)#1	89.48(16)	C(8)-W(1)-C(11)	58.4(2)
W(1)-W(1)#1	2.7473(10)	C(9)-W(1)-S(3)#1	87.1(4)	S(3)-W(1)-C(7)	89.1(4)
W(1)-W(1)#2	2.7473(10)	C(10)-W(1)-S(3)#1	111.4(5)	C(9)-W(1)-C(7)	58.6(2)
S(3)-Sn(2)	2.814(3)	S(3)-W(1)-S(4)	107.02(10)	C(10)-W(1)-C(7)	58.6(2)
Sn(2)-S(2)	2.524(3)	C(9)-W(1)-S(4)	123.6(5)	S(3)#1-W(1)-C(7)	133.4(5)
Sn(2)-S(2)#2	2.524(3)	C(10)-W(1)-S(4)	90.8(4)	S(4)-W(1)-C(7)	118.0(5)

C(8)-W(1)-C(7)	34.97(19)	C(2)-C(1)-Sn(1)	117.8(5)	S(2)-Sn(2)-S(2)#2	103.22(8)
C(11)-W(1)-C(7)	34.96(19)	C(6)-C(1)-Sn(1)	122.2(5)	S(2)-Sn(2)-S(2)#1	103.22(8)
S(3)-W(1)-W(1)#1	96.54(8)	C(11)-C(7)-W(1)	71.8(5)	S(2)#2-Sn(2)-S(2)#1	103.22(8)
C(9)-W(1)-W(1)#1	121.5(4)	C(8)-C(7)-W(1)	71.8(6)	S(2)-Sn(2)-S(3)	155.49(10)
C(10)-W(1)-W(1)#1	115.7(4)	C(9)-C(8)-W(1)	71.2(6)	S(2)#2-Sn(2)-S(3)	84.87(10)
S(3)#1-W(1)-W(1)#1	53.66(8)	C(7)-C(8)-W(1)	73.2(6)	S(2)#1-Sn(2)-S(3)	97.19(10)
S(4)-W(1)-W(1)#1	53.87(7)	C(10)-C(9)-W(1)	72.2(6)	S(2)-Sn(2)-S(3)#1	84.87(10)
C(8)-W(1)-W(1)#1	150.1(5)	C(8)-C(9)-W(1)	73.4(6)	S(2)#2-Sn(2)-S(3)#1	97.19(10)
C(11)-W(1)-W(1)#1	136.5(5)	C(9)-C(10)-W(1)	72.2(6)	S(2)#1-Sn(2)-S(3)#1	155.49(10)
C(7)-W(1)-W(1)#1	171.2(5)	C(11)-C(10)-W(1)	73.5(6)	S(3)-Sn(2)-S(3)#1	71.07(11)
S(3)-W(1)-W(1)#2	53.85(8)	C(7)-C(11)-W(1)	73.2(5)	S(2)-Sn(2)-S(3)#2	97.19(10)
C(9)-W(1)-W(1)#2	176.2(4)	C(10)-C(11)-W(1)	71.2(6)	S(2)#2-Sn(2)-S(3)#2	155.49(10)
C(10)-W(1)-W(1)#2	140.8(5)	W(1)-S(4)-W(1)#1	72.26(13)	S(2)#1-Sn(2)-S(3)#2	84.87(10)
S(3)#1-W(1)-W(1)#2	96.40(8)	W(1)-S(4)-W(1)#2	72.26(13)	S(3)-Sn(2)-S(3)#2	71.07(11)
S(4)-W(1)-W(1)#2	53.87(7)	W(1)#1-S(4)-W(1)#2	72.26(13)	S(3)#1-Sn(2)-S(3)#2	71.07(11)
C(8)-W(1)-W(1)#2	144.8(5)	W(1)-S(3)-W(1)#2	72.49(10)	Sn(1)-S(2)-Sn(2)	112.16(12)
C(11)-W(1)-W(1)#2	117.5(4)	W(1)-S(3)-Sn(2)	99.79(12)		
C(7)-W(1)-W(1)#2	119.3(4)	W(1)#2-S(3)-Sn(2)	99.64(11)		

Symmetry transformations used to generate equivalent atoms:

#1 -x+y+1,-x,z #2 -y,x-y-1,z

3. Single-Crystal X-Ray Crystallography of Compound 3

Compound **3** crystallizes as deep red hexagonal plates. Data of the X-Ray diffraction analysis was collected on a STOE STADIVARI diffractometer using Cu K_α radiation (λ = 1.54186 Å) from an X-ray micro source with X-ray optics and a Pilatus 300K Si hybrid pixel array detector at 100 K. Reflection data were processed with X-Area 1.77.[1] Structure solution was performed by direct methods and full-matrix-least-squares refinement against F^2 using SHELXT[2] and SHELXL-2014[3] software. All non-hydrogen atoms were refined anisotropically, although C7 – C11 were refined using an EADP restraint due to their disorder. Hydrogen atom positions were calculated. **3** reproducibly crystallizes as inversion twin and was refined accordingly. Cocrystallized toluene could not be refined and was thus removed using the SQUEEZE routine. The void is located at 0.0, 0.0, 0.5, has a volume of 270 $Å^3$ and contains 92 electrons, corresponding to 0.46 molecules of toluene per formula unit.

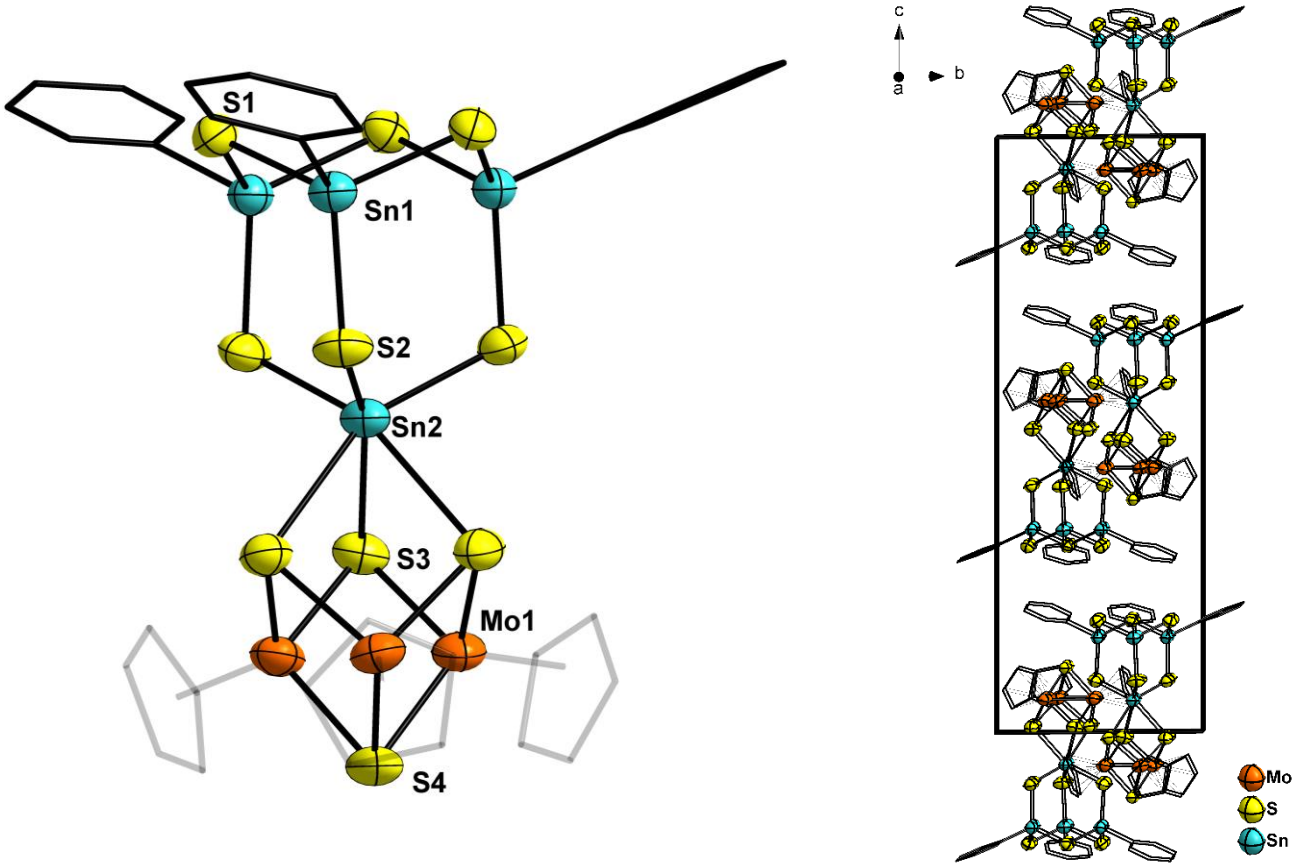

Figure S3: Left: Molecular structure of **3**. Right: Crystal structure of **3**, viewed along the crystallographic *a* axis. Ellipsoids are drawn at 50% probability, hydrogen atoms are omitted for clarity.

Table S7: Crystal data and structure refinement for **3**.

Empirical formula	$C_{33}H_{30}Mo_3S_{10}Sn_4$	
Formula weight	1509.92	
Temperature	100(2) K	
Wavelength	1.54178 Å	
Crystal system	Trigonal	
Space group	$P\bar{3}c1$	
Unit cell dimensions	a = 12.90680(10) Å	α = 90°.
	b = 12.90680(10) Å	β = 90°.
	c = 32.3654(4) Å	γ = 120°.
Volume	4.66927(9) nm^3	
Z	4	
Density (calculated)	2.152 Mg/m^3	
Absorption coefficient	27.598 mm^{-1}	
F(000)	2860	
Crystal size	0.06 x 0.04 x 0.01 mm^3	
Theta range for data collection	2.730 to 69.999°.	
Index ranges	-13<=h<=13, -15<=k<=15, 0<=l<=39	
Reflections collected	2963	
Independent reflections	2963 [R(int) = ?]	
Completeness to theta = 67.679°	100.0 %	
Absorption correction	Sphere	
Max. and min. transmission	0.0203 and 0.0013	
Refinement method	Full-matrix least-squares on F^2	
Data / restraints / parameters	2963 / 0 / 119	
Goodness-of-fit on F^2	1.005	
Final R indices [I>2sigma(I)]	R1 = 0.0400, wR2 = 0.1059	
R indices (all data)	R1 = 0.0479, wR2 = 0.1103	
Largest diff. peak and hole	1.206 and -0.804 e.$Å^{-3}$	

Table S8: Atomic coordinates (x 10^4) and equivalent isotropic displacement parameters ($Å^2$x 10^3) for **3**. U(eq) is defined as one third of the trace of the orthogonalized U^{ij} tensor.

	x	y	z	U(eq)
Mo(1)	7067(1)	4713(1)	5552(1)	62(1)
S(1)	6587(2)	1522(2)	3115(1)	51(1)
S(2)	4823(2)	1669(2)	4126(1)	61(1)
S(3)	8291(2)	4485(3)	5080(1)	60(1)
Sn(1)	4954(1)	1695(1)	3395(1)	48(1)
Sn(2)	6667	3333	4451(1)	54(1)
C(1)	3545(10)	-848(9)	3030(3)	64(3)
C(2)	3425(8)	144(8)	3144(2)	54(2)
C(3)	2379(10)	72(10)	3109(3)	65(2)
C(4)	1380(11)	-1001(14)	2951(4)	85(4)
S(4)	6667	3333	6077(1)	69(1)
C(5)	1509(10)	-1935(10)	2843(3)	71(3)
C(6)	2599(12)	-1865(10)	2877(3)	70(3)
C(7)	6987(11)	5981(9)	6073(3)	110(2)
C(8)	8194(10)	6310(9)	5990(3)	110(2)
C(9)	8453(8)	6718(9)	5575(3)	110(2)
C(10)	7407(11)	6642(10)	5401(3)	110(2)
C(11)	6501(8)	6187(9)	5709(4)	110(2)

Table S9: Bond lengths [Å] and angles [°] for **3**.

Mo(1)-C(9)	2.296(10)	C(1)-C(6)	1.363(16)	C(9)-Mo(1)-C(10)	35.54(14)
Mo(1)-S(3)#1	2.318(3)	C(1)-C(2)	1.412(16)	S(3)#1-Mo(1)-C(10)	93.1(2)
Mo(1)-C(8)	2.318(9)	C(2)-C(3)	1.311(16)	C(8)-Mo(1)-C(10)	58.92(16)
Mo(1)-S(3)	2.318(3)	C(3)-C(4)	1.434(19)	S(3)-Mo(1)-C(10)	102.7(3)
Mo(1)-S(4)	2.324(3)	C(4)-C(5)	1.34(2)	S(4)-Mo(1)-C(10)	144.5(2)
Mo(1)-C(10)	2.353(11)	C(5)-C(6)	1.368(19)	C(9)-Mo(1)-C(7)	58.71(15)
Mo(1)-C(7)	2.388(9)	C(9)-Mo(1)-S(3)#1	125.5(3)	S(3)#1-Mo(1)-C(7)	119.2(3)
Mo(1)-C(11)	2.409(9)	C(9)-Mo(1)-C(8)	35.84(13)	C(8)-Mo(1)-C(7)	35.08(13)
Mo(1)-Mo(1)#2	2.7480(15)	S(3)#1-Mo(1)-C(8)	148.4(2)	S(3)-Mo(1)-C(7)	144.8(3)
Mo(1)-Mo(1)#1	2.7480(15)	C(9)-Mo(1)-S(3)	88.2(2)	S(4)-Mo(1)-C(7)	86.6(3)
S(1)-Sn(1)	2.404(2)	S(3)#1-Mo(1)-S(3)	88.49(13)	C(10)-Mo(1)-C(7)	57.97(15)
S(1)-Sn(1)#1	2.407(2)	C(8)-Mo(1)-S(3)	110.6(3)	C(9)-Mo(1)-C(11)	58.40(16)
S(2)-Sn(1)	2.371(2)	C(9)-Mo(1)-S(4)	126.1(3)	S(3)#1-Mo(1)-C(11)	90.6(2)
S(2)-Sn(2)	2.505(2)	S(3)#1-Mo(1)-S(4)	106.82(8)	C(8)-Mo(1)-C(11)	58.12(15)
S(3)-Sn(2)	2.762(3)	C(8)-Mo(1)-S(4)	92.0(3)	S(3)-Mo(1)-C(11)	137.2(3)
Sn(1)-C(2)	2.148(9)	S(3)-Mo(1)-S(4)	106.80(9)	S(4)-Mo(1)-C(11)	114.3(3)

C(10)-Mo(1)-C(11)	34.67(13)	Mo(1)#2-S(3)-Sn(2)	99.90(10)	S(3)-Sn(2)-S(3)#1	71.70(9)
C(7)-Mo(1)-C(11)	34.43(12)	Mo(1)-S(3)-Sn(2)	99.89(9)	C(6)-C(1)-C(2)	121.1(11)
C(9)-Mo(1)-Mo(1)#2	123.9(3)	C(2)-Sn(1)-S(2)	109.8(2)	C(3)-C(2)-C(1)	119.3(10)
S(3)#1-Mo(1)-Mo(1)#2	96.04(7)	C(2)-Sn(1)-S(1)	102.2(3)	C(3)-C(2)-Sn(1)	122.1(9)
C(8)-Mo(1)-Mo(1)#2	115.6(2)	S(2)-Sn(1)-S(1)	115.75(9)	C(1)-C(2)-Sn(1)	118.5(8)
S(3)-Mo(1)-Mo(1)#2	53.64(7)	C(2)-Sn(1)-S(1)#2	106.8(3)	C(2)-C(3)-C(4)	119.6(12)
S(4)-Mo(1)-Mo(1)#2	53.76(5)	S(2)-Sn(1)-S(1)#2	110.74(9)	C(5)-C(4)-C(3)	120.4(12)
C(10)-Mo(1)-Mo(1)#2	154.2(3)	S(1)-Sn(1)-S(1)#2	110.93(10)	Mo(1)-S(4)-Mo(1)#2	72.47(11)
C(7)-Mo(1)-Mo(1)#2	134.1(3)	S(2)#2-Sn(2)-S(2)	103.58(6)	Mo(1)-S(4)-Mo(1)#1	72.47(11)
C(11)-Mo(1)-Mo(1)#2	167.6(3)	S(2)#2-Sn(2)-S(2)#1	103.58(6)	Mo(1)#2-S(4)-Mo(1)#1	72.47(11)
C(9)-Mo(1)-Mo(1)#1	175.6(2)	S(2)-Sn(2)-S(2)#1	103.58(6)	C(4)-C(5)-C(6)	120.3(10)
S(3)#1-Mo(1)-Mo(1)#1	53.66(7)	S(2)#2-Sn(2)-S(3)#2	155.69(8)	C(1)-C(6)-C(5)	119.3(11)
C(8)-Mo(1)-Mo(1)#1	142.2(3)	S(2)-Sn(2)-S(3)#2	84.52(8)	C(11)-C(7)-Mo(1)	73.6(4)
S(3)-Mo(1)-Mo(1)#1	96.02(7)	S(2)#1-Sn(2)-S(3)#2	96.51(8)	C(8)-C(7)-Mo(1)	69.8(4)
S(4)-Mo(1)-Mo(1)#1	53.76(5)	S(2)#2-Sn(2)-S(3)	96.52(8)	C(9)-C(8)-Mo(1)	71.2(4)
C(10)-Mo(1)-Mo(1)#1	141.5(3)	S(2)-Sn(2)-S(3)	155.69(8)	C(7)-C(8)-Mo(1)	75.1(4)
C(7)-Mo(1)-Mo(1)#1	117.4(2)	S(2)#1-Sn(2)-S(3)	84.52(8)	C(10)-C(9)-Mo(1)	74.4(4)
C(11)-Mo(1)-Mo(1)#1	117.3(3)	S(3)#2-Sn(2)-S(3)	71.70(9)	C(8)-C(9)-Mo(1)	72.9(4)
Sn(1)-S(1)-Sn(1)#1	102.38(8)	S(2)#2-Sn(2)-S(3)#1	84.52(8)	C(9)-C(10)-Mo(1)	70.0(4)
Sn(1)-S(2)-Sn(2)	112.14(9)	S(2)-Sn(2)-S(3)#1	96.51(8)	C(11)-C(10)-Mo(1)	74.8(4)
Mo(1)#2-S(3)-Mo(1)	72.70(8)	S(2)#1-Sn(2)-S(3)#1	155.69(8)	C(7)-C(11)-Mo(1)	72.0(4)
		S(3)#2-Sn(2)-S(3)#1	71.70(9)	C(10)-C(11)-Mo(1)	70.5(4)

Symmetry transformations used to generate equivalent atoms:

#1 -x+y+1,-x+1,z #2 -y+1,x-y,z

4. XRF Spectra

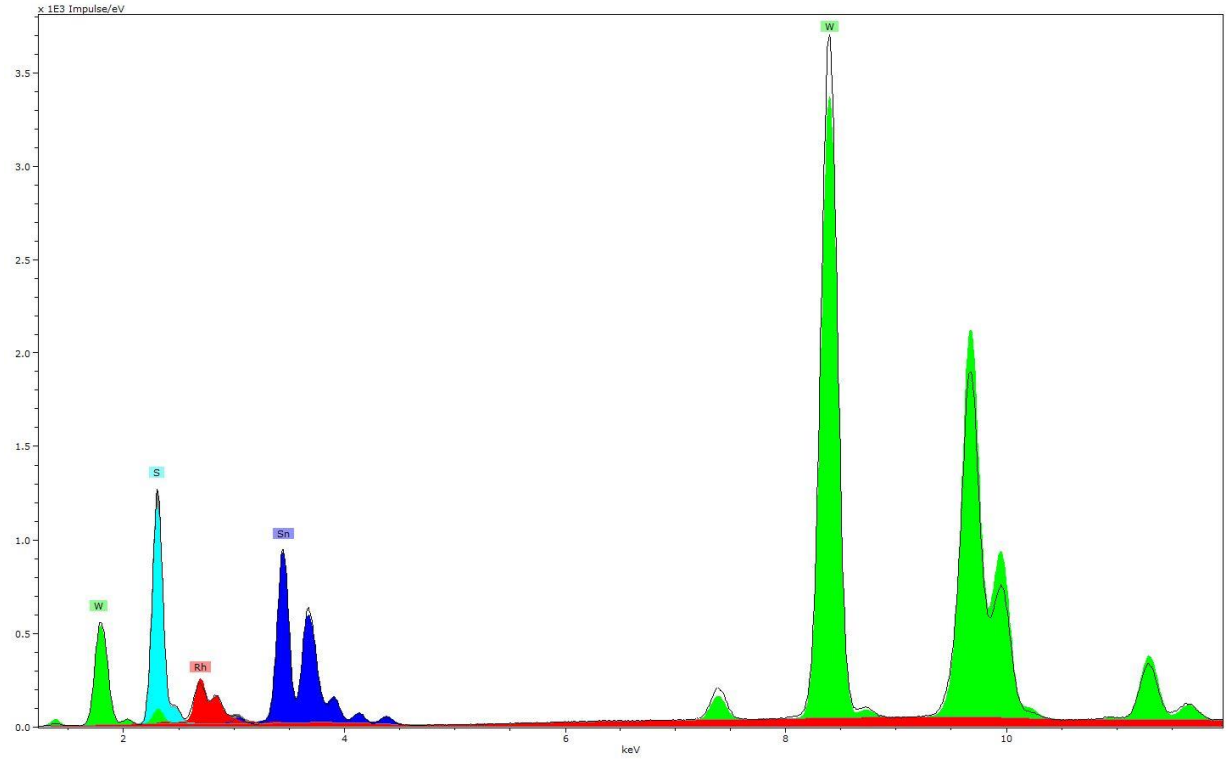

Figure S4: µ-XRF spectrum of **2**.

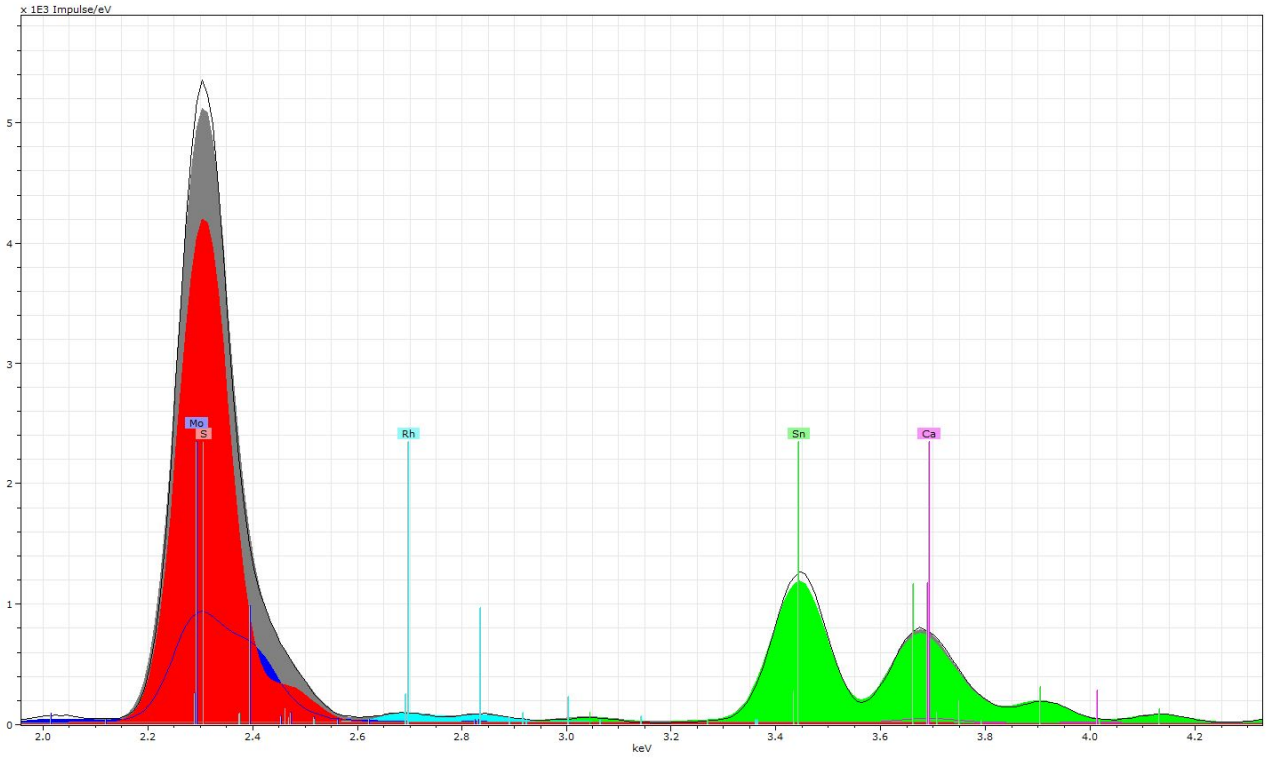

Figure S5: µ-XRF spectrum of **3**.

5. Mass spectra

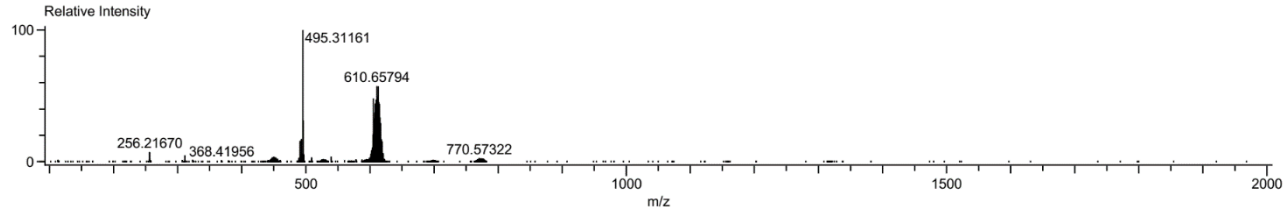

Figure S6: LIFDI mass spectrum of **3**.

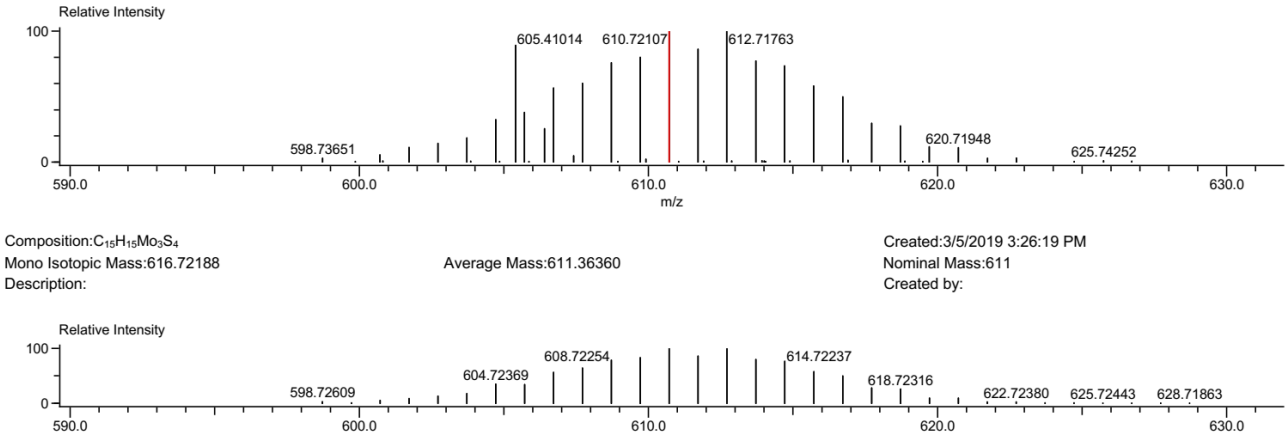

Figure S7: High resolution of the mass signal at 610.72107 m/z, corresponding to a fragment with the formula [$C_{15}H_{15}Mo_3S_4$].

6. IR spectra

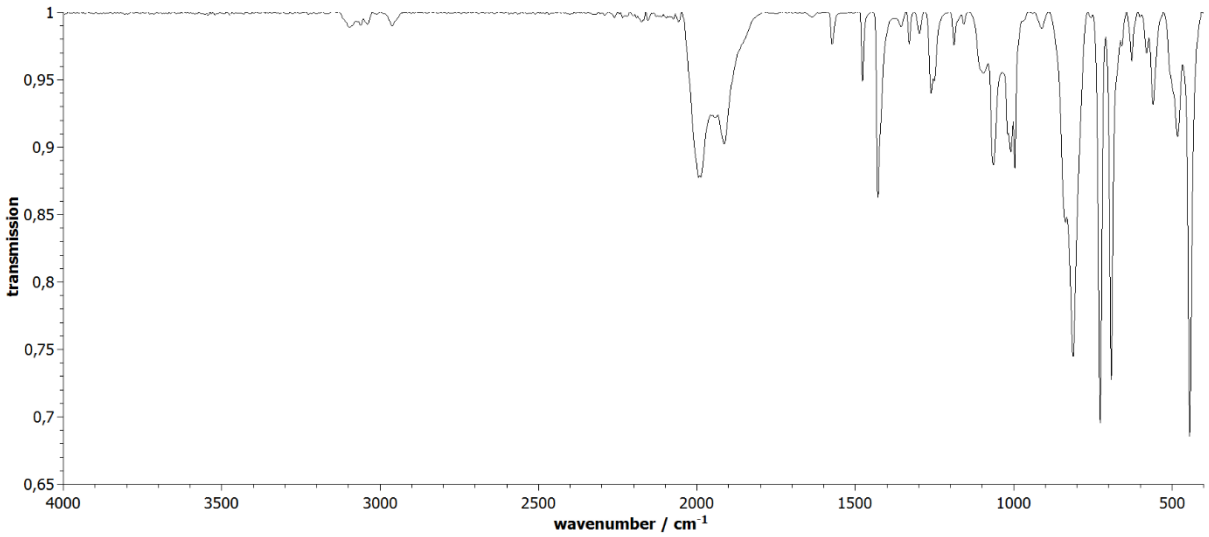

Figure S8: IR spectrum of **2**.

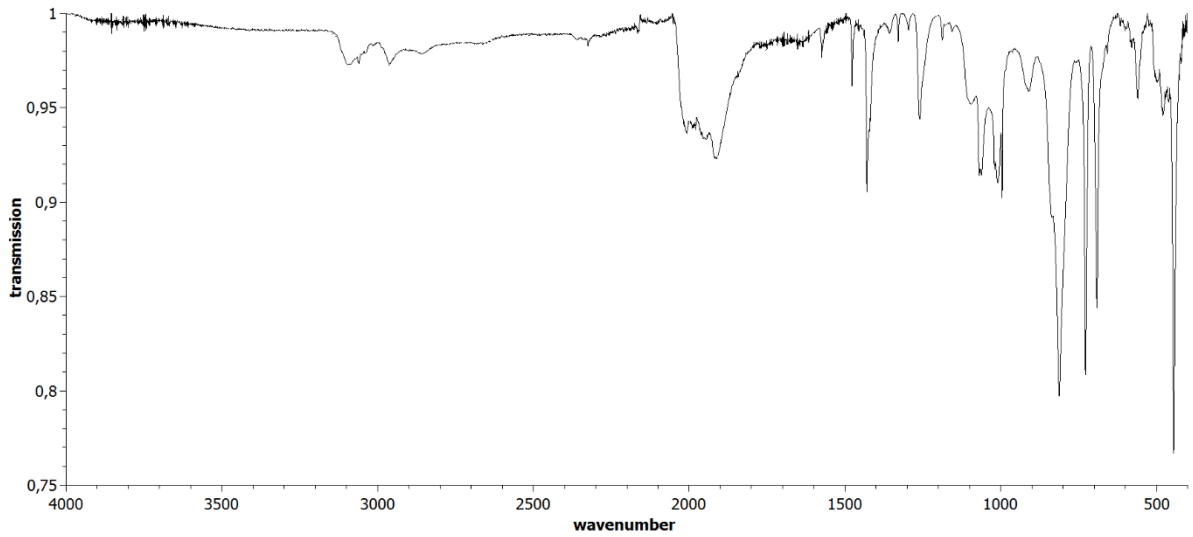

Figure S9: IR spectrum of **3**.

7. UV-Vis spectra

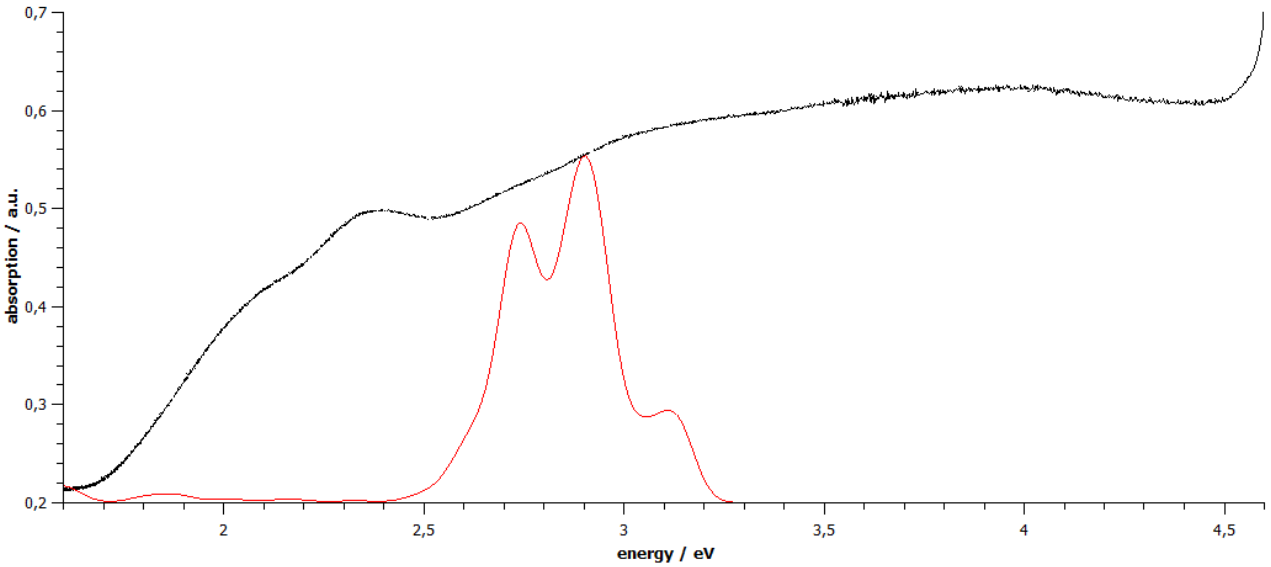

Figure S10: Black: Measured UV-Vis spectrum of **2**. Red: Simulated UV-Vis spectrum, obtained from a TD-DFT calculation including the first 200 electronic excitations.

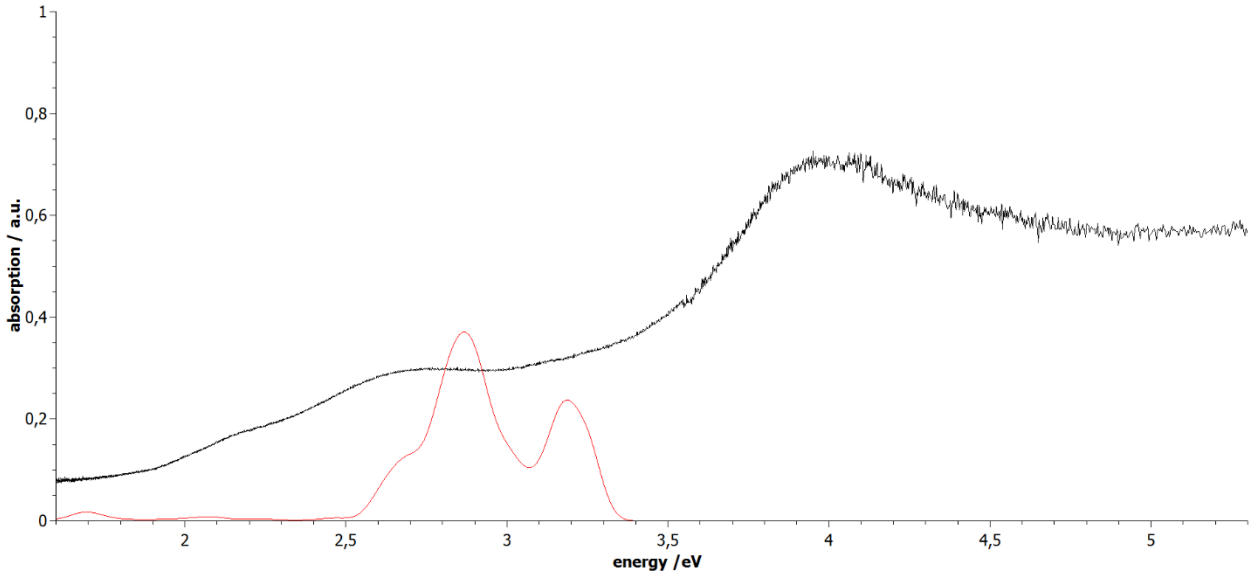

Figure S11: Black: Measured UV-Vis spectrum of **3**. Red: Simulated UV-Vis spectrum, obtained from a TD-DFT calculation including the first 200 electronic excitations.

8. DFT calculations

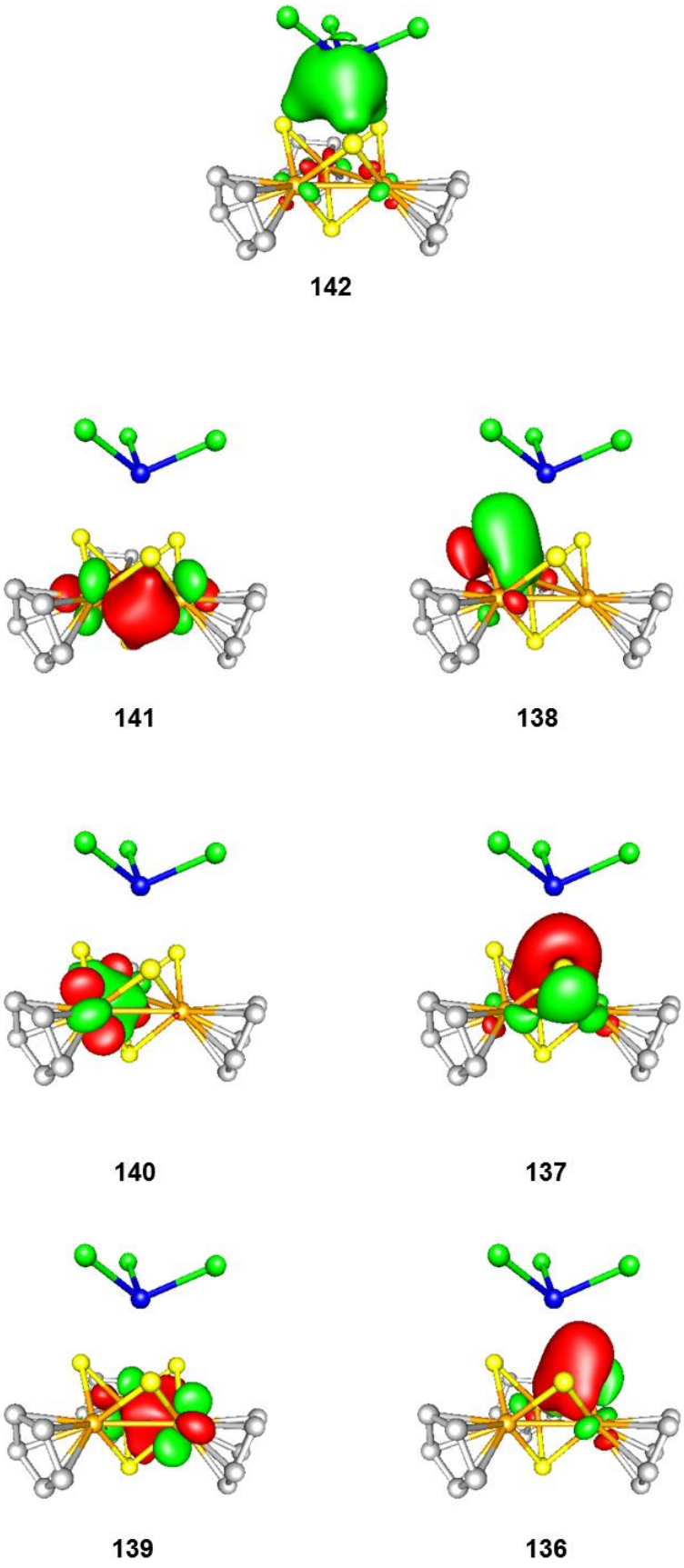

Figure S12: DFT calculated LMOs for **1**. The contour value was chosen to be 0.05 a.u.

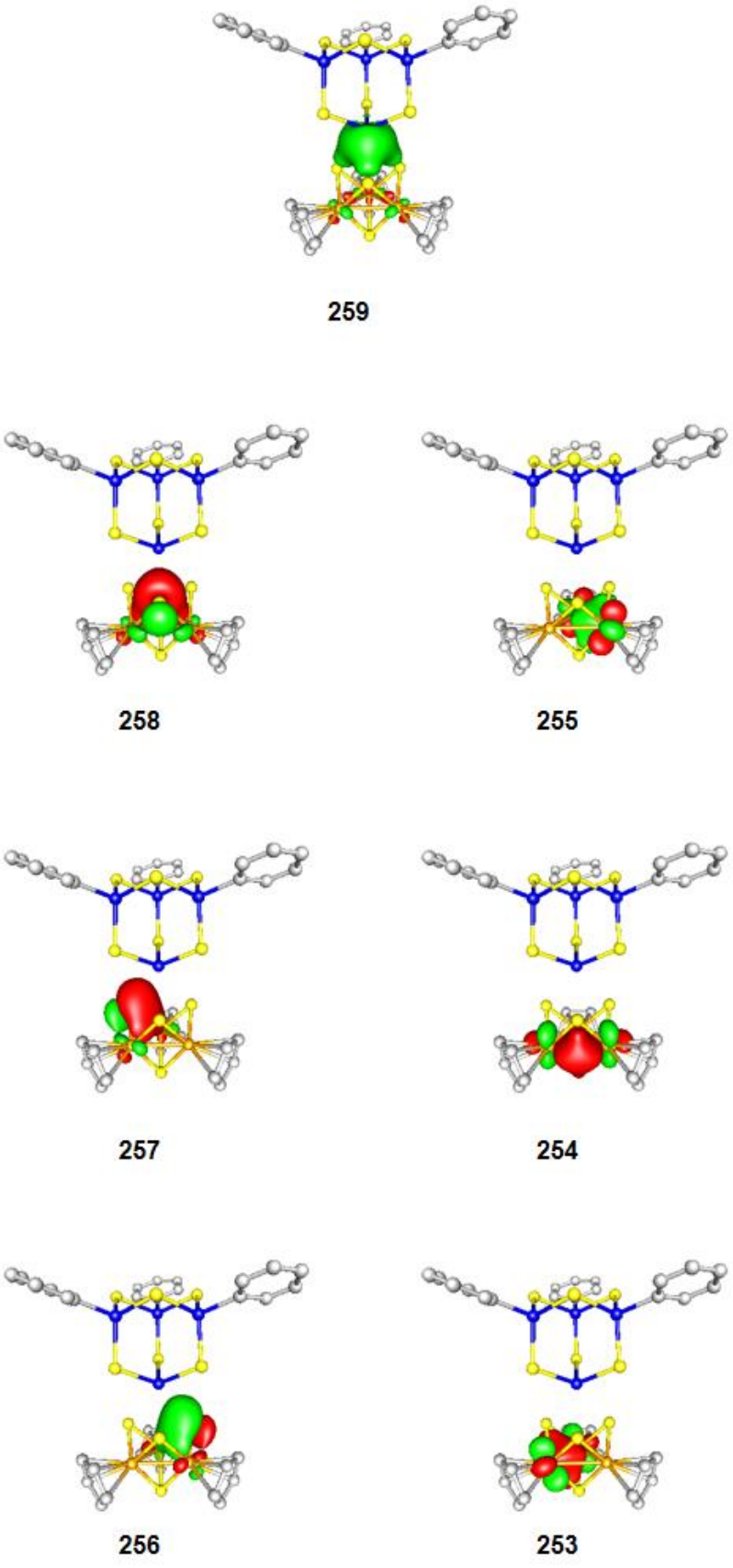

Figure S13: DFT calculated LMOs for **2**. The contour value was chosen to be 0.05 a.u.

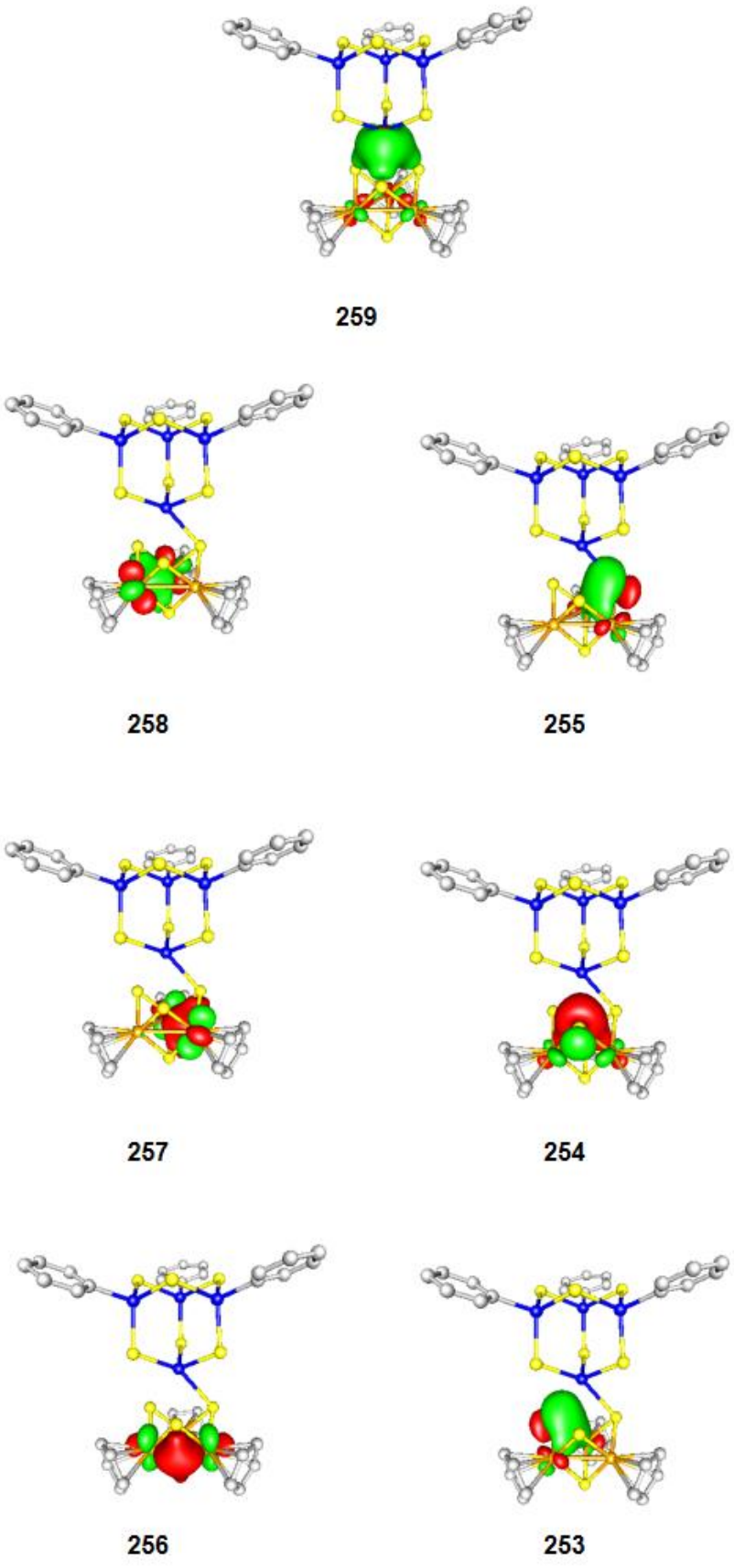

Figure S14: DFT calculated LMOs for **3**. The contour value was chosen to be 0.05 a.u.

Table S10: Mulliken atomic charges for **1**.

1c	-0.12957
2h	0.1353
3c	-0.16674
4h	0.13835
5c	-0.1291
6h	0.13486
7c	-0.13134
8h	0.16358
9c	-0.123
10h	0.16336
11c	-0.12689
12h	0.13092
13c	-0.15255
14h	0.13779
15c	-0.14882
16h	0.13327
17c	-0.11761
18h	0.16744
19c	-0.1295
20h	0.158
21c	-0.1313
22h	0.13237
23c	-0.11876
24h	0.16087
25c	-0.11824
26h	0.16269
27c	-0.15559
28h	0.13263
29c	-0.14727
30h	0.13803
31cl	-0.39404
32cl	-0.39347
33cl	-0.39488
34sn	0.6985
35w	0.54608
36w	0.57989
37w	0.57002
38s	-0.32162
39s	-0.32239
40s	-0.32378
41s	-0.40752

Table S11: Mulliken atomic charges for **2**.

1c	-0.17091	41c	-0.09355
2c	-0.14277	42c	-0.21582
3c	-0.1266	43s	-0.49007
4c	-0.10538	44c	-0.01301
5c	-0.13262	45c	-0.23647
6w	0.57774	46c	-0.09402
7s	-0.33835	47c	-0.10902
8w	0.54706	48c	-0.09547
9w	0.5434	49c	-0.21793
10c	-0.15857	50s	-0.48462
11c	-0.13628	51h	0.1234
12c	-0.13561	52h	0.10748
13c	-0.1145	53h	0.10747
14c	-0.14311	54h	0.10835
15s	-0.40965	55h	0.12309
16s	-0.329	56h	0.15849
17c	-0.1168	57h	0.16474
18c	-0.11922	58h	0.13246
19c	-0.13871	59h	0.13513
20c	-0.15516	60h	0.13204
21c	-0.14608	61h	0.12012
22s	-0.32347	62h	0.10763
23sn	0.62014	63h	0.10729
24s	-0.48494	64h	0.10831
25sn	0.82887	65h	0.12744
26c	-0.00589	66h	0.13059
27c	-0.23917	67h	0.16447
28c	-0.09008	68h	0.16346
29c	-0.10643	69h	0.13076
30c	-0.10233	70h	0.13751
31c	-0.21806	71h	0.12108
32s	-0.48495	72h	0.10684
33sn	0.83097	73h	0.10665
34s	-0.48705	74h	0.10857
35s	-0.48809	75h	0.12249
36sn	0.83929	76h	0.13124
37c	-0.0184	77h	0.16018
38c	-0.23889	78h	0.16135
39c	-0.09407	79h	0.13
40c	-0.1105	80h	0.13553

Table S12: Mulliken atomic charges for **3**.

1c	-0.23564	41c	-0.09651
2c	-0.01387	42c	-0.1079
3c	-0.22075	43c	-0.08911
4c	-0.09421	44c	-0.24743
5c	-0.10723	45c	-0.01553
6c	-0.09769	46c	-0.22513
7sn	0.83858	47c	-0.09787
8s	-0.4868	48c	-0.10558
9sn	0.8299	49c	-0.09801
10s	-0.47733	50c	-0.22169
11sn	0.84221	51h	0.12099
12s	-0.49031	52h	0.12544
13s	-0.47522	53h	0.10803
14sn	0.66666	54h	0.10737
15s	-0.47617	55h	0.10963
16s	-0.28798	56h	0.13758
17mo	0.43303	57h	0.13007
18s	-0.31387	58h	0.15929
19mo	0.41438	59h	0.16553
20c	-0.1463	60h	0.13061
21c	-0.11738	61h	0.12236
22c	-0.14919	62h	0.12233
23c	-0.1163	63h	0.10806
24c	-0.12157	64h	0.10744
25mo	0.42131	65h	0.10896
26s	-0.28657	66h	0.13702
27c	-0.15798	67h	0.13097
28c	-0.12913	68h	0.16695
29c	-0.13645	69h	0.16137
30c	-0.12223	70h	0.13097
31c	-0.11598	71h	0.12374
32c	-0.13381	72h	0.12211
33c	-0.1095	73h	0.10803
34c	-0.16921	74h	0.10686
35c	-0.11788	75h	0.10982
36c	-0.1219	76h	0.13891
37s	-0.29109	77h	0.13133
38s	-0.47986	78h	0.16117
39c	-0.0171	79h	0.16382
40c	-0.21356	80h	0.132

Table S13: Calculated bond lengths for **1**.

dist 36 w -- 40 s = 4.4235 au = 234.08 pm
dist 35 w -- 38 s = 4.4245 au = 234.14 pm
dist 37 w -- 40 s = 4.4251 au = 234.16 pm
dist 36 w -- 39 s = 4.4255 au = 234.19 pm
dist 37 w -- 38 s = 4.4255 au = 234.19 pm
dist 35 w -- 39 s = 4.4273 au = 234.28 pm
dist 36 w -- 41 s = 4.4601 au = 236.02 pm
dist 37 w -- 41 s = 4.4602 au = 236.02 pm
dist 35 w -- 41 s = 4.4606 au = 236.05 pm
dist 29 c -- 36 w = 4.5200 au = 239.19 pm
dist 13 c -- 37 w = 4.5205 au = 239.21 pm
dist 27 c -- 36 w = 4.5223 au = 239.31 pm
dist 3 c -- 35 w = 4.5227 au = 239.33 pm
dist 21 c -- 36 w = 4.5230 au = 239.35 pm
dist 11 c -- 37 w = 4.5232 au = 239.36 pm
dist 5 c -- 35 w = 4.5237 au = 239.39 pm
dist 15 c -- 37 w = 4.5240 au = 239.40 pm
dist 1 c -- 35 w = 4.5250 au = 239.45 pm
dist 23 c -- 36 w = 4.5368 au = 240.08 pm
dist 9 c -- 35 w = 4.5373 au = 240.10 pm
dist 17 c -- 37 w = 4.5376 au = 240.12 pm
dist 25 c -- 36 w = 4.5391 au = 240.20 pm
dist 7 c -- 35 w = 4.5402 au = 240.26 pm
dist 19 c -- 37 w = 4.5422 au = 240.36 pm
dist 32 cl -- 34 sn = 4.5897 au = 242.87 pm
dist 31 cl -- 34 sn = 4.5904 au = 242.92 pm
dist 33 cl -- 34 sn = 4.5913 au = 242.96 pm

Table S14: Calculated bond lengths for **2**.

33 sn -- 44 c = 4.0806 au = 215.94 pm
25 sn -- 26 c = 4.0808 au = 215.95 pm
36 sn -- 37 c = 4.0813 au = 215.97 pm
6 w -- 22 s = 4.4285 au = 234.34 pm
8 w -- 16 s = 4.4293 au = 234.39 pm
9 w -- 22 s = 4.4300 au = 234.42 pm
6 w -- 7 s = 4.4303 au = 234.44 pm
9 w -- 16 s = 4.4302 au = 234.44 pm
7 s -- 8 w = 4.4311 au = 234.48 pm
8 w -- 15 s = 4.4602 au = 236.02 pm
6 w -- 15 s = 4.4611 au = 236.07 pm
9 w -- 15 s = 4.4613 au = 236.08 pm
9 w -- 10 c = 4.5193 au = 239.15 pm
8 w -- 20 c = 4.5197 au = 239.17 pm
1 c -- 6 w = 4.5202 au = 239.20 pm
9 w -- 14 c = 4.5229 au = 239.34 pm
8 w -- 21 c = 4.5230 au = 239.35 pm
2 c -- 6 w = 4.5236 au = 239.38 pm
8 w -- 19 c = 4.5236 au = 239.38 pm
5 c -- 6 w = 4.5242 au = 239.41 pm
9 w -- 11 c = 4.5250 au = 239.45 pm
8 w -- 18 c = 4.5396 au = 240.23 pm
4 c -- 6 w = 4.5401 au = 240.25 pm
3 c -- 6 w = 4.5410 au = 240.30 pm
8 w -- 17 c = 4.5416 au = 240.33 pm
9 w -- 12 c = 4.5428 au = 240.39 pm
9 w -- 13 c = 4.5426 au = 240.39 pm
35 s -- 36 sn = 4.5545 au = 241.02 pm
24 s -- 25 sn = 4.5566 au = 241.12 pm
32 s -- 33 sn = 4.5580 au = 241.20 pm
25 sn -- 50 s = 4.6085 au = 243.87 pm
36 sn -- 43 s = 4.6092 au = 243.91 pm
33 sn -- 34 s = 4.6107 au = 243.99 pm
36 sn -- 50 s = 4.6184 au = 244.40 pm
25 sn -- 34 s = 4.6212 au = 244.54 pm
33 sn -- 43 s = 4.6231 au = 244.64 pm
23 sn -- 35 s = 4.7523 au = 251.48 pm
23 sn -- 24 s = 4.7545 au = 251.60 pm
23 sn -- 32 s = 4.7567 au = 251.72 pm

Table S15: Calculated bond lengths for **3.**

9 sn -- 45 c = 4.0783 au = 215.82 pm
2 c -- 7 sn = 4.0790 au = 215.85 pm
11 sn -- 39 c = 4.0806 au = 215.93 pm
19 mo -- 37 s = 4.3944 au = 232.54 pm
17 mo -- 37 s = 4.3946 au = 232.55 pm
16 s -- 17 mo = 4.3947 au = 232.56 pm
16 s -- 25 mo = 4.3948 au = 232.56 pm
25 mo -- 26 s = 4.3958 au = 232.62 pm
19 mo -- 26 s = 4.3980 au = 232.73 pm
18 s -- 19 mo = 4.4137 au = 233.56 pm
18 s -- 25 mo = 4.4145 au = 233.60 pm
17 mo -- 18 s = 4.4152 au = 233.64 pm
19 mo -- 21 c = 4.5015 au = 238.21 pm
17 mo -- 33 c = 4.5028 au = 238.28 pm
25 mo -- 28 c = 4.5033 au = 238.30 pm
17 mo -- 34 c = 4.5058 au = 238.44 pm
25 mo -- 27 c = 4.5060 au = 238.45 pm
19 mo -- 22 c = 4.5065 au = 238.47 pm
19 mo -- 20 c = 4.5076 au = 238.53 pm
17 mo -- 32 c = 4.5080 au = 238.55 pm
25 mo -- 29 c = 4.5082 au = 238.57 pm
17 mo -- 36 c = 4.5196 au = 239.17 pm
25 mo -- 30 c = 4.5196 au = 239.17 pm
25 mo -- 31 c = 4.5209 au = 239.23 pm
19 mo -- 24 c = 4.5216 au = 239.27 pm
17 mo -- 35 c = 4.5231 au = 239.35 pm
19 mo -- 23 c = 4.5234 au = 239.37 pm
7 sn -- 38 s = 4.5576 au = 241.18 pm
11 sn -- 13 s = 4.5590 au = 241.25 pm
9 sn -- 15 s = 4.5611 au = 241.36 pm
7 sn -- 8 s = 4.6084 au = 243.87 pm
11 sn -- 12 s = 4.6100 au = 243.95 pm
9 sn -- 10 s = 4.6102 au = 243.96 pm
10 s -- 11 sn = 4.6175 au = 244.35 pm
8 s -- 9 sn = 4.6183 au = 244.39 pm
7 sn -- 12 s = 4.6186 au = 244.41 pm
13 s -- 14 sn = 4.7404 au = 250.85 pm
14 sn -- 15 s = 4.7422 au = 250.95 pm
14 sn -- 38 s = 4.7471 au = 251.20 pm

9. Magnetic measurements

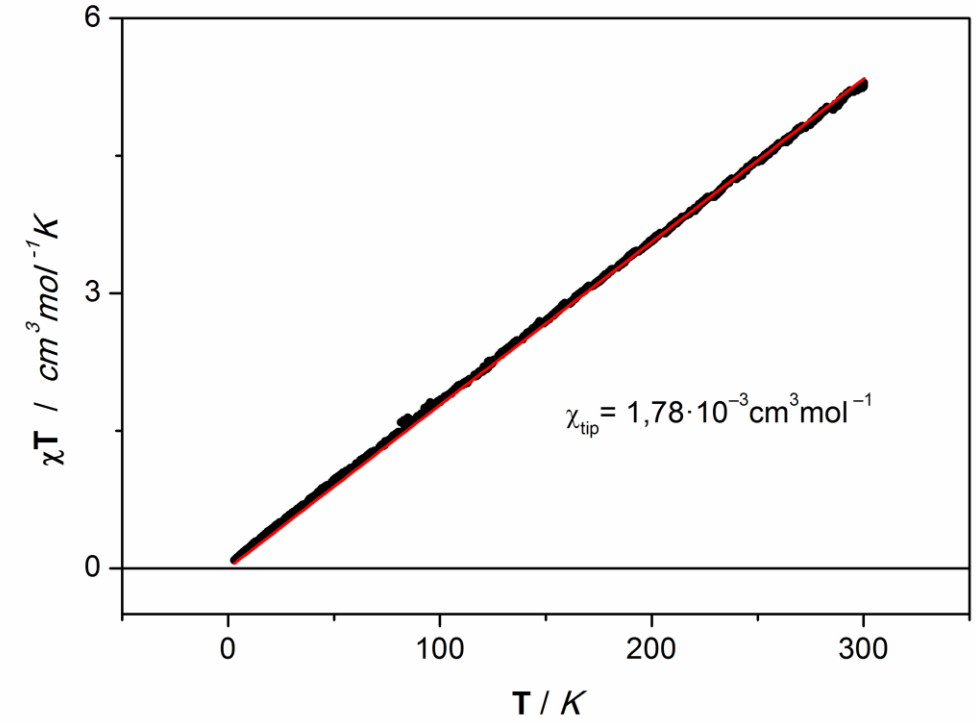

Figure S15: χT vs. T plot for **2**.

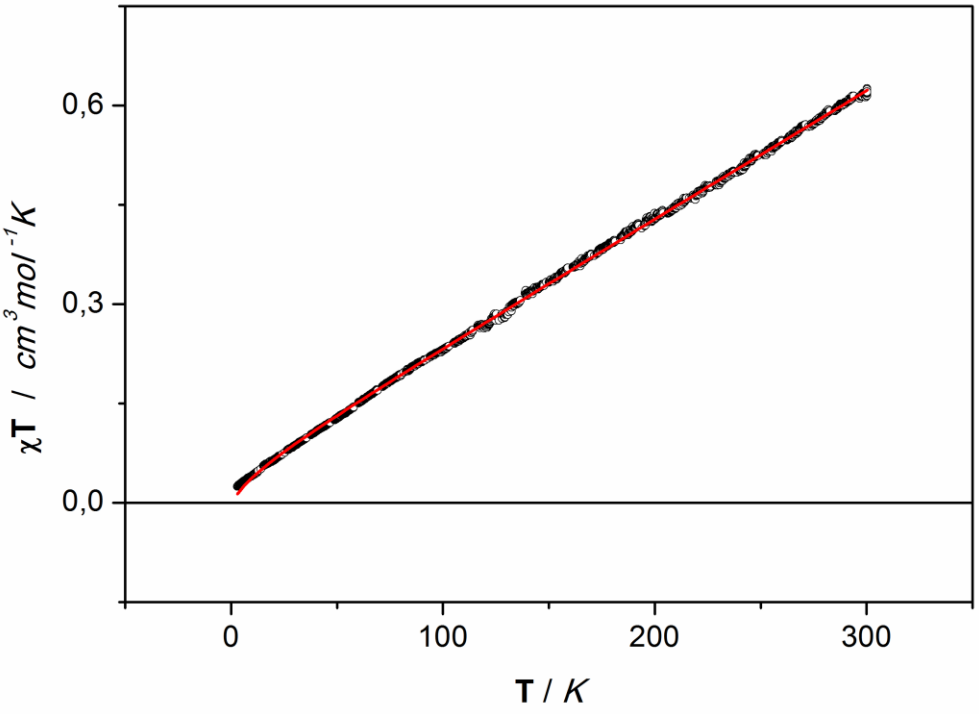

Figure S16: χT vs. T plot for **3**.

10. References for the Supporting Information

[1] Stoe and Cie GmbH, *X-Area*, *Version 1.77*, **2016**.
[2] Sheldrick, G. M., *Acta Crystallogr A* **2015**, *71*, 3-8.
[3] Hübschle, C. B., Sheldrick, G. M., Dittrich, B., *J. Appl. Cryst.* **2011**, 1281-1284.

4.6 How Organotin Sulfide Clusters Behave in the Presence of Zinc Compounds – a Reactivity Study

Zitat: E. Dornsiepen, S. Dehnen, *Eur. J. Inorg. Chem.* **2019**, DOI:10.1002/ejic.201900508.

Abstract

The reactivity of the organotin sulfide clusters $[(R^1Sn)_3S_4Cl]$ (**A**, $R^1 = CMe_2CH_2COMe$) and $[(R^1Sn)_4S_6]$ (**B**) towards different zinc chloride phosphine complexes $[ZnCl_2(PR_3)_2]$ as well as diphenylzinc $ZnPh_2$ was investigated in detail. The study revealed a wide landscape of possible reaction pathways, which ended up with a diversity of different reaction products. In reactions starting from **A**, the tinsulfide cluster core was retained as a cation upon release of the chloride ligand, but side reactions occurred that yielded various chlorostannate or chlorozincate anions to crystallize along with the cations in the salts $[(R^2Sn)_3S_4][SnCl_3]$ (**1**, $R^2 = CMe_2CH_2C(NNH_2)Me$), $[(R^3Sn)_3S_4]_2[dppe(ZnCl_3)_2]$ (**2**, $R^3 = CMe_2CH_2(NNHPh)Me$), and $[(R^2Sn)_3S_4]_2[ZnCl_4]$ (**3**). In one case, transfer of the organic substituent R^3 from tin to phosphorus was observed, resulting in the phosphonium salt $[R^3PMe_3][HPMe_3][ZnCl_4]$ (**4**). When reacting cluster compound **B** with different zinc species, no zinc-containing compounds were isolated. Instead, in one case we observed hydrolysis of **B** and subsequent formation of the adamantane-type mixed oxide/sulfide cluster $[(R^2Sn)_4S_5O]$ (**5**) as a consequence of the Lewis acidity of $ZnCl_2$. In the reaction of **B** with $ZnPh_2$, rearrangement of the cluster was observed under transmetallation of the phenyl substituent, yielding the dinuclear complex $[(R^2PhSn)_2S_2]$ (**6**).

Eigener Anteil

Alle Synthesen wurden von mir geplant und von Anna Reuter im Rahmen eines von mir betreuten Forschungspraktikums durchgeführt. Alle analytischen Daten wurden von mir ausgewertet. Die Aufnahme der röntgenographischen Daten wurde von mir durchgeführt. ^{1}H- und ^{13}C-NMR-Spektren wurden von mir, ^{31}P- und ^{119}Sn-NMR-Experimente von der zentralen NMR-Abteilung des Fachbereichs Chemie an der Philipps-Universität unter Leitung von Dr. Xiulan Xie gemessen. Massenspektrometrie und CHNS-Analysen wurden von der entsprechenden Serviceabteilung des Fachbereichs unter Leitung von Dr. Uwe Linne durchgeführt. Das Manuskript wurde gemeinsam von Stefanie Dehnen und mir verfasst.

EurJIC
European Journal of Inorganic Chemistry

A Journal of ChemPubSoc Europe

Accepted Article

Title: Behavior of Organotin Sulfide Clusters Towards Zinc Compounds

Authors: Eike Dornsiepen and Stefanie Dehnen

To be cited as: *Eur. J. Inorg. Chem.* 10.1002/ejic.201900508

Link to VoR: http://dx.doi.org/10.1002/ejic.201900508

WILEY-VCH

10.1002/ejic.201900508

WILEY-VCH

FULL PAPER

Behavior of Organotin Sulfide Clusters Towards Zinc Compounds

*Eike Dornsiepen and Stefanie Dehnen**

Abstract: The reactivity of the organotin sulfide clusters $[(R^1Sn)_3S_4Cl]$ (**A**, $R^1 = CMe_2CH_2COMe$) and $[(R^1Sn)_4S_6]$ (**B**) towards different zinc chloride phosphine complexes $[ZnCl_2(PR_3)_2]$ as well as diphenylzinc $ZnPh_2$ was investigated. A diversity of different reaction products was obtained. In reactions starting from **A**, the tinsulfide cluster core was retained as a cation upon release of the chloride ligand, but side reactions occurred that yielded various chlorostannate or chlorozincate anions to crystallize along with the cations in the salts $[(R^2Sn)_3S_4][SnCl_3]$ (**1**, $R^2 = CMe_2CH_2C(NNH_2)Me$), $[(R^3Sn)_3S_4]_2[dppe(ZnCl_3)_2]$ (**2**, $R^3 = CMe_2CH_2(NNHPh)Me$), and $[(R^2Sn)_3S_4]_2[ZnCl_4]$ (**3**). In one case, transfer of the organic substituent R^3 from tin to phosphorus was observed, resulting in the phosphonium salt $[R^3PMe_3][HPMe_3][ZnCl_4]$ (**4**). When reacting cluster compound **B** with different zinc species, no zinc-containing compounds were isolated. Instead, in one case we observed hydrolysis of **B** and subsequent formation of the adamantane-type mixed oxide/sulfide cluster $[(R^2Sn)_4S_5O]$ (**5**), as a consequence of the Lewis acidity of $ZnCl_2$. In the reaction of **B** with $ZnPh_2$, rearrangement of the cluster was observed under transmetallation of the phenyl substituent, yielding the dinuclear complex $[(R^2PhSn)_2S_2]$ (**6**).

Introduction

Organotin chalcogenides are a class of hybrid compounds comprising an inorganic core derived from chalcogenidostannate anions, yet being surrounded by organic ligands that are covalently attached to the tin atoms.[1] The properties of these compounds can be tuned and adjusted finely, but in abroad range, by the elemental combination within the inorganic core on the one hand,[2] and by variation of the organic substituents on the other hand.[3]

Our group employs mainly two types of organic substituents. The first are simple alkyl or aryl substituents without functional groups that lead to the formation of adamantane-type (AD) clusters $[(RSn)_4E_6]$ with extreme nonlinear optical properties.[4] The second type of substituents is based on a CMe_2CH_2COMe (R^1) moiety and its derivatives. This substituent allows the stabilization of a "double-decker"-type (DD) topology that is isomeric to the adamantane-type architecture, by Lewis acid-base interactions between the carbonyl oxygen atoms and the tin atoms. Furthermore, it enables derivatization of the organic ligand sphere by condensation reactions with hydrazines, hydrazones or hydrazides. This way, many different versions of ligand extensions have been realized, including biomolecules,[5] chelating ligands[6] and metallocenes,[7] which were successfully attached to the clusters.

The reactivity of functionalized ligands like R^1 allows for the targeted alteration of the organic shell, but the inorganic core of the clusters can also be derivatized. This can be achieved by reactions of the binary organotinsulfide clusters with transition metal complexes (usually upon activation by an additional sulfide source like $S(SiMe_3)_2$) to form clusters with ternary inorganic cores. While most of these ternary clusters include coinage metal atoms,[8] examples containing palladium[9] or iridium[10] have also been reported. Regarding group 12 metals, only few examples of Zn/Sn/E (E = O, S, Se) clusters exist, although they may potentially serve as ternary precursors for the preparation of copper zinc tin sulfide solar cells.[11]

In order to gain further insight into the reactivity of organotinsulfide clusters towards zinc compounds, we reacted the clusters $[(R^1Sn)_3S_4Cl]$ (**A**) and $[(R^1Sn)_4S_6]$ (**B**) with different zinc chloride phosphine complexes and diphenylzinc. The formation of a ternary Zn/Sn/S cluster core was not observed. We assume that the formation of binary sulfides (ZnS, SnS_2), which form in all cases in the reaction mixtures, outperforms the formation of ternary clusters. However we isolated six new compounds, as shown in Scheme 1.

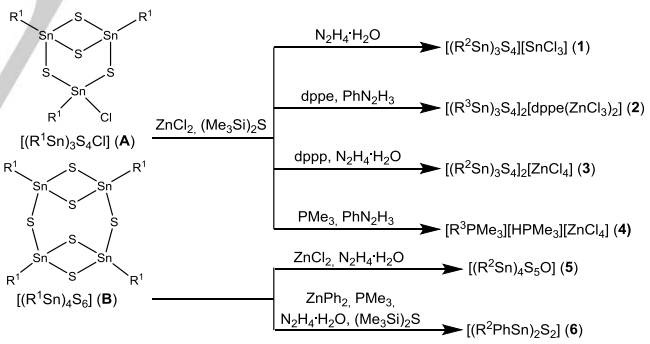

Scheme 1: Synthesis of compounds **1**–**6** in dichloromethane (DCM), with subsequent layering by n-hexane for crystallization. Starting compounds are $[(R^1Sn)_3S_4Cl]$ (**A**, $R^1 = CMe_2CH_2COMe$) and $[(R^1Sn)_4S_6]$ (**B**).

Results and Discussion

For the study, the clusters **A** or **B**, respectively, zinc chloride and the chosen phosphine ligand were dissolved in dichloromethane (DCM), After addition of $(Me_3Si)_2S$, the resulting solutions were stirred at room temperature for 24 hours, filtered and partitioned in three aliquots, of which one was reacted with hydrazine hydrate and one with phenylhydrazine, for post-functionalization of the organic substituent R. The third aliquot was not post-

[a] E. Dornsiepen, Prof. Dr. S. Dehnen
Fachbereich Chemie and Wissenschaftliches Zentrum für Materialwissenschaften (WZMW)
Philipps-Universität Marburg
Hans-Meerwein-Straße 4, 35043 Marburg, Germany
E-mail: dehnen@chemie.uni-marburg.de
Homepage: www.uni-marburg.de/fb15/ag-dehnen

Supporting information for this article is given via a link at the end of the document.

10.1002/ejic.201900508

functionalized. The following phosphine ligands were employed: the bidentate phosphines bis(diphenylphosphino)ethane (dppe) and bis(diphenylphosphino)propane (dppp), as well as the monodentate phosphine PMe_3. From these reactions, we isolated five new compounds – three of them being salts of the $[(RSn)_3S_4]^+$ cations with different anions, namely $[(R^2Sn)_3S_4][SnCl_3]$ (**1**), $[(R^3Sn)_3S_4]_2[dppe(ZnCl_3)_2]$ (**2**), and $[(R^2Sn)_3S_4]_2[ZnCl_4]$ (**3**). The fourth new compound represents the phosphonium salt $[R^3PMe_3][HPMe_3][ZnCl_4]$ (**4**), in which the substituent R^3 was transferred from a tin to a phosphorus atom. Another new compound was obtained with the adamantane-type cluster $[(R^2Sn)_4S_5O]$ (**5**), in which the "double-decker"-type cage of **B** was partially hydrolyzed and rearranged. The molecular structures of compounds **1** – **5** are shown in Figure 1.

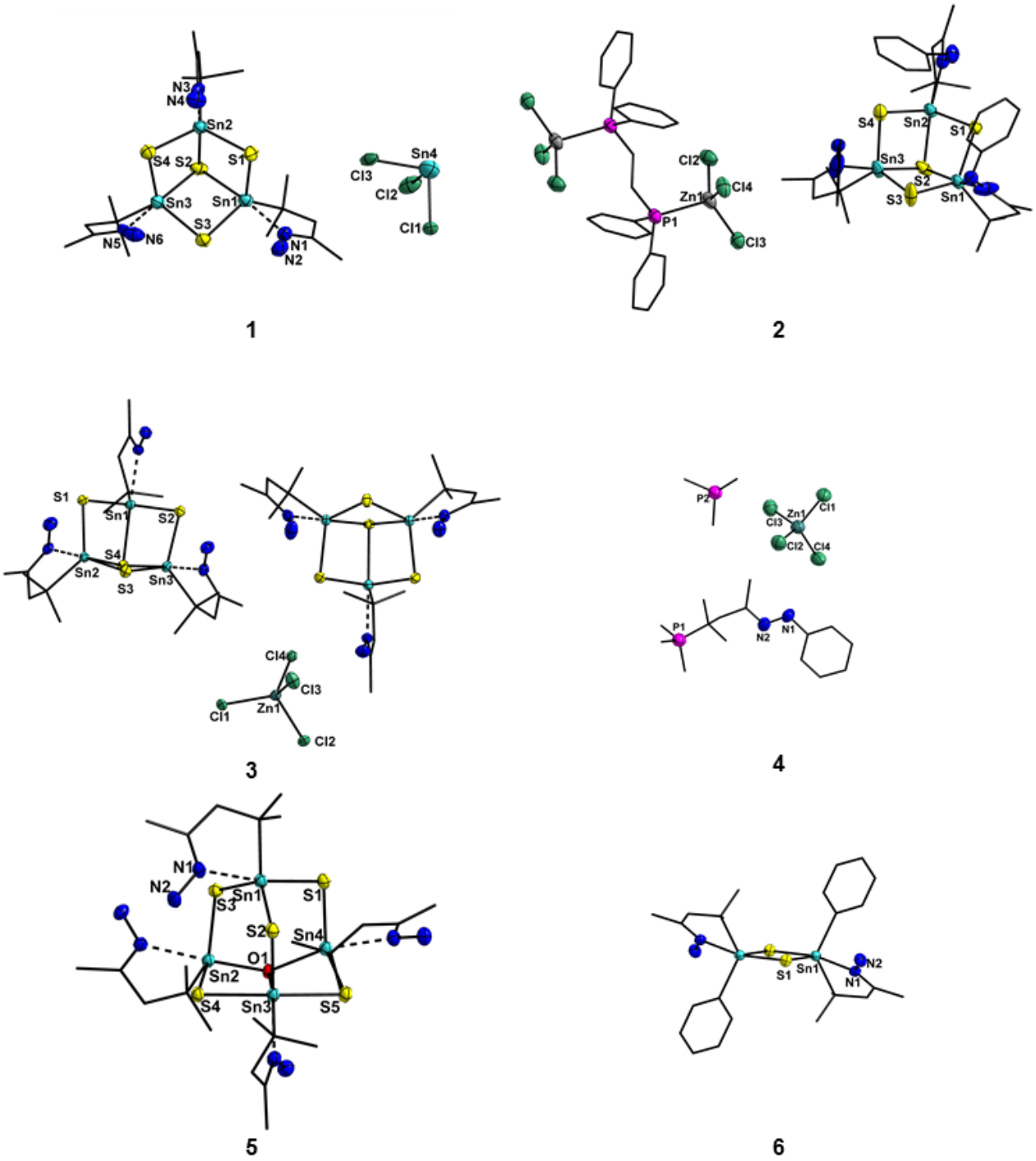

Figure 1. Molecular structures of compounds **1** – **6**, shown for the entire the formula units. Ellipsoids are drawn at 50 % probability, hydrogen atoms are omitted for clarity. Relevant structural parameters are given in the main text; a full collection of structural parameters is provided in the Supporting information (Tables S1-S18).

10.1002/ejic.201900508

Compound **1** is obtained from the reaction of **A** with $ZnCl_2$ and $(Me_3Si)_2S$ after subsequent addition of hydrazine hydrate. Layering of the reaction solution yields colorless plates of **1**·0.7 n-hexane. The compound crystallizes in the triclinic crystal system in the space group $P\bar{1}$. It consists of a defect-heterocubane type $[(R^2Sn)_3S_4]^+$ cation and a trichlorostannate anion. All tin atoms of the cation show trigonal-bipyramidal coordination, with S1 and N1 being the apical ligands, while C1, S2 and S3 occupy the equatorial positions. The N1–Sn1–S1 angle (173.7(2)°) deviates from the ideal value of 180°. Although being slight, the distortion of the coordination sphere is more distinct than in the literature-known cluster $[(R^2Sn)_3S_4Cl]$ (178.5(3)°),[2a] and the Sn–N distances are shorter (2.280(8) – 2.321(7) Å in **1** vs. 2.331(6) – 2.369(10) Å in $[(R^2Sn)_3S_4Cl]$), indicating a slightly stronger intramolecular coordination in **1**.

From the reaction of **A**, $ZnCl_2$, dppe, $(Me_3Si)_2S$ and phenylhydrazine, **2**·$2CH_2Cl_2$ crystallizes as orange blocks after layering with *n*-hexane. The structure was solved and refined in the triclinic crystal system in the space group $P\bar{1}$. The asymmetric unit consists of one defect-heterocubane type $[(R^3Sn)_3S_4]^+$ cation and one half of the $[dppe(ZnCl_3)_2]^{2-}$ dianion. The cation shows the same slight distortion of the trigonal-bipyramidal coordination of the tin sites as in **1**. The molecular structure of the anion shows no significant deviation from the neutral $[dppeZnCl_2]_n$ coordination polymer.[12]

In the corresponding reaction of **A** with $ZnCl_2$, dppp, $(Me_3Si)_2S$ and hydrazine hydrate, colorless crystals of **3**·$3.5CH_2Cl_2$·hexane were obtained after layering with *n*-hexane. Compound **3** also crystallizes in the space group $P\bar{1}$ and comprises two $[(R^2Sn)_3S_4]^+$ cations and one tetrachlorozincate anion per formula unit. The molecular structure of the cation is very similar to the one found in compound **1**. In contrast to the corresponding reaction with dppe, the stable $[ZnCl_4]^{2-}$ anions act as counterions in **3** instead of trichlorozincate anions coordinated by a bridging dppp ligand. This may be due to the higher flexibility of such molecules, which are unfavorable for crystallization, while the tetrachlorozincate anion represents a very good counterion. The $[ZnCl_4]^{2-}$ unit shows a slight distortion from a perfect tetrahedron, with Cl–Zn–Cl angles of 107.86(4) and 111.22(4)°, respectively.

Upon the use of the smaller monodentate ligand trimethylphosphine instead of bidentate phosphine ligands, another product is obtained. In the reaction of **A** with $ZnCl_2$, PMe_3, and $(Me_3Si)_2S$ and subsequent post-functionalization with phenylhydrazine, one observes the transfer of the organic substituent R^3 from a tin atom to a phosphorus atom, leading to formation of the phosphonium salt **4**. When the reaction solution is layered with *n*-hexane, **4** crystallizes in the orthorhombic crystal system in the space group $Pca2_1$. The asymmetric unit comprises one protonated $[HPMe_3]^+$ cation, one $[R^3PMe_3]^+$ cation and one $[ZnCl_4]^{2-}$ anion.

Since ligand transfer reactions from tin to phosphorus atoms are, to the best of our knowledge, unknown, and we did not recover any organotinsulfide cluster within the product, the most plausible explanation for the formation of **4** is based on the decomposition of **A** to yield R^3Cl and a lower-valent tin species, as has been observed before.[2a,8c] The Lewis-acidic zinc chloride, or a corresponding monophosphine complex $[(Me_3P)ZnCl_2]$, forms an adduct with R^3Cl by coordination to the chlorine atom. After nucleophilic attack of free PMe_3 at the chlorine-substituted carbon atom, the phosphonium salt **4** is formed (Scheme 2). This kind of mechanism has been proposed before for the formation of $[R_3P(CHCl)]^+$ cations by reaction of PR_3 with dichloromethane in the presence of $BeCl_2$.[13] To get more evidence that this mechanism occurs here as well, we prepared R^1Cl – similar to the intermediate R^3Cl proposed above – according to a literature procedure,[14] and reacted it with $[ZnCl_2(PMe_3)_2]$. After subsequent functionalization with phenylhydrazine, we were able to obtain $[R^3PMe_3]_2[ZnCl_4]$ (**4b**).

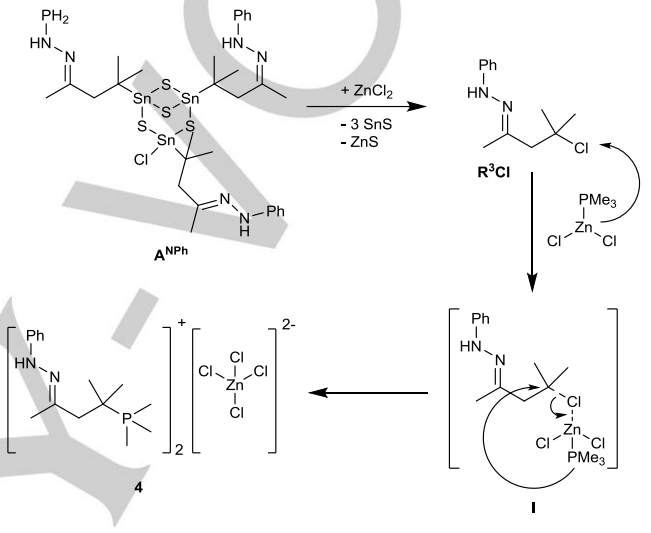

Scheme 2: Proposed course of the transfer of the organic substituent from a tin atom to a phosphorus atom during the reaction of **A** with $ZnCl_2$, PMe_3, $(Me_3Si)_2S$, and phenylhydrazine, leading to formation of the phosphonium salt **4**.

Compound **5** is obtained from **B**, $ZnCl_2$, and hydrazine hydrate. **5**·H_2O·$2CH_2Cl_2$ crystallizes in the triclinic crystal system in the space group $P\bar{1}$ after the reaction solution was layered with *n*-hexane. The inorganic core of **5** shows an adamantane-type topology, in which one of the sulfur atoms is replaced by an oxygen atom. The formation of this compound is the result of a partial hydrolysis of **B** that leads to rearrangement of the inorganic core. The water required for the hydrolysis is introduced by addition of hydrazine hydrate, which not only contains water itself, but also generates water upon the desired condensation reaction with the keto group of R^1. Usually, we do not observe hydrolysis of our clusters upon addition of hydrazine hydrate, yet, in the presence of zinc chloride, the hydrolytic cleavage of **B** seems to be facilitated upon formation of strongly acidic $[ZnCl_2(H_2O)_2]$ in situ.[15]

The product of this reaction, compound **5**, is remarkable for two reasons. First, the observation of an adamantane-type (AD) inorganic core is unexpected for clusters with the ligand R^2, as it allows for an intramolecular back-coordination of the hydrazone nitrogen atom to the tin atom, which stabilizes and thus favors the isomeric double-decker-type topology, for which the increased coordination number of 5 at the tin atom is more stable than for the adamantane-type topology. An adamantane-type cluster with

10.1002/ejic.201900508

the ligand R^2 has been observed before, but in this case the organotinsulfide cluster was co-crystallized with [(dppe)Au]Cl, and the hydrazone groups were involved in intermolecular hydrogen bonding to the chloride anion; here, the tin atoms retained four-coordinate.[16] The hydrazone groups in **5** do form coordinative bonds with the tin atoms, though they are slightly elongated (2.382(3) – 2.471(3) Å vs. 2.331(6) – 2.369(10) Å in $[(R^2Sn)_3S_4Cl]$), reflecting an only weak stabilization by additional N···Sn bonding interaction. Consequently, DFT calculations show no clear preference for either of the possible isomers. While a "double-decker"-type cluster with the oxygen atom in one of the four-membered rings ($DD^{O\text{-}r}$) is less stable than the adamantane by 7 kJ/mol, the other possible isomer with the oxygen atom being one of the chalcogen atoms bridging between the two rings ($DD^{O\text{-}b}$) is more stable than the adamantane-type by 10 kJ/mol. In general, the potential energy surface seems to be rather flat, so that small packing effects may be favoring the crystallization of **5**. The results of the calculations are summarized in Figure 2.

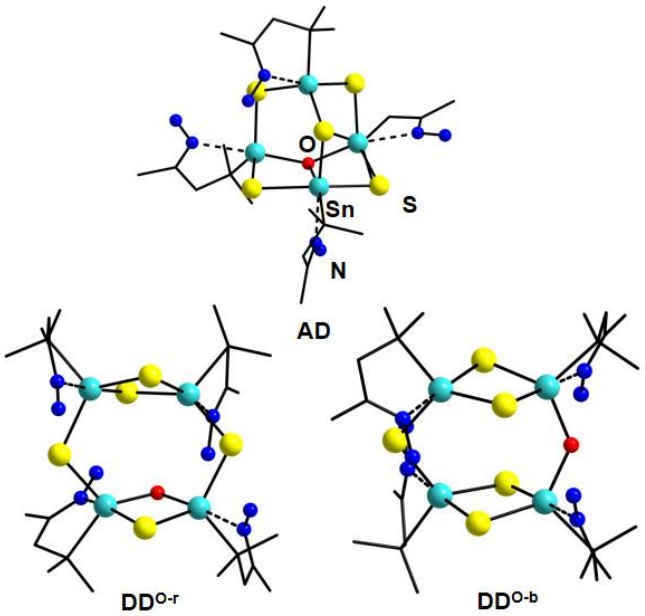

Figure 2: Calculated structure of the cluster in compound 5 and its potential isomers, as resulting from geometry optimizations using DFT methods; note that the adamantane-type structure does not converge, but form the shown distorted version during geometry optimizations. From left: adamantane-type (AD), "double-decker"-type structure with O in the four ring ($DD^{O\text{-}r}$), "double-decker"-type topology with the O atom in the bridge ($DD^{O\text{-}b}$).

The second remarkable feature of **5** is the inclusion of an oxygen atom into the adamantane core, leading to a $[Sn_4S_5O]$ core composition which has not yet been observed in the $[Sn_4E^1_{6-x}E^2_x]$ family of cluster cores (E^1, E^2 = O, Se, Se, Te; $E^1 \neq E^2$). The replacement also comes along with a significant distortion of the cage, as the oxygen atom is shifted inwards on a μ_3-bridging position between Sn2, Sn3, and Sn4 (see Figure 3). This can, on the one hand, be attributed to the much smaller atomic radius of oxygen, resulting in Sn–O bond lengths of 2.097(2) – 2.137(2) Å (as compared to 2.3699(9) – 2.5867(9) Å for the Sn–S bonds).

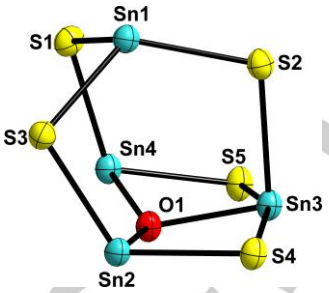

Figure 3. Side view of the inorganic core of **5**, highlighting the distortion caused by the oxygen atom.

On the other hand, this distortion may also be due to the increased coordination number of the tin sites: a penta-coordinate tin atom aims at a trigonal-bipyramidal coordination environment, which is highly distorted in an adamantane-type cage topology und thus unfavorable. The distortion, however, causes all of the four tin atoms to realize the trigonal-bipyramidal coordination. A similar distortion has recently been observed for an $[Sn_4S_6]$ cage, to which two $[Cu(PPh_3)_2]$ coordinate, such that two of the tin sites are additionally part of an $[SnS_2Cu]$ four-membered ring attached to the original cage.[17]

Since the formation of chlorozincate anions seems to be a thermodynamic sink that cannot be easily overcome, we also explored a reaction with a halide-free source of zinc atoms, namely diphenylzinc. We repeated the aforementioned reactivity study with $ZnPh_2$, thereby obtaining only one isolable compound, which is a dinuclear tin complex, $[(R^2SnPh)_2S_2]$ (**6**). Notably, the formation of **6** took place under transmetalation of the phenyl substituent from the zinc to the tin atom. Other reactions with $ZnPh_2$ did not yield any new crystalline compounds. From this we conclude a lower reactivity of diphenylzinc as compared to the zinc chloride phosphine complexes.

6 is obtained from the reaction of **B** with diphenylzinc, $(Me_3Si)_2S$, and PMe_3, yet only after subsequent post-functionalization with hydrazine hydrate. This can be attributed to the general observation that clusters functionalized with hydrazine hydrate have a higher tendency towards crystallization.[18] The compound crystallizes in the monoclinic crystal system in the space group $P2_1/c$. Its molecular structure can be derived from the literature-known complex $[(R^1SnCl)_2S_2]$,[2a] but the two chloride substituents are replaced with phenyl moieties (upon the said transmetalation). The central $[Sn_2S_2]$ four-membered ring is nearly square-planar, as in the chloride-substituted complex that, however, possesses crystallographic inversion symmetry, which the complex in compound **6** does not. Transmetalation processes of aryl substituents from zinc to tin atoms are not unknown in the literature;[19] yet, with one exception,[19a] they employ arylzinc halides. The formation of **6** requires a partial decomposition of the starting material **B**, which may have taken place according to the following reaction pathway [equation (1); note that the R^1 substituent is transformed to the R^2 substituent plus water, by condensation reaction with N_2H_4, which was added as $N_2H_4 \cdot H_2O$; PMe_3 and $(Me_3Si)_2S$ were omitted from the reaction scheme, as both reactants were obviously not involved in the formation of **6**]:

10.1002/ejic.201900508

$[(R^1Sn)_4S_6]$ (**B**) + 2 $ZnPh_2$ + 4 $N_2H_4{\cdot}H_2O$
$\rightarrow$ 2 $[(R^2SnPh)_2S_2]$ (**6**) + 8 H_2O + 2 ZnS (1)

In all of these cases, no zinc-containing compounds could be isolated from reactions starting from compound **B**. Since zinc has no spin ½ nucleus, investigations of the species in solution is not easily achieved by NMR spectroscopy, so isolation of single crystals and subsequent structural analysis is the main tool to get insight into the reaction products.

Conclusions

The reactivity of the organotinsulfide clusters $[(R^1Sn)_3S_4Cl]$ (**A**) and $[(R^1Sn)_4S_6]$ (**B**) towards different zinc chloride phosphine complexes $[(R_3P)_2ZnCl_2]$ as well as diphenylzinc was investigated. In reactions starting from **A**, chloride was released from the otherwise unaltered organotin sulfide core, yielding ionic compounds of the respective cations with different chlorostannate or chlorozincate anions $[(R^2Sn)_3S_4][SnCl_3]$ (**1**), $[(R^3Sn)_3S_4]_2[dppe(ZnCl_3)_2]$ (**2**) and $[(R^2Sn)_3S_4]_2[ZnCl_4]$ (**3**). Decomposition of **A** under formation of RCl and subsequent reaction with $[ZnCl_2(PMe_3)_2]$ led to formation of the phosphonium salt $[R^3PMe_3][HPMe_3][ZnCl_4]$ (**4**), that was also prepared purposefully as $[R^3PMe_3]_2[ZnCl_4]$ (**4b**). In reactions of **B** with different zinc species, no products containing zinc atoms could be isolated in crystalline form. Instead, we observed (partial) hydrolysis of **B** and subsequent formation of a distorted adamantane-type, mixed oxide/sulfide cluster $[(R^2Sn)_4S_5O]$ (**5**), upon reaction with $[ZnCl_2(H_2O)_2]$ formed in situ from $ZnCl_2$ and water (from $N_2H_2{\cdot}H_2O$). In a reaction of **B** with $ZnPh_2$, rearrangement of the cluster occurs, under transmetallation of the phenyl substituent and formation of a dinuclear complex, $[(R^2PhSn)_2S_2]$ (**6**).

Experimental Section

General. All synthetic steps were carried out under exclusion of oxygen and moisture by use of standard Schlenk procedures. **A**,[20] B,[2a] $(Me_3Si)_2S$,[21] PMe_3[22] and $ZnPh_2$[23] were prepared according to literature procedures. $ZnCl_2$ (Alfa) was dried overnight in vacuum before use, dppe (Ventron), dppp (abcr), $N_2H_4{\cdot}H_2O$ (Merck) and phenylhydrazine (Sigma-Aldrich) were used as received. Yields of the syntheses are calculated based on the Sn content and refer to the amount of product isolated as single crystals. IR spectra were recorded on a Bruker Tensor 37 ATR spectrometer. ^{1}H, ^{13}C and ^{119}Sn NMR spectroscopy was carried out at 25°C using a Bruker DRX 300 MHz spectrometer. The chemical shifts are given in ppm relative to the residual protons of deuterated solvents for ^{1}H spectra, relative to the solvent signal for ^{13}C spectra and relative to Me_4Sn for ^{119}Sn spectra. High-resolution ESI mass spectra were acquired with a LTQ-FT Ultra mass spectrometer (Thermo Fischer Scientific). The resolution was set to 100.000.

$[(R^2Sn)_3S_4][SnCl_3]$ (1): A (430 mg, 0.53 mmol) and $ZnCl_2$ (218 mg, 1.60 mmol) were suspended in dichloromethane (45 mL). $(Me_3Si)_2S$ (0.35 mL, 1.67 mmol) was added and the orange suspension stirred for 24 hours. After filtration, hydrazine hydrate (0.1 mL, 2.00 mmol) was added to the colorless filtrate and the resulting colorless suspension stirred at room temperature for another 24 hours. Filtration and subsequent layering with *n*-hexane (1:1 v/v) gave colorless crystals of **1** after two days.

Yield: 110 mg (0.11 mmol, 21%). **^{1}H-NMR** (300 MHz, $CDCl_3$): δ = 1.33 (s, 18H, CMe_2), 1.91 (s, 9H, CH_3), 2.59 (s, 6H, CH_2), 5.63 (s, br, 6H, NH_2) ppm. **^{13}C-NMR** (75 MHz, $CDCl_3$): δ = 17.4 (CH_3), 25.9 ($SnCMe_2$), 26.8 (CMe_2), 50.7 (CH_2), 154.3 ($C(N_2H_3)$) ppm. A ^{119}Sn NMR spectrum could not be obtained due to the compound's low solubility. **HRMS (ESI+):** m/z calcd: 822.9176 found: 822.9194 for $[C_{18}H_{39}N_6Sn_3S_4]^+$.

$[(R^3Sn)_3S_4]_2[dppe(ZnCl_3)_2]$ (2): A (200 mg, 0.25 mmol), $ZnCl_2$ (100 mg, 0.73 mmol) and dppe (290 mg, 0.73 mmol) were suspended in dichloromethane (24 mL). $(Me_3Si)_2S$ (0.15 mL, 0.71 mmol) was added and the orange suspension stirred at room temperature for three days. After filtration and addition of phenylhydrazine (0.1 mL, 1.03 mmol), the colorless suspension was stirred for another three hours, then filtrated again and layered with *n*-hexane (1:1 v/v). Light orange crystals of **2**$\cdot CH_2Cl_2$ were obtained within ten days.

Yield: 17 mg (6 µmol, 5%). **^{1}H-NMR** (300 MHz, CD_2Cl_2): δ = 1.36 (s, 36 H, CMe_2), 1.64 (s, 4 H, dppeCH_2), 2.06 (s, 12 H, CH_2), 2.40 (s, 6 H, N*H*), 2.92 (s, 12 H, CH_3), 6.62 (d, *J*= 7.9 Hz, 12 H, H_{arom}), 6.97 (t, *J*= 7.2 Hz, 12 H, dppeH_{arom}), 7.20 (t, *J*= 7.9 Hz, 18 H, H_{arom}), 7.39 (m, 8 H, dppe-H_{arom}) ppm. **^{119}Sn-NMR** (187 MHz, CD_2Cl_2): δ = -119 ppm. **HRMS (ESI+):** m/z calcd: 1051.0121 found: 1051.0126 for $[C_{36}H_{51}N_6Sn_3S_4]^+$.

$[(R^2Sn)_3S_4]_2[ZnCl_4]$ (3): A (220 mg, 0.27 mmol), $ZnCl_2$ (110 mg, 0.81 mmol) and dppp (330 mg, 0.80 mmol) were dissolved in dichloromethane (24 mL). After addition of $(Me_3Si)_2S$ (0.17 mL, 0.81 mmol), the orange suspension was stirred at room temperature for 24 hours. After filtration and addition of $N_2H_4{\cdot}H_2O$ (40 µl, 0.80 mmol), the colorless suspension was stirred for another 24 hours. Filtration and subsequent layering with *n*-hexane (1:1 v/v) gave colorless crystals of **3**$\cdot 2.5\ CH_2Cl_2$ after three weeks.

Yield: 3 mg (3 µmol, 1%). **IR:** $\tilde{\nu}$ = 3313 (m), 3260 (w), 3080 (m, br), 2957 (w), 2663 (w), 1668 (w), 1609 (w), 1571 (m), 1524 (m), 1507 (s), 1457 (w), 1402 (m), 1179 (w), 1112 (m), 1078 (s), 962 (s), 946 (s), 801 (m), 612 (w), 480 (w), 420 (w) cm^{-1}. **^{1}H-NMR** (300 MHz, CD_2Cl_2): δ = 1.31 (s, 36 H, CMe_2), 2.23 (s, 12 H, CH_2), 2.89 (s, 18 H, CH_3). The hydrazone protons are not visible due to the low solubility of **3**, thus the (usually very broad) signal could not be found. For the same reason, ^{13}C and ^{119}Sn NMR spectra could not be obtained. **HRMS (ESI+):** m/z calcd: 822.9176 found: 822.9279 for $[C_{18}H_{39}N_6Sn_3S_4]^+$.

$[R^3PMe_3][HPMe_3][ZnCl_4]$ (4): A (238 mg, 0.29 mmol) and $ZnCl_2$ (120 mg, 0.88 mmol) were suspended in dichloromethane (24 mL). After addition of $(Me_3Si)_2S$ (0.19 mL, 0.91 mmol) and PMe_3 (0.18 mL, 1.80 mmol), the colorless suspension was stirred at room temperature for eight days, during which it changed its color to a deep purple. After filtration and addition of phenylhydrazine (0.1 mL, 1.03 mmol), stirring was continued for five days. After filtration, the clear reddish solution was layered with *n*-hexane (1:1 v/v). A few crystals of **4** were obtained within one week.

Yield: 2 mg (3.6 µmol, 0.4 %). **HRMS (ESI+):** m/z calcd: 265.1828, found: 265.1830 $[C_{15}H_{26}N_2P]^+$.

$[R^3PMe_3]_2[ZnCl_4]$ (4b): Tetraethylammonium chloride (760 mg, 4.58 mmol) was dissolved in trifluoroacetic acid (4 mL). Mesityl oxide (0.40 mL, 3.46 mmol) was added, the resulting deep red solution stirred for 2 hours at room temperature and then extracted with *n*-hexane (2 x 20 mL). After solvent removal from the combined hexane extracts in vacuo, the remaining yellow oil was dissolved in dichlormethane (20 mL) and added to a solution of zinc chloride (239 mg, 1.75 mmol) and trimethylphosphine

(0.35 mL, 3.50 mmol) in dichloromethane (20 mL). The colorless solution was stirred at room temperature. A colorless precipitate formed within few minutes. After 4 hours, phenylhydrazine (0.20 mL, 2.04 mmol) was added and the yellow suspension stirred for another 15 hours during which all precipitate had dissolved. **4b** was isolated by crystallization, for which the reaction solution was layered with *n*-hexane (1:1, v/v).

Yield: 178 mg (0.24 mmol, 23%). **HRMS:** m/z calcd: 265.1828, found: 265.1830 $[C_{15}H_{26}N_2P]^+$ **^{1}H-NMR** (250 MHz, CD_2Cl_2): δ = 1.34 (d, 6H, CMe, J_{P-H} = 7.5 Hz), 1.87 (d, 9H, PMe3,J_{P-H} = 6.3 Hz), 1.98 (s, 3H, CH_3), 2.56 (d, 2H, CH_2, J_{P-H} = 6.3 Hz), 6.85 (m, H_{arom}), 7.05 (m, Ha_{rom}), 7.22 (m, H_{arom}). A clean integration of the aromatic protons was not possible due to the underlying hydrazone proton. **^{13}C-NMR** (75 MHz, CD_2Cl_2): δ = 6.7 (d, 3C, PMe_3), 18.3 (s, CH_3), 22.5 (s, 2C, CMe_2), 33.3 (d, PCMe_2), 45.8 (CH_2), 113.4 (2C, C_{arom}), 120.6 (C_{arom}), 129.8 (2C, C_{arom}), 140.8 (C_{arom}), 145.6 (C(NN)) ppm. **^{31}P-NMR** (101 MHz, CD_2Cl_2): δ = 38.4 (s, 1P) ppm.

$[(R^2Sn)_4S_5O]$ (5): B (200 mg, 0.19 mmol) and $ZnCl_2$ (100 mg, 0.73 mmol) were suspended in dichloromethane (24 mL) and the colorless suspension stirred at room temperature for 24 hours. After filtration and addition of $N_2H_4{\cdot}H_2O$ (40 µl, 0.80 mmol), the colorless suspension was stirred another 24 hours after which it was filtered and layered with *n*-hexane (1:1, v/v). Colorless blocks of $\mathbf{5}{\cdot}H_2O{\cdot}2CH_2Cl_2$ were obtained after one day.

Yield: 29 mg (26 µmol, 14%) **IR**: $\tilde{\nu}$ = 3349 (m), 3195 (m), 3003 (w), 2959 (w), 2930 (w), 2902 (w), 2841 (s), 2807 (w), 2714 (w), 1659 (w), 1614 (m), 1452 (m), 1415 (w), 1364 (m), 1260 (m), 1197 (m), 1154 (m), 1098 (s), 1014 (s), 796 (s), 724 (s), 694 (m), 657 (m), 529 (w), 515 (w), 470 (w) cm^{-1}. **^{1}H-NMR** (300 MHz, CD_2Cl_2): δ = 1.32 (s, 24 H, CMe_2), 1.79 (s, 12H, CH_3), 2.50 (s, 8 H, CH_2) ppm. **^{13}C-NMR** (75 MHz, CD_2Cl_2): δ = 16.9, 26.8, 36.9, 51.3, 152.6 ppm. **^{119}Sn-NMR** (187 MHz, CD_2Cl_2): δ = -73 ppm. **Elemental Analysis:** found % (calcd. %): C 25.87 (26.11), H 4.71 (4.75), N 9.70 (10.15), S 14.40 (14.52).

$[(R^2PhSn)_2S_2]$ (6): B (200 mg, 0.19 mmol) and $ZnPh_2$ (160 mg, 0.73 mmol) were suspended in dichloromethane (24 mL). After addition of $(Me_3Si)_2S$ (0.16 mL, 0.76 mmol) and PMe_3 (0.16 mL, 1.60 mmol), the resulting colorless suspension was stirred at room temperature for thee days. After filtration and addition of $N_2H_4{\cdot}H_2O$ (40 µl, 0.80 mmol), the colorless suspension was stirred another three days. Filtration and subsequent layering with *n*-hexane (1:1, v/v) afforded crystals of **6** within four weeks.

Yield: 33 mg (48 µmol, 12%) **^{1}H-NMR** (300 MHz, CD_2Cl_2): δ = 1.33 (m, 12 H, CMe_2), 1.87 (s, 6 H, CH_3), 2.48 (m, 4 H, CH_2), 5.15 (s, 4 H, NH_2), 7.55 (m, 10 H, H_{arom}) ppm. **^{13}C-NMR** (75 MHz, $CDCl_3$): δ = 16.9, 27.2, 33.9, 34.0, 51.8, 128.5, 129.0, 136.1, 154.2 ppm. **^{119}Sn-NMR** (187 MHz, CD_2Cl): δ = -89, -87 ppm. The observation of two signals with nearly identical intensity hints to a symmetry reduction in solution, resulting in slightly different coordination environments for both tin atoms. **HRMS (ESI+):** m/z calcd: 683.0499, found: 683.0501 $[C_{24}H_{36}N_4Sn_2S_2H]^+$.

Quantum Chemical Investigations. Density functional theory calculations were carried out with TURBOMOLE[24] using def2-TZVP basis sets[25] and taking advantage of the multipole-accelerated resolution-of the-identity method.[26] Structures were optimized with the functional TPSSH.[27]

X-Ray Diffraction Studies. Data of the X-Ray diffraction analyses were collected either on a STOE IPDS2 (**1**, **4**–**6**) or IPDS2T (**2**, **3**) imaging plate diffractometer using $Mo_{K\alpha}$ radiation with graphite monochromatization. (λ = 0.71073 Å) at 100 K. Reflection data were processed with X-Area 1.77.[28] Structure solution was performed by direct methods and full-matrix-least-squares refinement against F^2 using SHELXT[29] and SHELXL-2014.[30] CCDC 1914529-1914534 contains the supplementary crystallographic datafor this paper. These data can be obtained free of charge atwww.ccdc.cam.ac.uk/conts/retrieving.html [or from the CambridgeCrystallographic Data Center, 12 Union Road, CambridgeCB2 1EZ, UK; fax: (internat.) +44-1223/336-033; E-mail:deposit@ccdc.cam.ac.uk].

Acknowledgments

This work was financially supported by the DFG (Deutsche Forschungsgemeinschaft) within the framework of GRK 1782. We thank Anna Reuter for her help with the syntheses.

Keywords: tin chalcogenide clusters • zinc • cluster reactivity • X-ray crystallography • DFT calculations

[1] a) H.-J. Jacobsen, B. Krebs, *J. Organomet. Chem.* **1977**, *136*, 333-338; b) H. Berwe, A. Haas, *Chem. Ber.* **1987**, *120*, 1175-1182; c) R. Hauser, K. Merzweiler, *Z. Anorg. Allg. Chem.* **1998**, *624*, 10-12; c) K. Wraage, T. Pape, R. Herbst-Irmer, M. Noltemeyer, H.-G. Schmidt, H. W. Roesky, *Eur. J. Inorg. Chem.* **1999**, 869-872; d) J. Janssen, J. Magull, H. W. Roesky, *Angew. Chem. Int. Ed.* **2002**, *41*, 1365-1367; e) M. Saito, H. Hashimoto, T. Tajima, M. Ikeda, *J. Organomet. Chem.* **2007**, *692*, 2729-2735; f) Z. Padelkova, H. Vankatova, I. Cisarova, M. S. Neachaev, T. A. Zevaco, O. Walter, A. Ruzicka, *Organometallics* **2009**, *28*, 2629-2632; g) M. Wagner, C. Dietz, M. Bouska, L. Dostal, Z. Padelkova, R. Jambor, K. Jurkschat, *Orgaometallics* **2013**, *32*, 4973-4984; h) M. Wagner, T. Zoller, W. Hiller, M. H. Prosenc, K. Jurkschat, *Chem. Eur. J.* **2013**, *19*, 9463-9467; i) M. Zhong, Z. Yang, Y. Yi, D. Zhang, K. Sun, H. W. Roesky, Y. Yang, *Dalton Trans.* **2015**, *46*, 19800-19804.

[2] a) J. P. Eußner, B. E. K. Barth, E. Leusmann, Z. You, N. Rinn, S. Dehnen, *Chem. Eur. J.* **2013**, *19*, 13792-13802; b) N. Rinn, J. P. Eußner, W. Kaschuba, X. Xie, S. Dehnen, *Chem. Eur. J.* **2016**, *22*, 3094-3104; c) J. P. Eußner, R. O. Kusche, S. Dehnen, *Chem. Eur. J.* **2015**, *21*, 12376-12388; d) E. Dornsiepen, E. Geringer, N. Rinn, S. Dehnen,* *Coord. Chem. Rev.* **2019**, *380*, 136–169.

[3] a) B E. K. Barth, B. A. Tkachenko, J. P. Eußner, P. R. Schreiner, S. Dehnen, *Organometallics* **2014**, *33*, 1678-1688; b) E. Leusmann, N. W. Rosemann, B. Weinert, S. Chatterjee, S. Dehnen, *Eur. J. Inorg. Chem.* **2016**, 5300-5304; c) Z. Hassanzahdeh Fard, M. R. Halvagar, S. Dehnen, *J. Am. Chem. Soc.* **2010**, *132*, 2848-2849.

[4] a) N. W. Rosemann, J. P. Eußner, A. Beyer, S. W. Koch, K. Volz, S. Dehnen, S. Chatterjee, *Science* **2016**, *352*, 1301-1304; b) N. W. Rosemann, J. P. Eußner, E. Dornsiepen, S. Chatterjee, S. Dehnen, *J. Am. Chem. Soc.* **2016**, *138*, 16224-16227.

[5] a) N. Rinn, J. P. Berndt, A. Kreher, R. Hrdina, M. Reinmuth, P. R. Schreiner, S. Dehnen, *Organometallics* **2016**, *35*, 3215-3220; b) J. P. Berndt, A. Engel, R. Hrdina, S. Dehnen, P. R. Schreiner, *Organometallics* **2019**, *38*, 329-335.

[6] E. Leusmann, F. Schneck, S. Dehnen, *Organometallics* **2015**, *34*, 3264-3271.

[7] a) E. Leusmann, M. Wagner, N. W. Rosemann, S. Chatterjee, S. Dehnen, *Inorg. Chem.* **2014**, *53*, 4228-4233; b) Z. You, S. Dehnen, *Inorg. Chem.* **2013**, *52*, 12332-12334.

[8] a) R. Hauser, K. Merzweiler, *Z. Anorg. Allg. Chem.* **2002**, *628*, 905-906; b) M. R. Halvagar, Z. Hassanzahdeh Fard, S. Dehnen, *Chem Commun.* **2010**, *46*, 4716-4718; c) J. P. Eußner, S. Dehnen, *Chem. Commun.* **2014**, *50*, 11385-11388.

[9] M. R. Halvagar, Z. Hassanzahdeh Fard, L. Xiong, S. Dehnen, *Inorg. Chem.* **2009**, *48*, 7373-7377.

Content

1) NMR spectra

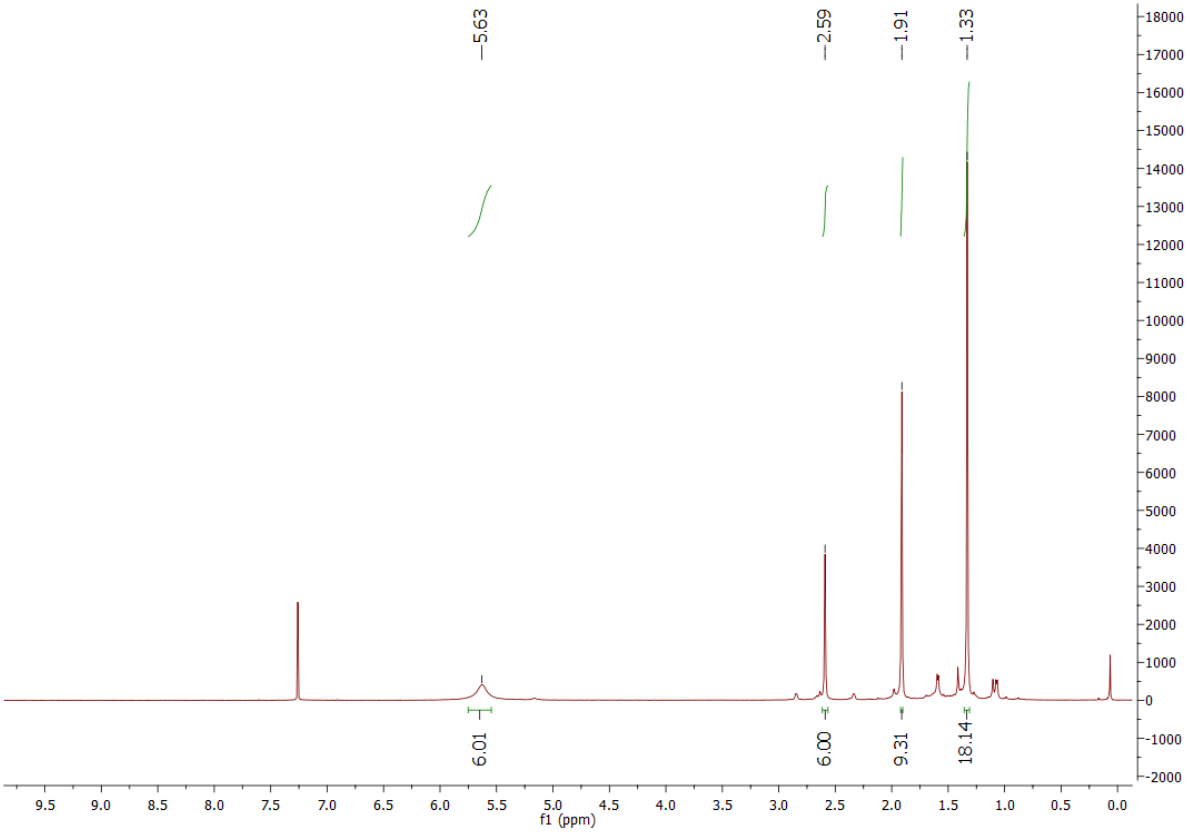

Figure S1. ^{1}H-NMR spectrum of **1** (300 MHz, $CDCl_3$).

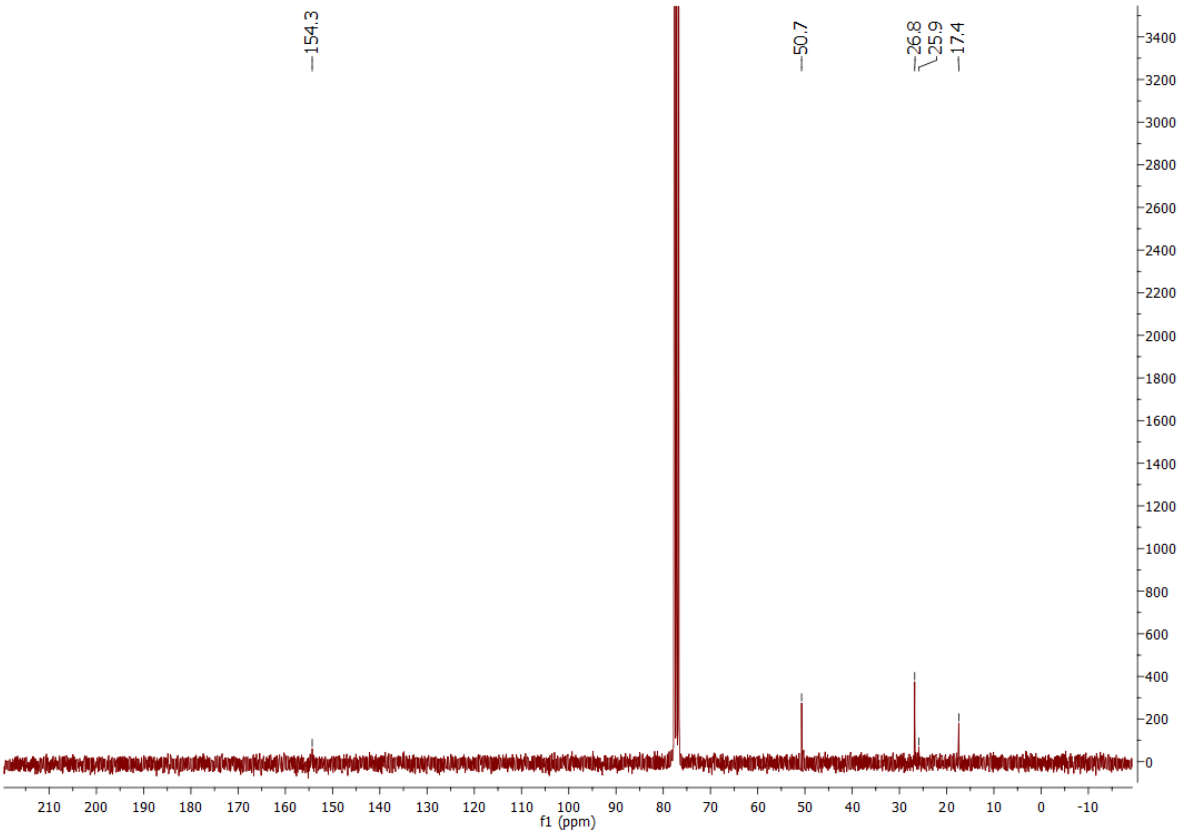

Figure S2. ^{13}C-NMR spectrum of **1** (75MHz, $CDCl_3$).

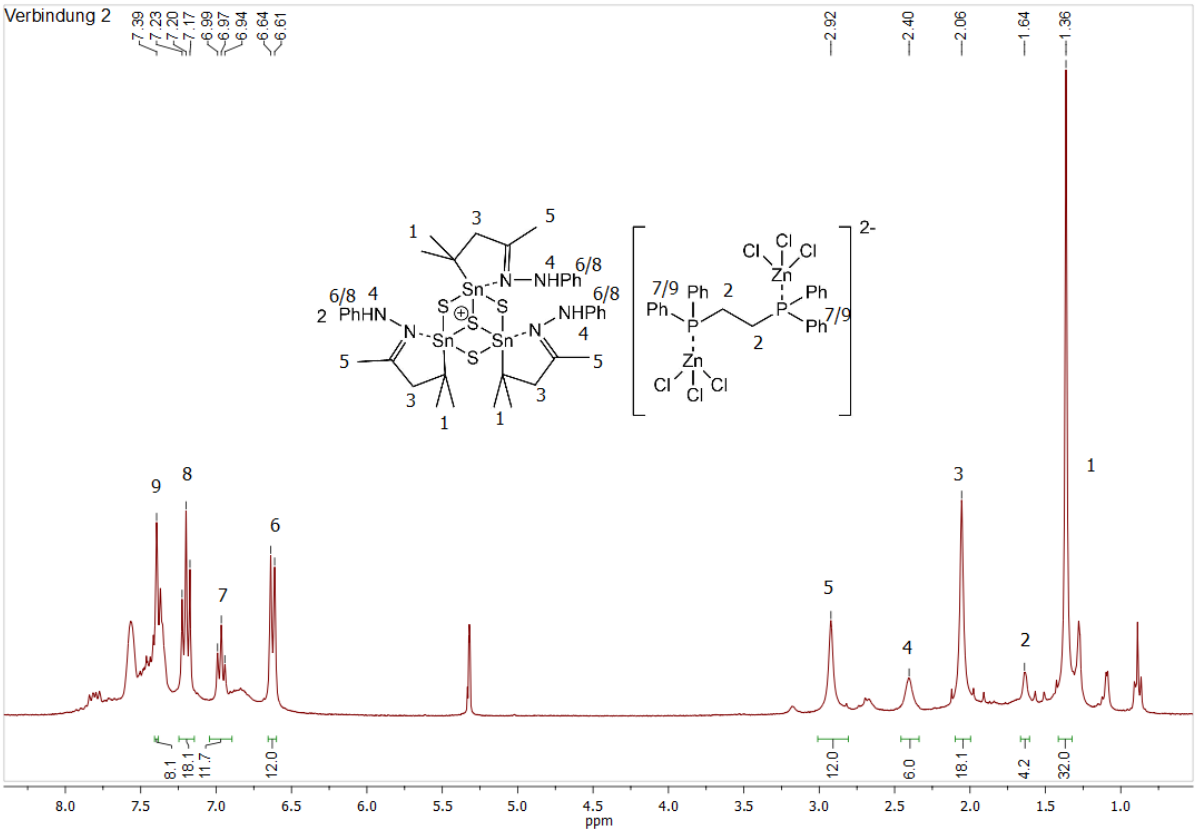

Figure S3. ^{1}H-NMR spectrum of **2** (300 MHz, CD_2Cl_2).

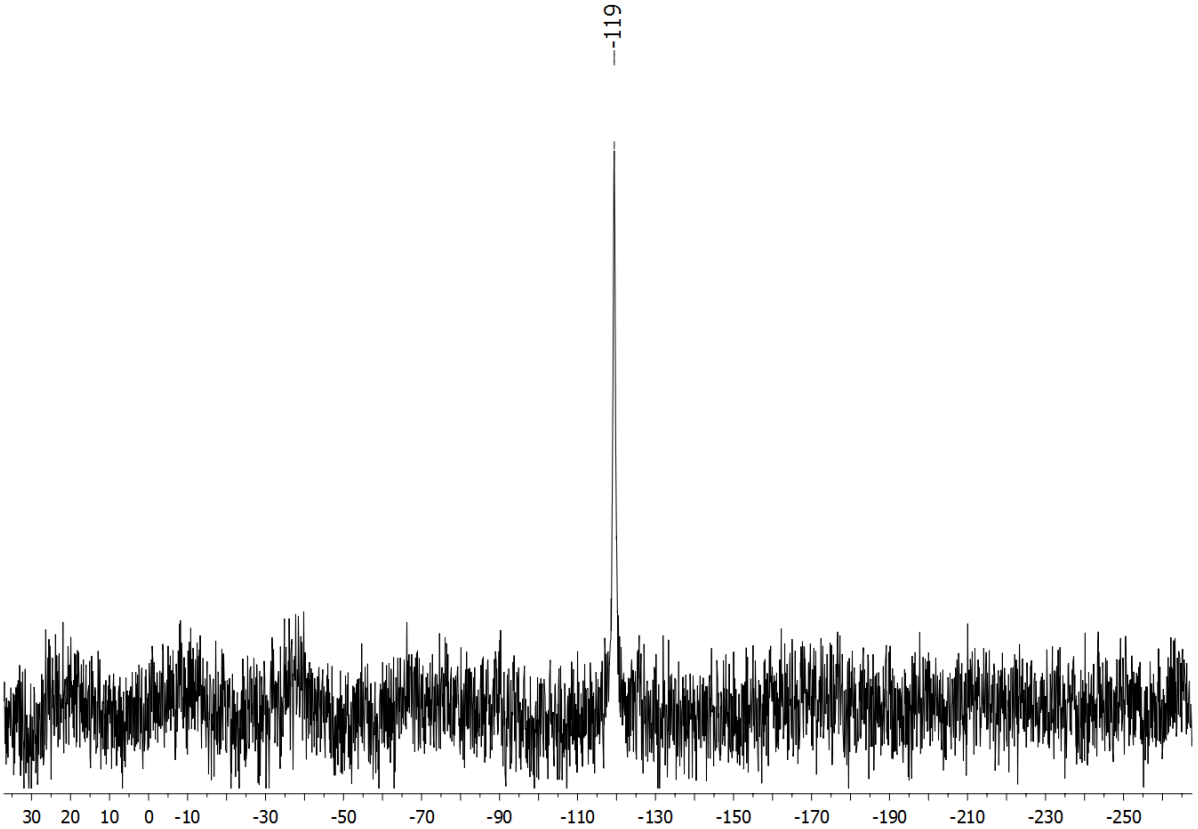

Figure S4. ^{119}Sn-NMR spectrum of **2** (187 MHz, CD_2Cl_2).

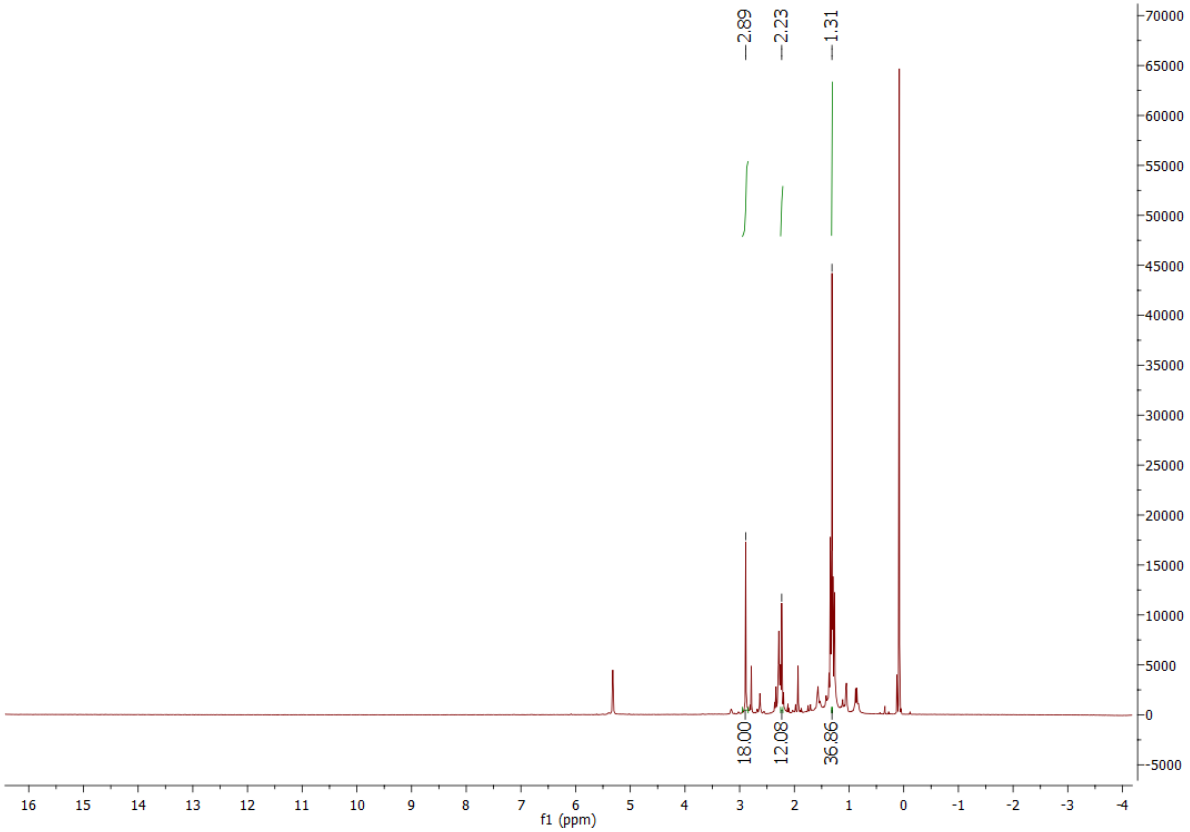

Figure S5. ^{1}H-NMR spectrum of **3** (300 MHz, CD_2Cl_2).

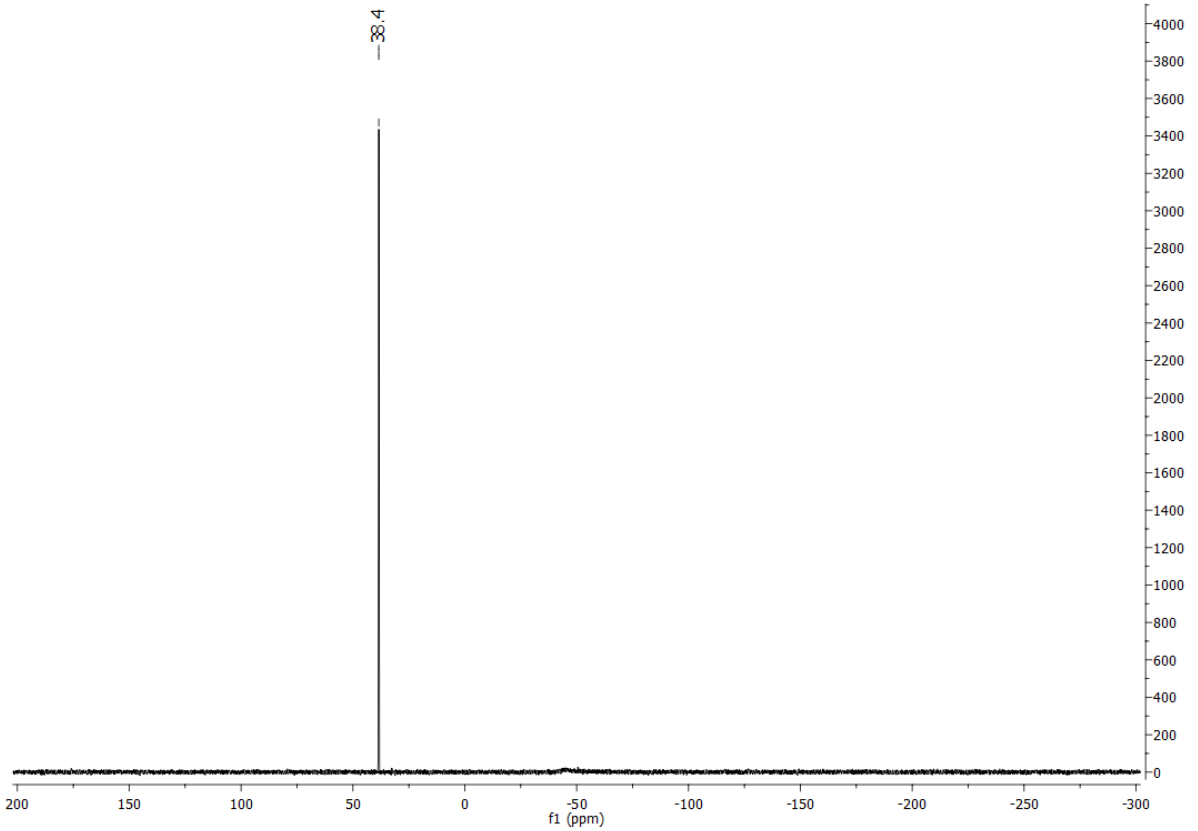

Figure S6. ^{31}P-NMR spectrum of **3** (101 MHz, CD_2Cl_2).

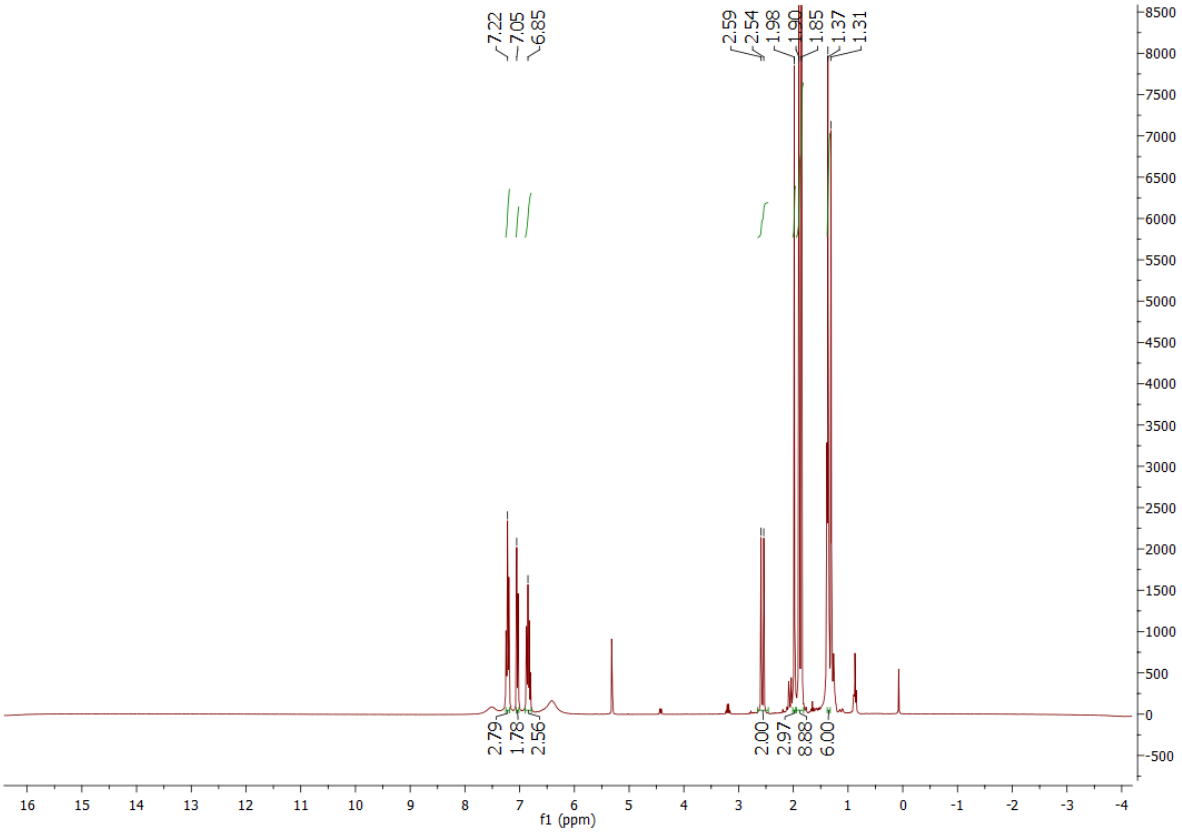

Figure S7. ^{1}H-NMR spectrum of **4b** (300MHz, CD_2Cl_2).

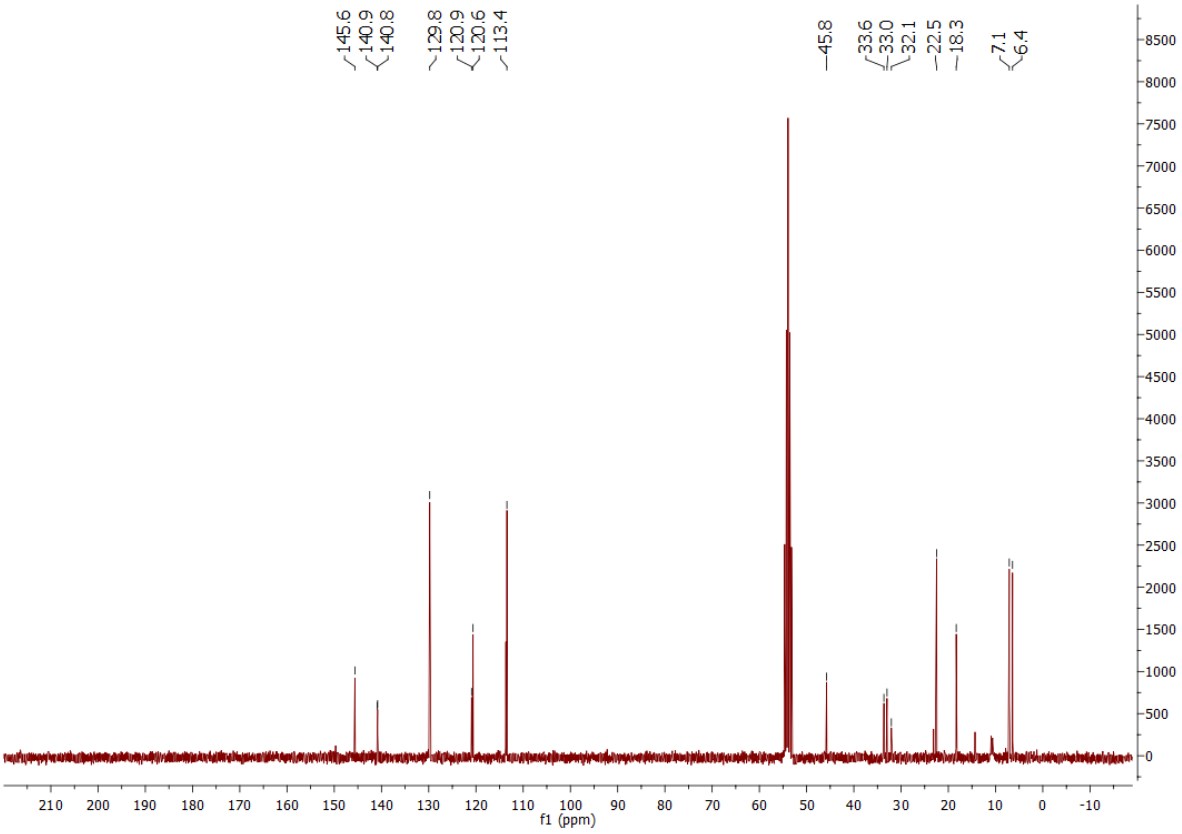

Figure S8. ^{13}C-NMR spectrum of **4b** (75MHz, CD_2Cl_2).

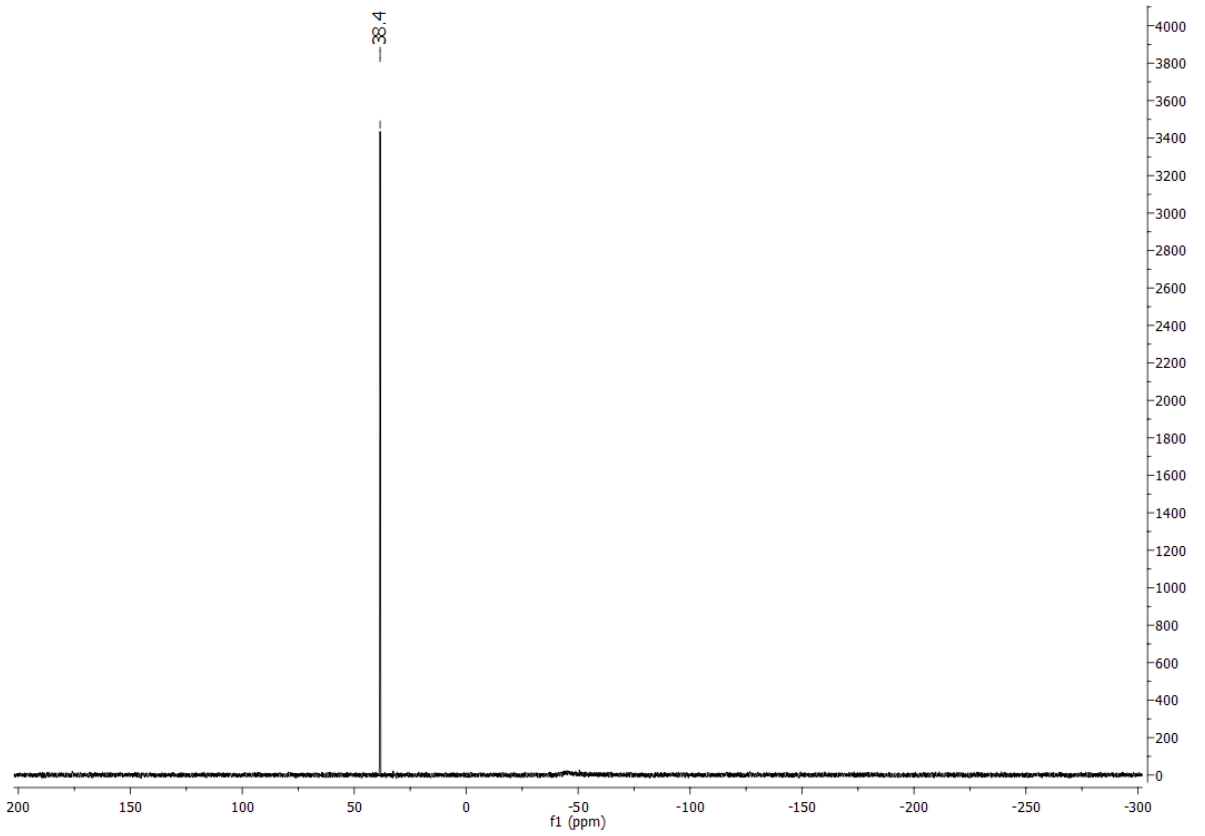

Figure S9. ^{13}C-NMR spectrum of **5** (75MHz, CD_2Cl_2).

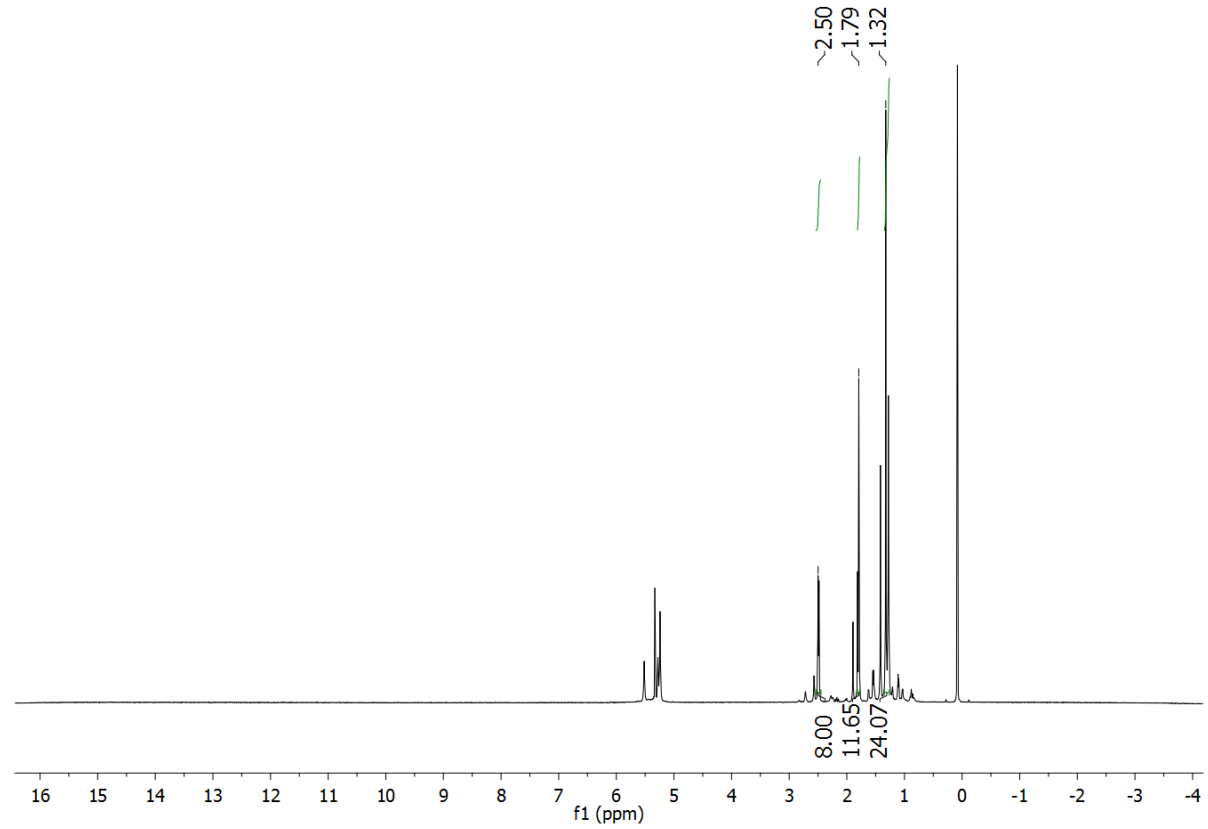

Figure S10. ^{1}H-NMR spectrum of **5** (300 MHz, CD_2Cl_2).

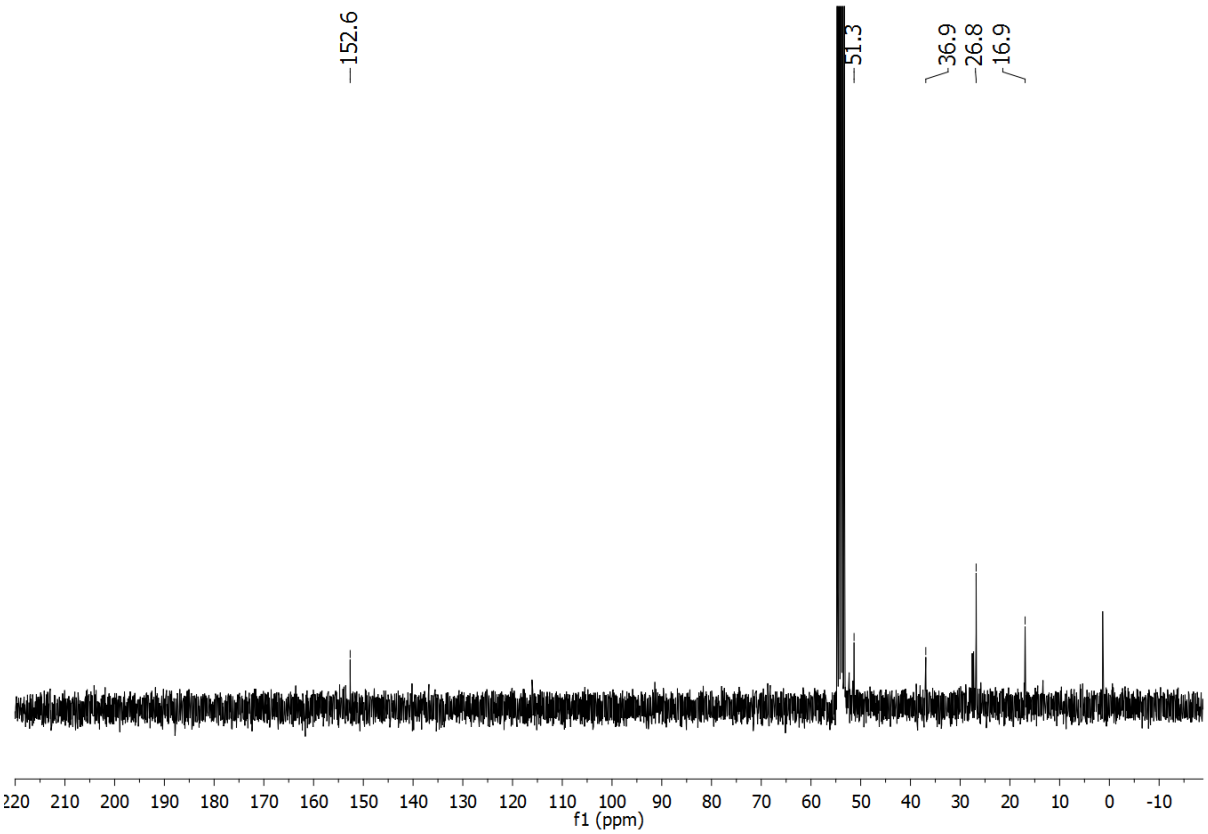

Figure S11. ^{13}C-NMR spectrum of **5** (75MHz, CD_2Cl_2).

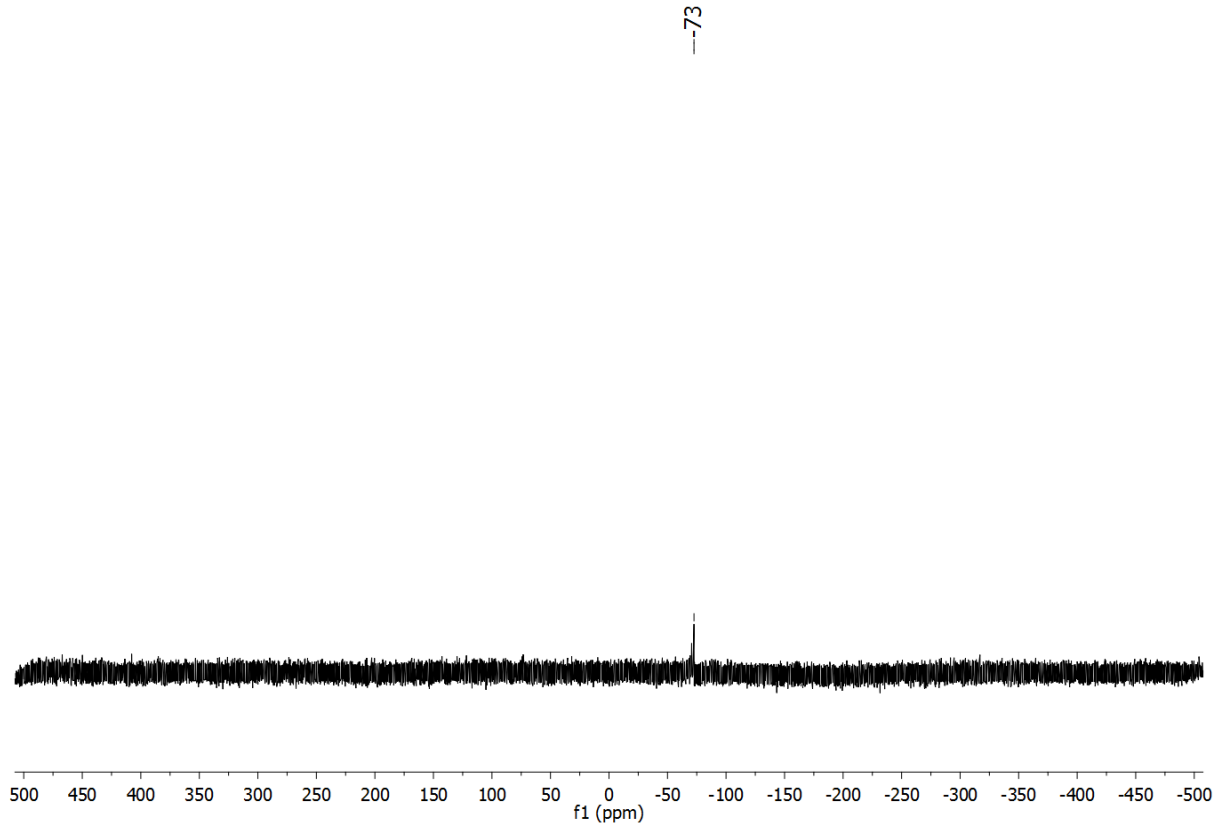

Figure S12. ^{119}Sn-NMR spectrum of **5** (187 MHz, CD_2Cl_2).

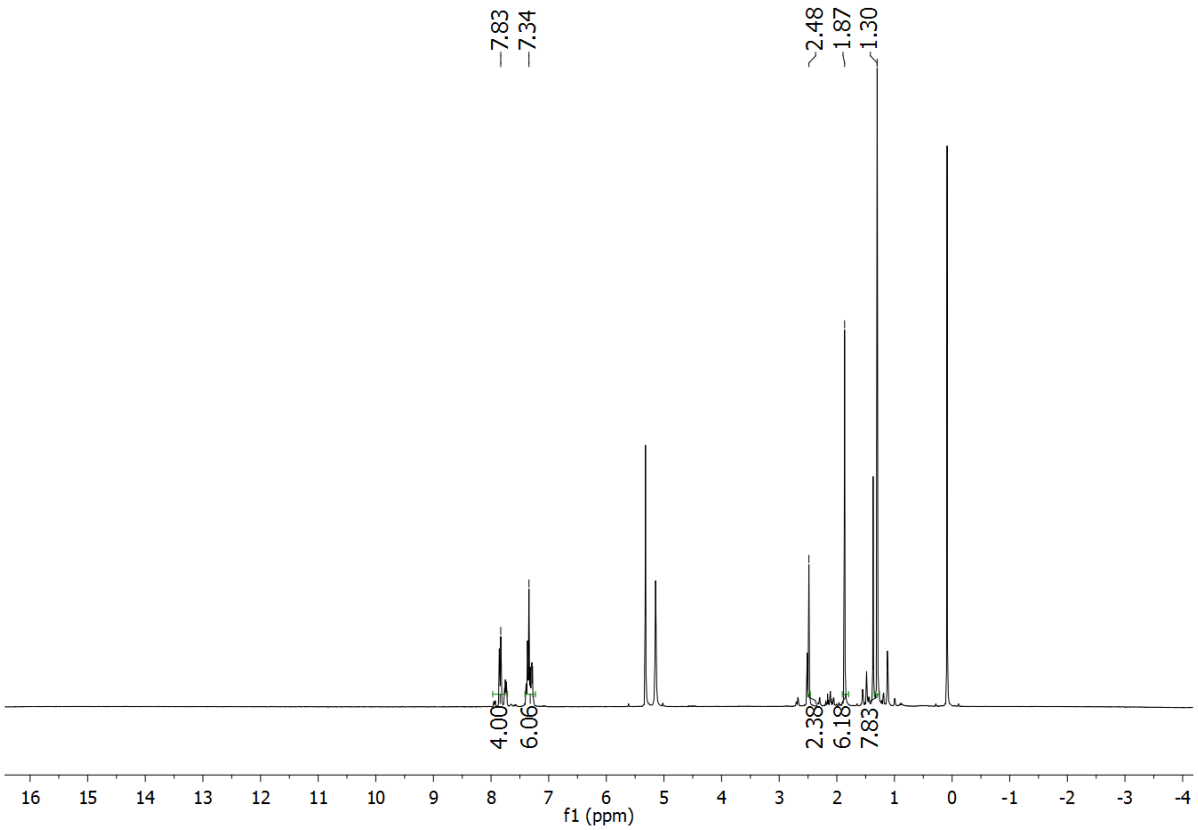

Figure S13. ^{1}H-NMR spectrum of **6** (300 MHz, CD_2Cl_2).

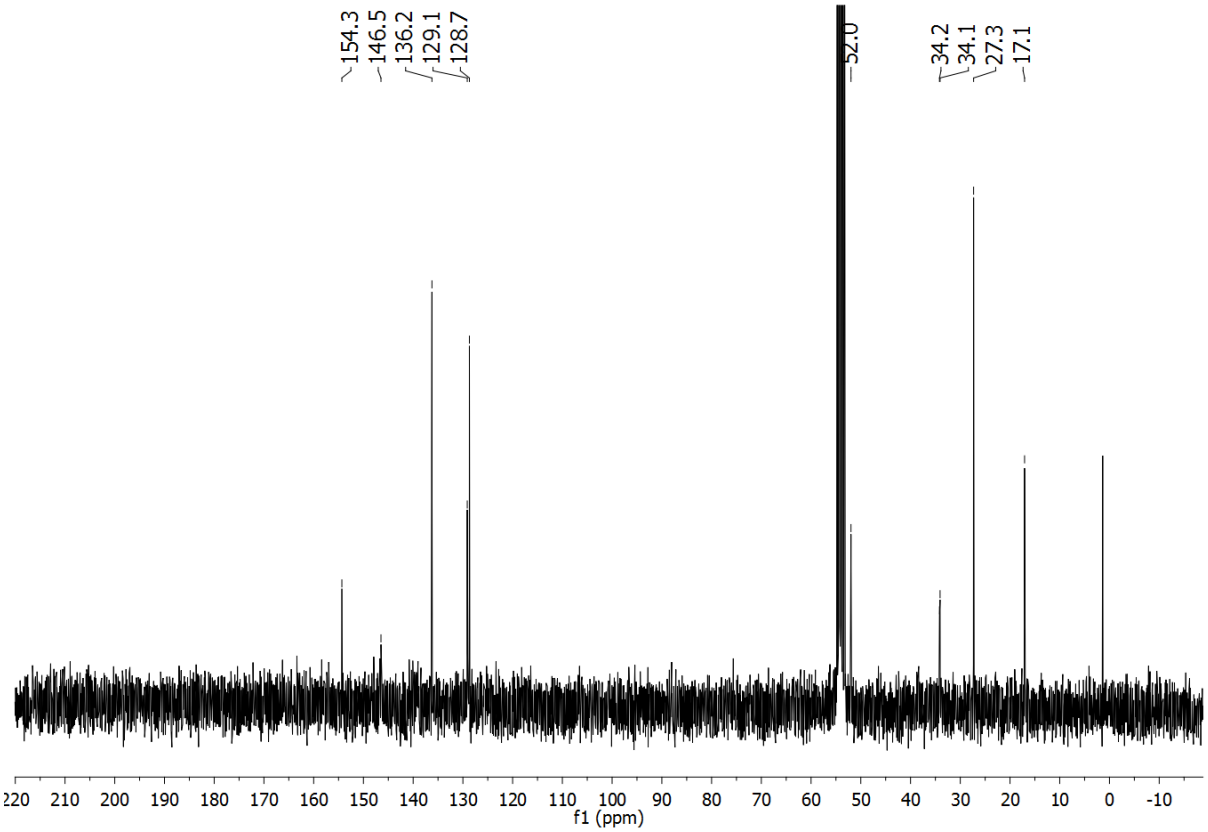

Figure S14. ^{13}C-NMR spectrum of **6** (75 MHz, CD_2Cl_2).

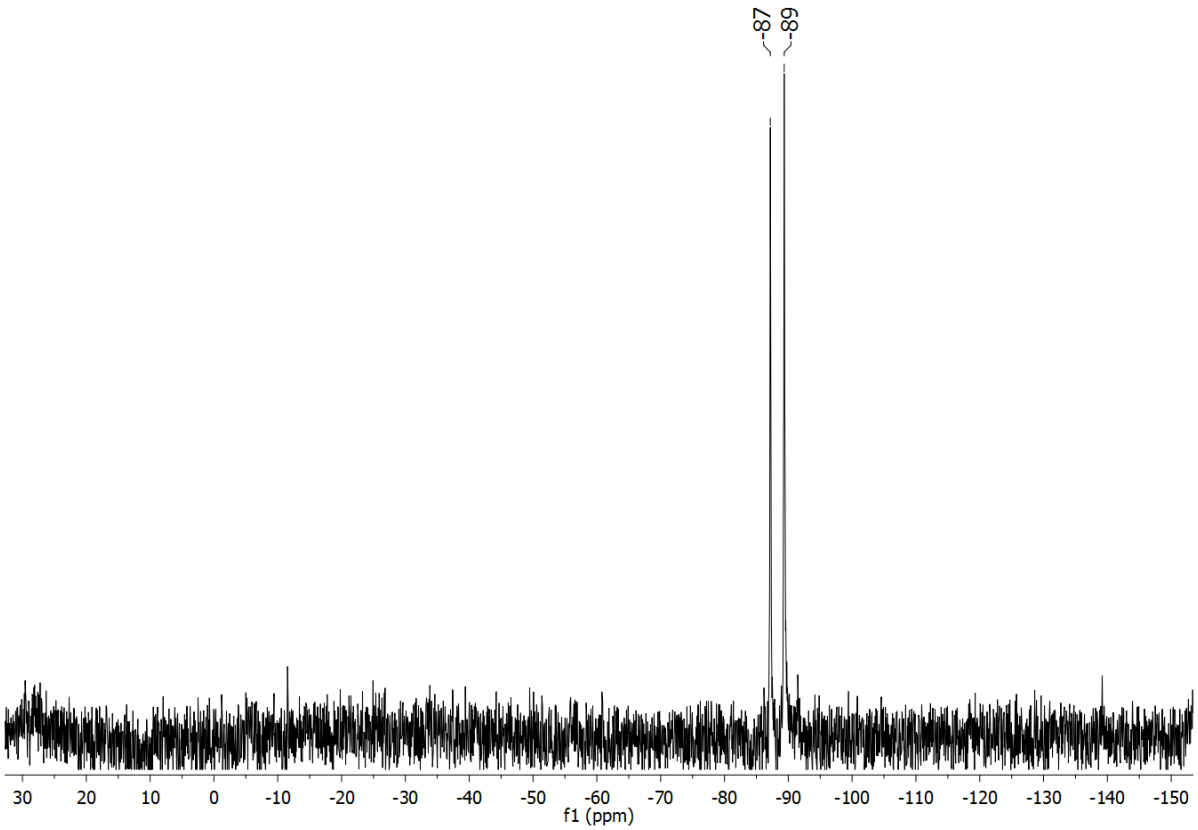

Figure S15. ^{119}Sn-NMR spectrum of **5** (187 MHz, CD_2Cl_2).

2) Mass spectra

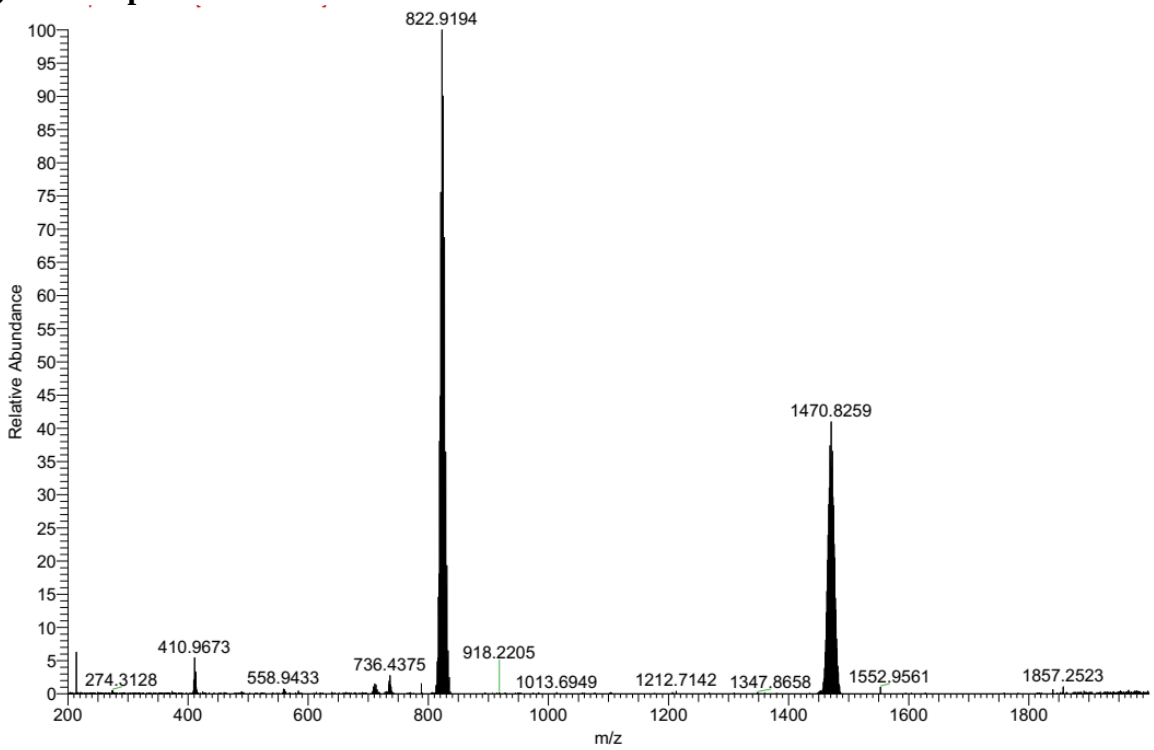

Figure S16. ESI(+) mass spectrum of **1**.

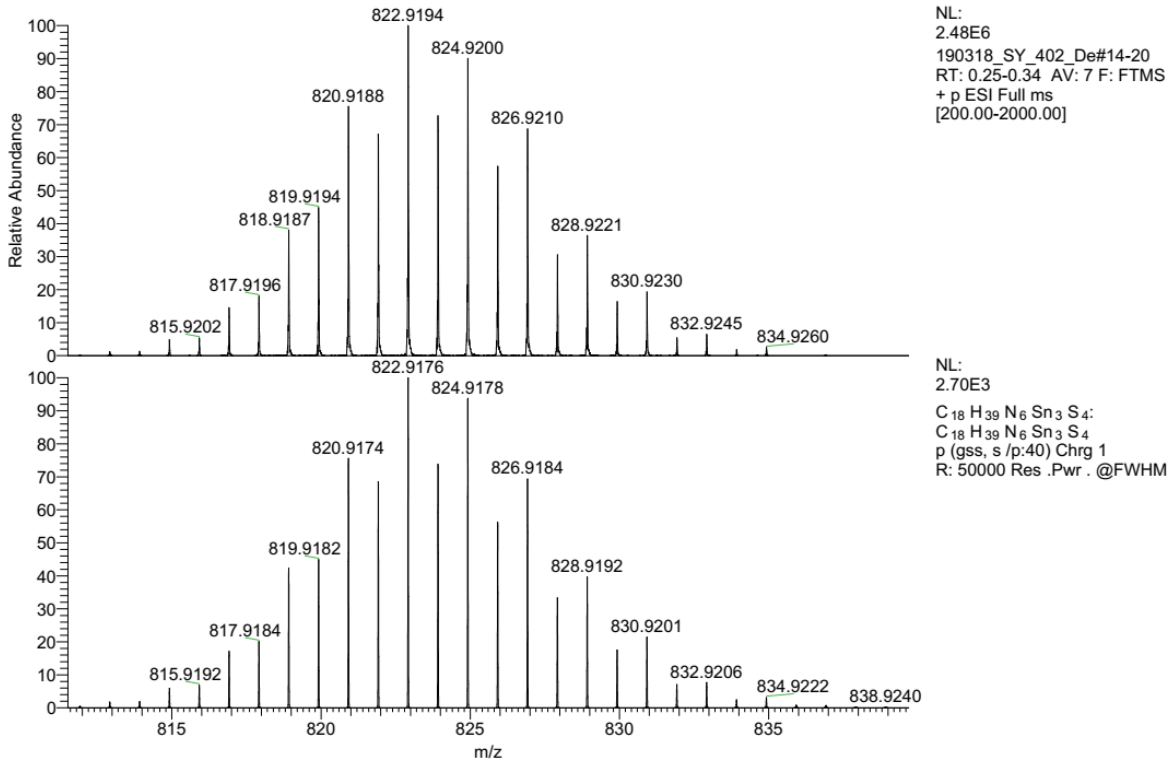

Figure S17. High resolution of the mass signal at 822.9194 m/z, corresponding to the formula $[C_{18}H_{39}N_6Sn_3S_4]^+$.

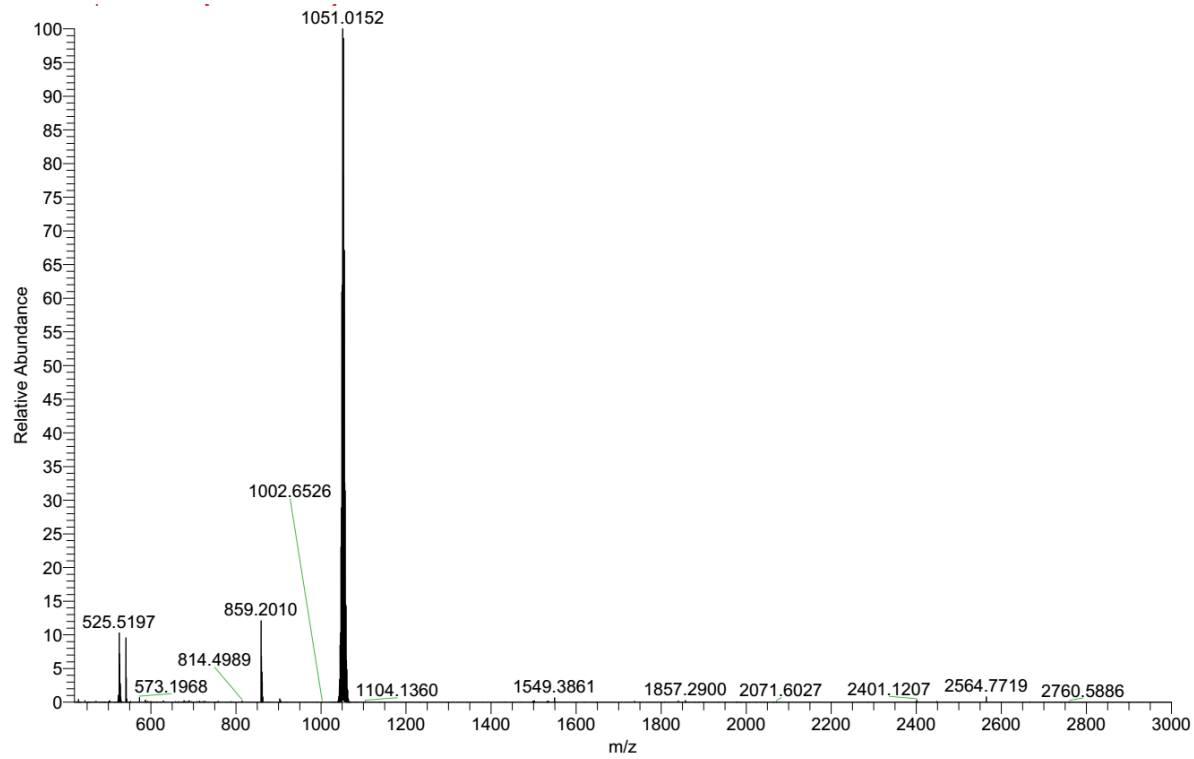

Figure S18. ESI(+) mass spectrum of **2**.

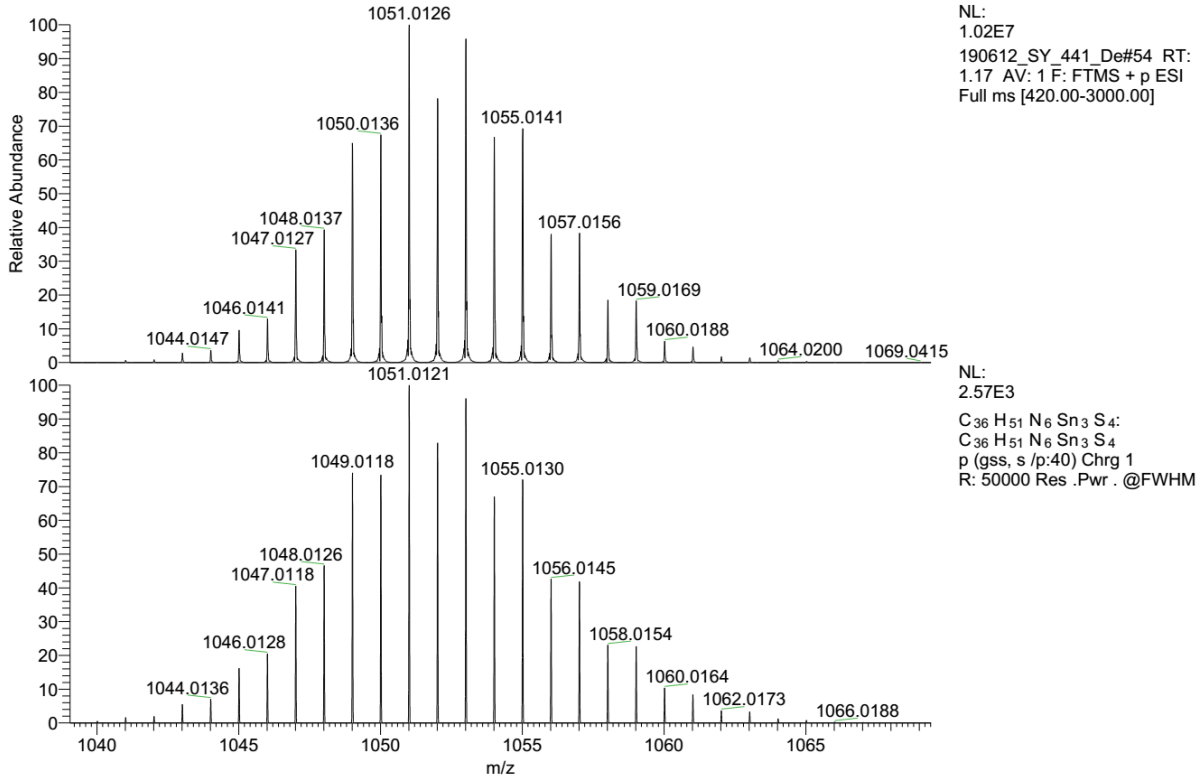

Figure S19. High resolution of the mass signal at 1051.0126 m/z, corresponding to the formula $[C_{36}H_{51}N_6Sn_3S_4]^+$.

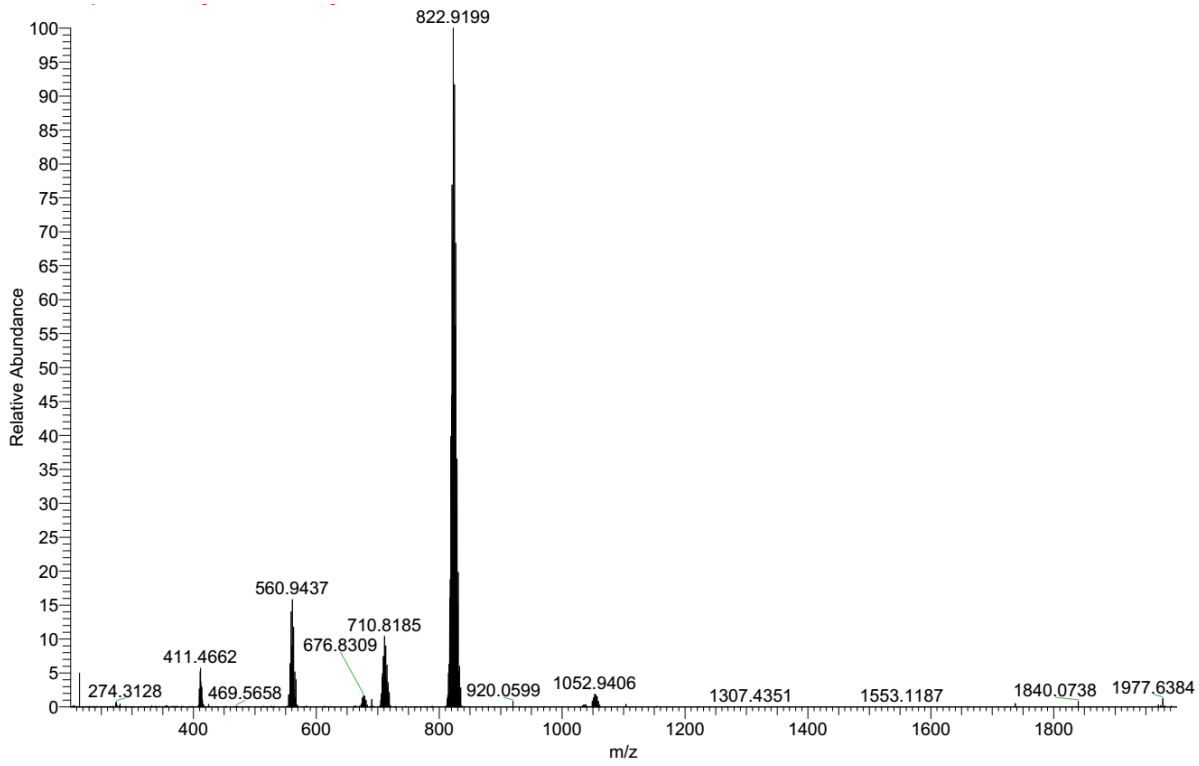

Figure S20. ESI(+) mass spectrum of **3**.

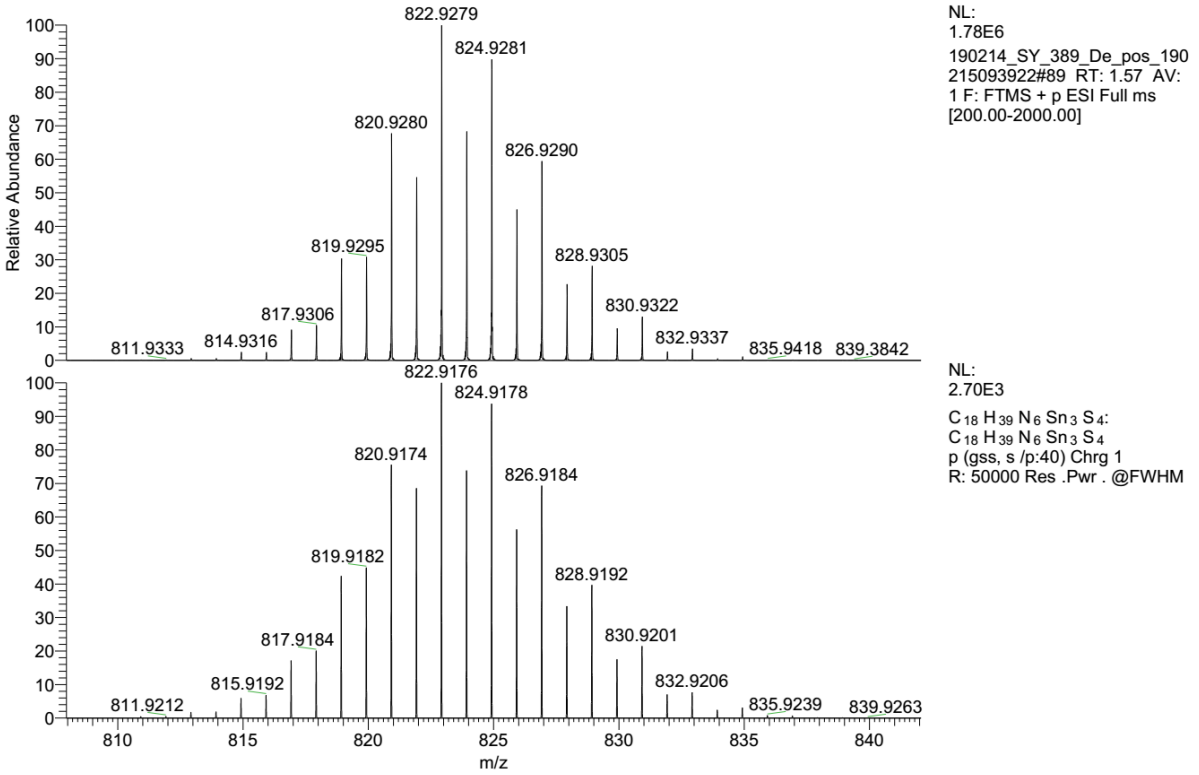

Figure S21. High resolution of the mass signal at 822.9279 m/z, corresponding to the formula $[C_{18}H_{39}N_6Sn_3S_4]^+$.

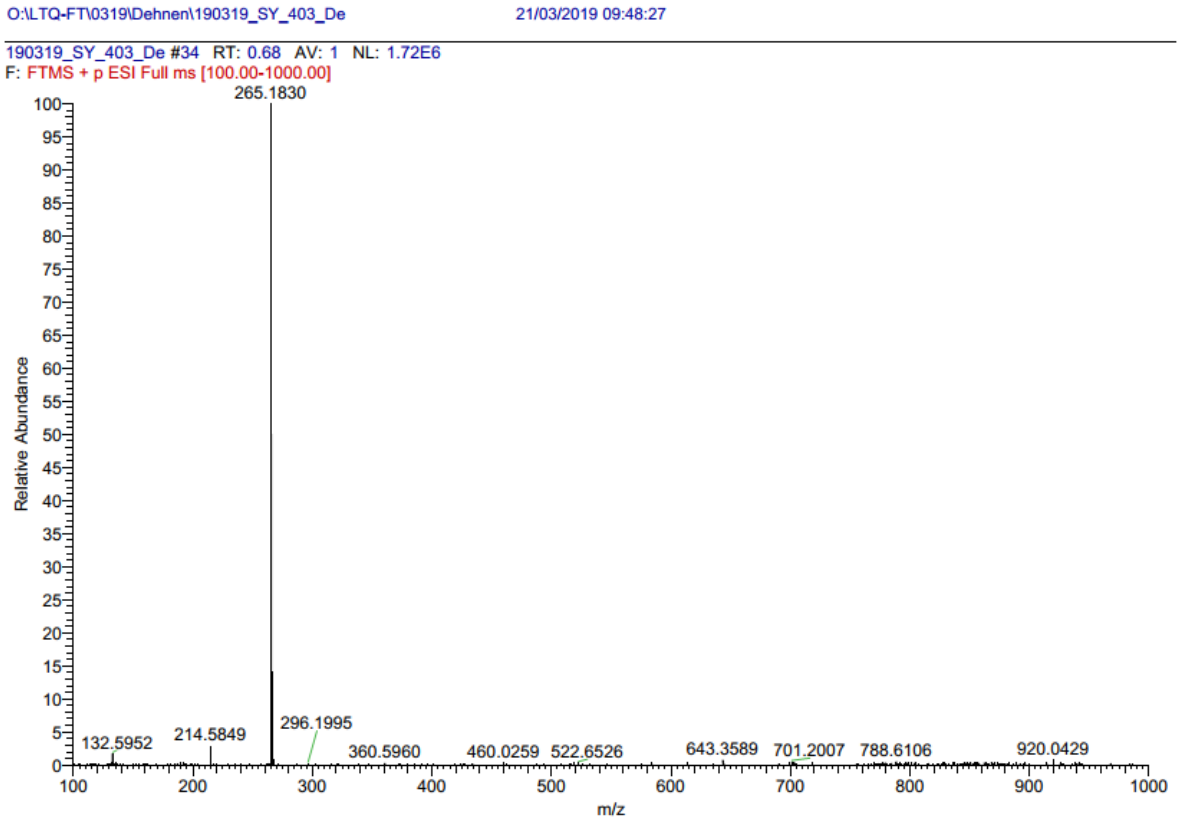

Figure S22 ESI(+) mass spectrum of **4b**.

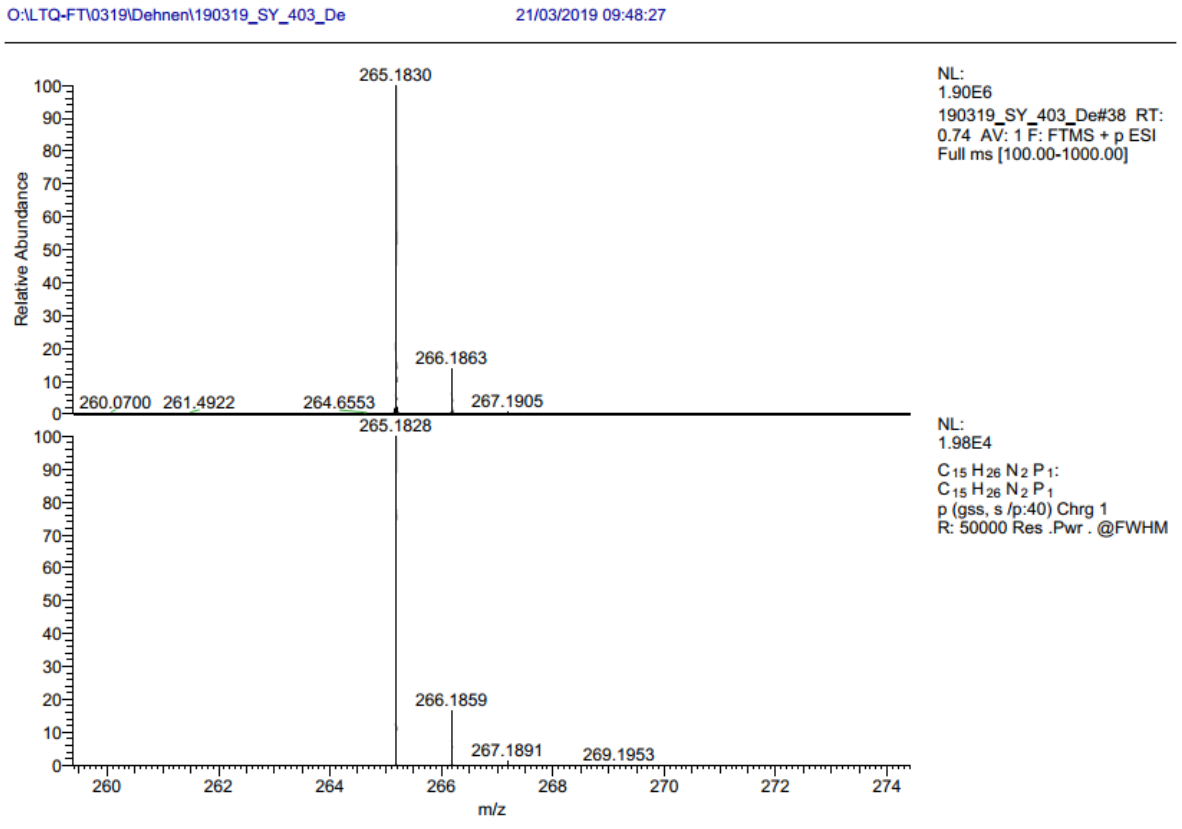

Figure S23. High resolution of the mass signal at 265.1830 m/z, corresponding to the formula $[C_{15}H_{26}N_2P]^+$.

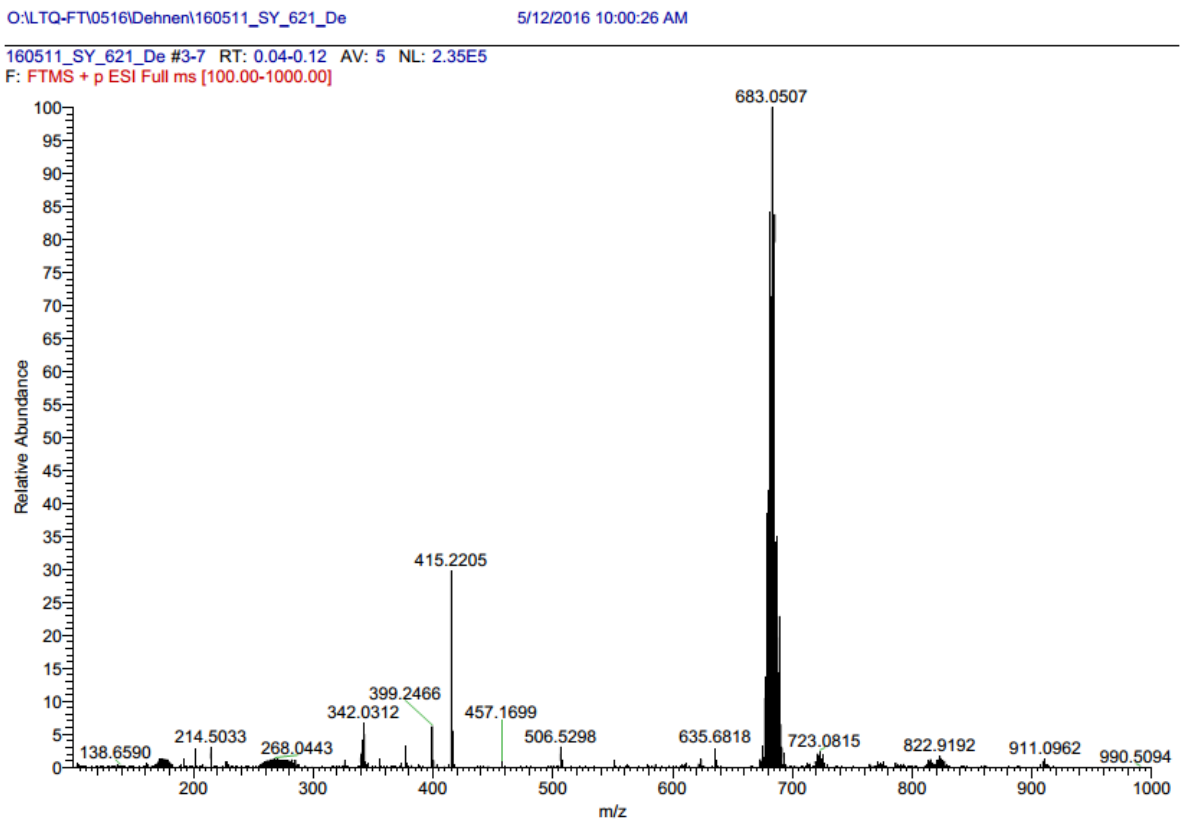

Figure S24. ESI(+) mass spectrum of **6**.

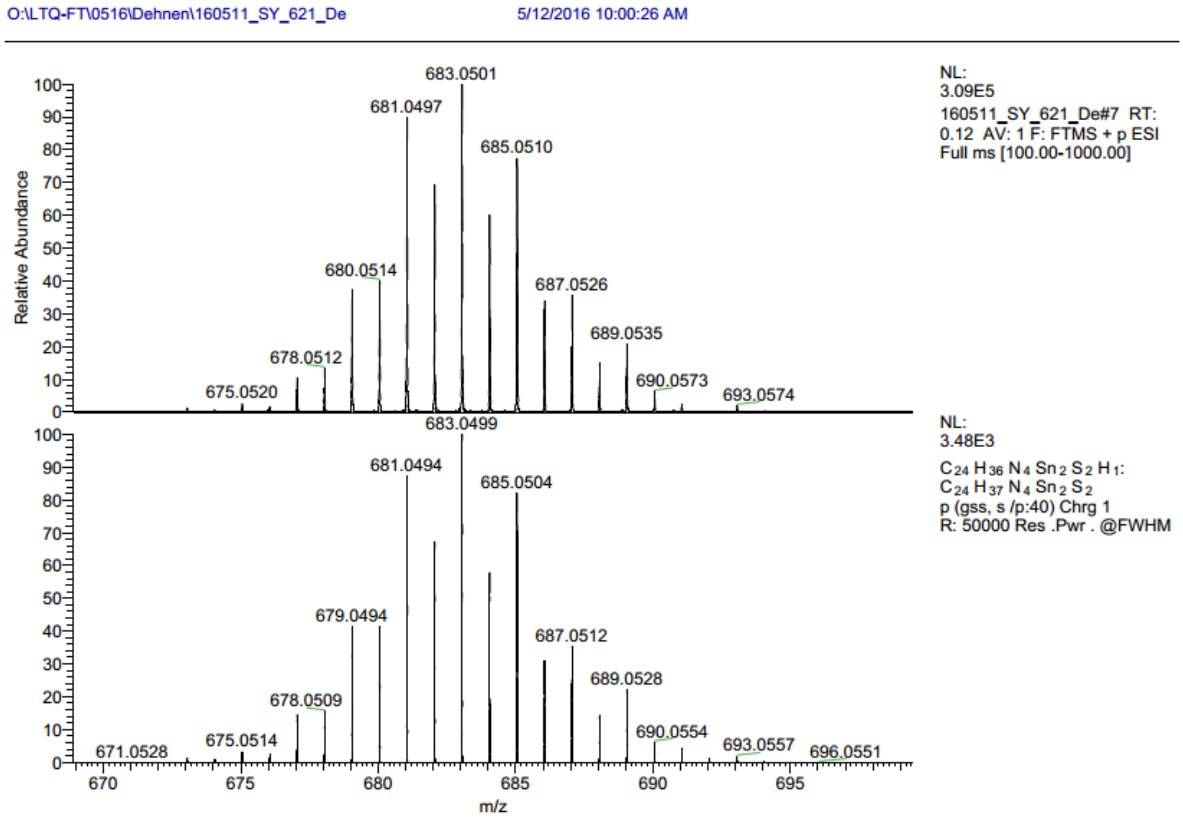

Figure S25. High resolution of the mass signal at 683.0501 m/z, corresponding to the formula $C_{24}H_{37}N_4Sn_2S_2$ ([**6**H]$^+$).

3) IR spectra

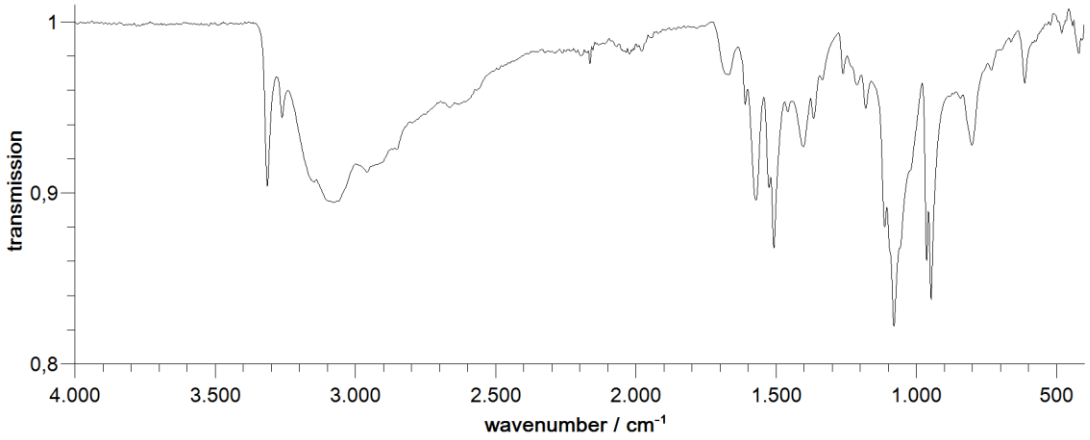

Figure S26. IR spectrum of **3**.

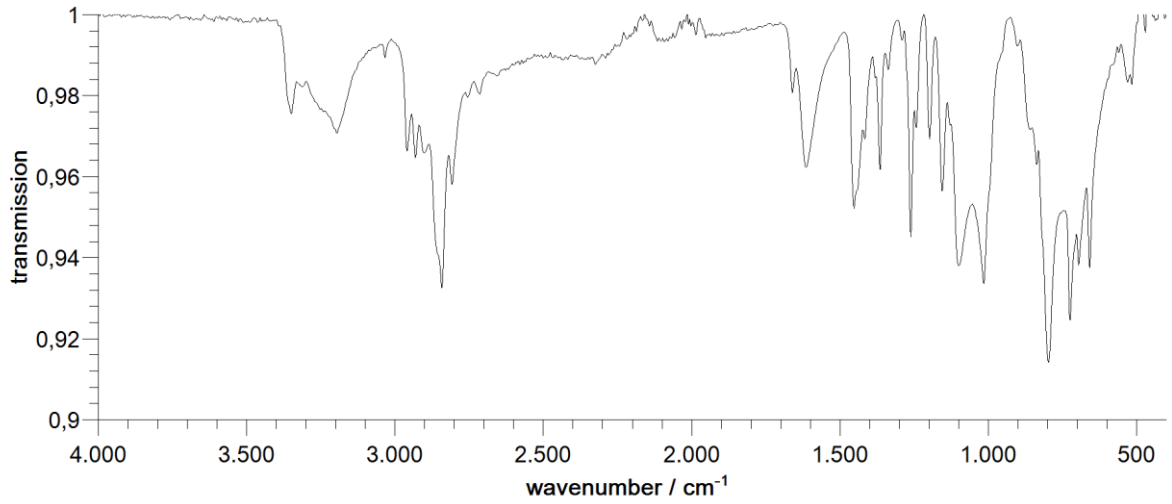

Figure S27. IR spectrum of **5**.

4) Single-crystal X-ray Crystallography of Compound 1

Compound **1** crystallizes as colorless plates. Data of the X-Ray diffraction analyses were collected on a STOE IPDS2 imaging plate diffractometer using $Mo_{K\alpha}$ radiation with graphite monochromatization. (λ = 0.71073 Å) at 100 K. Reflection data were processed with X-Area 1.77.[1] Structure solution was performed by direct methods and full-matrix-least-squares refinement against F^2 using SHELXT[2] and SHELXL-2014.[3] All non-hydrogen atoms were refined anisotropically, hydrogen atom positions were calculated. One cocrystallized, partially occupied hexane molecule per formula unit could not be refined and was thus removed by the SQUEEZE routine. The void is located at 0.5, 0.0, 1.0, has a volume of 256 $Å^3$ and contains 71 electrons, corresponding to 0.7 molecules hexane per formula unit. The carbon atoms C8 and C9 are disordered on two positions each.

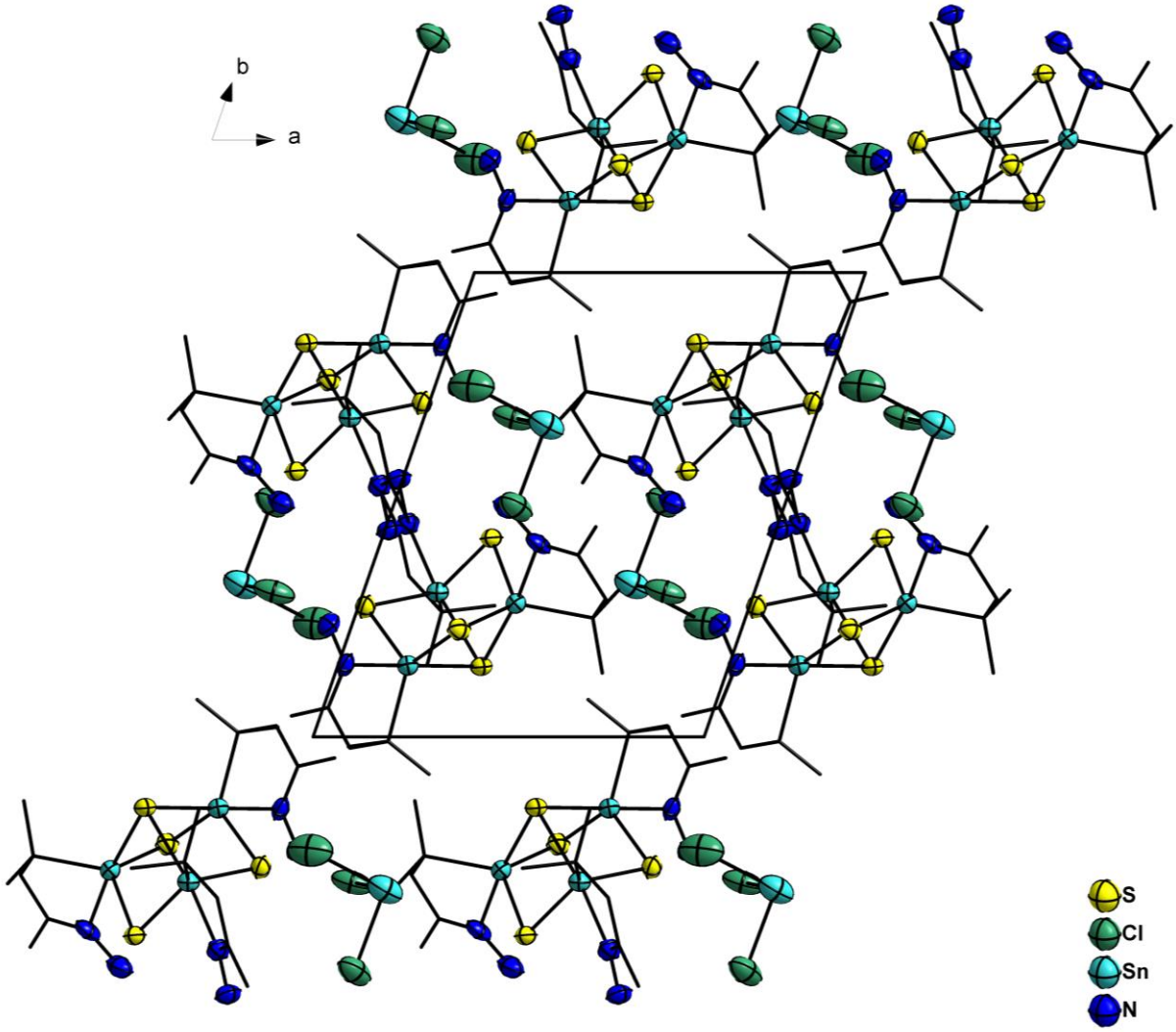

Figure S28. Crystal structure of **1** along the *c* axis.

Table S1. Crystal data and structure refinement for **1**.

Empirical formula	$C_{18}H_{39}Cl_3N_6S_4Sn_3Zn_1$	
CCDC number	1914529	
Formula weight	995.65	
Temperature	100(2) K	
Wavelength	0.71073 Å	
Crystal system	Triclinic	
Space group	$P\bar{1}$	
Unit cell dimensions	a = 10.7708(8) Å	α = 75.149(4)°.
	b = 13.9915(8) Å	β = 87.818(4)°.
	c = 14.1040(8) Å	γ = 70.912(4)°.
Volume	1939.1(2) $Å^3$	
Z	2	
Density (calculated)	3.173 Mg/m^3	
Absorption coefficient	9.525 mm^{-1}	
F(000)	1674	
Crystal size	0.1 x 0.1 x 0.1 mm^3	
Theta range for data collection	1.496 to 26.794°.	
Index ranges	-13<=h<=12, -17<=k<=15, -17<=l<=17	
Reflections collected	16410	
Independent reflections	8206 [R(int) = 0.0716]	
Completeness to theta = 25.242°	99.8 %	
Absorption correction	Sphere	
Max. and min. transmission	0.2738 and 0.0102	
Refinement method	Full-matrix least-squares on F^2	
Data / restraints / parameters	8206 / 2 / 334	
Goodness-of-fit on F^2	0.940	
Final R indices [I>2sigma(I)]	R1 = 0.0592, wR2 = 0.1397	
R indices (all data)	R1 = 0.1125, wR2 = 0.1602	
Largest diff. peak and hole	2.567 and -1.630 $e.Å^{-3}$	

Table S2. Atomic coordinates (x 10^4) and equivalent isotropic displacement parameters ($Å^2$x 10^3) for **1**. U(eq) is defined as one third of the trace of the orthogonalized U^{ij} tensor.

	x	y	z	U(eq)
C(1)	2179(10)	2695(8)	2572(8)	46(3)
C(2)	2279(16)	1533(10)	2753(10)	80(4)
C(3)	3476(13)	2827(10)	2230(10)	70(4)
C(4)	1024(12)	3463(10)	1877(11)	71(2)
C(5)	323(9)	4493(8)	2092(8)	44(2)
C(6)	-537(11)	5368(9)	1295(9)	59(3)
C(7)	1961(10)	-97(7)	6734(8)	46(3)
C(8A)	3295(18)	-803(15)	6739(18)	60(7)
C(9A)	990(17)	-211(16)	5883(14)	52(6)
C(8B)	3190(20)	-502(16)	7570(20)	43(7)
C(9B)	2400(20)	-659(19)	5964(18)	47(8)
C(10)	1041(12)	-240(10)	7475(11)	71(2)
C(11)	125(10)	632(8)	7827(9)	48(3)
C(12)	-737(11)	453(9)	8612(9)	60(3)
C(13)	6096(9)	2562(8)	6064(9)	47(3)
C(14)	6828(10)	1377(9)	6278(11)	73(4)
C(15)	6507(10)	3159(11)	5138(11)	75(4)
C(16)	6257(12)	2971(10)	6955(11)	71(2)
C(17)	5162(12)	3916(10)	7055(9)	57(3)
C(18)	5364(14)	4525(12)	7740(10)	79(4)
S(1)	182(2)	2805(2)	5037(2)	39(1)
S(2)	3672(2)	1518(2)	5067(2)	37(1)
S(3)	2796(2)	4279(2)	4501(2)	37(1)
S(4)	2778(2)	2313(2)	7243(2)	38(1)
Cl(1)	3137(4)	4954(3)	10104(3)	76(1)
Cl(2)	944(5)	7557(3)	9901(3)	99(1)
Cl(3)	2287(4)	6871(2)	7756(2)	72(1)
Sn(1)	1896(1)	3119(1)	3973(1)	32(1)
Sn(2)	1790(1)	1538(1)	6277(1)	32(1)
Sn(3)	4002(1)	2873(1)	5864(1)	34(1)
Sn(4)	3192(1)	6719(1)	9386(1)	76(1)
N(1)	528(7)	4589(6)	2930(6)	38(2)
N(2)	-114(8)	5546(6)	3192(7)	45(2)
N(3)	191(6)	1553(6)	7429(6)	36(2)
N(4)	-602(8)	2420(6)	7710(7)	47(2)
N(5)	4046(8)	4164(6)	6589(6)	42(2)
N(6)	2903(9)	4950(7)	6719(7)	51(2)

Table S3. Bond lengths [Å] and angles [°] for **1**.

C(1)-C(3)	1.513(16)	C(3)-C(1)-C(2)	109.5(10)	C(1)-Sn(1)-S(3)	126.8(3)
C(1)-C(4)	1.530(16)	C(4)-C(1)-C(2)	114.2(10)	N(1)-Sn(1)-S(3)	86.2(2)
C(1)-C(2)	1.547(16)	C(3)-C(1)-Sn(1)	105.5(7)	S(1)-Sn(1)-S(3)	109.62(9)
C(1)-Sn(1)	2.187(11)	C(4)-C(1)-Sn(1)	106.6(7)	C(1)-Sn(1)-S(2)	99.7(3)
C(4)-C(5)	1.494(16)	C(2)-C(1)-Sn(1)	108.8(7)	N(1)-Sn(1)-S(2)	173.4(2)
C(5)-N(1)	1.259(13)	C(5)-C(4)-C(1)	118.1(11)	S(1)-Sn(1)-S(2)	91.74(8)
C(5)-C(6)	1.501(14)	N(1)-C(5)-C(4)	117.6(10)	S(3)-Sn(1)-S(2)	90.01(8)
C(7)-C(10)	1.435(16)	N(1)-C(5)-C(6)	123.3(10)	C(7)-Sn(2)-N(3)	78.6(3)
C(7)-C(8A)	1.45(2)	C(4)-C(5)-C(6)	119.0(10)	C(7)-Sn(2)-S(4)	121.6(3)
C(7)-C(9B)	1.48(3)	C(10)-C(7)-C(8A)	125.2(13)	N(3)-Sn(2)-S(4)	87.6(2)
C(7)-C(8B)	1.66(3)	C(10)-C(7)-C(9B)	128.4(13)	C(7)-Sn(2)-S(1)	123.0(3)
C(7)-C(9A)	1.69(2)	C(10)-C(7)-C(8B)	91.6(12)	N(3)-Sn(2)-S(1)	90.98(18)
C(7)-Sn(2)	2.158(10)	C(9B)-C(7)-C(8B)	108.1(15)	S(4)-Sn(2)-S(1)	113.58(9)
C(10)-C(11)	1.481(16)	C(10)-C(7)-C(9A)	91.0(10)	C(7)-Sn(2)-S(2)	101.8(3)
C(11)-N(3)	1.292(13)	C(8A)-C(7)-C(9A)	110.3(14)	N(3)-Sn(2)-S(2)	176.7(2)
C(11)-C(12)	1.443(15)	C(10)-C(7)-Sn(2)	109.2(7)	S(4)-Sn(2)-S(2)	89.41(8)
C(13)-C(15)	1.495(17)	C(8A)-C(7)-Sn(2)	113.7(10)	S(1)-Sn(2)-S(2)	91.54(8)
C(13)-C(14)	1.539(15)	C(9B)-C(7)-Sn(2)	114.0(11)	C(13)-Sn(3)-N(5)	78.0(4)
C(13)-C(16)	1.546(18)	C(8B)-C(7)-Sn(2)	98.6(9)	C(13)-Sn(3)-S(3)	118.7(3)
C(13)-Sn(3)	2.168(9)	C(9A)-C(7)-Sn(2)	102.9(9)	N(5)-Sn(3)-S(3)	86.3(2)
C(16)-C(17)	1.490(17)	C(7)-C(10)-C(11)	123.2(11)	C(13)-Sn(3)-S(4)	119.7(3)
C(17)-N(5)	1.292(13)	N(3)-C(11)-C(12)	121.8(10)	N(5)-Sn(3)-S(4)	86.2(2)
C(17)-C(18)	1.506(17)	N(3)-C(11)-C(10)	116.3(10)	S(3)-Sn(3)-S(4)	117.74(8)
S(1)-Sn(1)	2.415(2)	C(12)-C(11)-C(10)	121.8(11)	C(13)-Sn(3)-S(2)	108.4(3)
S(1)-Sn(2)	2.416(2)	C(15)-C(13)-C(14)	112.2(10)	N(5)-Sn(3)-S(2)	173.6(2)
S(2)-Sn(3)	2.559(3)	C(15)-C(13)-C(16)	112.0(10)	S(3)-Sn(3)-S(2)	90.77(8)
S(2)-Sn(1)	2.590(2)	C(14)-C(13)-C(16)	110.4(10)	S(4)-Sn(3)-S(2)	90.15(8)
S(2)-Sn(2)	2.598(2)	C(15)-C(13)-Sn(3)	106.4(7)	Cl(1)-Sn(4)-Cl(3)	95.12(11)
S(3)-Sn(3)	2.415(2)	C(14)-C(13)-Sn(3)	109.8(7)	Cl(1)-Sn(4)-Cl(2)	93.16(14)
S(3)-Sn(1)	2.416(3)	C(16)-C(13)-Sn(3)	105.7(7)	Cl(3)-Sn(4)-Cl(2)	90.65(14)
S(4)-Sn(2)	2.406(3)	C(17)-C(16)-C(13)	115.0(10)	C(5)-N(1)-N(2)	120.8(8)
S(4)-Sn(3)	2.415(3)	N(5)-C(17)-C(16)	119.3(10)	C(5)-N(1)-Sn(1)	114.9(7)
Cl(1)-Sn(4)	2.437(3)	N(5)-C(17)-C(18)	121.6(12)	N(2)-N(1)-Sn(1)	124.2(6)
Cl(2)-Sn(4)	2.492(4)	C(16)-C(17)-C(18)	119.0(11)	C(11)-N(3)-N(4)	121.3(8)
Cl(3)-Sn(4)	2.462(4)	Sn(1)-S(1)-Sn(2)	91.22(8)	C(11)-N(3)-Sn(2)	112.7(7)
Sn(1)-N(1)	2.280(8)	Sn(3)-S(2)-Sn(1)	83.95(7)	N(4)-N(3)-Sn(2)	126.0(6)
Sn(2)-N(3)	2.321(7)	Sn(3)-S(2)-Sn(2)	83.34(8)	C(17)-N(5)-N(6)	124.4(9)
Sn(3)-N(5)	2.305(8)	Sn(1)-S(2)-Sn(2)	83.45(7)	C(17)-N(5)-Sn(3)	111.1(7)
N(1)-N(2)	1.426(11)	Sn(3)-S(3)-Sn(1)	90.93(8)	N(6)-N(5)-Sn(3)	122.5(6)
N(3)-N(4)	1.379(11)	Sn(2)-S(4)-Sn(3)	90.65(9)		
N(5)-N(6)	1.401(11)	C(1)-Sn(1)-N(1)	78.4(3)		
		C(1)-Sn(1)-S(1)	122.0(3)		
C(3)-C(1)-C(4)	111.8(10)	N(1)-Sn(1)-S(1)	94.6(2)		

5) Single-crystal X-ray Crystallography of Compound 2

Compound **2** crystallizes as orange blocks. Data of the X-Ray diffraction analyses were collected on a STOE IPDS2T imaging plate diffractometer using $Mo_{K\alpha}$ radiation with graphite monochromatization. (λ = 0.71073 Å) at 100 K. Reflection data were processed with X-Area 1.77.[1] Structure solution was performed by direct methods and full-matrix-least-squares refinement against F^2 using SHELXT[2] and SHELXL-2014.[3] All non-hydrogen atoms were refined anisotropically, hydrogen atom positions were calculated. A second dichloromethane molecule could not be refined due to its disorder and was removed with the SQUEEZE routine. The void is located at 0.0, 0.0, 0.0, has a volume of 165 $Å^3$ and contains 79 electrons. The organic substituent at Sn3 is disordered on two positions.

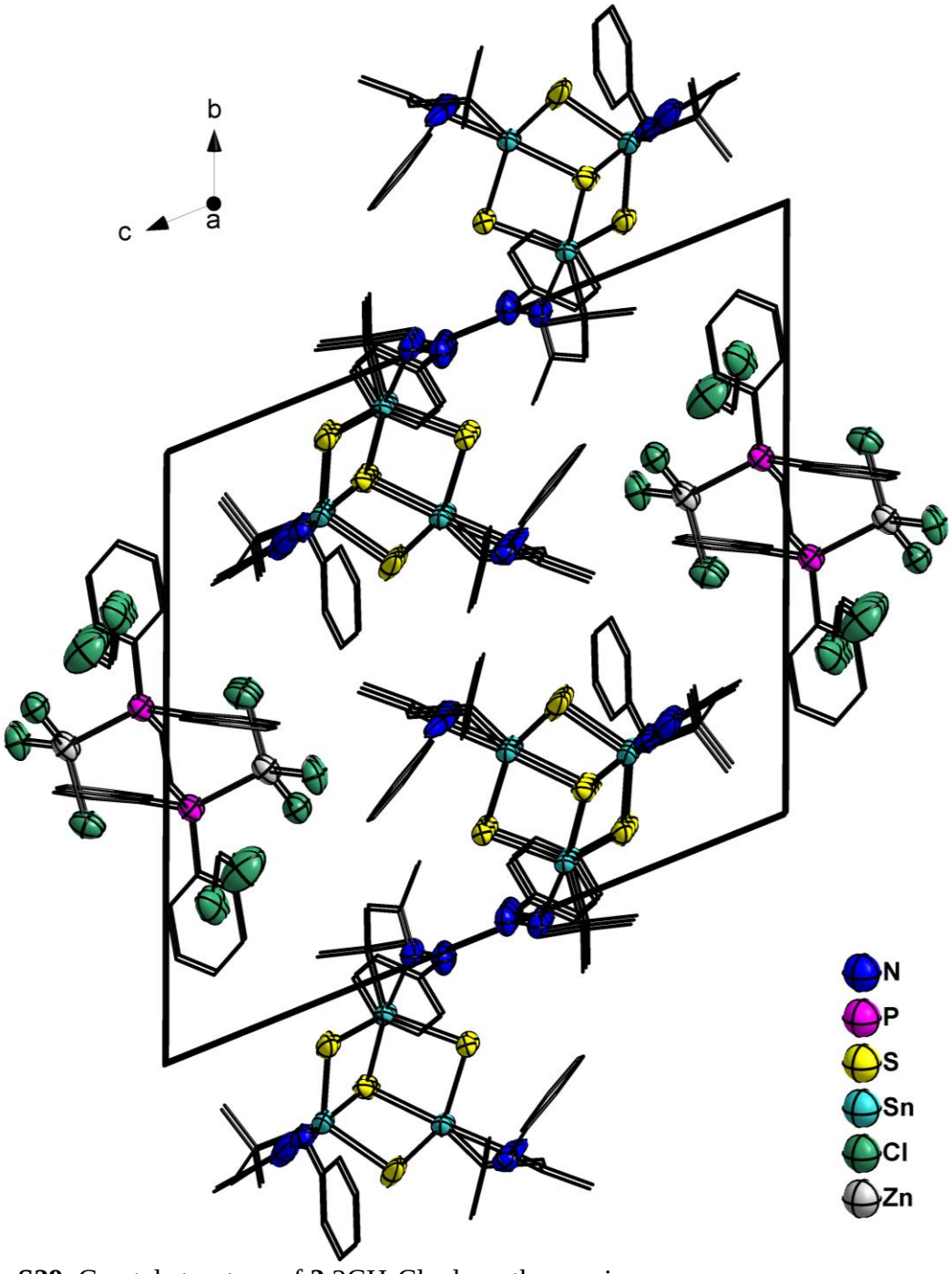

Figure S29. Crystal structure of **2**·2CH_2Cl_2 along the *a* axis.

Table S4. Crystal data and structure refinement for **2**·$2CH_2Cl_2$.

Empirical formula	$C_{50}H_{61}Cl_5N_6P_1S_4Sn_3Zn_1$	
CCDC number	1914530	
Formula weight	1503.94	
Temperature	100(2) K	
Wavelength	0.71073 Å	
Crystal system	Triclinic	
Space group	$P\bar{1}$	
Unit cell dimensions	a = 11.3687(4) Å	α = 110.2990(10)°.
	b = 16.8991(5) Å	β = 98.085(2)°.
	c = 18.4946(5) Å	γ = 98.664(2)°.
Volume	3222.41(17) $Å^3$	
Z	2	
Density (calculated)	1.550 Mg/m^3	
Absorption coefficient	1.915 mm^{-1}	
F(000)	1494	
Crystal size	0.1 x 0.1 x 0.1 mm^3	
Theta range for data collection	1.852 to 26.807°.	
Index ranges	-14<=h<=14, -21<=k<=21, -23<=l<=19	
Reflections collected	27258	
Independent reflections	13593 [R(int) = 0.0564]	
Completeness to theta = 25.242°	99.6 %	
Absorption correction	Sphere	
Max. and min. transmission	1.000 and 1.000	
Refinement method	Full-matrix least-squares on F^2	
Data / restraints / parameters	13593 / 5 / 721	
Goodness-of-fit on F^2	1.125	
Final R indices [I>2sigma(I)]	R1 = 0.0569, wR2 = 0.1572	
R indices (all data)	R1 = 0.0699, wR2 = 0.1662	
Largest diff. peak and hole	2.364 and -2.597 e.$Å^{-3}$	

Table S5. Atomic coordinates (x 10^4) and equivalent isotropic displacement parameters ($Å^2$x 10^3) for **2**·2CH_2Cl_2. U(eq) is defined as one third of the trace of the orthogonalized U^{ij} tensor.

	x	y	z	U(eq)
C(31A)	-123(6)	7162(3)	7466(4)	42(2)
C(32A)	-620(5)	6348(4)	7444(4)	42(3)
C(33A)	-44(7)	5667(3)	7161(4)	46(2)
C(34A)	1029(6)	5800(3)	6898(4)	57(3)
C(35A)	1526(5)	6613(4)	6919(4)	61(3)
C(36A)	950(6)	7294(3)	7203(4)	55(2)
N(6)	-609(6)	7889(4)	7770(4)	37(2)
C(30A)	-667(9)	7605(6)	9195(5)	49(2)
C(29)	-1757(11)	7682(6)	8646(7)	57(4)
C(28)	-2927(13)	7606(9)	8927(6)	63(3)
C(27)	-3909(12)	8880(6)	9089(6)	57(3)
C(32B)	-581(11)	6040(7)	7274(7)	45(5)
C(35)	-982(10)	6810(7)	7475(5)	48(4)
C(34)	-979(10)	7265(6)	6977(6)	55(4)
C(33)	-574(11)	6950(7)	6277(6)	61(5)
C(32)	-173(10)	6180(7)	6076(5)	58(5)
C(31)	-176(10)	5725(6)	6574(7)	64(6)
N(7)	-1355(14)	7118(11)	8212(9)	62(4)
C(30B)	-1350(15)	7978(11)	9705(10)	55(4)
C(29B)	-2170(20)	7981(13)	9018(12)	63(8)
C(28B)	-3201(17)	8496(12)	9227(9)	58(5)
C(27B)	-5170(20)	8804(12)	8769(12)	71(5)
C(1)	-6865(5)	6194(3)	4882(4)	51(1)
P(1)	8285(1)	4002(1)	9603(1)	37(1)
C(2)	-7925(6)	6571(5)	4830(5)	62(1)
C(3)	-6993(6)	5438(4)	5083(5)	62(1)
C(4)	-6601(6)	5879(4)	3967(4)	57(1)
C(5)	-5453(8)	5740(4)	3923(4)	67(2)
C(6A)	-6469(14)	5147(8)	3126(9)	28(4)
C(6B)	-5167(8)	5144(5)	3153(5)	49(2)
C(7)	-2617(6)	6558(4)	4163(5)	70(2)
C(8)	-3160(6)	6937(5)	3690(5)	73(3)
C(9)	-2468(7)	7319(5)	3293(5)	71(2)
C(10)	-1277(6)	7324(5)	3372(4)	64(2)
C(11)	-702(5)	6960(5)	3841(4)	63(2)
C(12)	-1359(6)	6569(4)	4235(5)	60(2)
C(13)	-4740(5)	10510(4)	6764(4)	51(1)

C(14)	-5126(6)	10740(4)	7555(3)	48(1)
C(15)	-5828(5)	10346(3)	6101(3)	42(1)
C(16)	-3725(6)	11212(4)	6773(4)	57(1)
C(17)	-2895(5)	10956(3)	6233(3)	44(1)
C(18)	-2256(6)	11588(4)	5942(4)	58(2)
C(19)	-876(5)	9732(4)	5903(3)	44(1)
C(20)	-174(6)	10346(4)	6608(4)	60(2)
C(21)	895(6)	10188(5)	6954(4)	66(2)
C(22)	1258(6)	9423(6)	6592(5)	69(2)
C(23)	568(7)	8827(6)	5895(5)	77(2)
C(24)	-507(6)	8973(4)	5541(4)	57(2)
C(26)	-5155(8)	7362(5)	8477(5)	81(2)
C(37)	-3227(6)	6914(5)	10867(5)	67(2)
C(38)	7596(5)	4465(3)	10422(3)	40(1)
C(39)	6338(5)	4416(4)	10270(4)	49(1)
C(40)	5769(6)	4747(5)	10886(4)	61(2)
C(41)	6440(6)	5153(5)	11643(4)	61(2)
C(42)	7657(6)	5191(5)	11803(4)	63(2)
C(43)	8252(5)	4855(4)	11204(4)	49(1)
C(44)	7582(7)	1647(4)	9821(4)	60(2)
C(45)	8028(6)	1144(4)	9208(4)	61(2)
C(46)	8556(6)	1491(4)	8745(4)	58(2)
C(47)	8644(5)	2362(4)	8880(3)	47(1)
C(48)	8212(4)	2883(3)	9489(3)	38(1)
C(49)	7670(5)	2531(4)	9962(4)	52(1)
C(86)	9902(5)	4517(4)	9933(3)	41(1)
S(1)	-4427(1)	8295(1)	5144(1)	38(1)
S(2)	-5587(1)	8257(1)	6786(1)	45(1)
S(3)	-3727(2)	6702(1)	6335(1)	74(1)
S(4)	-2407(2)	9210(1)	7386(1)	48(1)
Sn(1)	-5180(1)	7137(1)	5543(1)	35(1)
Sn(2)	-4049(1)	9336(1)	6479(1)	36(1)
Sn(3)	-3635(1)	7973(1)	7475(1)	51(1)
Cl(2)	7399(1)	5560(1)	8742(1)	57(1)
Cl(3)	5571(1)	3291(1)	7904(1)	45(1)
Cl(4)	8763(1)	3733(1)	7611(1)	56(1)
Cl(5)	-1674(2)	7329(2)	11255(2)	115(1)
Cl(6)	-3999(2)	7696(2)	10767(1)	86(1)
Zn(1)	7435(1)	4137(1)	8395(1)	43(1)
N(1)	-4635(6)	6228(3)	4451(4)	74(2)
N(2A)	-3278(5)	6158(4)	4510(4)	39(2)

N(2B)	-4458(12)	6601(9)	3754(8)	34(4)
N(3)	-2768(4)	10165(3)	6037(3)	41(1)
N(4)	-1951(4)	9878(3)	5519(3)	48(1)
N(5)	-1765(7)	7791(4)	8068(4)	88(3)
C(25)	-4027(9)	7987(5)	8573(4)	80(3)

Table S6. Bond lengths [Å] and angles [°] for **2**·2CH_2Cl_2.

C(31A)-C(32A)	1.3900	C(4)-C(5)	1.369(10)	C(41)-C(42)	1.360(10)
C(31A)-C(36A)	1.3900	C(5)-N(1)	1.205(9)	C(42)-C(43)	1.378(9)
C(31A)-N(6)	1.396(8)	C(5)-C(6B)	1.544(10)	C(44)-C(45)	1.375(10)
C(32A)-C(33A)	1.3900	C(5)-C(6A)	1.631(15)	C(44)-C(49)	1.408(9)
C(33A)-C(34A)	1.3900	C(5)-N(2B)	1.847(14)	C(45)-C(46)	1.351(10)
C(34A)-C(35A)	1.3900	C(7)-N(2A)	1.310(10)	C(46)-C(47)	1.391(9)
C(35A)-C(36A)	1.3900	C(7)-C(8)	1.383(12)	C(47)-C(48)	1.371(8)
N(6)-N(5)	1.503(11)	C(7)-C(12)	1.414(9)	C(48)-C(49)	1.380(8)
C(30A)-C(29)	1.539(13)	C(8)-C(9)	1.383(12)	C(86)-C(86)#1	1.541(10)
C(29)-N(5)	1.145(12)	C(8)-N(2B)	1.536(15)	S(1)-Sn(1)	2.4039(13)
C(29)-C(28)	1.499(16)	C(9)-C(10)	1.339(10)	S(1)-Sn(2)	2.4162(13)
C(28)-C(25)	1.646(14)	C(10)-C(11)	1.374(10)	S(2)-Sn(1)	2.5735(14)
C(27)-C(25)	1.451(12)	C(11)-C(12)	1.367(10)	S(2)-Sn(3)	2.5927(16)
C(32B)-C(35)	1.3900	C(13)-C(16)	1.520(8)	S(2)-Sn(2)	2.5969(14)
C(32B)-C(31)	1.3900	C(13)-C(14)	1.524(9)	S(3)-Sn(3)	2.4074(15)
C(35)-C(34)	1.3900	C(13)-C(15)	1.531(8)	S(3)-Sn(1)	2.4172(15)
C(35)-N(7)	1.430(18)	C(13)-Sn(2)	2.166(6)	S(4)-Sn(3)	2.4018(16)
C(34)-C(33)	1.3900	C(16)-C(17)	1.472(9)	S(4)-Sn(2)	2.4136(14)
C(33)-C(32)	1.3900	C(17)-N(3)	1.295(7)	Sn(1)-N(1)	2.304(5)
C(32)-C(31)	1.3900	C(17)-C(18)	1.493(8)	Sn(2)-N(3)	2.295(5)
N(7)-N(5)	1.384(17)	C(19)-C(24)	1.384(9)	Sn(3)-C(25)	2.133(7)
C(30B)-C(29B)	1.47(2)	C(19)-C(20)	1.390(8)	Sn(3)-N(5)	2.366(6)
C(29B)-C(28B)	1.58(3)	C(19)-N(4)	1.424(7)	Cl(2)-Zn(1)	2.2721(18)
C(29B)-N(5)	1.81(3)	C(20)-C(21)	1.397(10)	Cl(3)-Zn(1)	2.2367(15)
C(28B)-C(25)	1.341(17)	C(21)-C(22)	1.389(11)	Cl(4)-Zn(1)	2.2559(16)
C(27B)-C(25)	2.02(2)	C(22)-C(23)	1.368(11)	N(1)-N(2A)	1.557(9)
C(1)-C(3)	1.442(8)	C(23)-C(24)	1.399(10)	N(1)-N(2B)	1.643(14)
C(1)-C(2)	1.452(9)	C(26)-C(25)	1.480(10)	N(3)-N(4)	1.441(7)
C(1)-C(4)	1.673(9)	C(37)-Cl(6)	1.738(8)	C(32A)-C(31A)-N(6)	123.9(5)
C(1)-Sn(1)	2.185(6)	C(37)-Cl(5)	1.745(7)		
P(1)-C(38)	1.793(6)	C(38)-C(43)	1.402(8)	C(36A)-C(31A)-N(6)	116.0(5)
P(1)-C(48)	1.817(6)	C(38)-C(39)	1.402(8)		
P(1)-C(86)	1.829(5)	C(39)-C(40)	1.380(9)	C(31A)-N(6)-N(5)	118.7(6)
P(1)-Zn(1)	2.4064(15)	C(40)-C(41)	1.374(10)		

N(5)-C(29)-C(28)	118.2(11)	C(4)-C(5)-C(6A)	66.6(6)	N(4)	121.6(6)
N(5)-C(29)-C(30A)	127.8(10)	N(1)-C(5)-N(2B)	60.9(6)	C(19)-C(20)-C(21)	119.8(7)
C(28)-C(29)-C(30A)	114.0(9)	C(4)-C(5)-N(2B)	113.3(6)	C(22)-C(21)-C(20)	120.1(7)
C(29)-C(28)-C(25)	118.3(8)	C(6B)-C(5)-N(2B)	84.0(7)	C(23)-C(22)-C(21)	119.7(7)
C(34)-C(35)-N(7)	122.3(10)	N(2A)-C(7)-C(8)	120.0(7)	C(22)-C(23)-C(24)	121.0(8)
C(32B)-C(35)-N(7)	117.6(10)	N(2A)-C(7)-C(12)	120.5(8)	C(19)-C(24)-C(23)	119.5(7)
N(5)-N(7)-C(35)	93.4(10)	C(8)-C(7)-C(12)	119.4(7)	Cl(6)-C(37)-Cl(5)	112.6(4)
C(30B)-C(29B)-C(28B)	114(2)	C(9)-C(8)-C(7)	119.6(6)	C(43)-C(38)-C(39)	118.9(5)
C(30B)-C(29B)-N(5)	124(2)	C(9)-C(8)-N(2B)	145.0(9)	C(43)-C(38)-P(1)	123.1(4)
C(28B)-C(29B)-N(5)	118.2(11)	C(7)-C(8)-N(2B)	94.4(9)	C(39)-C(38)-P(1)	118.0(4)
C(25)-C(28B)-C(29B)	95.2(13)	C(10)-C(9)-C(8)	119.9(8)	C(40)-C(39)-C(38)	119.8(6)
C(3)-C(1)-C(2)	117.1(6)	C(9)-C(10)-C(11)	122.2(8)	C(41)-C(40)-C(39)	120.0(6)
C(3)-C(1)-C(4)	106.3(5)	C(12)-C(11)-C(10)	119.5(6)	C(42)-C(41)-C(40)	120.9(6)
C(2)-C(1)-C(4)	104.1(6)	C(11)-C(12)-C(7)	119.3(7)	C(41)-C(42)-C(43)	120.6(6)
C(3)-C(1)-Sn(1)	112.3(5)	C(16)-C(13)-C(14)	111.6(5)	C(42)-C(43)-C(38)	119.7(6)
C(2)-C(1)-Sn(1)	114.0(4)	C(16)-C(13)-C(15)	110.1(5)	C(45)-C(44)-C(49)	119.5(6)
C(4)-C(1)-Sn(1)	101.0(4)	C(14)-C(13)-C(15)	110.6(5)	C(46)-C(45)-C(44)	120.5(6)
C(38)-P(1)-C(48)	106.1(2)	C(16)-C(13)-Sn(2)	106.6(4)	C(45)-C(46)-C(47)	120.2(7)
C(38)-P(1)-C(86)	105.9(3)	C(14)-C(13)-Sn(2)	111.0(4)	C(48)-C(47)-C(46)	120.7(6)
C(48)-P(1)-C(86)	105.1(2)	C(15)-C(13)-Sn(2)	106.9(4)	C(47)-C(48)-C(49)	119.3(5)
C(38)-P(1)-Zn(1)	115.63(18)	C(17)-C(16)-C(13)	117.7(5)	C(47)-C(48)-P(1)	118.5(4)
C(48)-P(1)-Zn(1)	112.24(17)	N(3)-C(17)-C(16)	115.7(5)	C(49)-C(48)-P(1)	122.1(5)
C(86)-P(1)-Zn(1)	111.20(18)	N(3)-C(17)-C(18)	123.7(6)	C(48)-C(49)-C(44)	119.7(6)
C(5)-C(4)-C(1)	114.0(5)	C(16)-C(17)-C(18)	120.6(5)		
N(1)-C(5)-C(4)	116.9(7)	C(24)-C(19)-C(20)	120.0(6)		
N(1)-C(5)-C(6B)	120.0(8)	C(24)-C(19)-N(4)	118.4(5)		
C(4)-C(5)-C(6B)	121.6(6)	C(20)-C(19)-			
N(1)-C(5)-C(6A)	171.4(9)				

C(86)#1-C(86)-P(1)	110.7(5)	S(1)-Sn(2)-S(2)	88.26(5)	N(1)-N(2B)-C(5)	39.9(4)
Sn(1)-S(1)-Sn(2)	91.55(4)	C(25)-Sn(3)-N(5)	79.5(4)	C(17)-N(3)-N(4)	118.4(5)
Sn(1)-S(2)-Sn(3)	83.46(4)	C(25)-Sn(3)-S(4)	121.16(19)	C(17)-N(3)-Sn(2)	114.2(4)
Sn(1)-S(2)-Sn(2)	83.84(4)	N(5)-Sn(3)-S(4)	84.3(2)	N(4)-N(3)-Sn(2)	127.1(3)
Sn(3)-S(2)-Sn(2)	83.48(5)	C(25)-Sn(3)-S(3)	125.7(2)	C(19)-N(4)-N(3)	113.2(4)
Sn(3)-S(3)-Sn(1)	90.91(5)	N(5)-Sn(3)-S(3)	89.51(16)	C(29)-N(5)-N(6)	120.2(8)
Sn(3)-S(4)-Sn(2)	91.70(5)	S(4)-Sn(3)-S(3)	110.12(7)	N(7)-N(5)-C(29B)	81.9(11)
C(1)-Sn(1)-N(1)	75.8(2)	C(25)-Sn(3)-S(2)	103.8(3)	C(29)-N(5)-Sn(3)	115.6(9)
C(1)-Sn(1)-S(1)	121.09(17)	N(5)-Sn(3)-S(2)	175.5(2)	N(7)-N(5)-Sn(3)	135.3(7)
N(1)-Sn(1)-S(1)	86.75(14)	S(4)-Sn(3)-S(2)	91.29(5)	N(6)-N(5)-Sn(3)	123.9(5)
C(1)-Sn(1)-S(3)	117.32(16)	S(3)-Sn(3)-S(2)	90.90(5)	C(29B)-N(5)-Sn(3)	94.7(8)
N(1)-Sn(1)-S(3)	87.4(2)	Cl(3)-Zn(1)-Cl(4)	113.03(6)	C(28B)-C(25)-C(26)	130.0(10)
S(1)-Sn(1)-S(3)	117.50(7)	Cl(3)-Zn(1)-Cl(2)	112.17(6)	C(27)-C(25)-C(26)	117.9(9)
C(1)-Sn(1)-S(2)	109.67(17)	Cl(4)-Zn(1)-Cl(2)	112.58(7)	C(27)-C(25)-C(28)	108.6(8)
N(1)-Sn(1)-S(2)	174.33(14)	Cl(3)-Zn(1)-P(1)	109.38(5)	C(26)-C(25)-C(28)	104.6(8)
S(1)-Sn(1)-S(2)	89.07(4)	Cl(4)-Zn(1)-P(1)	104.27(5)	C(28B)-C(25)-C(27B)	93.0(12)
S(3)-Sn(1)-S(2)	91.15(5)	Cl(2)-Zn(1)-P(1)	104.72(6)	C(26)-C(25)-C(27B)	81.1(9)
C(13)-Sn(2)-N(3)	77.9(2)	C(5)-N(1)-N(2A)	124.1(6)	C(28B)-C(25)-Sn(3)	117.1(9)
C(13)-Sn(2)-S(4)	120.54(18)	C(5)-N(1)-N(2B)	79.2(7)	C(27)-C(25)-Sn(3)	108.1(5)
N(3)-Sn(2)-S(4)	93.17(12)	C(5)-N(1)-Sn(1)	116.7(6)	C(26)-C(25)-Sn(3)	112.7(5)
C(13)-Sn(2)-S(1)	121.75(19)	N(2A)-N(1)-Sn(1)	118.1(4)	C(28)-C(25)-Sn(3)	103.9(6)
N(3)-Sn(2)-S(1)	84.16(11)	N(2B)-N(1)-Sn(1)	116.2(6)	C(27B)-C(25)-Sn(3)	101.6(7)
S(4)-Sn(2)-S(1)	115.34(5)	C(7)-N(2A)-N(1)	117.5(6)		
C(13)-Sn(2)-S(2)	105.50(16)	C(8)-N(2B)-N(1)	118.4(9)		
N(3)-Sn(2)-S(2)	172.36(11)	C(8)-N(2B)-C(5)	144.8(11)		
S(4)-Sn(2)-S(2)	90.92(5)				

Symmetry transformations used to generate equivalent atoms:

#1 -x+2,-y+1,-z+2

6) Single-crystal X-ray Crystallography of Compound 3

Compound **3** crystallizes as colorless blocks. Data of the X-Ray diffraction analyses were collected on a STOE IPDS2T imaging plate diffractometer using $Mo_{K\alpha}$ radiation with graphite monochromatization. (λ = 0.71073 Å) at 100 K. Reflection data were processed with X-Area 1.77.[1] Structure solution was performed by direct methods and full-matrix-least-squares refinement against F^2 using SHELXT[2] and SHELXL-2014.[3] All non-hydrogen atoms were refined anisotropically, hydrogen atom positions were calculated. **3** crystallizes with 5 molecules dichloromethane and two molecules hexane per unit cell (2.5 CH_2Cl_2 and 1 hexane per formula unit). Two of the dichloromethane molecules and the hexane molecules could not be refined due to their disorder and were removed with the SQUEEZE routine. The void containing the hexane molecules is located at 0.0, 0.0 0.5, has a volume of 294 $Å^3$ and contains 96 electrons. The voids containing the two disordered dichloromethane molecules are located at 0.286, 0.349, 0.549 (147 $Å^3$, 42 electrons) and 0.714, 0.651, 0.451 (146 $Å^3$, 42 electrons).

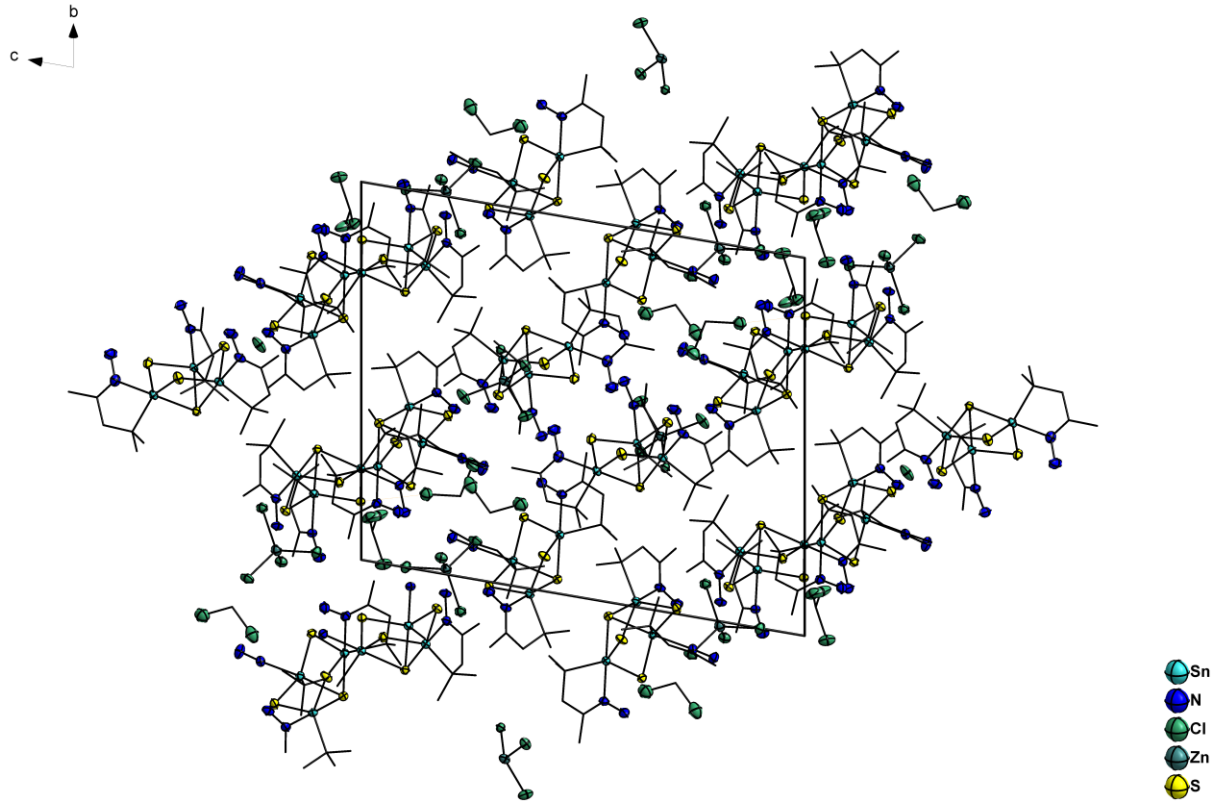

Figure S30. Crystal structure of **3**·3.5CH_2Cl_2·hexane along the *a* axis.

Table S7. Crystal data and structure refinement for **3**·3.5CH_2Cl_2·hexane.

Empirical formula	$C_{75}H_{136}Cl_{14}N_{24}S_{16}Sn_{12}Zn_2$	
CCDC number	1914531	
Formula weight	3938.62	
Temperature	100(2) K	
Wavelength	0.71073 Å	
Crystal system	Triclinic	
Space group	$P\bar{1}$	
Unit cell dimensions	a = 17.4428(2) Å	α = 76.5010(10)°.
	b = 20.6365(3) Å	β = 77.6320(10)°.
	c = 23.2995(3) Å	γ = 67.9930(10)°.
Volume	7485.89(18) $Å^3$	
Z	2	
Density (calculated)	1.826 Mg/m^3	
Absorption coefficient	2.864 mm^{-1}	
F(000)	3992	
Crystal size	0.1 x 0.1 x 0.1 mm^3	
Theta range for data collection	1.419 to 26.776°.	
Index ranges	-22<=h<=22, -26<=k<=26, -28<=l<=29	
Reflections collected	105251	
Independent reflections	31683 [R(int) = 0.0359]	
Completeness to theta = 25.242°	99.9 %	
Absorption correction	Sphere	
Max. and min. transmission	0.4284 and 0.0923	
Refinement method	Full-matrix least-squares on F^2	
Data / restraints / parameters	31683 / 0 / 1336	
Goodness-of-fit on F^2	1.025	
Final R indices [I>2sigma(I)]	R1 = 0.0326, wR2 = 0.1151	
R indices (all data)	R1 = 0.0358, wR2 = 0.1188	
Largest diff. peak and hole	2.006 and -1.618 e.$Å^{-3}$	

Table S8. Atomic coordinates (x 10^4) and equivalent isotropic displacement parameters ($Å^2$x 10^3) for **3**·3.5CH_2Cl_2·hexane. U(eq) is defined as one third of the trace of the orthogonalized U^{ij} tensor.

	x	y	z	U(eq)
Sn(1)	8638(1)	4267(1)	8911(1)	23(1)
C(1)	7539(2)	9188(2)	251(2)	35(1)
N(1)	7621(2)	4766(2)	8299(1)	24(1)
Cl(1)	6261(1)	5878(1)	6300(1)	26(1)
Zn(1)	5278(1)	5380(1)	6770(1)	24(1)
S(1)	8186(1)	3254(1)	9211(1)	28(1)
Sn(2)	9461(1)	2548(1)	9625(1)	20(1)
N(2)	7503(2)	4413(2)	7899(1)	29(1)
Cl(2)	5573(1)	4778(1)	7694(1)	40(1)
Zn(2)	688(1)	9865(1)	1916(1)	25(1)
S(2)	10664(1)	2175(1)	8884(1)	22(1)
Sn(3)	10734(1)	3358(1)	8621(1)	20(1)
N(3)	9163(2)	1562(2)	9650(1)	23(1)
Cl(3)	5244(1)	4533(1)	6295(1)	36(1)
S(3)	9773(1)	3695(1)	9598(1)	23(1)
Sn(4)	91(1)	5676(1)	6228(1)	19(1)
N(4)	8909(2)	1440(2)	9171(1)	34(1)
Cl(4)	3967(1)	6189(1)	6856(1)	23(1)
S(4)	9675(1)	4205(1)	8042(1)	26(1)
Sn(5)	1348(1)	6581(1)	5316(1)	20(1)
N(5)	11542(2)	3143(2)	7728(1)	24(1)
Cl(5)	-413(1)	9583(1)	1805(1)	29(1)
S(5)	1077(1)	4976(1)	6909(1)	23(1)
Sn(6)	1598(1)	5936(1)	6797(1)	19(1)
N(6)	11304(2)	2978(2)	7257(1)	36(1)
Cl(6)	1466(1)	9992(1)	1007(1)	32(1)
S(6)	718(1)	5764(1)	5190(1)	25(1)
Sn(9)	4249(1)	8437(1)	4478(1)	19(1)
N(9)	2247(2)	6371(2)	4451(1)	27(1)
Cl(9)	506(1)	7529(1)	2464(1)	56(1)
S(9)	2911(1)	9076(1)	4128(1)	25(1)
Sn(8)	5377(1)	9343(1)	3427(1)	18(1)
N(8)	499(2)	4087(2)	5928(2)	34(1)
Cl(8)	1471(1)	8985(1)	2573(1)	34(1)
S(8)	2511(1)	6021(1)	5874(1)	27(1)
Sn(7)	3264(1)	10142(1)	3794(1)	20(1)
N(7)	-125(2)	4676(2)	6148(1)	24(1)

Cl(7)	200(1)	10919(1)	2238(1)	28(1)
S(7)	319(1)	6821(1)	6283(1)	19(1)
S(00K)	4241(1)	10136(1)	2886(1)	23(1)
Sn(10)	4488(1)	11534(1)	1065(1)	19(1)
N(10)	2757(2)	5695(2)	4348(2)	43(1)
Cl(10)	-590(1)	7808(1)	3589(1)	53(1)
S(10)	5375(1)	8140(1)	3668(1)	22(1)
Sn(11)	5660(1)	12408(1)	5(1)	19(1)
N(11)	2700(2)	5209(2)	7263(1)	24(1)
Sn(12)	6038(1)	11939(1)	1456(1)	18(1)
N(12)	3313(2)	4609(2)	7058(2)	37(1)
S(12)	4465(1)	9629(1)	4425(1)	20(1)
S(13)	4689(1)	12724(1)	988(1)	20(1)
N(13)	2144(2)	10615(1)	3261(1)	22(1)
S(15)	5545(1)	10947(1)	1712(1)	22(1)
Cl(15)	6782(8)	8845(6)	187(5)	43(2)
Cl(20)	6794(6)	8761(6)	365(11)	66(3)
N(15)	6183(2)	9139(2)	2523(1)	24(1)
S(14)	5030(1)	11534(1)	17(1)	22(1)
N(14)	1986(2)	10269(2)	2880(1)	27(1)
S(16)	6892(1)	11949(1)	496(1)	22(1)
Cl(16)	7040(1)	10018(1)	503(1)	42(1)
N(16)	5920(2)	9004(2)	2049(1)	33(1)
N(17)	4131(2)	7360(1)	4523(1)	23(1)
Cl(17)	5207(1)	7972(1)	1464(1)	44(1)
Cl(18)	4854(1)	6981(1)	2512(1)	62(1)
N(18)	3916(2)	7143(2)	4069(1)	33(1)
N(19)	4302(2)	10482(1)	1110(1)	22(1)
C(020)	4370(2)	6923(2)	4988(2)	26(1)
N(20)	4943(2)	9872(2)	943(1)	30(1)
C(022)	9469(2)	2109(2)	10564(1)	26(1)
N(22)	6907(2)	11449(2)	-987(1)	34(1)
N(21)	6484(2)	12136(2)	-861(1)	23(1)
C(023)	3596(2)	10454(2)	1389(2)	24(1)
N(23)	7167(2)	11230(1)	1925(1)	23(1)
C(024)	6010(2)	12601(2)	2063(1)	21(1)
N(24)	7588(2)	10508(2)	1896(1)	26(1)
C(025)	6478(2)	9561(2)	3488(1)	22(1)
C(026)	5828(2)	13367(2)	1731(2)	27(1)
C(027)	2038(2)	11623(2)	3649(2)	26(1)
C(028)	6957(2)	9044(2)	2516(2)	25(1)

C(029)	5376(2)	13446(2)	-540(2)	24(1)
C(02A)	1991(2)	10934(2)	4688(2)	33(1)
C(02B)	1392(2)	6481(2)	7539(2)	25(1)
C(02C)	6549(2)	12676(2)	-1238(1)	25(1)
C(02D)	9175(2)	1162(2)	10157(2)	25(1)
C(02E)	7350(2)	11531(2)	2279(1)	22(1)
C(02F)	4362(2)	7982(2)	5409(1)	24(1)
C(02G)	3169(2)	11796(2)	1435(2)	23(1)
C(02H)	6860(2)	12308(2)	2274(2)	24(1)
C(02I)	4585(3)	7179(2)	5459(2)	32(1)
C(02J)	2555(2)	11120(2)	4134(2)	25(1)
C(02K)	1076(2)	11724(2)	2907(2)	30(1)
C(02L)	1760(2)	11277(2)	3267(2)	26(1)
C(02N)	5327(2)	12538(2)	2581(2)	28(1)
C(02O)	-1252(2)	5975(2)	6481(2)	26(1)
C(02P)	-1451(2)	5284(2)	6666(2)	28(1)
C(02Q)	11827(2)	3573(2)	8714(2)	27(1)
C(02R)	2140(2)	6904(2)	4040(1)	25(1)
C(02S)	6274(2)	10355(2)	3287(2)	29(1)
C(02T)	2963(2)	11109(2)	1600(2)	31(1)
C(02U)	6615(2)	5888(2)	7889(2)	31(1)
C(02V)	-852(2)	4661(2)	6383(2)	25(1)
C(02W)	1194(2)	7652(2)	4837(2)	28(1)
C(02X)	3129(2)	11454(2)	4270(2)	31(1)
C(02Y)	7238(2)	5432(2)	8292(2)	28(1)
C(02Z)	8948(2)	510(2)	10287(2)	28(1)
C(030)	2078(2)	6046(2)	7936(2)	33(1)
C(031)	1501(3)	7607(2)	4185(2)	38(1)
C(032)	5045(2)	8142(2)	5606(2)	33(1)
C(033)	2736(2)	5385(2)	7740(2)	26(1)
C(034)	7190(2)	9140(2)	3066(2)	28(1)
C(035)	3025(3)	12132(2)	1975(2)	36(1)
C(036)	12273(2)	3162(2)	7684(2)	29(1)
C(037)	4463(3)	6153(2)	5082(2)	36(1)
C(038)	4552(2)	13628(2)	-757(2)	38(1)
C(039)	2660(2)	12321(2)	966(2)	36(1)
C(03A)	8034(2)	11160(2)	2653(2)	29(1)
C(03B)	11549(3)	4382(2)	8643(2)	40(1)
C(03C)	1434(3)	7216(2)	7280(2)	34(1)
C(03D)	3389(3)	9788(2)	1543(2)	38(1)
C(03E)	536(2)	6523(2)	7889(2)	36(1)

C(03F)	3402(2)	4983(2)	8128(2)	31(1)
C(03G)	6680(2)	9338(2)	4122(2)	34(1)
C(03H)	7488(3)	5767(2)	8705(2)	37(1)
C(03I)	-1148(3)	4056(2)	6434(2)	37(1)
C(03J)	-1647(2)	6419(2)	5934(2)	38(1)
C(03K)	9428(3)	1360(2)	10649(2)	35(1)
C(03L)	8687(3)	2598(2)	10895(2)	41(1)
C(03M)	7091(3)	12630(2)	-1822(2)	42(1)
C(03N)	5321(3)	14004(2)	-177(2)	39(1)
C(03O)	10252(3)	2101(2)	10757(2)	38(1)
C(03P)	-1529(2)	6385(2)	6996(2)	36(1)
C(03Q)	6083(2)	13397(2)	-1063(2)	34(1)
C(03R)	7917(3)	5259(2)	9218(2)	45(1)
C(03S)	2569(2)	6882(2)	3404(2)	35(1)
C(03T)	3512(3)	8307(2)	5760(2)	38(1)
C(03U)	12899(3)	3052(2)	7139(2)	43(1)
C(03V)	12514(2)	3288(3)	8225(2)	43(1)
C(03W)	294(3)	8144(2)	4938(2)	41(1)
C(03X)	1756(3)	7895(2)	5091(2)	40(1)
C(03Y)	12075(3)	3236(3)	9327(2)	46(1)
C(03Z)	7624(3)	8812(2)	2011(2)	37(1)
C(040)	8493(5)	5564(3)	9402(3)	94(3)
C(043)	4804(5)	7866(3)	2235(2)	77(2)
C(045)	7299(4)	5107(3)	9757(2)	100(3)
C(046)	-126(4)	8169(3)	2911(2)	64(2)

Table S9. Bond lengths [Å] and angles [°] for **3**·3.5CH_2Cl_2·hexane.

Sn(1)-C(03R)	2.157(4)	Sn(5)-S(6)	2.4291(8)	Sn(11)-S(14)	2.4287(8)
Sn(1)-N(1)	2.296(3)	Sn(5)-S(7)	2.5812(8)	Sn(11)-S(13)	2.5974(8)
Sn(1)-S(4)	2.4006(9)	N(5)-C(036)	1.272(5)	N(11)-C(033)	1.266(5)
Sn(1)-S(1)	2.4087(9)	N(5)-N(6)	1.403(4)	N(11)-N(12)	1.404(4)
Sn(1)-S(3)	2.5687(9)	S(5)-Sn(6)	2.4138(8)	Sn(12)-C(024)	2.165(3)
C(1)-Cl(15)	1.761(13)	Sn(6)-C(02B)	2.172(3)	Sn(12)-N(23)	2.288(3)
C(1)-Cl(20)	1.771(8)	Sn(6)-N(11)	2.258(3)	Sn(12)-S(16)	2.4073(8)
C(1)-Cl(16)	1.782(4)	Sn(6)-S(8)	2.4006(9)	Sn(12)-S(15)	2.4121(8)
N(1)-C(02Y)	1.280(5)	Sn(6)-S(7)	2.6107(8)	Sn(12)-S(13)	2.6015(8)
N(1)-N(2)	1.397(4)	Sn(9)-C(02F)	2.174(3)	N(13)-C(02L)	1.279(4)
Cl(1)-Zn(1)	2.2766(9)	Sn(9)-N(17)	2.283(3)	N(13)-N(14)	1.386(4)
Zn(1)-Cl(4)	2.2696(9)	Sn(9)-S(10)	2.4175(8)	N(15)-C(028)	1.287(5)
Zn(1)-Cl(2)	2.2798(10)	Sn(9)-S(9)	2.4202(9)	N(15)-N(16)	1.402(4)
Zn(1)-Cl(3)	2.2998(9)	Sn(9)-S(12)	2.5974(8)	N(17)-C(020)	1.272(4)
S(1)-Sn(2)	2.4150(9)	N(9)-C(02R)	1.262(5)	N(17)-N(18)	1.405(4)
Sn(2)-C(022)	2.163(3)	N(9)-N(10)	1.390(4)	Cl(17)-C(043)	1.777(5)
Sn(2)-N(3)	2.266(3)	Cl(9)-C(046)	1.761(6)	Cl(18)-C(043)	1.764(5)
Sn(2)-S(2)	2.4168(8)	S(9)-Sn(7)	2.4168(8)	N(19)-C(023)	1.279(4)
Sn(2)-S(3)	2.6035(9)	Sn(8)-C(025)	2.170(3)	N(19)-N(20)	1.405(4)
Zn(2)-Cl(7)	2.2617(9)	Sn(8)-N(15)	2.302(3)	C(020)-C(02I)	1.491(5)
Zn(2)-Cl(6)	2.2740(9)	Sn(8)-S(10)	2.4148(8)	C(020)-C(037)	1.503(5)
Zn(2)-Cl(5)	2.2831(9)	Sn(8)-S(00K)	2.4223(8)	C(022)-C(03O)	1.520(5)
Zn(2)-Cl(8)	2.2889(9)	Sn(8)-S(12)	2.5746(8)	C(022)-C(03L)	1.534(5)
S(2)-Sn(3)	2.4177(8)	N(8)-N(7)	1.409(4)	C(022)-C(03K)	1.539(5)
Sn(3)-C(02Q)	2.177(3)	Sn(7)-C(02J)	2.164(3)	N(22)-N(21)	1.400(4)
Sn(3)-N(5)	2.286(3)	Sn(7)-N(13)	2.314(3)	N(21)-C(02C)	1.272(4)
Sn(3)-S(4)	2.4145(9)	Sn(7)-S(00K)	2.4141(8)	C(023)-C(03D)	1.495(5)
Sn(3)-S(3)	2.5896(8)	Sn(7)-S(12)	2.5694(8)	C(023)-C(02T)	1.499(5)
N(3)-C(02D)	1.273(4)	N(7)-C(02V)	1.278(5)	N(23)-C(02E)	1.289(4)
N(3)-N(4)	1.391(4)	Sn(10)-C(02G)	2.182(3)	N(23)-N(24)	1.405(4)
Sn(4)-C(02O)	2.171(3)	Sn(10)-N(19)	2.287(3)	C(024)-C(02H)	1.521(5)
Sn(4)-N(7)	2.287(3)	Sn(10)-S(15)	2.4095(8)	C(024)-C(02N)	1.523(5)
Sn(4)-S(5)	2.4091(8)	Sn(10)-S(14)	2.4207(8)	C(024)-C(026)	1.534(4)
Sn(4)-S(6)	2.4253(8)	Sn(10)-S(13)	2.5687(8)	C(025)-C(03G)	1.517(4)
Sn(4)-S(7)	2.5725(8)	Cl(10)-C(046)	1.747(5)	C(025)-C(02S)	1.520(5)
Sn(5)-C(02W)	2.175(3)	Sn(11)-C(029)	2.158(3)	C(025)-C(034)	1.526(5)
Sn(5)-N(9)	2.291(3)	Sn(11)-N(21)	2.266(3)	C(027)-C(02L)	1.509(5)
Sn(5)-S(8)	2.4106(9)	Sn(11)-S(16)	2.4179(8)	C(027)-C(02J)	1.534(5)

C(028)-C(03Z)	1.491(5)	C(030)-C(033)	1.510(5)	Cl(3)	112.95(4)
C(028)-C(034)	1.500(5)	C(033)-C(03F)	1.493(5)	Cl(2)-Zn(1)-Cl(3)	103.86(4)
C(029)-C(038)	1.509(5)	C(036)-C(03U)	1.488(5)	Sn(1)-S(1)-Sn(2)	91.16(3)
C(029)-C(03Q)	1.529(5)	C(036)-C(03V)	1.514(5)	C(022)-Sn(2)-N(3)	80.21(12)
C(029)-C(03N)	1.545(5)	C(03H)-C(03R)	1.516(6)	C(022)-Sn(2)-S(1)	122.32(10)
C(02A)-C(02J)	1.514(5)	C(03R)-C(045)	1.527(8)	N(3)-Sn(2)-S(1)	88.88(8)
C(02B)-C(03C)	1.519(5)	C(03R)-C(040)	1.540(8)	C(022)-Sn(2)-S(2)	122.62(10)
C(02B)-C(03E)	1.521(5)	C(03R)-Sn(1)-N(1)	77.45(14)	N(3)-Sn(2)-S(2)	90.47(7)
C(02B)-C(030)	1.541(5)	C(03R)-Sn(1)-S(4)	121.44(14)	S(1)-Sn(2)-S(2)	113.84(3)
C(02C)-C(03M)	1.482(5)	N(1)-Sn(1)-S(4)	88.96(7)	C(022)-Sn(2)-S(3)	99.93(10)
C(02C)-C(03Q)	1.509(5)	C(03R)-Sn(1)-S(1)	121.74(14)	N(3)-Sn(2)-S(3)	178.89(8)
C(02D)-C(02Z)	1.490(5)	N(1)-Sn(1)-S(1)	88.22(8)	S(1)-Sn(2)-S(3)	90.12(3)
C(02D)-C(03K)	1.498(5)	S(4)-Sn(1)-S(1)	114.26(3)	S(2)-Sn(2)-S(3)	90.37(3)
C(02E)-C(03A)	1.490(5)	C(03R)-Sn(1)-S(3)	103.03(12)	Cl(7)-Zn(2)-Cl(6)	107.80(4)
C(02E)-C(02H)	1.508(5)	N(1)-Sn(1)-S(3)	179.31(8)	Cl(7)-Zn(2)-Cl(5)	109.20(3)
C(02F)-C(03T)	1.519(5)	S(4)-Sn(1)-S(3)	91.21(3)	Cl(6)-Zn(2)-Cl(5)	108.28(4)
C(02F)-C(032)	1.528(5)	S(1)-Sn(1)-S(3)	91.10(3)	Cl(7)-Zn(2)-Cl(8)	111.23(4)
C(02F)-C(02I)	1.535(5)	Cl(15)-C(1)-Cl(16)	109.8(4)	Cl(6)-Zn(2)-Cl(8)	110.62(4)
C(02G)-C(035)	1.507(5)	Cl(20)-C(1)-Cl(16)	108.4(3)	Cl(5)-Zn(2)-Cl(8)	109.63(4)
C(02G)-C(039)	1.515(5)	C(02Y)-N(1)-N(2)	121.5(3)	Sn(2)-S(2)-Sn(3)	91.19(3)
C(02G)-C(02T)	1.534(5)	C(02Y)-N(1)-Sn(1)	114.1(2)	C(02Q)-Sn(3)-N(5)	79.19(12)
C(02J)-C(02X)	1.527(5)	N(2)-N(1)-Sn(1)	123.8(2)	C(02Q)-Sn(3)-S(4)	121.99(10)
C(02K)-C(02L)	1.489(5)	Cl(4)-Zn(1)-Cl(1)	112.83(3)	N(5)-Sn(3)-S(4)	86.23(8)
C(02O)-C(03J)	1.516(5)	Cl(4)-Zn(1)-Cl(2)	108.95(4)	C(02Q)-Sn(3)-S(2)	121.65(10)
C(02O)-C(03P)	1.520(5)	Cl(1)-Zn(1)-Cl(2)	110.84(4)	N(5)-Sn(3)-S(2)	92.77(7)
C(02O)-C(02P)	1.535(5)	Cl(4)-Zn(1)-Cl(3)	106.93(3)		
C(02P)-C(02V)	1.508(5)	Cl(1)-Zn(1)-			
C(02Q)-C(03Y)	1.511(5)				
C(02Q)-C(03V)	1.511(5)				
C(02Q)-C(03B)	1.533(5)				
C(02R)-C(03S)	1.514(4)				
C(02R)-C(031)	1.520(5)				
C(02U)-C(02Y)	1.486(5)				
C(02V)-C(03I)	1.492(5)				
C(02W)-C(031)	1.511(5)				
C(02W)-C(03W)	1.520(5)				
C(02W)-C(03X)	1.522(5)				
C(02Y)-C(03H)	1.520(5)				

S(4)-Sn(3)-S(2) 114.83(3)
C(02Q)-Sn(3)-S(3) 100.78(10)
N(5)-Sn(3)-S(3) 175.95(8)
S(4)-Sn(3)-S(3) 90.39(3)
S(2)-Sn(3)-S(3) 90.69(3)
C(02D)-N(3)-N(4) 122.7(3)
C(02D)-N(3)-Sn(2) 114.1(2)
N(4)-N(3)-Sn(2) 122.9(2)
Sn(1)-S(3)-Sn(3) 83.22(2)
Sn(1)-S(3)-Sn(2) 83.53(3)
Sn(3)-S(3)-Sn(2) 83.37(2)
C(02O)-Sn(4)-N(7) 78.82(12)
C(02O)-Sn(4)-S(5) 123.29(10)
N(7)-Sn(4)-S(5) 89.84(8)
C(02O)-Sn(4)-S(6) 121.49(10)
N(7)-Sn(4)-S(6) 88.92(7)
S(5)-Sn(4)-S(6) 113.50(3)
C(02O)-Sn(4)-S(7) 100.88(9)
N(7)-Sn(4)-S(7) 178.06(7)
S(5)-Sn(4)-S(7) 91.91(3)
S(6)-Sn(4)-S(7) 89.62(3)
Sn(1)-S(4)-Sn(3) 90.70(3)
C(02W)-Sn(5)-N(9) 78.10(12)
C(02W)-Sn(5)-S(8) 116.55(10)
N(9)-Sn(5)-S(8) 89.69(8)
C(02W)-Sn(5)-S(6) 128.32(10)
N(9)-Sn(5)-S(6) 90.19(8)
S(8)-Sn(5)-S(6) 113.47(3)
C(02W)-Sn(5)-S(7) 101.75(9)
N(9)-Sn(5)-S(7) 179.25(8)
S(8)-Sn(5)-S(7) 91.03(3)
S(6)-Sn(5)-S(7) 89.33(3)
C(036)-N(5)-N(6) 120.1(3)
C(036)-N(5)-Sn(3) 114.2(2)
N(6)-N(5)-Sn(3) 125.7(2)
Sn(4)-S(5)-Sn(6) 91.01(3)
C(02B)-Sn(6)-N(11) 80.37(12)
C(02B)-Sn(6)-S(8) 127.68(10)
N(11)-Sn(6)-S(8) 90.24(8)
C(02B)-Sn(6)-S(5) 120.41(10)
N(11)-Sn(6)-S(5) 91.10(7)
S(8)-Sn(6)-S(5) 111.05(3)
C(02B)-Sn(6)-S(7) 97.24(9)
N(11)-Sn(6)-S(7) 177.46(8)
S(8)-Sn(6)-S(7) 90.54(3)
S(5)-Sn(6)-S(7) 90.87(3)
Sn(4)-S(6)-Sn(5) 91.19(3)
C(02F)-Sn(9)-N(17) 79.12(12)
C(02F)-Sn(9)-S(10) 123.93(9)
N(17)-Sn(9)-S(10) 87.29(7)
C(02F)-Sn(9)-S(9) 122.46(9)
N(17)-Sn(9)-S(9) 92.63(8)
S(10)-Sn(9)-S(9) 112.19(3)
C(02F)-Sn(9)-S(12) 100.28(9)
N(17)-Sn(9)-S(12) 177.08(8)
S(10)-Sn(9)-S(12) 90.72(3)
S(9)-Sn(9)-S(12) 90.10(3)
C(02R)-N(9)-N(10) 122.0(3)
C(02R)-N(9)-Sn(5) 114.0(2)
N(10)-N(9)-Sn(5) 123.0(2)
Sn(7)-S(9)-Sn(9) 91.00(3)
C(025)-Sn(8)-N(15) 77.38(11)
C(025)-Sn(8)-S(10) 120.06(9)
N(15)-Sn(8)-S(10) 91.15(7)
C(025)-Sn(8)-S(00K) 125.59(9)
N(15)-Sn(8)-S(00K) 88.05(8)
S(10)-Sn(8)-S(00K) 112.25(3)
C(025)-Sn(8)-S(12) 101.69(9)
N(15)-Sn(8)-S(12) 177.49(7)
S(10)-Sn(8)-S(12) 91.33(3)
S(00K)-Sn(8)-S(12) 90.64(3)
Sn(6)-S(8)-Sn(5) 91.79(3)
C(02J)-Sn(7)-N(13) 77.75(11)
C(02J)-Sn(7)-S(00K) 120.66(9)
N(13)-Sn(7)-S(00K) 91.34(7)
C(02J)-Sn(7)-

S(9)	123.16(9)	S(14)-Sn(10)-S(13)	89.79(3)	S(15)	87.55(7)
N(13)-Sn(7)-S(9)	88.67(7)	Sn(8)-S(10)-Sn(9)	91.15(3)	S(16)-Sn(12)-S(15)	111.53(3)
S(00K)-Sn(7)-S(9)	114.50(3)	C(029)-Sn(11)-N(21)	79.52(12)	C(024)-Sn(12)-S(13)	99.84(9)
C(02J)-Sn(7)-S(12)	100.62(9)	C(029)-Sn(11)-S(16)	118.61(9)	N(23)-Sn(12)-S(13)	176.12(7)
N(13)-Sn(7)-S(12)	177.65(7)	N(21)-Sn(11)-S(16)	89.29(8)	S(16)-Sn(12)-S(13)	92.01(3)
S(00K)-Sn(7)-S(12)	90.96(3)	C(029)-Sn(11)-S(14)	125.69(9)	S(15)-Sn(12)-S(13)	90.09(3)
S(9)-Sn(7)-S(12)	90.84(3)	N(21)-Sn(11)-S(14)	90.39(7)	Sn(7)-S(12)-Sn(8)	83.72(2)
C(02V)-N(7)-N(8)	121.6(3)	S(16)-Sn(11)-S(14)	114.40(3)	Sn(7)-S(12)-Sn(9)	83.78(2)
C(02V)-N(7)-Sn(4)	113.5(2)	C(029)-Sn(11)-S(13)	100.09(9)	Sn(8)-S(12)-Sn(9)	83.71(2)
N(8)-N(7)-Sn(4)	124.4(2)	N(21)-Sn(11)-S(13)	178.82(7)	Sn(10)-S(13)-Sn(11)	84.42(2)
Sn(4)-S(7)-Sn(5)	84.59(2)	S(16)-Sn(11)-S(13)	91.87(3)	Sn(10)-S(13)-Sn(12)	83.92(2)
Sn(4)-S(7)-Sn(6)	83.17(2)	S(14)-Sn(11)-S(13)	88.94(3)	Sn(11)-S(13)-Sn(12)	82.49(2)
Sn(5)-S(7)-Sn(6)	83.43(2)	C(033)-N(11)-N(12)	120.7(3)	C(02L)-N(13)-N(14)	121.5(3)
Sn(7)-S(00K)-Sn(8)	90.43(3)	C(033)-N(11)-Sn(6)	114.5(2)	C(02L)-N(13)-Sn(7)	113.0(2)
C(02G)-Sn(10)-N(19)	79.28(11)	N(12)-N(11)-Sn(6)	124.8(2)	N(14)-N(13)-Sn(7)	124.5(2)
C(02G)-Sn(10)-S(15)	120.05(9)	C(024)-Sn(12)-N(23)	79.12(11)	Sn(10)-S(15)-Sn(12)	91.61(3)
N(19)-Sn(10)-S(15)	90.20(7)	C(024)-Sn(12)-S(16)	120.88(9)	C(028)-N(15)-N(16)	120.7(3)
C(02G)-Sn(10)-S(14)	124.88(9)	N(23)-Sn(12)-S(16)	91.72(7)	C(028)-N(15)-Sn(8)	113.5(2)
N(19)-Sn(10)-S(14)	89.07(7)	C(024)-Sn(12)-S(15)	125.98(9)	N(16)-N(15)-Sn(8)	124.9(2)
S(15)-Sn(10)-S(14)	113.59(3)	N(23)-Sn(12)-		Sn(10)-S(14)-Sn(11)	91.40(3)
C(02G)-Sn(10)-S(13)	100.79(9)				
N(19)-Sn(10)-S(13)	178.64(7)				
S(15)-Sn(10)-S(13)	90.94(3)				

Sn(12)-S(16)-Sn(11)	90.52(3)	C(03D)	123.0(3)	N(15)-C(028)-C(034)	116.7(3)
C(020)-N(17)-N(18)	120.7(3)	N(19)-C(023)-C(02T)	118.6(3)	C(03Z)-C(028)-C(034)	119.4(3)
C(020)-N(17)-Sn(9)	112.9(2)	C(03D)-C(023)-C(02T)	118.4(3)	C(038)-C(029)-C(03Q)	110.7(3)
N(18)-N(17)-Sn(9)	126.0(2)	C(02E)-N(23)-N(24)	120.8(3)	C(038)-C(029)-C(03N)	110.1(3)
C(023)-N(19)-N(20)	121.1(3)	C(02E)-N(23)-Sn(12)	114.0(2)	C(03Q)-C(029)-C(03N)	110.6(3)
C(023)-N(19)-Sn(10)	114.1(2)	N(24)-N(23)-Sn(12)	124.8(2)	C(038)-C(029)-Sn(11)	108.1(2)
N(20)-N(19)-Sn(10)	123.9(2)	C(02H)-C(024)-C(02N)	110.7(3)	C(03Q)-C(029)-Sn(11)	106.6(2)
N(17)-C(020)-C(02I)	118.8(3)	C(02H)-C(024)-C(026)	111.2(3)	C(03N)-C(029)-Sn(11)	110.5(2)
N(17)-C(020)-C(037)	123.1(3)	C(02N)-C(024)-C(026)	111.8(3)	C(03C)-C(02B)-C(03E)	111.1(3)
C(02I)-C(020)-C(037)	118.1(3)	C(02H)-C(024)-Sn(12)	107.2(2)	C(03C)-C(02B)-C(030)	111.6(3)
C(03O)-C(022)-C(03L)	110.3(3)	C(02N)-C(024)-Sn(12)	106.7(2)	C(03E)-C(02B)-C(030)	110.1(3)
C(03O)-C(022)-C(03K)	112.2(3)	C(026)-C(024)-Sn(12)	108.9(2)	C(03C)-C(02B)-Sn(6)	107.5(2)
C(03L)-C(022)-C(03K)	111.0(3)	C(03G)-C(025)-C(02S)	110.9(3)	C(03E)-C(02B)-Sn(6)	108.3(2)
C(03O)-C(022)-Sn(2)	109.4(2)	C(03G)-C(025)-C(034)	110.7(3)	C(030)-C(02B)-Sn(6)	108.0(2)
C(03L)-C(022)-Sn(2)	106.4(2)	C(02S)-C(025)-C(034)	111.7(3)	N(21)-C(02C)-C(03M)	123.6(3)
C(03K)-C(022)-Sn(2)	107.3(2)	C(03G)-C(025)-Sn(8)	110.7(2)	N(21)-C(02C)-C(03Q)	117.8(3)
C(02C)-N(21)-N(22)	121.1(3)	C(02S)-C(025)-Sn(8)	106.0(2)	C(03M)-C(02C)-C(03Q)	118.6(3)
C(02C)-N(21)-Sn(11)	113.7(2)	C(034)-C(025)-Sn(8)	106.5(2)	N(3)-C(02D)-C(02Z)	123.4(3)
N(22)-N(21)-Sn(11)	125.2(2)	C(02L)-C(027)-C(02J)	116.1(3)	N(3)-C(02D)-C(03K)	118.3(3)
N(19)-C(023)-		N(15)-C(028)-C(03Z)	123.7(3)	C(02Z)-C(02D)-	

C(03K)	118.3(3)	C(02X)-C(02J)-C(027)	109.9(3)	Sn(3)	105.0(2)
N(23)-C(02E)-C(03A)	123.4(3)	C(02A)-C(02J)-Sn(7)	106.5(2)	N(9)-C(02R)-C(03S)	124.3(4)
N(23)-C(02E)-C(02H)	116.4(3)	C(02X)-C(02J)-Sn(7)	111.4(2)	N(9)-C(02R)-C(031)	117.8(3)
C(03A)-C(02E)-C(02H)	120.1(3)	C(027)-C(02J)-Sn(7)	106.8(2)	C(03S)-C(02R)-C(031)	117.8(3)
C(03T)-C(02F)-C(032)	111.6(3)	N(13)-C(02L)-C(02K)	123.7(3)	C(023)-C(02T)-C(02G)	118.4(3)
C(03T)-C(02F)-C(02I)	111.1(3)	N(13)-C(02L)-C(027)	117.5(3)	N(7)-C(02V)-C(03I)	125.4(3)
C(032)-C(02F)-C(02I)	110.5(3)	C(02K)-C(02L)-C(027)	118.8(3)	N(7)-C(02V)-C(02P)	118.1(3)
C(03T)-C(02F)-Sn(9)	106.3(2)	C(03J)-C(02O)-C(03P)	111.6(3)	C(03I)-C(02V)-C(02P)	116.5(3)
C(032)-C(02F)-Sn(9)	110.6(2)	C(03J)-C(02O)-C(02P)	110.7(3)	C(031)-C(02W)-C(03W)	112.1(3)
C(02I)-C(02F)-Sn(9)	106.4(2)	C(03P)-C(02O)-C(02P)	110.6(3)	C(031)-C(02W)-C(03X)	110.2(3)
C(035)-C(02G)-C(039)	109.8(3)	C(03J)-C(02O)-Sn(4)	107.0(2)	C(03W)-C(02W)-C(03X)	110.1(3)
C(035)-C(02G)-C(02T)	111.3(3)	C(03P)-C(02O)-Sn(4)	110.0(2)	C(031)-C(02W)-Sn(5)	107.7(2)
C(039)-C(02G)-C(02T)	111.3(3)	C(02P)-C(02O)-Sn(4)	106.9(2)	C(03W)-C(02W)-Sn(5)	111.6(2)
C(035)-C(02G)-Sn(10)	108.1(2)	C(02V)-C(02P)-C(02O)	116.4(3)	C(03X)-C(02W)-Sn(5)	104.9(2)
C(039)-C(02G)-Sn(10)	108.1(2)	C(03Y)-C(02Q)-C(03V)	112.2(4)	N(1)-C(02Y)-C(02U)	124.3(3)
C(02T)-C(02G)-Sn(10)	108.2(2)	C(03Y)-C(02Q)-C(03B)	110.0(3)	N(1)-C(02Y)-C(03H)	116.3(3)
C(02E)-C(02H)-C(024)	117.6(3)	C(03V)-C(02Q)-C(03B)	111.8(3)	C(02U)-C(02Y)-C(03H)	119.3(3)
C(020)-C(02I)-C(02F)	117.8(3)	C(03Y)-C(02Q)-Sn(3)	109.8(3)	C(033)-C(030)-C(02B)	117.9(3)
C(02A)-C(02J)-C(02X)	111.5(3)	C(03V)-C(02Q)-Sn(3)	107.7(2)	C(02W)-C(031)-C(02R)	116.8(3)
C(02A)-C(02J)-C(027)	110.6(3)	C(03B)-C(02Q)-		N(11)-C(033)-C(03F)	124.3(3)

N(11)-C(033)-C(030)	119.1(3)	C(03R)-C(03H)-C(02Y)	115.6(3)	C(03H)-C(03R)-Sn(1)	107.4(2)
C(03F)-C(033)-C(030)	116.6(3)	C(02D)-C(03K)-C(022)	118.3(3)	C(045)-C(03R)-Sn(1)	107.3(3)
C(028)-C(034)-C(025)	116.4(3)	C(02C)-C(03Q)-C(029)	116.9(3)	C(040)-C(03R)-Sn(1)	110.3(3)
N(5)-C(036)-C(03U)	123.4(3)	C(03H)-C(03R)-C(045)	112.6(4)	C(02Q)-C(03V)-C(036)	118.3(3)
N(5)-C(036)-C(03V)	117.6(3)	C(03H)-C(03R)-C(040)	109.6(4)	Cl(18)-C(043)-Cl(17)	110.8(3)
C(03U)-C(036)-C(03V)	119.0(3)	C(045)-C(03R)-C(040)	109.6(5)	Cl(10)-C(046)-Cl(9)	113.2(3)

7) Single-crystal X-ray Crystallography of Compound 4

Compound **4** crystallizes as orange blocks. Data of the X-Ray diffraction analyses were collected on a STOE IPDS2 imaging plate diffractometer using $Mo_{K\alpha}$ radiation with graphite monochromatization. (λ = 0.71073 Å) at 100 K. Reflection data were processed with X-Area 1.77.[1] Structure solution was performed by direct methods and full-matrix-least-squares refinement against F^2 using SHELXT[2] and SHELXL-2014.[3] All non-hydrogen atoms were refined anisotropically, hydrogen atom positions were calculated.
Intrinsically low crystal quality, owing to a high tendency to grow together, caused low scattering intensities. As a consequence, the final R values remained relatively high, in contrast to all other compounds reported in this work.

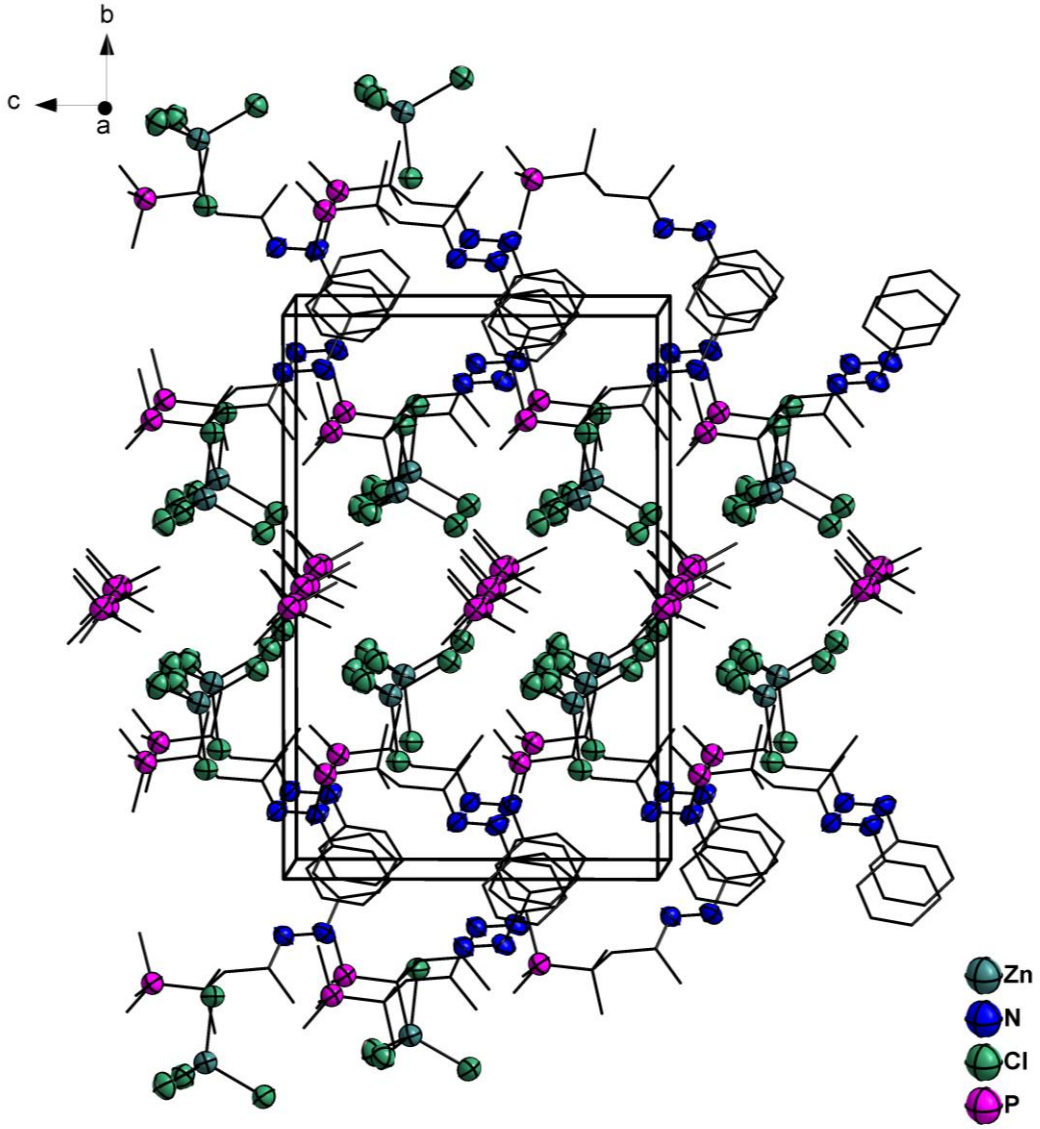

Figure S31. Crystal structure of **4** along the *a* axis.

Table S10. Crystal data and structure refinement for **4**.

Empirical formula	$C_{18}H_{35}Cl_4N_2P_2Zn_1$	
CCDC number	1914532	
Formula weight	548.62	
Temperature	100(2) K	
Wavelength	0.71073 Å	
Crystal system	Orthorhombic	
Space group	$Pca2_1$	
Unit cell dimensions	a = 11.0740(12) Å	□ = 90°.
	b = 19.1093(19) Å	□ = 90°.
	c = 12.6525(19) Å	□ = 90°.
Volume	2677.5(6) $Å^3$	
Z	4	
Density (calculated)	1.358 Mg/m^3	
Absorption coefficient	1.443 mm^{-1}	
F(000)	1136	
Crystal size	0.1 x 0.1 x 0.1 mm^3	
Theta range for data collection	1.609 to 26.000°.	
Index ranges	-13<=h<=12, -23<=k<=20, -15<=l<=15	
Reflections collected	13783	
Independent reflections	5262 [R(int) = 0.1455]	
Completeness to theta = 25.242°	99.8 %	
Absorption correction	Sphere	
Max. and min. transmission	0.8083 and 0.0054	
Refinement method	Full-matrix least-squares on F^2	
Data / restraints / parameters	5262 / 1 / 254	
Goodness-of-fit on F^2	0.803	
Final R indices [I>2sigma(I)]	R1 = 0.1004, wR2 = 0.2448	
R indices (all data)	R1 = 0.1966, wR2 = 0.2909	
Absolute structure parameter	-0.09(3)	
Largest diff. peak and hole	1.611 and -1.298 e.$Å^{-3}$	

Table S11. Atomic coordinates (x 10^4) and equivalent isotropic displacement parameters ($Å^2$x 10^3) for **4**. U(eq) is defined as one third of the trace of the orthogonalized U^{ij} tensor.

	x	y	z	U(eq)
Zn(1)	-5581(2)	-6718(1)	-7888(2)	62(1)
C(1)	-4210(20)	-8830(12)	-952(18)	71(6)
N(1)	-4651(16)	-8851(8)	-5895(12)	62(5)
Cl(1)	-5461(6)	-6118(3)	-9452(4)	70(2)
P(1)	-4521(6)	-7951(3)	-1304(4)	59(1)
Cl(2)	-4027(5)	-6359(3)	-6847(5)	73(2)
C(2)	-3540(20)	-7410(14)	-593(17)	75(6)
N(2)	-4773(17)	-8805(8)	-4820(12)	57(4)
P(2)	-7134(6)	-5064(3)	-5403(4)	64(2)
Cl(3)	-7401(6)	-6405(3)	-7219(4)	73(2)
C(3)	-5970(20)	-7786(12)	-916(16)	62(5)
Cl(4)	-5460(6)	-7898(3)	-8082(4)	79(2)
C(4)	-4338(18)	-7841(9)	-2707(14)	56(5)
C(9)	-5810(20)	-7663(13)	-5116(17)	72(7)
C(8)	-5323(19)	-8252(12)	-4440(16)	64(6)
C(7)	-5410(20)	-8187(13)	-3267(16)	70(6)
C(6)	-4344(18)	-7067(9)	-2966(18)	60(5)
C(5)	-3100(20)	-8138(12)	-3044(17)	77(6)
C(10)	-3984(19)	-9449(10)	-6281(15)	55(5)
C(11)	-3960(20)	-9553(11)	-7338(18)	73(6)
C(12)	-3200(30)	-10086(10)	-7780(20)	90(8)
C(13)	-2580(20)	-10542(11)	-7040(20)	81(7)
C(14)	-2680(20)	-10417(10)	-5950(20)	85(8)
C(15)	-3360(20)	-9873(10)	-5563(19)	68(6)
C(16)	-6240(20)	-5670(12)	-4720(18)	73(6)
C(17)	-7670(20)	-4430(11)	-4504(17)	69(6)
C(18)	-6330(20)	-4695(11)	-6461(15)	70(6)

Table S12. Bond lengths [Å] and angles [°] for **4**.

Zn(1)-Cl(3)	2.267(7)	C(12)-C(13)	1.46(4)	C(18)-P(2)-	
Zn(1)-Cl(4)	2.270(5)	C(13)-C(14)	1.40(4)	C(17)	112.8(10)
Zn(1)-Cl(2)	2.274(6)	C(14)-C(15)	1.37(3)	C(6)-C(4)-C(7)	108.6(17)
Zn(1)-Cl(1)	2.291(6)	Cl(3)-Zn(1)-Cl(4)	110.8(2)	C(6)-C(4)-C(5)	107.7(17)
C(1)-P(1)	1.77(2)	Cl(3)-Zn(1)-Cl(2)	112.1(2)	C(7)-C(4)-C(5)	113.6(17)
N(1)-N(2)	1.37(2)	Cl(4)-Zn(1)-Cl(2)	108.6(3)	C(6)-C(4)-P(1)	109.1(14)
N(1)-C(10)	1.44(2)	Cl(3)-Zn(1)-Cl(1)	104.0(2)	C(7)-C(4)-P(1)	108.6(14)
P(1)-C(3)	1.71(2)	Cl(4)-Zn(1)-Cl(1)	113.6(2)	C(5)-C(4)-P(1)	109.2(14)
P(1)-C(2)	1.75(2)	Cl(2)-Zn(1)-Cl(1)	107.8(2)	N(2)-C(8)-C(7)	117(2)
P(1)-C(4)	1.799(19)	N(2)-N(1)-		N(2)-C(8)-C(9)	123.9(18)
N(2)-C(8)	1.31(3)	C(10)	115.9(15)	C(7)-C(8)-C(9)	119(2)
P(2)-C(16)	1.75(2)	C(3)-P(1)-C(2)	109.0(10)	C(8)-C(7)-C(4)	116.5(17)
P(2)-C(18)	1.75(2)	C(3)-P(1)-C(1)	106.5(11)	C(11)-C(10)-C(15)	123(2)
P(2)-C(17)	1.76(2)	C(2)-P(1)-C(1)	108.2(12)	C(11)-C(10)-	
C(4)-C(6)	1.52(2)	C(3)-P(1)-C(4)	111.6(10)	N(1)	117.6(19)
C(4)-C(7)	1.53(3)	C(2)-P(1)-C(4)	111.6(10)	C(15)-C(10)-	
C(4)-C(5)	1.54(3)	C(1)-P(1)-C(4)	109.7(10)	N(1)	119.4(17)
C(9)-C(8)	1.51(3)	C(8)-N(2)-N(1)	117.6(16)	C(10)-C(11)-C(12)	120(2)
C(8)-C(7)	1.49(3)	C(16)-P(2)-		C(11)-C(12)-C(13)	117(2)
C(10)-C(11)	1.35(3)	C(18)	110.8(11)	C(14)-C(13)-C(12)	120(2)
C(10)-C(15)	1.40(3)	C(16)-P(2)-		C(15)-C(14)-C(13)	122(2)
C(11)-C(12)	1.43(3)	C(17)	109.0(12)	C(14)-C(15)-C(10)	118(2)

8) Single-crystal X-ray Crystallography of Compound 5

Compound **5** crystallizes as colorless blocks. Data of the X-Ray diffraction analyses were collected on a STOE IPDS2 imaging plate diffractometer using $Mo_{K\alpha}$ radiation with graphite monochromatization. (λ = 0.71073 Å) at 100 K. Reflection data were processed with X-Area 1.77.[1] Structure solution was performed by direct methods and full-matrix-least-squares refinement against F^2 using SHELXT[2] and SHELXL-2014.[3] All non-hydrogen atoms were refined anisotropically, hydrogen atom positions were calculated.

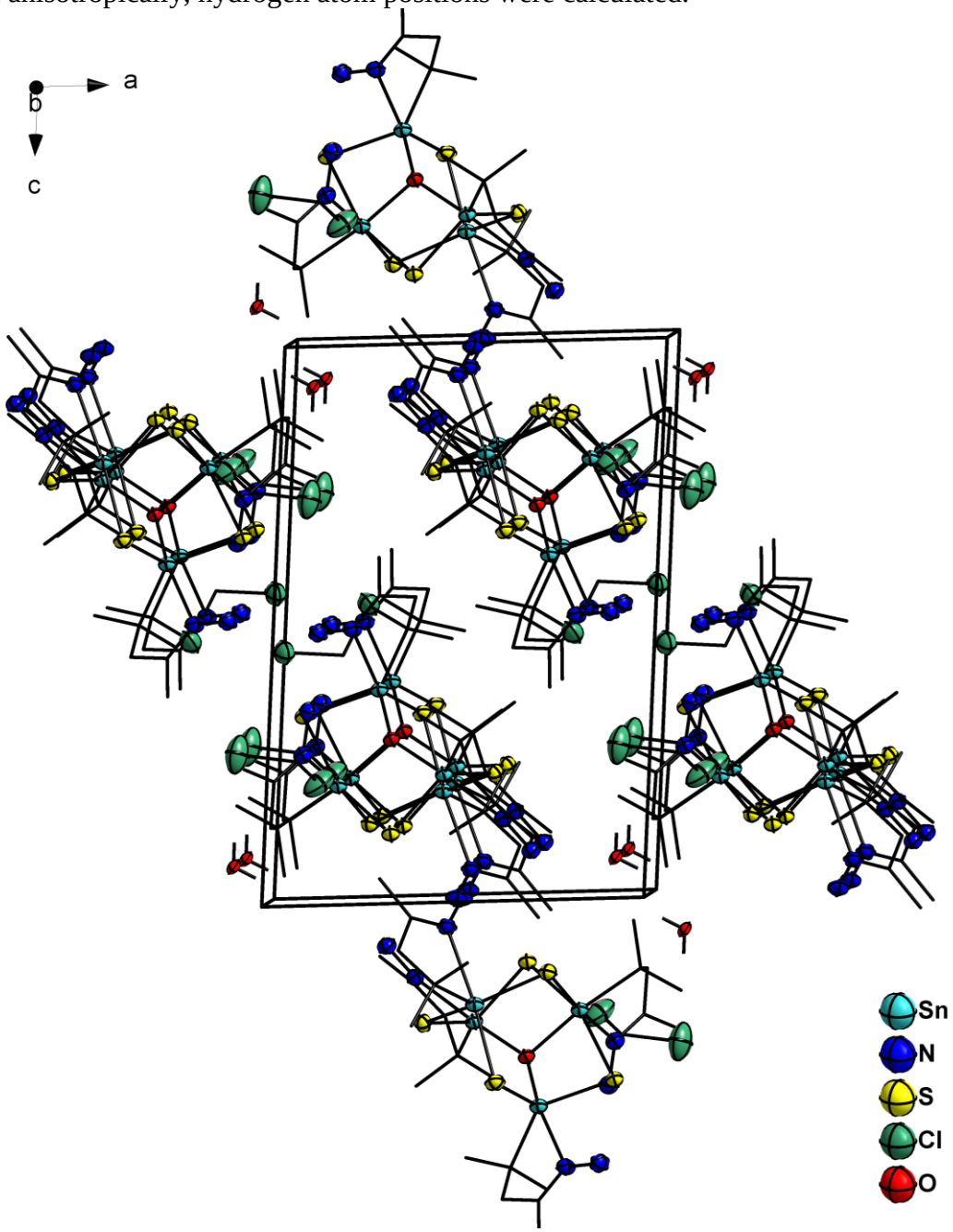

Figure S32. Crystal structure of **5**·H_2O·$2CH_2Cl_2$ along the *b* axis.

Table S13. Crystal data and structure refinement for **5**·H_2O·$2CH_2Cl_2$.

Empirical formula	$C_{26}H_{50}Cl_4N_8O_2S_5Sn_4$	
CCDC number	1914533	
Formula weight	1283.68	
Temperature	100(2) K	
Wavelength	0.71073 Å	
Crystal system	Triclinic	
Space group	$P\bar{1}$	
Unit cell dimensions	a = 11.3177(5) Å	α = 102.869(4)°.
	b = 12.6882(6) Å	β = 92.146(4)°.
	c = 16.9983(8) Å	γ = 98.155(4)°.
Volume	2349.56(19) $Å^3$	
Z	2	
Density (calculated)	1.811 Mg/m^3	
Absorption coefficient	2.585 mm^{-1}	
F(000)	1248	
Crystal size	0.1 x 0.1 x 0.1 mm^3	
Theta range for data collection	1.666 to 29.340°.	
Index ranges	-15<=h<=15, -17<=k<=17, -23<=l<=22	
Reflections collected	31659	
Independent reflections	12698 [R(int) = 0.0499]	
Completeness to theta = 25.242°	99.7 %	
Absorption correction	Sphere	
Max. and min. transmission	0.1237 and 0.0178	
Refinement method	Full-matrix least-squares on F^2	
Data / restraints / parameters	12698 / 2 / 462	
Goodness-of-fit on F^2	1.016	
Final R indices [I>2sigma(I)]	R1 = 0.0471, wR2 = 0.1278	
R indices (all data)	R1 = 0.0531, wR2 = 0.1313	
Largest diff. peak and hole	2.099 and -2.189 e.$Å^{-3}$	

Table S14. Atomic coordinates (x 10^4) and equivalent isotropic displacement parameters ($Å^2$x 10^3) for **5**·H_2O·$2CH_2Cl_2$. U(eq) is defined as one third of the trace of the orthogonalized U^{ij} tensor.

	x	y	z	U(eq)
Sn(1)	4516(1)	6349(1)	8068(1)	23(1)
N(1)	5357(3)	7216(3)	9462(2)	27(1)
C(1)	5558(3)	5210(3)	8461(2)	25(1)
S(1)	3866(1)	5267(1)	6678(1)	27(1)
Cl(1)	-680(1)	3836(2)	7214(2)	84(1)
O(1)	3155(2)	8015(2)	7091(2)	23(1)
Sn(2)	4603(1)	9164(1)	7723(1)	22(1)
C(2)	6093(4)	4537(3)	7744(2)	30(1)
S(2)	2642(1)	6630(1)	8608(1)	26(1)
N(2)	5018(3)	8149(3)	9952(2)	33(1)
O(2)	-627(2)	4875(3)	9206(2)	29(1)
Cl(2)	1460(2)	3096(1)	7776(1)	66(1)
Sn(3)	1811(1)	7950(1)	7903(1)	23(1)
C(3)	4694(3)	4470(3)	8845(2)	29(1)
S(3)	5891(1)	7822(1)	7741(1)	25(1)
N(3)	6238(3)	10356(3)	8528(2)	26(1)
Cl(3)	32(1)	1494(1)	5574(1)	48(1)
N(4)	7003(3)	10099(3)	9108(2)	30(1)
Sn(4)	2735(1)	6493(1)	6219(1)	23(1)
C(4)	6564(3)	5850(3)	9077(2)	28(1)
S(4)	3286(1)	9582(1)	8761(1)	26(1)
Cl(4)	2190(1)	1105(1)	4757(1)	53(1)
N(5)	889(3)	9204(3)	7315(2)	28(1)
C(5)	6293(3)	6865(3)	9646(2)	26(1)
S(5)	780(1)	6542(1)	6662(1)	27(1)
N(6)	1011(3)	9370(3)	6532(2)	33(1)
C(6)	7177(3)	7429(3)	10348(2)	32(1)
C(9)	3951(4)	10678(4)	6636(3)	37(1)
C(8)	6089(4)	10314(4)	6585(3)	35(1)
N(8)	1001(3)	4116(3)	5205(2)	32(1)
C(7)	5044(3)	10501(3)	7114(2)	28(1)
N(7)	1908(3)	4976(3)	5144(2)	27(1)
C(10)	5448(3)	11505(3)	7810(2)	30(1)
C(11)	6334(3)	11341(3)	8435(2)	28(1)
C(12)	7241(4)	12261(3)	8895(3)	33(1)

C(13)	270(3)	8300(3)	8620(2)	27(1)
C(15)	-836(3)	7516(3)	8217(2)	30(1)
C(14)	503(3)	8192(4)	9479(2)	32(1)
C(17)	175(3)	9693(3)	7777(2)	29(1)
C(16)	135(3)	9477(3)	8604(2)	30(1)
C(19)	3416(3)	6880(3)	5131(2)	27(1)
C(18)	-599(4)	10443(4)	7529(3)	46(1)
C(20)	4616(3)	7631(4)	5318(3)	35(1)
C(21)	2505(4)	7428(4)	4738(3)	35(1)
C(22)	3566(3)	5796(3)	4582(2)	30(1)
C(23)	2582(3)	4861(3)	4558(2)	28(1)
C(24)	2498(4)	3869(4)	3885(3)	36(1)
C(25)	1597(4)	1730(5)	5648(3)	46(1)
C(26)	888(5)	4099(4)	7368(3)	50(1)

Table S15. Bond lengths [Å] and angles [°] for **5**·H_2O·$2CH_2Cl_2$.

Sn(1)-C(1)	2.187(4)	N(5)-N(6)	1.402(5)	C(4)-C(1)-Sn(1)	109.4(2)
Sn(1)-S(2)	2.3850(9)	C(5)-C(6)	1.506(5)	C(3)-C(1)-Sn(1)	106.4(2)
Sn(1)-S(3)	2.4330(10)	C(9)-C(7)	1.524(5)	Sn(4)-S(1)-Sn(1)	99.79(3)
Sn(1)-N(1)	2.471(3)	C(8)-C(7)	1.525(5)	Sn(3)-O(1)-Sn(2)	106.40(10)
		N(8)-N(7)	1.412(5)	Sn(3)-O(1)-Sn(4)	103.93(10)
Sn(1)-S(1)	2.4793(9)	C(7)-C(10)	1.535(5)	Sn(2)-O(1)-Sn(4)	142.65(11)
N(1)-C(5)	1.261(5)	N(7)-C(23)	1.273(5)	O(1)-Sn(2)-C(7)	110.99(12)
N(1)-N(2)	1.399(4)	C(10)-C(11)	1.502(5)	O(1)-Sn(2)-S(4)	86.11(7)
C(1)-C(2)	1.524(5)	C(11)-C(12)	1.490(5)	C(7)-Sn(2)-S(4)	112.55(10)
C(1)-C(4)	1.524(5)	C(13)-C(14)	1.514(5)	O(1)-Sn(2)-N(3)	174.57(11)
C(1)-C(3)	1.525(5)	C(13)-C(15)	1.519(5)	C(7)-Sn(2)-N(3)	74.44(13)
S(1)-Sn(4)	2.3872(10)	C(13)-C(16)	1.529(6)	S(4)-Sn(2)-N(3)	91.67(8)
Cl(1)-C(26)	1.757(6)	C(17)-C(16)	1.493(6)	O(1)-Sn(2)-S(3)	94.19(7)
O(1)-Sn(3)	2.097(2)	C(17)-C(18)	1.497(6)	C(7)-Sn(2)-S(3)	121.90(10)
O(1)-Sn(2)	2.111(2)	C(19)-C(22)	1.515(5)	S(4)-Sn(2)-S(3)	120.92(3)
O(1)-Sn(4)	2.137(2)	C(19)-C(20)	1.523(5)	N(3)-Sn(2)-S(3)	82.70(8)
Sn(2)-C(7)	2.187(4)	C(19)-C(21)	1.533(6)	Sn(1)-S(2)-Sn(3)	106.68(4)
Sn(2)-S(4)	2.3699(9)	C(22)-C(23)	1.499(6)	H(1)-O(2)-H(2)	113(10)
Sn(2)-N(3)	2.382(3)	C(23)-C(24)	1.490(5)	O(1)-Sn(3)-C(13)	162.88(13)
Sn(2)-S(3)	2.3975(9)	C(1)-Sn(1)-S(2)	120.40(10)	O(1)-Sn(3)-N(5)	88.83(11)
S(2)-Sn(3)	2.5263(10)	C(1)-Sn(1)-S(3)	108.68(10)	C(13)-Sn(3)-N(5)	74.42(13)
O(2)-H(1)	0.98(2)	S(2)-Sn(1)-S(3)	122.25(3)	O(1)-Sn(3)-S(2)	96.17(7)
O(2)-H(2)	1.01(2)	C(1)-Sn(1)-N(1)	72.79(12)	C(13)-Sn(3)-S(2)	100.58(11)
Cl(2)-C(26)	1.764(6)	S(2)-Sn(1)-N(1)	84.37(7)	N(5)-Sn(3)-S(2)	175.00(8)
Sn(3)-C(13)	2.205(3)	S(3)-Sn(1)-N(1)	82.77(8)	O(1)-Sn(3)-S(5)	79.95(7)
Sn(3)-N(5)	2.393(3)	C(1)-Sn(1)-S(1)	98.68(10)	C(13)-Sn(3)-S(5)	101.13(10)
Sn(3)-S(5)	2.5593(9)	S(2)-Sn(1)-S(1)	101.39(3)		
Sn(3)-S(4)	2.5867(9)	S(3)-Sn(1)-S(1)	99.23(3)		
N(3)-C(11)	1.285(5)	N(1)-Sn(1)-S(1)	171.38(8)		
N(3)-N(4)	1.410(4)	C(5)-N(1)-N(2)	120.8(3)		
Cl(3)-C(25)	1.750(5)	C(5)-N(1)-Sn(1)	112.8(2)		
Sn(4)-C(19)	2.159(4)	N(2)-N(1)-Sn(1)	125.1(2)		
Sn(4)-S(5)	2.3683(9)	C(2)-C(1)-C(4)	109.2(3)		
Sn(4)-N(7)	2.391(3)	C(2)-C(1)-C(3)	110.5(3)		
C(4)-C(5)	1.505(5)	C(4)-C(1)-C(3)	110.6(3)		
Cl(4)-C(25)	1.751(5)	C(2)-C(1)-Sn(1)	110.6(2)		
N(5)-C(17)	1.275(5)				

N(5)-Sn(3)-S(5)	83.39(8)	N(6)-N(5)-Sn(3)	126.4(2)	N(5)-C(17)-C(16)	116.3(3)
S(2)-Sn(3)-S(5)	97.61(3)	N(1)-C(5)-C(4)	116.2(3)	N(5)-C(17)-C(18)	123.6(4)
O(1)-Sn(3)-S(4)	81.03(7)	N(1)-C(5)-C(6)	124.6(3)	C(16)-C(17)-C(18)	120.1(3)
C(13)-Sn(3)-S(4)	94.98(10)	C(4)-C(5)-C(6)	119.0(3)	C(17)-C(16)-C(13)	113.2(3)
N(5)-Sn(3)-S(4)	89.18(8)	Sn(4)-S(5)-Sn(3)	85.08(3)	C(22)-C(19)-C(20)	110.1(3)
S(2)-Sn(3)-S(4)	91.44(3)	C(9)-C(7)-C(8)	112.0(4)	C(22)-C(19)-C(21)	110.6(3)
S(5)-Sn(3)-S(4)	159.69(3)	C(9)-C(7)-C(10)	109.7(3)	C(20)-C(19)-C(21)	110.2(3)
Sn(2)-S(3)-Sn(1)	101.25(3)	C(8)-C(7)-C(10)	108.6(3)	C(22)-C(19)-Sn(4)	105.9(3)
C(11)-N(3)-N(4)	119.9(3)	C(9)-C(7)-Sn(2)	111.3(3)	C(20)-C(19)-Sn(4)	110.8(3)
C(11)-N(3)-Sn(2)	113.1(3)	C(8)-C(7)-Sn(2)	111.1(3)	C(21)-C(19)-Sn(4)	109.1(2)
N(4)-N(3)-Sn(2)	126.8(2)	C(10)-C(7)-Sn(2)	103.9(3)	C(23)-C(22)-C(19)	115.9(3)
O(1)-Sn(4)-C(19)	103.18(12)	C(23)-N(7)-N(8)	120.5(3)	N(7)-C(23)-C(24)	125.3(4)
O(1)-Sn(4)-S(5)	83.75(7)	C(23)-N(7)-Sn(4)	111.3(3)	N(7)-C(23)-C(22)	116.0(3)
C(19)-Sn(4)-S(5)	128.08(10)	N(8)-N(7)-Sn(4)	125.9(2)	C(24)-C(23)-C(22)	118.6(3)
O(1)-Sn(4)-S(1)	105.84(7)	C(11)-C(10)-C(7)	115.0(3)	Cl(3)-C(25)-Cl(4)	112.1(3)
C(19)-Sn(4)-S(1)	110.43(10)	N(3)-C(11)-C(12)	124.1(4)	Cl(1)-C(26)-Cl(2)	112.1(3)
S(5)-Sn(4)-S(1)	116.91(4)	N(3)-C(11)-C(10)	114.3(3)		
O(1)-Sn(4)-N(7)	167.14(10)	C(12)-C(11)-C(10)	121.6(4)		
C(19)-Sn(4)-N(7)	74.43(13)	C(14)-C(13)-C(15)	110.4(3)		
S(5)-Sn(4)-N(7)	87.93(8)	C(14)-C(13)-C(16)	110.7(3)		
S(1)-Sn(4)-N(7)	86.67(8)	C(15)-C(13)-C(16)	110.5(3)		
C(5)-C(4)-C(1)	116.7(3)	C(14)-C(13)-Sn(3)	110.8(2)		
Sn(2)-S(4)-Sn(3)	85.54(3)	C(15)-C(13)-Sn(3)	109.0(2)		
C(17)-N(5)-N(6)	120.7(3)	C(16)-C(13)-Sn(3)	105.1(2)		
C(17)-N(5)-Sn(3)	112.7(3)				

9) Single-crystal X-ray Crystallography of Compound 6

Compound **6** crystallizes as colorless blocks. Data of the X-Ray diffraction analyses were collected on a STOE IPDS2 imaging plate diffractometer using $Mo_{K\alpha}$ radiation with graphite monochromatization. (λ = 0.71073 Å) at 100 K. Reflection data were processed with X-Area 1.77.[1] Structure solution was performed by direct methods and full-matrix-least-squares refinement against F^2 using SHELXT[2] and SHELXL-2014.[3] All non-hydrogen atoms were refined anisotropically, hydrogen atom positions were calculated.

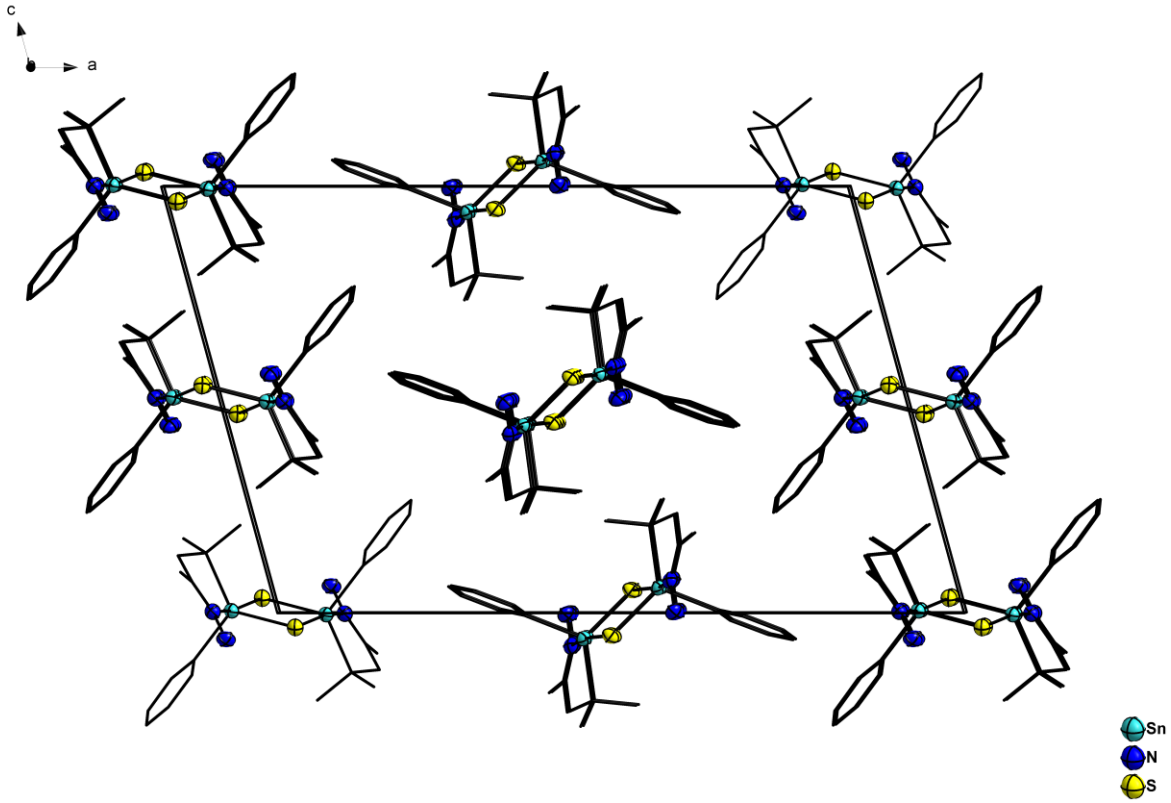

Figure S33. Crystal structure of **6** along the *b* axis.

Table S16. Crystal data and structure refinement for **6**.

Empirical formula	$C_{24}H_{32}N_4S_2Sn_2$	
CCDC number	1914534	
Formula weight	678.09	
Temperature	100(2) K	
Wavelength	0.71073 Å	
Crystal system	Monoclinic	
Space group	$P2_1/c$	
Unit cell dimensions	a = 23.3073(9) Å	α = 90°.
	b = 8.5530(2) Å	β = 105.246(3)°.
	c = 14.9965(6) Å	γ = 90°.
Volume	2884.30(18) $Å^3$	
Z	4	
Density (calculated)	1.561 Mg/m^3	
Absorption coefficient	1.894 mm^{-1}	
F(000)	1344	
Crystal size	0.1 x 0.1 x 0.1 mm^3	
Theta range for data collection	2.548 to 26.708°.	
Index ranges	-23<=h<=29, -10<=k<=9, -18<=l<=18	
Reflections collected	15703	
Independent reflections	6085 [R(int) = 0.0294]	
Completeness to theta = 25.242°	99.8 %	
Absorption correction	Sphere	
Max. and min. transmission	0.7568 and 0.3281	
Refinement method	Full-matrix least-squares on F^2	
Data / restraints / parameters	6085 / 0 / 295	
Goodness-of-fit on F^2	0.894	
Final R indices [I>2sigma(I)]	R1 = 0.0275, wR2 = 0.0596	
R indices (all data)	R1 = 0.0459, wR2 = 0.0613	
Largest diff. peak and hole	0.694 and -0.786 $e.Å^{-3}$	

Table S17. Atomic coordinates (x 10^4) and equivalent isotropic displacement parameters ($Å^2$x 10^3) for **6**. U(eq) is defined as one third of the trace of the orthogonalized U^{ij} tensor.

	x	y	z	U(eq)
Sn(1)	5651(1)	5935(1)	5596(1)	25(1)
N(1)	5865(1)	8678(3)	5774(2)	29(1)
C(1)	5774(1)	6415(4)	7062(2)	29(1)
S(1)	4769(1)	6793(1)	4471(1)	30(1)
Sn(2)	9324(1)	811(1)	5047(1)	26(1)
S(2)	10190(1)	1843(1)	4660(1)	29(1)
N(2)	5810(1)	9765(3)	5040(2)	34(1)
C(2)	6033(1)	5005(4)	7656(2)	34(1)
N(3)	9058(1)	3552(3)	5031(2)	28(1)
C(3)	5152(2)	6796(5)	7165(2)	41(1)
C(5)	6123(1)	9063(4)	6603(2)	33(1)
C(4)	6185(2)	7829(4)	7327(2)	35(1)
N(4)	9146(1)	4684(3)	4387(2)	34(1)
C(6)	6382(2)	10655(4)	6878(3)	48(1)
C(7)	6415(1)	5575(4)	5053(2)	27(1)
C(8)	6777(1)	6795(4)	4930(2)	30(1)
C(9)	7267(2)	6534(5)	4591(2)	37(1)
C(10)	7403(2)	5042(5)	4376(2)	41(1)
C(11)	7057(2)	3819(5)	4495(2)	42(1)
C(12)	6561(2)	4081(4)	4830(2)	37(1)
C(13)	9181(2)	1229(4)	6404(2)	31(1)
C(14)	9791(2)	1569(4)	7055(2)	42(1)
C(15)	8907(2)	-200(4)	6737(2)	40(1)
C(16)	8771(2)	2664(4)	6343(2)	35(1)
C(17)	8878(1)	3955(4)	5730(2)	30(1)
C(18)	8755(2)	5603(4)	5962(2)	36(1)
C(19)	8580(1)	306(4)	3889(2)	26(1)
C(20)	8483(2)	-1199(4)	3534(2)	32(1)
C(21)	8010(2)	-1552(5)	2782(2)	38(1)
C(22)	7626(1)	-379(4)	2363(2)	37(1)
C(23)	7711(2)	1127(4)	2700(2)	39(1)
C(24)	8184(1)	1470(4)	3462(2)	34(1)

Table S18. Bond lengths [Å] and angles [°] for **6**.

Sn(1)-C(7)	2.167(3)	C(7)-Sn(1)-C(1)	120.16(11)	C(19)-Sn(2)-S(2)#2	100.92(9)
Sn(1)-C(1)	2.180(3)	C(7)-Sn(1)-N(1)	90.73(11)	C(13)-Sn(2)-S(2)#2	99.03(9)
		C(1)-Sn(1)-N(1)	74.65(11)	S(2)-Sn(2)-S(2)#2	90.33(3)
Sn(1)-N(1)	2.399(3)	C(7)-Sn(1)-S(1)	114.54(8)	N(3)-Sn(2)-S(2)#2	166.91(6)
Sn(1)-S(1)	2.4048(8)	C(1)-Sn(1)-S(1)	120.77(9)	Sn(2)-S(2)-Sn(2)#2	89.67(3)
Sn(1)-S(1)#1	2.5213(9)	N(1)-Sn(1)-S(1)	83.94(7)	C(17)-N(3)-N(4)	120.8(3)
N(1)-C(5)	1.273(4)	C(7)-Sn(1)-S(1)#1	101.65(9)	C(17)-N(3)-Sn(2)	113.1(2)
N(1)-N(2)	1.421(4)	C(1)-Sn(1)-S(1)#1	99.29(9)	N(4)-N(3)-Sn(2)	125.7(2)
C(1)-C(2)	1.526(4)	N(1)-Sn(1)-S(1)#1	167.59(7)	N(1)-C(5)-C(4)	117.2(3)
C(1)-C(4)	1.529(5)	S(1)-Sn(1)-S(1)#1	90.19(3)	N(1)-C(5)-C(6)	123.7(3)
C(1)-C(3)	1.532(4)	C(5)-N(1)-N(2)	120.7(3)	C(4)-C(5)-C(6)	119.1(3)
Sn(2)-C(19)	2.150(3)	C(5)-N(1)-Sn(1)	113.1(2)	C(5)-C(4)-C(1)	115.8(3)
Sn(2)-C(13)	2.178(3)	N(2)-N(1)-Sn(1)	125.45(19)	C(8)-C(7)-C(12)	117.8(3)
Sn(2)-S(2)	2.4085(9)	C(2)-C(1)-C(4)	110.4(3)	C(8)-C(7)-Sn(1)	122.2(2)
Sn(2)-N(3)	2.423(3)	C(2)-C(1)-C(3)	110.4(3)	C(12)-C(7)-Sn(1)	120.0(2)
Sn(2)-S(2)#2	2.5226(9)	C(4)-C(1)-C(3)	110.5(3)	C(9)-C(8)-C(7)	121.2(3)
N(3)-C(17)	1.275(4)	C(2)-C(1)-Sn(1)	111.5(2)	C(10)-C(9)-C(8)	120.0(3)
N(3)-N(4)	1.420(4)	C(4)-C(1)-Sn(1)	108.6(2)	C(11)-C(10)-C(9)	120.1(3)
C(5)-C(4)	1.494(5)	C(3)-C(1)-Sn(1)	105.4(2)	C(10)-C(11)-C(12)	120.0(3)
C(5)-C(6)	1.502(4)	Sn(1)-S(1)-Sn(1)#1	89.81(3)	C(7)-C(12)-C(11)	120.9(3)
C(7)-C(8)	1.385(4)	C(19)-Sn(2)-C(13)	119.90(12)	C(15)-C(13)-C(14)	110.1(3)
C(7)-C(12)	1.385(4)	C(19)-Sn(2)-S(2)	115.36(8)	C(15)-C(13)-C(16)	110.6(3)
C(8)-C(9)	1.384(4)	C(13)-Sn(2)-S(2)	120.58(9)	C(14)-C(13)-C(16)	110.2(3)
C(9)-C(10)	1.374(5)	C(19)-Sn(2)-N(3)	92.08(11)	C(15)-C(13)-Sn(2)	110.8(2)
C(10)-C(11)	1.361(5)	C(13)-Sn(2)-N(3)	75.44(11)	C(14)-C(13)-Sn(2)	106.5(2)
C(11)-C(12)	1.394(5)	S(2)-Sn(2)-N(3)	82.64(7)	C(16)-C(13)-Sn(2)	108.6(2)
C(13)-C(15)	1.523(5)				
C(13)-C(14)	1.525(4)				
C(13)-C(16)	1.543(5)				
C(16)-C(17)	1.499(5)				
C(17)-C(18)	1.497(4)				
C(19)-C(20)	1.388(4)				
C(19)-C(24)	1.394(4)				
C(20)-C(21)	1.388(4)				
C(21)-C(22)	1.380(5)				
C(22)-C(23)	1.378(5)				
C(23)-C(24)	1.395(5)				

C(17)-C(16)-C(13)	115.0(3)	C(20)-C(19)-C(24)	117.7(3)	C(22)-C(21)-C(20)	119.5(3)
N(3)-C(17)-C(18)	124.8(3)	C(20)-C(19)-Sn(2)	120.7(2)	C(21)-C(22)-C(23)	119.9(3)
N(3)-C(17)-C(16)	116.6(3)	C(24)-C(19)-Sn(2)	121.6(2)	C(22)-C(23)-C(24)	120.2(3)
C(18)-C(17)-C(16)	118.5(3)	C(21)-C(20)-C(19)	121.9(3)	C(23)-C(24)-C(19)	120.8(3)

Symmetry transformations used to generate equivalent atoms:

#1 -x+1,-y+1,-z+1 #2 -x+2,-y,-z+1

10) References for the Supporting Information

[1] Stoe and Cie GmbH, *X-Area*, *Version 1.77*, **2016**.
[2] Sheldrick, G. M. SHELXT – Integrated space-group and crystal-structure determination, *Acta Crystallogr A* **2015**, *71*, 3-8.
[3] Hübschle, C. B., Sheldrick, G. M., Dittrich, B. ShelXle: a Qt graphical user interface for SHELXL, *J. Appl. Cryst.* **2011**, 1281-1284.

4.7 Dinuclear organogermanium chalcogenide complexes as intermediates towards functionalized clusters

Zitat: E. Dornsiepen, S. Dehnen, *Dalton Trans.* **2019**, *48*, 3671-3675.

Abstract

Reactions of R^1GeCl_3(R^1=CMe_2CH_2COMe) with $(Me_3Si)_2E$(E=SSeTe) yield three new organogermanium chalcogenide complexes $[(R^1GeCl)_2S_2]$ (**1**), $[(R^1GeCl)_2Se_2]$ (**2**), and $[(R^1GeCl)_2Te_2]$ (**3**) with functionalized ligands. NMR titration experiments clearly demonstrate that these dimeric complexes are intermediates in the formation of the well-known sesquichalcogenide clusters $[(R^1Ge)_4E_6]$. In striking contrast to related tin compounds that were recently reported, the mono-bridged complexes of the type "$[(R^1GeCl_2)_2E]$" and defect-heterocubane-type clusters "$[(R^1Ge)_3E_4Cl]$" do not form on the NMR time scale for E = S or Te, and only in traces for E = Se.

Eigener Anteil

Alle Synthesen wurden von mir geplant und durchgeführt, alle analytischen Daten wurden von mir ausgewertet. Die Aufnahme der röntgenographischen Daten sowie der IR- und UV/Vis-Spektren wurde von mir durchgeführt. ^{1}H- und ^{13}C-NMR-Spektren wurden von mir, ^{31}P- und ^{119}Sn-NMR-Experimente von der zentralen NMR-Abteilung des Fachbereichs Chemie an der Philipps-Universität unter Leitung von Dr. Xiulan Xie gemessen. Massenspektren wurden von der entsprechenden Serviceabteilung des Fachbereichs unter Leitung von Dr. Uwe Linne aufgenommen. Das Manuskript wurde gemeinsam von Stefanie Dehnen und mir verfasst.

Dalton Transactions

PAPER

View Article Online
View Journal | View Issue

Cite this: *Dalton Trans.*, 2019, **48**, 3671

Dinuclear organogermanium chalcogenide complexes as intermediates towards functionalized clusters†

Eike Dornsiepen and Stefanie Dehnen *

Received 22nd January 2019,
Accepted 15th February 2019

DOI: 10.1039/c9dt00310j

rsc.li/dalton

Reactions of R^1GeCl_3 (R^1 = CMe_2CH_2COMe) with $(Me_3Si)_2E$ (E = S, Se, Te) yield three new organogermanium chalcogenide complexes $[(R^1GeCl)_2S_2]$ (**1**), $[(R^1GeCl)_2Se_2]$ (**2**), and $[(R^1GeCl)_2Te_2]$ (**3**) with functionalized ligands R^1 = CMe_2CH_2COMe. NMR titration experiments clearly demonstrate that these dimeric complexes are intermediates in the formation of the well-known sesquichalcogenide clusters $[(R^1Ge)_4E_6]$. In striking contrast to related tin compounds that were recently reported, the mono-bridged complexes of the type "$[(R^1GeCl_2)_2E]$" and defect-heterocubane-type clusters "$[(R^1Ge)_3E_4Cl]$" do not form on the NMR time scale for E = S or Te, and only in traces for E = Se.

Introduction

In recent years, organotetrelchalcogenide clusters comprising a chalcogenidotetrelate core surrounded by organic ligands have attracted interest due to their intriguing structural, chemical and physical properties.[1] Organogermanium chalcogenide complexes with the general composition $[(RGe)_xE_y]$ (R = organic substituent, E = S, Se, Te) were first prepared in 1903,[2] and their first structural characterization dates back to 1968.[3]

Contemporary research in this field has focused on organogermanium sulfides with organic substituents bearing reactive functional groups[4] or with ligands that allow for extreme nonlinear optical properties,[5] as well as the extension towards their heavier congeners with selenium[6] and tellurium.[7] In these studies, three different topologies were reported for the inorganic cluster core. The two predominant architectures are the adamantane-type (AD) topology (Scheme 1, left) and an isomeric "double-decker"-type (DD) variant (Scheme 1, center), which consists of two Ge_2E_2 four-membered rings connected by two μ-bridging chalcogenide ligands.

These two competing topologies can be selectively obtained by choice of organic substituents, although in some cases, transformation of the DD topology into the thermodynamically more stable AD topology by heating in solution is possible.[8]

For selenide and telluride clusters, a noradamantane-type (NA) topology (Scheme 1, right) is also known, which is derived from the AD type by removal of one chalcogenide atom in the formation of a Ge–Ge bond, thus resulting in a mixed-valence situation with two Ge atoms in the +IV oxidation state and two in the +III oxidation state.[6,8] In all of these studies, alkali metal chalcogenides were employed as chalcogenide sources.

For the tin homologues, we recently investigated the stepwise cluster formation upon reaction of organotintrichlorides $RSnCl_3$ with different stoichiometric amounts of $(Me_3Si)_2E$ (Scheme 2).[9] In these studies, a stepwise growth of the final to $[(RSn)_4E_6]$ clusters was monitored that included the formation of compounds $[(RSnCl_2)_2E]$, $[(RSnCl)_2E_2]$, $[(RSn)_3E_4Cl]$ (E = S, Se, Te).

To shed light on the formation of the homologous germanium chalcogenide clusters $[(R^1Ge)_4E_6]$, we studied the reactivity of R^1GeCl_3 (R^1 = CMe_2CH_2COMe) towards $(Me_3Si)_2E$ at varying stoichiometric ratios (Scheme 3). We obtained new dimeric organogermanium chalcogenide complexes $[(R^1GeCl)_2S_2]$ (**1**), $[(R^1GeCl)_2Se_2]$ (**2**) and $[(R^1GeCl)_2Te_2]$ (**3**) in

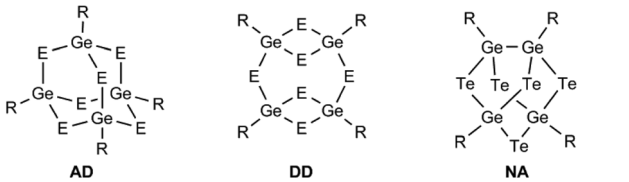

Scheme 1 Known topologies of organogermanium chalcogenide clusters.

Fachbereich Chemie and Wissenschaftliches Zentrum für Materialwissenschaften (WZMW), Philipps-Universität Marburg, Hans-Meerwein-Straße 4, D-35043 Marburg, Germany. E-mail: dehnen@chemie.uni-marburg.de

†Electronic supplementary information (ESI) available: Details on NMR, IR and ESI MS, and single-crystal XRD. CCDC 1891726-1891728. For ESI and crystallographic data in CIF or other electronic format, see DOI: 10.1039/c9dt00310j

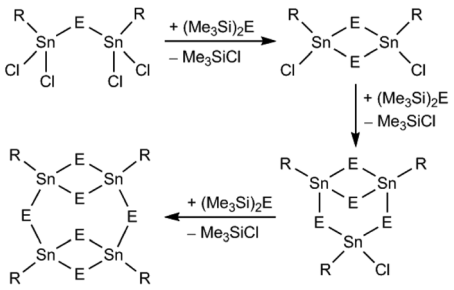

Scheme 2 Formation mechanism for organotin chalcogenide clusters by stepwise addition of $(Me_3Si)_2E$, according to a combination of NMR titration experiments, crystallographic studies and quantum chemical calculations.[9]

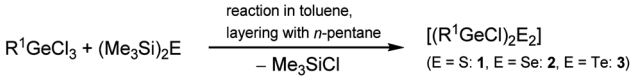

Scheme 3 Preparation of compounds **1–3**.

the crystalline form (CCDC 1891726–1891728†), all of which feature a central Ge_2E_2 four-membered ring.

In contrast to the findings with T = Sn illustrated in Scheme 2, neither the V-shaped, mono-bridged $[(RTCl_2)_2E]$ intermediates, nor the defect-heterocubane-type clusters $[(RT)_3E_4Cl]$ were formed for T = Ge – at least not on the NMR time-scale, as confirmed by NMR titration experiments. However, the NMR studies indicate that the reactions proceed until the formation of $[(R^1Ge)_4E_6]$. Consequently, **1–3** can indeed be understood as intermediates on the way towards larger cluster formation.

Results and discussion

The reaction of R^1GeCl_3 with one equivalent of $(Me_3Si)_2S$ in toluene yields colorless crystals of **1** upon layering of the reaction solution with *n*-pentane. Compound **1** crystallizes in the monoclinic crystal system (space group $P2_1/n$) with two formula units per unit cell. The molecular structure of **1** consists of a dinuclear germanium complex connected by two μ-bridging sulfur atoms (Fig. 1, top left). Each germanium atom bears one chlorine atom and one organic substituent. The carbonyl oxygen atom of the substituent coordinates back to the germanium atom, thus extending its coordination number to five, hereby stabilizing the compound. The central Ge_2S_2 ring shows a slight distortion with Ge–S bond lengths ranging from 2.2057(4) to 2.386(10) Å and bond angles varying between 81.7(2) and 95.089(13)°. The bond lengths are in the same range as those for the literature-known compound $[(R^1Ge)_4S_6]$ (2.207(2)–2.246(2) Å).[4b]

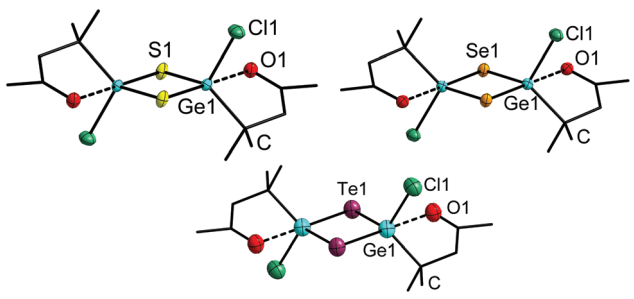

Fig. 1 Molecular structure of compounds **1–3**.

The analogous reaction with $(Me_3Si)_2Se$ yields colorless to light yellow crystals of **2**, which are isostructural to **1** (Fig. 1, top right). The unit cell volume is slightly larger (955 *vs.* 945 Å^3, respectively), reflecting the larger atom size of Se that causes longer Ge–Se bonds (2.3354(4) and 2.3866(3) Å) at nearly identical bond angles for **1** and **2**.

The corresponding reaction with $(Me_3Si)_2Te$ needs to be conducted under exclusion of day-light due to the light sensitivity of tellurium compounds. An orange solid precipitates from the reaction solution. After dissolution in dichloromethane and layering with *n*-pentane, **3** is obtained as blocks of intense orange color. **3** is isostructural to both **1** and **2**, with an again larger cell volume of 1003 Å^3 due to the larger Te atomic size and, consequently, larger Ge–Te bond lengths of 2.5466(9) and 2.5896(10) Å.

In preliminary studies, all three compounds were obtained from reactions where R^1GeCl_3 and $(Me_3Si)_2E$ were combined in a 1 : 1 stoichiometric ratio. However, upon having received the series of analogous tin compounds, we were left with the question if compounds of the composition $[(R^1GeCl_2)_2E]$ could be isolated from reactions with 0.5 equivalents of the chalcogenide source. These reactions also yielded single crystals of **1–3**, but in lower yields. We also tried to isolate clusters of the composition $[(R^1Ge)_3E_4Cl]$ from a 1 : 1.33 ratio of the reagents, but these reactions only afforded the known DD-type clusters $[(R^1Ge)_4E_6]$.

From these findings, the question arose if the intermediate products do not exist at all, or whether they could just not be isolated by crystallization. To answer this, we carried out an NMR study, in which we titrated R^1GeCl_3 with 0.5, 1.0 and 1.5 equivalents of $(Me_3Si)_2E$ each. Due to the lack of a useful nuclear spin at Ge ($I = 7/2$), we resorted to monitoring the reactions by ^{1}H NMR spectroscopy. The spectra are shown in Fig. 2–4.

For E = S, the spectra indicate the formation of **1** only, for 0.5 and 1 equivalent of the sulfide source, while the reaction carried out with 1.5 equivalents yields a mixture of **1** and $[(R^1Ge)_4S_6]$ (Fig. 2).[4b]

In the case of E = Se, the main product of all reactions is **2**. Yet, according to the spectra, this reaction becomes significantly less selective with increasing amount of $(Me_3Si)_2Se$, leading to the formation of a variety of different species in small amounts (Fig. 3).

For E = Te, the selectivity increases; besides **3** as the main product, a second species is formed upon increase of the Te concentration in the reaction solution, which we claim to be $[(R^1Ge)_4Te_6]$ (Fig. 4).

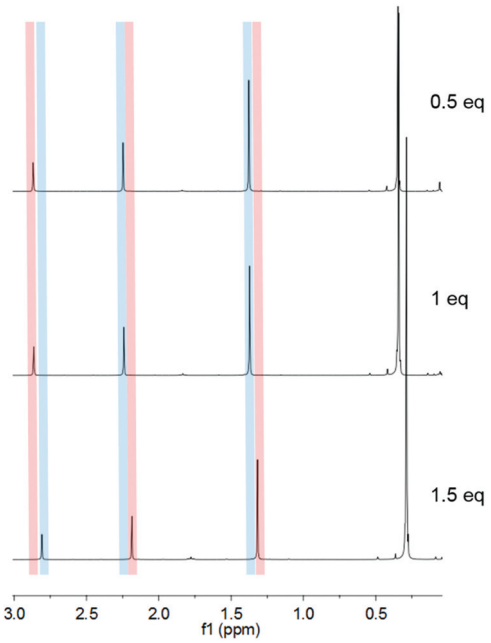

Fig. 2 ^{1}H NMR spectra of the reaction of $R^{1}GeCl_3$ with different stoichiometric amounts of $(Me_3Si)_2S$ in $CDCl_3$. The signal set marked with red highlight corresponds to **1**, and the one marked with blue highlight corresponds to $[(R^{1}Ge)_4S_6]$.[4b]

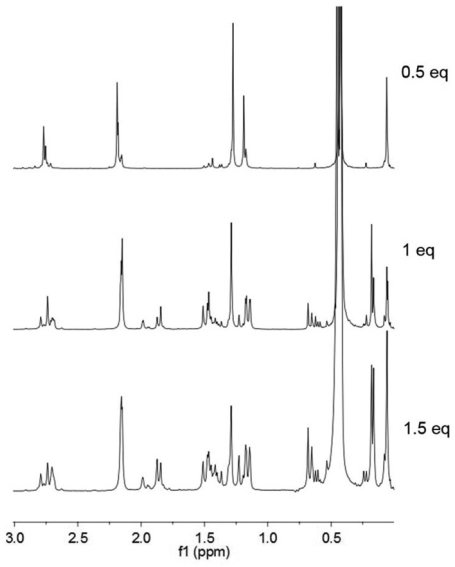

Fig. 3 ^{1}H NMR spectra of the reaction of $R^{1}GeCl_3$ with different stoichiometric amounts of $(Me_3Si)_2Se$ in $CDCl_3$.

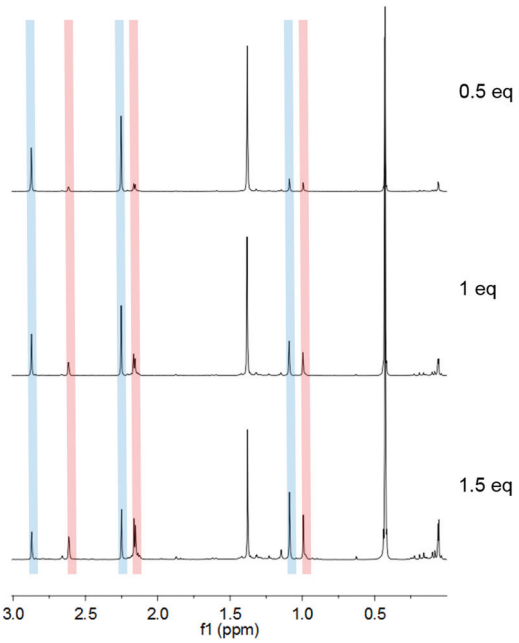

Fig. 4 ^{1}H NMR spectra of the reaction of $R^{1}GeCl_3$ with different stoichiometric amounts of $(Me_3Si)_2Te$ in $CDCl_3$. The signal set marked with red highlight corresponds to **3**, and the one marked with blue highlight corresponds to $[(R^{1}Ge)_4Te_6]$.

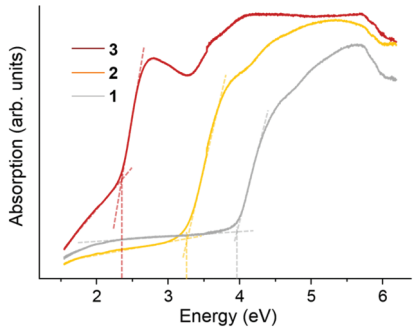

Fig. 5 UV-Vis spectra of compounds **1**–**3**. The tangential fits for the determination of the optical excitation energies are also shown. The dents at 3.4 eV are caused by the light source change.

At least for E being S and Te, the formation of yet unknown species "$[(R^{1}GeCl_2)_2E]$" and "$[(R^{1}Ge)_3E_4Cl]$" can be ruled out. In the case of S = Se, these two types of compounds may be formed as side products in small yields; so far, they could not be isolated, however, upon formation of **2** as the main product.

For a more comprehensive knowledge about the nature of compounds **1**–**3**, UV-Vis spectra were recorded on solid samples (Fig. 5). For the colorless compound **1**, the optical absorption sets on at around 4 eV. A tangential fit reveals an optical excitation energy of 3.95 eV (314 nm).

For compound **2**, the spectrum is red-shifted to an excitation energy of 3.25 eV (381 nm). The spectrum of **3** shows an excitation energy of 2.35 eV (528 nm) according to the tangent method, which correlates well with the orange color of the crystals. Two more absorption features can be seen below 2.35 eV and between 3.2 and 3.8 eV, which may be attributed to minor impurities upon light-induced decomposition of the light-sensitive tellurium compounds. The recorded spectra demonstrate the general and expected trend of decreasing optical excitation energies for homologous chalcogenide compounds when going from S through Se to Te.[9c] UV-Vis spectra in solution were also recorded, showing nearly the same absorption features (see Fig. S20†).

Experimental section

General

All synthetic steps were carried out under exclusion of oxygen and moisture by the use of standard Schlenk procedures. $(Me_3Si)_2E$ (E = S, Se, Te)[10,11] was prepared according to literature procedures. The yields of the syntheses were calculated based on the Ge content and refer to the amount of product isolated as single crystals. IR spectra were recorded on a Bruker Tensor 37 ATR spectrometer. ^{1}H and ^{13}C spectroscopy was carried out at 25 °C using a Bruker DRX 300 MHz spectrometer. The chemical shifts are given in ppm relative to the residual protons of deuterated solvents for ^{1}H spectra and relative to the solvent signal for ^{13}C spectra. High-resolution ESI mass spectra were acquired with an LTQ-FT Ultra mass spectrometer (Thermo Fischer Scientific). The resolution was set to 100 000. UV-visible absorption spectroscopy was performed by analyses of the diffuse reflection of powdered samples. The measurements were carried out using a Varian Cary 5000 dual-beam spectrometer with a Praying Mantis sample holder from Harrick.

R^1GeCl_3 (A). Compound **A** was prepared according to a modified literature procedure.[6a] 1,1,3,3-Tetramethyldisiloxane (7.50 mL, 42.5 mmol) was added to a solution of $GeCl_4$ (5.00 mL, 42.5 mmol) in diethyl ether (15 mL). After refluxing for 1.5 hours, mesityl oxide (3.60 mL, 43 mmol) was added dropwise, and the resulting solution was stirred at room temperature for 15 hours. After solvent removal *in vacuo*, the remaining oil was freeze-dried and taken up in *n*-pentane (5 mL) and the resulting solid was filtered, washed with *n*-pentane (2 × 5 mL) and dried. **Yield**: 8.14 g (29.3 mmol, 69%). All analytical data are in accordance with the literature values.[6a]

$[(R^1GeCl)_2S_2]$ (1). $(Me_3Si)_2S$ (0.40 mL, 1.91 mmol) was added to a solution of **A** (530 mg, 1.91 mmol) in toluene (10 mL). The colorless solution was stirred at room temperature for 15 hours, concentrated to a volume of 5 mL, layered with *n*-pentane (10 mL) and stored at 5 °C. Colorless crystals of **1** were obtained within one day.

Yield: 273 mg (0.57 mmol, 60%) **IR:** $\tilde{\nu}$ = 2949 (w), 1695 (s), 1454 (w), 1418 (w), 1401 (w), 1386 (w), 1364 (s), 1339 (m), 1247 (w), 1188 (s), 1128 (w), 1014 (w), 1000 (w), 961 (w), 843 (w), 797 (w), 613 (s), 542 (w), 497 (w), 487 (w), 451 (m), 424 (s) cm^{-1}. **^{1}H-NMR** (300 MHz, CD_2Cl_2): δ = 1.32 (s, 12H, C*Me*$_2$), 2.20 (s, 6H, CO*Me*), 2.82 (s, 4H, CH_2) ppm. **^{13}C-NMR** (75 MHz, CD_2Cl_2): δ = 23.7 (C*Me*$_2$), 30.1 (CO*Me*), 40.0 (GeC), 54.8 (CH_2), 201.1 (CO) ppm. **HRMS (ESI+)**: *m*/*z* calcd: 442.9177 $[C_{12}H_{22}O_2Ge_2S_2Cl]^+$, found: 442.9175; calcd: 626.9198 $[C_{18}H_{33}O_3Ge_3S_3O]^+$, found: 626.9196.

$[(R^1GeCl)_2Se_2]$ (2). $(Me_3Si)_2Se$ (0.40 mL, 1.60 mmol) was added to a solution of **A** (444 mg, 1.60 mmol) in toluene (10 mL). The yellow solution was stirred at room temperature for 15 hours and subsequently layered with *n*-pentane (10 mL). Colorless crystals of **2** were obtained within one day.

Yield: 224 mg (0.45 mmol, 56%) **IR:** $\tilde{\nu}$ = 2949 (w), 1695 (s), 1450 (w), 1399 (m), 1362 (s), 1335 (m), 1247 (w), 1184 (m), 1124 (m), 1013 (w), 1001 (w), 956 (w), 842 (w), 793 (w), 612 (s), 540 (w), 483 (w), 444 (w) cm^{-1}. **^{1}H-NMR** (300 MHz, CD_2Cl_2): δ = 1.25 (s, 12H, C*Me*$_2$), 2.18 (s, 6H, CO*Me*), 2.76 (s, 4H, CH_2) ppm. **^{13}C-NMR** (75 MHz, CD_2Cl_2): δ = 23.9 (C*Me*$_2$), 30.2 (CO*Me*), 38.8 (GeC), 54.4 (CH_2), 210.0 (CO) ppm. **HRMS (ESI−)**: *m*/*z* calcd: 320.8573 $[C_6H_{11}GeSeCl_2]^-$, found: 320.8581; calcd: 472.6968 $[C_6H_{11}OGe_2Se_2Cl_2]^-$, found: 472.6975; calcd: 570.7699 $[C_{12}H_{21}O_2Ge_2Se_2Cl_2]^-$, found 570.7707.

$[(R^1GeCl)_2Te_2]$ (3). $(Me_3Si)_2Te$ (0.40 mL, 1.42 mmol) was added to a solution of **A** (394 mg, 1.42 mmol) in toluene (10 mL). The red suspension was stirred at room temperature under exclusion of light (by wrapping all reaction vessels in aluminium foil) for 15 hours and filtered subsequently. The orange solid was dissolved in dichloromethane (10 mL) and layered with *n*-pentane (10 mL). Orange crystals of **3** were obtained within two days.

Yield: 191 mg (0.32 mmol, 45%) **IR:** $\tilde{\nu}$ = 2962 (w), 2917 (w), 2858 (w), 1696 (s), 1454 (m), 1410 (m), 1397 (m), 1361 (s), 1338 (m), 1238 (m), 1183 (m), 1120 (m), 1014 (m), 980 (w), 954 (w), 859 (w), 840 (w), 793 (w), 611 (m), 531 (w), 480 (w), 443 (w) cm^{-1}. **^{1}H-NMR** (300 MHz, CD_2Cl_2): δ = 1.07 (s, 12H, C*Me*$_2$), 2.16 (s, 6H, CO*Me*), 2.61 (s, 4H, CH_2) ppm. **^{13}C-NMR** (75 MHz, CD_2Cl_2): δ = 24.3 (C*Me*$_2$), 30.3 (CO*Me*), 34.1 (GeC), 53.5 (CH_2), 210.1(CO) ppm. **HRMS (ESI+)**: *m*/*z* calcd: 307.0513 $[C_{12}H_{22}O_2GeCl]^+$, found 307.0516; calcd: 634.7837 $[C_{12}H_{22}O_2Ge_2Te_2Cl]^+$, found 634.7879.

Conclusions

Three new organogermanium chalcogenide complexes $[(R^1GeCl)_2E_2]$ (E = S, Se, Te) with functionalized ligands R^1 = CMe_2CH_2COMe were prepared and characterized. NMR titration experiments show that these dimeric complexes represent intermediates along the formation of larger sesquichalcogenide clusters $[(R^1Ge)_4E_6]$. In contrast to the homologous tin compounds, complexes of the composition $[(R^1GeCl_2)_2E]$ and $[(R^1Ge)_3E_4Cl]$ are not formed for E = S and Te, and only in traces for E = Se. The optical absorption energies correlate well with the visible colors of the crystals. All compounds will be subject to an extension of the organic ligands with complementarily functionalized organic molecules, and of the inorganic moieties by addition of further metal ions.

Conflicts of interest

There are no conflicts to declare.

Acknowledgements

This work was funded by the Deutsche Forschungsgemeinschaft within the framework of GRK1782.

References

1 (*a*) B. Krebs, *Angew. Chem., Int. Ed. Engl.*, 1983, **22**, 113; (*b*) W. Ando, T. Kadowaki, Y. Kabe and M. Ishii, *Angew. Chem., Int. Ed. Engl.*, 1994, **31**, 59; (*c*) M. G. Kanatzidis, *Science*, 2007, **317**, 490; (*d*) S. Dehnen and M. Melullis, *Coord. Chem. Rev.*, 2007, **251**, 1259; (*e*) L. Nicole, C. Laberty-Robert, L. Rozes and C. Sanchez, *Nanoscale*, 2014, **6**, 6267; (*f*) E. Dornsiepen, E. Geringer, N. Rinn and S. Dehnen, *Coord. Chem. Rev.*, 2019, **380**, 136.

2 P. Pfeiffer and R. Lehnardt, *Chem. Ber.*, 1903, **36**, 3027.

3 C. Dorfelt, A. Janeck, D. Kobelt, E. F. Paulus and H. Scherer, *J. Organomet. Chem.*, 1968, **14**, P22.

4 (*a*) Z. Hassanzahdeh Fard, C. Müller, T. Harmening, R. Pöttgen and S. Dehnen, *Angew. Chem., Int. Ed.*, 2009, **48**, 4441; (*b*) Z. Hassanzahdeh Fard, L. Xiong, C. Müller, M. Holynska and S. Dehnen, *Chem. – Eur. J.*, 2009, **15**, 6596.

5 N. W. Rosemann, J. P. Eußner, E. Dornsiepen, S. Chatterjee and S. Dehnen, *J. Am. Chem. Soc.*, 2016, **138**, 16224.

6 (*a*) S. Heimann, M. Holynska and S. Dehnen, *Z. Anorg. Allg. Chem.*, 2012, **638**, 1663; (*b*) S. Heimann, G. Thiele and S. Dehnen, *J. Organomet. Chem.*, 2016, **813**, 36.

7 S. Heimann, M. Holynska and S. Dehnen, *Chem. Commun.*, 2011, **47**, 1881.

8 M. Unno, Y. Kawai, H. Shioyama and H. Matsumoto, *Organometallics*, 1997, **16**, 4428.

9 (*a*) J. P. Eußner, B. E. K. Barth, E. Leusmann, Z. You, N. Rinn and S. Dehnen, *Chem. – Eur. J.*, 2013, **19**, 13792; (*b*) N. Rinn, J. P. Eußner, W. Kaschuba, X. Xie and S. Dehnen, *Chem. – Eur. J.*, 2016, **22**, 3094; (*c*) J. P. Eußner, R. O. Kusche and S. Dehnen, *Chem. – Eur. J.*, 2015, **21**, 12376.

10 J.-H. So and P. Boudjouk, *Synthesis*, 1989, 306.

11 M. W. DeGroot, N. J. Taylor and J. F. Corrigan, *J. Mater. Chem.*, 2004, **14**, 654.

Dinuclear organogermanium chalcogenide complexes as intermediates towards functionalized clusters

Eike Dornsiepen and Stefanie Dehnen*

Fachbereich Chemie and Wissenschaftliches Zentrum für Materialwissenschaften, Philipps-Universität Marburg, Hans-Meerwein-Straße, D-35043 Marburg, Germany

SUPPORTING INFORMATION

Content

1. NMR spectra

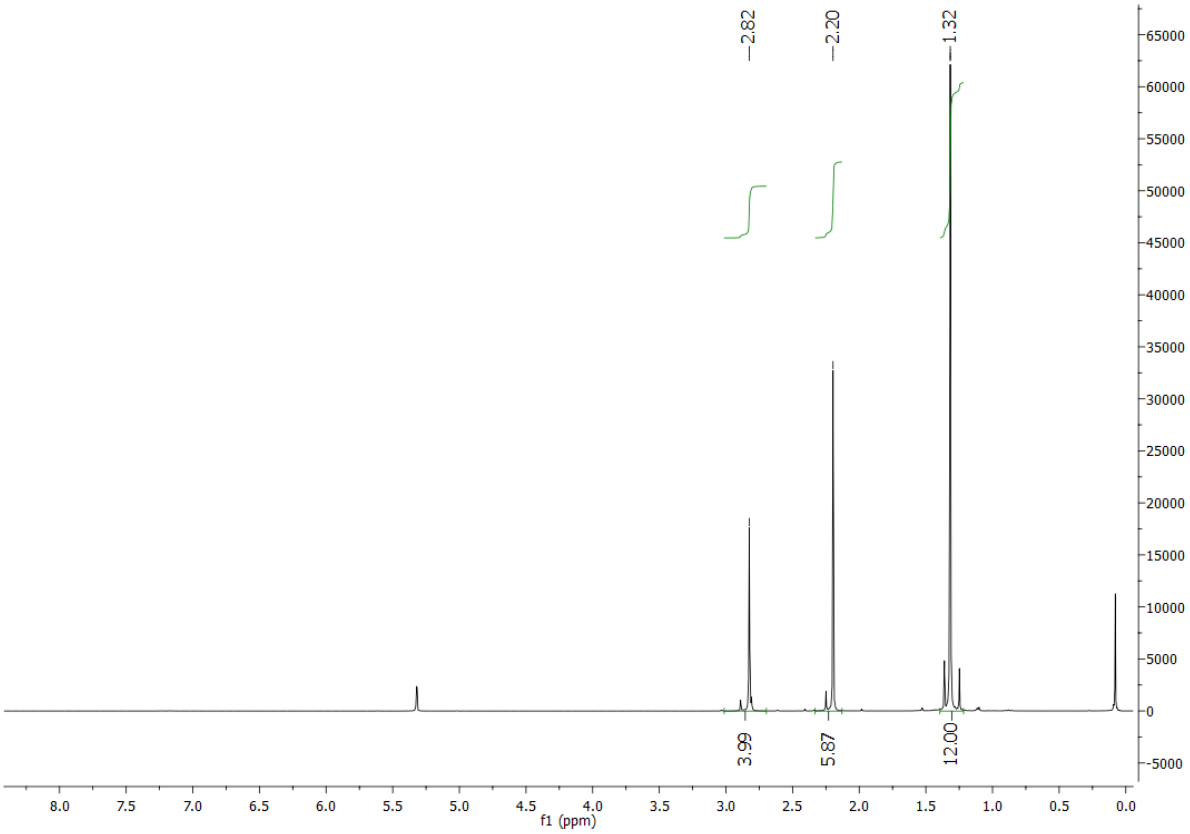

Figure S1: ^{1}H-NMR spectrum of **1** (300 MHz, CD_2Cl_2).

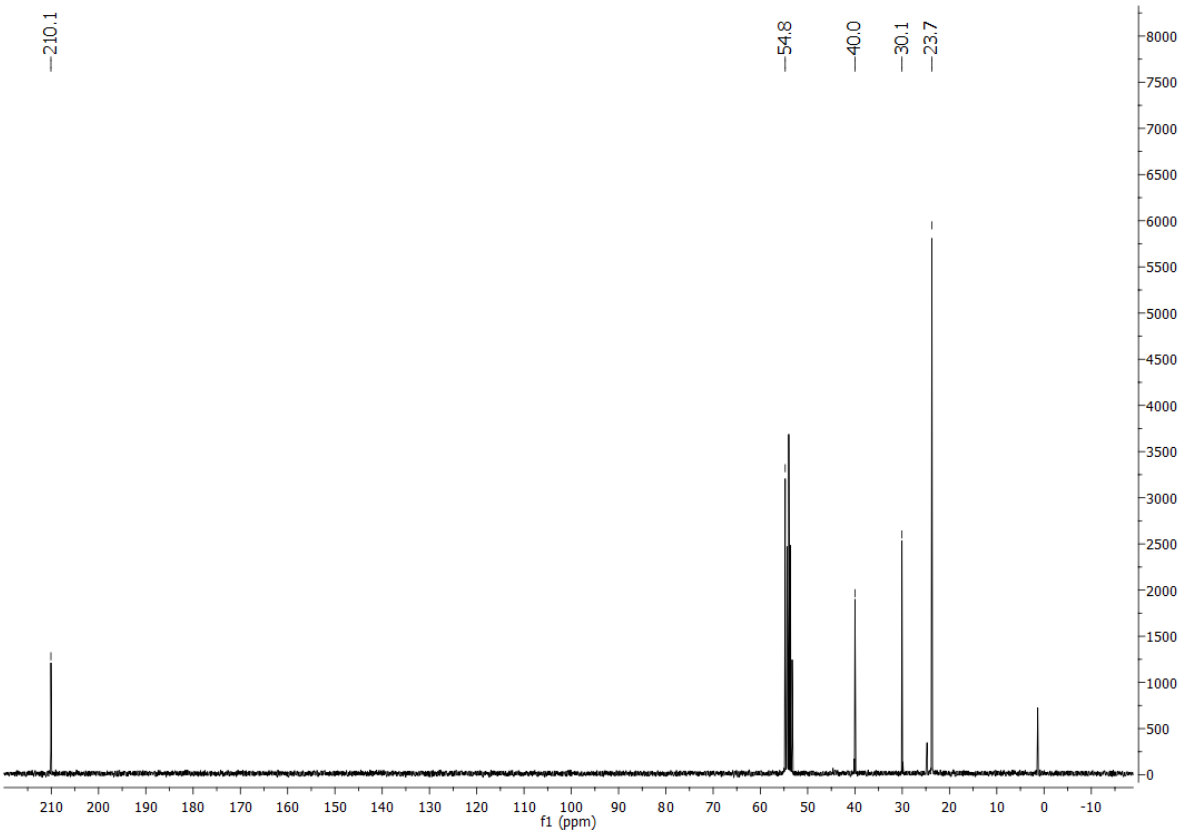

Figure S2: $^{13}C\{^{1}H\}$-NMR spectrum of **1** (75 MHz, CD_2Cl_2).

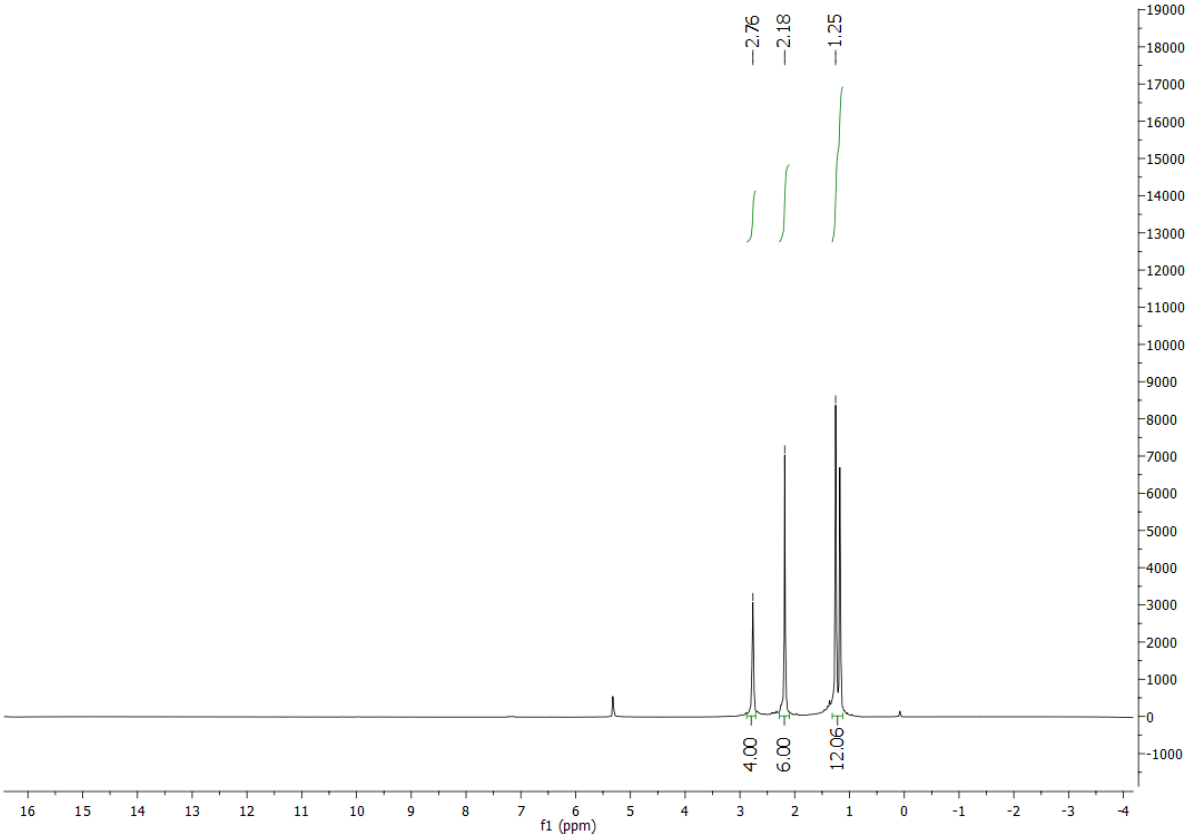

Figure S3: ^{1}H-NMR spectrum of **2** (300 MHz, CD_2Cl_2).

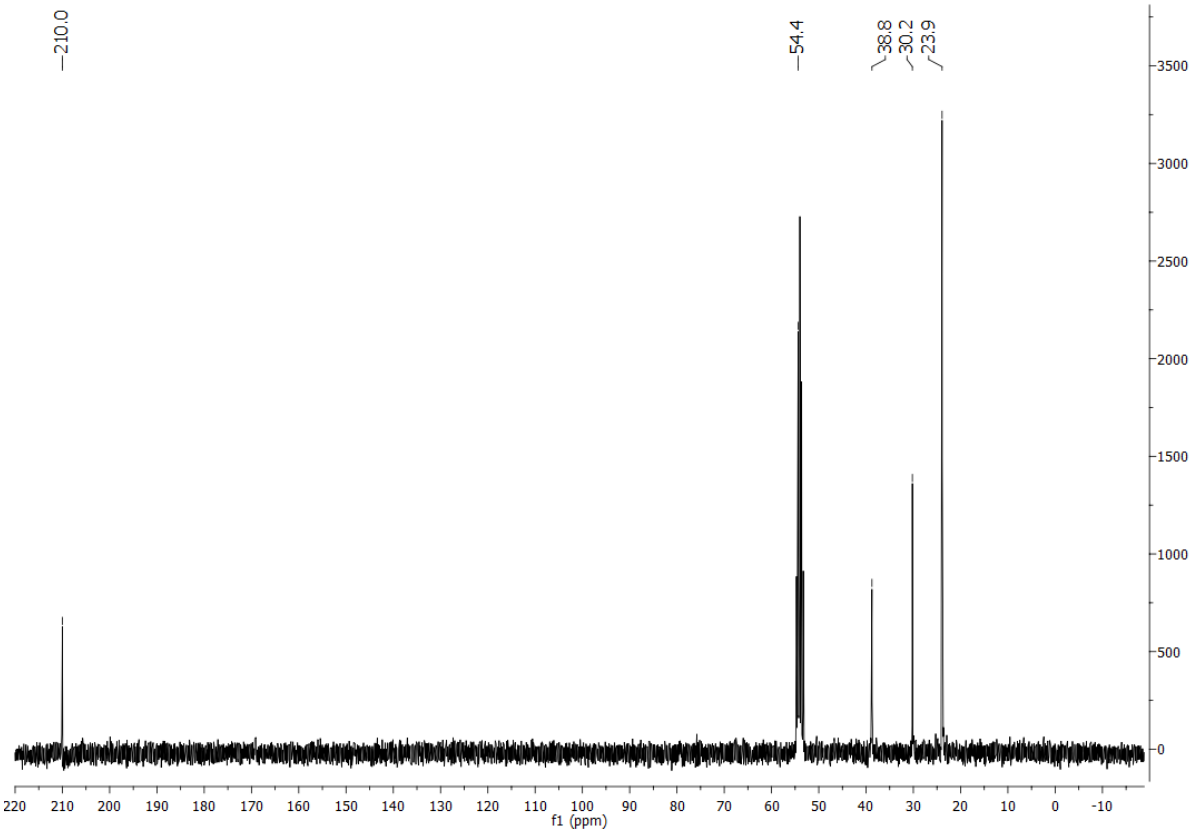

Figure S4: ^{13}C{^{1}H}-NMR spectrum of **2** (75 MHz, CD_2Cl_2).

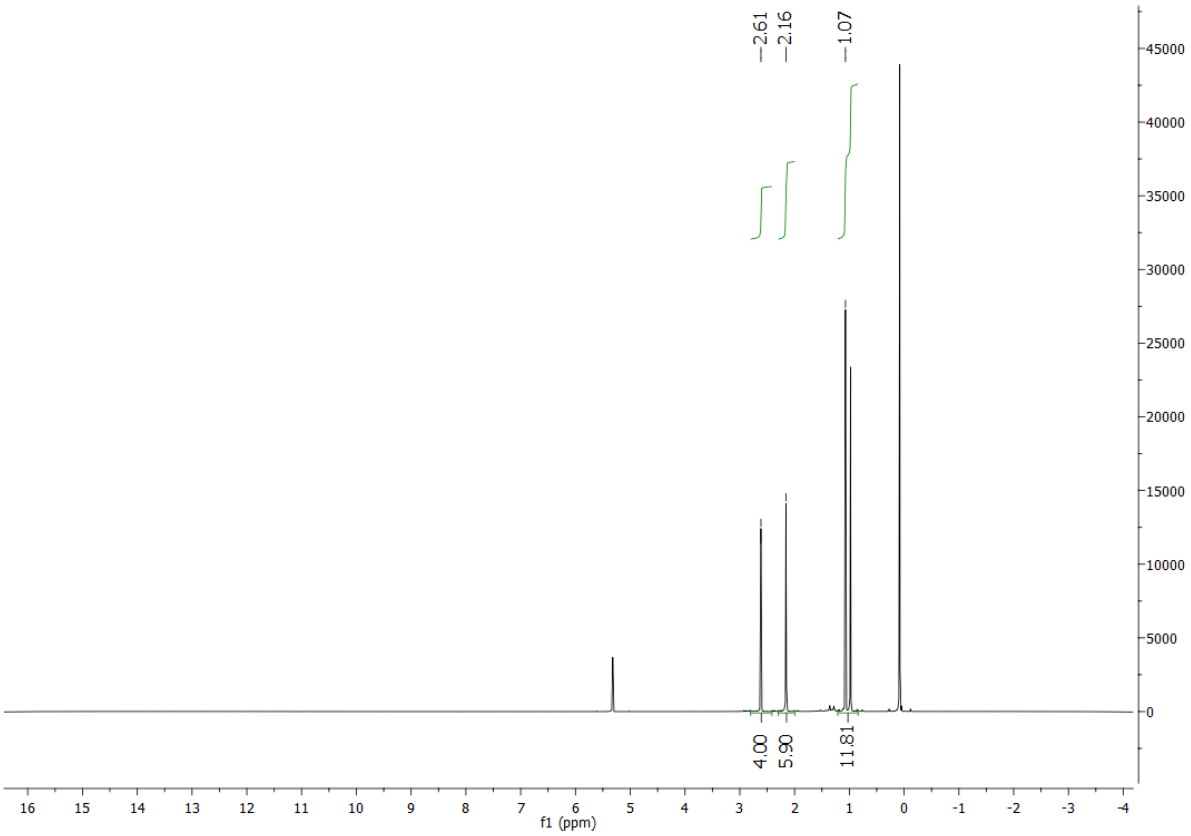

Figure S5: ^{1}H-NMR spectrum of **3** (300 MHz, CD_2Cl_2).

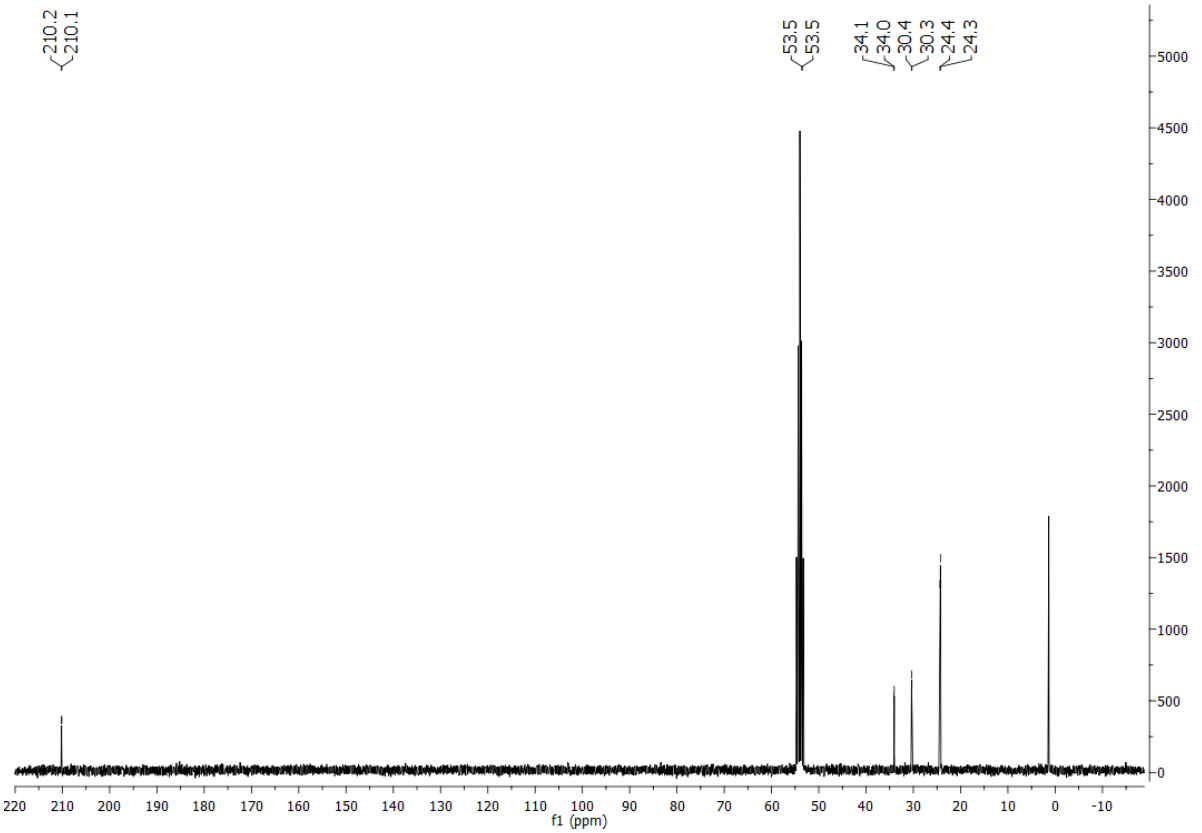

Figure S6: ^{13}C{^{1}H}-NMR spectrum of **3** (300 MHz, CD_2Cl_2).

2. Mass spectra

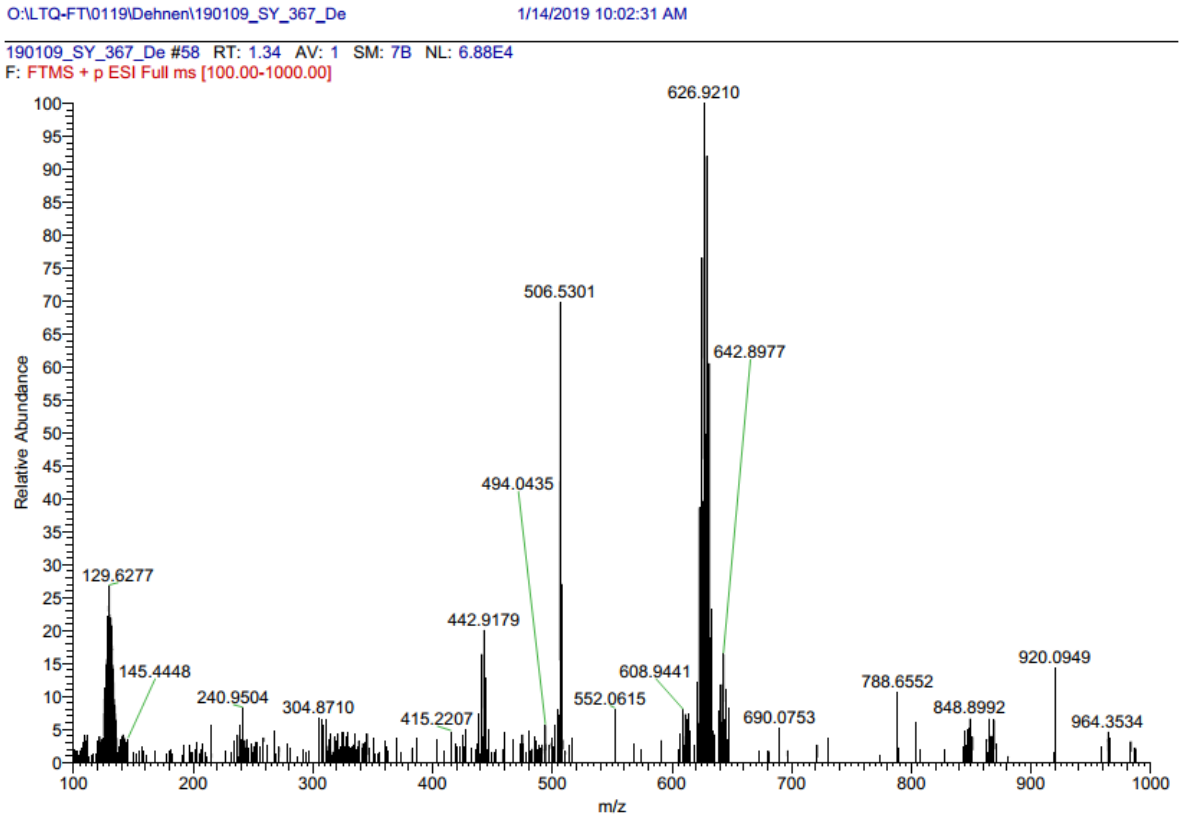

Figure S7: ESI(+) mass spectrum of **1**.

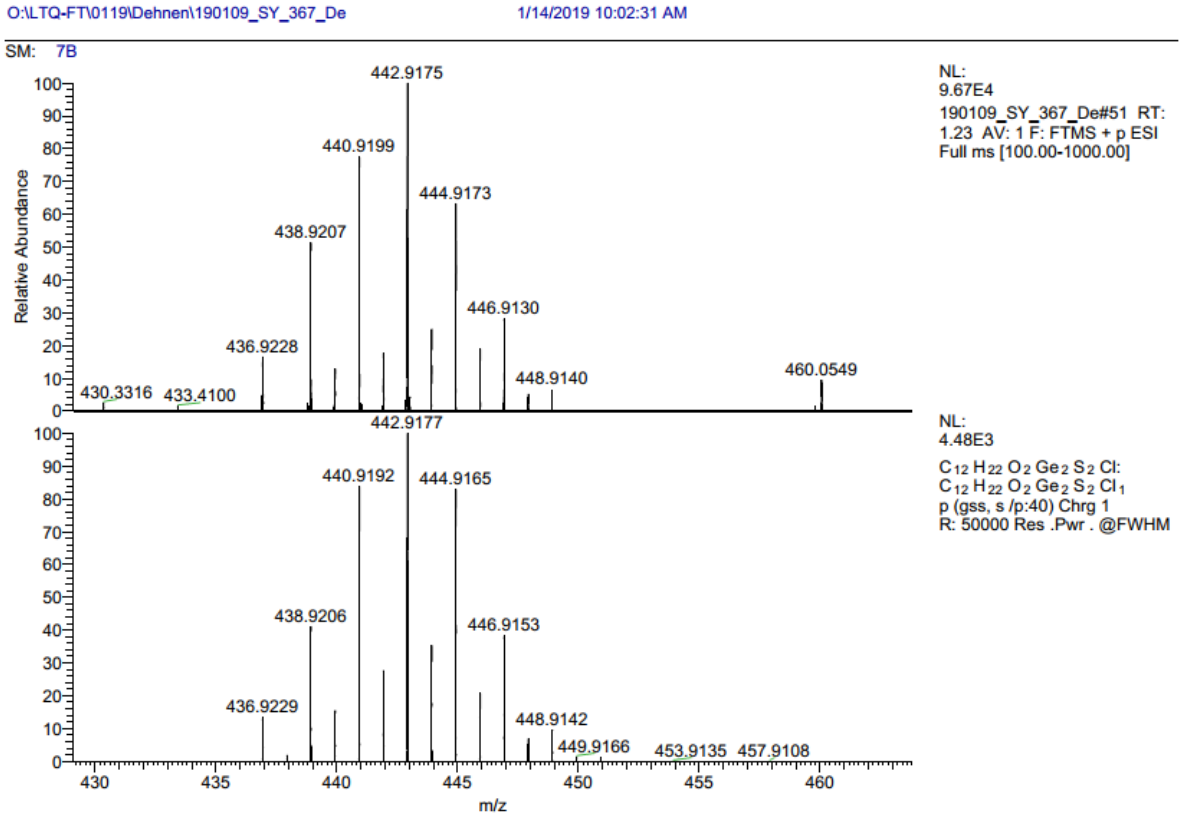

Figure S8: HRMS from the signal at 442.9175 m/z corresponding to the sum formula $[C_{12}H_{22}O_2Ge_2S_2Cl]^+$.

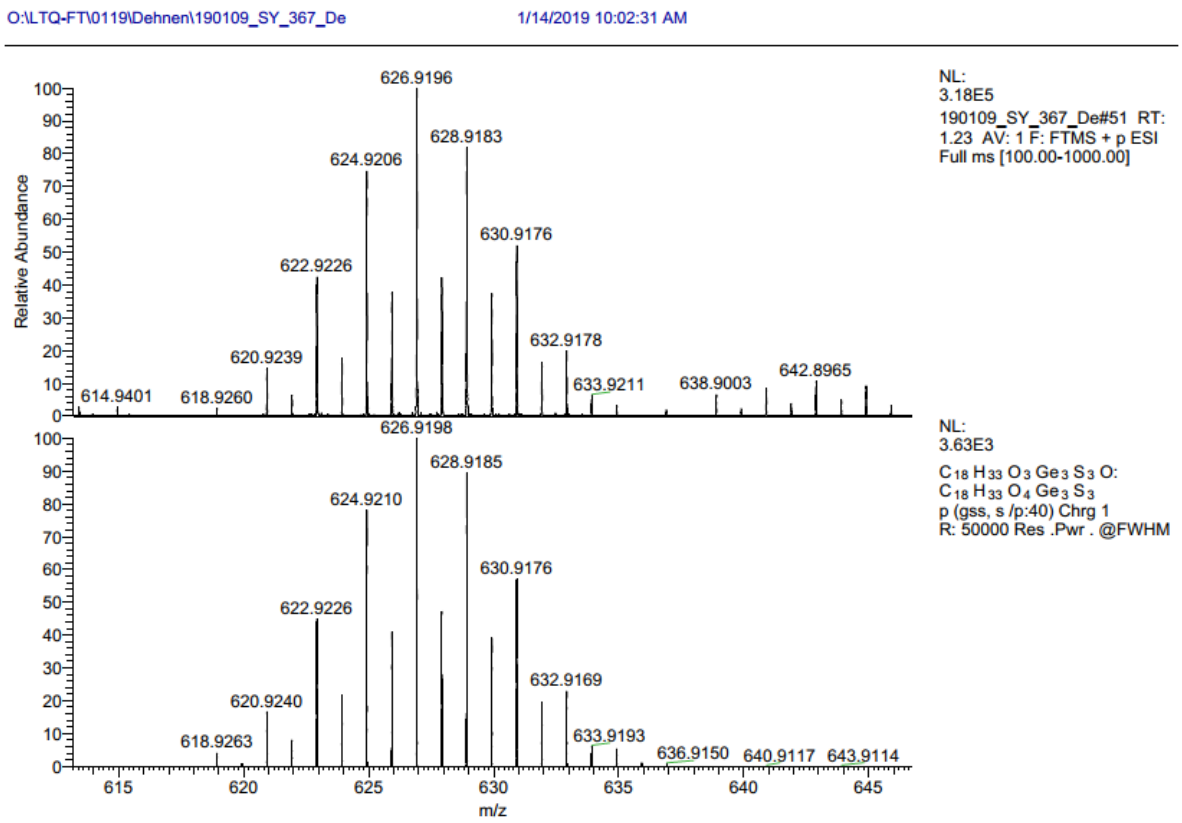

Figure S9: HRMS from the signal at 626.9196 m/z corresponding to the sum formula $[C_{18}H_{33}O_3Ge_3S_3O]^+$, formed by hydrolysis of **1** due to water traces in the mass spectrometer.

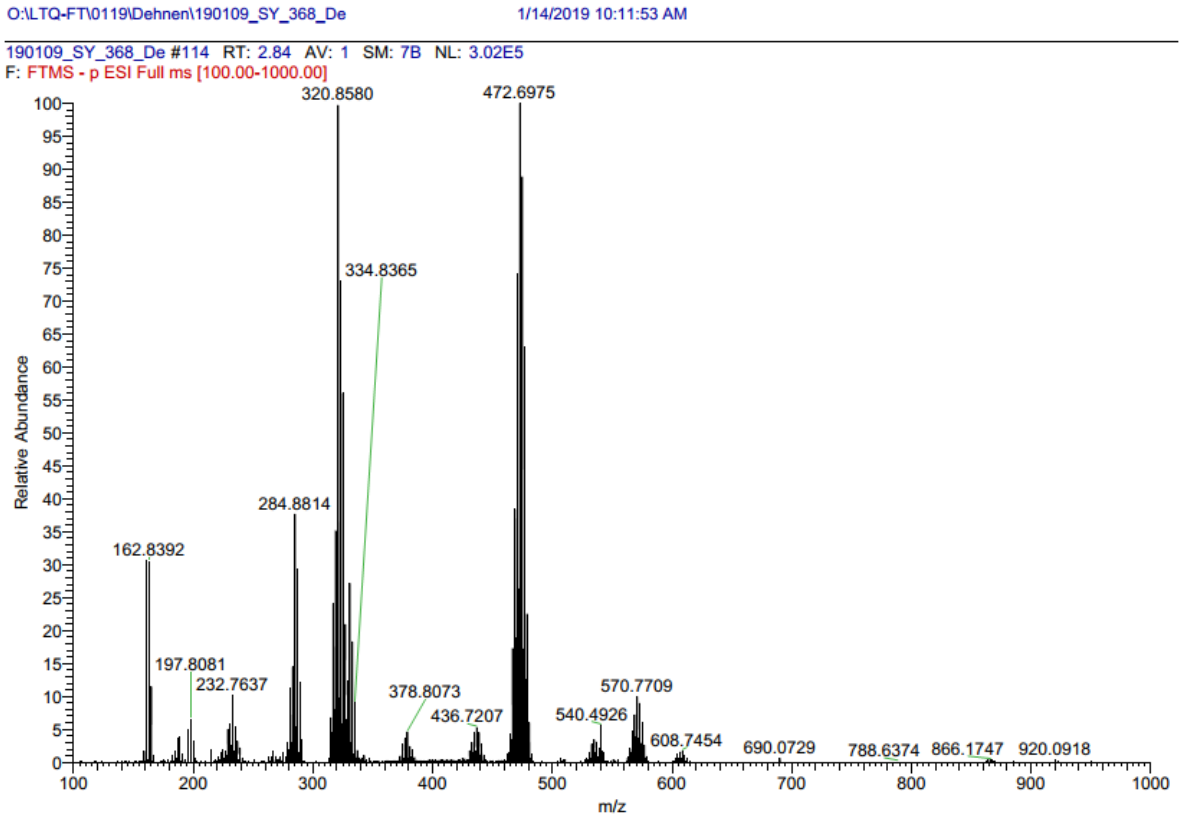

Figure S10: ESI(-) mass spectrum of **2**.

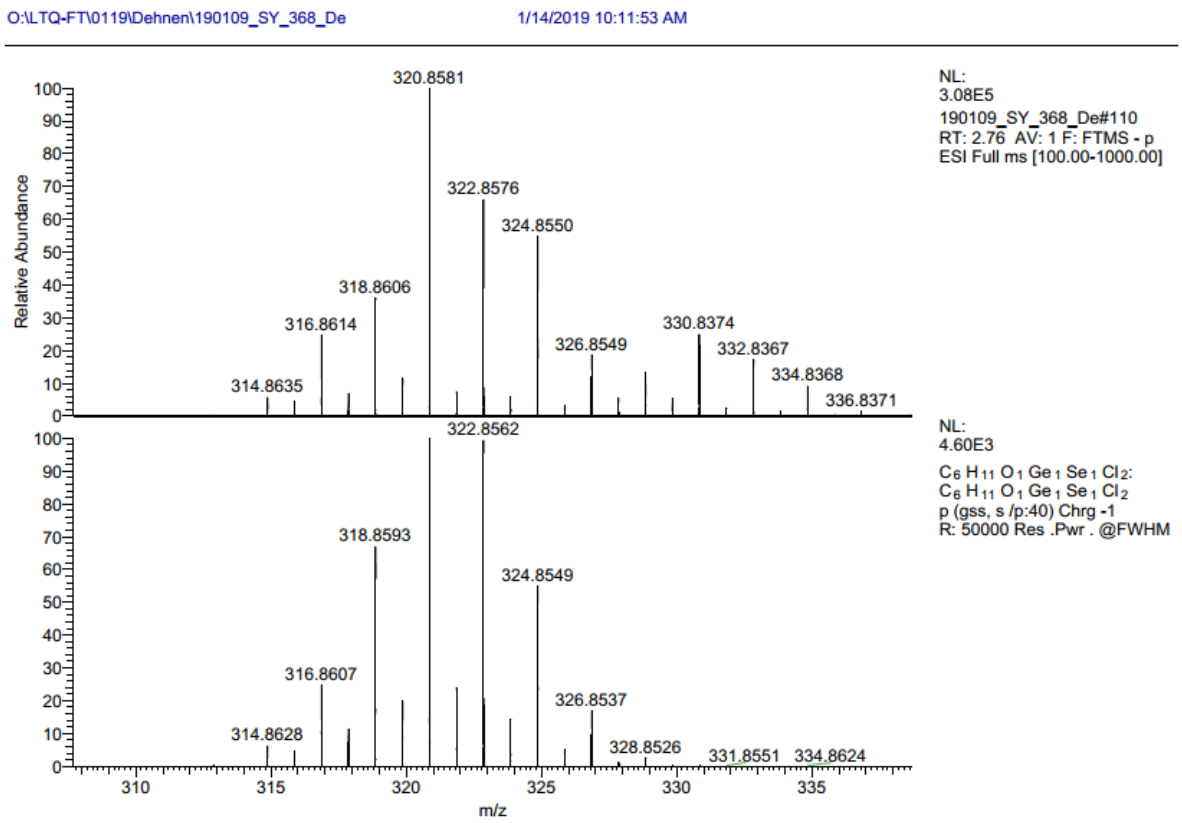

Figure S11: HRMS from the signal at 320.8581 m/z corresponding to the sum formula $[C_6H_{11}O_1Ge1Se_1Cl_2]^-$.

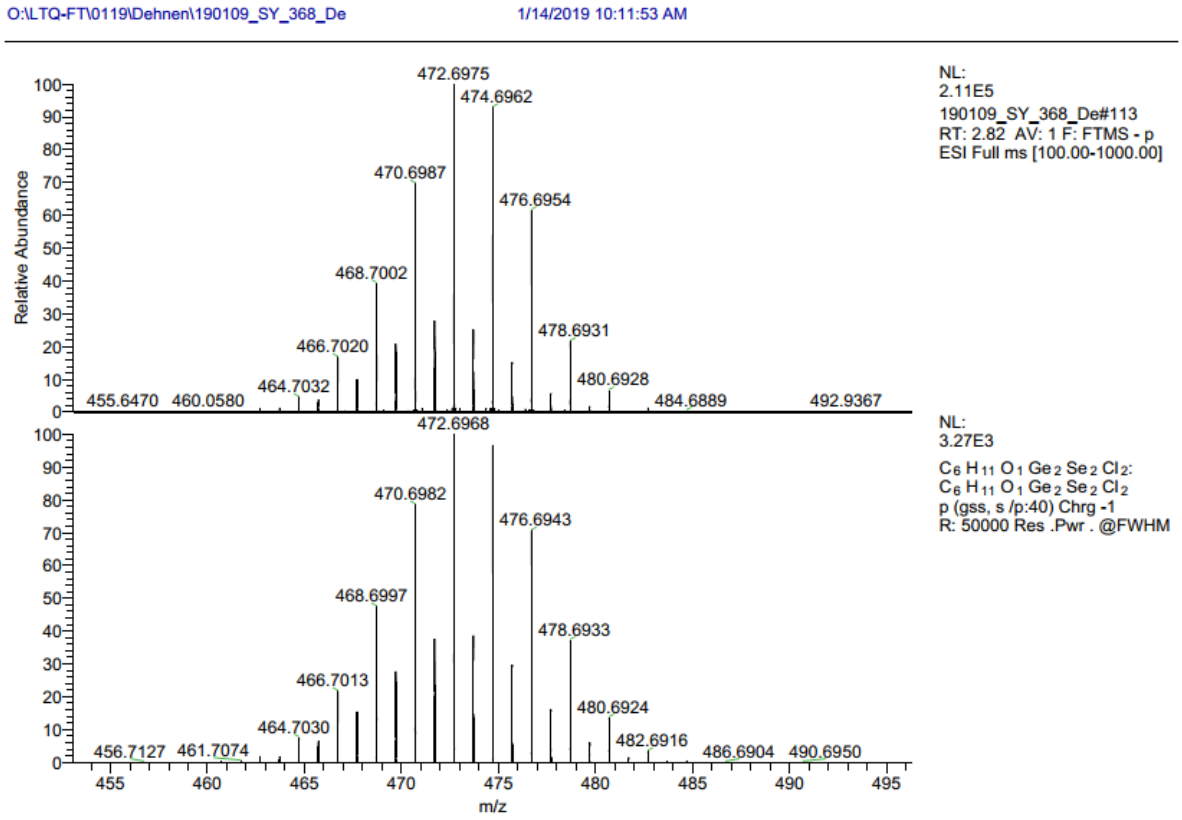

Figure S12: HRMS from the signal at 472.6975 m/z corresponding to the sum formula $[C_6H_{11}O_1Ge_2Se_2Cl_2]^-$.

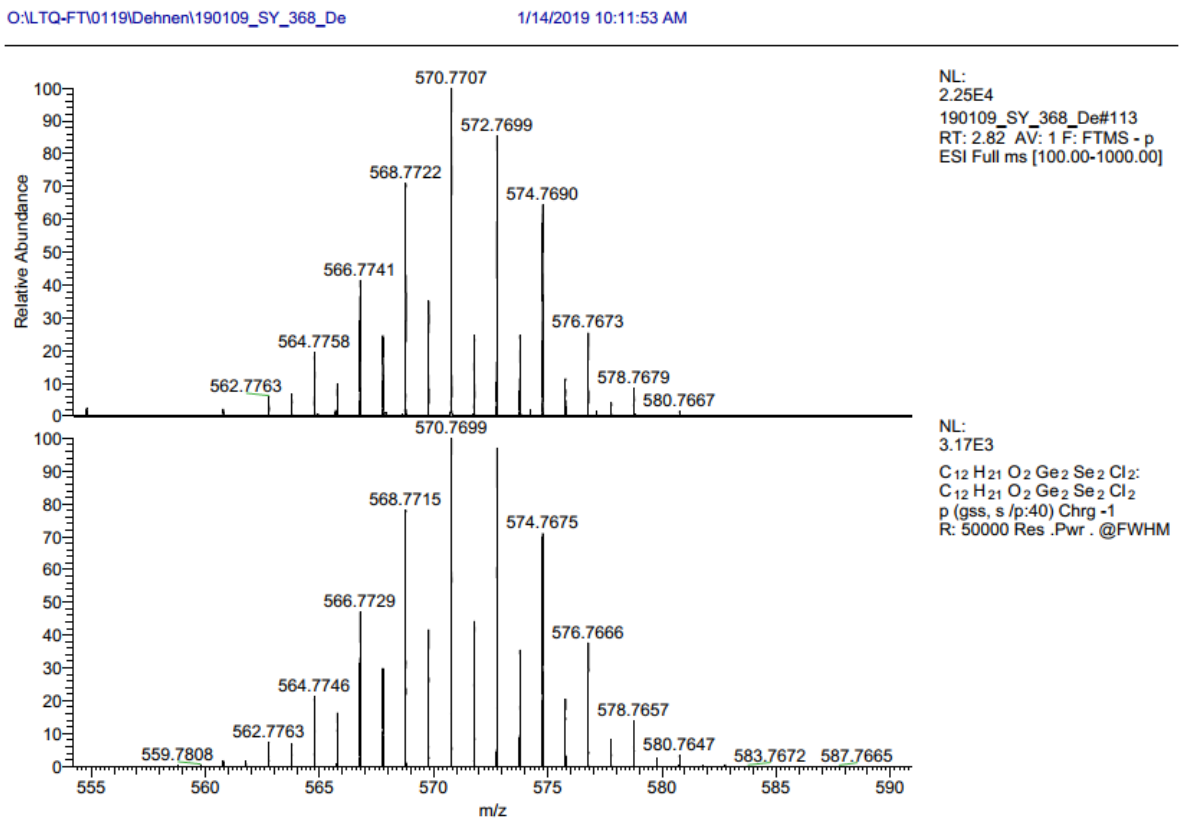

Figure S13: HRMS from the signal at 570.7707 m/z corresponding to the sum formula $[C_{12}H_{21}O_2Ge_2Se_2Cl_2]^-$.

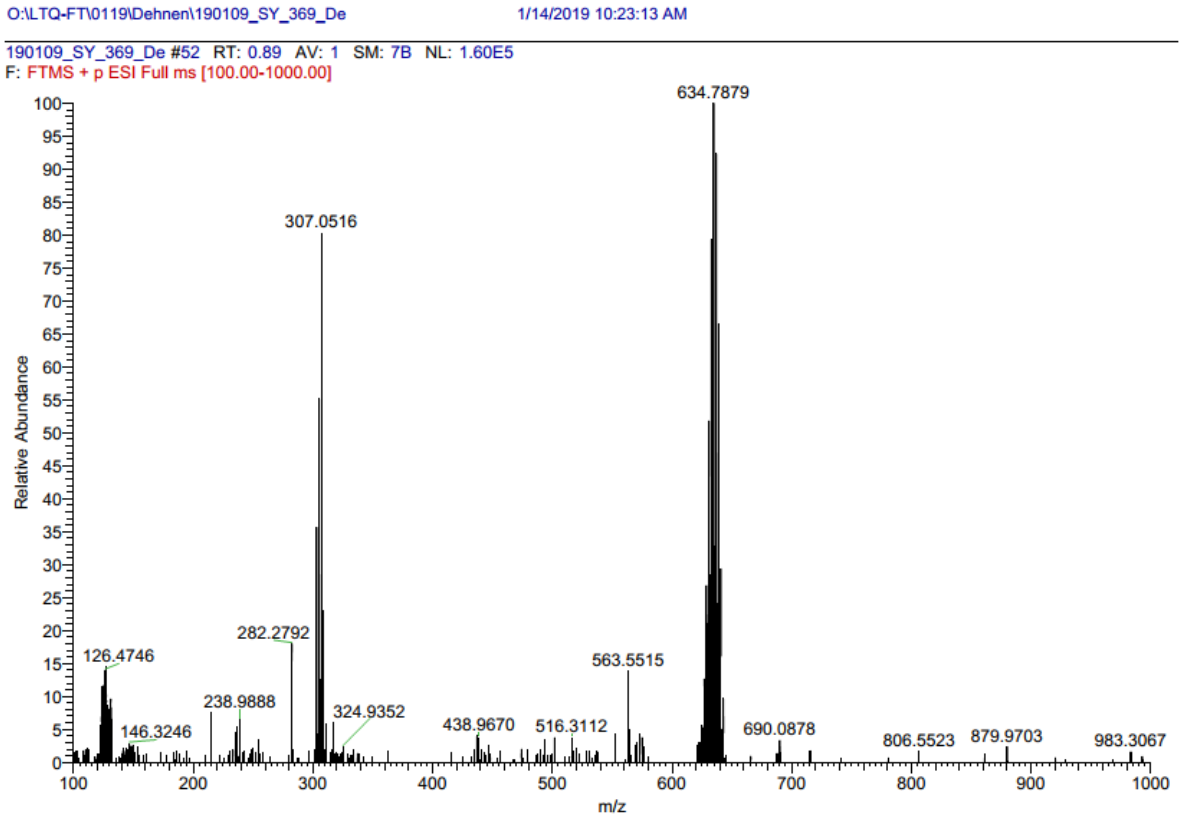

Figure S14: ESI(+) mass spectrum of **3**.

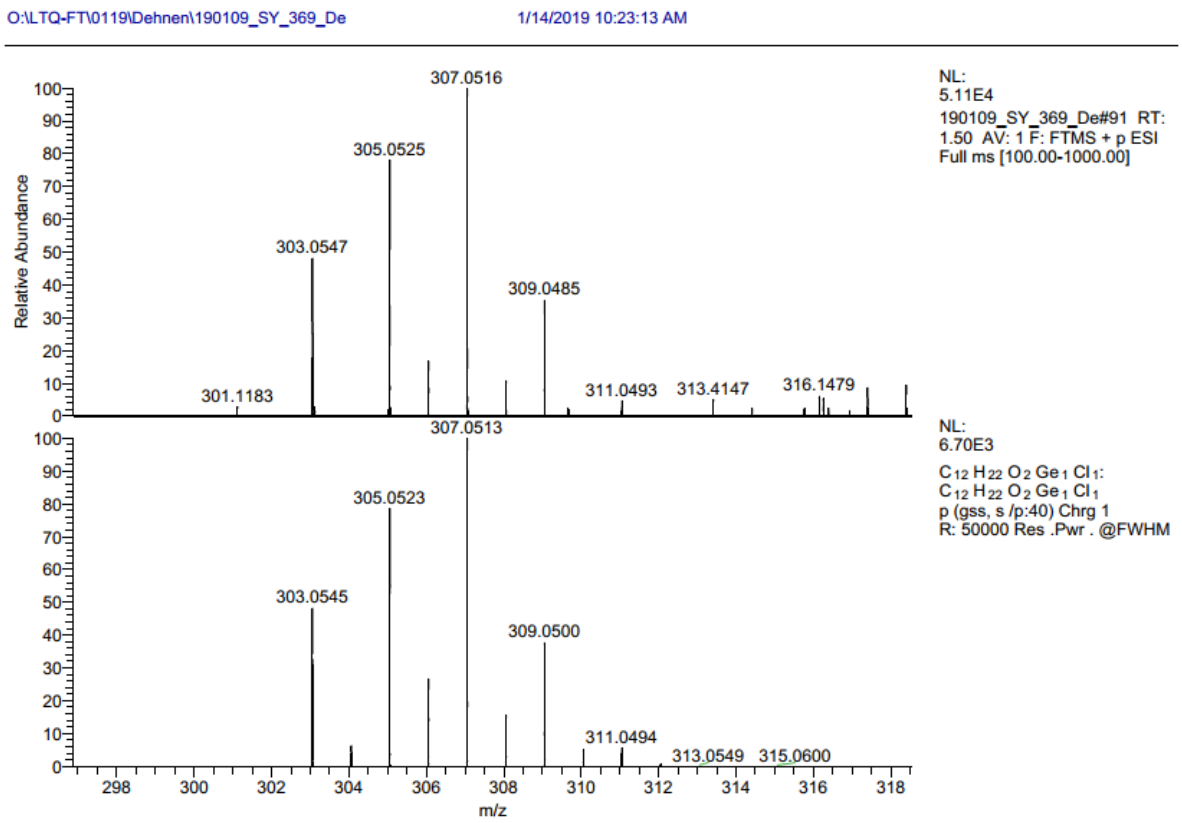

Figure S15: HRMS from the signal at 307.0516 m/z corresponding to the sum formula $[C_{12}H_{22}O_2Ge1Cl_1]^+$.

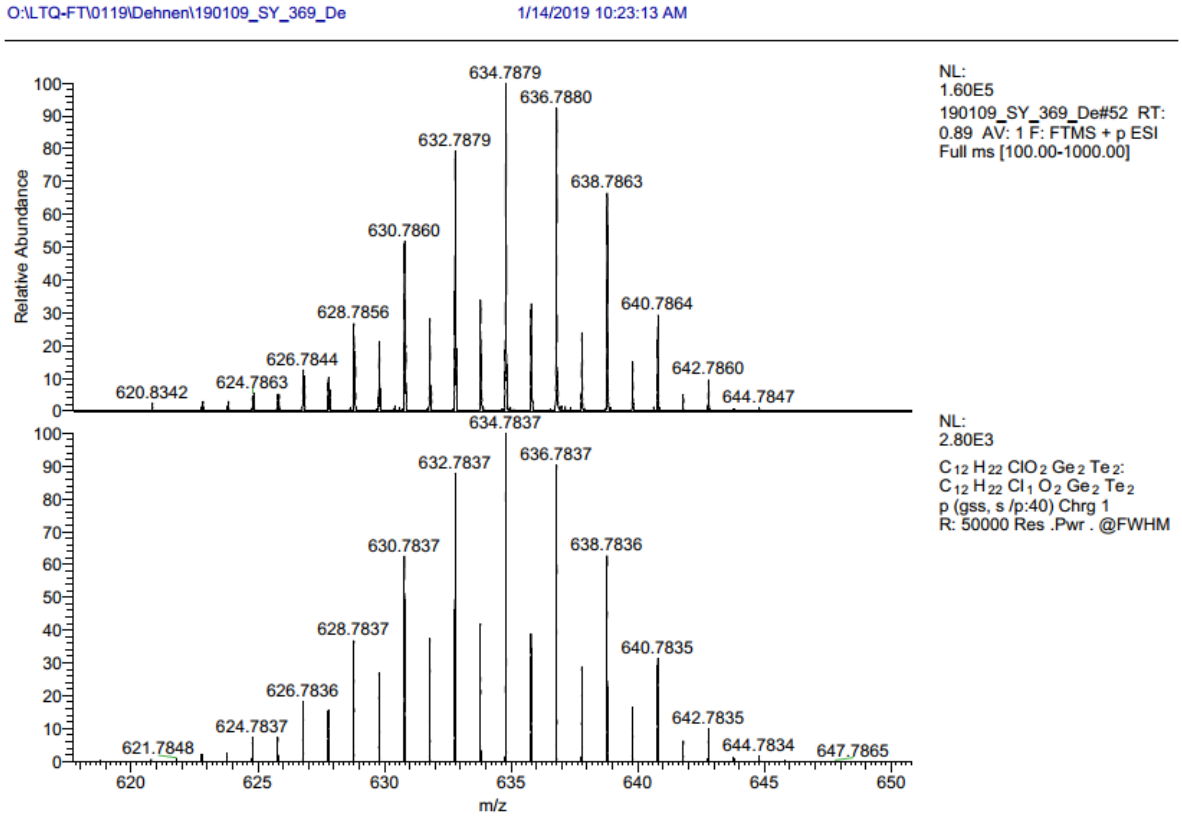

Figure S16: HRMS from the signal at 634.7879 m/z corresponding to the sum formula $[C_{12}H_{21}O_2Ge_2Te_2Cl]^+$.

3. IR spectra

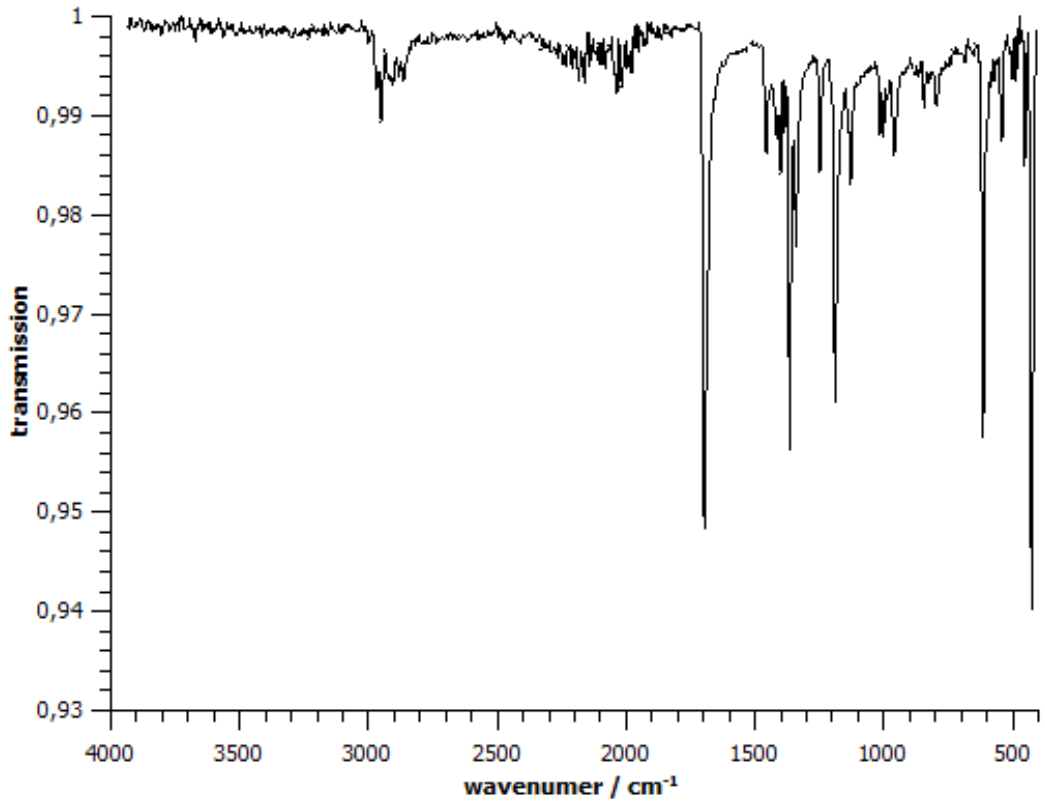

Figure S17: IR spectrum of **1**.

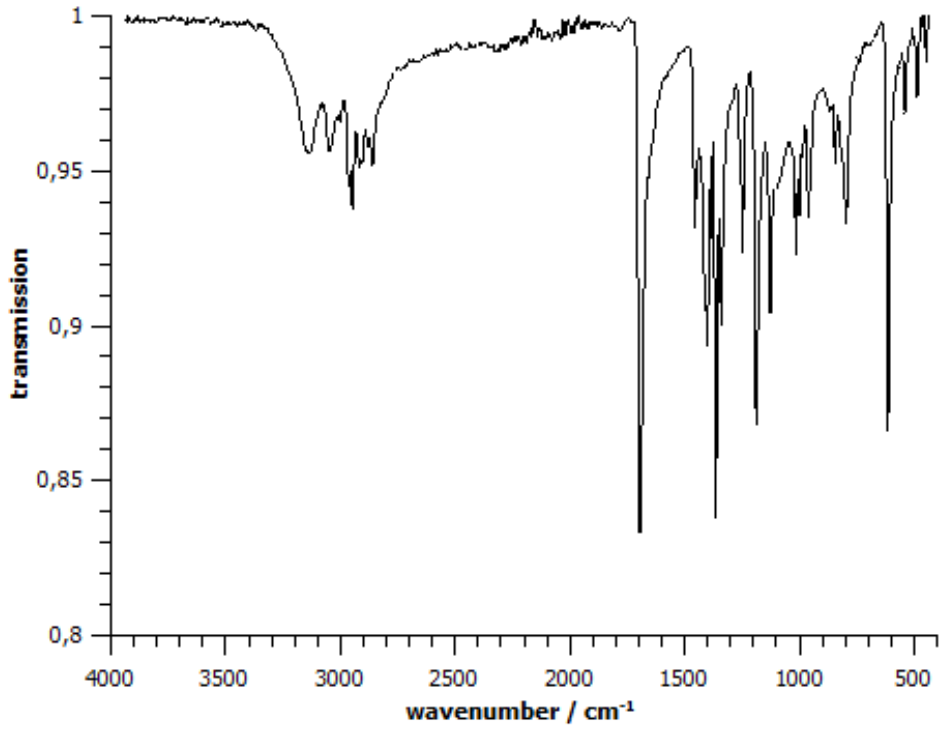

Figure S18: IR spectrum of **2**.

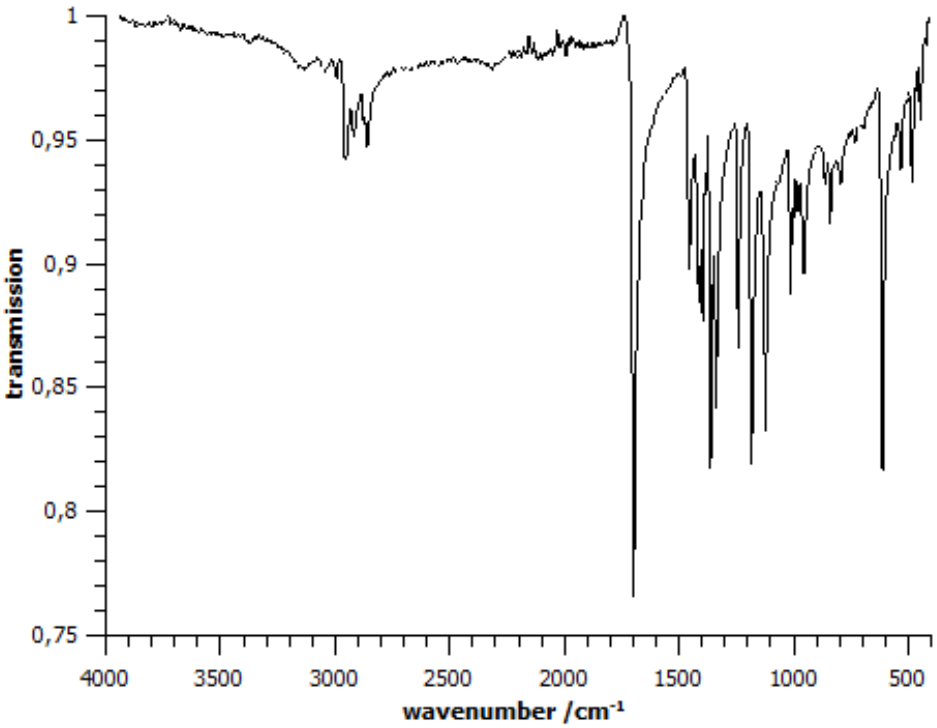

Figure S19: IR spectrum of **3**.

4. Solution UV-Vis Spectra

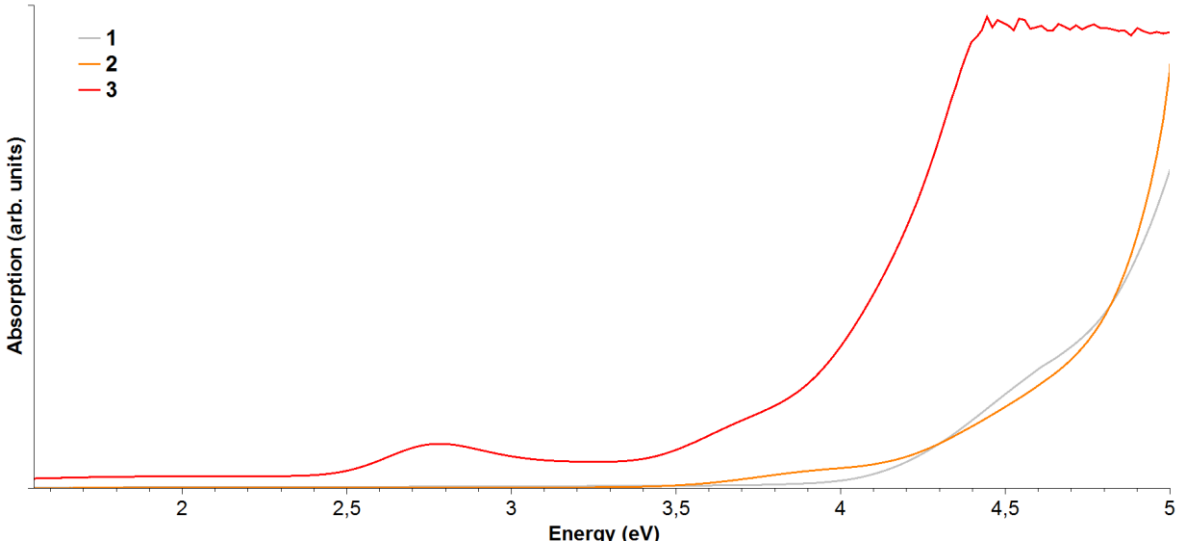

Figure S20: UV-Vis spectra of compounds **1**–**3**. The spectra were recorded in dichloromethane solutions (c = 2 mg/mL).

5. Single-crystal X-ray Crystallography of Compound 1

Compound **1** crystallizes as colorless blocks. Data of the X-Ray diffraction analyses were collected on a STOE IPDS 2T imaging plate diffractometer using $Mo_{K\alpha}$ radiation with graphite monochromatization (λ = 0.71073 Å) at 100 K. Reflection data were processed with X-Area 1.77.[1] Structure solution was performed by direct methods and full-matrix-least-squares refinement against F^2 using SHELXT[2] and SHELXL-2014[3] software. All non-hydrogen atoms were refined anisotropically, hydrogen atom positions were calculated.

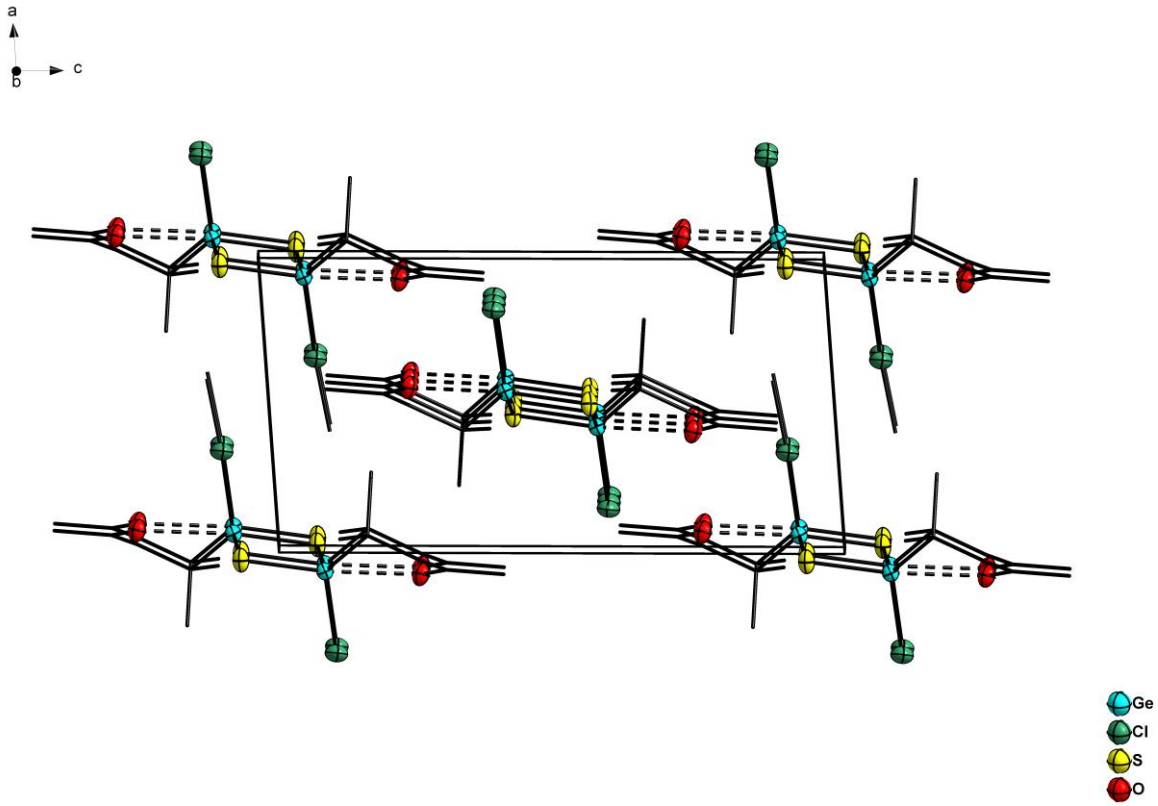

Figure S21: View of the crystal structure of **1** along the *b* axis.

Table S1: Crystal data and structure refinement for **1**.

Empirical formula	$C_{12}H_{22}Cl_2Ge_2O_2S_2$	
Formula weight	478.49	
Temperature	100(2) K	
Wavelength	0.71073 Å	
Crystal system	Monoclinic	
Space group	$P2_1/n$	
Unit cell dimensions	a = 7.6877(2) Å	α= 90°.
	b = 8.3778(3) Å	β= 94.275(2)°
	c = 14.7178(4) Å	γ = 90°.
Volume	945.28(5) $Å^3$	
Z	2	
Density (calculated)	1.681 Mg/m^3	
Absorption coefficient	3.681 mm^{-1}	
F(000)	480	
Crystal size	0.34 x 0.22 x 0.12 mm^3	
Theta range for data collection	2.776 to 30.502°.	
Index ranges	-10<=h<=10, -11<=k<=11, -20<=l<=20	
Reflections collected	21585	
Independent reflections	2873 [R(int) = 0.0735]	
Completeness to theta = 25.242°	100.0 %	
Absorption correction	Integration	
Max. and min. transmission	0.8295 and 0.3167	
Refinement method	Full-matrix least-squares on F^2	
Data / restraints / parameters	2873 / 0 / 99	
Goodness-of-fit on F^2	1.058	
Final R indices [I>2sigma(I)]	R1 = 0.0283, wR2 = 0.0456	
R indices (all data)	R1 = 0.0351, wR2 = 0.0478	
Largest diff. peak and hole	0.489 and -0.300 $e.Å^{-3}$	

Table S2: Atomic coordinates (x 10^4) and equivalent isotropic displacement parameters ($Å^2$x 10^3) for **1**. U(eq) is defined as one third of the trace of the orthogonalized U^{ij} tensor.

	x	y	z	U(eq)
C(1)	5641(2)	2475(2)	6591(1)	20(1)
Ge(1)	4387(1)	4050(1)	5785(1)	17(1)
Ge(2)	5453(16)	3942(11)	5901(7)	16(3)
C(2)	5557(3)	864(2)	6103(1)	30(1)
C(3)	7535(2)	3059(2)	6719(1)	28(1)
C(6)	4308(3)	3903(2)	8945(1)	36(1)
Cl(1)	1605(1)	3813(1)	5888(1)	31(1)
S(1)	5227(1)	6557(1)	5682(1)	23(1)
C(4)	4806(2)	2325(2)	7496(1)	25(1)
C(5)	4454(2)	3897(2)	7940(1)	22(1)
O(1)	4268(2)	5102(1)	7481(1)	26(1)

Table S3: Bond lengths [Å] and angles [°] for **1**.

C(1)-C(4)	1.527(2)	C(4)-C(1)-Ge(1)	111.10(10)
C(1)-C(2)	1.5277(19)	C(2)-C(1)-Ge(1)	107.84(10)
C(1)-C(3)	1.534(2)	C(3)-C(1)-Ge(1)	106.07(10)
C(1)-Ge(2)	1.594(10)	C(1)-Ge(1)-Cl(1)	109.72(5)
C(1)-Ge(1)	1.9768(14)	C(1)-Ge(1)-S(1)	122.99(4)
Ge(1)-Cl(1)	2.1644(4)	Cl(1)-Ge(1)-S(1)	112.839(17)
Ge(1)-S(1)	2.2057(4)	C(1)-Ge(1)-S(1)#1	109.25(4)
Ge(1)-S(1)#1	2.2600(4)	Cl(1)-Ge(1)-S(1)#1	104.315(17)
Ge(2)-S(1)	2.219(10)	S(1)-Ge(1)-S(1)#1	95.089(13)
Ge(2)-S(1)#1	2.386(10)	C(1)-Ge(2)-S(1)	148.9(6)
C(6)-C(5)	1.492(2)	C(1)-Ge(2)-S(1)#1	119.3(5)
C(4)-C(5)	1.503(2)	S(1)-Ge(2)-S(1)#1	91.3(4)
C(5)-O(1)	1.2173(18)	Ge(1)-S(1)-Ge(1)#1	84.911(13)
C(4)-C(1)-C(2)	109.38(12)	Ge(1)-S(1)-Ge(2)#1	81.7(2)
C(4)-C(1)-C(3)	112.08(12)	Ge(1)#1-S(1)-Ge(2)#1	20.3(3)
C(2)-C(1)-C(3)	110.25(13)	C(5)-C(4)-C(1)	114.09(12)
C(4)-C(1)-Ge(2)	126.5(4)	O(1)-C(5)-C(6)	122.20(14)
C(2)-C(1)-Ge(2)	112.5(4)	O(1)-C(5)-C(4)	120.21(13)
C(3)-C(1)-Ge(2)	82.7(4)	C(6)-C(5)-C(4)	117.57(13)

Symmetry transformations used to generate equivalent atoms:

#1 -x+1,-y+1,-z+1

6. Single-crystal X-ray Crystallography of Compound 2

Compound **2** crystallizes as colorless blocks. Data of the X-Ray diffraction analyses were collected on a STOE IPDS 2T imaging plate diffractometer using $Mo_{K\alpha}$ radiation with graphite monochromatization (λ = 0.71073 Å) at 100 K. Reflection data were processed with X-Area 1.77.[1] Structure solution was performed by direct methods and full-matrix-least-squares refinement against F^2 using SHELXT[2] and SHELXL-2014[3] software. All non-hydrogen atoms were refined anisotropically, hydrogen atom positions were calculated.

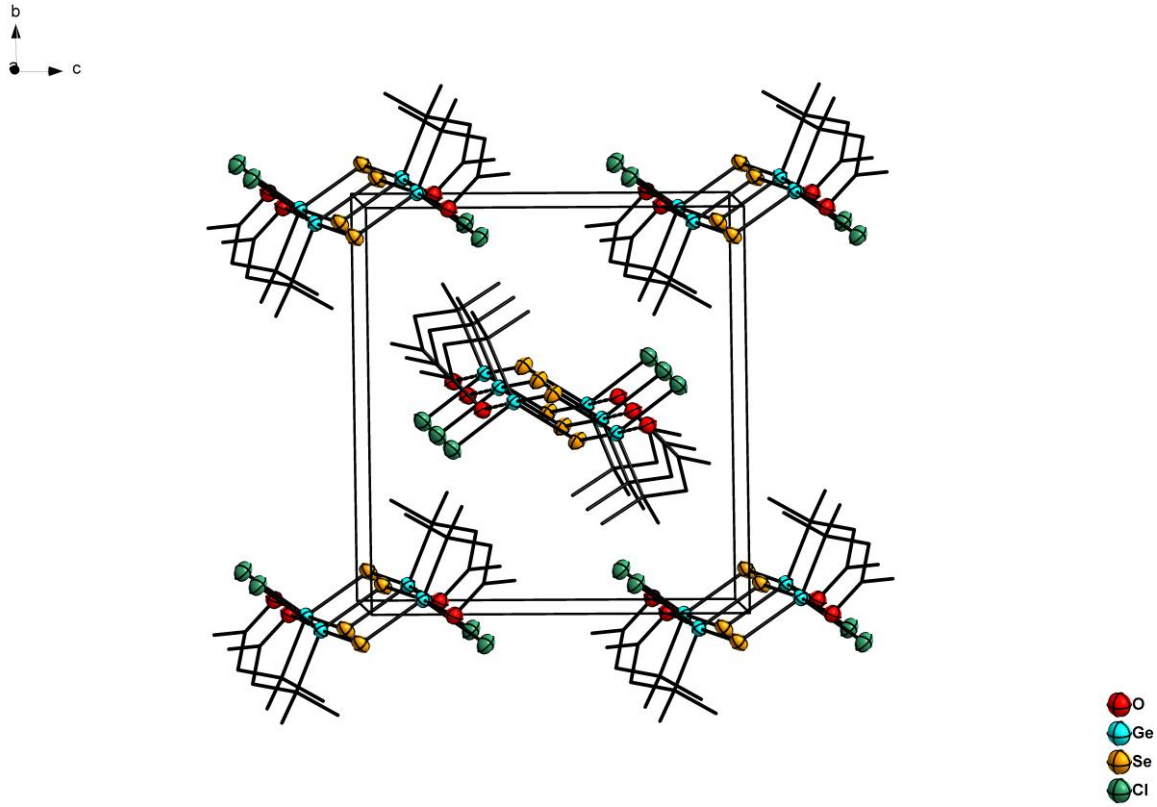

Figure S22: View of the crystal structure of **2** along the *a* axis.

Table S4: Crystal data and structure refinement for **2**.

Empirical formula	$C_{12}H_{22}Cl_2Ge_2O_2Se_2$	
Formula weight	572.29	
Temperature	100(2) K	
Wavelength	0.71073 Å	
Crystal system	Monoclinic	
Space group	$P2_1/n$	
Unit cell dimensions	a = 8.1795(5) Å	α= 90°
	b = 11.2847(6) Å	β= 104.226(5)°
	c = 10.6812(6) Å	γ = 90°
Volume	955.67(10) $Å^3$	
Z	2	
Density (calculated)	1.989 Mg/m^3	
Absorption coefficient	7.231 mm^{-1}	
F(000)	552	
Crystal size	0.22 x 0.17 x 0.11 mm^3	
Theta range for data collection	2.670 to 26.731°.	
Index ranges	-10<=h<=10, -14<=k<=13, -13<=l<=13	
Reflections collected	7041	
Independent reflections	2019 [R(int) = 0.0532]	
Completeness to theta = 25.242°	99.5 %	
Absorption correction	Integration	
Max. and min. transmission	0.3910 and 0.2254	
Refinement method	Full-matrix least-squares on F^2	
Data / restraints / parameters	2019 / 0 / 94	
Goodness-of-fit on F^2	1.070	
Final R indices [I>2sigma(I)]	R1 = 0.0236, wR2 = 0.0544	
R indices (all data)	R1 = 0.0281, wR2 = 0.0557	
Largest diff. peak and hole	0.500 and -0.637 $e.Å^{-3}$	

Table S5: Atomic coordinates (x 10^4) and equivalent isotropic displacement parameters ($Å^2$x 10^3) for **2**. U(eq) is defined as one third of the trace of the orthogonalized U^{ij} tensor.

	x	y	z	U(eq)
C(1)	4089(3)	3078(2)	6992(2)	22(1)
C(2)	2888(3)	2464(2)	5855(3)	25(1)
C(3)	5723(3)	2379(2)	7447(3)	27(1)
C(4)	3255(3)	3252(2)	8109(3)	24(1)
C(5)	1829(3)	4136(2)	7848(3)	23(1)
C(6)	535(3)	4016(3)	8621(3)	33(1)
O(1)	1769(2)	4914(2)	7057(2)	26(1)
Ge(1)	4700(1)	4620(1)	6339(1)	20(1)
Se(1)	2971(1)	5642(1)	4611(1)	24(1)
Cl(1)	5659(1)	5755(1)	8029(1)	29(1)

Table S6: Bond lengths [Å] and angles [°] for **2**.

C(1)-C(4)	1.525(3)	C(5)-C(4)-C(1)	114.5(2)
C(1)-C(3)	1.525(3)	O(1)-C(5)-C(6)	122.4(2)
C(1)-C(2)	1.528(4)	O(1)-C(5)-C(4)	120.4(2)
C(1)-Ge(1)	1.984(2)	C(6)-C(5)-C(4)	117.2(2)
C(4)-C(5)	1.508(3)	C(1)-Ge(1)-Cl(1)	107.02(8)
C(5)-O(1)	1.212(3)	C(1)-Ge(1)-Se(1)	123.73(7)
C(5)-C(6)	1.500(3)	Cl(1)-Ge(1)-Se(1)	112.73(2)
Ge(1)-Cl(1)	2.1951(7)	C(1)-Ge(1)-Se(1)#1	109.70(7)
Ge(1)-Se(1)	2.3354(4)	Cl(1)-Ge(1)-Se(1)#1	105.11(2)
Ge(1)-Se(1)#1	2.3866(3)	Se(1)-Ge(1)-Se(1)#1	96.696(13)
C(4)-C(1)-C(3)	110.0(2)	Ge(1)-Se(1)-Ge(1)#1	83.304(13)
C(4)-C(1)-C(2)	110.9(2)	Symmetry transformations used to generate equivalent atoms:	
C(3)-C(1)-C(2)	111.1(2)	#1 -x+1,-y+1,-z+1	
C(4)-C(1)-Ge(1)	111.23(16)		
C(3)-C(1)-Ge(1)	106.79(16)		
C(2)-C(1)-Ge(1)	106.67(16)		

7. Single-crystal X-ray Crystallography of Compound 3

Compound **3** crystallizes in the shape of orange blocks. Data of the X-Ray diffraction analysis was collected on a STOE STADIVARI diffractometer using Cu K_α radiation (λ = 1.54186 Å) from an X-ray micro source with X-ray optics and a Pilatus 300K Si hybrid pixel array detector at 100 K. Reflection data were processed with X-Area 1.77.[1] Structure solution was performed by direct methods and full-matrix-least-squares refinement against F^2 using SHELXT[2] and SHELXL-2014[3] software. All non-hydrogen atoms were refined anisotropically, hydrogen atom positions were calculated.

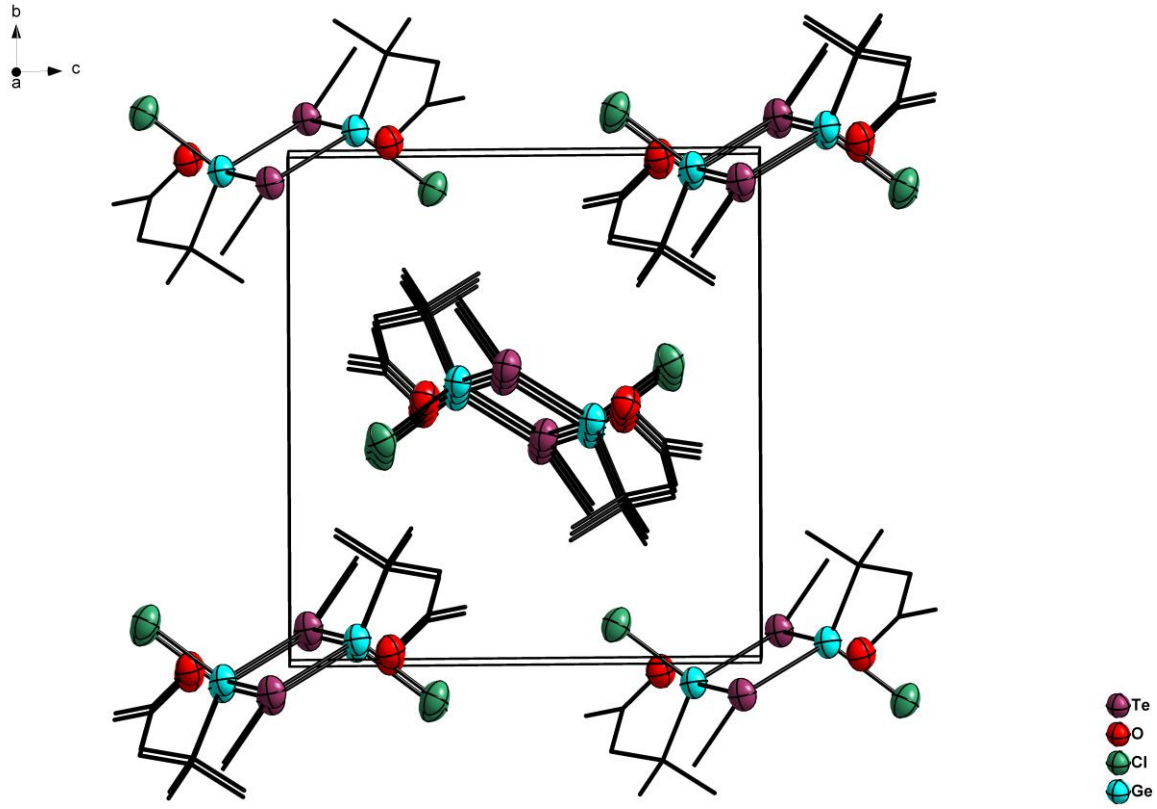

Figure S23: View of the crystal structure of **3** along the *a* axis.

Table S7: Crystal data and structure refinement for **3**.

Empirical formula	$C_{12}H_{22}Cl_2Ge_2O_2Te_2$	
Formula weight	669.57	
Temperature	100(2) K	
Wavelength	1.54178 Å	
Crystal system	Monoclinic	
Space group	$P2_1/n$	
Unit cell dimensions	a = 8.2073(3) Å	α= 90°
	b = 11.4851(4) Å	β= 104.500(3)°
	c = 10.9961(4) Å	γ = 90°
Volume	1003.50(6) $Å^3$	
Z	2	
Density (calculated)	2.216 Mg/m^3	
Absorption coefficient	28.612 mm^{-1}	
F(000)	624	
Crystal size	0.1 x 0.1 x 0.1 mm^3	
Theta range for data collection	5.666 to 74.860°	
Index ranges	-10<=h<=9, -14<=k<=14, -11<=l<=13	
Reflections collected	2037	
Independent reflections	2037 [R(int) = 0.0301]	
Completeness to theta = 25.242°	99.7 %	
Absorption correction	Sphere	
Max. and min. transmission	0.25191 and 0.0000	
Refinement method	Full-matrix least-squares on F^2	
Data / restraints / parameters	2037 / 0 / 95	
Goodness-of-fit on F^2	1.404	
Final R indices [I>2sigma(I)]	R1 = 0.0539, wR2 = 0.1564	
R indices (all data)	R1 = 0.0596, wR2 = 0.1692	
Largest diff. peak and hole	1.946 and -2.747 $e.Å^{-3}$	

Table S8: Atomic coordinates (x 10^4) and equivalent isotropic displacement parameters ($Å^2$x 10^3) for **3**. U(eq) is defined as one third of the trace of the orthogonalized U^{ij} tensor.

	x	y	z	U(eq)
Te(01)	2748(1)	4347(1)	4601(1)	31(1)
Ge(02)	4756(1)	5383(1)	6421(1)	29(1)
Cl(03)	5670(3)	4240(2)	8063(2)	39(1)
O(004)	1739(7)	5111(5)	7119(5)	38(1)
C(005)	623(11)	5960(9)	8695(9)	44(2)
C(006)	5780(10)	7575(8)	7576(8)	41(2)
C(007)	1883(9)	5838(7)	7922(8)	31(2)
C(008)	2969(10)	7528(7)	5989(7)	35(2)
C(009)	4112(9)	6890(7)	7086(7)	32(2)
C(00A)	3308(9)	6700(7)	8176(7)	34(2)

Table S9: Bond lengths [Å] and angles [°] for **3**.

Te(01)-Ge(02)	2.5466(9)	Te(01)-Ge(02)-Te(01)#1	98.13(3)
Te(01)-Ge(02)#1	2.5896(10)	O(004)-C(007)-C(005)	121.8(8)
Ge(02)-C(009)	2.001(8)	O(004)-C(007)-C(00A)	121.6(7)
Ge(02)-Cl(03)	2.207(2)	C(005)-C(007)-C(00A)	116.5(7)
O(004)-C(007)	1.199(10)	C(008)-C(009)-C(00A)	113.0(6)
C(005)-C(007)	1.501(11)	C(008)-C(009)-C(006)	110.3(7)
C(006)-C(009)	1.553(10)	C(00A)-C(009)-C(006)	108.5(6)
C(007)-C(00A)	1.505(10)	C(008)-C(009)-Ge(02)	107.1(5)
C(008)-C(009)	1.518(10)	C(00A)-C(009)-Ge(02)	111.7(6)
C(009)-C(00A)	1.522(11)	C(006)-C(009)-Ge(02)	105.9(5)
Ge(02)-Te(01)-Ge(02)#1	81.87(3)	C(007)-C(00A)-C(009)	114.7(7)
C(009)-Ge(02)-Cl(03)	106.4(2)	Symmetry transformations used to generate equivalent atoms:	
C(009)-Ge(02)-Te(01)	120.9(2)	#1 -x+1,-y+1,-z+1	
Cl(03)-Ge(02)-Te(01)	112.68(7)		
C(009)-Ge(02)-Te(01)#1	111.4(2)		
Cl(03)-Ge(02)-Te(01)#1	106.38(7)		

7. References for the Supporting Information

[1] Stoe and Cie GmbH, *X-Area*, *Version 1.77*, 2016.

[2] G. M. Sheldrick, *Acta Crystallogr*. *A*, 2015, **71**, 3.

[3] C. B. Hübschle, G. M. Sheldrick, B. Dittrich, *J. Appl. Cryst.*, 2011, 1281.

5 Zusammenfassung

Im Rahmen dieser Dissertation wurden die in der Zielsetzung vorgestellten drei Teilprojekte bearbeitet, die in Schema 10 nochmals zusammengefasst sind.

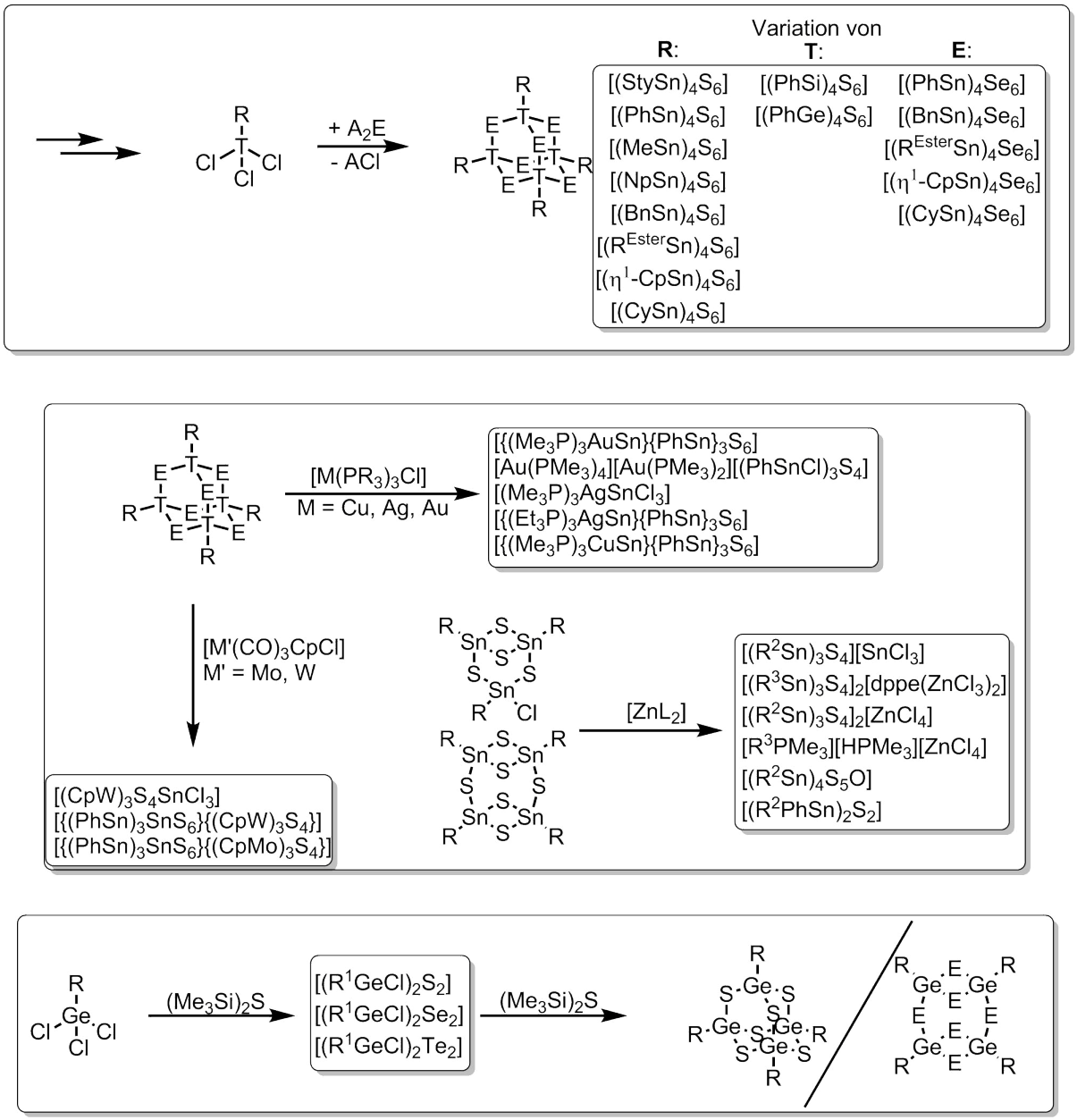

Schema 10: Übersicht über alle im Rahmen der einzelnen Teilprojekte untersuchten Verbindungen ($R^{Ester} = C_2H_4(C_6H_4)CO_2Et$).

Im ersten Teilprojekt wurde die erstmals an $[(StySn)_4S_6]$ beobachtete Weißlichtemission an Organotetrelchalkogenidclustern mit adamantanartiger Struktur näher untersucht. Hierzu wurde vor allem die Substanzbibliothek deutlich erweitert, um durch systematische Variation sowohl der Kernzusammensetzung als auch der organischen Substituenten zu

analysieren, welche Voraussetzungen die Clusterverbindungen für den Effekt mitbringen müssen, um den zugrunde liegenden Mechanismus weiter zu erforschen, und um zu testen, ob und wie sich die Emissionsspektren gezielt modifizieren lassen. In einer ersten Arbeit konnte durch Variation des Tetrelelements sowie der Substituenten gezeigt werden, dass die Amorphizität der Verbindungen Grundvoraussetzung für die Weißlichtemission ist, da andernfalls phasengleiche Emission in Form einer Frequenzverdopplung auftritt. Durch weitere Variation der organischen Substituenten und Substitution der Schwefelatome im anorganischen Kern durch Selenatome wurde weiterhin festgestellt, dass - anders als anfangs angenommen - kein π-Elektronensystem, sondern lediglich ein cyclischer organischer Substituent erforderlich ist. Weiterhin deuten die neuen Untersuchungen darauf hin, dass die Emission durch das HOMO-LUMO-Gap der Verbindung limitiert wird, wodurch ausgeschlossen werden kann, dass es sich um eine Anregung in reale elektronische Zustände handelt. Der beobachtete Effekt ist stattdessen als Anregung in extrem kurzlebige virtuelle Zustände, die innerhalb des Gaps liegen, zu verstehen.

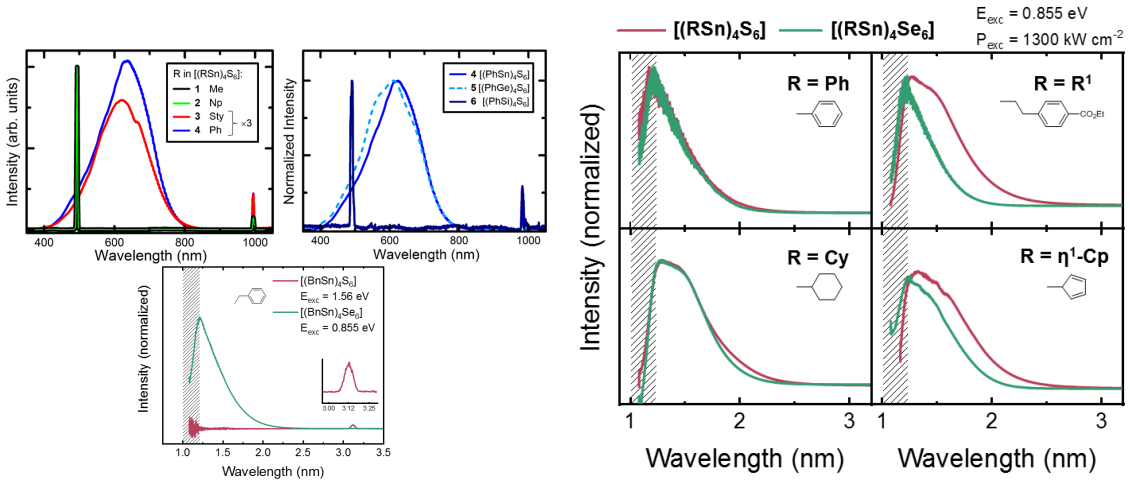

Abbildung 27: Emissionsspektren der untersuchten Verbindungen.

Im zweiten Teilprojekt wurde die Reaktivität von $[(PhSn)_4S_6]$ gegenüber Übergangsmetallkomplexen untersucht, wobei verschiedene ternärer Cluster erhalten werden konnten. In Umsetzungen mit Münzmetallkomplexen mit sterisch wenig anspruchsvollen Phosphanliganden wurden Cluster synthetisiert, bei denen das anorganische Grundgerüst des Edukts erhalten bleibt, während einer der Phenylreste in einer Redoxreaktion durch ein Münzmetall-Komplexfragment substituiert wird. Die so erhaltenen Cluster haben die Zusammensetzung $[\{(R_3P)_3MSn\}\{PhSn\}_3S_6]$ (M/R = Cu/Me, Ag/Et, Au/Me). Bei Verwendung des sterisch anspruchsvolleren Phosphanliganden PPh_3 kommt es hingegen zur Zersetzung des Organozinnsulfidclusters und anschließendem Aufbau eines größeren ternären Clusters der Zusammensetzung $[(CuPPh_3)_4(PhSn)_{18}Cu_6S_{31}Cl_2]$, bei dem es sich um den

ersten Cluster mit ternärem Grundgerüst handelt, der ohne Zusatz einer zusätzlichen Sulfidquelle erhalten wurde. Wahlweise durch Oxidation der Reaktionslösung mit Luftsauerstoff oder durch gezielten Einsatz von $[Cu(PPh_3)_2Cl_2]$ wurde zudem mit $[\{Cu(PPh_3)_2\}(PhSn)_3(SnCl)S_8]$ der erste ternäre Cu/Sn/S-Cluster erhalten, in dem die Kupferatome in der Oxidationsstufe +II vorliegen.

Bei der Übertragung der mit Münzmetallkomplexen durchgeführten Ligandenaustauschreaktionen auf Komplexe der Gruppe 6 konnten Cluster der Zusammensetzung $[\{(PhSn)_3SnS_6\}\{(CpM)_3S_4\}]$ (M = Mo, W) dargestellt werden, bei denen ein Phenylsubstituent des adamantanartigen Organozinnsulfidclusters durch einen Thiowolframat- oder Thiomolybdat-Käfig substituiert wurde. Die Thiometallat-Käfige entsprechen dabei minimalen Ausschnitten aus einer MoS_2- bzw. WS_2-Schicht, womit die Verbindungen als molekulare Modellsysteme für die Adsorption von Organozinnsulfidclustern auf entsprechenden Oberflächen betrachtet werden können. Die Bindungssituation in den Molekülen wurde durch DFT-Rechnungen untersucht, was eine gemischtvalente Situation und die Ausbildung einer ungewöhnlichen 2-Elektronen-4-Zentren-Bindung zwischen den genannten Untereinheiten zutage brachte.

Neben diesen ternären Clustern, deren Synthesen stets ausgehend von $[(PhSn)_4S_6]$ erfolgten, wurde die Reaktivität der bereits zuvor intensiv untersuchten Cluster $[(R^1Sn)_3S_4Cl]$ und $[(R^1Sn)_4S_6]$ gegenüber verschiedenen Zinkverbindungen untersucht. Dabei konnte kein ternärer Cluster mit Zink isoliert werden, jedoch wurden verschiedene Salze des defektheterokubanartigen $[(RSn)_3S_4]^+$-Kations mit Chlorostannat- und Chlorozinkat-Anionen erhalten. Zudem wurde durch Hydrolyse von $[(R^2Sn)_4S_6]$ mit *in situ* entstandenem $[ZnCl_2(H_2O)_2]$ der erste gemischte Oxid-/Sulfid-Cluster mit adamantanartiger Struktur, $[(R^2Sn)_4S_5O]$, erhalten.

Im dritten Teilprojekt wurden durch Umsetzung des Organogermaniumtrichlorids R^1GeCl_3 mit den Bis(trimethylsilylchalkogeniden) die entsprechenden zweikernigen Komplexe $[(R^1GeCl)_2E_2]$ (E = S, Se, Te) erhalten, die für das schwere Homologe Zinn bereits bekannt waren. Durch NMR-Titrationsexperimente konnte gezeigt werden, dass die für die Zinnverbindungen bekannten, in der Reaktionskaskade zu größeren Clustern auftretenden Intermediate $[(R^1GeCl_2)_2E]$ und $[(R^1Ge)_3E_4Cl]$ nicht gebildet werden.

6 English Summary

In the framework of this dissertation, the three sub-projects presented in the objective were investigated. The investigated results are summarized in figure 28.

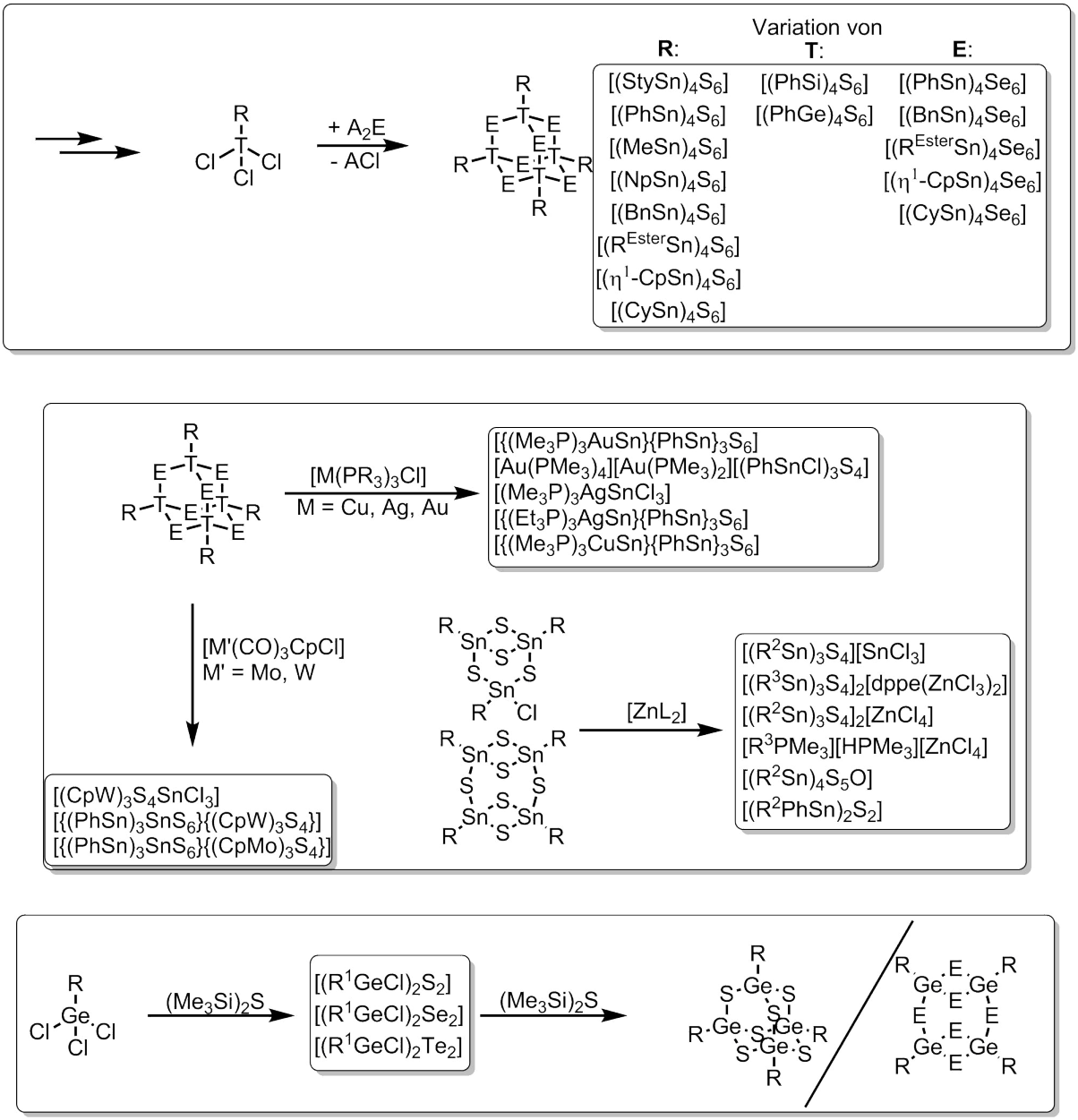

Figure 28: Overview of all compounds that were investigated within the individual sub-projects ($R^{Ester} = C_2H_4(C_6H_4)CO_2Et$).

In the first sub-project, the white light generation (WLG) first observed on $[(StySn)_4S_6]$ for organotetrel chalcogenide clusters with an adamantane-type structure was investigated in more detail. For this purpose, the substance library was significantly extended, in particular in order to analyze necessary prerequisites for the white-light emission. By

systematic variation of both the core composition and the organic substituents the understanding of the underlying mechanism was improved, and possible ways to selectively modify the emission spectra were found. In a first study, it could be shown by varying the tetrel element and the substituents that the amorphicity of the compounds is a basic requirement for the WLG, since otherwise emission occurs in phase as second harmonic generation (SHG). By further variation of the organic substituents and replacement of the sulfur atoms in the inorganic core by selenium atoms, it was further found that - opposing the initial hypothesis - no π electron system, but only a cyclic organic substituent is required, and that the emission seems to be limited by the HOMO-LUMO gap of the compound. By this it can be ruled out that the WLG is caused by an excitation into real electronic states. Instead, the observed effect is to be understood as an excitation into extremely short-lived virtual states that lie within the gap.

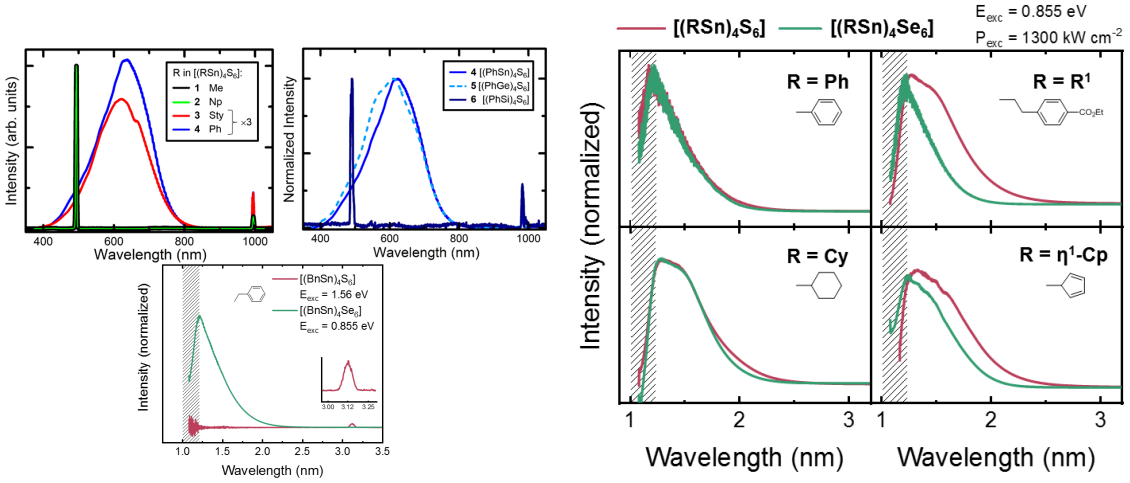

Figure 29: Emission spectra of the investigated compounds.

In the second part of the project, the reactivity of $[(PhSn)_4S_6]$ towards transition metal complexes was investigated, whereby different ternary clusters were obtained. In reactions with coinage metal complexes with sterically less demanding phosphine ligands, clusters were synthesized in which the inorganic core of the starting material is retained and one of the phenyl substituents is replaced with a coinage metal complex fragment. The resulting clusters have the composition $[\{(R_3P)_3MSn\}\{PhSn\}_3S_6]$ (M/R = Cu/Me, Ag/Et, Au/Me). However, by use of the more bulky phosphine ligand PPh_3 the organotin sulfide cluster is decomposed and subsequently rearranged to a larger ternary cluster with the composition $[(CuPPh_3)_4(PhSn)_{18}Cu_6S_{31}Cl_2]$, which is the first cluster with ternary inorganic core which was obtained without an additional source of sulfide. Either by oxidation of this reaction solution or by deliberate use of $[Cu(PPh_3)_2Cl_2]$, the first Cu/Sn/S cluster with copper atoms in the +II oxidation state was obtained.

Transferring the ligand-exchange reactions carried out with coinage metal complexes to Group 6 complexes allowed for the preparation of clusters with the composition $[\{(PhSn)_3SnS_6\}\{(CpM)_3S_4\}]$ (M = Mo, W) in which an adamantane-type organotinsulfide cluster is substituted with a thiotungstate or thiomolybdate cage. The thiometalate cages correspond to sections of a MoS_2 or WS_2 layer, which allows the compounds to be considered as molecular model systems for the adsorption of organotin sulfide clusters on corresponding surfaces. The binding situation in the molecules was rationalized by DFT calculations, which revealed a mixed-valence situation and an unusual two-electron-four-center bond connecting the two subunits of the molecules.
In addition to these ternary clusters, whose syntheses always proceeded from $[(PhSn)_4S_6]$, the reactivity of the already intensely studied clusters $[(R^1Sn)_3S_4Cl]$ and $[(R^1Sn)_4S_6]$ towards various zinc compounds was investigated. It was not possible to isolate any ternary cluster with zinc, but various salts of the defect-heterocubane-type $[(RSn)_3S_4]^+$ cations were obtained with chlorostannate and chlorozincate anions. In addition, hydrolysis of $[(R^2Sn)_4S_6]$ with $[ZnCl_2(H_2O)_2]$ generated *in situ* resulted in the first mixed oxide/sulfide cluster with adamantane-type structure, $[(R^2Sn)_4S_5O]$.
In the third sub-project, reactions of the organogermanium trichloride R^1GeCl_3 with the bis(trimethylsilyl)chalcogenides gave the dinuclear $[(R^1GeCl)_2E_2]$ (E = S, Se, Te) complexes, which were already known for the heavy homologue tin. It was shown by NMR titration experiments that the intermediates in the reaction cascade known for the tin compounds $[((R^1GeCl_2)_2E]$ and $[(R^1Ge)_3E_4Cl]$ are not formed in the case of germanium.

7 Literatur

[1] L. Nicole, C. Laberty-Robert, L. Rozes, C. Sanchez, *Nanoscale* **2014**, *6*, 6267–6292.

[2] M. Zhong, Z. Yang, Y. Yi, D. Zhang, K. Sun, H. W. Roesky, Y. Yang, *Dalton Trans.* **2015**, *44*, 19800–19804.

[3] G. Kickelbick, *Hybrid Materials: Synthesis, Characterization and Applications*, Wiley-VCH, Weinheim, **2007**.

[4] A. F. Holleman, N. Wiberg, *Lehrbuch der Anorganischen Chemie*, Walter De Gruyter, Berlin, **2007**.

[5] X. Bu, N. Zheng, Y. Li, P. Feng, *J. Am. Chem. Soc.* **2002**, *124*, 12646–12647.

[6] W.-W. Xiong, J.-R. Li, B. Hu, B. Tan, R.-F. Li, X.-Y. Huang, *Chem. Sci* **2012**, *3*, 1200–1204.

[7] T. Wu, X. Bu, P. Liao, L. Wang, S.-T. Zheng, R. Ma, P. Feng, *J. Am. Chem. Soc.* **2012**, *134*, 3619–3622.

[8] M. Ribes, J. Olivier-Fourcade, E. Philipott, M. Maurin, *J. Solid. State. Chem.* **1973**, *8*, 195–205.

[9] K. Tsamourtzi, J.-H. Song, T. Bakas, A. J. Freeman, P. N. Tritikalis, M. G. Kanatzidis, *Inorg. Chem.* **2008**, *47*, 11920–11929.

[10] G. Thiele, T. Krüger, S. Dehnen, *Angew. Chem. Int. Ed.* **2014**, *53*, 4699.

[11] W. S. Sheldrick, B. Schaaf, *Z. Naturforsch. B* **1995**, *50*, 1469.

[12] J. Hilbert, W. Bensch, C. Näther, *Curr. Inorg. Chem.* **2016**, *6*, 181.

[13] Y.-Y. Pu, X. Zhang, L.-S. You, G.-Q. Bian, Q.-Y. Zhu, J. Dai, *Z. Anorg. Allg. Chem.* **2012**, *638*, 2498.

[14] B. Krebs, S. Pohl, W. Schiwy, *Angew. Chem. Int. Ed. Engl.* **1970**, *9*, 897–898.

[15] J. P. H. J. C. Huffman, and, A. M. Umarij, G. K. Shenoy, R. C. Haushalter, *Inorg. Chem.* **1984**, *23*, 2312–2315.

[16] B. Eisenmann, J. Hansa, *Z. Kristallogr.* **1993**, *203*, 299–300.

[17] C. Zimmermann, M. Melullis, S. Dehnen, *Angew. Chem. Int. Ed.* **2002**, *41*, 4269–4272.

[18] S. Dehnen, M. K. Brandmayer, *J. Am. Chem. Soc.* **2003**, *125*, 6618–6619.

[19] M. Melullis, C. Zimmermann, C. E. Anson, S. Dehnen, *Z. Anorg. Allg. Chem.* **2003**, *629*, 2325–2329.

[20] M. K. Brandmayer, R. Clerac, F. Weigend, S. Dehnen, *Chem. Eur. J.* **2004**, *10*, 5147–5157.

[21] E. Ruzin, A. Fuchs, S. Dehnen, *Chem. Commun.* **2006**, *38*, 4796–4798.

[22] E. Ruzin, C. Zimmermann, P. Hillebrecht, S. Dehnen, *Z. Anorg. Allg. Chem.* **2007**, *633*, 820–829.

[23] F. Lips, S. Dehnen, *Inorg. Chem.* **2008**, *47*, 5561–5563.

[24] S. Santner, S. Dehnen, *Inorg. Chem.* **2015**, *54*, 1188–1190.

[25] A. Fehlker, R. Blachnik, *Z. Anorg. Allg. Chem.* **2001**, *627*, 411–418.

[26] S. Santner, J. Heine, S. Dehnen, *Angew. Chem.* **2016**, *128*, 886–904.

[27] Y. Lin, W. Massa, S. Dehnen, *J. Am. Chem. Soc.* **2012**, *134*, 4497–4500.

[28] S. Santner, S. Yogendra, J. J. Weigand, S. Dehnen, *Chem. Eur. J.* **2017**, *23*, 1999.

[29] Q. Lin, X. Bu, P. Feng, *Chem. Commun.* **2014**, *50*, 4044.

[30] J. B. Parise, Y. Ko, J. Rijssenbeek, D. M. Nellis, K. Tan, S. Koch, *J. Chem. Soc. Chem. Commun.* **1994**, 527.

[31] N. Kamaya, K. Hooma, Y. Yamakawa, M. Hirayama, R. Kanno, M. Yonemura, T. Kamiyama, Y. Kato, S. Hama, K. Kawamoto, A. Mitsui, *Nature Mater.* **2011**, *10*, 682–686.

[32] T. Kaib, S. Haddadpour, M. Kapitein, P. Bron, C. Schröder, H. Eckert, B. R. S. Dehnen, *Chem. Mater.* **2013**, *24*, 2211–2219.

[33] P. Bron, S. Johansson, K. Zick, J. S. auf der Günne, S. Dehnen, B. Roling, *J. Am. Chem. Soc.* **2013**, *135*, 15694–15697.

[34] M. Duchardt, U. Ruschewitz, S. Adams, S. Dehnen, *Angew. Chem.* **2018**, *129*, 8906–8910.

[35] M. Duchardt, S. Neuberger, U. Ruschewitz, T. Krauskopf, W. Zeier, J. S. auf der Günne, S. Adams, B. Roling, S. Dehnen, *Chem. Mater.* **2018**, *30*, 4134–4139.

[36] Y. Lin, D. Xie, W. Massa, L. Mayrhofer, S. Lippert, B. Evers, A. Chernikov, M. Koch, S. Dehnen, *Chem. Eur. J.* **2013**, *19*, 8806–8813.

[37] B. D. Yuhas, A. L. Smeigh, A. P. Samuel, Y. Shim, S. Bag, A. P. Douvalis, M. R. Wasielewski, M. G. Kanatzidis, *J. Am. Chem. Soc.* **2011**, *133*, 7252–7255.

[38] P. Pfeiffer, R. Lehnhardt, *Ber. Dtsch. Chem. Ges.* **1903**, *36*, 3027–3030.

[39] N. Kakimoto, M. Matsui, T. Takada, M. Akiba, *Heterocycles* **1985**, *23*, 2681–2684.

[40] R. H. Benno, C. J. Fritchie, *J. Chem. Soc. Dalton Trans.* **1973**, 543–546.

[41] W. Klemm, H. Sodomann, P. Langmesser, *Z. Anorg. Allg. Chem.* **1939**, *241*, 281.

[42] G. Brauer, *Handbuch der Präparativen Anorganischen Chemie*, Ferdinand Enke Verlag, Stuttgart, **1975**.

[43] J.-H. So, P. Boudjouk, *Synthesis* **1989**, 306–307.

[44] M. W. DeGroot, N. J. Taylor, J. F. Corrigan, *J. Mater. Chem.* **2004**, *14*, 654–660.

[45] B. M. Moore, S. M. Ramirez, G. R. Yandek, T. S. Haddad, J. M. Mabry, *J. Organomet. Chem.* **2011**, *696*, 2676–2680.

[46] C. Honacker, Z.-W. Qu, J. Tannert, M. Layh, A. Hepp, S. Grimme, W. Uhl, *Dalton Trans.* **2016**, *45*, 6159–6174.

[47] U. Schröer, H.-J. Albert, W. P. Neumann, *J. Organomet. Chem.* **1975**, *102*, 291–295.

[48] K. A. Kocheshkov, *Ber. Dtsch. Chem. Ges.* **1929**, *62*, 996–999.

[49] K. A. Kocheshkov, *Ber. Dtsch. Chem. Ges.* **1933**, *66*, 1661–1665.

[50] H. Zimmer, H.-W. Sparmann, *Chem. Ber.* **1954**, *87*, 42–48.

[51] C. Zeppek, J. Pichler, A. Torvisco, M. Flock, F. Uhlig, *J. Organomet. Chem.* **2013**, *740*, 41–49.

[52] B. Jousseaume, M. Lahcini, M.-C. Rascle, *Organometallics* **1995**, *14*, 685–689.

[53] B. Jousseaume, H. Riague, T. .Toupance, *Organometallics* **2002**, *21*, 4590–4594.

[54] H. Alhamzaoui, B. Jousseaume, T. Toupance, H. Allouchi, *Organometallics* **2007**, *26*, 3902–3917.

[55] M. Seibert, K. Merzweiler, C. Wagner, H. Weichmann, *J. Organomet. Chem.* **2002**, *650*, 25–36.

[56] C. W. Still, *J. Am. Chem. Soc.* **1978**, *100*, 1481–1487.

[57] R. J. Linderman, J. M. Siedlecki, *J. Org. Chem.* **1990**, *61*, 6492–6493.

[58] G. Villaca, K. Barathieu, B. Jousseaume, T. Toupance, *Organometallics* **2003**, *22*, 4584–4592.

[59] C. Gosmini, J. Perichon, *Org. Biomol. Chem.* **2005**, *3*, 216–217.

[60] J. W. Burley, R. E. Hutton, V. Oakes, *J. Chem. Soc. Chem. Commun.* **1976**, *20*, 803–804.

[61] R. E. Hutton, J. W. Burley, *J. Organomet. Chem.* **1978**, *156*, 369–382.

[62] K. v. Werner, H. Blank, K. Yasufuku, *J. Organomet. Chem.* **1979**, *165*, 187–198.

[63] J. P. Eußner, S. Dehnen, *Z. Anorg. Allg. Chem.* **2014**, *640*, 295–299.

[64] S. H. L. Thoonen, B.-J. Deelman, G. van Koten, *J. Organomet. Chem.* **2004**, *689*, 2145–2157.

[65] G. Shangguan, F. Xing, X. Qu, J. Mao, D. Zhao, X. Zhao, J. Ren, *Bioorg. Med. Chem. Lett.* **2005**, *15*, 2962–2965.

[66] S. Mahboob, R. Gill, M. Mazhar, G. Kociok-Köhn, K. C. Molloy, *Monatsh. Chem.* **2008**, *139*, 1019–1024.

[67] S. Heimann, M. Holynska, S. Dehnen, *Z. Anorg. Allg. Chem.* **2012**, *638*, 1663–1666.

[68] S. Heimann, G. Thiele, S. Dehnen, *J. Organomet. Chem.* **2016**, *813*, 36–40.

[69] H. Berwe, A. Haas, *Chem. Ber.* **1987**, *120*, 1175–1182.

[70] Z. Hassanzahdeh Fard, C. Müller, T. Harmening, R. Pöttgen, S. Dehnen, *Angew. Chem. Int. Ed.* **2009**, *48*, 4441–4444.

[71] Z. You, J. Bergunde, B. Gerke, R. Pöttgen, S. Dehnen, *Inorg. Chem.* **2014**, *53*, 12512–12518.

[72] K. Wraage, T. Pape, R. Herbst-Irmer, M. Noltemeyer, H.-G. Schmidt, H. W. Roesky, *Eur. J. Inorg. Chem.* **1999**, 869–872.

[73] Z. Hassanzadeh Fard, L. Xiong, C. Müller, M. Holynska, S. Dehnen, *Chem. Eur. J.* **2009**, *15*, 6595–6604.

[74] J. A. Forstner, E. L. Muetterties, *Inorg. Chem.* **1966**, *4*, 552–554.

[75] U. Herzog, U. Bohme, G. Roewer, G. Rheinwald, H. Lang, *J. Organomet. Chem.* **2000**, *602*, 193–207.

[76] S. R. Bahr, P. Boudjouk, *Inorg. Chem.* **1992**, *31*, 712–713.

[77] U. Herzog, G. Rheinwald, *J. Organomet. Chem.* **2001**, *628*, 133–143.

[78] J. Eußner, B. Barth, E. Leusmann, Z. You, N. Rinn, S. Dehnen, *Chem. Eur. J.* **2013**, *19*, 13792–13802.

[79] J. Eußner, R. O. Kusche, S. Dehnen, *Chem. Eur. J.* **2015**, *21*, 12376–12388.

[80] N. Rinn, J. Eußner, W. Kaschuba, X. Xie, S. Dehnen, *Chem. Eur. J.* **2016**, *22*, 3094–3104.

[81] B. Menzebach, P. Bleckmann, *J. Organomet. Chem.* **1975**, *91*, 291.

[82] L. Pazdernik, F. Brisse, R. Rivest, *Acta Crystallogr.* **1977**, *B33*, 1780.

[83] a. A. B. M. Drager, H.-J. Jacobsen, B. Krebs, *J. Organomet. Chem.* **1978**, *161*, 319.

[84] P. Boudjouk, M. P. R. jr., D. G. Grier, W. Triebold, B. R. Jarabek, *Organometallics* **1999**, *18*, 4534.

[85] U. Herzog, H. Lange, H. Borrmann, B. Walfort, H. Lang, *J. Organomet. Chem.* **2004**, *689*, 4909.

[86] I. S. Nizamov, G. G. Sergeenko, I. D. Nizamov, Y. E. Poppovich, R. N. Khaibulin, L. A. Afmetkina, B. E. Abalonin, E. S. Batyeva, D. B. Krivolapov, I. A. Litvinov, *Heteroat. Chem.* **2004**, *15*, 225.

[87] G. Gupta, T.-M. Jeong, C. G. Kim, J. Kim, *Mater. Lett.* **2015**, *156*, 121.

[88] P. G. Jones, H. W. Roesky, Y. Zhi, *CSD Communication* **2015**.

[89] C. Dorfelt, A. Janeck, D. Kobelt, E. F. Paulus, H. Scherer, *J. Organomet. Chem.* **1968**, *14*, P22–P24.

[90] E. Wiberg, W. Simmler, *Z. Anorg. Chem.* **1955**, *282*, 330.

[91] K. Moedritzer, *Inorg. Chem.* **1967**, *6*, 1248–1249.

[92] J. C. J. Bart, J. J. Daly, *Dalton Trans.* **1975**, 2063–2068.

[93] A. Haas, H.-J. Kutsch, C. Krüger, *Chem. Ber.* **1987**, *120*, 1045–1048.

[94] H. Puff, K. Braun, S. Franken, T. Riza, W. Schuh, *J. Organomet. Chem.* **1987**, *335*, 167–168.

[95] M. Weidenbruch, J. Schlaefke, *Angew. Chem.* **1994**, *106*, 1938–1939.

[96] C. Wagner, C. Raschke, K. Merzweiler, *Appl. Organomet. Chem.* **2004**, *18*, 147.

[97] W. Ando, T. Kadowaki, Y. Kabe, M. Ishii, *Angew. Chem.* **1992**, *104*, 84–85.

[98] R. A. Varga, C. Silvestru, *Acta Crystallogr.* **2007**, *E63*, m2789–m2789.

[99] O. J. Scherer, K. Andres, C. Krüger, Y. H. Tsay, G. Wolmershäuser, *Angew. Chem.* **1980**, *92*, 563–564.

[100] M. Unno, Y. Kawai, H. Shioyama, H. Matsumoto, *Organometallics* **1997**, *16*, 4428–4434.

[101] Z. Hassanzahdeh Fard, *Dissertation*, Philipps-Universität Marburg, **2010**.

[102] J. P. Eußner, B. E. K. Barth, U. Justus, N. W. Rosemann, S. Chatterjee, S. Dehnen, *Inorg. Chem.* **2015**, *54*, 22–24.

[103] S. Heimann, M. Holynska, S. Dehnen, *Chem. Commun.* **2011**, *47*, 1881–1883.

[104] S. Heimann, *Dissertation*, Philipps-Universität Marburg, **2013**.

[105] E. Leusmann, *Dissertation*, Philipps-Universität Marburg, **2015**.

[106] B. E. K. Barth, E. Leusmann, K. Harms, S. Dehnen, *Chem. Commun.* **2013**, *49*, 6590–6592.

[107] B. E. K. Barth, K. Harms, S. Dehnen, *Eur. J. Inorg. Chem.* **2014**, 2406–2411.

[108] E. Leusmann, F. Schneck, S. Dehnen, *Organometallics* **2015**, *34*, 3264–3271.

[109] E. Leusmann, N. W. Rosemann, B. Weinert, S. Chatterjee, S. Dehnen, *Eur. J. Inorg. Chem.* **2016**, 5300–5304.

[110] E. Geringer, pers. Mitteilung, **2019**.

[111] E. Leusmann, E. Geringer, B. Weinert, S. Dehnen, *Dalton Trans.* **2016**, *45*, 15298–15302.

[112] E. Geringer, S. Dehnen, *Z. Anorg. Allg. Chem.* **2018**, *644*, 920–924.

[113] Z. You, S. Dehnen, *Inorg. Chem.* **2013**, *52*, 12332–12334.

[114] Z. You, D. Fenske, S. Dehnen, *Dalton Trans.* **2013**, *42*, 8179–8182.

[115] E. Leusmann, M. Wagner, N. W. Rosemann, S. Chatterjee, S. Dehnen, *Inorg. Chem.* **2014**, *53*, 4228–4233.

[116] C. Pöhlker, I. Schellenberg, R. .Pöttgen, S. Dehnen, *Chem. Commun.* **2010**, *46*, 2605–2607.

[117] Z. You, K. Harms, S. Dehnen, *Eur. J. Inorg. Chem.* **2015**, 5322–5328.

[118] Z. You, R. Möckel, J. Bergunde, S. Dehnen, *Chem. Eur. J.* **2015**, *20*, 13491–13496.

[119] Z. Hassanzahdeh Fard, M. R. Halvagar, S. Dehnen, *J. Am. Chem. Soc.* **2010**, *132*, 2848–2849.

[120] K. Hanau, N. Rinn, M. Argentari, S. Dehnen, *Chem. Eur. J.* **2018**, *24*, 11711–11716.

[121] B. E. K. Barth, B. A. Tkachenko, J. P. Eußner, P. R. Schreiner, S. Dehnen, *Organometallics* **2014**, *33*, 1678–1688.

[122] J.-P. Berndt, A. Engel, R. Hrdina, S. Dehnen, P. R. Schreiner, *Organometallics* **2019**, *38*, 329–335.

[123] A. Engel, E. Dornsiepen, S. Dehnen.

[124] N. Rinn, J.-P. Berndt, A. Kreher, R. Hrdina, P. R. Schreiner, S. Dehnen, *Organometallics* **2016**, *35*, 3215–3220.

[125] A. Engel, S. Dehnen, Manuskript eingereicht, **2019**.

[126] A. Engel, A. Reuter, J. Boche, S. Dehnen, Manuskript in Vorbereitung, **2019**.

[127] J. Keuter, K. Schwedtmann, A. Hepp, K. Bergander, O. Janka, C. Doerenkamp, H. Eckert, C. Mück-Lichtenfeld, F. Lips, *Angew. Chem. Int. Ed.* **2017**, *56*, 13866–13871.

[128] M. Saito, H. Hashimoto, T. Tajima, M. Ikeda, *J. Organomet. Chem.* **2007**, *692*, 2729–2735.

[129] C. Gaffney, P. G. Harrison, T. J. King, *J. Chem. Soc. Chem. Commun.* **1980**, 1251–1252.

[130] A. Eichhoefer, *Eur. J. Inorg. Chem.* **2005**, 1683–1688.

[131] R. Hauser, K. Merzweiler, *Z. Anorg. Allg. Chem.* **2002**, *628*, 905–906.

[132] R. Hauser, K. Merzweiler, *Z. Anorg. Allg. Chem.* **1998**, *624*, 10–12.

[133] M. R. Halvagar, Z. Hassanzahdeh Fard, S. Dehnen, *Chem. Commun.* **2010**, *46*, 4716–4718.

[134] J. P. Eußner, S. Dehnen, *Chem. Commun.* **2014**, *50*, 11385–11388.

[135] N. Rinn, L. Guggolz, J. Lange, S. Chatterjee, T. Block, R. Pöttgen, S. Dehnen, *Chem. Eur. J.* **2018**, *24*, 5840–5848.

[136] N. Rinn, L. Guggolz, K. Gries, K. Volz, J. Senker, S. Dehnen, *Chem. Eur. J.* **2017**, *23*, 15607–15611.

[137] E. Dornsiepen, J. P. Eußner, N. W. Rosemann, S. Chatterjee, S. Dehnen, *Inorg. Chem.* **2017**, *56*, 11326–11335.

[138] M. R. Halvagar, Z. Hassanzahdeh Fard, L. Xiong, S. Dehnen, *Inorg. Chem.* **2009**, *48*, 7373–7377.

[139] N. Rinn, K. Hanau, L. Guggolz, A. Rinn, S. Chatterjee, S. Dehnen, *Z. Anorg. Allg. Chem.* **2017**, *643*, 1508–1512.

[140] Y. Matsuhashi, N. Tokitoh, R. Okazaki, *Organometallics* **1994**, *13*, 4387–4397.

[141] J. S. L. Yeo, J. J. Vittal, T. S. A. Hor, W. Henderson, *Dalton Trans.* **2001**, 315–321.

[142] H. P. Nayek, W. Massa, S. Dehnen, *Inorg. Chem.* **2008**, *47*, 9146–9148.

[143] A. Eichhöfer, J. Jiang, S. Lebedkin, D. Fenske, D. G. McDonald, J. F. Corrigan, C.-Y. Su, *Dalton Trans.* **2012**, *41*, 3321–3327.

[144] A. Eichhöfer, M. Kühn, S. Lebedkin, M. Kehry, M. M. Kappes, F. Weigend, *Inorg. Chem.* **2017**, *56*, 9339–9336.

[145] W. Zinth, U. Zinth, *Optik*, De Gruyter, Berlin, **2018**.

[146] W. Demtröder, *Experimentalphysik 2 - Elektrizität und Optik*, Springer, **2017**.

[147] J. Heintze, P. Bock, *Lehrbuch zur Experimentalphysik - Band 4: Wellen und Optik*, Springer, **2017**.

[148] P. W. Atkins, J. de Paula, *Physikalische Chemie*, Wiley-VCH, Weinheim, **2010**.

[149] J. P. Eußner, *Dissertation*, Philipps-Universität Marburg, **2015**.

[150] N. Rosemann, J. Eußner, A. Beyer, S. Koch, K. Volz, S. Dehnen, S. Chatterjee, *Science* **2016**, *352*, 1301–1304.

8 Publikationsliste

Publikationen

Die in dieser Arbeit enthaltenen Publikationen sind durch fett gedruckte Titel gekennzeichnet.

13. **"Controlling the White-Light Generation of $[(RSn)_4E_6]$: Effects of substituent and chalcogenide variation"**
E. Dornsiepen, F. Dobener, N. Mengel, S. Chatterjee, S. Dehnen, **2019** *Manuskript in Vorbereitung.*

12. **"$[\{(PhSn)_3SnS_6\}\{(CpM)_3S_4\}]$ (M = Mo, W): Minimal Molecular Models of Covalent Attachment of Metalchalcogenide Clusters on Layered Transition Metal Dichalcogenides (TMDCs)"**
E. Dornsiepen, S. Dehnen, **2019**, *Manuskript in Vorbereitung.*

11. **"How Organotin Sulfide Clusters Behave in the Presence of Zinc Compounds – a Reactivity Study"**
E. Dornsiepen, S. Dehnen, *Eur. J. Inorg. Chem.* **2019**, DOI:10.1002/ejic.201900508.

10. "Click Reactions and Intramolecular Condensation Reactions on Azido-Adamantyl-Functionalized Tin Sulfide Clusters"
A. Engel, E. Dornsiepen, S. Dehnen, *Inorg. Chem. Front.* **2019**, DOI:10.1039/C9QI00424F.

9. **"White-Light Generation Upon In-Situ Amorphization of Single Crystals of $[\{(Me_3P)_3AuSn\}(PhSn)_3S_6]$ and $[\{(Et_3P)_3AgSn\}(PhSn)_3S_6]$"**
E. Dornsiepen, F. Dobener, N. Mengel, O. Lenchuk, C. Dues, S. Sanna, D. Mollenhauer, S. Chatterjee, and S. Dehnen,*Adv. Opt. Mater.* **2019**, *7*, 1801793.

8. **"Dinuclear organogermanium chalcogenide complexes as intermediates towards functionalized clusters"**
E. Dornsiepen, S. Dehnen, *Dalton Trans.* **2019**, *48*, 3671–3675.

7. **"Transition-Metal-Induced Rearrangement of $[(PhSn)_4S_6]$ Towards Ternary $Cu^I/Sn/S$ or $Cu^{II}/Sn/S$ Clusters"**
E. Dornsiepen, F. Weigend, S. Dehnen, *Chem. Eur. J.* **2019**, *25*, 2486–2490.

6. “Coordination chemistry of organometallic or inorganic binary group 14/16 units towards transition metal atoms”
E. Dornsiepen, E. Geringer, N. Rinn, S. Dehnen, *Coord. Chem. Rev.* **2019**, *380*, 136–169.

5. “Impact of the Exchange of the Coordinating Solvent Shell in $[Bi_{38}O_{45}(OMc)_{24}(dmso)_9]$ by Alcohols: Crystal Structure, Gas Phase Stability, and Thermoanalysis”
M. Weber, G. Thiele, E. Dornsiepen, D. P. Weimann, C. A. Schalley, S. Dehnen, M. Mehring, *Z. Anorg. Allg. Chem.* **2018**, *644*, 1796–1804.

4. “Structure Determination of a new Molecular White-Light Source”
B. D. Klee, E. Dornsiepen, J. R. Stellhorn, B. Paulus, S. Hosokawa, S. Dehnen, W.-C. Pilgrim, *Phys. Status Solidi B* **2018**, *255*, 1800083.

3. “Syntheses and Properties of Gold-Organotin Sulfide Clusters”
E. Dornsiepen, J. P. Eußner, N. W. Rosemann, S. Chatterjee, S. Dehnen, *Inorg. Chem.* **2017**, *56*, 11326–11335.

2. “Synthesis, structure and thermolysis of oxazagermines and oxazasilines”
F. Dannenberg, G. Thiele, E. Dornsiepen, S. Dehnen, M. Mehring, *New J. Chem.* **2017**, *41*, 4990–4997.

1. **“Organotetrel Chalcogenide Clusters: Between Strong Second-Harmonic and White-Light Continuum Generation”**
N.W. Rosemann, J.P. Eußner, E. Dornsiepen, S. Chatterjee, S. Dehnen, *J. Am. Chem. Soc.* **2016**, *138*, 16224–16227.

Tagungsbeiträge

12. “Binary and Ternary Organotetrel Sulfide Clusters with Extreme Optical Nonlinearity”
Posterbeitrag bei der 17. Vortragstagung der Wöhler-Vereinigung vom 24.09. - 27.09.2018 in Regensburg.

11. “Organotetrel Chalcogenide Clusters with Nonlinear Optical Properties”
Vortrag bei der GRK-Jahrestagung vom 02.09 - 06.09.2018 in Volkenroda

10. “Binary and Ternary Organotetrel Sulfide Clusters with Extreme Optical Nonlinearity”
Posterbeitrag bei der EuChems 2018 vom 26.08. - 30.08.2018 in Liverpool

9. “Organotetrel Sulfide Clusters with Optical Nonlinearity”
Posterbeitrag beim SFB Student Poster Day am 01.03.2018 in Marburg

8. “Binary and Ternary Organotetrel Chalcogenide Clusters”
Vortrag bei der GRK-Jahrestagung vom 02.10. - 06.10.2017 in Stadland

7. “Binary and Ternary Organotetrel Sulfide Clusters”
Posterbeitrag beim GDCh-Wissenschaftsforum vom 10.09. - 14.09.2017 in Berlin

6. “Organozinnchalkogenid-Cluster mit Heteroadamantanstruktur”
Vortrag beim Seminar von Arbeitsgruppen für Anorganische Chemie vom 20.08. - 25.08.2017 in Hirschegg (Kleinwalsertal)

5. “Binary and Ternary Organotetrel Sulfide Clusters”
Posterbeitrag bem Anglo-German Inorganic Chemistry Meeting (Agichem) vom 06.08. - 09.08.2017 in Göttingen

4. “Synthesis and Properties of Inorganic/Organic Core-Shell-Shell Clusters”
Vortrag bei der SFB Winter School vom 17.01. - 18.01.2017 in Rauischholzhausen

3. “Binary and Ternary Organotin Chalcogenide Clusters”
Posterbeitrag bei der 16. Vortragstagung der Wöhler-Vereinigung vom 26.09. - 28.09.2016 in Berlin

2. “Binary and Ternary Organotin Chalcogenide Clusters”
Posterbeitrag bei der International Conference on the Coordination and Organometallic Chemistry of Germanium, Tin and Lead (GTL) vom 28.08. - 02.09.2016 in Pardubice (Tschechische Republik)

1. “Functional Binary and Ternary Organotin Sulfide Clusters”
Posterbeitrag bei der International Conference on Internal Interfaces (ICII) vom 31.05. - 03.06.2016 in Marburg

9 Wissenschaftlicher Lebenslauf

Persönliche Daten

Name:	Eike Dornsiepen
Geburtsdatum:	23.04.1991
Geburtsort:	Bad Wildungen

Promotion

02/2016 - 07/2019	Promotion in der Arbeitsgruppe von Prof. Dr. Stefanie Dehnen "Organotetrelchalkogenidcluster mit Heteroadamantanstruktur"

Studium

10/2013 - 01/2016	Chemiestudium (M. Sc.) an der Philipps-Universität Marburg Masterarbeit in der Arbeitsgruppe von Prof. Dr. Stefanie Dehnen "Beiträge zur Derivatisierung von Organozinnsulfid-Clustern"
10/2010 - 09/2013	Chemiestudium (B. Sc.) an der Philipps-Universität Marburg Bachelorarbeit in der Arbeitsgruppe von Prof. Dr. Bernd Harbrecht "Low-temperature, size-selective synthesis and characterization of Mn_3O_4 nanoparticles"

Schulische Ausbildung

06/2010	Abitur am Gustav-Stresemann-Gymnasium, Bad Wildungen

10 Abdruckgenehmigungen der im kumulativen Teil enthaltenen Publikationen

Im Folgenden sind die Abdruckgenehmigungen der Publikationen 4.1, 4.2 und 4.4 beigefügt. Die Publikation 4.7 darf ohne explizite Genehmigung der Royal Society of Chemistry abgedruckt werden; die restlichen Publikationen waren zum Druckzeitpunkt dieser Dissertation noch nicht gedruckt.

Title: Organotetrel Chalcogenide Clusters: Between Strong Second-Harmonic and White-Light Continuum Generation

Author: Nils W. Rosemann, Jens P. Eußner, Eike Dornsiepen, et al

Publication: Journal of the American Chemical Society

Publisher: American Chemical Society

Date: Dec 1, 2016

PERMISSION/LICENSE IS GRANTED FOR YOUR ORDER AT NO CHARGE

This type of permission/license, instead of the standard Terms & Conditions, is sent to you because no fee is being charged for your order. Please note the following:

- Permission is granted for your request in both print and electronic formats, and translations.
- If figures and/or tables were requested, they may be adapted or used in part.
- Please print this page for your records and send a copy of it to your publisher/graduate school.
- Appropriate credit for the requested material should be given as follows: "Reprinted (adapted) with permission from (COMPLETE REFERENCE CITATION). Copyright (YEAR) American Chemical Society." Insert appropriate information in place of the capitalized words.
- One-time permission is granted only for the use specified in your request. No additional uses are granted (such as derivative works or other editions). For any other uses, please submit a new request.

JOHN WILEY AND SONS LICENSE TERMS AND CONDITIONS

May 16, 2019

This Agreement between Eike Dornsiepen ("You") and John Wiley and Sons ("John Wiley and Sons") consists of your license details and the terms and conditions provided by John Wiley and Sons and Copyright Clearance Center.

License Number	4590800647833
License date	May 16, 2019
Licensed Content Publisher	John Wiley and Sons
Licensed Content Publication	Advanced Optical Materials
Licensed Content Title	White-Light Generation Upon In-Situ Amorphization of Single Crystals of [{(Me3P)3AuSn}(PhSn)3S6] and [{(Et3P)3AgSn}(PhSn)3S6]
Licensed Content Author	Eike Dornsiepen, Florian Dobener, Nils Mengel, et al
Licensed Content Date	Apr 2, 2019
Licensed Content Volume	0
Licensed Content Issue	0
Licensed Content Pages	10
Type of use	Dissertation/Thesis
Requestor type	Author of this Wiley article
Format	Print and electronic
Portion	Full article
Will you be translating?	No
Title of your thesis / dissertation	Organotetrelchalkogenidcluster mit Heteroadamantanstruktur
Expected completion date	May 2019
Expected size (number of pages)	380
Requestor Location	Eike Dornsiepen Kantstraße 10 Marburg, Hessen 35039 Germany Attn: Eike Dornsiepen
Publisher Tax ID	EU826007151
Total	0.00 EUR
Terms and Conditions	

TERMS AND CONDITIONS

This copyrighted material is owned by or exclusively licensed to John Wiley & Sons, Inc. or one of its group companies (each a"Wiley Company") or handled on behalf of a society with which a Wiley Company has exclusive publishing rights in relation to a particular work (collectively "WILEY"). By clicking "accept" in connection with completing this licensing transaction, you agree that the following terms and conditions apply to this transaction (along with the billing and payment terms and conditions established by the Copyright Clearance Center Inc., ("CCC's Billing and Payment terms and conditions"), at the time that you opened your RightsLink account (these are available at any time at http://myaccount.copyright.com).

JOHN WILEY AND SONS LICENSE TERMS AND CONDITIONS

May 16, 2019

This Agreement between Eike Dornsiepen ("You") and John Wiley and Sons ("John Wiley and Sons") consists of your license details and the terms and conditions provided by John Wiley and Sons and Copyright Clearance Center.

License Number	4590801187329
License date	May 16, 2019
Licensed Content Publisher	John Wiley and Sons
Licensed Content Publication	Chemistry - A European Journal
Licensed Content Title	Transition-Metal-Induced Rearrangement of [(PhSn)4S6] Towards Ternary CuI/Sn/S or CuII/Sn/S Clusters
Licensed Content Author	Eike Dornsiepen, Florian Weigend, Stefanie Dehnen
Licensed Content Date	Jan 25, 2019
Licensed Content Volume	25
Licensed Content Issue	10
Licensed Content Pages	5
Type of use	Dissertation/Thesis
Requestor type	Author of this Wiley article
Format	Print and electronic
Portion	Full article
Will you be translating?	No
Title of your thesis / dissertation	Organotetrelchalkogenidcluster mit Heteroadamantanstruktur
Expected completion date	May 2019
Expected size (number of pages)	380
Requestor Location	Eike Dornsiepen Kantstraße 10 Marburg, Hessen 35039 Germany Attn: Eike Dornsiepen
Publisher Tax ID	EU826007151
Total	0.00 EUR
Terms and Conditions	

TERMS AND CONDITIONS

This copyrighted material is owned by or exclusively licensed to John Wiley & Sons, Inc. or one of its group companies (each a"Wiley Company") or handled on behalf of a society with which a Wiley Company has exclusive publishing rights in relation to a particular work (collectively "WILEY"). By clicking "accept" in connection with completing this licensing transaction, you agree that the following terms and conditions apply to this transaction (along with the billing and payment terms and conditions established by the Copyright Clearance Center Inc., ("CCC's Billing and Payment terms and conditions"), at the time that you opened your RightsLink account (these are available at any time at http://myaccount.copyright.com).

Danksagung

Hiermit möchte ich mich ganz herzlich bei all denjenigen bedanken, die in den letzten dreieinhalb Jahren meinen Weg zur Promotion begleitet haben. Es war eine wirklich schöne Zeit und ich habe immer gerne Zeit mit euch verbracht.
Bei meiner Doktormutter *Prof. Dr. Stefanie Dehnen* möchte ich mich für das stete Vertrauen, die große Freiheit bei der Bearbeitung meines Themas und viele lehrreiche Diskussionen bedanken.
Herrn *PD Dr. Ralf Tonner* danke ich für die Übernahme des Zweitgutachtens dieser Arbeit. Ebenso danke ich Herrn *Prof. Dr. Michael Gottfried* für die Mitwirkung in der Prüfungskommission.
Dem Sonderforschungsbereich 1083 „*Struktur und Dynamik innerer Grenzflächen*“ und dem Graduiertenkolleg 1782 „*Funktionalisierung von Halbleitern*“danke ich für die Finanzierung meiner Arbeit.
Meinen Kooperationspartnern *Dr. Nils W. Rosemann, Florian Dobener, Nils Mengel, Prof. Dr. Sangam Chatterjee, Olena Lenchuk, Prof. Dr. Doreen Mollenhauer, Christof Dues, Prof. Dr. Simone Sanna, Benjamin Klee, Prof. Dr. Wolf-Christian Pilgrim* und *PD Dr. Florian Weigend* danke ich für die Messung der komischen Verbindungen, die wir Anorganiker so fabrizieren, und die umfangreiche Unterstützung durch theoretische Rechnungen, die erheblich zum Verständnis der experimentellen Ergebnisse beigetragen haben.
Den Mitarbeitern der Serviceabteilungen des Fachbereichs Chemie, insbesondere in den Abteilungen für Kristallstrukturanalyse, Massenspektrometrie und NMR-Spektroskopie sei für die vielen Stunden an Messzeit gedankt.
Bei allen aktuellen und ehemaligen Mitarbeitern der Arbeitsgruppe, allen voran meinen Laborkollegen *Dr.(!) Niklas Rinn, Annikka Engel* und *Eugenie Geringer*, aber auch
Mario Argentari, Andreas Bäcker, Josefin Boche, Natalie Dehnhardt, Dr. Carsten Donsbach, Armin Eulenstein, Dr. Jens Eußner, Felix Fischer, Kimon Flosdorf, Stephanie Göbeler-Scheuer, Dr. Lukas Guggolz, Katharina Hanau, Dr. Johanna Heine, Uwe Justus, Dr. Istemi Kuzu, Dr. Robert Langer, Dr. Niels Lichtenberger, Leon Maser, Jakob Möbs, Igor Müller, Jörn Münzer, Simon Nier, Isabell Nußbruch, Bertram Peters, Jonathan Pfeiffer, Dr. Dejan Premuzic, Alexander Reckziegel, Anna Reuter, Dr. Silke Santner, Christian Schneider, Gregoire Sieg, Ursula Siepe, Dr. Frank Tambornino, Dr. Günther Thiele, Andrea Tschirch, Dr. Lisa Vondung, Bettina Wagner, Dr. Bastian Weinert, Ruth Weller, Dr. Gunnar Werncke und *Dr. Robert Wilson*
möchte ich für das sehr angenehme Arbeitsklima und die schöne Zeit sowohl im Labor als auch außerhalb davon danken.
Natürlich danke ich auch meinen Bachelor- und Vertiefungsstudenten *Anna Reuter, Falk*

Krauss, Igor Müller und *Andres Gonzales* für die Unterstützung.
Mein ganz besonderer Dank gilt meinen Freunden und vor allem meiner Familie, die mir in allen Phasen des Entstehens dieser Arbeit jede nur denkbare Unterstützung entgegenbrachten.